ULTRASONIC AND THERMO-KINETIC CHARACTERIZATION OF CURING EPOXY RESIN

By

SHEIKH MOHAMMOD ALI, MSc.

Thesis submitted to the University of Nottingham

for the degree of Doctor of Philosophy

JULY 2013

ABSTRACT

This study combines cure kinetics modelling and thermal and ultrasonic cure monitoring to characterize the cure state of a complex commercial modified epoxy thermosetting system of industrial importance containing two epoxies, diethylene triamine hardener, external catalyst, aliphatic reactive diluent, and mica. Both catalyst and reactive diluent in the formulation of two epoxy resin mixture keep this complex system odd from others and to some extent a new one to report cure kinetics to the best of our knowledge. The cure was monitored using differential scanning calorimetry (DSC) and broadband ultrasonic techniques over a group of isothermal cure temperatures within corresponding acceptable time scales. The sensitivities of both techniques to the *chemical, physical,* and *mechanical* changes associated with each part of the cure was discussed *comprehensively* and *critically* together with an inspection of the similarities between them coupled with *qualitative* and *quantitative* correlations.

An in depth details analysis of the chemical cure kinetics of the investigated system was presented utilizing the model free iso-conversional method coupled with the light of physics of advanced kinetics research. The modelling of the calorimetric cure kinetics of the epoxy system under study was developed utilizing the empirical approach of fitting of the experimental data to various kinetic models. The best fit model which best possibly describe the *non-typical autocatalytic* cure behaviour of the resin system and predicts the reaction course was evaluated and analyzed in details. Utilization of the maximum attained conversion at a specific curing temperature enables this model to *most closely* simulate the curing reaction under both chemical controlled and diffusion controlled conditions with almost a reasonable degree of satisfaction over the entire range of conversion and temperature studied without the *a priori* need of a glass transition temperature model. The non-conventional autocatalytic effect and prediction of the *trimolecular catalysis mechanism* of the curing reaction was found to be manifested in *temperature dependence of reaction orders*, which was elucidated and justified. In comparison to other epoxy resins without reactive diluents, the analysis of our data shows that most possibly, the reactive diluent increased the maximum value of calorimetric conversion and reaction rate, reduced the viscosity, while the values of activation energy and process parameters remained within the typical values of epoxy formulations and the crosslink density was unaffected.

The performance of each particular model tested was discussed along with their comparisons. Implementing diffusion factor in conventional models some useful information associated with the diffusion controlled kinetics related to our data were explored. The cure kinetics was also analyzed from both kinetic and thermodynamic viewpoint in the context of Horie model. This approach we employed, is, to some extent uncommon, can *contribute* towards a *new way of characterization* and the critical understanding of the cure reaction from the *micro-kinetic standpoint* providing information of the effect of reactive diluent on kinetics, regarding reaction pathways, kinetic homogeneity / inhomogeneity associated with reaction phase and the properties of the end product which are important to monitor and ultimately control the cure to attain desired properties in the end material. A TTT diagram of the cure process of this system was also constructed.

The ultrasonic compression wave velocity was demonstrated to be the most interesting and potential parameter for monitoring and characterizing the cure process at all stages which provided with the information of *degree of mechanical property development* and can detect gelation and vitrification that occur during cure. Therefore, ultrasonic velocity measurement could be exploited for *non-destructive on-line process control* in an industrial environment. It was demonstrated that ultrasonic compression wave velocity can be used as a predictor of calorimetric conversion measurements and thus can be used *to track chemical reaction on-line* which is of potential importance for cure monitoring. Though system specific, the methodology we utilized, at least in part, constitutes a *novel way* of quantifying the degree of cure of a commercial epoxy thermoset network from ultrasonic longitudinal velocity measurements which is interesting and promising. It was found that the DSC is much more sensitive to changes occurring at the early stages of the cure but is relatively insensitive to the changes occurring at the latter stage. Ultrasonic compression wave velocity shows a better sensitivity at the end of the cure. It was also demonstrated that ultrasonic compression wave attenuation, real and imaginary parts of compression modulus, ultrasonic loss tangent and associated central relaxation time, also provided information of the material state and the cure process as well. The end of cure ultrasonic data, in general, provide a convenient assessment of final product quality.

ACKNOWLEDGEMENTS

Table of Contents

Chapter 1   Introduction

1.1 Introduction

Epoxy resins are used in a wide range of applications across a diverge range of industries. They are playing an ever-increasing role in modern technology displaying series of interesting characteristics, with bonding applications ranging from toys and table tops to supersonic transports, with applications as primary structural materials in composite structures ranging from critical safety components and structures in the sector of automotive and aerospace industries to exciting space vehicle like *"Space ship One"* the primary structure of which is manufactured using an epoxy/graphite system, with applications in *"joining and fastening technology"* in many industries in full swing, with applications including coatings, electronic components and enclosures and as high-grade synthetic resins in engineering sectors, and also in *repairing 'human'* in medical sectors (e.g. the use of UV-curing cements in dentistry and acrylic bond cements in orthopaedic surgery) etc. and the list is virtually endless.

Epoxy resin consumption has grown, not only because of its performance capabilities but also because of its simplicity in use and its availability in a wide range of outstanding physical properties with remarkable advantages, making it adaptable for the rapid evolving stream of new applications.

1.2 The Importance of the Knowledge of Cure Kinetics

The thermosetting materials undergo an irreversible chemical process called *cure*. During cure the thermoset changes from low viscous liquid to visco-elastic rubber, and finally, to a glassy insoluble solid. On the microscopic level, polymer molecules grow into longer chains with branches and also crosslinking occurs. During the curing process of the epoxy resin, complex chemical and thermal reactions take place between the chemical species present in the thermosetting system. The overall effect of these reactions is generally attributed to a single reaction scheme, called the curing reaction. The progress of the curing reaction affects the properties of the thermoset and subsequently imposes limitations on its processability.

Thermosetting systems are characterized by their ability to form *'tailor-made'* products for particular applications. The properties and performance of the end products depend on the cure mechanism, extent of the cure reaction, process parameters like process time, temperature and pressure, the chemical mixture and thermoset volume. Optimal curing schedules are key to achieve efficiently the desired properties of the cured materials. Although companies manufacturing commercial epoxy thermoset materials usually suggest cure cycles for custom applications, their curing cycles may not be the optimal ones for special applications. The knowledge of the cure kinetics associated with the progress of the cure reaction and the evolution of the physical properties as the structure of the macromolecule forms during cure is highly important and essential on an *industrial scale* to the establishment of an optimum process cycle for a thermosetting system to attain the desired properties of the final product. In particular, the study of the reaction kinetics of thermosetting systems as a function of the processing conditions, from a macro-kinetic point of view, is very important for the analysis and design of processing operations. For the full potential of a thermosetting system to be realized it is vital to have a proper understanding of the chemistry (chemical nature) of the individual components of the resin system being used, as the reaction kinetics will have a direct impact on the nature of the final polymer (and hence component) produced.

Moreover, the optimization of the process can enhance cost effectiveness either by reducing the overall time of the heat treatment, or by changing the imposed thermal profile. By optimizing the cure process, it is also possible to increase overall manufacturing efficiency. The lack of knowledge of the optimum cure time can prolong product manufacturing times and therefore has economic consequences. In this connection, here, the common manufacturing process for the cure of structural adhesives can be mentioned which is generally based on a rigorous compliance to the cure schedule recommended by the supplier. Like mechanical fastening or welding most of the structural adhesives cannot produce maximum bond strength instantly. The assembled joint must be supported for at least part of the time period during which the strength of the bond is developing. In reality, sometimes the manufacturer needs to compromise efficiency to ensure that the bond is supported for an adequate length of time to completely avoid the possibility of under-curing and consequently the reduced mechanical strength. Therefore, this lack of knowledge of the optimum

time of cure lengthen product manufacturing times and thus bears economic consequences. If the cure temperature and time are not optimum the adhesive may be *overcured* or *undercured* during the cure. Overcured adhesives generally become brittle and fragile, whereas undercured adhesives may be rubbery thus lacking in mechanical strength. In the interest of component quality and reliability, it is becoming increasingly important to monitor the cure of many industrial resins in order to achieve the optimum curing condition for a given manufacturing process. Monitoring enables the user to follow the physical, chemical and structural changes that occur during the cure. Thus, it allows the detection of the state of the material including any abnormality during the curing process and ensure consistency in properties and performance of the final product.

The importance of the knowledge of cure kinetics becomes more obvious from the perspectives of its financial implications. As for example, fiber-reinforced composites are still the most common applications of epoxy resin. The superior strength-to-weight ratio make them suitable for applications ranging from sporting goods to aircraft components and space vehicles. However, they are relatively expensive and cannot be recycled owing to the irreversible nature of the cure. Without the aid of an adequate manufacturing process to produce the desired product, the final product can only be scrapped leading to high production costs. The knowledge of kinetics of cure enables to reduce the volume of scrap by simulating the process and limiting the range of the controlling parameters prior to the start of manufacture. Cure monitoring can ensure minimum amount of waste which may caused by accidental fluctuations of control parameters during cure and intentional destruction of the composite materials for the purposes of verification of their mechanical properties.

Proper understanding of the cure kinetics is one of the vital requirements for the development of a reliable monitoring system. The knowledge of the curing process, coupled with an appropriate monitoring technique can provide a better comprehensive insight of the cure.

Epoxy resins form the mainstay of the aerospace and automotive resin market and continue to find increasing use both as adhesives and as primary structural materials to form safety critical structural components or adhesive layers in aerospace, automotive, and marine assemblies. This give rise to increased demand of *quality assurance*. In fact, in the interest of component quality and reliability and manufacturing process economy, there is a requirement for techniques to monitor the cure of the resins during the component forming process to provide essential quality assurance data and eventually to provide the basis for real-time control of the process itself. The proper understanding of the kinetics of cure including the chemistry/chemical nature of the individual components of the thermosetting system under study, coupled with major advances in instrumentation and online non-destructive cure monitoring techniques, could pave the way of a new era of responsive and intelligent process control. Optimized process control will require a sensor to gather real-time process data, a cure model based on reaction mechanisms and physical changes, correlations between molecular structure and macroscopic properties, and an expert system to control the fabrication device. Once determined, setting the fixed quality assurance data for each thermoset, can be used as an input for the system.

1.3 Various Techniques of Cure Monitoring

As has already been stated cure monitoring enables the user to follow the physical, chemical and structural changes that occur during the cure and thus allows to *'see'* the state of the material during the progress of cure. Basically, the monitoring of cure process is done through recording and analysis of a selected material property that is related to the material *chemistry* and *microstructure*. There are a number of candidate techniques that could be used to monitor the cure of thermosetting materials and indeed have been suggested and used so to do. The varieties of techniques are based on the material properties which are measured in order to assess the state of the cure process. It will be helpful to categorize these into generic types of technique, and they are shown in table 1.1 along with the particular techniques and corresponding parameter/ material property measured during cure.

Table 1.1 Techniques of cure monitoring.

Generic Category	Techniques	Parameter/material property monitored
Chemical Techniques	Fourier Transform Infrared (FTIR) Spectroscopy	Functional group
	Raman Spectroscopy	Functional group
	Nuclear Magnetic Resonance (NMR) Spectroscopy	Chemical shift
	Chromatography	Molecular weight
Thermal Techniques	Differential Scanning Calorimetry (DSC)	Heat generation (enthalpy)
Electrical Techniques	Dielectric Analysis (DEA)	Conductivity, permittivity, loss tangent
Ultrasonic Techniques	Standard Ultrasonic Technique	Compression or shear velocity and attenuation
Mechanical Techniques	Dynamic Mechanical Analysis (DMA)	Viscosity, complex elastic or shear modulus, resonance frequency
Optical Techniques	Fourier Transform Infrared (FTIR) Spectroscopy using fiber optics	Refractive index and chemical functional group
	Raman Spectroscopy using fiber optics	Refractive index and chemical functional group
	Fluorescence Spectrometry	Intensity
Hypersonic (GHz) Technique	Brillouin Spectroscopy (BS)	Hypersonic velocity and attenuation
Microstructural Imaging Techniques	Wide angle X-ray Scattering (WAXS)	X-ray diffraction pattern
	Scanning Electron Microscopy (SEM) with Energy dispersive X-ray analysis (EDXA)	Intensity of electron (commonly secondary and back scattered electron) and X-ray diffraction pattern
	Transmission Electron Microscopy (TEM)	Intensity of electron (transmitted) diffraction pattern
	Standard Optical Microscopy	Intensity of light

Among the techniques mentioned in table 1.1 the most frequently used cure monitoring techniques are differential scanning calorimetry (DSC) [1,2,3,4,5,6], Raman Spectroscopy [3], nuclear magnetic resonance (NMR) [7,8], wide angle X-ray scattering (WAXS) [8], dynamic mechanical analysis (DMA) [1,5], dielectric measurements [7], and ultrasound [4,5,6,7,8].Since the design of a process cycle depends mostly on the *thermo-mechanical properties*, the thermal and mechanical techniques — these two generic methods based on the measurement of heat generation (enthalpy) and the complex elastic or shear moduli and viscosity respectively are of prime interest.

1.4 Characterization of Curing Process using DSC

The most common type of cure monitoring technique is differential scanning calorimetry. In this technique a sample is heated at a constant rate (dynamic scanning) or to a particular temperature (isothermal scanning) and the heat flow to or from the material is monitored. Since the crosslinking reaction in thermosetting polymers is exothermic and generates heat, the DSC can monitor this exothermic flow of heat and a characterization of the cure state of the material is made [1,2,3,4,5,6]. The rate of heat generation is measured in DSC. The completion of cure is then indicated by the lack of heat generation. The heat generated to the present time is compared with the total heat of reaction to determine the calorimetric degree of cure.

The results obtained from DSC on a thermosetting resin system can be easily analyzed to obtain the kinetic information and thermodynamic properties. For thermosetting resins, this technique provides valuable information on *glass transition temperature* (observed as an enthalpic relaxation peak/endothermic peak), *onset of cure* (observed as an exothermic event), *heat of cure* (integration of the area under the exothermic peak), *maximum rate of cure* (the exothermic peak), *completion of cure* (observed when DSC response returns to linear behaviour) and *degree of cure*.

The aim of the kinetic investigation of a curing thermoset resin system is, in general, the construction of a kinetic model which can predict characteristic features of the curing system for a given time-temperature profile. The object of modelling is to

optimize the processing parameters to obtain high-quality parts with greater consistency and to minimize the experimental work required to establish a cure cycle for any new parts. In the study of cure kinetics by DSC, the approach to describe the cure behaviour by an empirical kinetic model is, at present, the most flexible, simple and fast solution concerning the fitting of the experimental data (e.g. reaction rate profiles). This solution allows valid predictions despite the extreme variety of chemical reaction mechanisms.

In spite of the complexity of commercial epoxy thermosetting systems, the use of phenomenological models to describe the chemical reaction kinetics can still be useful in providing empirical parameters for modelling and controlling the curing process. By taking into account the kinetic equation empirically the researchers found the curing kinetic model to provide a very convenient way to describe the overall curing behaviour of commercial thermal-cure epoxy thermosets. These descriptions are useful for the modification and optimization of the cure cycle of the epoxy and other thermosetting systems for their particular applications.

It is worth mentioning that a thermosetting TTT(Time -Temperature -Transformation) cure diagram permits cure time-temperature paths to be chosen properly, so that the different material state transitions occur in a controlled manner and consequently give rise to predictable properties. Hence, such a TTT diagram might form the basis of a molecular model to aid a manufacturer in selecting an *optimum cure schedule* (cure time-temperature) to produce a cured resin with the desired properties. The diagram indicates suitable combinations of cure temperatures / cure times required to reach the significant events such as macromolecular gelation, vitrification and devitrification. Such information has to be considered in selecting the optimum cure profile for a composite part, especially if the main consideration is minimization of the duration of cure. This is particularly important in large and complex components, where there may be considerable variations in the thickness of the laminate. Minimization of the duration of cure shortens product manufacturing times leading to reduction of production costs. DSC, however, does not provide any information on mechanical behaviour.

1.5 Basis of Mechanical Technique

The mechanical techniques are based on the change of mechanical properties of the curing material which are measured in order to assess the state of cure [5]. The mechanical properties frequently measured are the complex shear moduli and the viscosity. Both the storage modulus and the shear viscosity increase with cure, the type of increase being sigmoidal for the former and exponential for the latter. The mechanical loss modulus initially increases to a peak and then decreases. The measurements of the complex moduli are usually taken in a low frequency range of up to 30 Hz.

Many of these techniques cannot be applied for on-line process monitoring (real time assessment) in an industrial setting that can form the basis of quality assurance procedures for adhered engineering components and structures. As for example, dielectric and mechanical methods are unsuitable since they require a special sample (DMA) or an insert in the joint (an electrode for the dielectric technique) and are as such not truly non-invasive which is highly desirable for process monitoring in an industrial setting.

1.6 Ultrasonic the state of the art

Among the techniques mentioned in table 1.1, ultrasound has the advantage that it is non-invasive, can be transmitted through the walls of a thermoset forming tool and can be applied to all cure states. This brings the opportunity to carry out on line, non-destructive process monitoring because ultrasonic detection can be done without pre-treatment of the material. However, the scientific basis for ultrasonic wave propagation through curing thermosets is not as well established as for dielectric spectroscopy which also have potential for applications in an industrial manufacturing setting. Other distinct advantages of this technique include the ability of the ultrasonic wave to propagate through a broad range of samples, including opaque materials (in contrast to optical spectroscopy), and the high resolution in measurements of velocity, allowing detection of concentrations down to ppm level.

Ultrasonic spectroscopy allows simultaneous measurements of two independent parameters of materials — velocity and attenuation, both of which are very sensitive to changes in intermolecular interactions and molecular organization. Attenuation is a measure of the energy loss in the compressions and decompressions produced as an ultrasonic wave passes through a material and gives information on the microscopic structural organization of the material. Ultrasonic velocity is a measurement of the density and elastic response of the material to the oscillating pressure and provides information regarding its molecular organization. Ultrasonic techniques have been shown to be an excellent tool for studying many key properties of polymer materials either in the context of a study of the materials themselves or for the purposes of in-process non-destructive evaluation.

First, both velocity and attenuation of ultrasound are known to be sensitive to the viscoelastic properties, polymer chain segment motions, and the structure of polymers [6,8]. Therefore, measurements of ultrasound absorption and phase velocity as functions of frequency and cure time can lead to important information about the extent of thermoset curing reaction, mechanical modulus, mechanical relaxation processes, phase transition phenomena and structural or morphological information in polymer systems.

Second, knowledge of the frequency dependence of the absorption co-efficient and of the wave propagation velocity can yield values for material viscoelastic parameters that can be incorporated into the simulation and design of adhered engineering components and structures and can be used for industrial process control of thermosetting materials.

Third, they may give indirect information on other process parameters for example, temperature or pressure and

Fourth, ultrasonic waves may be used on-line for inspection of part quality.

Fifth, because of the nature of the ultrasonic wave's propagation, ultrasonic technique directly measures the relation between ultrasonic wave behaviour and material characteristics on *microscopic scale* [4,6]. The measurement of ultrasonic parameters

reflect these changes in mechanical properties of the material during the cure process and correspondingly in the physical state of the material in terms of the *interplay between molecular and ultrasonic architecture of the growing network*. The term *'ultrasonic architecture'* is meant to include the type and concentration of ultrasonically active species as well as the various specific interactions that can affect the ultrasonic signal response.

In this study, the ultrasonic properties of the curing epoxy thermoset were measured using a broadband goniometric system. A sample of the uncured thermoset was formed in an aluminium frame and sandwiched between two thin polyamide layers. The sample was then positioned in a temperature-controlled heated water-filled test cell between two conventional compression wave transducers and cured at a fixed temperature between 30°C and 70°C. The pulser-receiver used was a Desktop Ultrasonic Instrument (DUI, NDT Solutions Ltd.) which is combined with inbuilt amplifier and digitizer. Fourier analysis of the transmitted pulses were utilized to calculate the frequency dependent compression wave phase velocity and corresponding attenuation coefficient throughout the cure process.

Ultrasonic wave propagation technique can also be applied for dynamic mechanical analysis (DMA) or characterization of polymers and composites. The propagation of ultrasonic waves acting as a dynamic mechanical deformation at high frequencies can be used for the calculation of complex longitudinal bulk and shear moduli during the cure of epoxy and other thermosetting systems. The evolution of attenuation and velocity during cure can be related to the strong physical and mechanical changes occurring during the cure process. The ultrasonic attenuation can be considered as the equivalent of a damping factor in a dynamic-mechanical experiment representing a measure of the energy loss as the wave travels through the polymer [6].

Measurements of the process parameters and material properties make possible the control of process variables to achieve the required material properties. For thermosetting materials the overall requirement of its final cured state is that the physical and engineering properties of its molecular, microscopic and macroscopic structure remain within specified limits. In order to achieve this it is required to

monitor and ultimately control the cure reactions where ultrasound has great potential to play a vital role.

In many cases, epoxy resin material forms part of a composite engineering structure which itself may need to be analyzed using ultrasound for the purpose of non-destructive testing, for example in the case of adhesive bonds and carbon fibre composites. In order to understand and model the interaction of ultrasound with composite materials it is necessary to characterize the propagation characteristics of the epoxy resin itself. To characterize completely material properties, the acoustic behaviour over a wide range of frequencies must be examined.

1.7 The Midous touch of Ultrasonic in Characterization of Polymers

For the purpose of maritime and defence applications, in April 1912 [9], ironically at almost the same time as the *Titanic* disaster, when the first ultrasonic echo traveled deep sea, then from *'far across the ocean' (the song of Titanic film)* who had then anticipated that perturbing through very long chain polymeric materials ultrasonic wave can bring the wealth of information (which is much more than a simple propagation speed available from an ultrasonic pulse) hidden inside the complex structure of polymers? Detect their behaviour? Sketch their states in terms of the viscoelastic parameters?

Who had then dreamt of the revolutionary look .... that with its vital spark of potential and midous touch a wide range of important things ultrasonic wave can perform? Latin word *'ultra'* means *'beyond'*; *sonic* means *sound*. Infact, ultrasound *sounds well* for performing a wide variety of important things *apart from sound*. Thus, really ultrasound is *'beyond sound' — the wave of the present and future*. We can see that ultrasound cooks, ultrasound heats, ultrasound heals, ultrasound treats, ultrasound cures, ultrasound repairs, ultrasound cleans, ultrasound tests, ultrasound inspects, ultrasound detects, ultrasound welds, ultrasound drills, ultrasound does not destroys but tests (NDT), ultrasound tastes, ultrasound hard, ultrasound soft, ultrasound moves, ultrasound relaxes, ultrasound controls, ultrasound monitors etc. and so on — a long list.

In 1955, acting as dynamic mechanical deformation, ultrasonic – first step into the realm of polymer when Sofer and Hauser [10] transmitted MHz –range pulsed wave trains through a curing polyester resin. Since then research have been carried out into ultrasonic wave propagation characteristics, the development of transducers, electronic systems and signal processing.

We are now bearing the fruits of *marriage* of developed ultrasonic technology and non-destructive evaluation which ensure precise measurements over a wider range of frequencies and hence brought such measurements into the realms of routine possibility. The increasing use of ultrasound for non-destructive testing of composite engineering structures that, in most cases, incorporate polymer components, has brought about the need for analyzing the ultrasonic propagation characteristics of the polymer itself. Therefore, researches on ultrasonic characterization of polymers are in advance.

It is now well known that ultrasound has the potential to monitor cure, detect gelation and vitrification and the molecular state of the curing material. Ultrasonic identification now offers a fast, economical, reliable, inherently safe approach, which has great potential for providing one of the best all-round method of characterization of polymer.

1.8 Background, Project Material, and Objectives of the Present Investigation

1.8.1 Background

One of the most basic and fundamental requirements in engineering is to join components together. The structural adhesives that have been widely used in the aerospace, automotive, and rail industries, are not only able to bond conventional metallic substrates, but can also join diverse substrates like plastic, wood, glass, and ceramic materials. Adhesive bonding offers a number of advantages over traditional joining techniques. The advantages include improved stress distribution, improved corrosion resistance, ability to join dissimilar materials, lighter weight, lower cost, greater flexibility in manufacturing etc. As a result the industrial use of epoxy resins as load bearing structural adhesives has grown rapidly, but to some extent their use

has been hampered by *three* factors — (i) a lack of through knowledge of the cure kinetics, (ii) an inability to measure the degree of cure *online*, and (iii) inadequate post-cure inspection procedures. As a result high safety factors have to be engineered in at the design stage and the full potential of the benefits of adhesive bonding are not being realized, thus there is a need for improved non-destructive evaluation (NDE) and non-destructive testing (NDT) methods.

Despite the considerable current research effort in the field of cure of epoxy resins, numerous issues have yet to be addressed. As for example, (i) from a microscopic standpoint, our understanding of the way in which a cross-linked epoxy structure develops has lagged behind the extent to which joining technologies use these adhesives, leaving a gap in our basic scientific understanding of the cure process. (ii) Also, there is a number of partially conflicting explanations proposed for the reaction mechanisms of the cure of epoxy systems. (iii) Moreover, determination of the reaction order from experimental data can be difficult and confusing in some reaction systems and hence, reaction kinetics differing from first to third order have been reported. (iv) Furthermore, though the focus of much research has been on the study and understanding of cure kinetics of epoxy-amine reaction, almost little effort has been made to establish the relationship between chemical extent (or degree) of cure and physical properties of epoxy-amine thermosets, which are of prime importance to achieve optimum process control for industrial setting.

1.8.2 Project Material

There are mainly six chemical types of structural adhesives available commercially; epoxy, polyurethane, polyimide, poly or vinyl ester, phenolic and acrylic. The most common structural adhesives used in safety critical applications are epoxies and polyurethanes. Among these various types of structural adhesives, epoxy has been the standard chosen adhesive employed by industry for applications where high strength over a wide operating temperature range and chemical tolerance are required.

The resin system under study is a complex modified epoxy system containing epoxy (DGEBA/DGEBF mixture), diethylene triamine (DETA) curing agent, external catalyst 2,4,6 - tris (dimethylaminomethyl) phenol, epoxy-based reactive diluent 1,4

Butane diol diglycidyl ether (BDGE), and mica which usually is used in epoxy system as filler. Epoxy resin has been chosen as the material of study in this project for its extensive use in safety critical applications in the automotive (British motor industry) and aerospace (Airbus) industry with which our Applied Ultrasonic Laboratory at University of Nottingham has several collaborations through UK Research Council for Non-Destructive Evaluation (RCNDE).

The curing reaction of the catalyzed multifunctional unmodified epoxy-amine system has been described by various authors, but there is less information when both catalyst and reactive diluent is used in the formulation of two epoxy resin mixture. This keeps the system odd from others and, to some extent, a new complex one to report cure kinetics to the best of our knowledge.

Many modifications have been carried out on the resin by adding promoters, fillers, and plasticizers to suit the application environment and the manufacturing conditions. Reactive diluent is considered one of these structure modifiers which enables to reduce viscosity in order to aid general processability.

1.8.3 Objectives of the Present Investigation

The present investigation, in general, focuses on the ultrasonic and thermo-kinetic behaviour of a commercial structural stoichiometric ratio mixture modified epoxy resin system during the cure process over a group of isothermal cure temperatures within acceptable cure time scales.

With the aid of combination of Ultrasonic and DSC cure monitoring techniques, the present study attempts to narrow the gaps [(i)—(iv) mentioned under the 'background' section 1.8.1] in understanding, to some extent, by determining a quantitative correlation between degree of cure and ultrasonic compression wave velocity which can be considered the most interesting parameter for cure monitoring as it follows the growth and evolution of the mechanical stiffness (physical property) of the resin during cure.

The main objectives of the research are as follows —

1.8.3.1 Thermo-kinetic characterization using DSC

(1) To evaluate the cure kinetics and analyze the curing process of the epoxy system under study using isothermal differential scanning calorimetry (DSC) data with the aid of iso-conversional method which enables us to determine the exact effective activation energy value obtained as a function of conversion, and thus useful in predicting the curing behaviour coupled with the cure mechanism.

(2) Modelling of the isothermal calorimetric cure kinetics of the epoxy system under study utilizing the empirical approach of fitting of the isothermal experimental data to various kinetic models, in an effort to find the model which best possibly describe the reaction behaviour of the resin system and predicts the reaction course.

(3) To explore some in depth information associated with the diffusion controlled kinetics due to vitrification related to our isothermal data implementing diffusion factor in conventional models. To analyze and discuss the performance of each particular model tested along with their comparisons which will be interesting and useful from the perspective of kinetic modelling.

(4) To evaluate kinetic and thermodynamic parameters and analyze the cure kinetics from both kinetic and thermodynamic viewpoint in the context of associated model.

(5) To explore the overall effect of the reactive diluent in the cure kinetics of this modified epoxy system under study.

(6) To construct a TTT phase transition diagram of the isothermal cure process of this epoxy-amine system.

15

1.8.3.2. Ultrasonic characterization of curing and comparison with DSC characterization

(7) To characterize the curing process of the epoxy system under study using ultrasonic compression wave velocity and its corresponding attenuation data at a fixed frequency at various isothermal temperatures.

(8) To carry out secondary calculations from the ultrasonic velocity and attenuation data at the fixed frequency at the various isothermal temperatures so as to produce derived functions like real and imaginary parts of compression modulus, ultrasonic loss tangent and associated central relaxation time, to characterize the material state and the cure process.

(9) To analyze the effect of temperature and frequency on ultrasonic data (velocity, attenuation, modulus, loss tangent).

(10) To characterize the curing process using frequency-dependent ultrasonic compression wave velocity and its relative attenuation data.

(11) To inspect the potential of ultrasonic technique in predicting gelation and vitrification.

(12) To compare the results associated with ultrasonic and DSC techniques to elucidate the sensitivities of both of the techniques to the chemical, physical, and mechanical changes associated with each part of the curing process together with an examination of the similarities between them.

(13) To inspect the qualitative and quantitative correlations between ultrasonic and kinetic parameters, in particular, correlation between ultrasonic velocity and calorimetric conversion.

1.9 Overview of the Thesis

The thesis is structured as follows —

Following the present chapter (**chapter 1**), where the advantages of the knowledge of cure kinetics along with thermoset cure monitoring, associated techniques, the necessity of online non-destructive evaluation are highlighted and an brief overview of the project under study is presented,

Chapter 2 reviews epoxy resins focusing on their advantageous properties, applications, synthesis, modifications and chemical reactions and associated mechanisms of cure.

Chapter 3 is divided in three parts: First, a review of the theoretical background to kinetics model coupled with the modelling attempts, which have been developed to describe chemical cure kinetics of thermosetting systems is given. The second part reviews the effect of temperature and time on the evolution of the cure cycle in connection with Time - Temperature - Transformation (TTT) cure diagrams, which focuses on cure as a process involving physical transformations. Finally, in the third part, the factors and fundamentals behind the final cure properties of thermosets is reviewed.

Chapter 4 gives information about the epoxy material investigated in this study along with the differential scanning calorimetric experiments, which have been performed for the thermo-kinetic characterization and modelling of its curing behaviour.

Chapter 5 presents the results of the isothermal chemical cure kinetics behaviour and glass transition development of the epoxy system under study using differential scanning calorimetry. The results are interpreted and discussed. In addition, an in depth details analysis of the cure kinetics of the investigated system is also presented utilizing model free iso-conversional method coupled with the light of physics of advanced kinetics research.

Chapter 6 deals with the modelling of the isothermal calorimetric cure kinetics of the epoxy system under study utilizing the empirical approach of fitting of the experimental data to various kinetic models. The best fit model which best possibly describe the reaction behaviour of the resin system and predicts the reaction course has been evaluated and analyzed in details. The performance of each particular model tested has been discussed along with their comparisons. Implementing diffusion factor in conventional models some in depth information associated with the diffusion controlled kinetics related to our data is explored. The cure kinetics has also been analyzed from both kinetic and thermodynamic viewpoint in the context of Horie model based on mechanistic approach. The overall effect of the reactive diluent in the cure kinetics of this modified epoxy system under study is also explored. A TTT phase transition diagram (theoretical) of the isothermal cure process of this epoxy-amine system is constructed.

Chapter 7 gives the theory and fundamentals of ultrasonic wave propagation in polymers, reviews viscoelasticity and relaxation in polymers along with various viscoelastic models of wave propagation and distribution of relaxation times. This chapter also critically reviews typical ultrasonic results related to evolution of structure in curing thermosets, the effect of temperature and frequency on ultrasound data and the potential of ultrasonic technique in defining gelation and vitrification.

Chapter 8 gives a description of the experimental apparatus and techniques of ultrasonic measurements that have been used in this project for the characterization of the curing epoxy resin under study.

Chapter 9 presents the results and analysis of ultrasonic characterization of curing and comparison with DSC characterization. The sensitivities of DSC and ultrasonic techniques to the chemical, physical, and mechanical changes associated with each part of the curing process are discussed comprehensively and critically together with an examination of the similarities between them coupled with qualitative and quantitative correlations. The ultrasonic compression wave velocity (at 5MHz) has been demonstrated to be the most interesting and potential parameter for monitoring and characterizing the cure process at all stages of the cure including detecting the

material state transformations that occur during cure. Therefore, its measurement could be exploited for *non-destructive on-line process control* in an industrial environment. Also, it can be used as a predictor of calorimetric conversion measurements observed by DSC and thus used *to track chemical reaction on-line*.

Chapter 10 presents the conclusions of this study along with the suggestions for further investigation arising from this work.

1.10 References

1. Thomas, R., Durix, S., Sinturel, C., Omonov, T., Goossens, S., Groeninckx, G., Moldenaers, P., Thomas, S., Polymer, vol. 48, 2007, 1695-1710.

2. Montserrat, S., Cima, I., Thermochimica Acta, vol. 330, 1999, 189-200.

3. Puglia, D., Valentini, L., Armentano, I., Kenny, J.M., Diamond and Related Materials, vol.12, 2003, 827-832.

4. Pindinelli, C., Montagna, G., Luprano, V.A.M., and Maffezzoli, A., Macromolecular Symposia, vol. 180, 2002, 73-88.

5. White,S.R., Mather,P.T., Smith,M.J., Polymer Engineering and Science, vol.42, no.1, 2002, 51-67.

6. Maffezzoli,A., Quarta,E., Luprano,V.A.M., Montagna,G., Nicolais,L., Journal of Applied Polymer Science, vol-73,1999,1969-1977.

7. Challis,R.E., Unwin,M.E., Chadwick,D.L., Freemantle,R.J., Partridge,I.K., Dare,D.J., Karkanas,P.I., Journal of Applied Polymer Science, vol-88, 2003, 1665-1675.

8. Challis,R.E., Freemantle,R.J., Cocker,R.P., Chadwick,D.L., Dare,D.L., Martin,C., Mahendrasingam,A., and Fuller,W., Plastics, Rubber and Composites, vol-29, no-3, 2000, 109-118.

9. Cracknell, A.P., Ultrasonics, Wykeham, London, 1980.

10. Sofer, G.A., and Hauser, E.A., J. Polymer Science, vol-8, no-6, 1955.

Chapter 2   Epoxy Resins

2.1 Introduction

The epoxy resins are the most versatile of the modern plastics. In terms of complexity of technology, variety and breadth of application, epoxy resins are superior to all other plastics and resins. They have penetrated into more industries and more manufacturing operations in a shorter space of time than any of their predecessors. Many of these uses depend on the adhesion of epoxies to surfaces.

But epoxy resin adhesives have an interesting past, in that the basic resins were discovered in fields not concerned primarily with adhesives [5]. The 'first' epoxy resin saw the light of day in 1936 with Pierre Castan's (of Switzerland) development of epoxy resin resulting from the reaction of epichlorohydrin and bisphenol A. He was specifically interested in the manufacture of dentures and other casting applications and his discovery was eventually licensed to Ciba Corp., Ltd.

The first superglue of nature is *'gluons'* (carriers of the strong force, have properties like photons), which bind all things from here to eternity [1].The term 'epoxy' has come to mean a "superglue" which bonds almost anything to anything. Although this is certainly an exaggeration, epoxy adhesives will bond to a wide variety of materials without requiring heat or pressure in most cases.

Epoxy adhesives are probably the most commonly used structural adhesive at present. The terms 'epoxy resin' and 'structural adhesive' are today almost synonymous [4]. In addition to enjoying the general advantages of adhesive bonding (which is described elsewhere [5,6,7,9]) over mechanical fastening, epoxy resin adhesives offer clear advantages over the other synthetic bonding materials. They are used in a wide range of applications across a diverge range of industries. They are playing an ever-increasing role in modern technology, with bonding applications ranging from toys and table tops to supersonic transports, and also in repairing human beings and this includes the use of UV-curing cements in dentistry and acrylic bond cements in orthopaedic surgery [6].Epoxy-adhesive consumption has grown, not only because of

its performance capabilities but also because of its simplicity in use and its availability in a wide range of outstanding physical properties, making it adaptable for a constant stream of new applications.

2.2 Advantageous properties of epoxy resin

Thermosetting epoxy resins possess a number of unusually valuable properties immediately amenable to use throughout the world for a multitude of purposes. The more important of these properties are—

1. **Adhesion** – epoxies are one of the best adhesives for bonding a wide range of adherends, in both specific and mechanical adhesion. They adhere well to most metals, plastics, wood, glass, concrete, ceramics. This is due to their good wetting and penetrating ability, their low viscosity, and the presence of highly polar groups in the molecule. Wetting allows the adhesive, in a low-viscosity liquid form, to come into intimate contact with the adherend, which allows the adhesive forces to become active. In fact epoxy molecule also contains a variety of functional groups, both polar and nonpolar which provides good affinity between dissimilar substrates, such as metals to plastics or concrete to rubber. The chemical basis of adhesive properties of epoxy resin is discussed later.

2. **Cohesion** – The internal strength of epoxies to resist cohesive failure is generally good, although this may be affected somewhat by the choice of fillers, modifiers and bond-line thicknesses. When properly cured they have such a high cohesive strength that, when taken with their adhesive strength, failure in the adherends usually occurs before failure in the epoxy resin or at the interface. If preparation and application processes are properly done, the internal strength of epoxy will often surpass that of thin-gage metals, plastics, glass, concrete, and wood. However, with heavy metallic adherends, and surfaces properly prepared, cohesion strength will be lower than adhesive strength and will therefore be the limiting factor in adhesive-joint design.

3. **100 percent solids (reactive)**--Epoxies cure without releasing moisture or other by- products. Only in special instances are solvents necessary. A 100 percent solid (reactive) adhesive reduces drastically the possibility of entrapped gases, voids, and

porosity in the bond line which would significantly lower bond strengths. Solvents and entrapped moisture will cause serious corrosion problems in metal bonding. This is the reason it is possible to bond successfully to metal with epoxies using *only contact pressures*, because it is unnecessary to provide for water removal (as in phenolics) and solvent removal (as in elastomer emulsions). The 100 percent solids content of epoxy also makes it convenient for rapid assembly-line bonding to nonporous surfaces such as glass and metals.

4. Low shrinkage factor (very little weight-loss) during cure--- In the liquid state, the epoxy resins are highly associated. Cure is by direct addition, and shrinkage is on the order of < 2 per cent for an unmodified system, indicating that little internal rearrangement of the molecules is necessary. Consequently, shrinkage stresses are minimized, resulting in a stronger and more durable bond.

Low shrinkage stresses are important in bonding dissimilar materials. Because of the difference in coefficient of thermal expansion between dissimilar materials, major mechanical stresses are almost always present, and so epoxy adhesives which add little or no additional shrinkage stress are needed to prevent bond failure. The low shrinkage of epoxy during cure also aids in holding tolerances, and this becomes more important in operations where bond lines are thick or surfaces are poorly mated, especially with elevated-temperature cures.

5. Low-heat and-pressure cures (good handling characteristics)---Many epoxies can be cured with contact or low pressures at room temperature. However, there are also many epoxy adhesives (designed to do specific jobs in aerospace and other critical applications) that give better results if heat and/or pressure are used. The ratio of curing agent to resin is not as critical as with some thermosetting materials. In many cases, pot life, viscosity, and cure schedules can be accommodated to the production situation without seriously influencing the properties of the cured system.

Most epoxy adhesives are less sensitive to variations in bond-line thickness than other adhesives and so can tolerate wider variations in curing temperatures and pressures. Therefore, production methods are simpler, production rates faster, and production tolerances easier to maintain.

6. Low creep under load --- Epoxy, when cured, maintains its shape under prolonged stress and adverse environments longer than most adhesives, especially as compared with thermoplastic adhesive. *Creep*, or *'cold flow'*, is of serious concern where mechanical loading is high and where tolerances are critical. Because epoxy adhesives give excellent service under those conditions, they are the logical choice. At elevated temperatures polymers become more susceptible to creep [4].

7. Resistance to moisture and solvents --- Unlike many other adhesives, cured epoxies are practically insensitive to moisture. Although moisture will penetrate most epoxies and may create interfacial problems at the adherend faying surface (i.e.the surface of a material in contact with another to which it is or will be joined), moisture does not seriously degrade the cohesive properties of epoxy. It should be pointed out that problems with moisture which do occur in epoxy bonding are more apparent when epoxy is cured or used at elevated temperatures.

Due to very high chemical inertness, epoxies have outstanding resistance to solvents, weak acids, and alkali compounds. This accounts for their rapid growth in the coatings and sealants field. The ether groups, the benzene rings, and, when present, the aliphatic hydroxyls in the cured epoxy system are virtually invulnerable to caustic attack and extremely resistant to acids. The chemical inertness of the cured epoxy system is enhanced by the dense, closely packed structure of the resinous mass, which is extremely resistant to solvent action.

8. Versatility (Epoxies are readily modified)-- This is a major reason epoxies have rapidly grown in favour as bonding agents. Numerous curing agents for epoxies are available, and epoxies are compatible with a wide variety of modifiers. Their compatibility with many modifiers allows them to be formulated for a wide scope of applications, not only for new design concepts but also for improvements in established designs.

Under appropriate conditions the epoxy ring may react with at least *50 chemical groupings.* Because of the wide range of resins and curing agents, it is also possible to arrange for epoxy systems to cure at a variety of rates (rapidly or slowly) over a wide range of temperatures (temperature range from 0 to 200° C), and some control over

the final network structure is available through choice of curing reagent or mix of reagents. One noteworthy example is *polymercaptan* curing agent, which, when used with an accelerator, would cure resins at an acceptable rate at 0° C.

By the modification techniques (stated later), epoxy resin adhesives can also be produced in many different physical forms, such as liquids, pastes, putties, powders, rods and supported films with a wide range of properties. In rubber modified epoxy resin by adding rubber in an epoxy matrix substantially improves the toughness of the adhesive whilst retaining other properties such as stiffness, creep resistance and high temperature properties.

9. Good mechanical and electrical properties---Epoxy systems are especially valuable not only because of their good electrical properties (very high resistivity), but also because of their very good physical and mechanical properties at normal and elevated temperatures, and their ease of fabrication into complex shapes. Cured epoxides have a high level of mechanical strength, which is retained at elevated temperatures and also have outstanding toughness which has been attributed to the distance between crosslinking points and the presence of integral aliphatic chains. At present, certain epoxy systems are able to withstand long-term exposure to temperatures of the order of $210\text{-}260^0$ C [9].

10. Wide viscosity range--- Epoxies exhibit a wide range in viscosity, from less than 1000 centipoises to high-melting-point solids.

2.3 Structure of the basic epoxy-resin molecule

The epoxy-resin molecule is characterized by the reactive epoxy groups (also known as *ethoxyline* or *oxirane* groups)
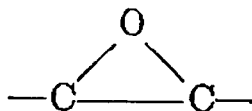
which serve as terminal linear polymerization points. By definition all epoxy resins must contain at least two epoxy groups per molecule within their structure. The

epoxide group consists of a planar three-membered ring of two carbon atoms singly bonded to an oxygen atom. It is the chief centre of reactivity of epoxy resins.

If this ring is reacted with suitable polyfunctional hardeners then a three dimensional structure may be developed . The geometry of the ring is such that reactions involving either electrophilic attack on the oxygen atom or nucleophilic attack on one of the carbon atoms are possible as shown in figure 2.1.
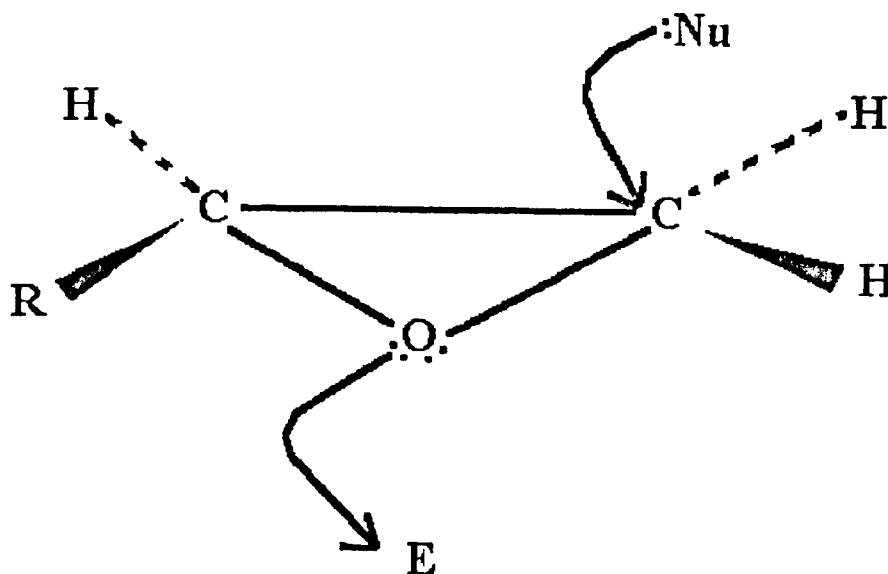
Figure 2.1 Mechanisms for the opening of the oxirane ring by either a nucleophile (NU) or an electrophile (E) (after Hamerton [19].)

In its simplest and idealized form, the epoxy molecule is represented by the diglycidyl ether of bisphenol A
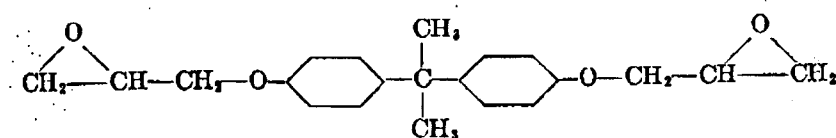
The most widely used liquid epoxy resins, those having viscosities in the 8,000 – to 20,000 – centipoise range, are predominantly of this structure. Since the commercial resins are not molecularly distilled, they contain some percentages of higher-weight

homologs, branched- chain molecules, isomers, and occasionally monoglycidyl ethers in combination with the basic structure. The high-viscosity liquid and the solid commercial resins are predominantly composed of more highly polymerized products considered as homologs of diglycidyl ether of bisphenol A.

2.4 Synthesis of the basic epoxy-resin molecule Diglycidyl ether of bisphenol A

Diglycidyl ether of bisphenol A is obtained by reacting epichlorohydrin with bisphenol A in the presence of a caustic:

(1) $\sim\!\!\!\big\langle\bigcirc\big\rangle\!\!-OH + CH_2\!-\!\!\!-CH\!-\!CH_2\!-\!Cl \xrightarrow{\ NaOH\ }$

$\sim\!\!\!\big\langle\bigcirc\big\rangle\!\!-O\!-\!CH_2\!-\!\overset{OH}{\underset{|}{C}H}\!-\!CH_2\!-\!Cl$

(2) $\sim\!\!\!\big\langle\bigcirc\big\rangle\!\!-O\!-\!CH_2\!-\!\overset{OH}{\underset{|}{C}H}\!-\!CH_2\!-\!Cl \xrightarrow{\ NaOH\ }$

$\sim\!\!\!\big\langle\bigcirc\big\rangle\!\!-O\!-\!CH_2\!-\!CH\!-\!\!\!-CH_2 + HCl$
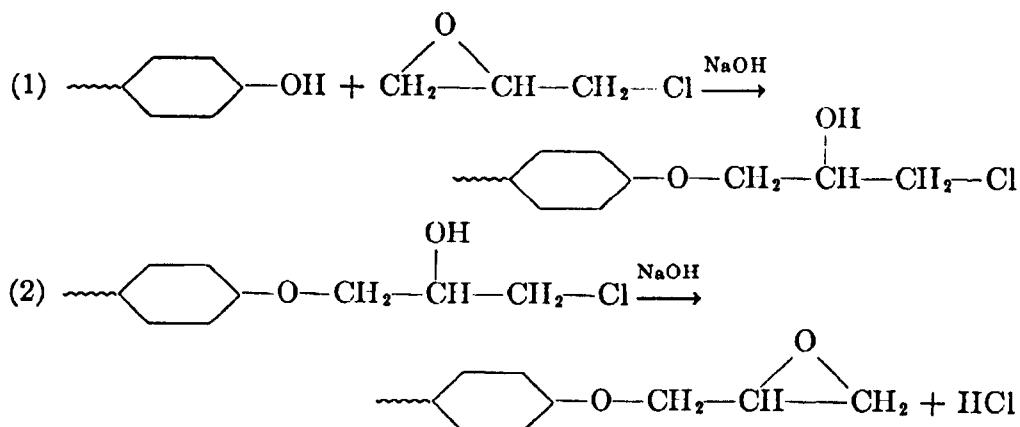
In order to obtain the diglycidyl ether of bisphenol A, 2 mols of epichlorohydrin are theoretically required for each mol of bisphenol A:

$2(CH_2\!-\!\!\!-CH\!-\!CH_2\!-\!Cl) + HO\!-\!\big\langle\bigcirc\big\rangle\!\!-\overset{CH_3}{\underset{\underset{CH_3}{|}}{C}}\!\!-\!\big\langle\bigcirc\big\rangle\!\!-OH \rightarrow$

$CH_2\!-\!\!\!-CH\!-\!CH_2\!-\!O\!-\!\big\langle\bigcirc\big\rangle\!\!-\overset{CH_3}{\underset{\underset{CH_3}{|}}{C}}\!\!-\!\big\langle\bigcirc\big\rangle\!\!-O\!-\!CH_2\!-\!CH\!-\!\!\!-CH_2$
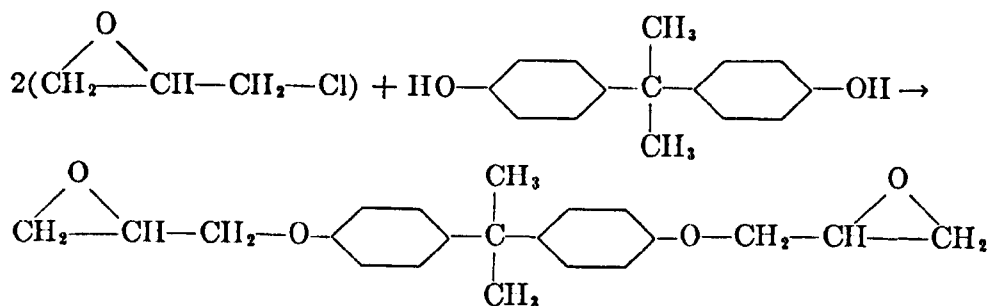
2.5 Synthesis of higher-molecular-weight epoxy resins

The general formula for higher-molecular-weight epoxy resin may be written:
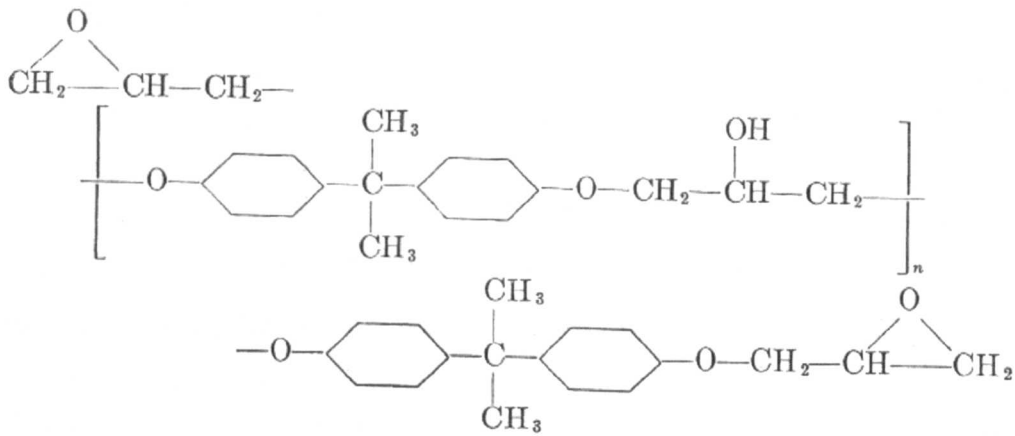
where n is the number of repeated units in the resin chain. Because of the varying number of repeat units (n) which can be incorporated into the resin, variation in the molecular weight of resin and thus, in turn, a variety of resin properties (especially the range of viscosities) can be achieved. When $n=0$, the molecular weight is 340; when $n=10$, about 3,000. For n going from 0 to 12 the resins change from liquids to low melting solids at room temperature. It should be noted that each such molecule contains as many alcoholic hydroxyls as there are n groups and, provided that the molecule is linear with no side branches, no more than two epoxy groups. Figure 2.2 shows the magnified atom model of epoxy-resin molecule compared with structural symbols.
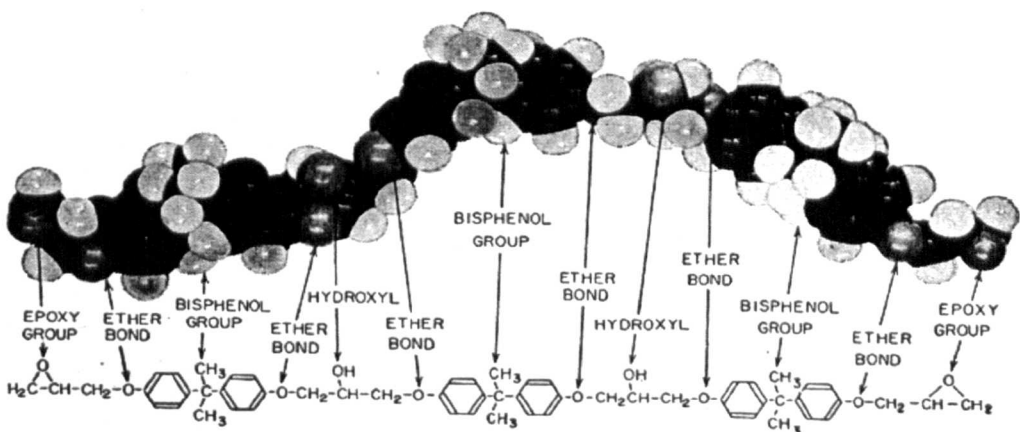
Figure 2.2 Atom model of epoxy-resin molecule compared with structural symbols (diglycidyl ether of bisphenol A, degree of polymerization of 2) (after Lee and Neville [10]).

27

2.6 Curing of epoxy-resins

Epoxy adhesives may be produced by either condensation polymerization or addition polymerization and cured by either *condensation polymerization* or *addition polymerization*. A condensation reaction is one in which monomers are joined through the elimination of water or other small molecules such as alcohols. The reaction of adipic acid and hexamethylenediamine to produce the polyamide nylon 6,6 and water is a well known example. Addition polymerization as the name suggests involves the addition of monomer units to one another to form the polymer. A well known example is the polymerization of propylene to form polypropylene. Addition reactions occur through either free radical, cationic or anionic mechanisms depending on how they are initiated. Three steps are involved to form the final polymer structure—chain initiation, chain propagation and chain termination.

In chemical curing process the epoxy adhesive is applied in the monomer or small polymer condition and a crosslinked structure forms during the cure by the use of either a curing agent or a catalyst. Curing agents, which are also called *accelerators*, are used up in the curing process. They become part of the final crosslinked structure. Catalysts are special chemicals added to make the adhesive components more reactive. They do not form a significant part of the final adhesive film. Figure 2.3 illustrates the functions of curing agents and catalysts.
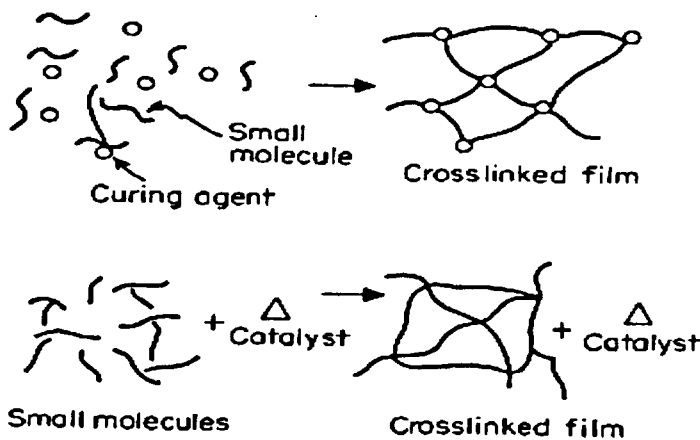
Figure 2.3 Functions of curing agent and catalyst.

Heat may be used with either accelerator- or catalyst-type systems to shorten the cure time. The curing reaction is exothermic, that is, heat is evolved during the crosslinking process, which causes an increase in the temperature of the system. This is often called *'exotherm'* and can reach high levels, perhaps $150\text{-}200^0C$ or above. When converted by a curing agent, the thermosetting resins become hard, infusible systems. The system may be visualized as a network cross-linked in all three dimensions. In a plane it might appear as in figure 2.4. It can be seen from the figure that movement of a molecule in any direction is opposed by the crosslinking arrangement.
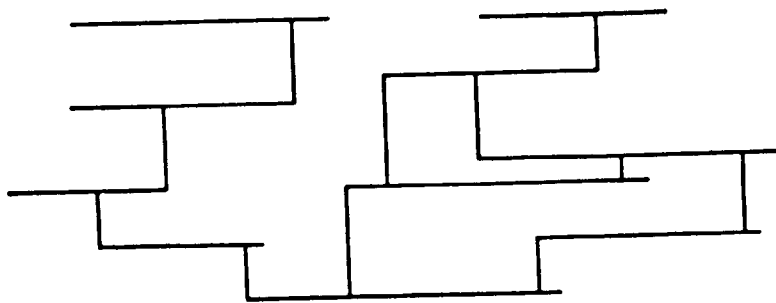
Figure 2.4 Schematic illustrating cured structure

2.6.1 Over-and under-curing

Regardless of the curing method used, it is important that the adhesive be neither undercured nor overcured. Overcuring results in adhesives which have too many crosslinks, they are generally brittle and do not adjust to mechanical impact or expansion and contraction with changing temperatures. Undercured adhesives do not have enough crosslinks. They may be 'cohesively weak' and may also be subject to excessive moisture absorption, further decreasing their cohesive strength.

2.6.2 Epoxy reaction mechanism

The resins cure into thermoset compounds by three reactions:

(1) Direct linkage between epoxy groups,

(2) Linkage of epoxy groups with aromatic or aliphatic hydroxyls, and

(3) Crosslinkage with the curing agent through various radicals.

It is obvious that in any highly crosslinked system there will be *reactive groups which are sterically hindered from reacting* [14].

2.6.3 Basic mechanism of opening of epoxy group

Epoxy resins in the pure or uncontaminated state possess indefinite shelf life. They are chemically stable at temperatures up to 200^0C. Once produced, the resin may react in one of two ways, either *anionically* or *cationically*.

1. Anionic Reaction

In the anionic reaction the epoxy group is opened to produce an anion as shown in figure 2.5. The anion produced is an active species and is therefore capable of further reaction.

Epoxy group   Epoxy anion
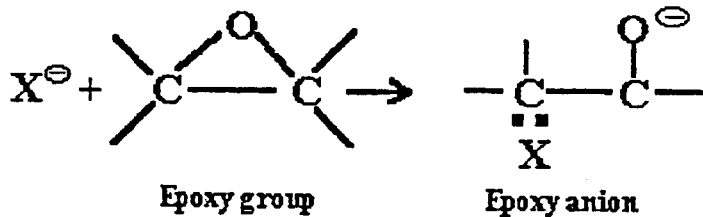
Figure 2.5 Anion formation from the epoxy group (after Lee and Neville [14]).

2. Cationic Reaction

During the cationic reaction the epoxy group is opened by an active hydrogen to give a new chemical bond and an hydroxyl group. This means there is a number of ways in which the cationic mechanism may proceed, and three possible routes are shown in figure 2.6. The two reaction mechanisms allow the epoxy group to react with many chemical groupings. The cationic route means that epoxy resins may be cured by basic curing agents. Basic curing agents commonly used are——Lewis bases, inorganic bases, amides and secondary and primary amines.
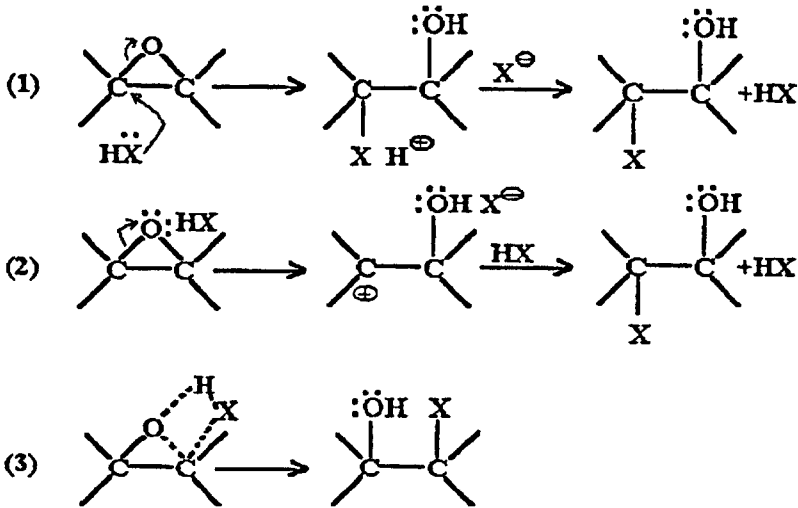
Figure 2.6 Possible cationic reactions (after Lee and Neville [14]).

2.6.4 Polymerization through epoxy groups

The reactivity of commercial epoxy resins is enhanced by the ether linkage, which even though separated by a methylene group (— CH_2 —) from the epoxy ring exerts an extremely strong activating effect. Because of this reactivity, the epoxy group may be readily opened not only by available ions and active hydrogens but even by tertiary (R_3N) amines. With tertiary amine cures, epoxy-epoxy polymerization may occur. The opening of the epoxy group is believed to take place in the following manner[10]:
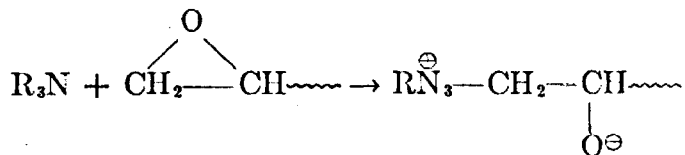
Assuming that this ion is capable of opening a new epoxy group as follows

31
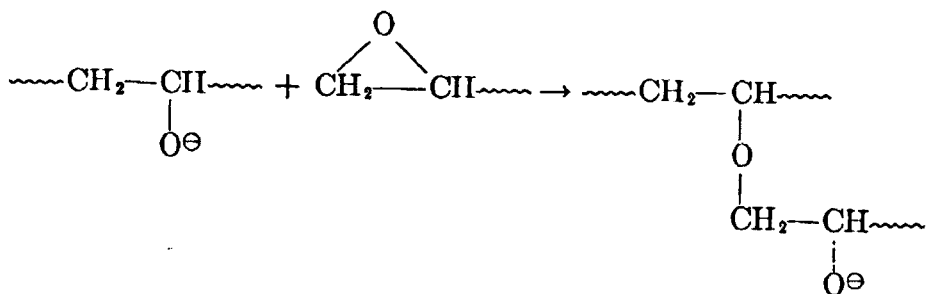
the reaction may then proceed to result in a very long chain system as shown below.

$$\sim\sim CH_2-CH\sim\sim$$
$$|$$
$$O$$
$$|$$
$$CH_2-CH\sim\sim$$
$$|$$
$$O$$
$$|$$
$$CH_2-CH\sim\sim$$
$$|$$
$$O$$
$$|$$
$$CH_2-CH\sim\sim$$
$$|$$
$$O$$
$$|$$
$$CH_2-CH\sim\sim$$
$$|$$
$$O^{\ominus}$$
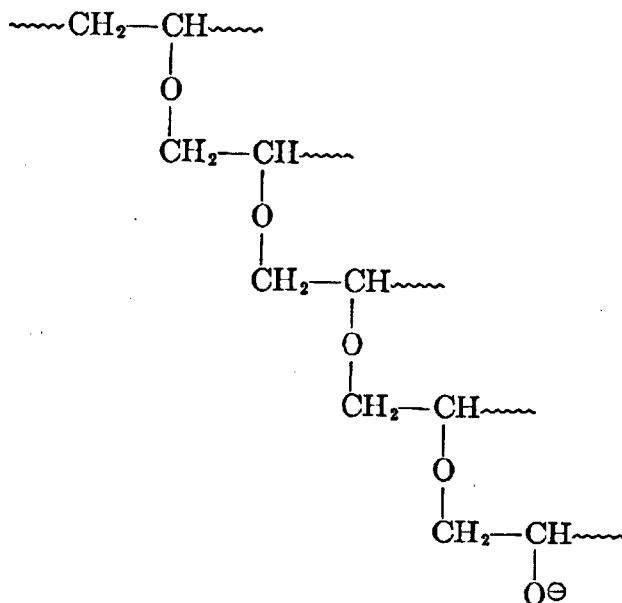
2.6.5 Polymerization through hydroxyl groups

Epoxy groups will react

(1) with hydroxyl groups introduced into the resin by the curing agent or modifiers,

(2) with hydroxyl groups present in the resin chain of higher–weight homologs,

(3) with hydroxyl groups formed as an epoxy group is opened by an active hydrogen during cure, and

(4) with various phenolic hydroxyls present as unreacted phenol, bisphenol, resorcinol, etc.

The epoxy groups, if uncatalyzed, do not react readily with the hydroxyl groups present along the higher-weight resin chain as evidenced by the stability of uncontaminated resins at temperatures up to 200^0C. However under suitable conditions, once the epoxy-hydroxyl polymerization is started, it proceeds very rapidly.

The first step of the epoxy-hydroxyl reaction may be represented [10]:

$$R\text{—}OH + \underset{CH_2\text{——}CH\sim\sim}{\overset{\overset{O}{/\backslash}}{}} \xrightarrow{\text{catalyst}} \begin{array}{l} RO\text{—}CH_2\text{—}\underset{\overset{|}{OH}}{CH}\sim\sim \quad \alpha \text{ isomer} \\[1.5em] HO\text{—}CH_2\text{—}\underset{\overset{|}{OR}}{CH}\sim\sim \quad \beta \text{ isomer} \end{array}$$
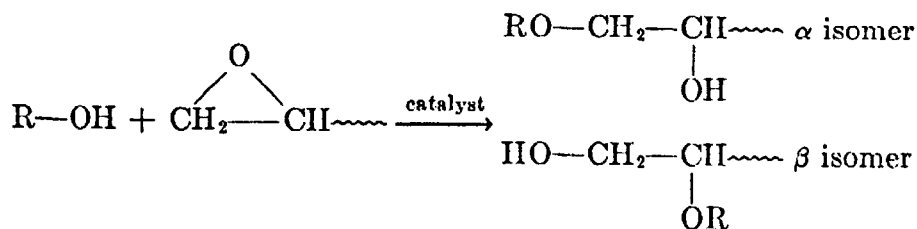
Although two isomers are possible, either provides a new hydroxyl group which is susceptible to continued polymerization. Showing further reaction of the α isomer, for example, to proceed through hydroxyls,

$$RO\text{—}CH_2\text{—}\underset{\overset{|}{OH}}{CH}\sim\sim + \underset{CH_2\text{——}CH\sim\sim}{\overset{\overset{O}{/\backslash}}{}} \rightarrow$$

$$RO\text{—}CH_2\text{—}\underset{\overset{|}{O\text{—}CH_2\text{-}\underset{\overset{|}{OH}}{CH}\sim\sim}}{CH}\sim\sim$$
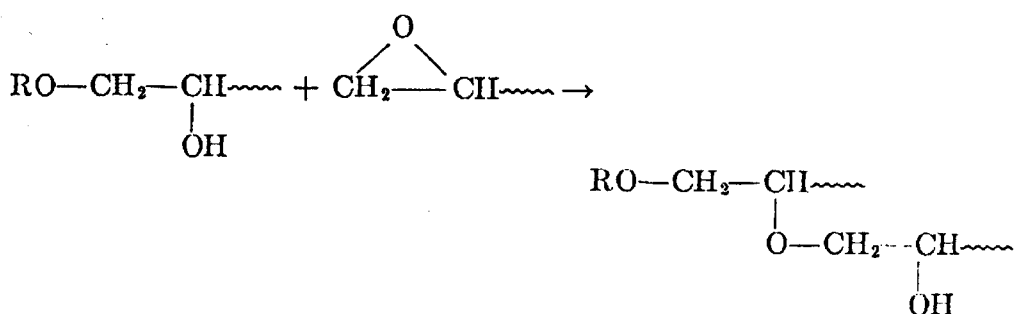
a structure very similar to that postulated for the epoxy-epoxy reaction cured compound will result [10]. The reaction, as before, can continue until a high degree of crosslinking is achieved.

2.6.6 Curing by crosslinking agents

Epoxy resins may be cured by using a reactive intermediate to join the resin chains. The principle reactive crosslinking agents are polyfunctional primary and secondary amines and dibasic acids or acid anhydrides. However, polyfunctional phenols such as bisphenol A and resorcinol have also been suggested as crosslinking agents and are sometimes used in conjunction with other curing agents.

2.6.6.1 Primary and secondary amines

Both aromatic and aliphatic amines are used as hardeners, and the stoichiometry is that *one epoxide ring will react with one amine-hydrogen atom* in a condensation

polymerization. Curing with aromatic amines requires elevated temperatures, the cured adhesives have higher glass transition temperatures and the joints tend to be more durable. Polyfunctional primary (RNH_2)and secondary (R_2NH) amines are widely used as curing agents for epoxy resins. Room–temperature curing epoxies are usually based on aliphatic amines or the polyamine-amide components marketed as *'Versamids'*. Each primary amine group is theoretically capable of reacting with two epoxy groups.

The reactions possible with primary amines are:

1. Reaction with an epoxy group to form a secondary amine

$$RNH_2 + \underset{CH_2\overline{}CH}{\overset{O}{\triangle}}\!\!\!\sim\!\!\sim \longrightarrow R\overset{H}{\underset{|}{N}}-CH_2-\underset{\underset{OH}{|}}{CH}\!\!\sim\!\!\sim$$
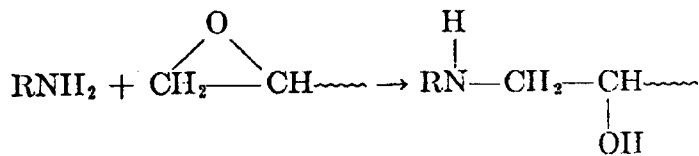
2. Reaction with another epoxy group to form a tertiary amine

$$R\overset{H}{\underset{|}{N}}-CH_2-\underset{\underset{OH}{|}}{CH}\!\!\sim\!\!\sim + \underset{CH_2\overline{}CH}{\overset{O}{\triangle}}\!\!\!\sim\!\!\sim \longrightarrow RN\!\!\Big\langle\begin{array}{l}CH_2-\underset{\underset{OH}{|}}{CH}\!\!\sim\!\!\sim\\ CH_2-\underset{\underset{OH}{|}}{CH}\!\!\sim\!\!\sim\end{array}$$
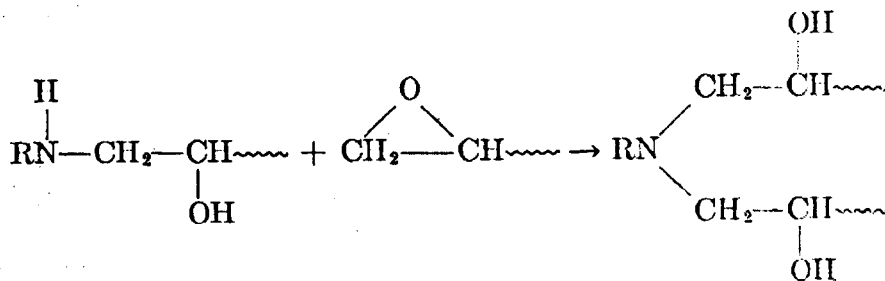
3. Reaction of hydroxyls so formed with epoxy

$$\sim\!\!\sim\!\!\underset{\underset{OH}{|}}{CH}\!\!\sim\!\!\sim + \underset{CH_2\overline{}CH}{\overset{O}{\triangle}}\!\!\!\sim\!\!\sim \longrightarrow \sim\!\!\sim\!\!\underset{\underset{\underset{\underset{OH}{|}}{CH_2-CH}\!\!\sim\!\!\sim}{|}}{\overset{}{\underset{O}{\underset{|}{CH}}}}\!\!\sim\!\!\sim$$
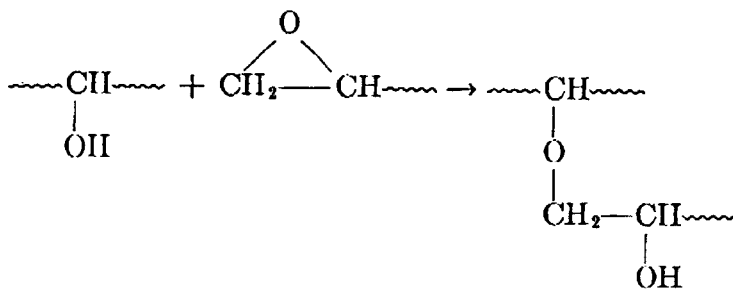
Under normal conditions, the two amine-epoxy reactions predominate and proceed at approximately equal rates. The resulting tertiary amine is too weak catalytically to react any further. Studies have shown that primary amines react about twice as fast as secondary amines [10] and figure 2.7 shows how the concentrations of the primary, secondary and tertiary amines change as a function of time.
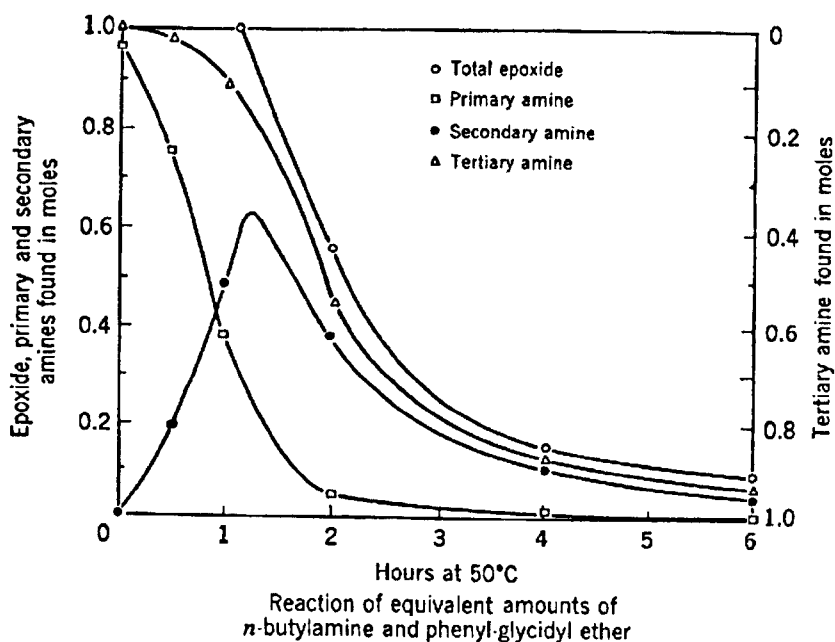
Figure 2.7 Progress of amine-epoxy reaction in terms of primary, secondary and tertiary amines (after Lee and Neville [10]).

As the primary diamine is difunctional with the resin, if more than one primary amine is present per molecule (as with a diamine), cross-linked structures will result through reaction with diepoxies as shown in figure 2.8.

The main reasons for using primary diamines as curing agents are –

(i) that a significant proportion of the hardener is incorporated into the cured resin which means the final structure may be varied by varying the amine used,

(ii) amines have low viscosity and are easily mixed with the resin and

(iii) they are reactive enough to react with the epoxide group at ambient temperatures. The reaction mechanisms of amido-polyamines are assumed to be similar to those of amines but with reduced reactivity due to steric hindrance.
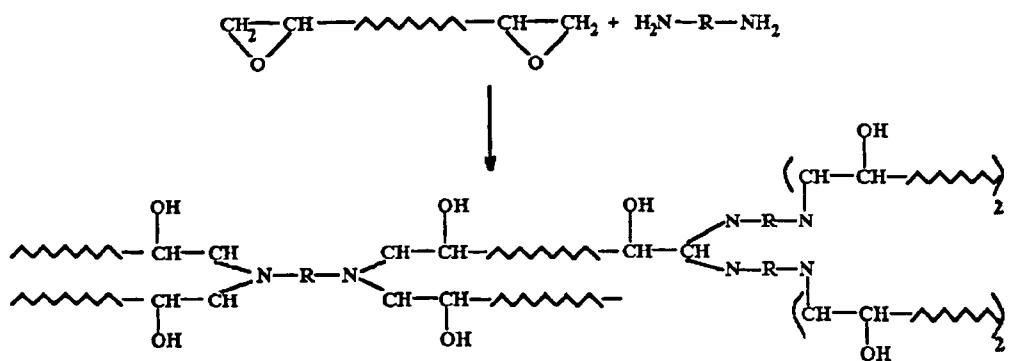
Figure 2.8 Reaction between an epoxy resin and a primary diamine hardener.

2.7 The adhesive properties of epoxy resins

The high adhesive strength of epoxy resins is said [12] to arise from the *polar groups* in the resin, *aliphatic hydroxyl* and *ether groups*. The epoxy groups are lost on curing [3]. These will also be present in the cured system as well as polar groupings from the curing agent, for example amino groups from amine curing agents. The polarity of these groups serves to create electromagnetic bonding forces between the epoxy molecule and the adjacent surface. The epoxy groups, likewise, will react to provide chemical bonds with surfaces, such as metals, where active hydrogens may be found. Since the resin passes relatively undisturbed (i.e. with only slight shrinkage) from the liquid to the solid state, the bonds initially established are 'preserved'.

By studying the static dielectric constant of epoxy resins in the liquid state de Bruyne [11](who, in 1939, first used the word 'adherend') concludes that, " *Epoxy resins behave as a collection of hydroxyl and epoxy groups acting quite independently of one another and without regard to the molecular weight of the hydrocarbon backbone to which they are attached* ".

Glazer [13] spread monolayers of epoxy resin onto a water surface to obtain a simplified model of an adhesive joint. He determined that the "epoxy groups and the hydrocarbon backbone" were factors determining the *cohesion* of the film but that *adhesion* (related to the collapse pressure of the film) was dependent on the

"hydroxyl group concentration". Although these studies were carried out on a model system with uncured resin it is conceivable that in a practical situation adsorption through hydrogen bonding of the hydroxyl groups to the metal oxide surface might occur before curing.

De Bruyne [11] prepared adhesive joints with resins of different epoxy content and found that the *breaking stress of the joints was proportional to (hydroxyl content)$^{2/3}$* . However, he also points out that *stresses formed in the joint on curing decrease with increasing hydroxyl content,* so that it would not be correct to ascribe adhesion directly to the adsorption of hydroxyl groups at the interface.

Hydrated oxide layers on metals all seem to be capable of forming good bonds with epoxide resins. This may be due to the formation of hydrogen bonds between the hydroxyl groups that are produced when epoxide adhesives are cured and similar groups on the surface [8]. However, water is a hydrogen-bonded liquid and it may compete with the adhesive in the formation of hydrogen bonds with the substrate with the result that the joint will be weakened by water.

Basically, a disadvantage of adhesives as a means of joining is that they are generally weakened by water and its vapour. Also, their service temperature ranges are less than for metal fasteners, being limited by their glass transition temperature (T_g) and chemical degradation. Indeed the basic reasons why water is generally aggressive to adhesive bonds is that it has a very high polar component of surface free-energy, and all adhesives contain polar groups. There are two processes involved in the deterioration of joints under the influence of moisture [3]. Those of *absorption of water* by the adhesive and its *adsorption at the interface* by displacement of adhesive.

In this connection it is interesting to mention the *De Proprietatibus Rerum (The properties of things)....1250 AD –*

"When a plate of gold shall be bonded with a plate of silver or joined thereto, it is necessary to beware of three things, of dust, of wind and of moisture: for if any come between the gold and silver they may not be joined together..." [1].

2.8 Modification of Epoxy resin

The simple resin-curing agent combination alone seldom provides a material with all the properties required for use in a given application. In commercial practice, in fact, seldom is the unmodified resin employed *except in laminating*. Therefore, basic epoxies are usually modified by one or more of the following methods:

1. Chemical modification of the base resins and/or curing agents.
2. Incorporation of various modifiers such as inert fillers and pigments, reactive diluents, flexibilisers, reinforcements etc. which will be discussed shortly.
3. Alloying with another resin (resinous modifiers).

Some modifying materials frequently perform more than one function at the same time, thus a diluent might also be a flexibiliser or a cure accelerator [9].

2.8.1 Chemical Modifications of base epoxy resin

Most commercial epoxy resins are diepoxides made from bisphenol A and epichlorohydrin, which are coreacted to an epoxy equivalent weight of 190 and a viscosity of 12,000 to16,000 centipoise. Modification to the base resin usually consists of varying the epoxy equivalent weight or increasing the viscosity and pendant hydroxyl content.

However, by using other reactive ingredients, a wide range of different epoxy resins can be manufactured with properties considerably different from the standard bisphenol A resins. Such as epoxy-novolac resins are two-step resins made by reacting epichlorohydrin with phenol formaldehyde condensates. They may have seven (7) or more epoxy groups per molecule which allow these resins to achieve high cross-link density in the cured resins resulting in excellent temperature, chemical and solvent resistance. They have superior performance at elevated temperature, superior electrical and mechanical properties, higher heat and humidity resistance and also higher viscosity.

Using diols and triols (i.e. two or three hydroxy groups in the molecule) gives flexible epoxy resins with high impact resistance but lower heat resistance. Using halogenated

reactants results in an epoxy that is self- extinguishing when removed from a flame but has higher specific gravity and cost. Using multifunctional ingredients gives resins with three or four epoxy groups, which results in more crosslinks during cure but reduces impact strength and increases cost. Cycloaliphatic reactants produce epoxy resins with superior electrical properties but reduced ability to be cured at room temperature. Each different epoxy resin occupies a place in the adhesive field where its advantages can be utilized best and its limitations can be tolerated or designed around.

2.8.2 Curing agents and their modification

Apart from curing agents, other reactive chemicals may be used to accelerate, promote, or retard the crosslinking reactions.

Each different curing agent will result in a different crosslinked molecular structure when cured, and so each will have different properties from all others. For example, using a primary and secondary amine gives fast, tight cures at room temperature, but the vapours are sensitizing and heat resistance is low. Amine adducts give easier mixing ratios and reduced sensitizing potential but increase the viscosity. Using polyamides gives excellent impact strength but lower heat resistance and chemical resistance. Aromatic amines give long pot life and increased heat and chemical resistance, but they must be oven-cured and many of them cause adverse skin reaction when handled. Lewis acid complexes give fast-setting adhesives (within seconds) but are weak mechanically and difficult to use in production lines. Anhydrides give high-temperature stability but the vapours are acidic and oven cures are required.These are only a few of the more than 100 curing agents available to the epoxy formulator, each one is appropriate for a limited range of uses.

2.8.3 Fillers

Fillers may be added to epoxy resins to reduce cost, lower the co-efficient of thermal expansion (that's why fillers are important in reducing stress in the bond area), lend toughness, reduce shrinkage, reduce flammability, increase electrical and thermal conductivity, alter surface hardness, increase or decrease density, reduce exotherms,

control the working time of adhesives, add colour or opacity, improve chemical, abrasion and arc resistance, improve adhesive properties, and/or change the handling characteristics of the resin system to impart the desired flow or thixotropic properties i.e. to thicken the mix so that it will not run off inclined surfaces but will flow when stirred.

These modifications will usually be achieved at the expense of other properties in the system, so that it can be said that most fillers will somewhat reduce over-all mechanical, electrical and/or chemical properties. For instance, some fillers may be corrosive to metals. Fillers chosen to improve high temperature properties often reduce low-temperature properties, and vice-versa. Many fillers, such as fibrous fillers, exhibit a wicking action for moisture which may degrade internal strength and chemically attack the adherends. Fillers may add undesired weight, which is of serious importance in aerospace, where a pound saved in an assembly may reduce fuel consumption by several thousand pounds during the life of an aircraft.

Fillers may be either organic or inorganic, metallic or non metallic and may range from cheap beach sand to moderately priced aluminum oxide to costly silver flake to ultra-expensive boron fibers.

2.8.4 Liquid modifiers

Liquid modifiers are used in epoxy systems for three main reasons, to reduce resin viscosity (diluents), to raise impact strength (flexibilisers and plasticisers), or to make the system cheaper (extenders).

2.8.5 Diluents

Diluents are free-flowing liquids used primarily to reduce the viscosity of the epoxy resin so that better penetration in casting and better wetting ability in laminate and adhesive formulations may be achieved and so that higher filler contents may be employed. The diluents may be either reactive (i.e. may contain epoxy groups or other reactive groups) or non-reactive. Reactive diluents are those which become permanently bound into the cured system and thus have the least degrading effect on

properties. Non-reactive diluents do not react chemically with either the epoxy resin or the curing agent and therefore may seriously alter properties. So, the reactive diluents are preferred over the non-reactive.

Use of a reactive diluent will somewhat decrease the tendency of the curing agent to volatilize during cure, and particularly in room-temperature curing adhesive formulations it is employed for this purpose. Diluents are also used for the following important reasons—

(i) increase or decrease impact and flexural strengths.

(ii) increase or decrease high-temperature or low- temperature capabilities.

(iii)improve or modify chemical resistance, electrical properties, and flame resistance.

(iv) Reduce or extend pot life, increase or decrease exotherm and extend storage life.

2.8.6 Flexibilisers and Plasticisers

Normally rigid epoxy systems may be made flexible by adding long-chain molecules to the mixture which are either nonreactive (plasticisers) or sparsely reactive (flexibilisers). The plasticisers may be considered as inert resinous or monomeric 'fillers'. The flexibilisers which my be either mono or polyfunctional become an integral part of the cured system.

The reactive long chains provide internal molecular-chain flexibility and lower the glass transition temperature (T_g), while the non-reactive plasticisers allow a measure of chain slippage and temporary distortion. Normally the reactive flexibilisers are much preferred in epoxy adhesives, since they are least likely to affect adhesive properties.

Flexibilisers for the epoxy resins are particularly useful where the high adhesion and low shrinkage of the unmodified resins cause strains in the system during cure. The function of a flexibiliser or plasticiser is to impart some degree of resiliency or toughness, which in turn may upgrade thermal and mechanical shock properties, increase impact resistance, improve peel and cleavage strengths, reduce internal stresses, decrease exotherm and shrinkage, and produce a better system for low temperature or cryogenic bonding. Some tackifiers and plasticisers contain

unsaturated bonds through which they can be polymerized or cross-linked once their initial task is completed [3]. It should be noted that some curing agents are also flexibilisers.

2.8.7 Flame/ Fire Retardants

Most plastics when exposed to a flame will ignite and burn, and epoxies are no exception. Self-extinguishing characteristics are obtained in epoxies by adding materials such as halogenated compounds in combination with antimony oxide. These two tend to change physical properties slightly, and if used in excessive amounts will cause serious brittleness, impairing peel and shock characteristics. Certain fillers and diluents are also valuable in this respect.

2.8.8 Cure accelerators

Certain simple substances can increase the rate of reaction between the epoxy resins and some curing agents, and wide variations in the rate of cure can be achieved by the addition of small amounts of catalyst. For example, phenol causes the rate of reaction between an epoxy resin and a simple aliphatic amine to increase by several orders of magnitude.

2.8.9 Reinforcements

These are inert, fibrous materials whose prime purpose is to increase the strength of the system. Glass and metal fibres are widely used, the glass being in fibrillar form or woven into a cloth or mat and the metal fibres being used as discrete fibres or whiskers. Carbon fibres are also important.The whole subject of polymeric composite materials is based on the combination of a resin matrix with a fibrous reinforcement, and epoxy resins play an important part in this particular technology.

2.8.10 Anti-degradants

Polymers, unlike minerals, have a strictly limited life and, like man himself who is also largely built of polymers, are subject to ageing processes. To counteract these or

at least delay them or to mitigate their effect on physical properties, various anti-degradants are used. Important in the list of additives therefore are anti-oxidants, anti-hydrolysis agents and stabilisers for halogenated polymers used against degradation by oxygen and UV.

2.8.11 Resinous modifiers

A wide range of other resins will react chemically with the epoxy resins to form a modified or 'alloyed' polymer system to gain advantages in specific physical properties, to simplify handling, or to obtain a distinct processing advantage. Common examples are the combinations of epoxy resins with polysulfide, phenolic, polyamide, nylon, urea melamine, polyester, polyurethane, silicone and vinyl resins. These systems have enhanced properties in certain respects over the properties of the individual, separate resins.

Other resins, although not reacting chemically with the epoxy resins, are also used to cheapen and alter the properties of the unmodified epoxy resins. Important examples are the addition of coal-tar pitch to yield epoxy paints with much improved water resistance, and petroleum-derived bitumens to cheapen anti-skid road surfacings.

2.9 Conclusion

It can be seen, therefore, that what is generally referred to as an epoxy resin is more properly a carefully formulated mixture of ingredients. The correct formulation of these ingredients is a skilled task and much of epoxy resin technology consists in the successful development of formulations 'tailor made' for particular applications. This could be because the final properties and eventual performance of the system require very specific characteristics, or because there is commercial advantage in so doing.

2.10 References

1. Lee, L.H., Fundamentals of Adhesion, Plenum Press, New York and London, 1991.

2. Brewis, D.M., and Briggs, D., Industrial Adhesion Problems, John Wiley and Sons, New York, 1985.

3. Wake, W. C., Adhesion and the formulation of Adhesives, Applied Science Publishers Limited, London, 1976.

4. Wake,W. C., Developments in Adhesives-1, Applied Science Publishers Limited, London, 1977.

5. DeLollis,N. J., Adhesives for Metals Theory and Technology, Industrial Press INC.

6. Comyn ,J., Adhesion Science, RSC Paperbacks.

7. Cagle ,C. V., Lee ,H., and Neville, K., Handbook of Adhesive Bonding, McGraw-Hill Book Company.

8. Adams, R. D., Comyn,J., and Wake,W.C., Structural Adhesive Joints in Engineering, Second Edition, 1997, Chapman and Hall.

9. Potter,W.G., Uses of Epoxy Resins, Newnes-Butterworths, 1975.

10. Lee,H., and Neville K., Epoxy Resins-their applications and technology, McGraw-Hill Book Company, INC 1957.

11. De Bruyne,N.A., Journal of Applied Chemistry, vol-6, 1956, 303.

12. Epstein,G., ACS Symposium, Atlantic City, September, 1956.

13. Glazer,J., Journal of Polymer Science, vol-13, 1954, 355.

14. Lee,H., and Neville,K., Handbook of Epoxy Resins, McGraw-Hill Book Company, 1967.

15. Hussain,A. , Paper 3, Plast. Rubb. Inst. 4th Conf. Res. Prog. Resin Plast. , 1976.

16. Batzer,H., Lohse,F., and Schmid,R., Angew. Makromol Chem. , vol- 29/30, 1973, 349.

17. Lohse,F., and Schmid,R., Chimia, vol-28, no-9, 1974, 576.

18. Mika,T.F., and Paradis,D.L., SAMPE, 2nd National Technical Conference, vol-2, 1970, 233.

19. Hamerton,I., Recent Developments in Epoxy Resins, Rapra Technology Ltd, England, 1996.

Chapter 3   Chemical Cure Kinetics, Modelling and Process Control

3.1 Introduction

This chapter is composed of three sections – cure kinetics, time, temperature and cure, and the factors and fundamentals behind final cured properties. These discussions shed some light on macroscopic and microscopic cure behaviour which can pave the way for better understanding of cure processes.

3.2 Cure Kinetics

Chemical reactions that take place during cure determine the molecular structure of cured resins that, in turn, determines the final physical, electrical and mechanical properties of the cured material. Thermoset cures, such as the cure of epoxy resins, are among the most difficult reactions to follow. This is due to the fact that—

(i)These materials generally start out as very low viscosity resins but then crosslink to form insoluble and rigid glassy materials. Therefore, the cure kinetics of the thermoset resin is complicated by the relative interaction between the chemical kinetics and the changing physical properties.

(ii) Moreover, the cure reaction of thermosetting materials is *exothermic* and as polymers exhibit low thermal conductivity, the temperature and rate of reaction can vary considerably within the curing mass. A further complicating matter is that these systems usually undergo more than one type of reaction.

(iii) Furthermore, in industrial formulations, a variety of additives are included in the cure system, resulting in complex cure kinetics.

(iv)Also, due to statistical variations present in the polymerization processes polymers are *polydisperse* or *heterogeneous* in molecular weight.

The overall requirement of the final cured state for thermosetting materials is that the physical and engineering properties of its microscopic and macroscopic structure remain within specified limits. Consequently, there is a need for more detailed understanding of the curing process and the evolution of structure-property relationship of cured material in order to control the curing economically and to

optimize the physical properties of final products. To allow a better understanding of reaction kinetics and the development of the engineering structure-properties on a microscopic scale, a combination of experimental monitoring techniques is required including ultrasound, X-ray analysis, NMR, DSC, dielectric, infrared spectrometry etc.

3.2.1 Perspectives of cure kinetics

The understanding of the mechanism and rate (kinetics) of cure is the first essential step in the process of evaluation of processing-morphology-property-durability relationships in thermosets and their composites. Knowledge of the rate that an adhesive cures and how that rate varies with cure temperature is useful and important from several standpoints.

Firstly, the most important point is to ensure that the adhesive is processed in an optimized manner compatible with its end use. Kinetics analysis helps the scientist, engineer or process control manager decide upon the most efficient temperature-time conditions for the generation of a component made from a thermosetting resin that has the optimum properties for any desired applications.

Secondly, the rate of cure defines the shelf-life of the adhesive for a given set of storage conditions and its working life by controlling its tack, wetting and flow properties.

Thirdly, the kinetics information is useful for balancing energy consumption versus the completeness of cure for a thermosetting product.

Fourthly, the modern kinetics software can be used to address the quality and consistency of thermosetting resins. This software provides the bench scientist with an easy-to-use, rapid, interactive method for the simulation of the kinetic behaviour of chemical reactions.

Fifthly, for a commercial adhesive, the manufacturers recommended cure schedule will, in general, yield an adequately cured material. It is often desired, however, to

cure the adhesive under a different set of conditions. This will occur, for instance, when several materials in an assembly are to be simultaneously cured or if temperature sensitive components are to be bonded. The cure kinetics in the form of a phenomenological rate law (discussed later) permit the cure cycle to be optimized for a given bonding situation. If, in addition, correlations between the degree of cure and the cohesive strength of the adhesive have been established, they help to make certain that the adhesive joint has not been compromised by cure cycle changes.

3.2.2 Molecular diffusion vs. chemical reaction -- Basic overall kinetics

According to Alig et al [73], the conversion of a thermoset from a liquid to a solid is a result of the *negative feedback* between the molecular diffusion and chemical reactions and it occurs when the product of the reaction has a lower configurational entropy and specific volume than the reactants. The decrease in the molecular diffusion co-efficient progressively reduces the probability of chemical reaction until such a time that neither diffusion nor reaction can take place at a significant rate and the resin is in effect cured.

During the initial phases of cure when the reaction mixture is of a low viscosity, the rate of chemical reaction is slower than molecular diffusion and therefore the rate of chemical reaction determines the rate at which network structure develops. During the later stages of cure when viscosity is high and the infinitely connected network or gel has formed it is molecular diffusion that is slower and therefore controls the rate at which the network densifies. Basically, in the last stage of the cure, reaction is no long associated with small molecules migration, but it involves displacements of long branched molecules and segmental mobility of the network. Therefore, steric hindrances and slow segmental diffusion lower the curing rate and lead to a reaction diffusion-controlled. Furthermore, segmental mobility is dramatically decreased by vitrification. It can be mentioned here that the amine-epoxy curing reactions referred to in the previous chapter have been studied by several authors and the reaction schemes are relatively well established.

3.2.3 Kinetic characterization using Differential Scanning Calorimetry

Differential scanning calorimetry is the most widely used technique in the investigation of the kinetics of cure of thermosetting resins. The basics of DSC in characterization of cure has already been mentioned in section 1.4 in chapter 1.

The aim of the kinetic investigation of a curing thermoset is, in general, based on the construction of a kinetic model, either *phenomenological* or *mechanistic*, which can predict characteristic features of the curing system, for instance, the rate or extent of reaction or the glass transition temperature for a given time-temperature profile. Therefore, from the standpoint of mathematical modelling, the correlation and representation of experimental data in the form of a simple kinetic expression is of considerable importance. In this respect differential scanning calorimetry has been extensively used as a convenient means to evaluate the rate equations and for estimation of the associated kinetic parameters [8, 18, 41, 42, 43, 50, 60, 62].

3.2.3.1 Treatment of DSC data

The basic assumption made in treating DSC data to follow reaction kinetics is that the heat of reaction evolved up to a time t, is proportional to the overall extent of reaction given by the fraction or number of moles of reactive groups (reactant) consumed. Following this approach the general expression for the degree of conversion, α, can be written as follows [22, 27, 42, 48, 49, 50, 54, 55]

$$\alpha = \frac{H(t)}{H_T} = \frac{\int_0^t \left(\frac{dH(t)}{dt}\right)dt}{\int_0^{t_f} \left(\frac{dH(t)}{dt}\right)dt} \tag{3.1}$$

Where, $H(t)$ is the total heat evolved up to a certain time t, in an isothermal experiment, $\frac{dH(t)}{dt}$ is the value of rate of heat generation at time t, and H_T is the total heat of reaction which can be estimated from the dynamic experiments that can take the reaction to complete or full conversion up to the final time t_f.

The rate of reaction, $\dfrac{d\alpha}{dt}$, thus can be obtained as a function of time from the isothermal rate of heat flow, $\dfrac{dH(t)}{dt}$, measured by DSC using the equation

$$\frac{d\alpha}{dt} = \frac{1}{H_T} \cdot \frac{dH(t)}{dt} \qquad\qquad (3.2)$$

assuming its proportionality to the rate of heat flow.

Here, it can be mentioned that since DSC measurements are based on the hypothesis of proportionality between the heat flow due to cure reaction and the overall rate of reaction, they do not enable individual reactions to be separated. Yang and Lee [68] utilized FTIR measurements to determine the multiple reaction mechanisms which would have been unresolved by conventional DSC methods using a polyurethane-polyester interpenetrating network (IPN) system. Consequently, DSC must be regarded as a useful complementary tool when a detailed reaction mechanism has already been established by more group specific techniques such as FTIR or NMR [4]. In such a case, exploiting the rich potential of DSC data, the kinetic analysis helps to determine those steps which most profoundly contribute to the overall process. This allows for the reduction of intricate mechanisms to an effective kinetic scheme. However, an advantage of the DSC technique is that by giving access to reaction rate it enables to detect *complex kinetic behaviour at low conversions* that would be almost undetectable by other experimental techniques [12].

3.2.3.2 DSC measurements – isothermal and non-isothermal tests

There are two experimental techniques for DSC measurements of thermoset reactions isothermal tests and non-isothermal scanning tests. In an isothermal test the rate of energy released is measured at constant temperature and the extent of reaction is calculated from equation (3.1). The major assumptions in this type of test are that the total heat of reaction can be determined accurately, and that all reactions contributing to the overall reaction have the same *enthalpy*. In non-isothermal scanning tests the heat of reaction is monitored over a linearly increasing temperature scan and kinetic data is obtained via various analysis of the DSC curve produced. These analysis

included deriving kinetic data from step integrals of the rate curve and deriving a relationship for kinetic parameters from exotherm maxima at various heating rates. Use of scanning DSC is very useful in obtaining kinetic data for commercial resin systems by fitting assumed empirical models to scanning data.

Isothermal measurements do have the advantage of a complete separation between the variables of time and temperature. Isothermal DSC measurement does not suffer from baseline problems. Nevertheless, an isothermal experiment is more time-consuming than a non-isothermal one, provides less information and despite seeming very easy theoretically, it is limited experimentally. It is hard to heat the sample instantaneously from ambient temperature to the desired cure temperature so that the data at the beginning of the measurement is not fully reliable. A significant advancement of the cure state can take place before DSC can reach and stabilize at the desired temperature, and at low temperatures, the reaction may not proceed to completion. So, isothermal DSC cannot be applied to systems that react too fast. However, the *multistep isothermal* cure experiment [12], which tests isothermal cure behaviour at different temperatures in only one experiment, takes less time than classic isothermal DSC experiments and enables isothermal curing to be studied even at high temperatures which can take the reaction to nearly *full conversion.* Also, isothermal DSC can introduce errors in cure modeling due to effects of unavoidable temperature ramping. Alternatively, dynamic data allow for a better capture of the kinetics at both the start and end of a reaction, and complex reaction mechanisms can be more easily interpreted by a comparison of measurements at different heating rates [9]. A brief outline of the various workers in the field of isothermal and non-isothermal DSC tests are given in the paper by Halley and Mackay [5].

3.2.3.3 Errors affecting in determination of kinetic parameters using DSC

Different errors may affect the accuracy of the cure kinetic parameter determination based on DSC measurements. Such as, the use of an inappropriate kinetic model function, intrinsic faults of the apparatus, or errors in the interpretation of the DSC thermogram. It is well known that the baseline (lying under the exothermal peak) of a DSC scan experiment for a thermoset is not a straight line, but obtaining its real shape is a complicated process.It can be obtained by heat capacity measurements

with *temperature modulated DSC*, which is an improvement of DSC apparatus where, a temperature modulation is added to the usual temperature ramp [12,42,59,60,61,62]. Nevertheless, this method is still not commonly used, and most kinetic studies are performed with conventional DSC. Moreover, the type of baseline used is generally a simple straight line drawn from the beginning to the end of the exothermic signal [8].

3.2.4 Theoretical background to kinetic modelling

In the study of cure kinetics by DSC, the essential step is fitting of the reaction rate profiles, obtained from isothermal and dynamic experiments, to a kinetic model. There are essentially two forms of kinetic models used to describe thermoset curing reactions—*phenomenological* or *empirical* and *mechanistic* models.

1. **Phenomenological or empirical model:** Phenomenological models assume an overall reaction order and fit this model to the kinetic data. They relate to the main features of the reaction kinetics and do not take into account individual reactions. This type of model provides no information on the kinetic mechanisms of the reaction and is predominantly used to provide models for industrial samples.

2. **Mechanistic model:** Mechanistic models are derived from an analysis of the individual reactions involved during curing which requires detailed measurements of the concentration of reactants, intermediates, and products. Essentially mechanistic models are intrinsically more complex than empirical models, however, they are not restricted by compositional changes, as are empirical models.

Determination of the most appropriate kinetic model for an application will depend on the type of system and the accuracy and form of results required. Due to the complex nature of thermosetting reactions, phenomenological models are the most popular for these systems.

3.2.4.1 Model-Fitting Method

The model-fitting technique is the most widely used approach. It consists of using empirical kinetic models and fitting them to experimental data. In phenomenological

modelling of the cure kinetics of thermosetting polymers, an internal state variable is defined to which all other properties are related. This state variable is the degree of cure (α) and ranges from 0 (uncured) to 1 (fully cured). Generally, researchers have related the extent of the chemical reaction to the other independent variables, that is, time and temperature. Therefore, evaluation of the appropriate kinetic model parameter from kinetic measurement defines the degree of conversion as a function of time and temperature, $\alpha(T, t)$.

In kinetic analysis, it is generally assumed that the rate of reaction can be described by the product of two separable functions, $K(T)$ and $f(\alpha)$, such that

$$\frac{d\alpha}{dt} = k(T).f(\alpha) \qquad (3.3)$$

where $\frac{d\alpha}{dt}$ is the rate of reaction, $K(T)$ is the temperature- dependent Arrhenius rate constant, and $f(\alpha)$ corresponds to the reaction model which gives the dependence of the reaction rate on the extent of reaction. Naturally, as the reactants are used up, the rate decreases. For *nth* order behaviour the function is expressed as

$$f(\alpha) = (1 - \alpha)^n$$

where n is the reaction order and α is the fraction reacted.

Basically, $f(\alpha)$ is a function that depends on the reaction mechanism. As mentioned before, a commercial epoxy adhesive formulation is a complex mixture of resins, hardeners, modifiers, accelerators, and fillers. As such, there is a little hope that insight into the nature of $f(\alpha)$ can be obtained without detailed and extensive chemical analysis. Nevertheless, chemical kinetic information is required for process definition which has already been stated, and study shows that $f(\alpha)$ *can be treated in a phenomenological manner* to rapidly and inexpensively obtain a useful kinetic model without requiring a thorough understanding of the cure chemistry.

The temperature dependence of the reaction rate constant is commonly described by the Arrhenius equation

$$k(T) = A.\exp\left(\frac{-E_a}{RT}\right)$$ (3.4)

where R is the universal gas constant, E_a is the activation energy, and A is the pre-exponential factor. It is understood that at higher temperatures the reaction rate is greater.

For non-isothermal conditions, when the temperature varies with time with a constant heating rate $\beta = \dfrac{dT}{dt}$, the explicit time dependence in equation (3.3) can be eliminated so that

$$\frac{d\alpha}{dT} = \frac{A}{\beta} \exp\left(\frac{-E_a}{RT}\right) f(\alpha)$$ (3.5)

A multivariate version of the Borchardt and Daniels method [69] is frequently used in the evaluation of dynamic DSC data. In this method, the kinetic parameters (A and E) are obtained by a linearizing transformation of equation (3.5) so that

$$\ln\frac{d\alpha/dT}{f(\alpha)} = \ln\left(\frac{A}{\beta}\right) - \frac{E_a}{RT}$$ (3.6)

This linear equation, which has the form $y = a_0 + a_1 x$ with $x = 1/T$, can be used to determine the optimal fit of the kinetic parameters by multiple linear regression [9].

Though the model fitting technique is the most widely used approach the problem is that usually quite different kinetic functions fit experimental data equally well (from a statistical point of view),whereas the numerical values of the corresponding Arrhenius parameters differ.

With a view to simulating the temperature field in thermoset thick pieces, this above mentioned effect can be a great problem as it is evident that even a small error in kinetic parameters, especially activation energy, can lead to totally wrong temperature predictions. Therefore, it is necessary to have information *a priori* about the reaction mechanism in order to choose a kinetic function with a physical meaning. This is the case when a kinetic scheme has already been established by other experimental techniques which have mentioned before.Traditional models which have been considered in relation to the curing kinetics of epoxy thermosets will be briefly discussed later.

3.2.4.2 Model-Free Isoconversional Method

The basic idea of the model-free isoconversional kinetic analysis of non-isothermal DSC experiments is to determine the apparent activation energy at each conversion without any assumption about kinetic function. In this alternative approach, the reaction rate at a constant conversion depends only on the temperature.This method assumes that both the activation energy and pre-exponential factor are functions of the degree of cure. Friedman's method [70] is the simplest means which is frequently used to determine the activation energy from the logarithmic form of the rate equation for each heating rate—

$$\ln\left[\beta_i\left(\frac{d\alpha}{dT}\right)_{\alpha,i}\right] = \ln[A_\alpha f(\alpha)] - \frac{E_\alpha}{RT_{\alpha,i}} \qquad (3.7)$$

where the subscript α is the value at a particular degree of cure and i refers to data from a given heating rate experiment. The activation energy at each degree of cure can be calculated with linear regression from a plot of $\ln\left[\beta_i\left(\frac{d\alpha}{dT}\right)_{\alpha,i}\right]$ versus $1/T_{\alpha i}$ (Friedman plot) across all of the heating rates tested. Similarly, the product of the cure- dependent pre-exponential factor and the reaction model can be obtained from the y intercept of the Friedman plot. These parameters can alternately be calculated by an integral iso-conversional method described by Flynn and Wall [71] and Ozawa [72].

The advantages of this model-free iso-conversional technique are twofold—on the one hand, one should be able to determine the exact apparent activation energy, and on the other hand, the evolution of apparent activation energy with conversion can be interpreted in terms of reaction mechanism, particularly in the case of multi-step reactions [12]. Therefore, the iso-conversional approach can be used to evaluate both simple and complex chemical reactions.

3.2.5 Kinetically controlled reaction models

A number of models have been considered in relation to the curing kinetics of thermosets. The main models that have been proposed in the literature to describe the chemical kinetics of the cure of thermosets are listed in table 3.1. A detailed chart and analysis of the kinetic models, both phenomenological and mechanistic, applied in the investigation of the cure kinetics of thermosets has been published by Halley and Mackay [5] in their review of chemorheology of thermosets.

In the case of a curing system which shows no autocatalytic phenomena and no complexity in the reaction mechanism, a simple nth order reaction model, such as that given by equation (3.8), is expected to hold. The epoxy cure reaction has sometimes been described by means of a simple *nth-order* kinetic expression governed by a single rate constant. Kinetic expressions describing the autocatalytic behaviour (i.e. maximum reaction rate $d\alpha/dt$ is observed for $t > 0$ in an isothermal cure) of epoxy cure have also been discussed in the literature. The simplest autocatalytic kinetic model proposed is given by equation (3.9).

The autocatalytic reaction models suggest that the curing process is governed by more than a single rate constant which, in turn, implies the presence of more than one reaction mechanism and activation energy in the system. The reaction rate constant, k_1 is generally assumed to correspond to the primary reaction which involves catalytic ring opening by the amino group through a ternary transition state of amine, epoxide, and hydrogen donor present in the reaction medium, and k_2 is generally assumed to correspond to the secondary reaction which involves autocatalytic ring opening involving amine, epoxide, and hydroxyl group formed by the opening of the first

epoxide ring. In the study of Sourour and Kamal [32] the overall reaction rate order (*m+n*) was assumed to be *2* and the validity of this assumption was confirmed elsewhere [21].

Table 3.1 kinetic models describing the chemical kinetics of thermoset cure.

Model	Euqation	Equation no.
*n*th order reaction	$\dfrac{d\alpha}{dt} = k(1-\alpha)^n$	(3.8)
Autocatalytic reaction	$\dfrac{d\alpha}{dt} = k\alpha^m(1-\alpha)^n$	(3.9)
*n*th order + autocatalytic reaction	$\dfrac{d\alpha}{dt} = (k_1 + k_2\alpha^m)(1-\alpha)^n$	(3.10)
General complex reaction model	$\left.\dfrac{d\alpha}{dt}\right\|_{overall} = \sum_{i=1}^{j} g_i A_i \exp\left(-\dfrac{E_i}{RT}\right)f_i(\alpha_i)$	(3.11)
Arrhenius dependence of rate constant	$k_i(T) = A\exp\left(-\dfrac{E}{RT}\right)$	(3.12)

where,

α = calorimetric conversion,

$\dfrac{d\alpha}{dt}$ = reaction rate,

m , n = reaction orders,

T = absolute temperature,

R = universal gas constant,

j = number of independent reactions,

A_i = pre-exponential factor of the ith reaction,

E_i = activation energy of the ith reaction,

$f_i(\alpha_i)$ = reaction function of the ith reaction,

g_i = normalized weighting factor of the ith reaction.

For the cure of most epoxy resins the proposed model is a combination of an autocatalyzed process with an nth order reaction. Because of the relative complexity of the epoxy-amine system and because of the autocatalytic effects of hydroxyl groups produced during the cure which have been mentioned before, a model that can describe the kinetics of the overall reaction is best described by an expression of the type shown in equation (10). Ryan and Dutta [20] and Sourour and Kamal [32] applied this model to an epoxy-amine cured system.

In the case of some thermosets very complex reactions occur during curing which produce unresolved thermal peaks in a DSC thermogram. Duswalt [74] suggested that for a complex reaction consisting of independent reactions, one or more of them can be eliminated by ageing the sample at a suitable temperature. By repeating this process at different temperatures, each reaction can be resolved so that the kinetic analysis can be applied to each reaction independently. For such a complex system the final kinetic model would then be of the form of equation (3.11) [6]. Chiou and Letton [26] applied this model to the study of the cure of a commercial epoxy system.

3.2.6 Estimation of kinetic parameters

In all of the above mentioned studies, the kinetic parameters have been determined by fitting the experimental rate data to the kinetic model using a linear or non-linear least-squares regression analysis fitting technique, or alternately, by combining the variables so as to produce a linear relationship from which the kinetic parameters could be estimated.

Other methods also have been developed to estimate the kinetic parameters associated with the cure kinetics of an epoxy system. Ryan and Dutta [20], for instance, developed what they termed a "rapid technique" for the estimation of the order of reaction and rate constants governing the autocatalytic behaviour of epoxy cure from isothermal initial and peak degree of cure rate DSC data; Arrhenius constants were subsequently estimated from these rate constants using linear regression. The advantage of this procedure is that it is simple; the disadvantage is that, since only two experimental data points are utilized in the determination of the isothermal kinetic parameters, experimental errors have a great impact on the estimates. Keenan [24]

proposed an extension to Ryan and Dutta's method [20] for the estimation of parameters of Sourour and Kamal's model [32] that requires neither data fitting nor prior knowledge of the reaction order.

Though the most commonly used method of determining kinetic parameters involves the use of *linear regression* and isothermal DSC data, one of the difficulties with this approach is that the Arrhenius constants cannot be estimated directly. This method first requires the estimation of the rate constants at different temperatures and then the estimation of the Arrhenius constants from the rate constants. A number of *non-linear estimation methods* which are basically statistical methods [6], also have been utilized to estimate the kinetic parameters associated with the kinetics of epoxy cure. Scott and Saad [19,2] have presented a new estimation procedure based on a new application of the Box-Kanemasu method in estimating kinetic parameters associated with the curing of an amine-epoxy system.

Most of the usual techniques for kinetic parameter determination of thermosets do not take into account the problems of sensitivity (and so of identifiability) of the kinetic parameters, or the problems of correlation between some of them. Scott and Saad [19,2] have made sensitivity studies for both isothermal and non-isothermal DSC experiments and shown that the problem of correlation between Arrhenius parameters is minimized for isothermal experiments when using the conversion degree as the modeled variable. They concluded that the degree of cure (α) rather than $d\alpha/dt$ should be treated as the dependent variable when using the Box-Kanemasu method. The Box-Kanemasu based method provides more accurate estimates of the kinetic parameters than the linear regression method, also it has the added advantage that the Arrhenius constants can be estimated directly [19].

3.2.7 Modifications for diffusion-controlled kinetics

It was previously mentioned that for the cure of most epoxy resins the proposed model is a combination of an autocatalyzed process with an nth order reaction. However, the autocatalytic reaction model has been found to be applicable over a wide conversion range for curing before vitrification. In those investigations, the

long-time results at low-temperature curing after vitrification typically deviated from the kinetic model predictions. Obviously, these deviations are expected as the reactions become diffusion limited after the materials vitrify. Therefore, the lack of agreement between experiment and theory is likely to be caused by the neglect of the existence of diffusion control in the later stages of the reactions.

Basically, the chemical kinetics of most thermosets at cure temperatures below $T_{g\infty}$ (the glass transition temperature of the fully cured network) is generally complicated by the fact that the reactions become diffusion-controlled in the later stages of cure, particularly after vitrification [16], where the rates of the chemical reactions become very low. In actuality, diffusion of chain segments can become a dominating factor especially when the T_g of the material rises beyond the cure temperature (i.e. after vitrification). Therefore, for meaningful characterization of the cure kinetics over the whole range of cure, in particular towards the later stages, it is necessary to incorporate the effects of diffusion control into the reaction kinetic model.

Mathematically there are two easy ways to modify the kinetic models in order to incorporate the effects of diffusion-controlled kinetics.

3.2.7.1 First method

A typical approach to the mathematical treatment of the diffusion phenomena is to express T_g in terms of conversion, α, using *Di Benedetto's equation* [15, 39] (which will be discussed later) and then introduce the modification of the kinetic rate constants according to Rabinowitch [75] as follows-

$$\frac{1}{k_e(\alpha,T)} = \frac{1}{k(T)} + \frac{1}{k_d(\alpha,T)}$$

(3.13)

where,

k_e = overall effective rate constant,

k = Arrhenius-dependent reaction rate constant in the kinetically controlled region, and

k_d = Specific rate constant for diffusion.

This equation shows that the overall rate constant is governed at one extreme by the Arrhenius rate constant (when $k_d >> k$), which is the case prior to vitrification, and at the other extreme by the diffusion rate constant (when $k >> k_d$), which is the case well after vitrification.

The basic idea of equation (3.13) is to find the mean duration of co-ordination of two molecules as a sum of the mean durations of co-ordinations due to reaction and diffusion. This idea is also known as the *"Law of the addition of kinetic resistances"*. It has been shown that the Arrhenius plot for a process complicated by diffusion is non-linear. To take into account the effect of both T and α on diffusion, Vyazovkin et al [4] developed an equation with separable variables T and α which is one of the most convenient way.

Now, there are three ways mentioned in literature by which the diffusion rate constant k_d can be expressed.

Expression 1

Simon and Gillham [76] give the expression for k_d by the following equation

$$k_d = A_d \exp\left(-\frac{E_d}{RT_c}\right)\exp\left(-\frac{b}{f}\right)$$ (3.14)

where,

A_d, b = adjustable parameters,

E_d = activation energy of the diffusion process,

T_c = cure temperature,

f = equilibrium fractional free volume given by-

$$f = 0.00048\left(T_c - T_g\right) + 0.025$$ (3.15)

where, T_g =instantaneous glass transition temperature of the curing system.

Expression 2

Wisanrakkit and Gillham [16] give an alternative expression for the diffusion rate constant (k_d) using a modified form of the *Williams-Landel-Ferry (WLF) equation*.

The usual form of the WLF equation applies only above T_g under equilibrium conditions. By including absolute value | T-T_0 | in the denominator the modified form shown in equation (3.16) allows application of this relationship below T_g and hence permit its application both above and below T_g.

$$\log(\alpha_T) \equiv \log \frac{\tau(T)}{\tau(T_0)} = \frac{-C_1(T - T_0)}{C_2 + |T - T_0|} \qquad (3.16)$$

where, T is the temperature of the experiment, T_0 is an arbitrary reference temperature, C_1 and C_2 are constants, τ (T) and τ (T_0) are the polymer segmental relaxation times at the temperatures T and T_0 respectively, and α_T is the time-temperature superposition factor.

From this modified form of WLF equation, Wisanrakkit and Gillham [16] give the expression for the diffusion rate constant (k_d) by the following equation-

$$\ln(k_d) = \ln(k_{do}) + \frac{40.2(T_c - T_g)}{51.6 + (T_c - T_g)} \qquad (3.17)$$

Expression 3

Chern and Poehlein [77] proposed a simpler semi-empirical relationship, based on free-volume considerations, to explain the diffusion control kinetics which have been widely used. According to their theory, when the degree of cure reaches a critical conversion value, α_c, diffusion becomes the controlling factor and the diffusion rate constant k_d is then given by—

$$k_d = k \exp[-C(\alpha - \alpha_c)] \qquad (3.18)$$

where k is Arrhenius-dependent reaction rate constant and C is a constant which has no discernible trend but α_c increases with temperature at a given composition, as in other studies [7].

Equation (3.18) corresponds to a rather "abrupt" onset of diffusion control at $\alpha = \alpha_c$, which typically occurs well beyond gelation, close to the vitrification point [3]. The latter is defined at the time or conversion at which the T_g of the resin reaches the curing temperature, and is thus only reached if the cure temperature is below $T_{g\infty}$. In reality, the onset of diffusion effects is somewhat more "gradual" and there is a region in which both chemical and diffusion factors control the kinetics. Combining equation (3.13) and equation (3.18), a diffusion factor $f_d(\alpha)$ can be defined as—

$$f_d(\alpha) = \frac{k_e}{k} = \frac{1}{1 + \exp[C(\alpha - \alpha_c)]}$$ (3.19)

For $\alpha \ll \alpha_c$, $f_d(\alpha)$ is close to unity and the effect of diffusion is negligible. Up to $\alpha = \alpha_c$, $f_d(\alpha)$ is almost constant and begins to decrease at $\alpha = \alpha_c$. Beyond this point, $f_d(\alpha)$ approaches zero as the reaction effectively stops. The effective reaction rate at any conversion is equal to the chemical reaction rate multiplied by $f_d(\alpha)$. The values of C and α_c can be obtained by fitting $f_d(\alpha)$ versus α data at each temperature and composition.

3.2.7.2 Second Method

The another mathematical method of modifying the kinetic model is empirical. In this case, the maximum degree of conversion achieved during an isothermal cure (α_{max}) is taken into account and its relationship with temperature is then modeled. For an nth order reaction scheme, the kinetic model can be expressed as follows [78]

$$\frac{d\alpha}{dt} = k(\alpha_{max} - \alpha)^n$$ (3.20)

3.2.8 Avrami phase change theory in cure kinetics

Apart from traditional kinetic models, Kim et al [22] used Avrami phase change theory to describe the cure kinetics of epoxy-amine system which gave even more satisfactory explanation to some experimental phenomena. This theory is basically based on the phase change and most often used to describe polymer crystallization kinetics. In a broad sense, crystallization can be considered as a physical form of crosslinking. In some aspects the behaviour of the amorphous crosslinked polymers at a higher degree of crosslinking is similar to that of at a higher degree of crystallinity. Therefore, it is also possible to predict the curing of epoxy resin based on the Avrami expression. The simple Avrami expression is given by the following equation [22]--

$$\alpha = 1 - \exp(-kt^n) \tag{3.21}$$

where α is the extent of cure at time t, k is the rate constant and n is Avrami exponent which provides qualitative information on the nature of the growth processes.

According to the study of Kim et al [22] the kinetic parameters obtained are consistent with that from other thermal analytical methods. Their study shows that the kinetic results from Avrami theory may present a combined effect of important physical phenomena that likely to take place in the system which are not taken into account in other kinetic investigations.

3.2.9 Variation in kinetic results

Even though many experimental techniques and studies relating to epoxy cure reactions have been reported in the literature with emphasis on the chemical, physical, and mechanical property changes with time [31,32], there are often conflicts in the kinetic parameters. Moreover, data can be interpreted by different methods to produce different results. The causes of these problems are twofold—(i) the assumptions used in the calculations and (ii) the neglection of the physical phenomena likely to take

place in the system. Therefore, it is essential to understand the fundamental principles that govern the cure process.

3.3 Time, Temperature, and Cure

The ultimate use of information on the reaction kinetics of thermoset polymerization is for the development of the desired final properties of thermosetting polymers. The states of the polymer throughout cure ultimately rely on the selected cure temperatures and times as well as the initial and ultimate glass transition temperatures of the polymer. In this section, the development of the glass transition temperature of a thermoset and its relation to the evolution of the cure cycle is discussed.

Temperature and time are the most important parameters to select in a cure cycle. As for example, producing an epoxy-based composite with the desired mechanical properties requires precise control of the heating schedule. Temperature not only *controls* cure rates, but also *reaction pathways*. Low cure temperatures favour chain-extension producing *flexible* composites, while high temperatures favour cross-linking producing *rigid* composites. Based on the knowledge gained by analyzing the thermoset, one can estimate these variables based previous generalizations made on thermosetting polymers. The importance of using thermal analysis techniques is considerable because the outcome of the resulting polymerization cannot be reversed. Therefore, it is imperative that an understanding of the relationships between the analysis and thermoset generalizations be obtained.

3.3.1 Gelation and Vitrification

Gelation and vitrification are the two principal events which are encountered in the transformation (cure) of liquid thermosetting multifunctional monomers to glassy network polymers.

3.3.1.1 Gelation

Gelation can be examined from both chemical and physical points of view. From a 'chemical' perspective, gelation is deemed as the point (the time or temperature) at

which covalent bonds connect across the network and an infinite molecular network is formed, which gives rise to long range elastic behaviour in the macroscopic fluid. It occurs at a specific point of chemical conversion for a given system according to *Flory's theory of gelation* [38], and depends on the curing system itself and the environment in which the reaction takes place. 'Physically' speaking, gelation occurs when the bulk polymer transforms from the liquid state to a rubbery state. This is noted by a divergence of the viscosity towards infinity. Gelation in both cases is an irreversible transformation. Chemical gelation usually takes place before physical gelation.

From macroscopic point of view, *macroscopic gelation* corresponds to the end of the processable fluid state on cure when gelation precedes vitrification. On the other hand, *molecular (theoretical) gelation* corresponds to a definite conversion for a given simple system; all molecules are finite at conversions lower than that at molecular gelation, whereas finite and infinite molecules occur together after the conversion corresponding to molecular gelation.

3.3.1.2 Vitrification

Vitrification is the process by which a polymer passes into the glassy state. This can happen in either the liquid state or the rubbery state i.e. vitrification can occur before or after gelation. Vitrification retards chemical conversion. Unlike gelation, vitrification can be undone by raising the temperature of the polymer. However, vitrification can reoccur as the degree of cure increases. The vitrification point of a reacting system is the point at which further reaction is prohibited. Work done by Wisanrakkit and Gillham [16] showed very slow diffusion-controlled reactions may occur in the vitrified state. Chemical ageing involves the slow continuation of chemical reactions beyond vitrification [30]. Basically, it is evident that *vitrification is not a point but a gradual process that extends over a large part of the cure* [17].

3.3.2 Cure diagram—representation of cure-property relationships

Identification of when gelation and vitrification will take place in a polymer can carry vital significance when deciding how to cure a polymer. The cure diagram is an

extremely useful tool in displaying this information in an understandable manner. There are four different types of cure diagrams that have been developed, utilizing appropriate analysis techniques on thermosetting polymers. Basically, generalizations on the cure and properties of thermosetting polymers, which have stemmed from cure monitoring technique (e.g. torsional braid analysis [29]), have been formulated in the cure diagrams in terms of *cure-property relationships*. They are—

1. Isothermal time-temperature- transformation (TTT) cure diagram [29]
2. Conversion-temperature-transformation (CTT) cure diagram [39] or,
   Continuous heating time-temperature- transformation (CHT) cure diagram [30]
3. Glass transition (conversion)- temperature-property (T_gT P) diagram [30,40]
4. Glass transition temperature versus conversion (T_g- α) relationship [16].

The relationships may be used to design time-temperature cure paths,that exploit gelation and vitrification, to optimize cure processes and glassy state properties. This allows one to select the optimum cure cycle settings based on the desired nature of the polymer under investigation. Prime [40] and Gillham [30] published examples of each type of cure diagram mentioned above. Here, we will limit our discussion to only the isothermal time-temperature-transformation (TTT) cure diagram.

3.3.2.1 Isothermal time-temperature-transformation (TTT) cure diagram

The most commonly recognized cure diagram is the well-known isothermal time-temperature-transformation (TTT) cure diagram, which was developed by Gillham [29], to relate the properties of thermosetting systems to process conditions. Gillham developed the TTT diagram using a form of Torsional Braid Analysis to identify when the onset of gelation and vitrification takes place in a polymer. It was also first adopted for the epoxy resin cure by Gillham.

The isothermal time-temperature-transformation (TTT) diagram provides a useful framework for the understanding of the curing process, particularly the effects of gelation and vitrification on the cure kinetics and properties and the optimization of the processing and the final material properties. A typical diagram of this kind is

shown schematically in figure 3.1. It displays the states of the material and characterizes the changes in the material during isothermal cure at different temperatures, T_{cure} vs time.
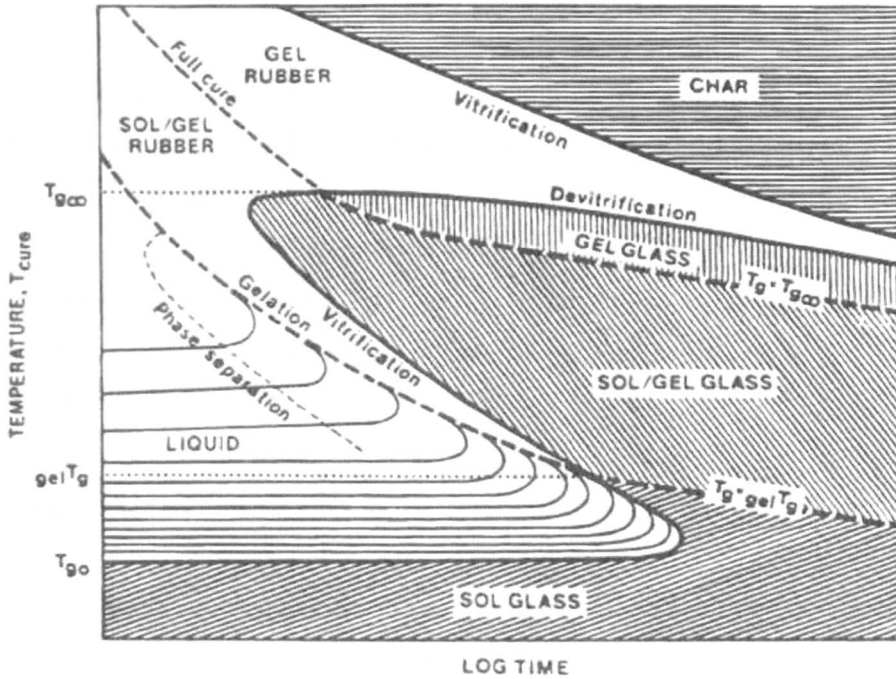
Figure 3.1 Schematic time-temperature-transformation (TTT) isothermal cure diagram for a thermosetting system (after J. K. Gillham [29]).

Material states (seven distinct regions) include – liquid, sol-gel rubber, gel-rubber (elastomer), sol-gel glass, gel-glass, ungelled (sol) glass, and char [29]. The various changes occurring in the material during isothermal cure at different temperatures T_{cure} are characterized by contours of the times to reach the events. The contours include the onset of phase separation, gelation, vitrification, full cure, devitrification and char formation [29]. The progress of the isothermal cure process and the state of the material can be clearly summarized in terms of these contours in the TTT diagram. Three critical temperatures are marked on the temperature axis of figure 3.1. They are T_{go} , the glass transition temperature of the uncured reactants, $_{gel}T_g$, the temperature at which molecular gelation and vitrification occur simultaneously, and $T_{g\infty}$,the glass transition temperature of the fully cured network. A thermoset cured in between T_{go} and $T_{g\infty}$ will develop a structure dependent on the cure temperature and

duration, represented on the diagram by the sol-gel, gel-glass regions. The information supplied on this diagram can be especially useful in determining the cure temperatures and times in the cure cycle.

3.4 Final cured properties—factors and fundamentals

This section sheds some light on three important points. Firstly, the factors affecting final cured properties are discussed. Secondly, the general concepts and relationship between the degree of cure and chemical crosslinking is explained. In this context, research on ultrasonic and thermal estimation of degree of reaction and crosslink density have been reviewed. Next, the relationship between the glass transition temperature, crosslink density and degree of cure is explained in the context of reaction kinetics and evolution of properties.

3.4.1 Factors affecting kinetics and final cured properties

The three-dimensional polymerization of multifunctional monomers or oligomers, traditionally, considered an available avenue for producing highly crosslinked polymer networks with desired structure and properties. In cured epoxies, the three-dimensional molecular network structure formed—which is a function of the prepolymers and curing agents, and of the stoichiometric ratio used and also of the extent to which crosslinking has advanced— determines the glass transition temperature and other physical properties of these materials. The curing conditions and degree of mixing [45] also have effects on cure kinetics and network formation. The functionality of the monomer units defines the microstructural characteristics of the network polymer. The crosslink density, which is dependent on the monomer functionality, ultimately defines the viscoelastic and mechanical properties (i.e. physical characteristics) of the thermosetting polymer. However, extensive research studies have shown that the polymerization is not limited to chemical crosslinking and that the relationship between initial oligomer and resulting polymer structure and properties is not so straightforward as it might appear [33].

Also, a complicating matter is that in many instances this polymerization process is accompanied by micro-phase separation, vitrification of reaction medium,

68

heterogeneous polymer network formation, and so called "caging effect" [34] which may lead to incomplete reaction of amine or epoxy group during the formation of high density thermoset network . Due to statistical variations present in the polymerization processes polymers are *polydisperse* or *heterogeneous* in molecular weight. Although it is generally recognized today that the model of coexisting regions of higher and lower crosslink density adequately describes the morphology of highly crosslinked thermosets [35], the concept of the formation of inhomogeneous (the microscopic inhomogeneity in the network structure which appears to be macroscopically homogeneous) thermoset network morphology still remains incompletely understood. The above mentioned physical and structural changes in turn often significantly affect both polymerization kinetics and the structure and properties of the resulting polymers [36,37].

3.4.1.1 Effects of curing agent

The curing agent determines the type of curing reaction which occurs, influences cure kinetics and thus the processing cycle—viscosity versus time – and gelation, and affects the final properties of the cured system. The difference in cured properties between aliphatic and aromatic amine cured epoxy resin, for example, will be mentioned later.

3.4.1.2 Effects of Stoichiometry

Stoichiometry is of critical importance in step polymerizations. Considering the epoxy system cured with amine curing agent, there should be no unreacted epoxy or amine when cure is completed in order to obtain the optimum properties. Each amine group can react with two epoxies. Thus, the ratio of amine to epoxy moieties must be 1:2. This proper ratio is termed the stoichiometric point and is calculated as follows

(MW of amine / available H for reaction) / (epoxide equivalent weight) * 100

This stoichiometric ratio is one important variable controlling the ultimate network structure and significantly affects properties including – glass transition temperature,

modulus, crosslinking density and strength. Systematically changing the stoichiometric ratio over a wide range, the effect of this important variable on the ultimate properties of the epoxy networks can be investigated.

3.4.1.3 Monomer functionality and its effect on crosslink density

The crosslinked networks formed in a thermosetting polymer grow in *three dimensions* having all of the monomers functionalities *greater than two*. This is what causes the fundamental property differences between thermosets and thermoplastics. Thermoplastics are linear polymers where the polymer chains grow in a *single direction* having all of the monomers functionalities of *two*. However, some thermoset monomers have a higher functionality than others. This has a significant effect on the potential crosslink density that a thermosetting polymer can have. A monomer with a functionality of three can only form half as many crosslinks in its network than a polymer with a monomer functionality of four. A higher crosslink density means more dimensional stability, high mechanical strength, as well as a higher glass transition temperature.

3.4.1.4 Effect of monomer's chemical structure and molecular weight

The size of the monomer unit plays a role in the crosslink density of a thermosetting polymer. If a monomer unit has long polymer chains between functional groups, the final polymer is much more limited in terms of the final crosslink density. The chemical structure heavily influences the glass transition by affecting mobility—

- flexible main chain components lower T_g .
- bulky side-groups raise T_g .
- increasing the length of flexible side-groups lowers T_g .
- increasing main chain polarity increases T_g .

A property derived from the monomer's chemical structure that affects the final glass transition temperature of a thermoset is the molecular weight between crosslinks. In general, a higher molecular weight between crosslinks leads to a lower glass transition temperature because of increased flexibility in the individual polymer chains.

Molecular weight influences T_g significantly at lower molecular weights where the excess of free volume associated with chain ends is significant. As molecular weight increases the concentration of chain ends decreases until its contribution to the free volume becomes negligible.

3.4.1.5 The effect of degree of mixing in cure kinetics

The degree of mixing of resin and hardener is an important parameter which will have a crucial effect on the kinetics of the cure process [45], and it is qualitatively well known that a higher degree of mixing leads to more rapid and complete development of the cross-linked network. So, this parameter needs to be quantified for complete analysis. Possible ways of quantifying the degree of mixing could include X-ray or optical techniques [45].

3.4.1.6 The effect of fillers on reaction kinetics

Many thermosetting compounds contain a variety of additives and ingredients including fillers and reinforcing agents. Fillers are used for various reasons and can have a significant effect on part shrinkage, flame retardancy, and cost which were mentioned previously. Therefore, the influence of fillers on the curing kinetics is of considerable interest. It is also vital to understanding the rheology of filled thermosets. For instance, the effects of filler concentration on viscosity can be used in process control to monitor batch to batch variations or to provide essential information for research into alternative filler/resin batches. Ng et al [66] examined an epoxy resin system with silica filler and established that the elastic modulus of the resin can be expressed in terms of filler concentration and the modulus of the matrix and that of the gel time is reduced as filler concentration increases. Dutta and Ryan [67] also examined the effects of fillers on the kinetics of an epoxy-diamine reaction, where they found that the type of filler can affect the reaction kinetics. According to them, carbon-black fillers increase the reaction rate via kinetic rate constants and silica fillers affect the reaction rate through activation energies. Carbon-black filled systems had an insignificant effect on the activation energy of the cure reaction. A brief overview of the effects of fillers on the chemoviscosity of thermosetting resins in connection with recent research is given in the paper by Halley et al [5].

3.4.1.7 The effect of temperature on cured properties

The effect of temperature on the rate and degree of polymerization is of prime importance in determining the manner of performing a polymerization. Increasing the reaction temperature usually increases the polymerization rate and decreases the final molecular weight of polymer [34].

3.4.1.8 Effect of amine structure on epoxy-amine system

Amines are often used as curing agents for epoxy resins to form crosslinked chemical structures possessing high glass transition temperature and strength. Research shows that the relative reactivity of primary amine versus secondary amine with epoxy is strongly dependent on the type of amine used. Moreover, variations in this relative rate of reaction can strongly influence processing behaviour of epoxy-amine systems by affecting viscosity development and the gel-point conversion.

Horie et al [52] argued that an increase in the number of methylene units in aliphatic diamines of the structure $H_2 N$ — $(C H_2)_n$ —$N H_2$ reacted with a DGEBA epoxy resin results in an increase in the final conversion, with near *100% conversion* being achieved by diamines with six or more methylene units. In their research study, the supposed lack of high conversions in shorter amines was attributed to the restriction of segmental mobility due to high levels of crosslinking.

3.4.1.9 Differences between aliphatic- and aromatic-amine cured epoxy resin

Previously it was mentioned that curing agents affect properties of the cured system. Research shows that epoxy resin cured with cyclo-aliphatic amine system shows a lower T_g , higher rubbery modulus and a wider glass transition than epoxy cured with aromatic amine system [17]. The lower T_g of the aliphatic system is to be expected from the lower stiffness of the cycloaliphatic moiety compared to its aromatic counterpart. The higher rubbery modulus of the aliphatic amine system shows that it has a somewhat higher crosslink density than the aromatic system which is further

indicated by the wider glass transition. These results reflect the fact that the two amines must react in different manners, producing networks with different structures.

It is well known that under extreme conditions of high cure temperature in the epoxy-amine reaction, *etherification side reaction* occurs [25] which *adversely affects network formation*. It is much more prevalent in aromatic amine systems than in aliphatic amine systems [46]. This is because of the lower basicity of aromatic amines which makes them less reactive towards epoxy groups and the higher cure temperatures employed with aromatic amines. The etherification reaction has a higher activation energy than the amine-epoxy addition [47], and thus competes more with the secondary amine reaction at higher cure temperatures. The lower tendency for etherification in the aliphatic amine leads to a higher fraction of tertiary-amine groups in this system compared to the aromatic amine system.

3.4.1.10 Inhomogeneity vs. final properties in epoxy system

The occurrence of different chemical reactions during cure is apt to lead to the formation of inhomogeneous network morphology which is a function of curing agent concentration [21]. Variations in morphology within the same system, in turn, would result in the local differences in physical/mechanical properties and durability of thermosets. An inhomogeneous morphology has been correlated to physical/ mechanical properties of amine cured-DGEBA type epoxies [35, 44]. However, a unifying concept of direct quantitative relationships between cure kinetics and the corresponding morphology has not been advanced.

3.4.1.11 Development of structure in rapid and longer cure epoxies

Dixon et al [45] had showed that there appears to be a fundamental difference in the way that the elastic moduli develop in the rapid cure and longer cure time epoxies. In terms of the reaction kinetics and the development of the structure on a microscopic scale Dixon et al [45] had showed that a generic difference exists between the curing reaction in rapid cure and longer cure epoxy adhesive systems. In case of rapid cure systems it would appear that the un-reacted polymer chains do not have sufficient time to reach locations on the network to which they can cross-link. The subsequent

cross-linking reactions occur at a much slower rate as the un-reacted polymers must orientate themselves or diffuse into a position where they can cross-link to the network. In longer cure epoxies, the rate of reaction is much slower and the un-reacted polymer chains have sufficient time to orientate or diffuse to the correct position for cross-linking reactions to occur.

3.4.2 Degree of cure

The amount of curing agent used is generally calculated on the assumption that for each reactive site in the resin there will be one in the curing agent. This gives a reasonable estimate of the relative proportions of each component and the optimum proportions can be obtained experimentally. Overcuring results in adhesives which have too many crosslinks, they are generally *brittle* and do not adjust to mechanical impact or expansion and contraction with changing temperatures. Undercured adhesives do not have enough crosslinks. They may be *cohesively weak* and may also be subject to excessive moisture absorption, further decreasing their cohesive strength. With amine cured systems it is generally found that too low a quantity of amine does not allow complete curing, whilst excess amine causes the final product to be brittle. Associated with this problem is the degree of cure. Not only is it necessary to employ the proper amount of curing agent to achieve thorough crosslinking of the system, but it is necessary to discover the cure time and/or cure temperature which will bring about this thorough crosslinking in a practical or convenient period of time.

The degree of cure can be defined where all reactive sites have been reacted during cure, or more realistically, until conversion has stopped. In the latter case some of the reactive sites are blocked by the solid network. For instance, in epoxy resins, the degree of cure has, by custom, come to refer to the extent to which the epoxy groups have been consumed, and, when present, the extent of consumption of the reactive elements in the curing agent. This definition of the degree of cure are based on *conversion of reactive sites*, is related to the reaction kinetics of cure.

The meaning of cure can also be considered in more pragmatic terms. In the real world of curing technology most of the users prefer as definition of (sufficient degree of) cure that— " *the cured product meets the needs of its functional properties to be*

commercial". Therefore, for practical purposes, a thoroughly cured system is considered one in which the degree of crosslinking is sufficient to *provide optimum physical properties for a particular application*. This varies widely depending on the nature of the constituents but generally aromatic amines are less reactive than aliphatic amines and higher temperatures are required for full cure. Complete cure, requiring consumption of all unsaturated elements, is seldom if ever obtained even under laboratory conditions.

During cure, there are two aspects to the reactions involved : *conversion* (the actual disappearance of reactive elements) and, more importantly, *crosslinking* (the coupling of the molecules into three-dimensional networks through reactive residues to form the desired thermoset resins). It is obvious that in any highly crosslinked system there will be reactive groups which are sterically hindered from reacting [51]. The development of a high density network may lead to incomplete reaction of amine or epoxy group as a consequence of the so called "caging effect" [34].

3.4.2.1 Post-cure heating and degree of cure

A higher degree of cure results in a higher crosslink density (higher rubber modulus) and hence in matrices with higher T_g . Post-curing at high temperatures increases the conversion of epoxy groups and modifies the crosslink density of the network. Wisanrakkit and Gillham [16] showed that when the glass transition temperature of a constructed network did not change with an increase in post-cure time or postcure temperature then the reaction had reached *full conversion*. Above the glass transition temperature entropic contributions are the key to determine the elastic behaviour of the material, whilst at temperatures lower than the glass transition temperature, the variations in the internal energy of the systems become considerable.

In recent years, intense research has been devoted to the development of *interpenetrating polymer networks (IPNs)*. In this class of materials, high post cure temperature cannot completely cure the material. IPNs are a new class of polymer blends that can be defined as a mixture of two or more crosslinked polymers held together predominantly by permanent entanglement of networks rather than by covalent bond grafting. Curing kinetics of simultaneous DGEBA/Unsaturated

polyester (UP) IPNs formation was studied by means of DSC [13]. A lower total heat of reaction developed during simultaneous polymerization in both dynamic and isothermal DSC tests was found, compared to the total heats developed during the cure of pure resins. For curing in dynamic conditions this phenomenon can be interpreted as an effect of "network interlock" that *could not be compensated completely by an increase of curing temperature.* Namely, the mutual entanglements of the two networks provide an extra sterically hindered environment to the curing reactions and restrained the mobilities of both components [13]. During isothermal cure the incomplete cure was attributed to both the "network interlock" and the vitrification of DGEBA resin.

3.4.2.2 Relation between chemical crosslinking and degree of cure

During the polymerization process the relaxation time τ increases spontaneously, which reflects an increase in the hinderance of molecular motions possibly caused by the increase in the chainlength and the number of crosslinks. The physical nature of chemical crosslinking is quantified and represented by two fundamentally different, but conceptually equivalent measurements. The most definitive value to represent cure is the *crosslink density*. The crosslink density is a quantitative measure of the number of crosslinks that exist in a given volume in the thermosetting polymer. The crosslink density is equal to the inverse of the molecular weight between crosslinks. The value of the crosslink density is related in some fashion to the degree of cure. Pollard predicted the gel point of multifunctional epoxy-amine system at which the deviation of experiment from theory occurred for the degree of cure [53]. The degree of cure does represent a certain level of chemical crosslinking in the thermoset, but the value obtained for the degree of cure is relative. In the research study of Pindinelli et al [1] and Maffezzoli et al [54], ultrasonic longitudinal modulus has been compared with the degree of reaction measured using differential scanning calorimetry and the ultrasonic longitudinal modulus is correlated well with the crosslinking density combining with degree of reaction. The development of the high frequency viscoelastic properties of the material is linked in an inextricable way to the degree of cure as the polymer structure develops, though the type or nature of this link is not known in a quantitative sense. The determination of the degree of cure from the

amount of chemical conversion is not satisfactory as the sole means for evaluating thermosets. The extent and character of the three-dimensional network formed during cure must be determined as well. Basically, *uncured* and *fully cured* states on the material must be defined to determine the degree of cure. Once these limits have been characterized, the degree of cure and the crosslink density become directly related. Thus the chemical crosslinking in a thermoset polymer corresponds to the physical nature of the polymer's cure. Obtaining the glass transition temperature of network polymers is crucial to understanding the relationship between the polymer and its crosslink density.

Another set of physical measurements that one can relate to the degree of crosslinking in a thermoset is the dielectric properties of the polymer during cure. Several instances are available in which researchers have related the changes of electrical conductivity in a thermoset to the change in degree of cure during the cure reaction.

3.4.2.3 Ultrasonic and DSC estimation of degree of reaction and crosslink density

In the research of amine cured epoxy resin by Pindinelli et al [1] and Maffezzoli et al [54], ultrasonic bulk longitudinal modulus (L) has been compared with the degree of reaction measured using differential scanning calorimetry. Furthermore, a correlation between the ultrasonic modulus and the crosslink density is presented combining DSC data with the stoichiometry of reactants according with the statistical theory of Miller and Macosko [56,57].

A comparison of time dependence of longitudinal modulus and the degree of reaction as per research of Pindinelli et al [1] is illustrated in figure 3.2. The experimental data [1] indicate that ultrasonic measurements (ultrasonic longitudinal modulus) show a limited sensitivity at the beginning of the cure whereas at the end of cure shows a better sensitivity than DSC which shows negligible changes of the degree of reaction (figure 3.2).Figure 3.3 illustrates a plot of L as a function of the degree of reaction α at corresponding times for three different cure temperatures. From these data it is evident that ultrasonic longitudinal modulus is mainly sensitive to the increasing

crosslinking density occurring after gelation rather than to the number of reacted groups.
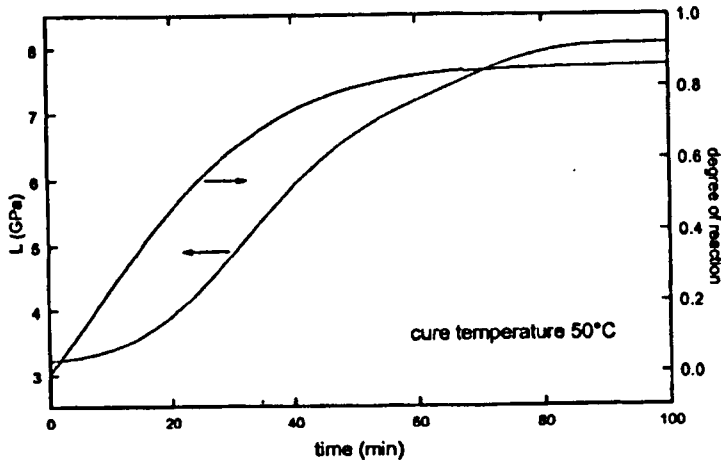
Figure 3.2 Comparison of time dependence of longitudinal modulus and degree of reaction (after Pindinelli et al [1]).
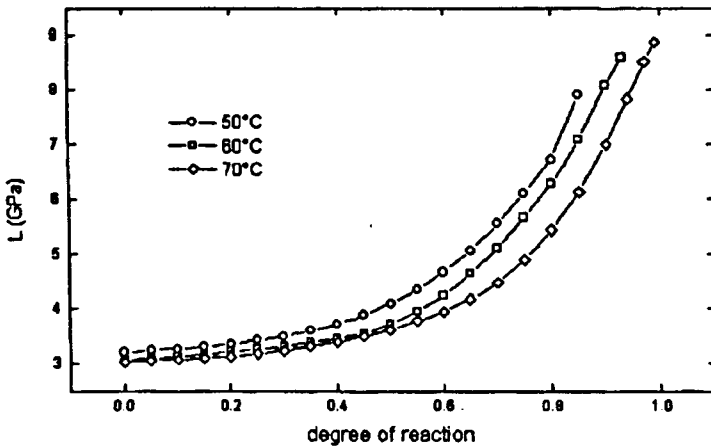
Figure 3.3 Longitudinal modulus as a function of the degree of reaction (after Pindinelli et al [1]).

Here, in view of comparison of different techniques of cure monitoring it can be mentioned that study shows [27] that DMA, is quite sensitive to the rubbery modulus (and as such, the cure state), but is limited practically to cure states above gelation. NMR and X-ray studies of the curing thermoset can measure structural changes and differences in composition [11]. Basically, NMR spectroscopy enables tracking of the

underlying chemistry of cure process and can relate the chemical structure of the thermoset to its mechanical properties. DSC shows apparent insensitivity to changes in the mechanical properties of a developing polymer network. Since the ultrasonic technique can be applied to all cure states it could be exploited for an on-line process monitoring ; particularly of postgel properties.

In the theory of rubber elasticity Flory [38] gives the theoretical prediction of the evolution of mechanical properties after gelation . Pindinelli et al [1] and Maffezzoli et al [54] computed it by applying the statistical approach of Macosko and Miller [56,57] for stepwise polymerization. Using a simple recursive method they derived the probability of a finite or dangling chain in a polymer network. Then finite chain probabilities are derived for a variety of networks as a function of type and extent of reaction. From these probabilities, useful post-gel properties of network polymers such as sol-fraction, cross-link density and the number of elastically effective network chains was readily developed. Then ultrasonic longitudinal modulus L was better correlated with the *degree of crosslinking, defined as the concentration of effective junction points in the infinite network,* rather than with the *degree of reaction.*

The two useful parameters considered are *crosslinking density* (μ) and the *concentration of active network chains* (v).The *crosslinking* is associated with a significant stiffening of the material and the *active network chain* represents only of the development of crosslinking segments which appear to significantly affect the stiffness of the resin [1]. It has already been mentioned that the cross-link density is considered as the concentration of effective network junctions. Taking rubber elasticity into account, a network chain can be considered "effective", act like an entropic spring, if it is long and if its ends are effective cross-links and are spaced such that it can assume a random coil conformation. Frequently a *front factor* is added to account for deviation from random coil behaviour. To count the effective network chains two types of crosslinks are considered as shown in figure 3.4.

In *chemical cross-links* (v_c) there is one defect – dangling ends or finite chains which result from incomplete reaction. This is taken into account in calculating crosslink density. Another type of possible crosslink is the *mechanically effective crosslink* (v_e)

or *physical crosslink* which is a "trapped entanglement" . In figures 3.2 and 3.3, a *mechanical response is observed also before gelation* when the velocity abruptly increases. This can be attributed to mechanically efffective crosslinks arising from trapped entanglements developed in the branched molecules of very high molecular weight [54].
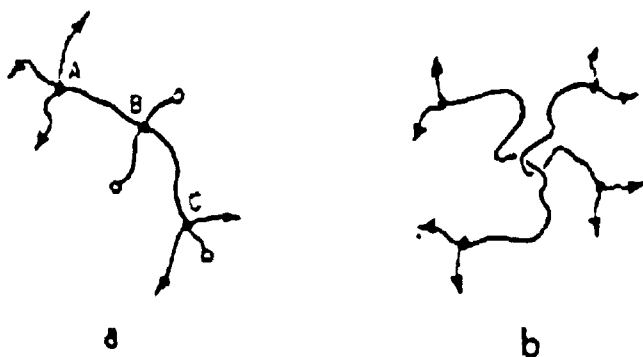
Figure 3.4 Network defects: (a) finite or dangling chain, —o ; (b) a physical cross-link, a trapped entanglement (after Miller and Macosko [56,57]).

Figure 3.5 shows a plot of crosslinking density, μ , and concentration of the active network chains, v_c , as a function of the amine groups conversion, P_A obtained by Pindinelli et al [1]. It was assumed that $P_A = \alpha_{DSC}$ and considered that α measures each reaction step either leading to a simple chain extension or to additional crosslinking during the network growth.
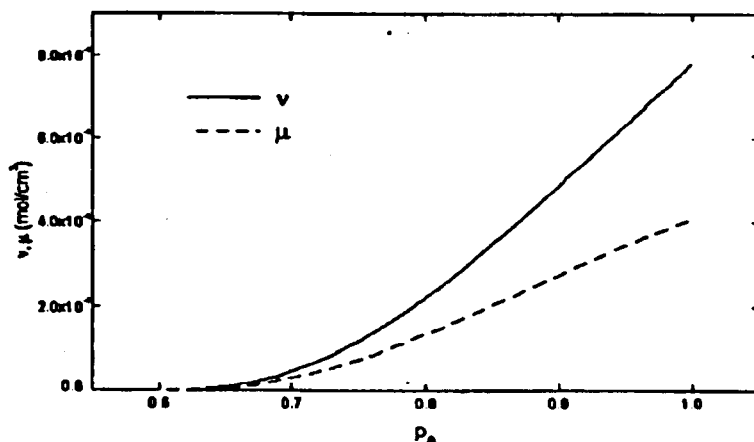
Figure 3.5 Crosslinking density, μ, and concentration of the active network chains, v, as a function of the amine groups conversion (after Pindinelli et al [1]).

80

The considerations regarding μ and ν have been mentioned before. The obtained correlation by Pindinelli et al [1] between L and the concentration of active network chains, ν, after the gel point is illustrated in figure 3.6.
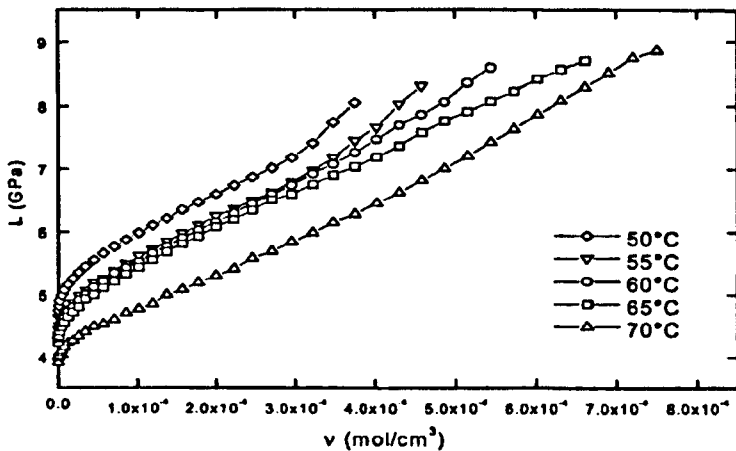
Figure 3.6 Correlation between L and the concentration of active network chains,ν, after the gel point (after Pindinelli et al [1]).

The longitudinal modulus plotted as a function of the concentration of active network chains showed a linear dependence in the rubbery region. In the final stage of the reaction, the transition to the glassy state is reflected in a sudden growth of the storage modulus. However, the linear growth of the modulus with temperature, predicted by the theory of rubber elasticity, was not observed. The longitudinal modulus, for each value of the crosslinking density, decreases with temperature, in contrast with the theory of rubber elasticity. Pindinelli et al [1] explained this phenomenon considering that the *very small deformation applied by ultrasonic wave propagation involves only energetic intrachain interactions rather than entropic effects* associated with macroscopic stretching of the chain segments [58] that control rubber elasticity.In fact, the energetic contribution to the elastic response of a rubber, not dependent on the strain, may be dominant at very small strains [58]. This result, in contrast with the observed linear dependence of L on ν, suggests that the entropic contribution to the ultrasonic bulk longitudinal modulus is not relevant as a consequence of the small deformation involved in the propagation of the ultrasonic waves.

Therefore, *the theory of rubber elasticity cannot be applied to the ultrasonic bulk longitudinal modulus.* However, it is already shown that ultrasonic longitudinal modulus is mainly sensitive to the increasing crosslinking density occurring after gelation and represents a sort of "statistical crosslinking".

3.4.3 Reaction Kinetics versus Development of glass transition

Research study on epoxy-amine resin systems show that T_g *advancement* follows a "single activation mechanism" during the build-up of the three-dimensional network, in contrast to the *reaction kinetics*, which follow "several activation mechanisms" depending on the nature of the individual cure reaction [14]. This result suggests that *the development of glass transition should be treated in a completely different way than the reaction kinetics.* There are several factors which influence the reaction kinetics, such as – the chemical constituents of the reactive system, the possible interactions that can be established between them and the relative distances between the various reactive species as these are determined by the positions that they hold in space during the development of the three dimensional network.

On the other hand, the "only factor" which seems to influence T_g is the "structural configuration" of the forming network itself. The possible reactions that can lead to this network have no influence on T_g.

3.4.3.1 Relation between segmental mobility and chemical conversion with T_g

The most comprehensive expression that correlates segmental mobility and chemical conversion with T_g, is the expression derived by Adabbo and Williams [39] using Di Benedetto's equation which has the form of

$$\frac{T_g - T_{go}}{T_{go}} = \frac{\left(\dfrac{E_x}{E_m} - \dfrac{F_x}{F_m}\right).\alpha_g}{1 - \left(1 - \dfrac{F_x}{F_m}\right).\alpha_g} \tag{3.22}$$

where, T_{go} and $T_{g\infty}$ are the glass transition temperature of the monomer and the fully reacted network, E_x and E_m are the lattice energies for crosslinked and uncrosslinked

polymer respectively, F_x and F_m are the corresponding segmental mobilities and α_g is the extent of conversion at T_g.

This expression can be used to consider the change of the reaction rate during vitrification, modelling of T_g equation and can be used to represent the relationship between T_g and the extent of conversion. The relationship between T_g and conversion given by equation (3.22) can be expressed as

$$\frac{T_g - T_{go}}{T_{g\infty} - T_{go}} = \frac{\lambda\alpha}{1 - (1 - \lambda)\alpha} \quad \text{where} \quad \lambda = \frac{F_x}{F_m} \tag{3.23}$$

by using

$$\frac{E_x / E_m}{F_x / F_m} = \frac{T_{g\infty}}{T_{go}} \tag{3.24}$$

Equation (3.23) can be used to model the T_g – conversion relationship by treating λ as an adjustable parameter.

Theoretically, the structure – dependent parameter λ is equated to $\dfrac{\Delta C_{p\infty}}{\Delta C_{po}}$, where

$\Delta C_{p\infty}$ and ΔC_{po} are the differences in heat capacity between the glassy and rubbery state for the fully cured network and monomer, respectively [15].

3.4.3.2 One-to-one relationship between T_g and conversion--- molecular basis

Many authors have shown that the T_g versus conversion relationship for thermosetting systems is one-to-one and independent of cure temperature [7,14,16,24,28,30]. An example is shown in figure 3.7. T_g has been used directly as a parameter for conversion in analysis of reaction kinetic models.

Figure 3.7 shows that T_g relates to conversion in a "non-linear fashion" with T_g rising more sharply with small increases in conversion at high conversions. This implies that T_g is a sensitive parameter and is particularly useful at high conversions and after vitrification because of the non-linearity of the T_g versus conversion relations. The

non-linearity also implies that very high conversions are necessary to attain maximum values of T_g.
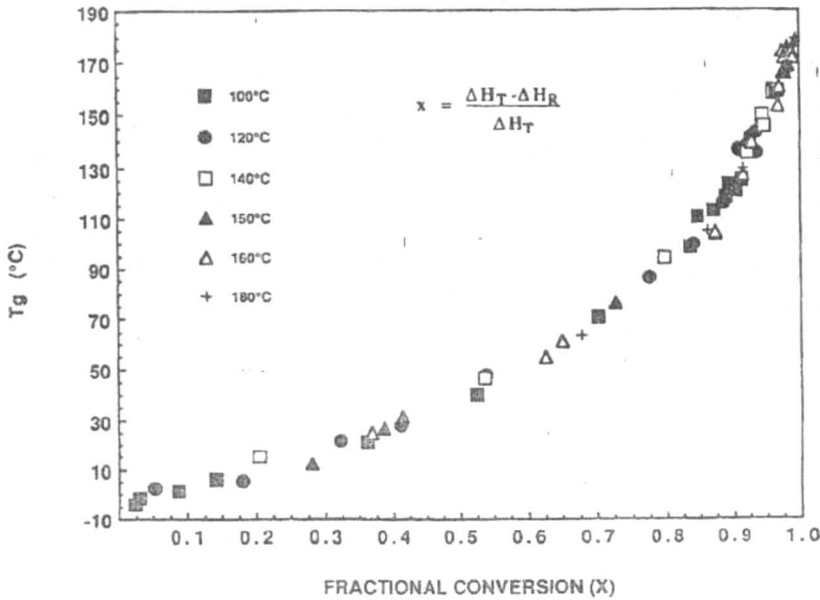
Figure 3.7 T_g versus fractional conversion (after Wisanrakkit and Gillham [16]).

This sharp rise of T_g in the high conversion range is considered to arise from the *dependence of T_g on the functionality of the crosslinking units* [16,24]. Higher-functional crosslinking units (such as tetrafunctional cross-linking unit) are more effective in raising T_g than are lower-functional crosslinking units (such as trifunctional cross-linking unit). An example is shown in figure 3.8. The concentration of the higher functional crosslinking units increases at high conversion at the expense of the lower functional crosslinking units, resulting in T_g rising more sharply at high conversion. This conception can be highlighted more fundamentally considering the molecular basis stated below.

During the cure of thermosets, low molecular weight liquids are transformed into an infinite network of amorphous solid polymer. In initial stage, all molecules are finite (sol). As the extent of reaction increases, T_g increases because of an increase in the molecular weight. After the chemical gel-point, the system is composed of both sol(finite molecule) and gel (infinite molecule) fractions. Both species contribute to

the overall increase of the T_g of the material. The T_g of the sol-fraction is considered to be a function of its number average molecular weight, whereas that of the gel-fraction depends on the crosslink concentration and depends more strongly on the higher functional crosslinking units than on the lower functional ones.
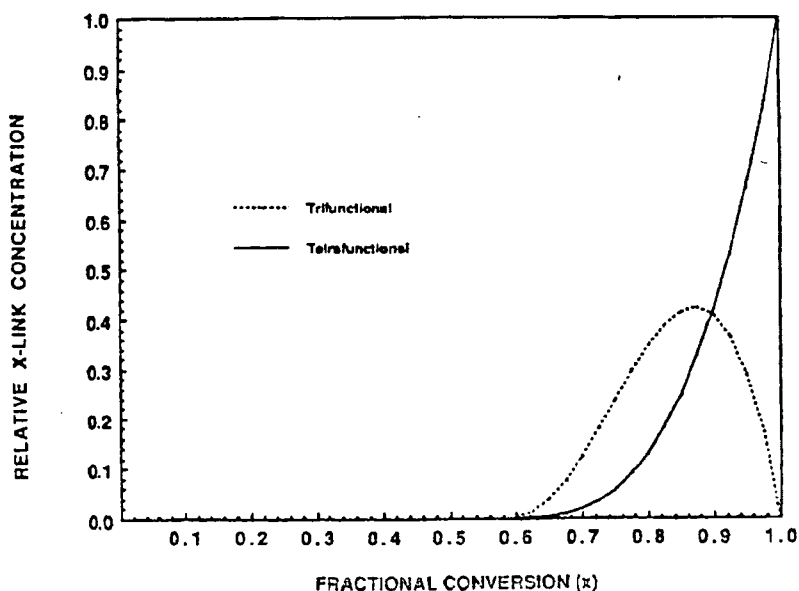
Figure 3.8 Relative concentrations of the amine crosslinking units of degree 3 and degree 4 vs. fractional conversion (after Wisanrakkit and Gillham [16]).

Conventionally, the unique one-to-one relationship between T_g and conversion implies either that the molecular structure of the materials cured at different cure temperature is the same or that the difference in the molecular structure for materials cured at different temperatures does not have a significant effect on the glass transition temperature [16, 30]. In another way it can be mentioned that the unique relationship suggests that there is either one reaction for polymerization or that the competing reactions have similar activation energies for the individual reaction rate constants [14,30]. For such cases a particular value of T_g corresponds to a particular conversion and to a particular molecular structure which can be calculated if the value of the rate constant [k $(= f(T)$] is known. Therefore, it is important to mention that the investigation of macroscopic properties versus conversion (T_g) corresponds to investigation of molecular structure-macroscopic property relations which is the principal theme of polymer materials science. In this case, the conversion-temperature-property (T_g T P) diagram can bear an important significance.

3.4.3.3 T_g – a practical parameter to monitor the extent of cure

It is usually difficult to accurately determine the extent of reaction for the final few percentage of reactive groups using conventional techniques such as DSC or infrared spectroscopy due to the insensitivity of them to low residual heat contents. Taking this into account, Wisanrakkit and Gillham [16] proposed using the glass transition temperature to monitor the extent of reaction because T_g can be measured more accurately than can the actual conversion data and displays significant changes over the entire range of conversion and in particular, extremely sensitive to the network structure changes occurring in the final stages of the curing process as has already been discussed. They showed that *when the glass transition temperature did not change with an increase in postcure time or postcure temperature then the reaction had reached full conversion.*

The combination of these facts suggest that T_g can be a "sensitive" and "practical" parameter for following the cure process of reactive thermosetting systems provided that the temperature history of the sample is known (i.e.no degradation has occurred) and factors such as the moisture content of the adhesive are accounted for [24]. The above mentioned features of T_g are also especially useful in the analysis of the diffusion–controlled kinetics for which the rate of change in chemical conversion is small. A kinetic model, in conjunction with T_g measurements, can be used for diagnostics as well as for quality control purposes in a production environment. However, the advantages of using T_g rely on the assumption that there is a unique one-to-one relationship between T_g and conversion. Since there are several reactions taking place at the same time and each reaction may be dominant at different temperatures, the network architecture should depend on the temperature histories. Therefore it is conceivable that the T_g versus conversion relationship is not unique for different temperature histories [26].

3.4.3.4 Factors associated with experimental determination of T_g

Choy and Plazek [63] considered the glass transition temperature T_g as a *material characterising parameter* which is meant to indicate the temperature below which a material exhibits properties typical of a glass. At temperatures higher than T_g the

molecular mobility is sufficient for the material to attain the properties such as enthalpy, specific volume etc.—characteristic of the equilibrium rubbery or liquid state.

Experiment shows that when, upon cooling, a glass transition temperature is determined, it *depends exclusively on the cooling rate* [15]. With faster cooling, T_g is evidenced at a higher temperature and with slower cooling, the end result is a lower T_g (Figure 3.9).
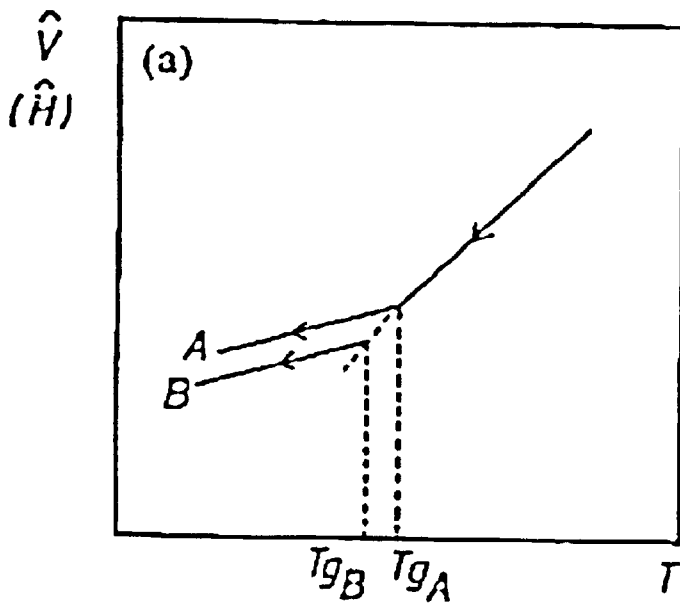
Figure 3.9 Specific volume (enthalpy) as a function of temperature for two different cooling rates (A > B) (after Pascault and Williams [15]).

This means that cooling at a slower rate requires a lower temperature to 'freeze in' the intermolecular associations that give the polymer the glassy state. From this point of view the *glass transition* phenomenon is *somewhat of a misnomer* since the term "transition" implies an "equilibrium phenomenon" that is invariant to the speed of the heating or cooling.

Basically, once the material enters the glassy condition its non-equilibrium state is determined by its thermal history, e.g. the particular state attained in its relaxation to equilibrium. The T_g determined by heating is not only a function of the rate of

temperature increase but also of the post thermal history. From that stand point, the T_g arising from a heating experiment is *not a material property* but a *specimen property* [63]. Therefore, we see that due to enthalpy relaxation, values of the T_g for partially reacted polymers may depend on the thermal history of samples and the heating rate used for measurements. Use of theoretical relations between T_g and the extent of reaction of a thermoset must take this fact into account.

It is well known that networks undergo physical aging like every polymer. For $t > t_{vit}$ two different effects are associated with the further increase of T_g. On the one hand, conversion continues to increase, although at a greatly diminished rate. On the other hand, annealing (physical aging) of the sample in the glassy state leads to an increase in the apparent T_g . In the DSC technique, measurements of T_g are disturbed by this effect of "physical aging" and also by the "residual heat of reaction". In order to get the T_g versus conversion relation all these basic factors are needed to be considered and these are nicely described in the paper by Pascault et al [15].

Another point is that, Differential thermal analysis (DTA) and Differential Scanning Calorimetry (DSC), can be quite insensitive to highly crosslinked polymers [64]. Furthermore, both methods require small masses of the sample for which T_g is to be determined, then *T_g depends strongly on the inhomogeneities of the sample* [65].

3.5 Conclusion

The knowledge of chemical kinetics of the polymerization and crosslinking reactions can be employed in curing the polymer to optimize the cure cycle. Also, the information obtained from cure diagrams and thermal analysis is very important in determining the physical characteristics of a thermosetting polymer through its cure cycle. The parameters that define the cure cycle ultimately determine the final physical properties of the thermoset. The items that must be determined in a cure cycle are the number of stages in the cure, the rate of temperature increase, the hold temperature at each stage, the pressure at which the cure takes place, and the time allotted for the cure cycle. Once the kinetics are understood and the underlying chemistry behind the cure is established, these cure cycle parameters can be chosen based on the desired polymer properties. Usually, the cure cycle seeks to achieve a

certain degree of cure, which is also quantified by means of the extent of reaction. For thermal curing polymers, these quantities can be calculated based on data from thermal analysis and the stoichiometry of the polymerization reaction. Ultimately, the resulting material must have the optimum properties to meet the needs of the desired application.

3.6 References

1. Pindinelli,C., Montagna,G., Luprano,V.A.M., and Maffezzoli,A., Macromolecular Symposia, vol. 180, 2002, 73-88.

2. Scott,E.P., and Saad,Z., Polymer Engineering and Science, vol. 33, no. 18, 1993,1165-1169.

3. Eom,Y., Boogh,L., Michaud,V., Sunderland,P.,and Manson,J.A., Polymer Engineering and Science, vol. 40, no. 6, 2000, 1281-1292.

4. Vyazovkin,S., and Sbirrazzuoli,N., Macromolecules, vol. 29, 1996, 1867-1873. 1867-1873.

5. Halley,P.J., and Mackay,M.E., Polymer Engineering and Science, vol.36, no.5, 1996, 593-609.
6. Karkanas,P.I., Partridge,I.K., and Attwood,D.,Polymer .International, vol.41, 1996, 183-191.

7. Han,S., Yoon,H.G., Suh,K.S., Kim,W.G., Moon,T.J., Journal of Polymer Science: Part A: Polymer Chemistry, vol. 37, 1999, 713-720.

8. Perrin, F.X., Nguyen, T.M.H., Vernet, J.L., Macromol. Chem. Phys., Vol. 208, 2007, 55-67.

9. Kessler,M.R., and White,S.R., Journal of Polymer Science: Part A: Polymer Chemistry, vol. 40, 2002, 2373-2383.

10. Kim,D.S.,and Kim,S.C., Polymer Engineering and Science, vol.34, no. 8, 1994, 625-631.

11. Hussain,A. , Paper 3, Plast. Rubb. Inst. 4th Conf. Res. Prog. Resin Plast. , 1976.

12. Leroy,E., Dupuy,J., Maazouz,A., Macromolecular Chemistry and Physics, vol. 202, no.4, 2001, 465-474.

13. Ivankovic,M., Dzodan,N., Brnardic,I., Mencer,H.J., Journal of Applied Polymer Science, vol. 83, 2002, 2689-2698.

14. Karkanas,P.I., Partridge,I.K., Journal of Applied Polymer Science, vol. 77, 2000,

2178-2188.

15. Pascault,J.P., and Williams,R.J.J., Journal of Polymer Science: Part B: Polymer Physics, vol. 28, 1990, 85-95.

16. Wisanrakkit,G., and Gillham,J.K., Journal of Applied Polymer Science, vol. 41, 1990, 2885-2929.

17. Lange,J., Ekelof,R., George,G.A., Polymer, vol. 40, 1998, 149-155.

18. Malek, J., Thermochimica Acta, vol. 200, 1992, 257-269.

19. Scott,E.P.,and Saad,Z., Polymer Engineering and Science, vol.33, no. 18, 1993, 1157-1164.

20. Ryan,M.E., and Dutta,A., Polymer, vol. 20, 1979, 203-206.

21. Mijovic,J., Kim,J., and Slaby,J., Journal of Applied Polymer Science, vol. 29, 1984, 1449-1462.

22. Kim,S., Lu,M., and Shim,M., Polymer Journal, vol. 30, no. 2, 1998, 90-94.

23. Ryan,M.E., Polymer Engineering and Science, vol. 24, no.9, 1984, 698-704.

24. Keenan,M.R., Journal of Applied Polymer Science, vol.33, 1987, 1725-1734.

25. Hseih,H.K., Su,C.C., and Woo,E.M., Polymer, vol. 39, no. 11, 1998, 2175-2183.

26. Chiou,P., and Alan Letton,A., Polymer, vol.33, n.o.18, 1992, 3925-3931.

27. White,S.R., Mather,P.T., Smith,M.J., Polymer Engineering and Science, vol.42, no.1, 2002, 51-67.

28. Lesser,A.J., and Crawford,E., Journal of Applied Polymer Science, vol. 66, 1997, 387-395.

29. Gillham,J.K., Polymer Engineering and Science, vol.26, no. 20 ,1986, 1429-1433.

30. Gillham, J.K.,Polymer International, vol. 44, 1997, 262-276.

31. Oishi,T., and Fujimoto,M., Journal of Po., Thermochimica Acta, vol.14, 1976, 41-59.

32. Sourour, S., and Kamal,M.R., Thermochimica Acta, vol.14, 1976, 41-59.

33. Berlin,A.A., and Matveyeva,N.G., Macromolecular Reviews, vol. 12, 1977, 1.

34. Odian,G., Principles of Polymeri.Azation, Hill,M., New York, 3rd edn., 1991.

35. Mijovic,J.,J and Koutsky,J.A., Polymer, vol.20, 1979, 1095.

36. Zhu,S., and Hamielec,A.E., Chemie,M., Macromolecular Symposia, vol 63, 1993, 135.

37. Liu,S.B., Liu,J.L., and Yu,T.L., Journal of Applied Polymer Science, vol. 53, 1994, 1165.

38. Flory,P.J., Principles of Polymer Chemistry, Cornell University Press, Ithaca, N. Y., 1953.

39. Adabbo, E,H., and Williams,R.J.J., Journal of Applied Polymer Science, vol. 27, 1982, 1327-1334.

40. Prime, Bruce,R., Thermal Characterization of Polymeric Materials, 2nd edition, Edith Turi, ed., vol. 2, 1379-1766.

41. Thomas, R., Durix, S., Sinturel, C., Omonov, T., Goossens, S., Groeninckx, G., Moldenaers, P., Thomas, S., Polymer, vol. 48, 2007, 1695-1710.

42. Villanueva, M., Nunez, L., Nunez, M.R., Rial, B., Fraga, L., and Montserrat, S., Journal of Thermal Analysis and Calorimetry, vol.70, 2002, 45-56.

43. Teil, H., Page, S.A., Michaud, V., Manson, J.A.E., Journal of Applied Polymer Science, vol.93, 2004, 1774-1787.

44. Mijovic,J., and Tsay,L., Polymer, vol. 22, 1981, 902.

45. Dixon,S., Jaques,D., and Palmer,S.B., Journal of Physics D : Applied Physics, vol-36, 2003, 753-759.

46. Hodd, K.,Epoxy Resins, In: Comprehensive Polymer Science, Chapter 37, vol. 5, 1989, 679, eds Allen, G and Bevington, J C Pergamon Press, Oxford.

47. Morgan,R.J., Mones, E.T., Journal of Applied Polymer Science, vol.33,1987,999.

48. Ma, Z.G., and Gao, J.G., Journal of Chemical Research, 2006, 236-239.

49. Samaras, Z.I., PhD Thesis, University of Carnfield, United Kingdom, 2005.

50. Skordos, A.A., and Partridge, I.K., Polymer Engineering and Science, vol.41, no.5, 2001, 793-805.

51. Lee,H., and Neville,K., Handbook of Epoxy Resins, McGraw-Hill Book Company, 1967.

52. Horie,K., Hiura,H., Sawads,M., Mita,I., and H Kambe,H., Journal of Polymer Science: Part A-1, vol. 8, 1970, 1357.

53. Pollard,M., and Kardos,J.L., Polymer Engineering and Science, vol. 27, 1987, 829.

54. Maffezzoli,A., Quarta,E., Luprano,V.A.M., Montagna,G., Nicolais,L., Journal of Applied Polymer Science, vol-73,1999,1969-1977.

55. Lionetto, F., Rizzo, R., Luprano, V.A.M., Maffezzoli, A., Materials Science and Engineering A, vol. 370, 2004, 284-287.

56. Miller, D.R., Macosko,C.W., Macromolecules, vol-9, 1976, p-206.

57. Macosko,C.V., Miller, D.R., Macromolecules, vol-9, 1976, p-199.

58. Aklonis,J.J.,and MacKnight,W.J., Introduction to Polymer Viscoelasticity, Wiley Interscience N Y, 1982.

59. Poljansek, I., Krajnc, M., Acta Chim. Slov., vol.50, 2003, 461-472.

60. Montserrat, S., Cima, I., Thermochimica Acta, vol. 330, 1999, 189-200.

61. Montserrat, S., Roman, F., Colomer, P., Polymer, vol. 44, 2003, 101-114.

62. Montserrat, S., Martin, J.G., Journal of Applied Polymer Science, vol.85, 2002, 1263-1276.

63. Choy,I.,C., and Plazek,D.J., Journal .of Polymer Science : Polymer Physics Edition, vol 24, 1986, 1303.

64. Schwarzl (Ed.),F.,R., Polymer- mechanik, Springer, Berlin, vol.113., 1990.
65. Povolo,F. , Jorge,G., Hermida,E.B., Journal of Alloys and Compounds, vol. 310, 2000, 388-391.

66. Ng,H., and Zloczower,L.,, Polymer Engineering and Science, vol. 33, 1993, 211.

67. Dutta ,A.,and Ryan,M.E., Journal of Applied Polymer Science, vol. 24, 1979, 635.

68. Yang,Y.S., and Lee,L.J., SPE ANTEC Technical Papers, vol. 32, 1986, 419.

69. Borchardt, H. J., Daniels, F., Journal of the American Chemical Society, vol. 79, 1957, 41-46.

70. Friedman, H.L., Journal of Polymer Science: Part C: Polymer Symposia, vol. 6, 1963, 183.

71. Flynn, J.H., Wall, L. A., Journal of Polymer Science : Part B : Polymer Letters, vol. 4, 1966, 323-328.

72. Ozawa, T., Bulletin of the Chemical Society of Japan, vol. 38, 1965, 1881.

73. Alig,I., Lellinger,D., and Johari,G.P., J. Appl. Polym. Sci : Part B, vol –30, 1992, 791-799.

74. Duswalt, A. A., Thermochimica Acta, vol. 8, 1974, 57.

75. Rabinowitch ,E., Transactions of the Faraday Society, vol. 33, 1937, 1225.

76. Simon, S. L., and Gillham J. K., Journal of Applied Polymer Science, vol. 47, 1993, 461.

77. Chern,C.S., and Poehlein,G.W., Polymer Engineering and Science, vol. 27, 1987, 782.

78. Kenny, J. M., and Trivisano, A., Polymer Engineering and Science, vol. 31, 1991, 1426.

Chapter 4　　Material and Experimental Techniques of DSC Measurements

4.1 Introduction

This chapter presents the details of the experimental material under investigation in this project along with the experimental methods of differential scanning calorimetry (DSC) used for the measurements of the curing kinetics of this material.

4.2 Material

In this study, Araldite 2015 modified epoxy based adhesive (Ciba Geigy, Vantico Ltd., Duxford, UK) is used for the thermo-kinetic and ultrasonic characterization of its curing state. Araldite 2015 is a commercially available two-part structural adhesive, which consists of AV 5308 (2015 A) (epoxy resin) and HV 5309-1(2015 B) (hardener) whose detailed compositions and contents are given in table 4.1. Generally, Araldite 2015 works after mixing these two components in a ratio of 1 to 1.Figure 4.1(a)—(e) shows the chemical structures of the components of Araldite 2015.

As shown in table 4.1, Araldite 2015 is a complex modified epoxy system containing two difunctional epoxies (DGEBA/DGEBF mixture), catalyzed pentafunctional diethylene triamine (DETA) curing agent, difunctional epoxy based aliphatic reactive diluent and mica [5] which usually is used in epoxy system as filler. Catalyst can accelerate ring opening without the need of raising the cure temperature to promote ring opening. There are various reasons for selecting this commercial epoxy system for this project. The curing reaction of the uncatalyzed and catalyzed multifunctional unmodified epoxy-amine system has been described by various authors, but there is less information when both catalyst and reactive diluent is used in the formulation of two epoxy resin mixture. This keeps our system odd from others and, to some extent, a new complex one to report cure kinetics to the best of our knowledge.

Table 4.1 Compositions and contents of (a) AV 5308 (2015 A) (epoxy resin); (b) HV 5309-1(2015 B) (hardener) which are components of Araldite 2015 [5].

Component (Chemical Name)	Concentration (%)
(a) Resin - DGEBA epoxy resin containing reactive diluent	
1,4 Butane diol diglycidyl ether (BDGE) (reactive diluent)	3—9 %
Diglycidyl ether of bisphenol-A (DGEBA) epoxy resin (number average molecular weight < 700)	30—40 %
Diglycidyl ether of bisphenol-F (DGEBF) epoxy resin	5—15%
Mica	1—10%
(b) Hardener - Formulated Polyaminoamide	
Diethylenetriamine (DETA)	3—9%
2,4,6-tris(dimethylaminomethyl) phenol (catalyst)	1—7%

The Araldite 2000 range is one of several structural adhesive ranges produced commercially and has bonding solutions for 95% of all structural bonding applications [6]. They are internationally recognized as the leading brand of industrial adhesives for high-performance bonding and joining, for chemical and high heat resistance, and for producing high strength bonds. The bonding process requires very little degreasing preparation and they can be cured at ambient temperatures. Airbus A320 series interior, Mangusta sports car door bonding, Swiss rail locomotive cabins to reduce weight and to increase strength are some of the important industrial applications of Araldite range [7].
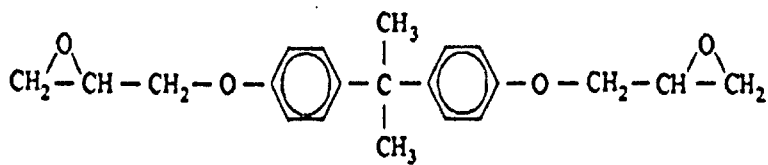
(a) Diglycidyl ether of bisphenol-A (DGEBA) epoxy resin
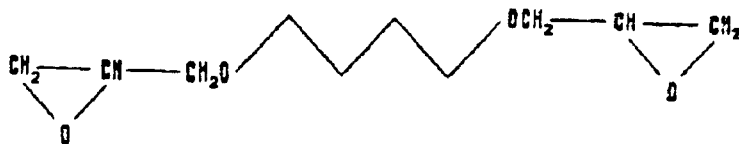
(b) Butane diol diglycidyl ether (BDGE) (reactive diluent)

(c) Diglycidyl ether of bisphenol-F (DGEBF) epoxy resin

$$NH_2-CH_2-CH_2-NH-CH_2-CH_2-NH_2$$
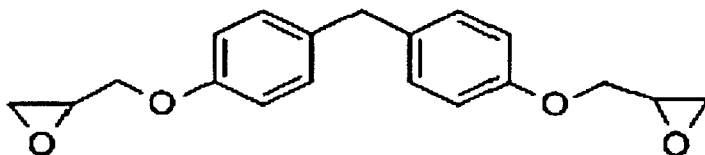
(d) Diethylenetriamine (DETA) hardener
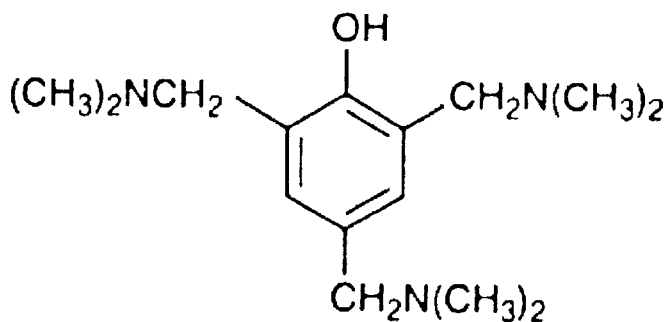
(e) 2,4,6-tris(dimethylaminomethyl) phenol (catalyst)

Figure 4.1(a)—(e) The chemical structures of the components of Araldite 2015.

The Araldite 2000 range includes rapid cure adhesives that can be cured in minutes as well as longer cure adhesives that require days for the cure to be completed. The adhesives also vary in terms of the range of substrates they can bond to. Araldite 2015 is chosen for this project as it is extensively used in bonding applications with most of the major substrates used in the automotive (British motor industry) and aerospace (Airbus) industries with which our Applied Ultrasonic Laboratory at University of Nottingham have several collaborations. Araldite 2015 is basically a toughened adhesive with fast bonding time. It requires 35 minutes at 60°C to obtain 10MPa lap shear strength. This provides for a combination of enough time to make reliable recordings of DSC and ultrasonic data and for the experiment to be completed within a fairly reasonable time. Araldite 2015 system was also chosen because preliminary studies had indicated that it was not prone to bubble formation (produces very few bubbles during cure), which would compromise the ultrasonic investigation, as it is well known that ultrasonic wave scattering at bubbles would strongly affect ultrasonic attenuation and phase velocity measurements. Thus, the cure could be successfully monitored by these two techniques.

4.3 Mixing and Dispensing of Araldite 2015 epoxy resin and hardener

The Araldite 2015 two-part 1:1 epoxy resin and hardener is commercially available in three sizes of 400 ml, 200 ml, and 50 ml of dual cartridges separating the resin and hardener. The 50 ml cartridge has a shelf life of up to 3 years when kept in an air-tight container between temperatures of 2°C to 40°C [5].

The dispensing and mixing is done by using the adhesive gun and mixing nozzle (RS Components Ltd., Corby, UK) as instructed by the manufacturer. Normally, the epoxy adhesive is dispensed by inserting the cartridge into a glue gun and then attaching the mixing nozzle in front of the cartridge. The mixing nozzle as recommended by the manufacturer is approximately 150 mm long, equipped with a plastic tube on the outside and a plastic mixing mesh on the inside. The resin and hardener will mix together while being pushed through the nozzle. The quite long length of the nozzle ensures good mixing of the resin and hardener. For optimum homogeneous mixing of the two

components, extra precaution was taken by discarding the first 30 mm length of mixed adhesive before making the sample. Here, it can be mentioned that as this setup for adhesive dispensing is as per recommendation of the manufacturer and used by the industry, the experimental results will to some extent resemble the industry practice.

4.4 Differential Scanning Calorimetry

Advancements in thermocouple technology and designs enhancing the temperature control capabilities led to the development of differential scanning calorimetry. DSC is an analytical tool in which the difference in thermal energy inputs into a sample and a reference material per unit of time is measured as a function of temperature while the sample and the reference material are subjected to a controlled temperature programme under both isothermal (constant temperature) and non-isothermal heating conditions (temperature varies with time with a constant heating rate, $\beta = dT/dt$ i.e. along a linear temperature ramp). The reference is an inert material such as alumina, or an empty aluminium pan.

DSC measures a sample's heat capacity at constant pressure, c_p. It measures the amount of heat (H) required to change the temperature of the sample by one degree while at constant pressure. The heat capacity is usually normalized by dividing the sample heat capacity by the weight of the sample (grams) to get the heat required to raise one gram of sample by one degree Celsius.

DSC enables the measurements of the transition such as the glass transition, melting, and crystallization. Furthermore, the chemical reaction such as thermal curing, heat history, specific heat capacity, and purity analysis are also measurable. DSC is one of the most frequently used analytical techniques for studying the kinetics of the curing reaction of thermosetting polymers and especially of epoxy resins. Recently, with the development of the highly-functional epoxy polymeric materials, the need of analysis of these thermal properties are increasing dramatically. Its basic advantages are — ease of operation and analysis of data, high speed of determination, requirement of very small sample masses in

the milligram range, ability to study many types of physical and chemical properties and phenomenon and chemical reactions. In general, the calorimetric accuracy of DSC is within 1-2%; *an accuracy that is more than sufficient for most polymer applications.* Hopefully, the DSC instrument is able to provide calorimetric accuracy to better than 1%.

4.4.1 Types of DSC Instruments

There are two basic types of commercially available differential scanning calorimeters, the heat flux DSC and the power compensation DSC, depending on the method of measurement used in detecting heat flux (the rate of heat flow per unit cross-sectional area).These two types are illustrated in figure 4.2(a,b).

| (a) Heat Flux DSC | (b) Power Compensation DSC |
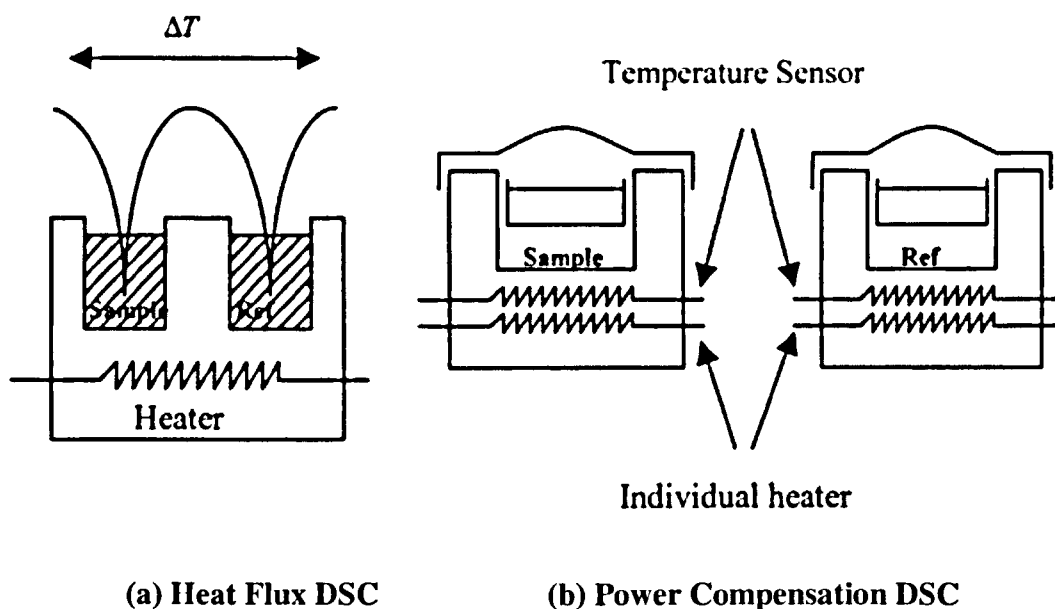
Figure 4.2 Simple schematic representation of the (a) Heat Flux DSC and (b) Power Compensation DSC in the differential scanning calorimetry techniques.

Heat flux DSC is based on slight modification of differential thermal analysis (DTA) system and utilizes the temperature difference required to determine the heat flow between a sample and a reference as a function of time and temperature in a controlled temperature programme. The sample and reference are enclosed in a same furnace with

99

only one heating source (figure 4.2(a)).Power compensation DSC measures the heat flow as a function of temperature utilizing the difference in power needed to equilibrate the temperature of a sample and a reference kept in separate but identical furnaces with separate individual heaters under controlled temperature programme (figure 4.2(b)).

4.4.2 Heat Flux DSC Instrument

Instead of maintaining equal temperatures and measuring differential heat flow as in the case of power compensation DSC, an alternative approach to heat flux DSC is to maintain constant heat flow and measure the difference in temperature between the reference and sample holders. The temperature difference gives a good measure of the heat capacity. Basically, heat flux DSC is a slight modification of differential thermal analysis (DTA) system. The difference between DTA and DSC is that in the DTA method the temperature sensor is placed in the sample, whilst in the DSC, the temperature sensors are placed external to the sample. DTA also requires a much larger amount of test material in comparison to the DSC and thus can cause thermal gradients within the sample.

Figure 4.3 shows the block diagram of heat flux DSC instrument. It can be seen from the figure that heat flux DSC comprises the sample and reference holder, the heat resistor, the heat sink, and the only single heater enclosed in the same furnace. The heat sink is a metallic block with high thermal conductivity (large heat capacity) that ensures good heat-flow path between the sample and the reference. Heat of heater is supplied into the sample and the reference through heat sink and heat resistor. Heat flow is proportional to the heat difference of heat sink and holders. Heat sink has the enough heat capacity compared to the sample. In case the sample occurs endothermic or exothermic phenomena such as transition and reaction, this endothermic or exothermic phenomena is compensated by heat sink. Thus the temperature difference between the sample and the reference is kept constant. The difference the amount of heat supplied to the sample and the reference is proportional to the temperature difference of both holders.
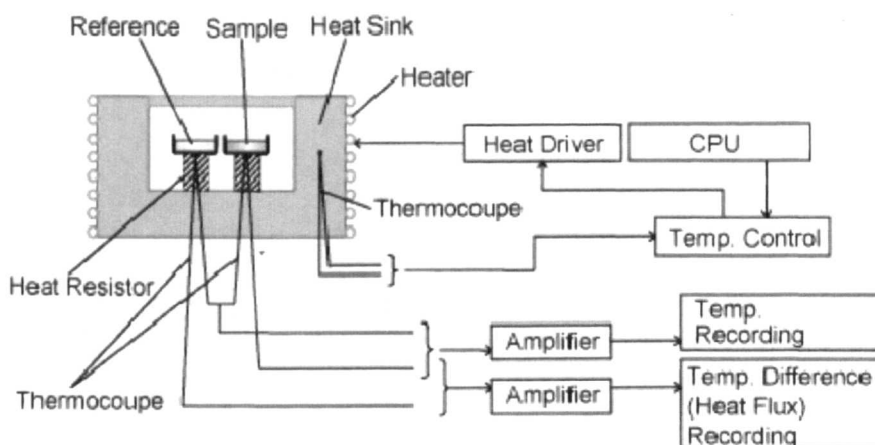
Figure 4.3 Block diagram of Heat Flux DSC.

When the heat capacity of the sample holder increases (because of a heat absorbing or endothermic transition) the temperature in the sample holder will lag behind the reference holder and there will be a negative temperature differential ($T_{sample} - T_{ref} < 0$). Conversely, when the heat capacity of the sample holder decreases (because of a heat generating or exothermic transition) the temperature in the sample holder will be ahead of the reference holder and there will be a positive temperature differential ($T_{sample} - T_{ref} > 0$). By calibrating the standard material, the quantitative measurement of the unknown sample is achievable. The thermal resistances of the heat-flux DSC system may change with temperature. But the DSC instruments may be used in the "calibrated" mode — the amplification of the DSC signal is then automatically varied with temperature to maintain a constant calorimetric sensitivity with temperature. The heat flux DSC has good baseline stability due to the presence of the heat sink.

4.4.3 Power Compensation DSC Instrument

A block diagram of power compensation DSC instrument is shown in figure 4.4. It can be seen that the sample and reference are controlled independently using separate, identical furnaces with separate individual heaters. Thus, it utilizes separate sample and reference

holders of low thermal mass, where the heat flux to the sample and to the reference are controlled by individual heaters.
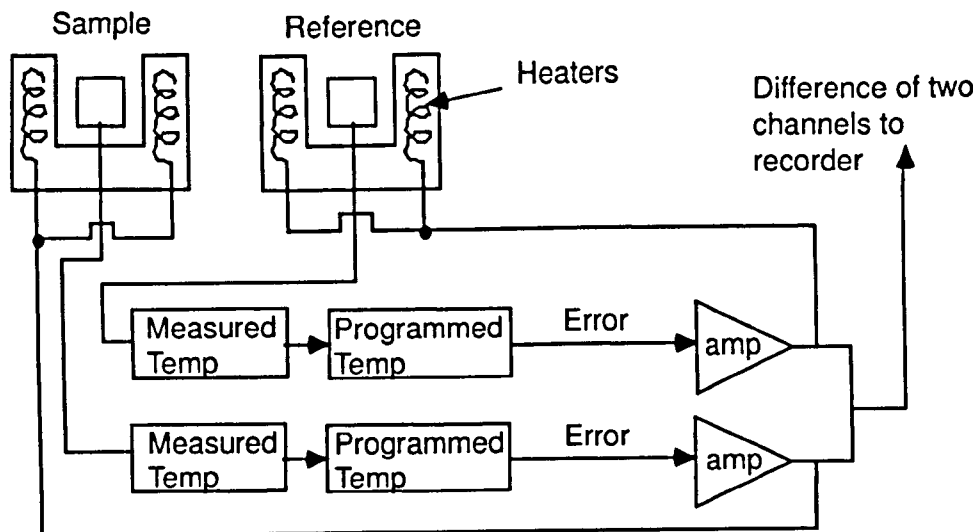
Figure 4.4 Block diagram of Power Compensation DSC.

When the temperature rises or falls in the sample, the temperatures of the sample and reference are made identical by varying the power (energy) input to the two furnaces to compensate for the sample energy. Both the two furnaces are then heated or cooled until they each reach the selected starting temperature. A temperature program is then begun; a typical temperature program would be to increase the temperature to some higher temperature at some fixed rate or fixed number of degrees Celsius per minute. As the program runs, the system monitors the temperature in each furnace. If the temperature differs from the programmed temperature in either furnace, heat or coolant is supplied to that furnace to make the temperature equal the program temperature. The difference in the energy supplied to the two furnaces per unit time (or, *dH/dt*) is proportional to the heat capacity of the sample. That energy difference is monitored electronically and output to the recorder. As a result, the system is maintained at a "thermal null" state at all times. The amount of power required to maintain system equilibrium is directly proportional to the energy or heat capacity changes occurring in the sample relative to the reference. No complex heat-flux equations are necessary with a power compensation DSC because the

102

system directly measures energy (heat) flow to and from the sample. The power compensation DSC has a feature of good heating and cooling response as both the sample holder and reference holder are directly heated and have small heat capacitance compared to the heat flux DSC.

4.4.4 Temperature Modulated Differential Scanning Calorimetry (TMDSC)

The calorimetric measurement of curing reaction by conventional DSC gives a unique heat flow signal, which *includes* the heat evolved during the curing and the so-called sensible heat due to the temperature dependence of the heat capacity of the sample. On the other hand, the measurements by TMDSC may give the heat of curing and the heat capacity of the system *separately*, apart from other properties. Modulated differential scanning calorimetry (MDSC) is a technique in which a small sinusoidal temperature oscillation is either superimposed on the linear temperature ramp of the conventional DSC which changes at a constant heating rate, or applied around a fixed average temperature resulting in a complex heat flow. The net effect is that the actual heating rate is sometimes greater than and sometimes less than the constant heating rate. A Fourier transformation is performed to deconvolute the total heat flow signal, which can be resolved into two parts— the *reversal heat flow* and the *non-reversal heat flow*. The *reversal heat flow* corresponds to a phase transition which can be used to detect specific heat, glass transition temperature etc. The *non-reversal heat flow* is dependent on irreversible effects such as chemical reactions and corresponds to the kinetic component caused by the exothermal reaction of the cure process. For isothermal experiments, the curve of the total heat flow is the same as the non-reversal heat flow because the reversal heat flow is zero (0).

Both, the frequency and the amplitude of modulation as well as the linear heating rate can be adjusted. The result is that the TMDSC, unlike DSC, is able to separate more complex transitions into more easily interpreted components, and to increase sensitivity in order to detect weaker transitions and melts. In addition, heat capacity and heat flow can be

directly measured in a single experiment. These properties can be determined due to the ability of TMDSC to separate *reversal* from *non-reversal* heat flows [2,3,4].

4.5 Experimental Techniques for DSC Measurements

Isothermal measurements and related dynamic scans which takes the reaction to complete or full conversion to determine the total heat of reaction, H_T were performed, using a heat flux DSC (Mettler-Toledo DSC 822e, Leicester, UK) under nitrogen purge. The glass transition temperature determinations were carried out using a heat flux temperature modulated differential scanning calorimeter (TMDSC) (TA Instruments, Model 2920, USA) in the modulated DSC mode.

The resin and hardener were mixed in a 1:1 equivalent ratio. The dispensing and mixing was done by using the adhesive gun and mixing nozzle (RS Components Ltd., Corby, UK) as instructed by the manufacturer as has already been mentioned. In every case bulk samples were prepared. From the bulk samples, 8—10 mg in size were used for calorimetric experiments. The samples were weighted accurately and sealed in aluminium pans covered with aluminium lids, using a press, before introducing them into the calorimeter.

In all experiments carried out in this study the weight of the sample was usually ranged from 8—10 mg, in order to ensure that the thermal gradients were negligible. Basically, this sample mass was selected as a compromise between the thermal detection limit and the existence of thermal gradients in the sample. As we know, much larger amount of samples can cause thermal gradients within the sample, where there is a temperature difference between measured temperature and the actual temperature inside the sample. Isothermal measurements were carried out by heat flux DSC (Mettler-Toledo DSC 822e, Leicester, UK) with the TSO80RO automatic sample robot. A highly sensitive ceramic sensor is used to measure the difference between the heat flows to the sample and the reference. With liquid nitrogen cooling the temperature range from -150°C up to 700°C with ±0.2°C accuracy can be investigated. The range of heating rate is from 0.02°K/min

up to 300°K/min and the range of cooling rate is from 0.02°K/min up to 50°K/min. Typical scanning rates range from 5 to 40°K/min. Generally, lower heating rates are more accurate and improve the peak resolution while higher heating rates improve sensitivity. This DSC is equipped with air cooling, cryostat cooling and intra cooler. It can automatically switches up to four gases— nitrogen, oxygen, argon, carbon dioxide.

The sample robot has a turn plate that allows up to 34 sample positions. The sample pans are made from aluminium with volume of 20μl. Typical polymer sample sizes are approximately 5 to 20 mg. Before the sample material is inserted into the pan, the sample pan is weighted on the MT XS105 dual range analytical balance which is calibrated before use. The sample material is then inserted into the pan and the weight of the material is noted. The aluminium lid is then placed onto the sample pan and sealed using the crucible sealing press. In order to preserve constant pressure during the experiment, a small hole is then pierced on top of the crucible using the piercing needle provided by the manufacturer. The crucible is then transferred to the automatic sample plate with a pair of tweezers. The sample can be inserted into the DSC furnace manually or using the sample robot. The STAR^e software provided by Mettler-Toledo is able to provide the DSC device with programmable temperature controls and an interactive monitoring window during experiments. The sample robot can retrieve the sample pan and place it onto the rotating sample plate after each experiment. Nitrogen was used as the purging gas. A flow of nitrogen gas of 50 ml/min was maintained over the samples during the isothermal and dynamic scans to create an inert and dry atmosphere. The nitrogen atmosphere also eliminates air oxidation of the samples at high temperatures. The instrument was calibrated for temperature, enthalpy and heat capacity using appropriate standard reference materials.

The isothermal measurements were conducted at the following temperatures — 30°C, 40°C, 50°C, 60°C, 70°C and 80°C. The furnace was preheated up to the desired fixed experimental temperature and kept for a certain period of time. When the system reached the equilibrium state, the sample pan was quickly placed on the calorimetric detector plate. The isothermal scan was stopped and the reaction was considered complete when

the isothermal heat flow curve leveled off to a baseline and reached a stable value. The total isothermal heat of reaction, $H(t)$, evolved up to a time t (in equation (3.1)), at a fixed temperature, was estimated by drawing a horizontal line, extrapolating the base line reached on the completion of the cure peak to the start of the peak and integrating the total enclosed area under the exothermal curve.

The total heat of reaction, H_T (in equation (3.1)), was estimated by heating the epoxy sample across the temperature range from 30°C to 300°C in a dynamic heating scan at a heating rate of 10°C/min, which took the reaction to complete or full conversion up to the final time t_f. A further heating run and rescan at the same heating rate was carried out in order to confirm that after achieving full conversion the reaction had stopped. The total heat of reaction, H_T, was estimated by drawing an integral tangential baseline connecting the base line before and after the exothermic peak and integrating the enclosed area under the heat flow thermogram.

Here, it can be mentioned that as the heat capacity of the sample is expected to change gradually from the initial to the final value and its value at intermediate point is considered linearly proportional to the degree of conversion, the integral tangential baseline is, therefore, considered here. Skordos and Partridge [1] have considered similar 'S' shaped sigmoidal baseline in their work. Basically, the shape of the baseline reflects the change in heat capacity, Δc_p, of the sample during cure. The 'line' baseline ignores any change in the heat capacity, whereas 'spline' and 'integral tangential' baselines go some way to taking into account of the change. In the laboratory environment, the baseline can be separated and categorized into several different shapes and is used to accommodate the changes shown by the DSC curves during a transition or reaction. The STAR^e curve analysis software provided by Mettler-Toledo DSC system (Usercom issue 25, Mettler Toledo) gives a list of selection of baseline types (e.g. line, tangential, horizontal, spline, integral tangential etc.) to choose from.

The degree of conversion, α, as defined in equation (3.1), as a function of cure time at a particular fixed temperature, was then determined by finding the ratio of the progressive

106

total iso-thermal heat of reaction up to the end of the isothermal cure to the total heat of reaction. The rate of reaction, $\frac{d\alpha}{dt}$, was, thus, obtained by differentiating the degree of cure, α with respect to time as given by equation (3.2).Hence, equations (3.1) and (3.2) lead to the estimation of the degree of conversion, α, and subsequently the rate of conversion, $\frac{d\alpha}{dt}$, for each iso-thermal cure temperature which are presented and discussed in the next chapter.

4.6 Determination of Glass Transition Development

The determination of the finally attained glass transition temperature ($T_{g\ final}$) for the Araldite 2015 samples, previously cured in extended isothermal conditions at specified temperatures, were conducted through dynamic test in the temperature modulated DSC (TMDSC) mode using a heat flux temperature modulated differential scanning calorimeter (TMDSC) (TA Instruments, Model 2920, USA). After the end of each isothermal run, the samples were then scanned at a heating rate of 10°C / min across the temperature range from -30°C to 275°C.The modulation conditions were 1°C of amplitude and a period of 60 Sec.

Through the TMDSC mode, the total heat flow of the sample was divided into the *reversal heat flow* and the *non-reversal heat flow* parts. The *reversal heat flow* corresponds to a *phase transition into a glassy state*, which can be used to detect T_g. The *non-reversal heat flow* is the *kinetic component* and is caused by the *exothermal reaction of the process* (i.e. cure reaction only).The exothermal reaction heat can be thought of as the residual heat of the sample.

In this study, the experimental T_g was defined as the *inflection point temperature* at the observed step in the reversing heat flux versus temperature curves in the TMDSC plots to get a *better clear resolution of T_g*, instead of the common approach in conventional DSC experiments to define it as the inflection point in the total heat flux versus temperature

curves where it is generally masked by the superposition of the glass transition signal upon the large residual reactivity peak. These two approaches of determination of the finally attained glass transition temperature corresponding to each isothermal curing are presented schematically and discussed in the next chapter.

4.7 References

1. Skordos, A.A., and Partridge, I.K., Polymer Engineering and Science, vol.41, no.5, 2001, 793-805.

2. Poljansek, I., Krajnc, M., Acta Chim. Slov., vol.50, 2003, 461-472.

3. Montserrat, S., Cima, I., Thermochimica Acta, vol. 330, 1999, 189-200.

4. Montserrat, S., Martin, J.G., Journal of Applied Polymer Science, vol.85, 2002, 1263-1276.

5. http://www.vantico.co.uk. Vantico — Safety data sheet for Araldite 2015 Composition of resin and hardener.

6. http://www.vantico.co.uk. Ciba Specially Chemicals — Performance Polymers Performance Application of Structural Adhesives — Araldite 2015.

7. Huntsman International LLC, http://www.huntsman.com/ advanced-materials /index.cfm? Page ID = 5416 & FAQ _ ID = 1133, 2008.

Chapter 5   Results and Discussions of
Calorimetric Investigation of Chemical Cure Kinetics and Model
Free Iso-Conversional Analysis of the Cure

5.1 Calorimetric Conversion

Figure 5.1 shows the fractional degrees of calorimetric conversion as a function of cure time of our epoxy system after an extended isothermal cure (after a long time, compared with usual cure schedules used for that system) at the different isothermal cure temperatures (30°C,40°C,50°C,60°C,70°C and 80°C) employed in the test. The shape of the curve is similar to that expected for an autocatalytic reaction and similar to that observed for other amine cured epoxy systems [1, 5, 7, 8, 9, 13, 25, 29].

As can be seen, the degree of calorimetric conversion increases rapidly in the early stages of cure until it asymptotically approaches a maximum value (α_{max}) which increases with isothermal cure temperature, T_{cure} , in the range of 0.80—0.98 for cure temperature range of 30°C—80°C. Also, at any given time, the degree of conversion increases with cure temperature. So, the curing reaction is a *thermally catalyzed* one and it is also seen that the maximum conversion is attained earlier at a higher curing temperature.

From figure 5.1 it can be noticed that the maximum calorimetric conversion did not reach 100%.This can be *partially* attributed to the slight partial loss of heat of curing (especially at higher curing temperatures) during the initial brief period of time required for the system to come into equilibrium to the desired isothermal curing temperature (i.e. initial period of system stabilization to the isothermal test temperature). This may cause incomplete recording (due to slight partial non-detection) of evolving heat of curing and consequently can *partially* be responsible for resulting in slightly lower values of conversion. Due to this slight partial loss of accuracy in the initial progressive isothermal heat of reaction the initial conversion data have some uncertainties. The probability of heat loss is increased at higher curing temperature as it takes more time for the system to reach the isothermal equilibrium. Therefore, as the isothermal temperature is increased from 30°C to 80°C, the

probability of heat loss will be more even if the heating cell is heated at a high ramp rate to the specified isothermal temperature. In addition, the decrease can be more realistically explained in the light of the incomplete cure at the isothermal temperature resulting from *vitrification* – which is certainly the case. The explanation is as follows.
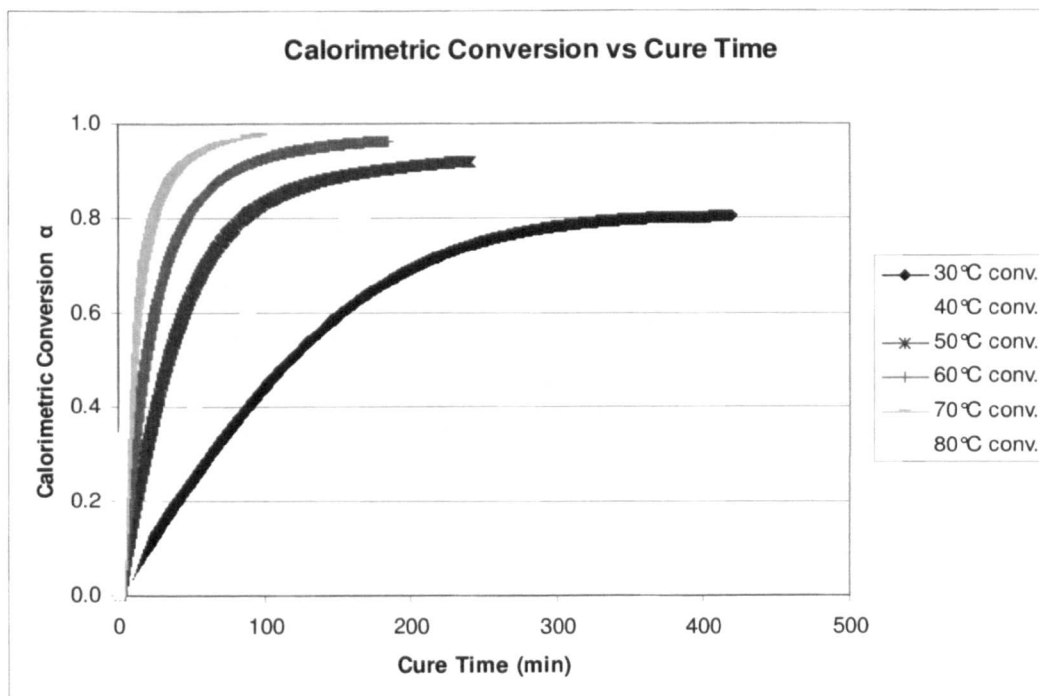
Figure 5.1 Degree of calorimetric conversion as a function of cure time at the different isothermal temperatures for Araldite 2015.

It is seen that at all investigated temperatures α_{max} for our system is lower than unity. Basically, when an epoxy system is cured at temperatures lower than the glass transition temperature of the completely cured system ($T_{g\infty}$),(i.e. $T_{cure} < T_{g\infty}$), *the extent of the reaction will almost never reach unity*. During the cure process some of the reactive groups indeed are *trapped* or *attached* to the cross-linked network. The incomplete cure of our DGEBA triamine system obtained in isothermal conditions can be attributed to the   influence of *diffusion control effects* on the reaction kinetics in the glass transition region.

During the isothermal cure the system changes from a viscous liquid to a highly crosslinked network. As the reaction occurs in a condensed phase, the rate of the cure reaction is controlled by the activity of the *functional groups* and additionally by their *mobility*. During the first stages of the reaction, when the rate of displacement of the groups is much faster than the rate of molecular collisions, the reaction is controlled by the chemical reactivity of these groups. As the reaction proceeds, there is an increase in chain branching until the system reaches gelation; further polymerization causes an increase of the crosslinking until the mobility of the reactive centres is progressively restricted and the reaction becomes diffusion controlled. Namely, the structural changes produced by the polymerization reactions are associated with an increase of the glass transition temperature, T_g , of our reactive system as the crosslinking degree progresses. When the increasing T_g of our DGEBA triamine system approaches the isothermal cure temperature, T_{cure} ,(i.e. $T_g \geq T_{cure}$),the molecular mobility is strongly reduced, the reaction becomes diffusion controlled and eventually stops before complete conversion of the epoxy occurs. This is the factor which limits the calorimetric conversion of our system at curing temperatures, T_{cure} , below the maximum glass transition temperature of the fully cured epoxy $T_{g\infty}$. As a result, the calorimetric conversion tends to a practically constant limiting value less than unity at all investigated isothermal temperatures.

In this connection it can be mentioned that subsequent exposure to temperatures greater than the previous isothermal cure temperature results in the increase of the molecular mobility of the cured system and further reaction. This will be discussed later on in the determination of finally attained glass transition temperatures after the isothermal cure at all isothermal temperatures employed in the test where it will be shown that re-scanning of the isothermally cured samples indicate a residual reactivity implying incomplete cure due to isothermal vitrification.

Further from figure 5.1 it is evident that vitrification occurs at lower conversions for lower temperatures of curing . As the isothermal cure temperature is increased, vitrification occurs at progressively higher degrees of conversion (i.e. vitrification is delayed further).Since the mobility of the reacting groups is less hindered in high temperature, vitrification occurs until high conversions, which leading to a high α_{max}.

5.1.1 Comments on obtained Conversion based on Reactive Diluent (modifier)

In our studied commercial epoxy-amine system Araldite 2015 (epoxy and amine are mixed in stoichiometric ratio mixture); catalyzed triamine (DETA) cured epoxy (DGEBA/DGEBF mixture) is *modified* with *difunctional* epoxy-based reactive diluent 1,4 Butane diol diglycidyl ether (BDGE) which enables to reduce viscosity in order to aid general processability. Because of the presence of epoxide groups, this epoxy-based reactive diluent—aliphatic diglycidyl ether can participate, together with DGEBA and DETA, in polymerization and crosslinking reactions thus become chemically bound into the cross-linked network. Basically, *the aliphatic chains of the reactive diluent (BDGE) are introduced / added into the main chain of the epoxy structure*. Therefore, the use of this aliphatic diepoxide type additive, can modify the properties of our catalyzed epoxy-triamine system during the curing reaction.

It is known that in the case of a mono epoxy reactive diluent, the curing reaction leads to a decrease of the crosslink density of the resin. But in the case of a *multifunctional / polyfunctional epoxy reactive diluent*, the behaviour of the diluent *can be considered to be similar to that of the basic epoxy component* [12,30] and, here; it can be seen from figure 5.1 that the crosslink density seems not to be affected for our studied resin system. This fact also reflected in the obtained final values of the glass transition temperatures after the isothermal cure at all isothermal temperatures employed in the test which will be discussed later.

The maximum value of calorimetric conversion (α_{max}) is in the range of 0.80—0.98 for isothermal cure temperature (T_{cure}) range of 30°C—80°C. This value of α_{max} is relatively *higher* than the typical values for DETA cured epoxy (DGEBA) (mixed in stoichiometric ratio mixture--like our studied resin system) without the reactive diluent [1, 5, 29] and other amine cured epoxy (DGEBA) formulations (mixed in stoichiometric ratio mixture--like our studied resin system) without the reactive diluent [7, 8, 9, 13, 25] or at least can be reached at similar higher temperatures or comparable at similar cure temperatures. A possible reason for that is the *higher mobility of the growing chain due to the addition of the aliphatic chains from the reactive diluent in the epoxy structure*. The curing agent can efficiently reach most of

the epoxy chains because of greater chain segmental mobility, and shifts the vitrification to longer times and thus a higher conversion value is observed.

5.2 Reaction Rate

A series of isothermal DSC thermograms of Araldite 2015 for various curing temperatures as a function of cure time is shown in figure 5.2.The similar features of isothermal heat flow curves illustrated in this figure is reflected in their corresponding reaction rates of cure plots as shown in figure 5.3(a,b) which will be discussed next.
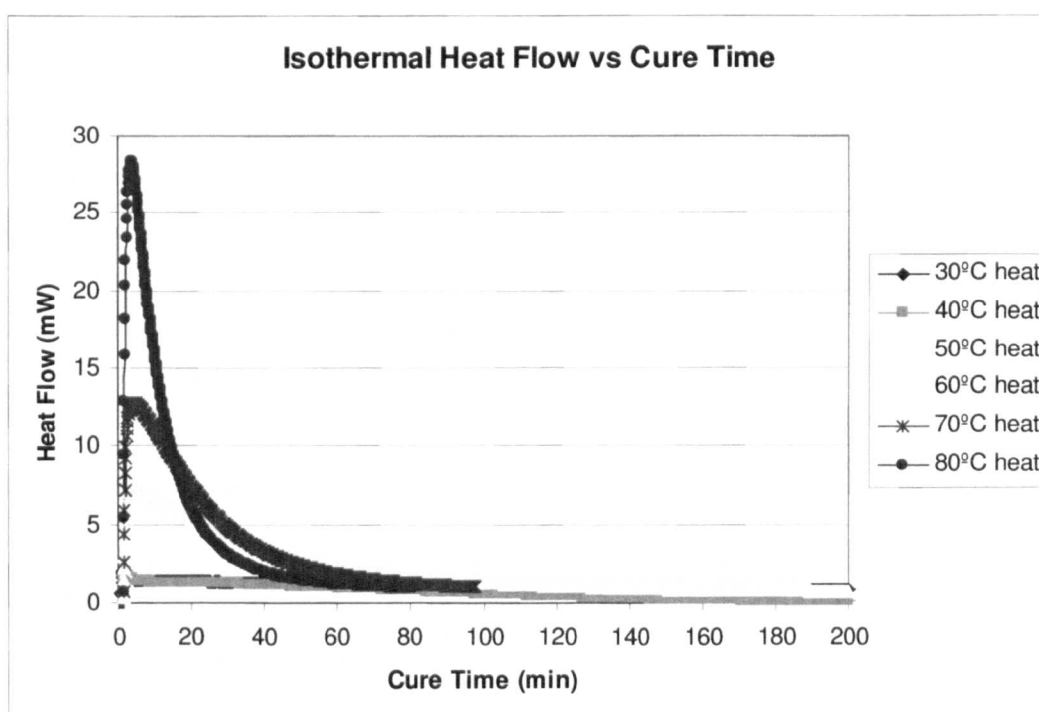
Figure 5.2 Isothermal heat flow (exotherm) curves of Araldite 2015 for various curing temperatures as a function of cure time.

In figure 5.3 (a,b) the reaction rate is plotted as a function of cure time at the different isothermal temperatures for Araldite 2015.From the figure it can be seen that

(i) Each of the reaction rate profiles shows a rapid increase at the early stage (due to *initial catalysis* by external catalyst present in the system and *autocatalysis*), passes through a maximum, followed by an exponential decrease with time.

(ii) The rate of reaction increases with increasing cure temperature showing the *thermal effect* of the curing reaction, and cure reactions take shorter times to

complete. On the contrary, the reaction time needed for complete cure increased with decreasing isothermal cure temperature.

(iii) The maximum reaction rate peak value increases and peak shifts to very slight lesser times with an increase in isothermal curing temperature. For higher curing temperatures (60°C,70°C,80°C) the time difference between the corresponding maximum reaction rate peaks are in the order of fraction of a minute (i.e. seconds) and for lower curing temperatures (30°C,40°C,50°C) they are in the order of approximately one minute to two minutes. In contrast, decreases in the maximum reaction rate peak value and peak shifts to very slight greater times are observed as the isothermal curing temperature is decreased.

The above mentioned characteristics along with the *bell shape* of these curves (the *bell shape* is more typical for the reaction rate profiles at higher curing temperatures (60°C,70°C,80°C)) suggested that in addition to the initial catalysis, *autocatalysis* is the reason for initial acceleration and that the reaction would be proceeded by an autocatalytic reaction mechanism where the products act as the catalysts for the chemical reaction.

5.2.1Comments on obtained Reaction Rate based on Reactive Diluent (modifier)

The maximum value of reaction rate $(d\alpha/dt)_{max}$ is in the range of 0.01/min—0.12/min for isothermal cure temperature (T_{cure}) range of 30°C—80°C. This value of $(d\alpha/dt)_{max}$ is relatively *higher* than the typical values for DETA cured epoxy (DGEBA) (mixed in stoichiometric ratio mixture--like our studied resin system) without the reactive diluent [1, 5, 29] and other amine cured epoxy (DGEBA) formulations (mixed in stoichiometric ratio mixture--like our studied resin system) without the reactive diluent [7, 8, 9, 13, 25] or at least can be reached at similar higher temperatures or comparable at similar cure temperatures. For more precise comparison, in particular, it can be mentioned that in our catalyzed triamine (DETA) cured modified epoxy (DGEBA) system the maximum cure rate $(d\alpha/dt)_{max}$ was reached at 80°C, 0.12/min. This value is significantly *higher* than the $(d\alpha/dt)_{max}$ values for catalyzed triamine (DETA) cured similar epoxy (DGEBA) formulation without the reactive diluent [1] and catalyzed diamine cured similar epoxy (DGEBA) formulation without the

reactive diluent [13] or comparable at similar cure temperature.
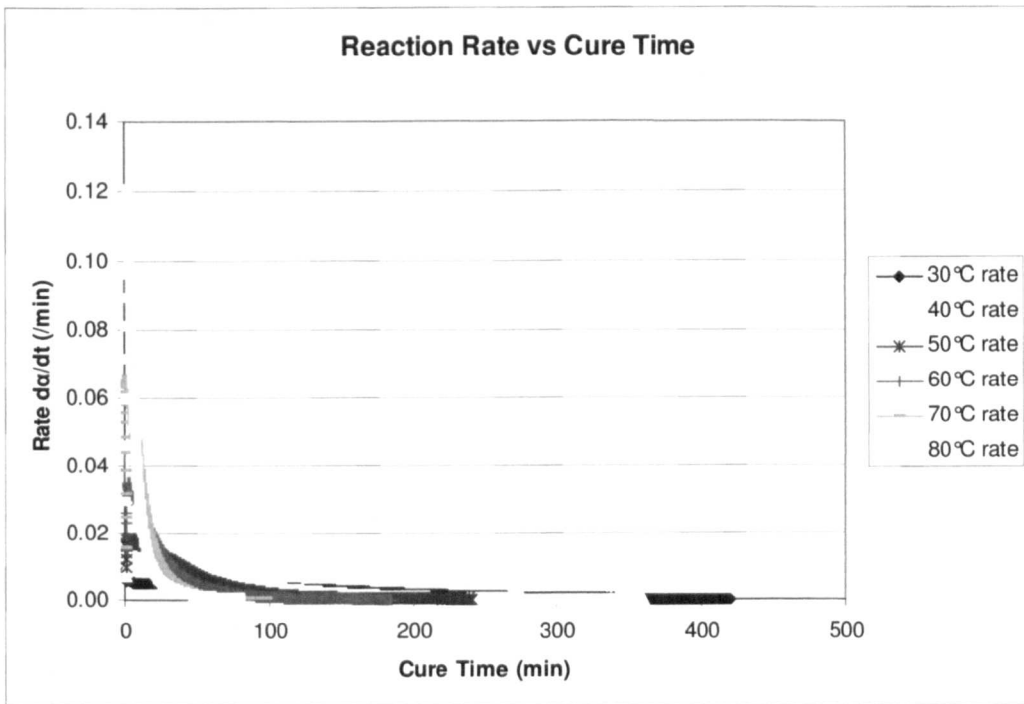
(a)
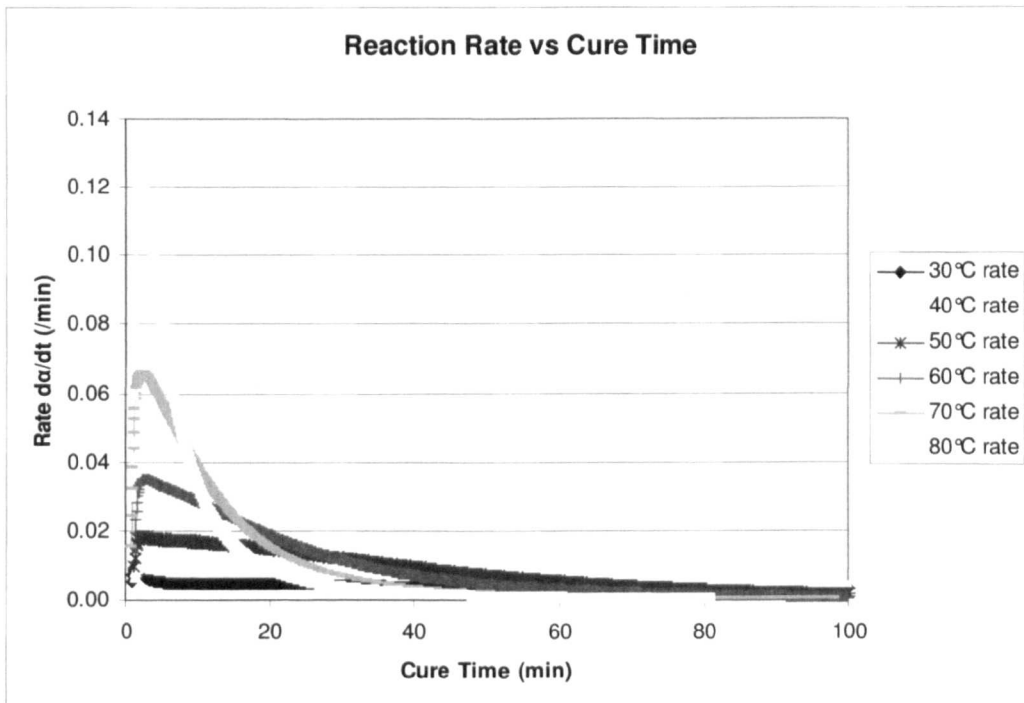
(b)

Figure 5.3 (a,b) Reaction rate as a function of cure time at the different isothermal temperatures for Araldite 2015.

As has previously been mentioned, a possible reason for that is the *higher mobility of the growing chain due to the addition of the aliphatic chains from the reactive diluent in the epoxy structure*. The curing agent can efficiently reach most of the epoxy chains because of greater chain segmental mobility and thus a higher conversion rate is observed.

5.2.2 General Mechanism of the Reactions from Reaction Rate Profiles

The maximum reaction rate peak has very important significance as it is related to the mechanisms of the reactions for both *nth order* and *autocatalytic* reactions. It can be seen from figure 5.3(b) that in the isothermal reaction rate profiles for our studied epoxy system, *the maximum reaction rate occurred for at times greater than zero* i.e. *at t>0* . This observation *negated the reaction mechanism based on the simple nth order kinetics* where the maximum reaction rate occurs at time zero i.e. at t=o. This nth order model assumes that the formed chain from each reaction step is not involved in further reactions and that the network formation occurs by only a unique reaction. This model cannot account for any autocatalytic effects and also unable to explain the entire curing reaction of a thermoset due to the physical transformations such as gelation and vitrification occurring during the curing reaction that lead to the network formation of the matrix.

Further, it can be seen from figure 5.3(a,b) that the rate of the reaction at t=0 is not zero (i.e. *non-zero initial rate*) and from the figure 5.4 that *the peaks of the maximum reaction rates is appeared approximately in the range of 3% —14% conversion* for isothermal temperature range of $30^{\circ}C$—$80^{\circ}C$.Therefore, we see that despite the *catalytic effect* of —OH groups of *external catalyst* 2,4,6 - tris (dimethylaminomethyl) phenol, for our *modified* complex-commercial epoxy–amine system Araldite 2015, the *usual autocatalytic character of epoxy-amine reactions is still perceptible*. In figure 5.4, the reaction rate profiles are plotted as a function of calorimetric conversion. As can be seen from this figure, the curves are *parabolic*, which is indicative of *autocatalytic* kinetics.

Autocatalytic reaction assumes that the *step reaction products are involved in the chain growth reaction*. This type of reactions normally have zero rate initially and
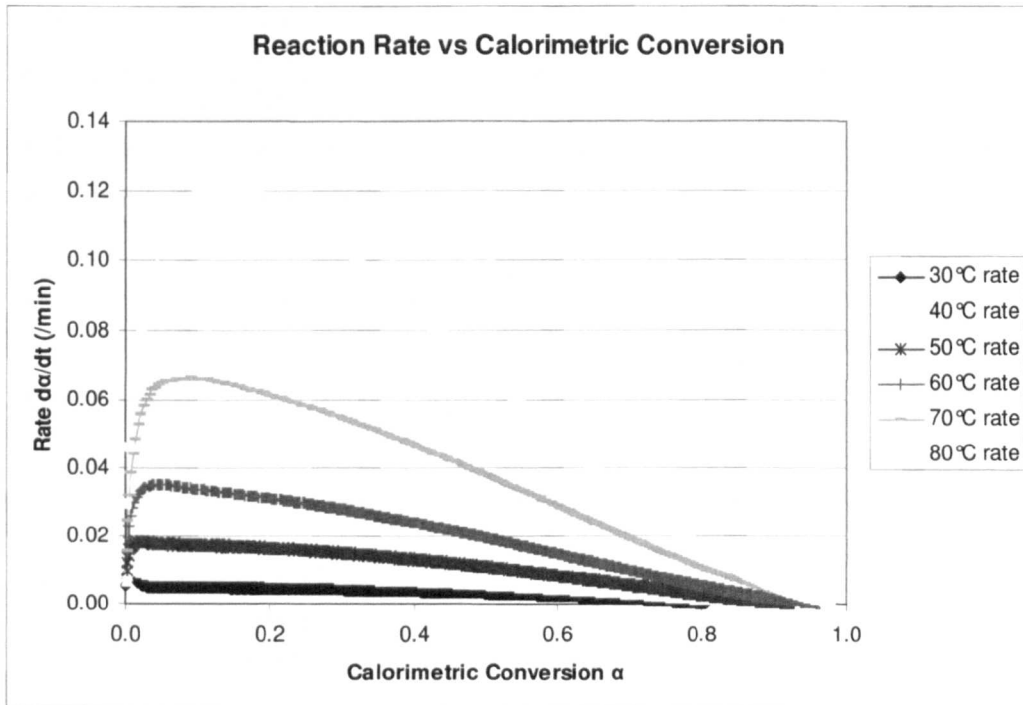
Figure 5.4 Reaction rate as a function of calorimetric conversion at the different isothermal temperatures for Araldite 2015.

attain a maximum value at some intermediate conversion. The autocatalyzed reactions are generally characterized by the *maximum reaction rate* at approximately **20%–40% conversion**[1] / 30%–40% conversion[28] although values **lower than 20% conversion** (similar to our case of catalyzed epoxy thermosetting system Araldite 2015 where the values are in the range of **3%–14% conversion**) have been reported [1,13,14,15,23,25] as mentioned with associated systems in table 5.1.

As has already been mentioned, the isothermal reaction rate profiles obtained in the present study for our studied resin system always gave a finite value of reaction rate when extrapolated to zero time. Such an occurrence of *non-zero initial reaction rate* in autocatalyzed curing in isothermal condition has been reported by several research workers [1,3,4,5,8,9,12,13,14,22,25,27,28]. It was attributed to some reactions or by external catalysts that are dominant only in the early stages of cure. In fact, the initial rate of autocatalytic reactions is not necessarily zero, since there is a possibility that reactants can be converted into products via *alternative paths* [28].

Table 5.1 Non-typical occurrence of the maximum reaction rate peak (i.e. appearance of $\dfrac{d\alpha}{dt}$ peak at a lower calorimetric conversion value than typical 20% —40% calorimetric conversion range) in autocatalytic cure kinetics for epoxy/amine, epoxy/ anhydride and other resin systems.

Investigator	System	Value / range(%) of conversion(α) at $\dfrac{d\alpha}{dt}$ peak
Perrin et al [1]	DGEBF/DGEBA mixture +Amine(Poly(oxypropylene)diamine (JEFF) / DETA) + BPA (Catalyst)	Nearly 10 %
Atarsia et al [13]	DGEBA (mixture) +Amine(4,4'-methylenedianiline) +Accelerator	5% —10%
Teil et al [14]	DGEBA +Methyl-hexahydrophthalic Anhydride (MHHPA) +Accelerator	20% (at higher Temperatures)
Ivankovic et al [25]	DGEBA +Amine(Poly(oxypropylene)diamine)	Nearly 10%
	DGEBA/ UP(Unsaturated Polyester) blend (50/50) (50/50-wt.ratio)	Nearly 10%
Leroy et al [23]	Dicyanate Ester Resin(aromatic prepolymer) +Catalyst	10% —15%
Mondragon et al[15]	Dicyanate Ester Resin +Catalyst	10%

5.3 Characteristics of Isothermal Reaction Rate vs Conversion Profiles

The unmodified epoxy-amine curing reaction mechanism is generally well known to be autocatalytic in nature. As was outlined in the present study, in spite of the catalytic effect of external catalyst 2,4,6 - tris (dimethylaminomethyl) phenol in our *modified* complex-commercial epoxy–amine system Araldite 2015, the usual autocatalytic character of epoxy-amine reactions is still perceptible. However, it is noteworthy to highlight some characteristics of the isothermal reaction rate profiles plotted as a function of calorimetric conversion as illustrated in figure 5.4.

(1) It is evident from the isothermal reaction rate vs conversion profiles of our modified epoxy-amine system in figure 5.4 that *the reaction rate profiles are not too well defined maximum typical autocatalytic in nature* (i.e. they does not clearly show the maximum typical characteristics of autocatalytic reaction) as the maximum rate of reactions occur at lower conversions (in the range of 3%—14% conversion) compared with data from the literature for typical autocatalyzed cure systems which is typically between 20% and 40% conversion [1,28] and curves are more defined as has already been mentioned.

In the present study, the occurrence of maximum reaction rate peak at nearly in the range of 3%—14% of conversion as shown in figure 5.4 suggests that when the cure reaction reaches its highest conversion rate at the temperature range of 30°C—80°C, nearly 3%—14% of the total epoxy groups have already been consumed.

(2) The typical characteristics of autocatalytic reactions is also not more evident for the studied system as it can be seen from figure 5.4 that at higher curing temperatures (at 60°C,70°C,80°C) the reaction reverts to a more autocatalytic reaction than the reaction at lower curing temperatures (at 30°C,40°C,50°C).This feature is in contrast to the conventional true autocatalytic characteristics of reaction which would be having a decreasing trend with increasing cure temperatures as found in literature. This feature will be discussed later.

(3) It is evident from the isothermal reaction rate vs conversion curve (figure 5.4) that at low curing temperatures (at 30°C,40°C,50°C) the reaction rates were not promoted

significantly and also the autocatalytical path seems to be retarded. The restrictions to carrying out the catalytical and autocatalytical reactions may be associated with the *difficulty in forming* the epoxy-external catalyst complex i.e. (epoxy–2,4,6-tris (dimethylaminomethyl) phenol) transition complex or simply (epoxy–phenol) transition complex and (epoxy – amine – —OH) transition complex respectively by the *reduced mobility* at low curing temperatures (at 30°C,40°C,50°C).

In contrast to lower curing temperatures, the observed high accelerating reaction rate at higher curing temperatures (at 60°C,70°C,80°C) can be attributed to---
(i) significant *thermal catalysis* at higher temperatures,
(ii)enhanced *chain segmental mobility* obtained by the introduction of aliphatic chains from the epoxy reactive diluent into the main chain of the epoxy as has previously been mentioned,
(iii) the *ease of formation* of epoxy-external catalyst complex i.e. (epoxy–2,4,6-tris (dimethylaminomethyl) phenol) transition complex or simply (epoxy–phenol) transition complex and (epoxy – amine – —OH) transition complex respectively at higher curing temperatures.

Also it is seen from figure 5.4 that at higher curing temperatures (at 60°C,70°C,80°C) the reaction reverts to a more autocatalytic reaction prior to vitrification due to the increased mobility of the reactive species.

Furthermore, as stated before, at higher curing temperatures (at 60°C,70°C,80°C) the *reaction reverts to a more autocatalytic reaction*; unlike the conventional true autocatalytic characteristics of reaction which would be having a *decreasing trend with increasing cure temperatures* as found in literature. This feature will be discussed in details in chapter 6 in the light of *trimolecular catalysis mechanism* involving (epoxy – amine – —OH) transition state complex in the context of the results associated with the temperature dependence of the reaction orders of the autocatalytic kinetic models that simulate the isothermal curing experimental data of the studied thermosetting system (Araldite 2015) with a reasonable degree of satisfaction and with scientifically reasonable associated best-fit parameter values.

5.4 Any Catalytic effect of Mica (filler) in the Reaction Rate profiles of Araldite 2015

Apart from 1,4 Butane diol diglycidyl ether (BDGE) epoxy reactive diluent, our studied thermosetting system catalyzed DETA cured modified DGEBA/DGEBF mixture also contains *mica* (1–10%) which usually used in epoxy system as *filler.*

Lu et al [16] reported the effects of filler on stoichiometric mixture of DGEBA-aromatic diamine system in the temperature range of 70°C–130°C and found that the *filler can catalyze the cure reactions of epoxy-amine system* by dispersing the curing agent and enhancing the cleavage of the carbon–oxygen bond depending on the cure temperature and would be retarded at low temperatures. Higher filler content can provide extra reaction regimes, thus further accelerating the reaction rate at higher temperatures.

But because of the low temperature range (30°C–80°C) that was employed in the present study and lower percentage (1 –10%) of mica content; any probable effect (may be small) of catalysis by mica acting as filler, as pointed out in literature by Lu et al [16] based on the research on stoichiometric mixture of epoxy-amine system (i.e. like our studied epoxy-amine mixture), is not considered here as a general possible point from a theoretical point of view in this context, in interpreting the cure kinetics of our epoxy-amine system.

5.5 Features of Reaction Rate Profiles based on the Peak of Maximum Reaction Rate

The maximum reaction rate peak has very important significance as it is related to the mechanisms of the reactions for both *nth order* and *autocatalytic* reactions as has previously been mentioned.

(i)The maximum isothermal reaction rate, (ii) the cure or reaction time required to attain the maximum reaction rate, and (iii) the degree of calorimetric conversion at the maximum reaction rate were found to be functions (basically *exponential functions*)

of isothermal cure temperatures for our studied thermosetting system as shown in the figure 5.5, figure 5.6 and figure 5.7 respectively.

Among them, (i)The maximum isothermal reaction rate and (ii) the cure or reaction time required to attain the maximum reaction rate are found to have *Arrhenius behaviour* as shown in figure 5.5 and figure 5.6.
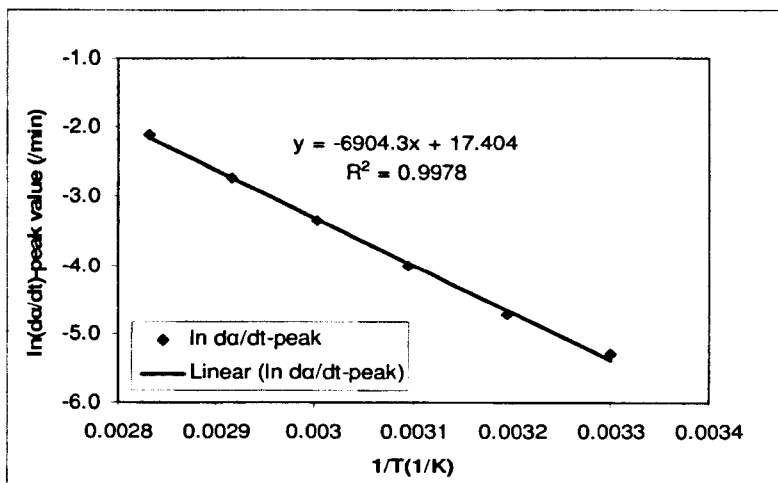
Figure 5.5 The isothermal reaction rate at the peak maximum as a function of the reciprocal of the absolute cure temperature.
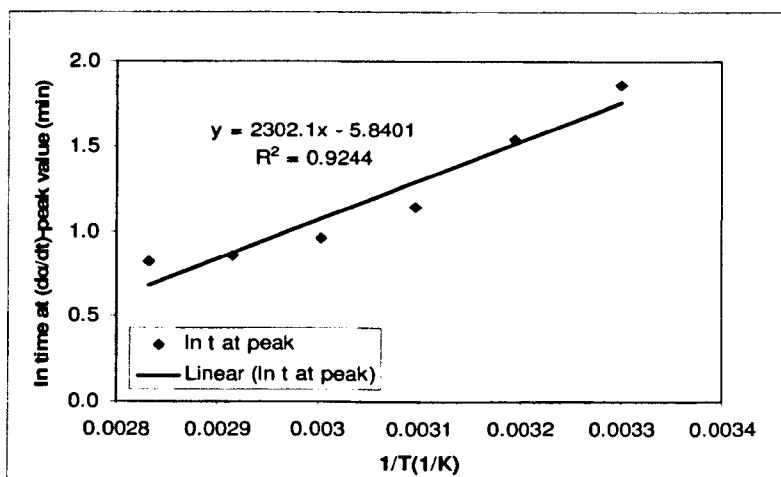
Figure 5.6 The cure time at the peak of the maximum reaction rate as a function of the reciprocal of the absolute cure temperature.
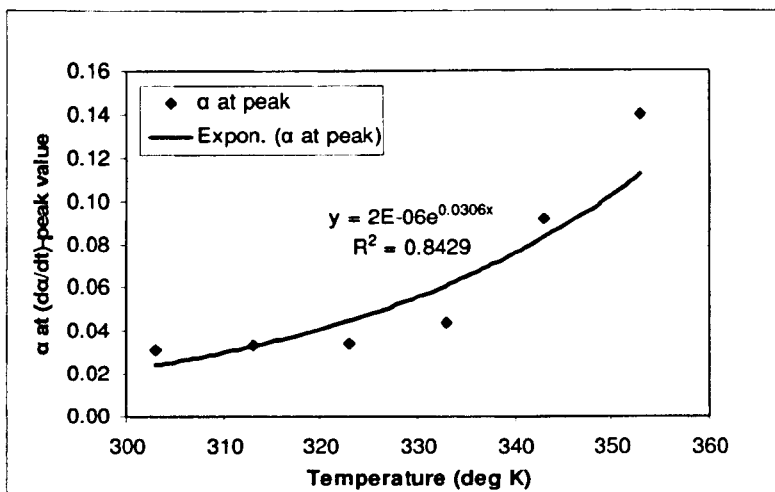
Figure 5.7 The degree of calorimetric conversion at the peak of
the maximum reaction rate as a function of cure temperature.

5.6 Model Free Iso-Conversional Analysis of Calorimetric Cure Kinetics

5.6.1 Significance of the determination of Activation Energy for Araldite 2015

For the quantitative evaluation of curing reaction of our DGEBA-triamine modified
epoxy thermosetting system (Araldite 2015) we need to determine the activation
energy. It can give valuable information on barriers to reaction (i.e. the overall
chemical threshold energy required for the initiation, propagation and termination in
the polymerization reaction of our studied epoxy resin system) and chemical
mechanism. Its *constancy* or *change* can enable us to understand the *molecular
aspects of curing*, effects of fillers, the stoichiometric variation of the resin and the
curing agent often encountered in practice. Being a time-temperature shift factor, it is
useful in predicting the curing behaviour in a real process.

The *true* value of activation energy, in fact, also is important (particularly for non-
isothermal curing condition of polymers) for a reliable determination of the
'appropriate' kinetic model, instead of an *'apparent'* one, because of the *correlation
of the kinetic parameters*, especially in the case of non-isothermal curing of polymers,
where it has been found that the activation energy, E_a and the pre-exponential factor

123

or frequency factor, A (which describes other physical factors related to the reaction condition) are strongly correlated [11,23,30,33,34].

5.6.2 Basic Principle of Iso-Conversional Kinetic Analysis

Iso-conversional kinetic analysis offers a viable alternative of determining the activation energy at a certain degree of conversion without knowing any explicit kinetic model nor its parameters.

Basically, this iso-conversional method compares the reaction rate $\frac{d\alpha}{dt}$ (in the case based on the conventional differential form of general kinetic model $\frac{d\alpha}{dt} = k(T)f(\alpha)$ as in equation (3.3) which, here, in this chapter, is entitled as Differential Method or the cure / reaction time t (in the case based on the integral form of general kinetic model which, here, in this chapter, is entitled as Integral Method) to reach the same degree of calorimetric conversion α at different temperatures (mainly in the conversion range of chemical controlled reaction regime i.e. below the conversion corresponding to the onset of vitrification---in the case of isothermal curing).

The basic idea of this type of analysis is that the reaction rate $\frac{d\alpha}{dt}$ (in the case of Differential Method) or the cure / reaction time t (in the case of Integral Method) to reach at a constant degree of conversion α is a *linear function of temperature only* i.e. depends only on the temperature.

To analyze the curing behaviour of our studied epoxy thermosetting system in isothermal conditions, it is *not necessary to know the exact equation for* $f(\alpha)$ in equation (3.3), which may vary during the isothermal curing process. For each isothermal temperature $k(T)$ becomes a *constant*. Applying the iso-conversional analysis at a series of temperatures, it is possible to determine the activation energy at different degrees of conversion which enables us to see how the reaction process evolves. Thus, it provide a means of detecting the kinetic changes through the reaction. Using this method an activation energy is obtained which depends on the

degree of conversion. On the other hand, when non-isothermal experiments are performed, the function $f(\alpha)$ has to be specified. In that case of non-isothermal conditions, where the temperature varies with time, the reaction rate $\dfrac{d\alpha}{dt}$ is not directly proportional to $f(\alpha)$, as the temperature dependent reaction rate constant $k(T)$ described by the common Arrhenius equation is not constant.

5.6.3 Advantageous features of Iso-Conversional Method

To analyze the curing kinetics of our studied epoxy thermosetting system, Araldite 2015, we choose the iso-conversional method for its rich potential associated with the following advantageous features.

Firstly, it enables us to determine the exact effective activation energy value at a given convesion for both simple and complex chemical reactions for isothermal and non-isothermal curing conditions. Also it has an identical approach to both isothermal and non-isothermal kinetic calculations. This exact effective activation energy value can be used in model fitting method.

Secondly, this iso-conversional method do not consider any specific mechanism and we *do not need to know any explicit kinetic model nor its parameters.* Therefore, the effective activation energy value obtained by this method should *contain information from the whole process*; in other words, information from any mechanism is independent of whether the curing reaction takes place by means of (i) the catalyzed and / or non-catalyzed reaction or (ii) a multi-mechanism process (chemical control and diffusion control).

Thirdly, as in this method, the effective activation energy is obtained as a function of the different degrees of conversion, therefore, this iso-conversional analysis *readily provides a check for the invariance of activation energy E_a with respect to conversion* α in the kinetic control regime for a *single-step process* and may have the meaning of the *intrinsic activation energy*, which (i.e. E_a should be independent of α) is one of the

basic assumptions in kinetic analysis of thermal analysis data. Hence, this method can be highly recommended for the reliable determination of activation energy.

Fourthly, the evolution of effective activation energy with conversion can be interpreted in terms of reaction mechanism, particularly in the case of *multi-step reactions* typical for epoxy systems.The analysis of which helps not only to disclose the complexity of a process but also to identify its kinetic scheme. Therefore, this method can provide us a wealth of information regarding *mechanism of the reaction.*

Basically, in case of multistep kinetics of epoxy curing, the variation of degree of cure reflects the variation in relative contribution of each single-step reaction to the reaction rate. Thus, the activation energy changes continuously with the change of degree of cure. Therefore, for monitoring the changes of degree of cure the activation energy has to be monitored continuously. Thus, the activation energy obtained as a function of the conversion in iso-conversional method, can be useful in predicting the curing behaviour coupled with the cure mechanism.

So, calculation of the effective activation energy from this method is highly reasonable. Here, it can be mentioned that the iso-conversional method has been used with success in the curing of epoxy and other polymer systems [7, 8, 9, 10, 15, 23, 30, 33, 34].

5.7 Iso-Conversional Analysis (Differential Method) of Cure Kinetics

As this method of iso-conversional analysis is based on the conventional differential form of general kinetic model $\dfrac{d\alpha}{dt} = k(T)f(\alpha)$ as in equation (3.3), here, we entitled it as Differential Method of iso-conversional analysis. As has already been stated, this method compares the reaction rate $\dfrac{d\alpha}{dt}$ to reach the same degree of conversion α at different temperatures (mainly in the conversion range of chemical controlled reaction regime in the case of isothermal curing). The basic idea of this type of analysis is that the reaction rate $\dfrac{d\alpha}{dt}$ at a constant degree of conversion α is a linear function of temperature only i.e. depends only on the temperature.

From equations (3.3) and (3.4) we know,

$$\frac{d\alpha}{dt} = k(T)f(\alpha) = A\exp\left(\frac{-E_a}{RT}\right)f(\alpha) \tag{5.1}$$

Taking the logarithms of equation (5.1) gives—

$$\ln\frac{d\alpha}{dt} = \ln A - \frac{E_a}{RT} + \ln f(\alpha) \tag{5.2}$$

By fixing the value of α and letting $k(T)$ as a variable, this equation can be written for a fixed or certain conversion α, in the following logarithmic form —

$$\ln\left(\frac{d\alpha}{dt}\right)_\alpha = \ln\{A \times f(\alpha)\} - \frac{E_{a,\alpha}}{R}\cdot\frac{1}{T} = constant - \frac{E_{a,\alpha}}{R}\cdot\frac{1}{T} \tag{5.3}$$

From equation (5.3), a plot of $\ln\left(\frac{d\alpha}{dt}\right)_\alpha$ versus $\frac{1}{T}$ values at the same degree of calorimetric conversion α, from a series of isothermal DSC experiments at different temperatures would result in a straight line with a slope of $-\frac{E_{a,\alpha}}{R}$ and an intercept of $\ln\{A \times f(\alpha)\}$. So, the slope of logarithmic rate of cure versus the reciprocal of the absolute temperature of cure at a fixed degree of conversion, gives the corresponding value of the effective activation energy divided by the universal gas constant

$$-\frac{E_{a,\alpha}}{R} = \frac{d\ln\left(\frac{d\alpha}{dt}\right)_\alpha}{d\left(\frac{1}{T}\right)} \tag{5.4}$$

Repeating this procedure for various values of α, the effective activation energy E_a and $\ln\{A \times f(\alpha)\}$ values corresponding to that different α can be obtained.

In this method, the calculation of E_a is performed from the results of the isothermal reaction rate versus calorimetric conversion data (figure 5.4) for the isothermal curing temperatures of 30°C, 40°C, 50°C, 60°C, 70°C and 80°C, using only the values of α below the conversion corresponding to the onset of vitrification. At 30°C and 80°C,

the α_{max} values are 0.8034 and 0.98 respectively. So, for the employed range of temperatures, vitrification takes place roughly at calorimetric conversion higher than 0.80, and equation (5.3) may not be applied because of the diffusion control kinetics.

The Arrhenius plots of $\ln\left(\dfrac{d\alpha}{dt}\right)$ versus $\dfrac{1}{T}$ for various values of α (α =0.1, 0.2, 0.3,

.....,0.8, 0.9) in the experimental range illustrated in figure 5.8, shows a linear temperature dependence, indicating a good fit to the experimental data based on equation (5.3). The effective activation energy E_a and $\ln\{A \times f(\alpha)\}$ values are obtained for each value of α from figure 5.8 by measuring the slope of the straight line fit of the data and the intercept as shown in equation (5.3).
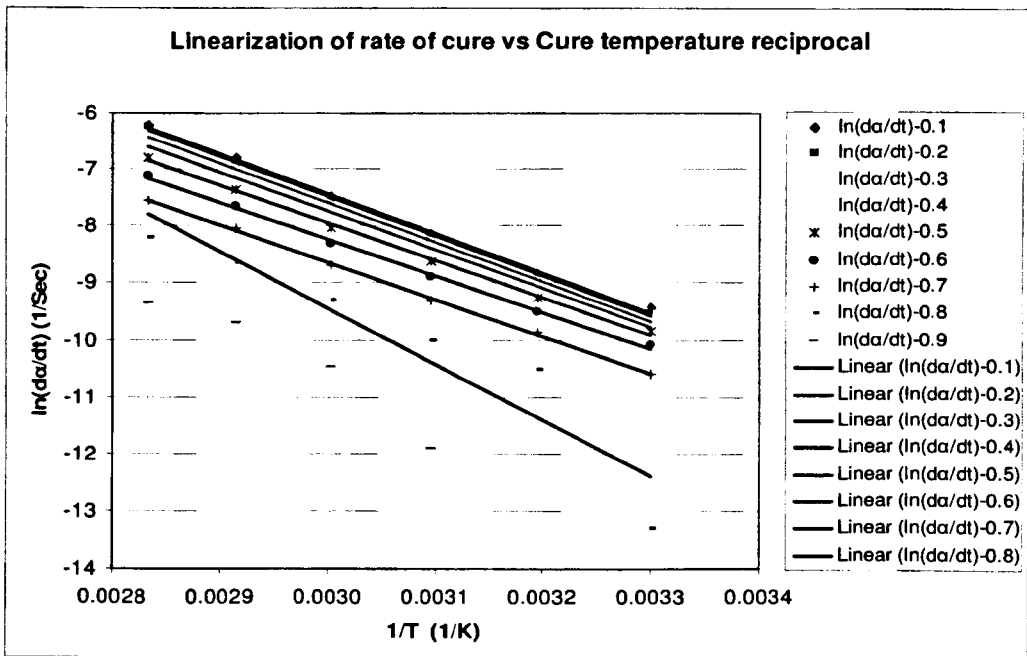
Figure 5.8 Linearization of the iso-conversional plots (Differential Method) of logarithm reaction rate as a function of the reciprocal of the absolute cure temperature---from which the effective activation energies are obtained at different degrees of conversion.

The corresponding equation of the linear expression of figure 5.8 for each value of α is presented in the table 5.2 along with its correlation co-efficient and calculated E_a value (in kJ/mol).The $\ln\{A \times f(\alpha)\}$ value (in / Sec) is the value of the intercept of the equation which is directly obtainable. An average value of the effective activation

128

energy, $E_{a(average)}$ = 55.50 kJ/mol calculated in the range of conversion (α) of $0.2 \leq \alpha \leq 0.7$ (for optimum reliability) is also indicated in table 5.2. These effective activation energy E_a and $\ln\{A \times f(\alpha)\}$ values are plotted in figure 5.9 (a,b) as a function of conversion.

Table 5.2 The effective activation energy (E_a) values for isothermal cure process of Araldite 2015 obtained from the iso-conversional analysis—equation(5.3) (Differential Method).

α	Linear expression of figure-5.8 $y = -$ (slope $=E_a/R$) x $+$ c	R^2 *	E_a (kJ/mol)
0.1	y = − 6967.48 x + 13.474	0.9976	57.9309
0.2	y = − 6968.37 x + 13.423	0.9965	57.9383
0.3	y = − 6887.34 x + 13.068	0.9965	57.2646
0.4	y = − 6753.91 x + 12.519	0.9975	56.1552
0.5	y = − 6563.36 x + 11.743	0.9971	54.5709
0.6	y = − 6389.86 x + 10.941	0.9979	53.1283
0.7	y = − 6488.82 x + 10.822	0.9990	53.9511
0.8	y = − 9861.42 x + 20.145	0.8895	81.9925
0.9	y = − 9730.03 x + 18.459	0.9344	80.9001

$$E_{a(average)}^{**} \mid_{\alpha=0.2-0.7} = 55.50 \text{ KJ/mol}$$

* Linear regression squared correlation co-efficient (i.e. co-efficient of determination).

** An average value of the effective activation energy calculated in the range of conversion (α) of $0.2 \leq \alpha \leq 0.7$.

Figure 5.9 (a,b) shows the variation of effective activation energy E_a and $\ln\{A \times f(\alpha)\}$ values with the calorimetric conversion. As can be seen from the figure, and associated table 5.2, the value of effective activation energy E_a, found by the iso-conversional analysis (Differential Method) applied to the isothermal DSC data of our

Activation Energy vs Conversion
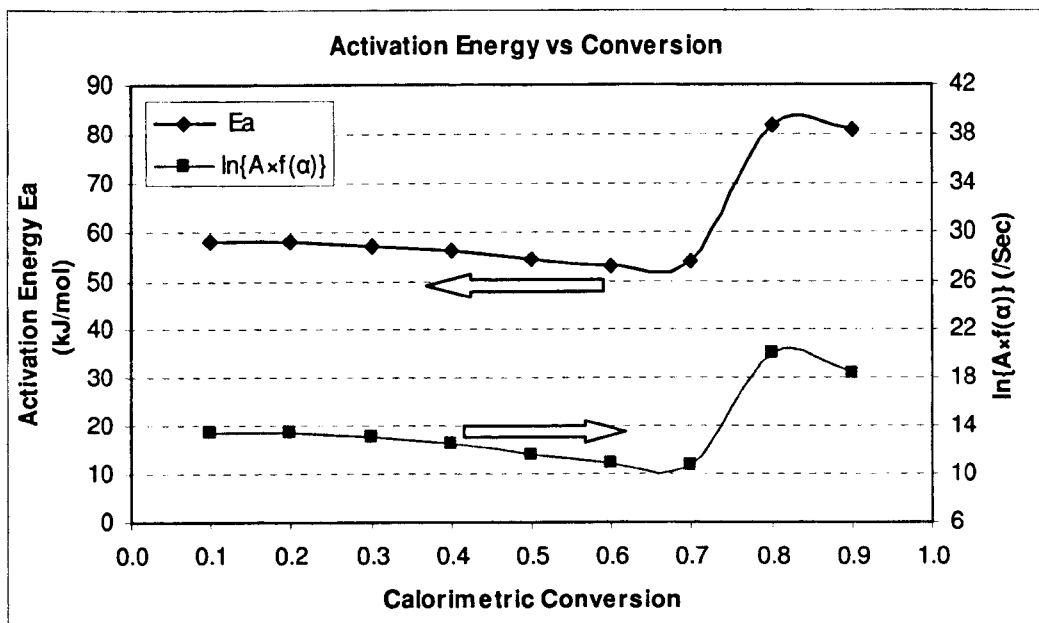
(a)
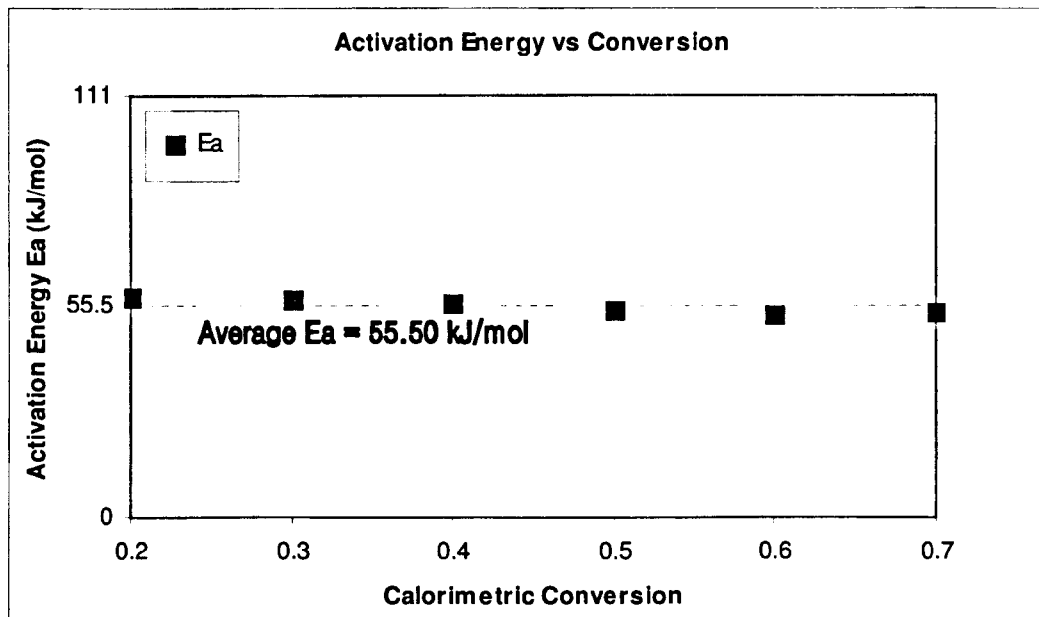
(b)

Figure 5.9 (a,b) The effective activation energy E_a and product $\ln\{A \times f(\alpha)\}$,obtained from the iso-conversional analysis (Differential Method),as a function of conversion. The broken line in figure **(b)** corresponds to an average value of the effective activation energy, $E_{a(average)} =$ **55.50 kJ/mol** calculated in the range of conversion (α) of $0.2 \leq \alpha \leq 0.7$.

studied thermosetting system Araldite 2015, decreases very slightly from $E_{a,a}$=57.93 kJ/mol at α=0.1 and α=0.2 to $E_{a,a}$=53.95 kJ/mol at α=0.7 with the increase in the degree of conversion, and an average value of the effective activation energy, $E_{a(average)}$ = **55.50 kJ/mol** is obtained in the chemical controlled reaction regime calculated in the range of conversion (α) of $0.2 \leq \alpha \leq 0.7$ (for optimum reliability) which is shown by the broken line in figure 5.9 (b). Data, analogous to this, has also been observed during the isothermal curing of epoxy-amine system [8,9].

It can be seen that the activation energy increases significantly for higher α values ($\alpha > 0.7$) and especially near the end of cure, similarly to data found for the cure of epoxy [30] and other polymer systems [15, 34].Probably it reflects the increasing difficulty of further reaction of the epoxy resin (DGEBA and DETA) after vitrification where the reaction becomes diffusion controlled.

Finally, it is evident from the figure 5.9 (a) that the plot of the product of $\ln\{A \times f(\alpha)\}$ appears to vary almost similarly to the activation energy with the calorimetric conversion showing a plateau in the range of conversion (α) of $0.2 \leq \alpha \leq 0.7$ .This correspondence can be explained in the light of the *iso-kinetic relationship* [23, 30, 34] or the so-called *kinetic compensation effect* [11, 30], which will be discussed shortly along with the interpretation and discussion of the above mentioned features illustrated in figure 5.9 (a,b).

5.7.1 Interpretation of E_a on α Dependence for isothermal cure of Araldite 2015

5.7.1.1 Analysis of the variation of E_a on α at $0.2 \leq \alpha \leq 0.7$

For *single-step reaction*, the value of the effective activation energy E_a should be practically *independent of the fractional conversion* α in the range of $0.2 \leq \alpha \leq 0.7$, and may have the meaning of the intrinsic activation energy. From figure 5.9 (a,b) and associated table 5.2, it is evident that the value of effective activation energy E_a, decreases very slightly from $E_{a,a}$=57.93 kJ/mol at α=0.2 to $E_{a,a}$=53.95 kJ/mol at α=0.7 with the increase in the degree of conversion, and an average value of the

effective activation energy, $E_{a(average)}$ = **55.50 ± 2 kJ/mol** is obtained in the chemical controlled reaction regime calculated in the range of conversion (α) of $0.2 \leq \alpha \leq 0.7$ (for optimum reliability).

Although the activation energy E_a for condensation or stepwise reactions should be constant in the range of $0.2 \leq \alpha \leq 0.7$, the very slight decrease in the activation energy E_a may indicates a *more complex mechanism of stepwise reactions*. Another possible explanation, is that the deviation in activation energy E_a might have magnified due to *error / uncertainty in baseline interpolation / approximation for peak tails* (figure 5.2). Peak tail here, in this figure, is represented by the declining heat flow after reaching the peak. If we look back at these heat flow curves in figure 5.2, we can find out that at lower isothermal temperatures (at 30°C, 40°C, 50°C and 60°C), the heat flow peak tail is extended. A possible reason for this behaviour is the beginning of vitrification and thus the change from kinetic-controlled to diffusion-controlled reaction. As the curing temperature increases, the rate increases rapidly and the peak tail diminishes. Furthermore, as the isothermal temperature is increased from 30°C to 80°C, the probability of heat loss will be more as it takes more time for the system to reach the isothermal equilibrium even if the heating cell is heated at a high ramp rate to the specified isothermal temperature.

In this case, such very slight variation in activation energy E_a is considerably lower than typical uncertainties for this type of analysis of experimental data [8,9] and because of the *small uncertainty* (~ ±2 kJ/mol) obtained (i.e. as it is not more pronounced variation), here, reasonably it can be assumed that the effective activation energy E_a is almost a *constant* with average value $E_{a(average)}$ = **55.50 ± 2 kJ/mol** in the conversion range of $0.2 \leq \alpha \leq 0.7$ (figure 5.9 (b)). This may be an indication that the reaction probably follows the same reaction mechanism that does not change with conversion up to α =0.7.

The average value of the effective activation energy $E_{a(average)}$ = **55.50 ± 2 kJ/mol** is within the range of 30—100 kJ/mol, usually found in the literature [21] and also well compared and very similar to the reported values in the literature obtained for similar epoxy-amine formulations by other researchers [1, 5, 7, 8, 9, 10, 11, 12, 24] as

mentioned with associated systems in table 5.3. This value also agrees well with that reported for DGEBA-diamine system in a stoichiometric ratio mixture obtained by conventional DSC from the non-isothermal scans [8], which is 57.7±0.6 kJ/mol, and that by the well known *Kissinger Method* of 58.7 kJ/mol, from the peak temperature T_p of non-isothermal DSC scans obtained at heating rates between 2.5 K/min and 20 K/min [8].Hence, the average E_a value which we obtained from iso-conversional analysis based on isothermal conditions, *agrees fairly well* with the values reported for similar epoxy-amine formulations obtained *for both isothermal and non-isothermal conditions* (i.e. unique value). Therefore, the average value of the effective activation energy $E_{a(average)}$ = **55.50 ± 2 kJ/mol** obtained for our studied resin system, *assures adequate statistical soundness of its validity*, and as a unique value, it provides a signature or characteristic fingerprint for our particular thermosetting system Araldite 2015.

So, it is a reasonable and good approximation to assume that the effective activation energy E_a is almost a constant with average value $E_{a(average)}$ = **55.50 ± 2 kJ/mol** between the conversion of α =0.2 and α =0.7, as illustrated by the broken line in figure 5.9 (b). Interestingly, in this connection it can be pointed out that Varley et al [31] has mentioned in their work, that the activation energy of aromatic amines cured DGEBA epoxies has been found to be relatively constant with cure conversion. Similar feature of nearly invariance of activation energy with respect to conversion, has also been found for the cure reactions of epoxies and aliphatic amines [7, 9].

We know that the secondary amine addition does not play an important role in the beginning of the cure. In all likelihood the primary amine addition controls the overall heat release at lower conversions. As evident from figure 5.9 (a,b) and associated table 5.2, the effective activation energy value of $E_{a,\alpha}$ =57.93 kJ/mol at α =0.1 can be ascribed to the *primary amine addition*. This value agrees well with the reported activation energy values of the autocatalyzed process of primary amine additions [33].

Since the effective activation energy E_a is almost *constant* with average value $E_{a(average)}$ = **55.50 ± 2 kJ/mol** in the conversion range of $0.2 \leq \alpha \leq 0.7$ (figure 5.9 (a,b)), we can use this value as an estimate for the activation energy of the *autocatalytic amine addition*. This value is in agreement with the literature values

Table 5.3 Activation energy values for several similar epoxy-amine systems exhibiting autocatalytic cure kinetics where in all the cases the resin and hardener are in stoichiometric ratio mixture and under isothermal curing. E_a is the average / overall activation energy value.

Investigator	System	E_a (kJ/mol)
Perrin et al [1]	DGEBF/DGEBA mixture +Amine(Poly(oxypropylene)diamine (JEFF) / DETA) + BPA (Catalyst)	E_{a1}=50 E_{a2}=58
Villanueva et al [12]	DGEBA (modified) +Amine(1,2 Diamine cyclohexane (DCH)) +Vinylcyclohexane dioxide (VCHD) (epoxy reactive diluent)	E_{a1} =58.86 ±7.48 E_{a2}=50.80 ±3.57
Poljansek et al [5]	DGEBA(Araldite 250) +Amine(Diethylene triamine (DETA))	E_a=51.2 ± 3.6
Montserrat et al [7]	DGEBA(Araldite F) +Polyoxypropylene triamine (Jeffamine T-430)	E_a=57.5
Montserrat et al [8,9]	DGEBA +Diamine(4,4'-diamino-3,3'-dimethyldicyclohexyl methane (3DCM)	E_a=57.9 ± 4.4
Verchere et al [10]	DGEBA +Diamine(4,4'-diamino-3,3'-dimethyldicyclohexyl methane (3DCM)	E_a=56—59
Malek [11]	DGEBA+ Amine	E_a=58
Pindinelli et al [24]	DGEBA +Triethylene tetraamine(TETA)	E_a=51.88

ascribed to the autocatalytic amine additions [7,8,9,33]. This value is also close to the activation energies of the autocatalyzed process of both the primary and the secondary amine additions [1,33]. In this connection, here, it can be mentioned that the activation energies of the primary and secondary amine addition were found to be same for several different amines, although substantially different values have also been reported [33].

In the light of the *advanced kinetics research*, here in this context, most interestingly it can be noted that variation of certain physical properties of the reaction medium may cause the experimental effective activation energy E_a value (estimated from the temperature dependence of the reaction rate) to vary significantly in liquid and solid phases even for single-step reactions [32].

So, in our context, in the liquid phase of epoxy-amine reaction in the conversion range of $0.2 \leq \alpha \leq 0.7$, the free energy barrier of electron transfer reactions of a chemical step can be affected by the variation in dielectric properties of the liquid phase epoxy medium (solvent) which can cause the experimental effective activation energy E_a value to vary significantly though the reaction involves a single chemical step [32].

This effect of *reaction medium induced significant variation of activation energy E_a in a single chemical step reaction* is obviously inconsistent with the concept of a constant activation energy and that of variable activation energy has been considered as an alternative, which permits a constant activation energy as a special case of a variable activation energy [32].This phenomenon, in fact, largely escapes our common attention.

As in our case, the variation of effective activation energy E_a with respect to α, in the conversion range of $0.2 \leq \alpha \leq 0.7$ in the chemical controlled reaction regime in liquid state kinetics, is *very slight* and *not so significant* (as has already been mentioned), it is unlikely the case, and therefore, we do not taking into account the conception of variable activation energy phenomenon, that above mentioned associated outcome of advanced kinetics research noted in other references[32],as a probable point or explanation in interpreting the observed slight variation of E_a with α in the conversion range of $0.2 \leq \alpha \leq 0.7$ for our studied thermosetting resin Araldite 2015.

5.7.1.2 Analysis of the variation of E_a on α at $\alpha > 0.7$ (at higher α)

As stated before, it can be seen from figure 5.9 (a,b) that the activation energy increases significantly for higher α values ($\alpha > 0.7$) near the end of cure, similarly to data found for the cure of epoxy [30] and other polymer systems [15, 34].Probably it reflects the increasing difficulty of further reaction of the epoxy resin (DGEBA and DETA) after vitrification where the reaction becomes diffusion controlled.

The increase in the effective activation energy E_a at higher conversions near the end of cure for our studied thermosetting resin system can be understood in terms of *cooperative motion of the chain segments*. As the cure reaction of our modified DGEBA (epoxy) and DETA (amine) proceeds, the system undergoes gelation (liquid-to-rubber) and vitrification (rubber-to-glass) transitions. Intensive cross-linking occurs and reduces molecular mobility, then the cure changes from a kinetic to a diffusion regime.

At the early stages of the transition, the packing is loose, which allows the chain segments to move independently (i.e. with a *lower degree of cooperativity*). As the cure reaction proceeds, the free volume decreases. At the glassy state, the small amount of free volume only allows for local motions of the chain segments. To initiate translational motion of the segments, it requires a *higher degree of cooperativity* between the chain segments, which is associated with a large energy barrier to the segmental motion as reflected in the higher value of effective activation energy E_a at the later stages of cure at higher conversions. As a result, the energetic constrains are intensified which is reflected in an increase of the value of effective activation energy E_a. In short, an increase in the molecular weight during the polymerization process of our modified epoxy-triamine system, augments or increase intermolecular rigidity and steric hindrance and at the later stages of cure (i.e. at higher values of α) alters the molecular architecture in the direction of higher cooperativity and activation energy.

Basically, reactions of epoxy in solid phase or glassy state tend to occur as multiple steps which may cause strong dependencies of the activation energy on temperature and/or degree of conversion which can be explained by the change in the reaction

mechanism from kinetic controlled to diffusion controlled as explained above considering the physics of *cooperative motion of the chain segments.*

In addition to diffusion limitation, the observed *significant variation in effective activation energy,* can also possibly be explained in the light of the *reacting solid medium induced activation energy variation,* mentioned in other references [32]. In fact, at higher conversions, in the solid phase epoxy reaction (i.e. in gelled glass state), the reacting solid medium (as for example, thermal expansion in solid phase) can cause an *alteration of the diffusion rate* that eventually causes the effective activation energy to vary. Moreover, due to the highly restricted molecular motion, the glassy state of epoxy reaction (i.e. reacting solid medium) allows a reactant to exist in *states of significantly different free energy* that are non-uniformly distributed throughout the solid phase (i.e. reacting solid). Because of this, the same reaction step may occur with different activation energies depending on the spatial location of the reaction centres. Here, it can be mentioned that kinetics of chemical reactions in solid phase may possibly be associated with the idea of *distribution of the activation energies* which has been successfully developed [32] to describe the solid phase reaction kinetics. This trend, coupled with above mentioned kinetic features of solid-phase reaction, ultimately give rise to significant dependencies of the activation energy on degree of conversion at $\alpha > 0.7$ for our epoxy reaction at glassy state.

5.7.1.3 Analysis of the variation of $\ln\{A \times f(\alpha)\}$ on α

As illustrated in figure 5.9 (a), the plot of the product of $\ln\{A \times f(\alpha)\}$ appears to vary almost similarly to the activation energy E_a with the degree of calorimetric conversion showing a plateau in the range of conversion (α) of $0.2 \leq \alpha \leq 0.7$.

This correspondence can be explained in the light of the *iso-kinetic relationship* [23, 30, 34] or the so-called *kinetic compensation effect* [11, 30], which suggests that especially in the non-isothermal curing of polymer there exists strong mutual correlation between both the activation energy E_a and the pre-exponential factor or frequency factor $\ln A$, which can be expressed by the following equation

$$\ln A = p_0 + q_0 E_a \tag{5.5}$$

Where, p_0 and q_0 are constants [11, 30].

Any change in the activation energy is therefore *"compensated"* by the change in ln A as expressed by equation (5.5).

Though basically in the case of non-isothermal curing ln A and E_a are found to be strongly correlated, however, in our case of isothermal curing, the plot of the product of ln$\{A \times f(\alpha)\}$ varies almost similarly to the activation energy E_a. It is worth noting that such a relationship implying a so-called *"compensation effect"* has been observed in the non-isothermal curing and decomposition of numerous other polymer systems [30,33,34].

5.8 Iso-Conversional Analysis (Integral Method) of Cure Kinetics

As this method of iso-conversional analysis is based on the Integral form of general kinetic model $\dfrac{d\alpha}{dt} = k(T)f(\alpha)$ as in equation (3.3), here, we entitled it as Integral Method of iso-conversional analysis. As has already been mentioned, this method compares the cure or reaction time t to reach the same degree of conversion α at different temperatures (mainly in the conversion range of chemical controlled reaction regime---in the case of isothermal curing). The basic idea of this type of analysis is that the cure or reaction time t to reach at a constant degree of conversion α is a *linear function of temperature only* i.e. depends only on the temperature.

From equation (5.1) we know,

$$\frac{d\alpha}{dt} = k(T)f(\alpha) = A\exp\left(\frac{-E_a}{RT}\right)f(\alpha)$$

Rearranging and integrating equation (5.1), the following equation is obtained which is the integral form of the general kinetic model—

$$g(\alpha) = \int_0^\alpha \frac{d\alpha}{f(\alpha)} = k(T)\int_0^t dt = k(T)t \tag{5.6}$$

Where $g(\alpha)$ is dependent only on the degree of calorimetric conversion.

Taking logarithms of equation (5.6) produces the following form of the equation

$$F(\alpha) = \ln g(\alpha) = \ln k(T) + \ln t = \ln A - \left(\frac{E_a}{RT}\right) + \ln t \tag{5.7}$$

Where $F(\alpha)$, which is also a function only of the conversion, describes the variation of the degree of conversion with the time and the curing temperature.

Rearranging equation (5.7) we get,

$$\ln t = F(\alpha) - \ln A + \left(\frac{E_a}{RT}\right) = \ln g(\alpha) - \ln A + \left(\frac{E_a}{RT}\right) = \ln\left\{\frac{g(\alpha)}{A}\right\} + \frac{E_a}{RT} \tag{5.8}$$

By fixing the value of α and letting $k(T)$ as a variable, this equation can be written for a fixed conversion α, in the following logarithmic form —

$$\ln(t)_\alpha = \ln\left\{\frac{g(\alpha)}{A}\right\} + \frac{E_{a,\alpha}}{R} \cdot \frac{1}{T} = constant + \frac{E_{a,\alpha}}{R} \cdot \frac{1}{T} \tag{5.9}$$

From equation (5.9), a plot of $\ln(t)_\alpha$ versus $\dfrac{1}{T}$ values at the same degree of calorimetric conversion α, from a series of isothermal DSC experiments at different temperatures would result in a straight line with a slope of $\dfrac{E_{a,\alpha}}{R}$ and an intercept of $\ln\{g(\alpha)/A\}$. So, the slope of $\ln(t)_\alpha$ versus $\dfrac{1}{T}$ at a constant conversion, gives the corresponding value of the effective activation energy divided by the universal gas constant

$$\frac{E_{a,\alpha}}{R} = \frac{d\ln(t)_\alpha}{d(1/T)} \tag{5.10}$$

Repeating this procedure for various values of α, the effective activation energy E_a and $\ln\{g(\alpha)/A\}$ values corresponding to that different α can be obtained. In this method, the calculation of E_a is performed from the results of the isothermal

calorimetric conversion versus cure time data (figure 5.1) for the isothermal curing temperatures of 30°C,40°C,50°C,60°C,70°C and 80°C, using only the values of α at times below the onset of vitrification. At 30°C and 80°C, the α_{max} values are 0.8034 and 0.98 respectively. So, for the employed range of temperature, vitrification takes place roughly at calorimetric conversion higher than 0.80, and equation (5.9) may not be applied because of the diffusion control kinetics.

The plots of $\ln t$ versus $\dfrac{1}{T}$ for various values of α (α =0.1, 0.2, 0.3, ...,0.8, 0.9) in the experimental range illustrated in figure 5.10, shows a linear temperature dependence, indicating a good fit to the experimental data based on equation (5.9). The effective activation energy E_a and $\ln\{g(\alpha)/A\}$ values are obtained for each value of α from figure 5.10 by measuring the slope of the straight line fit of the data and the intercept as shown in equation (5.9).
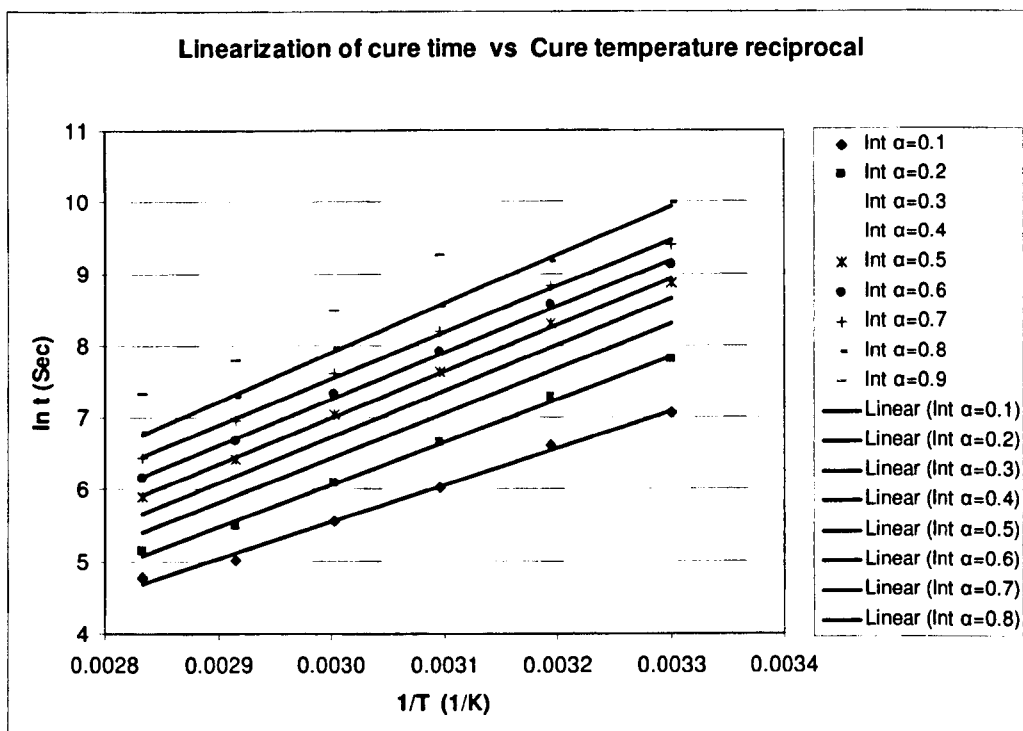
Figure 5.10 Linearization of the iso-conversional plots (Integral Method) of logarithm cure time as a function of the reciprocal of the absolute cure temperature--- from which the effective activation energies are obtained at different degrees of conversion.

The corresponding equation of the linear expression of figure 5.10 for each value of α is presented in the table 5.4 along with its correlation co-efficient and calculated E_a value (in kJ/mol).The $\ln\{g(\alpha)/A\}$ value (in / Sec) is the value of the intercept (c) of the equation which is directly obtainable. An average value of the effective activation energy, $E_{a(average)}$ = **52.35 kJ/mol** calculated in the range of conversion (α) of $0.2 \leq \alpha \leq 0.7$ (for optimum reliability) is also indicated in table 5.4. These effective activation energy E_a and $\ln\{g(\alpha)/A\}$ values are plotted in figure 5.11 (a,b) as a function of conversion.

Table 5.4 The effective activation energy (E_a) values for isothermal cure process of Araldite 2015 obtained from the iso-conversional analysis — equation (5.9) (Integral Method).

α	Linear expression of figure-5.10 $y = (slope = E_a/R) x + c$	R^2 *	E_a (kJ/mol)
0.1	y = 5146.030 x − 9.8923	0.9948	42.7865
0.2	y = 5898.837 x − 11.621	0.9974	49.0457
0.3	y = 6212.765 x − 12.202	0.9984	51.6558
0.4	y = 6368.074 x − 12.374	0.9984	52.9471
0.5	y = 6429.228 x − 12.292	0.9983	53.4556
0.6	y = 6434.244 x − 12.046	0.9982	53.4973
0.7	y = 6432.954 x − 11.762	0.9984	53.4866
0.8	y = 6805.667 x − 12.520	0.9987	56.5855
0.9	y = 7356.8705 x − 13.578	0.9918	61.1684

$E_{a(average)}$ ** $|_{\alpha=0.2-0.7}$ = **52.35 KJ/mol**

* Linear regression squared correlation co-efficient (i.e. co-efficient of determination).

** An average value of the effective activation energy calculated in the range of conversion (α) of $0.2 \leq \alpha \leq 0.7$.
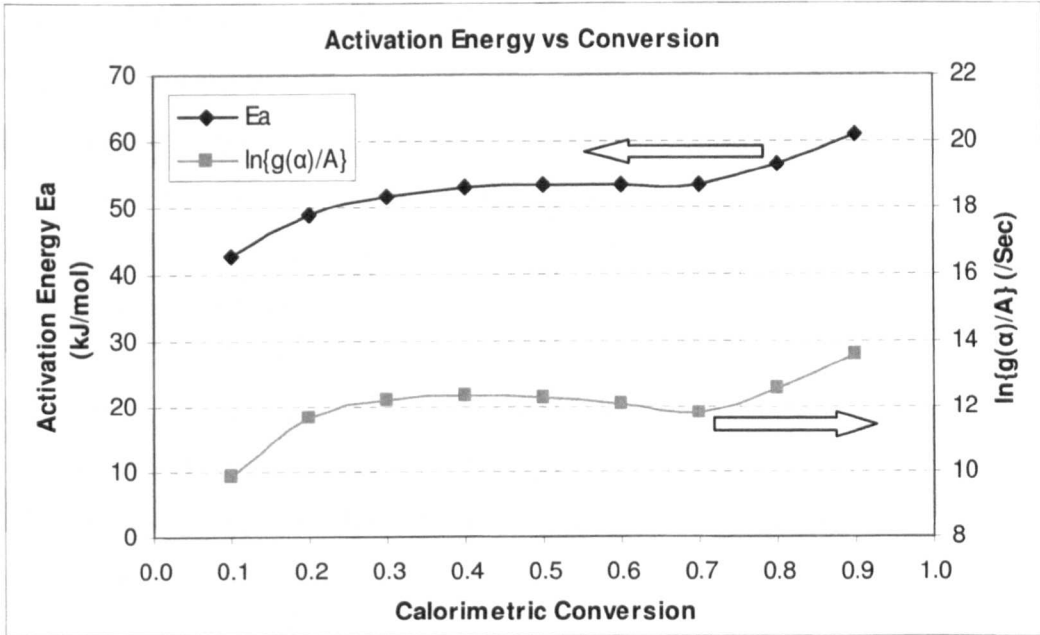
(a)
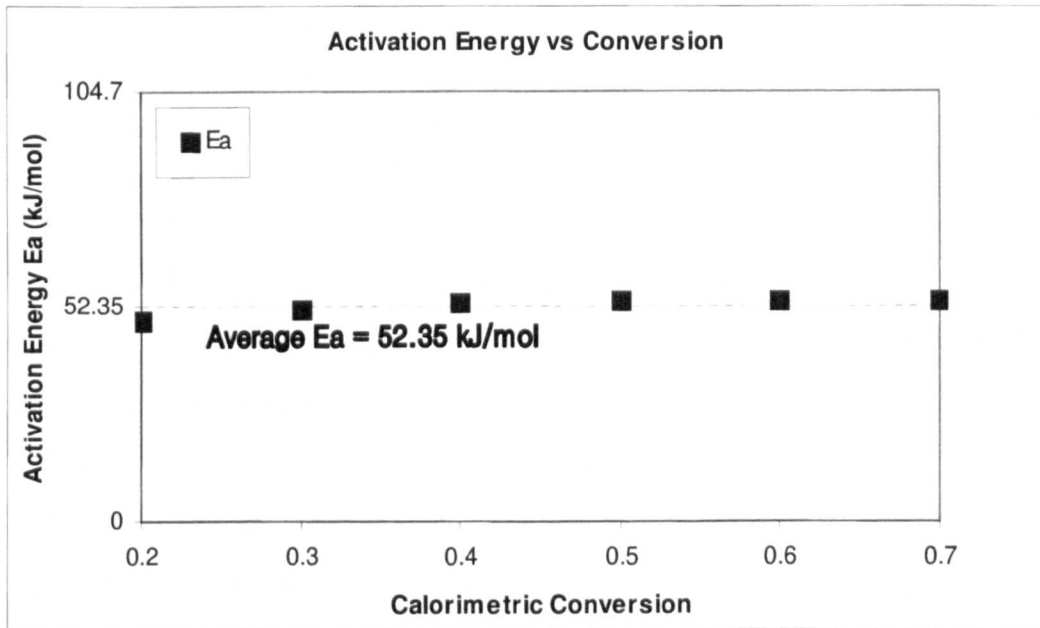
(b)

Figure 5.11 (a,b) The effective activation energy E_a and product $\ln\{g(\alpha)/A\}$, obtained from the iso-conversional analysis (Integral Method), as a function of conversion. The broken line in figure **(b)** corresponds to an average value of the effective activation energy, $E_{a(average)}$ **= 52.35 kJ/mol** calculated in the range of conversion (α) of $0.2 \leq \alpha \leq 0.7$.

Figure 5.11 (a,b) illustrates the variation of effective activation energy E_a and $\ln\{g(\alpha)/A\}$ values with the calorimetric conversion. As can be seen from the figure, and associated table 5.4, at low conversions, α =0.1—0.2, the value of effective activation energy E_a, found by the iso-conversional analysis (Integral Method) applied to the isothermal DSC data of our studied thermosetting system Araldite 2015, gradually increases to reach a plateau or constant with an average value $E_{a(average)}$ = **52.35 kJ/mol** from α =0.2 —0.7. This average value of the effective activation energy, $E_{a(average)}$ = **52.35 kJ/mol**, calculated in the chemical controlled reaction regime in the range of conversion (α) of $0.2 \leq \alpha \leq 0.7$ (for optimum reliability), is shown by the broken line in figure 5.11 (b). For higher α values ($\alpha >$ 0.7) especially near the end of cure, an increase in the activation energy E_a is noticed. Therefore, the values of activation energy E_a as a function of conversion show an almost *constant* value in the range of conversion (α) of $0.2 \leq \alpha \leq 0.7$, deviating from this at very low or very high conversions, similarly to data found for the cure of epoxy [30] and other polymer systems [15, 34]. It is evident from the figure 5.11 (a) that the plot of the product of $\ln\{g(\alpha)/A\}$ appears to vary almost similarly to the activation energy with the calorimetric conversion showing a plateau in the range of conversion (α) of $0.2 \leq \alpha \leq 0.7$.

Almost similar trend of the above mentioned variation of effective activation energy E_a and the product of $\ln\{A \times f(\alpha)\}$ on α has also been observed in the previously described Differential Method section of iso-conversional analysis. In that section, these observed features of---(i) almost constant effective activation energy E_a value (very slight variation of E_a) in the conversion range of $0.2 \leq \alpha \leq 0.7$, (ii) increased E_a value for higher conversions ($\alpha >$ 0.7) and (iii) like E_a on α dependence, nearly similar pattern of variation of the product of $\ln\{A \times f(\alpha)\}$ on α, have already been explained and discussed details.

However, as evident from figure 5.11(a), the low E_a value at the very beginning of the cure possibly reflects the effect of the catalyst 2,4,6 - tris (dimethylaminomethyl) phenol which is initially present in the system. Basically, at the beginning of the cure,

the increase in the concentration of —OH groups from the external catalyst possibly responsible for the initial decrease in the effective activation energy E_a.

The average value of the effective activation energy $E_{a(average)}$ = **52.35 kJ/mol**, is well compared and very similar to the reported values in the literature obtained for similar epoxy-amine formulations by other researchers [1, 5, 7, 8, 9, 10, 11, 12, 24] as has previously been mentioned with associated systems in table 5.3.

The average E_a value obtained from Integral Method ($E_{a(average)}$ = **52.35 kJ/mol**) is very similar to the average E_a value obtained by Differential Method ($E_{a(average)}$ = **55.50 kJ/mol**) of iso-conversional analysis calculated in the range of conversion (α) of $0.2 \leq \alpha \leq 0.7$. The slight difference between the average effective activation energy $E_{a(average)}$ values obtained by Differential Method and Integral Method of iso-conversional analysis possibly can be attributed to the difference associated with (i.e. variation induced by) the *dependent kinetic variables*, reaction rate $\left(\dfrac{d\alpha}{dt} \right)_\alpha$ and cure time $(t)_\alpha$ in equations (5.3) and (5.9), to reach at same degrees of calorimetric conversion α, in estimating $E_{a,\alpha}$, in the range of conversion (α) of $0.2 \leq \alpha \leq 0.7$ in kinetic controlled regime at the specified different isothermal cure temperatures (30°C,40°C,50°C,60°C,70°C and 80°C) employed in the test. This, in turn, may be due to the uncertainties / errors associated with the experimental determination of α and $\dfrac{d\alpha}{dt}$ values as a function of cure time t at the various isothermal test temperatures.

From tables 5.2 and 5.4 it is evident that the highest difference in the $E_{a,\alpha}$ values obtained by the two methods in the range of conversion (α) of $0.2 \leq \alpha \leq 0.7$ is at α =0.2, and at this conversion, the $E_{a,\alpha}$ values obtained from the Differential Method is 57.93 kJ/mol and from the Integral Method is 49.04 kJ/mol. The higher differences in the $E_{a,\alpha}$ values at lower conversions (α =0.2 and 0.3), probably due to higher experimental uncertainties, eventually plays vital role (i.e. put principal contribution) to introduce the small difference in the average effective activation energy $E_{a(average)}$ values obtained by the two methods.

However, from tables 5.2 and 5.4 it is also evident that the effective activation energy value E_a for various values of α obtained by the Differential Method always gives higher value than that obtained from the Integral Method which eventually results in slightly higher $E_{a(average)}$ value in the range of conversion (α) of $0.2 \leq \alpha \leq 0.7$. This is associated with the higher value of the slope of $\ln\left(\dfrac{d\alpha}{dt}\right)_\alpha$ versus $\dfrac{1}{T}$ in the case of Differential Method (equation(5.4) and figure 5.8) than the slope of $\ln(t)_\alpha$ versus $\dfrac{1}{T}$ in the case of Integral Method(equation(5.10) and figure 5.10), at fixed degrees of conversion α. This, in turn, implies that the reaction rate $\left(\dfrac{d\alpha}{dt}\right)_\alpha$ is *more sensitive to temperature* than the cure or reaction time $(t)_\alpha$ to reach at same degrees of calorimetric conversion α, in estimating $E_{a,\alpha}$.

Summarizing this section, it can be stated that the curing behaviour of our studied epoxy thermosetting system Araldite 2015 in isothermal conditions, is analyzed and discussed details using Differential and Integral Method of iso-conversional analysis based on differential and integral form of general kinetic model respectively. Applying the iso-conversional analysis at the series of isothermal temperatures (30°C,40°C,50°C,60°C,70°Cand80°C) employed in the test, effective activation energy values are obtained as a function of conversion which *readily provides a check of invariance of E_a with respect to* α, which is one of the basic assumptions in kinetic analysis of thermal analysis data. For both methods, the values of effective activation energy E_a as a function of conversion show an almost *constant* value in the range of conversion (α) of $0.2 \leq \alpha \leq 0.7$ in the chemical controlled reaction regime, and thus confirms the usual anticipated outcome of kinetic evaluations for single-step reaction.

So, the values of E_a obtained from iso-conversional analysis are highly reasonable and may have the meaning of the intrinsic activation energy and also fairly consistent with the literature estimates for the activation energies of similar epoxy-amine formulations in both isothermal and non-isothermal conditions as mentioned earlier. Without knowing the exact equation for $f(\alpha)$ in equation (3.3), which may vary during the isothermal curing process, from this method we reliably determined the

effective activation energy values at different degrees of conversion and interpret on the reaction process. As in this analysis we do not consider any specific kinetic model or mechanism, the average value of the effective activation energy $E_{a(average)}$ obtained by this method *contains information from the whole process* (i.e. independent of any mechanism).Therefore, we can use this value in model-fitting method.

5.9 Calorimetric Determination of Gelation (theoretical) and Glass Transition Development (finally attained) During Cure

5.9.1 Calorimetric Determination of Gelation (theoretical)

Gelation is a chemo-rheological event which had discussed before. The gel point of the cure process is closely related to rheological properties. It indicates the beginning of crosslinking for the cure reaction, where the resin system abruptly and irreversibly changes from a viscous liquid to an elastic gel or rubber. In chemically cross-linking system, it can be defined as the instant at which the weight average molecular weight diverges to infinity.

Ideal *molecular* or *microscopic* (theoretical) gelation is the incipient formation of infinite molecules that occurs at a specific conversion and at a corresponding T_g of $_{gel}T_g$ .So, it is an *iso-conversion* event which can be calculated if the chemistry is known. It may be detected as the point at which the reacting resin just becomes insoluble. In contrast, *macroscopic* gelation, related with macroscopic consequences of molecular gelation, include a rapid approach toward infinite viscosity and development of elastic properties not present in the pregel resin. Macroscopic means to approximate gelation include the time to reach a specific viscosity. So, it is an *iso-viscous* event. The gel time can be determined according to different criteria from the rheology or viscometric measurement.

According to *Flory's theory of gelation*, the degree of convesion α_{gel} at gel time depends on the functionalities and stoichiometric ratio of the epoxy systems only and is not related to the reaction temperature and other experimental conditions. So, it can be considered as a constant for a given epoxy system regardless the cure temperature $[i.e. \alpha(t_{gel},T) = \alpha_{gel}]$.This theory is based on two main assumptions – firstly, the

reactivity of all functional groups of a certain kind is the same and is independent of molecular size and secondly, there are no intramolecular connections. For epoxy-amine system, the theoretical value of the degree of conversion at the gel point is given by [24]--

$$\alpha_{gel} = \frac{1}{\sqrt{r_m(f_A - 1)(f_E - 1)}}$$ (5.11)

Where, f_A, f_E are respectively the functionalities of amine and epoxy reactants and r_m is their molar or stoichiometric ratio.

In our epoxy (DGEBA/DGEBF) amine (DETA) system which are mixed in stoichiometric ratio mixture i.e. $r_m = 1$, the theoretical functionality of both epoxy resins DGEBA and DGEBF, $f_E = 2$ and the theoretical functionality of Diethylenetriamine (DETA) hardener, $f_A = 5$ as this polyamine possesses five (5) active hydrogens, associated with two primary and one secondary amine, available for crosslinking. Therefore, according to equation (5.11), for our difunctional epoxy resin and pentafunctional aliphatic amine hardener in a stoichiometric ratio mixture, which react in *ideal* conditions, the *theoretical* gel point should achieved at a conversion

$$\alpha_{gel} = \frac{1}{\sqrt{1(5 - 1)(2 - 1)}} = \frac{1}{\sqrt{4}} = \frac{1}{2} = 0.50.$$

It can be mentioned that gelation in condensation systems typically occurs between 50% and 80% conversion (degree of conversion $\alpha = 0.5 - 0.8$).

In an *ideal* case, the same reactivity or *equireactivity* of the hydrogen atoms of the primary and secondary amino groups with epoxide are considered i.e. in absence of the *substitution effect* [35], the *reactivity ratio* $r_k = \frac{k_2}{k_1} = 1$ or, $k_1 = k_2$, where k_1 and k_2 are respectively the reaction rate constants of the primary amine and secondary amine hydrogens, and the gel point depends on this *ideal reactivity ratio*. In this case, the reaction rate constants are related to the hydrogen of the amino group. Basically, the reaction rate constants are related to the molecule and $r_k = \frac{k_2}{k_1} = \frac{1}{2}$ or, $2k_2 = k_1$

i.e. $k_1 > k_2$, in an ideal case, because the primary amino group contains two hydrogen atoms and hence, react about twice as fast as secondary amino group. Indeed, it was shown experimentally and theoretically that gel conversion depends on the magnitude of the *substitution effect* [35]. When the primary amine hydrogens are much more reactive than the secondary amine hydrogens i.e. $k_1 >> k_2$ (which is the usual case), gelation occurs of course at a conversion degree *higher* than that expected when equal reactivity of all amine hydrogens is assumed [35].In reality, the experimental value of the gel point conversion has been found to be greater than the theoretical value. Basically, shift or displacement of critical conversion at gelation from the ideal value (towards higher or lower values) can occur due to various non-ideal reaction conditions i.e. due to the possible difference in reactivity between the same types of functional groups, and the possibility that the curing system may be affected by intramolecular ring formation and other factors.

The critical calorimetric conversion at *theoretical* gelation is calculated from *Flory's theory of gelation* to be *50%* for our diepoxy-triamine stoichiometric ratio mixture system, which react in *ideal* conditions. The DSC measurements of the time to reach the calculated critical conversion of *50%* at the series of isothermal temperatures of 30°C, 40°C, 50°C, 60°C ,70°C and 80°C, employed in the test, are roughly taken as *theoretical gel time* ($t_{gel\ (theoretical)}$) at that specified temperature, obtained from calorimetric study. It is performed from the results of the isothermal calorimetric conversion versus cure time data (figure 5.1) for the isothermal curing temperatures of 30°C,40°C,50°C,60°C,70°C and 80°C and are listed in Table 5.5 along with corresponding activation energy value which will be discussed shortly. It has already been stated that the experimental gel point of the cure process is closely related to rheological properties which can be associated with an *iso-viscous* state. This *theoretical gel time* values do not bear or hold the traditional *rheological or viscometric signature of gelation.* An isothermal viscosity measurement could be used to determine the gel point. Due to limitation of the equipments in our laboratory, this experiment could not be performed at this stage.

The theoretical gel time obtained from calorimetric study as a function of isothermal cure temperature for our studied resin system Araldite 2015 is shown in figure 5.12(a,b). It can be seen from figure 5.12 (a) that the time to gel (*theoretical*) is a

decreasing exponential function with increasing temperature which is in accordance with *Flory's* standard theory of gelation. From figure 5.12(b) it is evident that the logarithm of time to gelation (*theoretical*) is inversely proportional to isothermal cure temperature, which implies the same thing akin to figure 5.12 (a).

Table 5.5 Theoretical gel time ($t_{gel\ (theoretical)}$) at different isothermal cure temperatures obtained from calorimetric study and the corresponding apparent activation energy $E_{a\ gel\ (theoretical)}$ obtained for isothermal cure process of Araldite 2015.

T_{cure} (°C)	30	40	50	60	70	80
$t_{gel\ (theoretical)}$ (min)	117.66	67.10	34.62	19.29	10.14	6.12
$E_{a\ gel\ (theoretical)}$ (kJ/mol)			53.435			
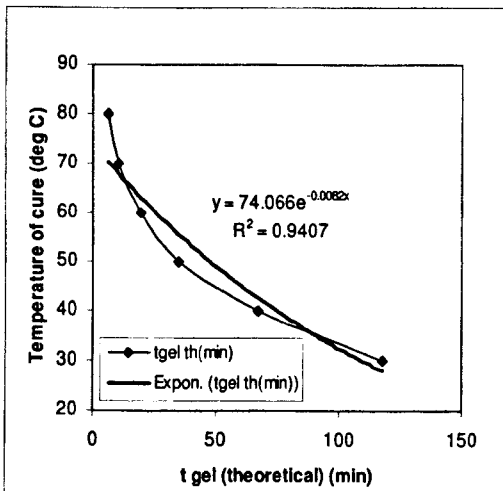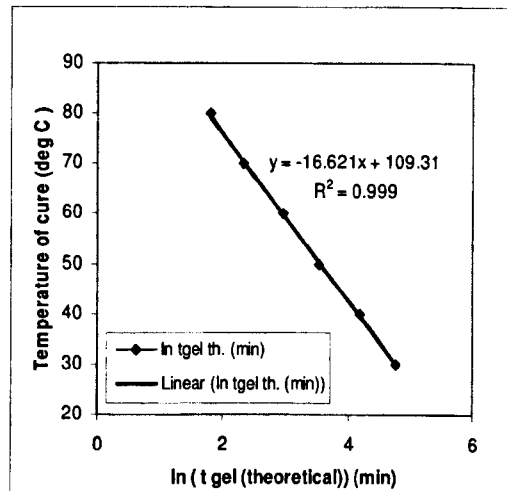
(a)   (b)

Figure 5.12 (a,b) Theoretical gel time obtained from calorimetric study as a function of isothermal cure temperature for isothermal cure process of Araldite 2015.

5.9.1.1 Determination of Activation Energy from Gel time

As the degree of convesion α_{gel} at gel time is a *constant* for a given epoxy system regardless the cure temperature, equation (5.9) can be particularly rewritten for gel

time t_{gel} as —

$$\ln\left(t_{gel}\right) = constant + \frac{E_a}{R} \cdot \frac{1}{T}$$ (5.12)

From equation (5.12), the overall apparent activation energy E_a of the curing process can be calculated from the slope of the curve of $\ln\left(t_{gel}\right)$ *versus* $\frac{1}{T}$.

As we do not have the experimental values of gel time data, according to equation (5.12), the plots of logarithm of *theoretical gel time* ($t_{gel\ (theoretical)}$) values obtained from calorimetric study, listed in Table 5.5, versus the reciprocal of the absolute cure temperature for our studied epoxy system Araldite 2015 is drawn in figure 5.13. It can be seen that a good linear fit of the *theoretical gel time* data allow us to calculate the apparent activation energy from the slope of the straight line which gives a value of the apparent activation energy at the theoretical gel point $E_{a\ gel\ (theoretical)}$ of **53.435 kJ/mol**, which is mentioned in Table 5.5.
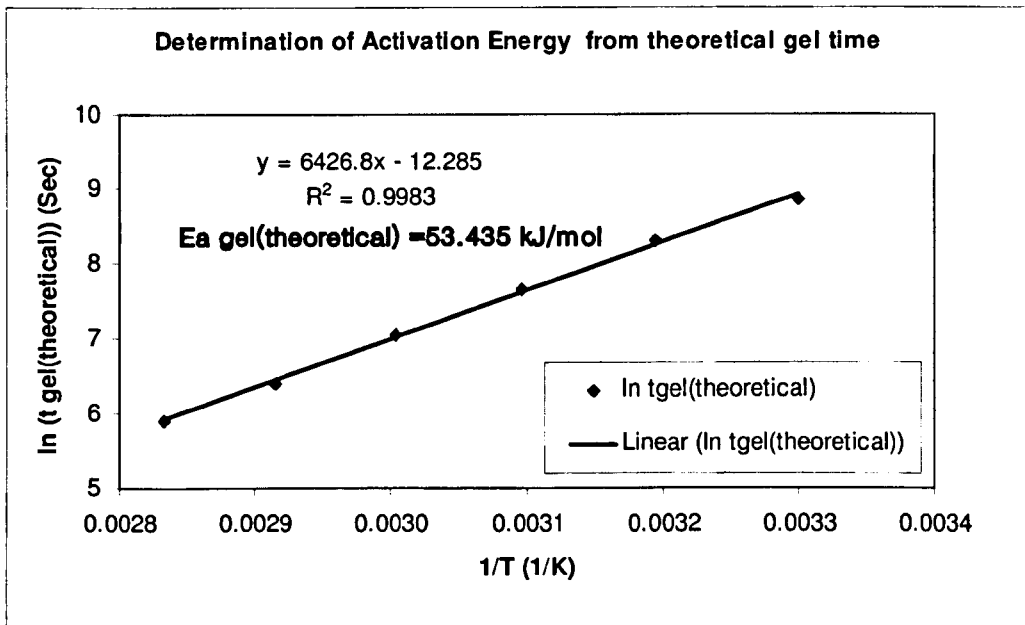
Figure 5.13 Plots of the logarithm of theoretical gel time obtained from calorimetric study as a function of the reciprocal of the absolute cure temperature for isothermal cure process of Araldite 2015.

150

5.9.2 Calorimetric Determination of Glass Transition Development (finally attained) During Cure

As we know, calorimetrically, the glass transition of a thermosetting system is manifested by a discontinuity either on the first derivative of a thermodynamic function such as *enthalpy*, $\dfrac{dH}{dT}$, or on a physical property such as the heat capacity, c_p. This phenomenon occurs over a range of temperature requiring the definition of T_g within that range. In this study, the determination of the finally attained glass transition temperature ($T_{g\ final}$) for the Araldite 2015 samples, previously cured in extended isothermal conditions at specified temperatures, were conducted through dynamic test in the temperature modulated DSC (TMDSC) mode. Here, it can be mentioned that the glass transition temperature determined by DSC is usually called *thermal* or *conventional glass transition*. It is heating rate dependent. The TMDSC allows us to determine the *dynamic glass transition temperature*. It is frequency dependent.

In this study, the experimental T_g was defined as the *inflection point temperature* at the observed step in the reversing heat flux versus temperature curves in the TMDSC plots, instead of the common approach in conventional DSC experiments to define it as the inflection point in the total heat flux versus temperature curves.

In conventional DSC, the measurement of T_g (*thermal* or *conventional glass transition*), which is determined through the change of the heat capacity c_p during reaction, is masked by the superposition of the glass transition signal upon the large exothermal reaction peak or the residual reactivity peak. TMDSC can measure the T_g (*dynamic glass transition temperature*) from the heat capacity directly in a single experiment with *better clear resolution of T_g* as it is able to separate overlapping phenomena and thus eliminate any physical ageing peak even at very slow underlying heating rates [5].

Figure 5.14(a)—(d) illustrates the two approaches of determination of the finally attained glass transition temperature along with residual heat of reaction through dynamic test in the TMDSC mode, at an underlying heating rate of 10°C / min, an

amplitude of 1°C and a period of 60 Sec, across the temperature range from -30°C to 275°C, performed on Araldite 2015 samples, previously cured in extended isothermal conditions where cure finally attained to---(a) 80% conversion at 30°C, (b) 89% conversion at 40°C, (c) 92% conversion at 50°C and (d) 96% conversion at 60°C. From the figure it can be seen that the finally attained T_g corresponding to the respective isothermal curing, appears as an endothermic shift over a limited temperature interval in the TMDSC scan. The T_g values determined in this study as the *inflection point temperature* at the observed step in the reversing heat flux versus temperature curves in the TMDSC plots agree well with the values reported in the data sheet of manufacturer [37].

It can also be seen in figure 5.14(a)—(d) that at the later stages of the cure, when the resin has reached vitrification, the residual reaction exotherm of the remaining reactants starts in the immediate vicinity of the glass transition region. In fact, when the isothermally cured Araldite 2015 epoxy system reaches the vicinity of the glass transition temperature, molecular mobility produces two effects, as evident in the TMDSC thermograms. While the characteristic small peak associated with the glass transition begins to appear, the increased molecular mobility allows the previously frozen (glassy state) reactive system to react again, giving an exothermic signal which reflects the residual reactivity.

In this connection, here, it can be mentioned that the presence of overlapping endothermic peaks in the glass transition region near the exothermic residual reactivity peak attributed to *enthalpic relaxation* or *physical ageing* are often seen in glassy polymers (i.e. the partially cured polymer samples that had vitrified during isothermal cure) as a result of slow cooling through the glass transition region or annealing below T_g [34]. The annealing time and temperature have a large effect on the position and magnitude of these annealing peaks. The presence of these superimposed annealing peaks mask the true T_g values making the measurements difficult and also complicates the determination of the residual heat of reaction causing some inaccuracy in the evaluation of the residual reactivity peak area. However, apart from using TMDSC, which is able to separate overlapping phenomena as has already been mentioned, from an experimental point of view, this so-called *enthalpy relaxation* effect would no longer be observed if the sample were

152
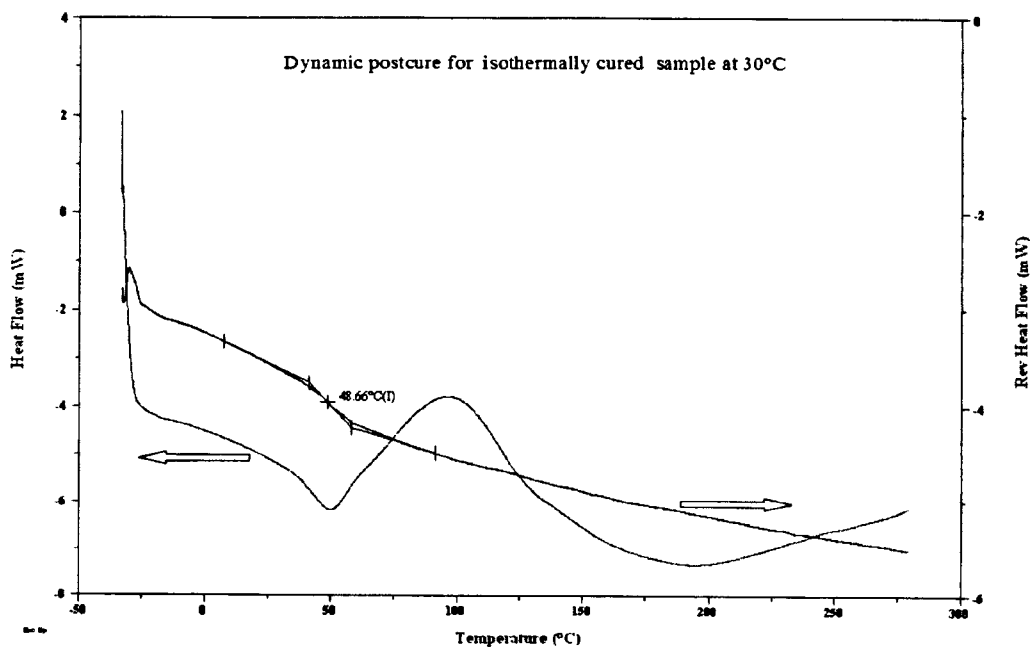
(a)
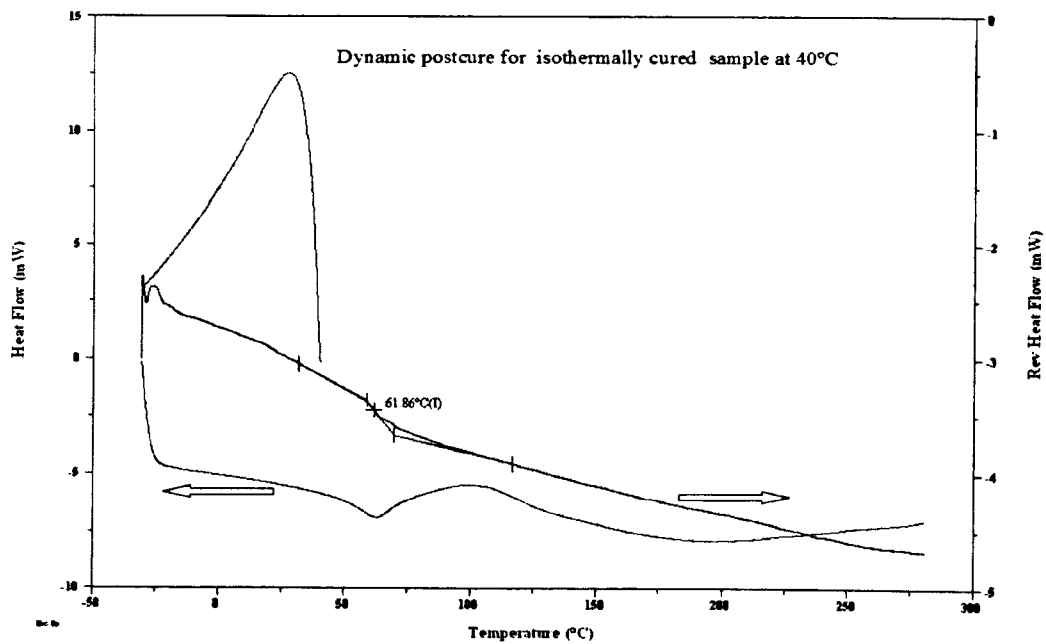
(b)
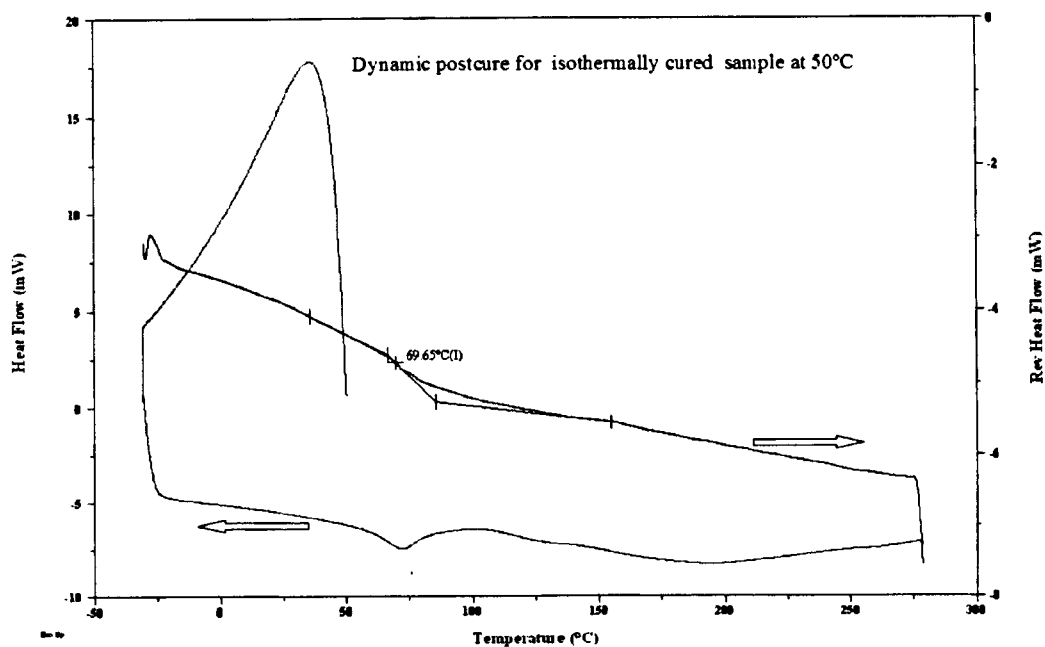
(c)
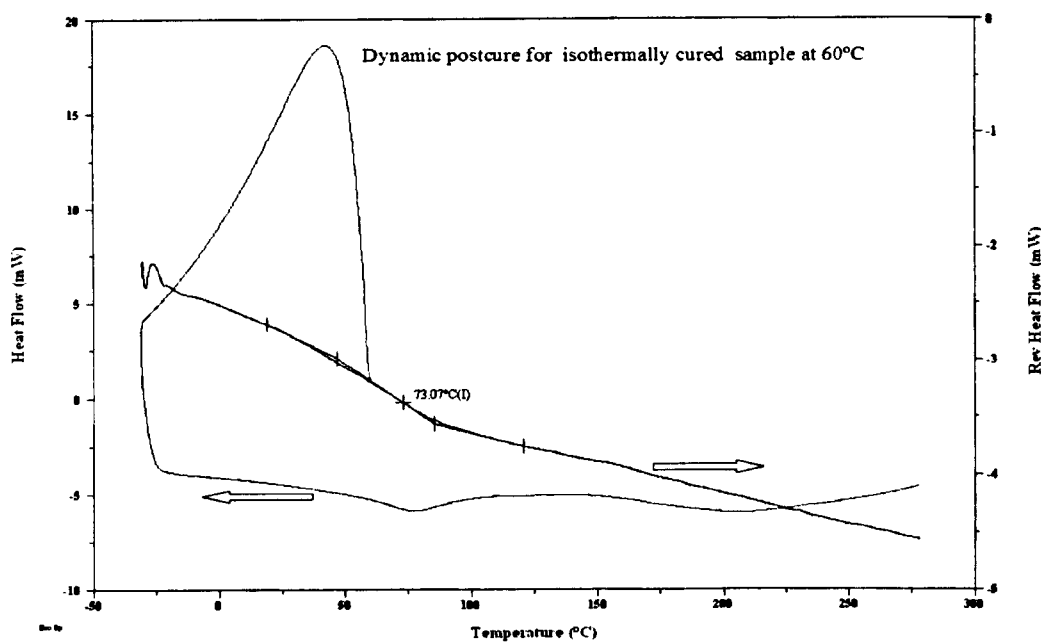
(d)

Figure 5.14 (a)—(d) Two approaches of determination of the attained glass transition temperature along with residual heat of reaction by means of dynamic test in the temperature modulated DSC mode, at an underlying heating rate of 10°C / min, an amplitude of 1°C and a period of 60 Sec, performed on Araldite 2015 samples, previously cured in extended isothermal conditions where cure finally attained to---**(a)** 80% conversion at 30°C, **(b)** 89% conversion at 40°C, **(c)** 92% conversion at 50°C, **(d)** 96% conversion at 60°C.

immediately measured again after cooling. Alternatively, first scanned up the sample to just beyond the ageing peak, then quenched it at a rapid rate and then re-scanned at a heating rate for measurement. It had shown that this procedure did not affect the measured value of T_g by more than 1-2°C [36].

Figure 5.14 (a)—(d) illustrates the two ways to define the glass transition temperature. Both the reversing heat flow and non-reversing heat flow signals are overlaid in respect of temperature. It can be seen that reversing heat flow could determine this transition better because it can override the influences of any exothermic curing reaction that may occur in the vicinity of the glass transition and hence obtain a *clear resolution of the T_g*. Therefore, reversing heat flow can follow the phenomenon at higher temperatures without the latter being hindered. On the other hand, from the non-reversing heat flux versus temperature curves in the TMDSC plots, it can be seen that the finally attained T_g corresponding to the respective isothermal curing, appears as an endothermic shift over a limited temperature interval near the beginning of the exothermic peak of the residual heat of cure. It is evident from the figure that both approaches of determination of T_g almost closely agrees well with each other.

From the curve of the non-reversal heat flow versus the cure temperature, the heat of the exothermal cure reaction can be determined by drawing a base line between the onset and the end point of the peak and integrating the peak curve based on the base line. The value of the integrated area represents the residual heat. Post curing effects are, however, difficult to detect if the degree of cure is much higher, such as, when the degree of conversion is already more than 95% as reflected in figure 5.14 (d). Figure 5.15 shows the determination of finally attained glass transition temperatures corresponding to the respective isothermal curing obtained through reversing heat flux versus temperature curves in the TMDSC mode. The T_g values are listed in Table 5.6 along with corresponding maximum conversion values obtained.

The maximum degree of conversion obtained under several isothermal cure temperatures as a function of corresponding final value of glass transition temperature for our studied resin system is shown in figure 5.16. A *linear relationship* between the maximum degree of conversion and final value of glass transition temperature is observed. So, the T_g *can be thought of as an index of the degree of conversion* for the
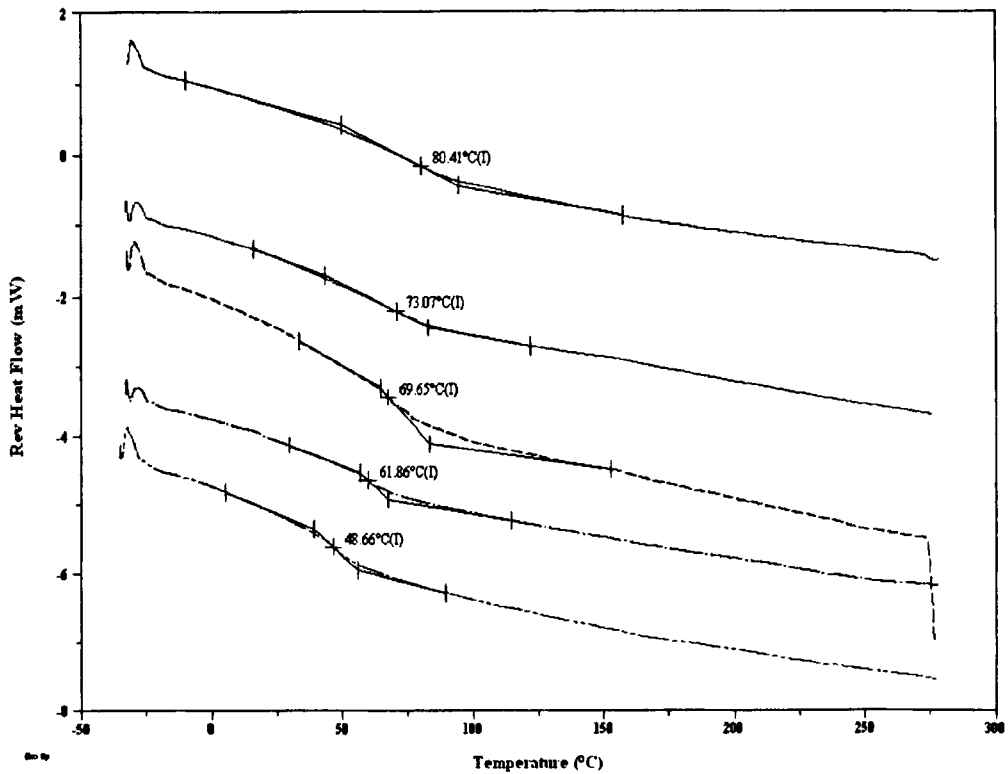
Figure 5.15 Determination of the finally attained glass transition temperature through Reversal heat flow curve as a function of temperature in the temperature modulated DSC mode, at an underlying heating rate of 10°C / min, an amplitude of 1°C and a period of 60 Sec, performed on Araldite 2015 samples, previously cured in extended isothermal conditions at, from bottom to top, 30°C, 40°C, 50°C, 60°C and 70°C, where in all the cases obtained conversions are less than 100% .

Table 5.6 Maximum degree of conversion (α_{max}) and corresponding final value of glass transition temperature ($T_{g\ final}$) obtained in isothermal cure process of Araldite 2015.

T_{cure} (°C)	30	40	50	60	70	80
α_{max}	0.8034	0.893	0.921	0.963	0.975	0.980
$T_{g\ final}$ (°C)	48.66	61.86	69.65	73.07	80.41	

epoxy system. This behaviour resembles the dependence between the maximum degree of conversion as a function of the isothermal cure temperature for a reactive polymer. In fact, it is possible to assume that the value of the T_g reached by the polymeric matrix during the isothermal cure process is of the order of the test temperature. This feature is reflected in figure 5.17, where, an almost a *linear dependence* between the final value of the glass transition temperature and corresponding cure temperature is observed. Basically, it is well known that the curing temperature controls the glass transition temperature of the polymerization material. This occurs because as the glass transition temperature rises during cure, the diffusion rate slows until the reaction becomes diffusion controlled. From figure 5.17 it can be seen that the final glass transition temperatures rise with increasing curing temperature and, in addition, they are always *higher* than the corresponding curing temperature. Table 5.6 shows that in our DETA / DGEBA system at cure temperatures below the T_g of the fully cured material ($T_{g\infty}$), the measured T_g was 18.66°C, 21.86°C, 19.65°C, 13.07°C and 10.41°C above the respective isothermal curing temperature.
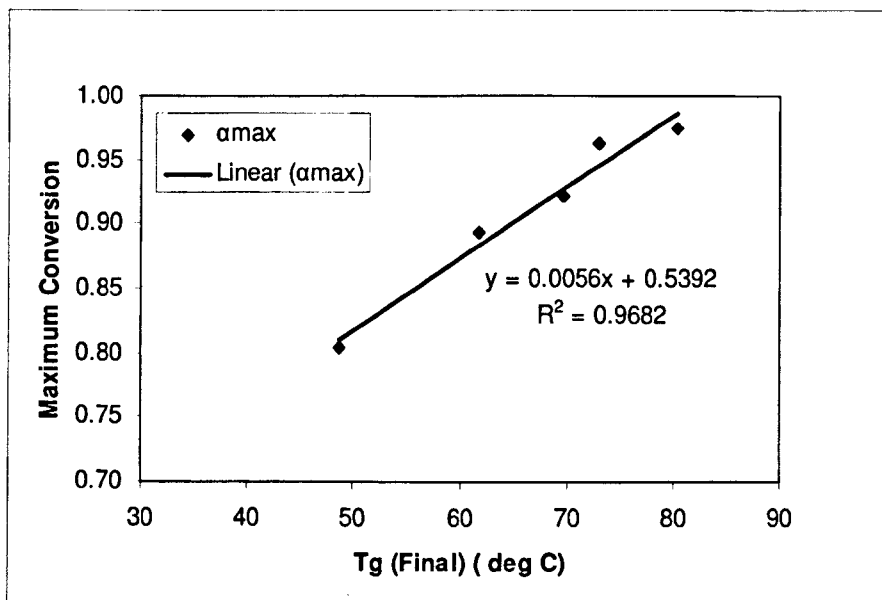
Figure 5.16 Maximum degree of conversion obtained under several isothermal cure temperatures as a function of corresponding final value of glass transition temperature for isothermal cure process of Araldite 2015.
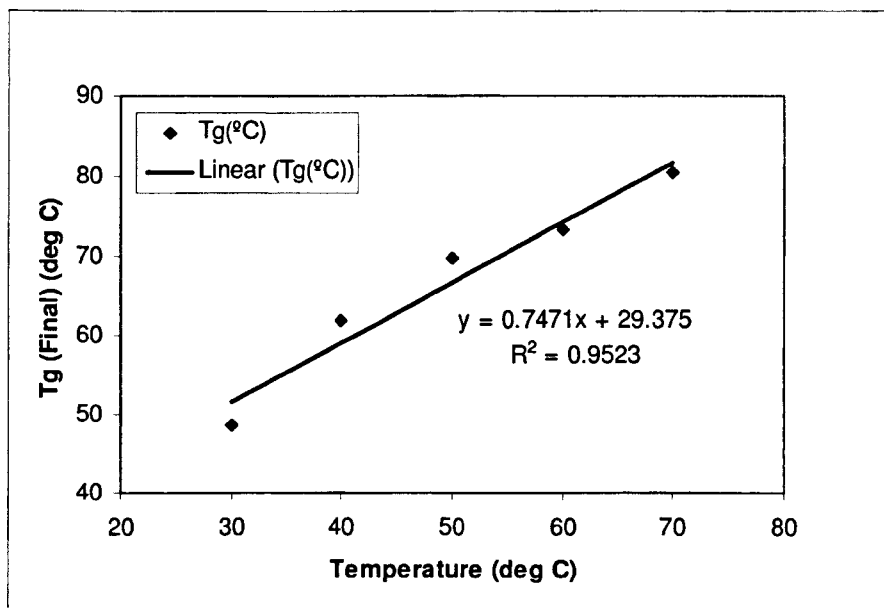
Figure 5.17 Dependence of the values of final glass transition temperatures after isothermal curing at different temperatures on curing temperature for Araldite 2015.

5.10 References

1. Perrin, F.X., Nguyen, T.M.H., Vernet, J.L., Macromol. Chem. Phys., Vol. 208, 2007, 55-67.

2. Gillham, J. K., Polymer Engineering and Science, vol.26, no. 20, 1986, 1429-1433.

3. Gualpa, M.C., Riccardi, C.C., and Vazquez, A., Polymer, vol. 39, no.11, 1998, 2247-2253.

4. Thomas, R., Durix, S., Sinturel, C., Omonov, T., Goossens, S., Groeninckx, G., Moldenaers, P., Thomas, S., Polymer, vol. 48, 2007, 1695-1710.

5. Poljansek, I., Krajnc, M., Acta Chim. Slov., vol.50, 2003, 461-472.

6. Denq, B.L., Hu, Y.S., Chen, L.W., Chiu, W.Y., Wu, T.R., Journal of Applied Polymer Science, vol.74, 1999, 229-237.

7. Montserrat, S., Cima, I., Thermochimica Acta, vol. 330, 1999, 189-200.

8. Montserrat, S., Roman, F., Colomer, P., Polymer, vol. 44, 2003, 101-114.

9. Montserrat, S., Martin, J.G., Journal of Applied Polymer Science, vol.85, 2002, 1263-1276.

10. Verchere, D., Sautereau, H., Pascault, J.P., Riccardi, C.C., Moschiar, S.M., and Williams, R.J.J., Macromolecules, vol.23, 1990, 725-731.

11. Malek, J., Thermochimica Acta, vol. 200, 1992, 257-269.

12. Villanueva, M., Nunez, L., Nunez, M.R., Rial, B., Fraga, L., and Montserrat, S., Journal of Thermal Analysis and Calorimetry, vol.70, 2002, 45-56.

13. Atarsia, A., and Boukhili, R., Polymer Engineering and Science, vol.40, no.3, 2000, 607-620.

14. Teil, H., Page, S.A., Michaud, V., Manson, J.A.E., Journal of Applied Polymer Science, vol.93, 2004, 1774-1787.

15. Mondragon, I., Solar, L., Recalde, I.B., Gomez, C.M., Thermochimica Acta, vol. 417, 2004, 19-26.

16. Lu, M., Shim, M., and Kim, S., Polymer Engineering and Science, vol.39, no.2, 1999, 274-285.

17. Ma, Z.G., and Gao, J.G., Journal of Chemical Research, 2006, 236-239.

18. Farquharson, S., Smith, W., Rose, J., Shaw, M., Journal of Process Analytical Chemistry, 45-53.
19. Smith, I.T., Polymer, vol.2, 1961, 95.

20. Horie, K., Hiura, H., Sawada, M., Mita, I., and Kambe, H., Journal of Polymer Science, part A-1, vol.8, 1970, 1357.

21. Costa, M. L., Pardini, L.C., Rezende, M.C., Materials Research, vol.8, no.1, 2005, 65-70.

22. Han, S., Yoon, H., G., Suh, K. S., Kim, W.G., Moon, T. J., Journal of Polymer Science: Part A: Polymer Chemistry, vol. 37, 1999, 713-720.

23. Leroy, E., Dupuy, J., Maazouz, A., Macromolecular Chemistry and Physics, vol. 202, no.4, 2001, 465-474.

24. Pindinelli, C., Montagna, G., Luprano, V.A.M., and Maffezzoli, A., Macromolecular Symposia, vol. 180, 2002, 73-88.

25. Ivankovic, M., Dzodan, N., Brnardic, I., Mencer, H.J., Journal of Applied Polymer Science, vol. 83, 2002, 2689-2698.

26. Hseih, H.K., Su, C.C., and Woo, E.M., Polymer, vol. 39, no. 11, 1998, 2175-2183.

27. Ryan, M.E., and Dutta, A., Polymer, vol. 20, 1979, 203-206.

28. Mijovic, J., Kim, J., and Slaby, J., Journal of Applied Polymer Science, vol. 29, 1984, 1449-1462.

29. Puglia, D., Valentini, L., Armentano, I., Kenny, J.M., Diamond and Related Materials, vol.12, 2003, 827-832.

30. Montserrat, S., Andreu, G., Cortes, P., Calventus, Y., Colomer, P., Hutchinson, J.M., and Malek, J., Journal of Applied Polymer Science, vol. 61, 1996, 1663-1674.

31. Varley, R. J., Hodgkin, J.H., Hawthorne, D.G., Simon, G.P., McCulloch, D., Polymer, vol. 41, 2000, 3425-3436.

32. Vyazovkin, S., New journal of Chemistry, vol. 24, 2000, 913-917.

33. Vyazovkin, S., and Sbirrazzuoli, N., Macromolecules, vol. 29, 1996, 1867-1873.
34. Kessler, M.R., and White, S.R., Journal of Polymer Science: Part A: Polymer Chemistry, vol. 40, 2002, 2373-2383.

35. Pascault, J.P., and Williams, R.J.J., Journal of Polymer Science: Part B: Polymer Physics, vol. 28, 1990, 85-95.

36. Karkanas, P.I., Partridge, I.K., and Attwood, D., Polymer International, vol.41, 1996, 183-191.

37. http://www.vantico.co.uk.

Chapter 6   Results and Discussions of
Calorimetric Chemical Cure Kinetics Modelling and Process Control

6.1 Modelling of Isothermal Calorimetric Cure Kinetics

6.1.1 Empirical Approach

In chapter 3 the details of kinetic modelling was discussed including the theoretical background. Our aim is to find a model which can *describe the reaction behaviour* of our studied thermosetting resin system as observed by the experimental result of DSC *as well as possible* and permits the prediction of the reaction course. We favour this approach to describe the cure behaviour by a formal-kinetic model as it is, at present, the most flexible, simple and fast solution concerning the fitting of reaction curves. This solution allows valid predictions despite the extreme variety of chemical reaction mechanisms.

As we know, in the case of non-isothermal conditions, where the temperature varies with time, the reaction rate $d\alpha/dt$ is not directly proportional to $f(\alpha)$ in the general form of kinetic model $d\alpha/dt = k(T)f(\alpha)$ as in equation (3.3), as the temperature dependent reaction rate constant $k(T)$ described by the common Arrhenius equation is not constant. But as in our case of isothermal experiments, for each isothermal temperature the value of the rate constant $k(T)$ is a *constant*. Therefore, the numerical solution should be straight forward. All kinetic models can be used to fit the experimental data. Also it is known that the evaluation of our isothermal DSC measurements can allow us the description of the time-dependent cross-linking kinetics.

6.1.2 Basis of Selection of Model

It has already been stated that based on the literature, the possible mechanism of epoxy cured with amine curing agents is as follows—

1. The primary and secondary amines react with epoxy.
2. The hydroxyl groups produced catalyze the reaction.

3. The hydroxyl groups themselves can react with epoxy rings to form ether linkages(*etherification*) and

4. The epoxy ring can undergo *homopolymerization*.

The extent of reaction depends on the reactivity of the amine, reaction temperature, and the ratio of epoxy equivalent mole to amine equivalent mole i.e. stoichiometric ratio of epoxy and amine. The reactions 1 and 2 *occur* under normal curing conditions. The reaction 3 is an etherification reaction which is a competitive side reaction that may occur usually under extreme conditions of high cure temperatures and at the later stages of cure, where the amine functional groups have been depleted. With excess epoxy (non-stoichiometric ratio mixture), etherification reactions can become operational as well [25]. High activation energies are characteristics of this etherification reaction process[33].Additionally, etherification can occur *intermolecularly* to form *crosslinks* or *intramolecularly* to form *cyclic rings (cyclization)*[26].Many studies have been carried out to detect the validity of etherification in the curing of epoxy resins. It is fair to point out that the etherification reaction is not significant for difunctional epoxy systems but plays an important role in the multifunctional epoxy/aromatic amine systems that need to be cured at high temperature typically higher than 150°C [16].

However, as pointed out in literature, the reactions 3 and 4 i.e. the etherification and epoxy homopolymerization reactions *do not occur* at molar stoichiometric conditions of the epoxy/amine mixture (i.e. no excess of epoxy groups) [1,6] and/or, when low curing temperatures typically below 150°C are employed [1,6,16], and when Lewis base (or acid) type catalysts are absent[1].This is especially true for aliphatic amines (such as our case of DETA) cured with DGEBA. In fact, the resin system studied for the present investigation is taken in the stoichiometric ratio and the cure temperature employed is in the range of 30°C—80°C, which is much lower than 150°C. Hence, for our studied resin system the etherification due to epoxy/hydroxyl reaction and the epoxy homopolymerization reaction need not be considered as they have almost no possibility to occur.

As has already been discussed before in chapter 5, from the observation of the isothermal reaction rate profiles of our studied resin system Araldite 2015, based on

the definition, we negated the reaction mechanism based on the simple *nth order kinetics* and logically considered *autocatalytic reaction kinetics* for describing the curing behaviour of our modified epoxy-amine system. As just mentioned in this section, further simplifications in selecting appropriate kinetic model for our epoxy-amine i.e. (DGEBA/DGEBF)-DETA system consist of neglecting *etherification* (including *intramolecular* or *intermolecular etherification*) and epoxy *homopolymerization* reaction. Hence, extended autocatalytic treatment as implemented by few authors [38] for epoxy-amine system cured at high temperature which includes side reactions-- like *etherification, homopolymerization* etc. can be neglected for our case. The autocatalytic reaction mechanism described by equation (3.10) of Kamal as previously had mentioned in chapter 3, which takes only the first two events (i.e. reactions 1 and 2) into account in the epoxy-amine reaction as has mentioned in this section, including non-zero initial reaction rate is, therefore, used in the first instance to analyze the isothermal cure kinetics of our studied epoxy-amine system.

6.1.3 Analysis of the Data by Means of Some Existing Autocatalytic Kinetic Models

6.1.3.1 Kamal Model

As had mentioned before in chapter 3, the autocatalytic model of Kamal for the isothermal cure process as given by equation (3.10), has the following form

$$\frac{d\alpha}{dt} = \left(k_1 + k_2\alpha^m\right)\left(1-\alpha\right)^n$$

This empirical expression implies that the reaction at the beginning is uncatalyzed and/or catalyzed by initial impurity or external catalyst present in the system and has a rate constant of k_1 (*initiation*).Subsequently, the reaction proceeds via autocatalysis by —OH group with a rate constant of k_2 (*autocatalysis*). As the —OH group is formed during the curing reaction, this term is multiplied by the degree of cure α^m (i.e. $k_2\alpha^m$).So, the term $k_2\alpha^m$ in this equation expresses the influence of the reaction

products on the reaction rate. Finally, the reaction becomes slower and eventually stops when α approaches to 1(*inhibition*).

According to this equation, the thermosetting resins behave between *two* extremes. At one extreme, when the concentration of the initial impurity or external catalyst is zero, k_1 becomes zero (i.e. $k_1 = 0$) and the cure would be *autocatalyzed*, exhibiting an induction time. At the other extreme, where $k_1 >> k_2\alpha^m$, curing would behave according to *nth order* kinetics, with the maximum rate at $t = 0$.Therefore, this equation combines both *nth order* and *autocatalytic* reaction kinetics.

Our studied commercial structural epoxy system relevant to practical applications is complicated and contains two mixtures of epoxy monomers, triamine hardener, catalyst, filler and reactive diluent modifier. In spite of complexity of our epoxy thermosetting system, the use of phenomenological models to describe the chemical reaction kinetics of our practical curing system can still be useful in providing *empirical parameters for modelling and controlling the curing process*. By taking into account the autocatalytic equation *empirically* (i.e. by treating m and n as variables or freely optimizing parameters and thus the value of ($m+n$) being allowed to float without any constraints on them) rather than *mechanistically* based (where $m+n = 3$; as in the case of Horie model [20] for stoichiometric ratio mixture of resin and hardener), or implementing *constraints of common convention* of $m+n = 2$ which have widely been used, the researchers found the curing kinetic model to provide a very convenient way to describe the overall curing behaviour of commercial thermal-cure epoxy thermosets. These descriptions are useful for curing cycle modification and optimization.

As this equation (3.10) of Kamal is non-linear in nature, the parameters cannot be estimated directly. To estimate the kinetic parameters of this equation for isothermal cure process of our studied thermosetting system Araldite 2015 as observed from isothermal kinetics data, we have chosen the most widely used non-linear regression analysis based on least-square method. It is most convenient due to its simplicity, relative ease, reasonable accuracy and efficiency. Several other methods for the estimation of kinetic parameters are also have mentioned in chapter 3.

During the process of non-linear regressions, the sum of the squares of the deviations between the theoretical values (i.e. model predictions) and the experimental values, which is called χ^2, decreases and the parameters change. The regression stops when χ^2 converges to a minimum value. Basically, this method minimizes the sum of the squares of the *vertical distances* between the experimental data points and the curve and finds the values of those parameters that generate the curve that comes closest to the data. The parameters thus obtained achieve the best values for the model. The best fit values of the parameters must make scientific sense (i.e. scientifically reasonable) in the light of the range of the data. The sum of squares is a measure of goodness-of-fit in non-linear regression analysis.

Ordinary least squares (OLS) = $\sum_{i} [(\text{experimental data}) - (\text{model prediction})]_i^2$ (6.1)

For successful convergence of a non-linear regression model, the selection of initial values for the parameters of the model and ranges of the experimental data is very important. Initial estimates should always be scientifically realistic and reasonable for the physical phenomena (in our case, the isothermal curing of thermosetting resin) that are being described.

To obtain an initial estimates of the four parameters (k_1, k_2, m, n) of the autocatalytic kinetic model of Kamal as in equation (3.10), we first simplify the model by linearizing it and then used the multiple linear regression option to determine the parameter values that can then be used as the initial estimates for the non-linear regression.

At first, the reaction rate constant k_1 was calculated from the initial reaction rate at time $t = 0$, given by the intercept of the reaction rate profiles in figure 5.3 and 5.4.

$$\left(\frac{d\alpha}{dt} \right)_{t=0} = k_1 \qquad (6.2)$$

Equation (3.10) can be re-written in the following forms which can be applied to the multiple linear regression model :

165

$$\ln(d\alpha/dt) = \ln(k_1 + k_2\alpha^m) + n\ln(1-\alpha) \qquad (6.3)$$

$$\{((d\alpha/dt)/(1-\alpha)^n) - k_1\} = k_2\alpha^m \qquad (6.4)$$

$$\ln\{((d\alpha/dt)/(1-\alpha)^n) - k_1\} = \ln k_2 + m\ln\alpha \qquad (6.5)$$

$$\ln\{(d\alpha/dt)/(k_1 + k_2\alpha^m)\} = n\ln(1-\alpha) \qquad (6.6)$$

At first observation the reaction order n was determined from the slope of a plot of $\ln(d\alpha/dt)$ versus $\ln(1-\alpha)$, as predicted in equation (6.3).Then, using previously computed k_1 and n values, the reaction order m and the reaction rate constant k_2 was determined respectively from the slope and the intercept of a plot of $\ln\{((d\alpha/dt)/(1-\alpha)^n) - k_1\}$ versus $\ln\alpha$, as predicted in equation (6.5). Here, it can be mentioned that to obtain more precise values, an iterative procedure can be applied aided with computer codes. If k_1, k_2, and m values are given, the new value of n can be determined from equation (6.6). The same iterative procedure can be repeated until apparent convergence of m and n values.

The preliminary kinetic parameters thus obtained on the first trial were used as the initial values for the non-linear regression analysis software and the curve fitting procedure was carried out simultaneously using the results of all the six isothermal runs which had performed at 30°C, 40°C,50°C, 60°C, 70°C and 80°C . We employed **SPSS 14.0.1** software to do non-linear least squares curve fitting to the experimental data. Using this statistical software, non-linear regression analysis which is basically a statistical method, was performed based on well known *Levenberg-Marquardt algorithm* (used in SPSS for unconstrained model) and *Sequential Quadratic Programming algorithm* (used in SPSS for constrained and unconstrained models) as well. Both algorithms gave same results in every case.

For the Kamal autocatalytic model as given by the semi-empirical equation (3.10), when the isothermal reaction rate data were fit as a function of conversion this approach gave reasonably good fits to the experimental data over the entire range of

conversions α at all of the six isothermal temperatures employed in the test. The comparisons of experimental data with model predictions are illustrated in the figure 6.1(a − f).

However, in order to achieve these fits *it was necessary to assume negative values for the rate constant k_1 (!)* at higher temperatures of 70°C and 80°C as it is evident by the variation in sign of best fit values of k_1 at 70°C and 80°C. Also, the best fit values for the rate constant k_2 did not show any discernible trend with temperature though the obtained values of $k_2 >> k_1$. Hence, the Arrhenius-type of relationship or trend with temperature was not observed for the best fit k_2 values. The values of m and n varied significantly with temperature having values in a broad range. Basically, our studied resin system Araldite 2015 is a complex commercial mixture containing DGEBA and DGEBF— these two epoxies, 1,4 Butane diol diglycidyl ether (BDGE) epoxy reactive diluent modifier, DETA hardener, *mica* which usually used in epoxy system as *filler*, as well as 2,4,6 - tris (dimethylaminomethyl) phenol — an external catalyst. As a result, the isothermal curves of $d\alpha/dt$ versus α do not clearly show the maximum typical of an autocatalytic reaction, which equation (3.10) was designed to represent.

In this connection, here, it is interesting to mention that the occurrence of *negative values of reaction rate constant k_1* and k_2 has been reported in literature [39, 38] as best fit values when fitting the isothermal experimental data of commercial thermosetting epoxy product with empirical kinetic models as a function of temperature. As for example, during characterizing the calorimetric and rheological behaviour of three commercial thermosetting prepreg epoxies (Hexcel 3501-6, Bryte BT250E-1 and Newport NC301) Hargis et al [39] have mentioned the incidence of *variation in sign of rate constant k_1 (!) as a function of temperature* while fitting the DSC isothermal experimental data for $d\alpha/dt$ versus α with autocatalytic model of Kamal as given by the equation (3.10) which is similar to our case. Cole et al [38] have reported in their research giving reference to the work of Springer et al that *negative values of rate constant k_2 (!)* were obtained on fitting the DSC experimental data of commercial thermosetting epoxy product (Hercules 3501-6) with the autocatalytic model of Horie et al [20] as a function of temperature. The autocatalytic model of Horie will be used later on to analyze our data.
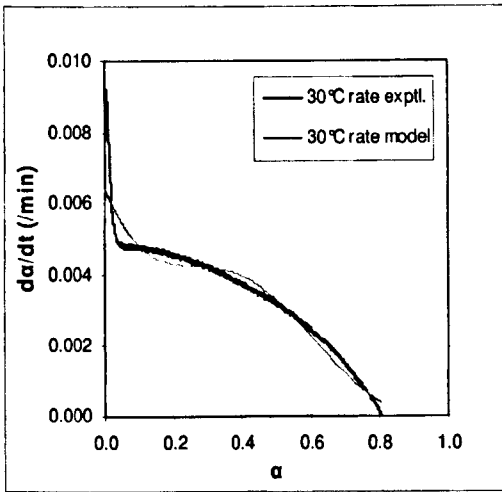
(a) 30°C **(b) 40°C**
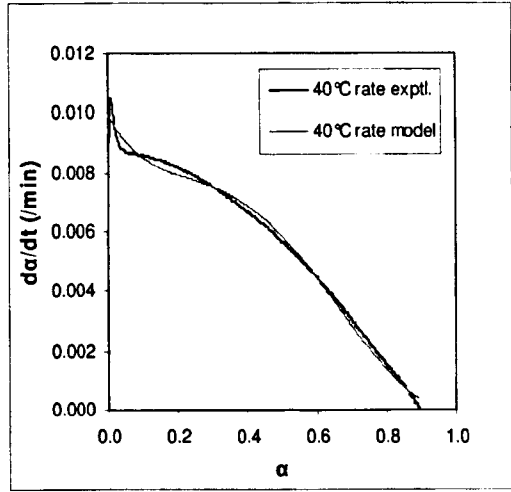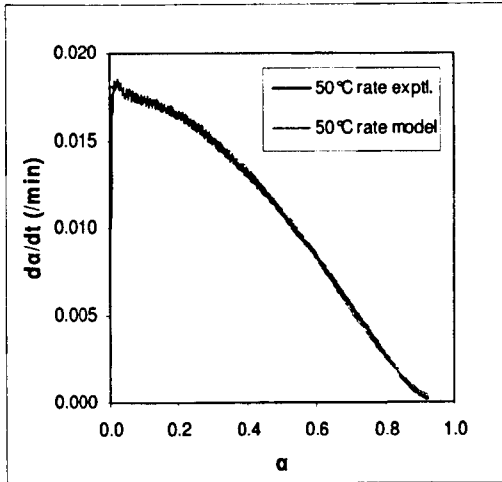
(c) 50°C **(d) 60°C**
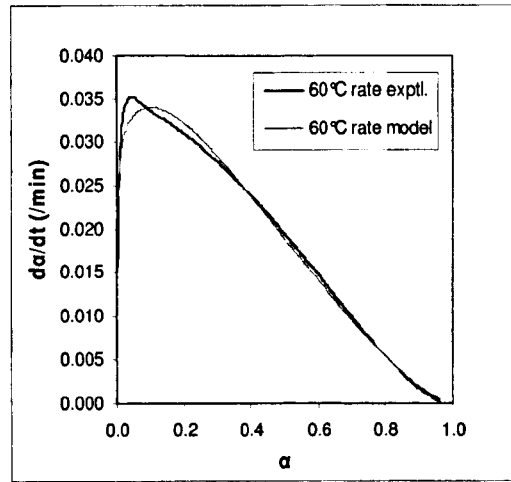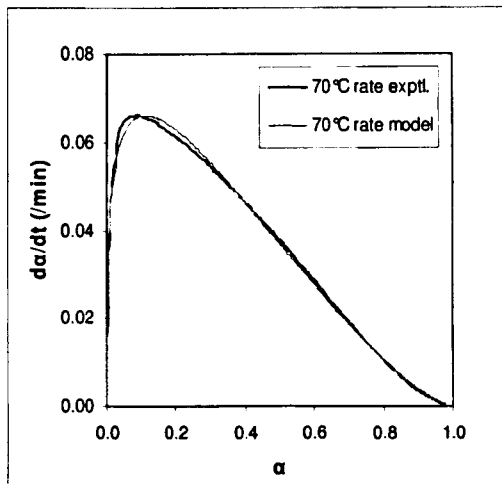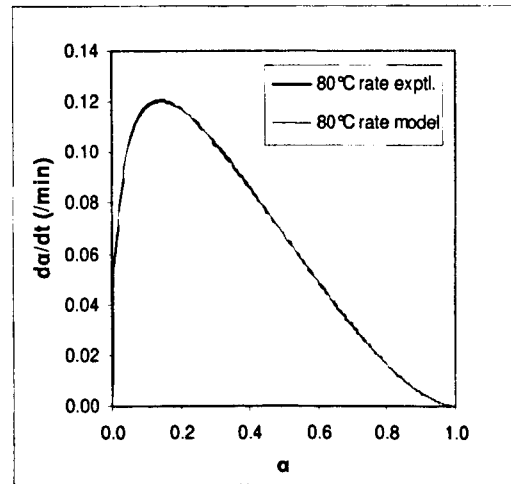
(e) 70°C **(f) 80°C**

Figure 6.1 (a—f) Isothermal reaction rates as a function of conversion — comparisons of experimental data with the predictions of Kamal model $d\alpha/dt = \left(k_1 + k_2\alpha^m\right)\left(1 - \alpha\right)^n$ at cure temperatures of :(a) 30°C, (b) 40°C, (c) 50°C, (d) 60°C, (e) 70°C and (f) 80°C.

From the figure 6.1(a – f) it can be seen that when the isothermal reaction rate data were fit as a function of conversion with the autocatalytic model of Kamal as given by the equation (3.10), this approach gave reasonably good fits to the experimental data over the entire range of conversions at all of the six isothermal temperatures employed in the test. However, as has mentioned, k_1 varied in sign and hence fitting k_1 as a function of temperature was not possible.

6.2 Kamal Model (where α_{max} was used instead of complete conversion 1)

In chapter 3, the methods associated with the modifications for diffusion-controlled kinetics have discussed. The modelling methodologies stated there to describe the final stages of cure are categorized into two generic groups — (i) methodologies that utilize the Rabinowitch model for serial reactions and (ii) methodologies that use maximum attained conversion expressions.

As has mentioned in the second methodology, instead of complete conversion 1, incorporating the empirical term α_{max} in equation (3.10) we get —

$$\frac{d\alpha}{dt} = \left(k_1 + k_2 \alpha^m\right)\left(\alpha_{\mathrm{max}} - \alpha\right)^n \tag{6.7}$$

Where, α_{max} is the maximum conversion value reached at a specific isothermal curing temperature after an extended ("infinite") isothermal cure (i.e. $\alpha_{\mathrm{max}(t=\infty)}$) compared with usual cure schedules used for that thermosetting system. *It is not treated as a fitting parameter.*

When the isothermal reaction rate data of our studied thermosetting system were fit as a function of conversion, this approach, as represented by equation (6.7), gave reasonably good fits to the experimental data over the entire range of conversions α at all of the six isothermal temperatures similar to the case before. However, in order to obtain these fits again *it was necessary to assume negative values for the rate constant k_1(!)* at higher temperatures of 60°C, 70°C and 80°C. Also, the best fit values for the rate constant k_2 did not show any discernible trend with temperature though the

obtained values of $k_2 \gg k_1$. As k_1 varied in sign fitting k_1 as a function of temperature was not possible. Therefore, k_1 was set to zero.

6.3 Kamal Model (where α_{max} was used instead of full conversion 1 and k_1 set to 0)

Setting k_1 to 0 and denoting k_2 as k equation (6.7) becomes

$$\frac{d\alpha}{dt} = k\alpha^m (\alpha_{max} - \alpha)^n \tag{6.8}$$

This modified autocatalytic reaction rate expression in equation (6.8) *accounts for partial conversion, through including the empirical term* α_{max}, taking into account the incomplete cure when the cure process occurs at isothermal temperatures lower than the glass transition temperature of the completely cured system $(T_{g\infty})$. As the term α_{max} does not allow fractional conversion to exceed the degree of cure associated with vitrification at the specific isothermal temperature, therefore, equation (6.8) results in lower reaction rates denoting the end of the reaction as the material approaches vitrification, thus satisfying any diffusion limitations in the cure kinetics. Here it can be mentioned that in practice the cure of epoxy resins is performed at a temperature lower than the glass transition temperature of the completely cured system $(T_{g\infty})$ because of processing constraints [14].

The selection of this model is logical, as at all the investigated isothermal temperatures α_{max} obtained for our system is lower than 1, and, as the reactive diluent reactions and the epoxy - amine reactions enter in the propagation of the chain cross linking, which has already been mentioned in chapter 5. In addition, the experimental data shows a rapid acceleration of the cure rate as illustrated in figure 5.4, which agrees with the kinetic model in equation (6.8).

Most of the attempts to incorporate the diffusion limitations into the kinetic model, under both mechanistic and phenomenological approaches, adopt empirical expressions based on the development of the glass transition temperature during cure.

Modelling methodology based on the maximum conversion values, $\alpha_{max}(T)$, that thermosetting material can attain at a specific temperature T, is used here, in this model in equation (6.8), in order to take into account the limitations that vitrification imposes on the cure kinetics. It has the advantage that *no prior knowledge of a T_g model is needed*. Therefore, this approach minimizes the experimental effort usually required for the incorporation of a T_g submodel.

In our present study, considering the total value of the heat of reaction determined from dynamic heating scan which took the reaction to full conversion, the maximum conversion value α_{max} for Araldite 2015 at each isothermal curing temperature was determined after an extended ("infinite") isothermal cure (i.e. $\alpha_{max(t=\infty)}$) compared with usual cure schedules used for this thermosetting system. It can be mentioned here that for modelling purposes, it is adequate to consider the total value of the heat of reaction determined in dynamic tests to be of the same order (or closely equal) as the value obtained from the sum of isothermal and residual reactivity tests. Therefore, this amount of heat can be considered an intrinsic property for the curing reaction of the thermosetting system studied, and is independent of the heating mode. However, in general, some probability of inaccuracy can be associated with these values due to two different effects. The first one can be associated with the sum of integration errors of two different peaks — isothermal exothermic peak and residual reactivity peak. The second one can be associated with the superposition of the glass transition signal upon the residual reactivity peak which can cause a greater inaccuracy in the evaluation of the peak area. Implementing the temperature modulated DSC (TMDSC) mode, as had employed in our study, this second problem can be eliminated, which has discussed details in chapter 5.

6.3.1 Expression of Maximum Obtainable Conversion α_{max} (T)

For modelling purposes it is convenient to determine the behaviour of α_{max} as a function of the isothermal test temperature. So, the model represented by equation (6.8) requires the incorporation of a relation connecting the maximum fractional conversion α_{max} to the curing temperature.

The expression of $\alpha_{max}(T)$ is derived by plotting the maximum conversion values obtained isothermally versus the curing temperature as shown in figure 6.2 and *it is not treated as a fitting parameter*. As has mentioned before this term is incorporated into the model equation instead of unity to denote the end of the reaction attributed to vitrification.

In figure 6.2 two temperature regions are denoted. In each of the regions, the experimentally determined α_{max} exhibits a linear temperature dependency. A Least square linear regression was applied to the two linear segments of the curve observed at the low and high curing temperature ranges respectively, while the transition from the one segment to the other was achieved by implementing the *Cumulative Normal Distribution Function*, expressed as the NORMDIST function of Microsoft Excel.
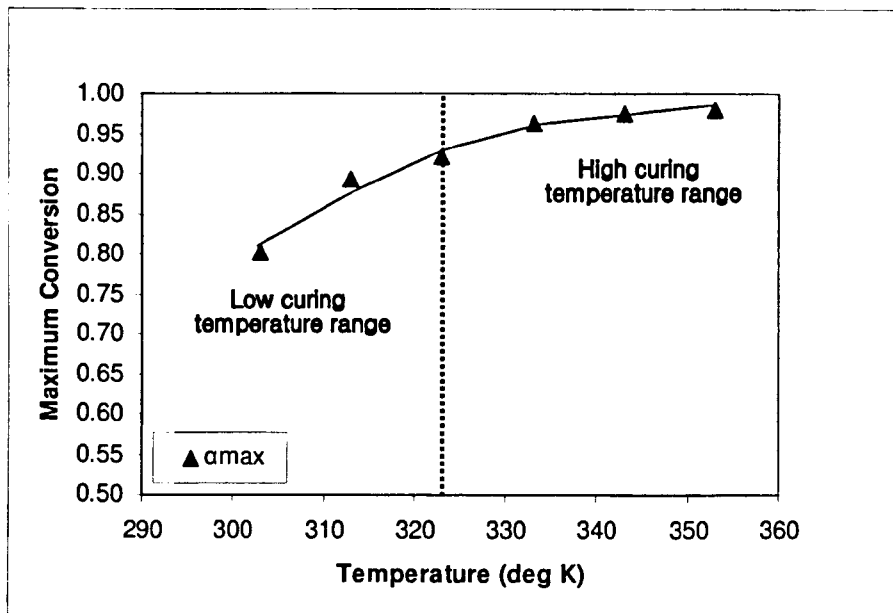
Figure 6.2 The maximum attained calorimetric conversion values for the case of Araldite 2015 cure under isothermal heating conditions as a function of the relevant isothermal cure temperature. The mathematical representation of α_{max} is shown as a line.

The normal distribution is a continuous probability distribution whose shape is determined by its mean and standard deviation. **NORMDIST(x, a, s, c)** function of

Microsoft Excel with the TRUE or 1 option in the last argument (i.e. in *c*) returns the normal cumulative probability distribution for a given sample value for the specified arithmetic mean and standard deviation. Here —

x – is the numeric value for which we want the distribution.

a – is the arithmetic mean of the distribution. It is numeric.

s – is the standard deviation of the distribution. It is numeric and must be greater than 0 (i.e. requirement is $s > 0$).

c – is a logical value that determines the form of the function.

(i) If cumulative is set to TRUE or 1(which is the most generally used case), NORMDIST returns the *Cumulative Normal Distribution Function, F(x,a,s)* given by the following equation

$$F(x,a,s) = NORMDIST(x,a,s,1(orTRUE)) = \frac{1}{\sqrt{2\pi}s} \int_{-\infty}^{x} \exp\left\{-\frac{(x-a)^2}{2s^2}\right\} dx \qquad (6.9)$$

So, for $c = 1$; the NORMDIST function returns the cumulative probability that the observed value of a Normal random variable with mean *a* and standard deviation *s* will be less than or equal to *x* (i.e. $\leq x$).This simply means that NORMDIST returns the proportion of the distribution that is less than or equal to an observed value, with the specified mean and standard deviation. The probability that a value that is less than or equal to *x* (i.e. $\leq x$) will occur (i.e. cumulative probability up to *x*) is the area under the familiar bell-shaped Normal probability density curve to the left of *x* (-∞, *x*). If $a = 0$, $s = 1$, and $c = 1$, NORMDIST returns the *Standard Normal Distribution*, NORMSDIST (*z*), where $z = (x - a)/s$.

(ii) If cumulative is set to FALSE or 0, NORMDIST returns the individual probability that *x* will occur according to the *Probability Density Function* or *Probability Mass function, f (x,a,s)* given by the following well known equation

$$f(x,a,s) = NORMDIST(x,a,s,0(orFALSE)) = \frac{1}{\sqrt{2\pi}s} \exp\left\{-\frac{(x-a)^2}{2s^2}\right\} \qquad (6.10)$$

So, for $c = 0$; the NORMDIST function returns to the height of the familiar bell-shaped probability density curve where the probability is distributed with the total area under the whole curve = 1, as every individual is represented in the graph. As already has mentioned that the probability that a value that is less than or equal to x (i.e. $\leq x$) will occur (also called cumulative probability up to x) is the area under this curve to the left of x; therefore, the probability that the value of a normal random variable that is greater than x (i.e. $> x$) will occur will be $= (1 - F(x,a,s))$ $= (1 - NORMDIST(x,a,s,1))$; which is the area under this curve to the right of x, and represents the tail probability of the Normal Gaussian distribution.

The *Cumulative Normal Distribution Function* takes values ranging from 0 to 1 depending on the proximity of the function values to the specified mean value. We can go back and forth between individual probabilities distribution. In our case, temperature was used to provide the function values, $x = T$, and the mean value of the distribution was taken as 323°K.The constructed normal distribution function acts as a temperature dependent weight factor for the transition from the one linear relationship to the other.

For our studied resin system Araldite 2015, the isothermal kinetics data provide information about the maximum attained conversion for temperatures up to 353°K where $\alpha_{max} = 0.98$. A normal distribution function is applied to ensure the continuity of the α_{max} expression during the transition from the low curing temperature range to the high curing temperature range as illustrated in figure 6.2.

Use of the constructed normal distribution function as a temperature dependent weighting factor for the transition from the one linear relationship to the other leads to the final form of the α_{max} equation which can be expressed as follows—

$$\alpha_{max} = (1 - NORMDIST(T,323,8.5,1))(59 \times 10^{-4}T - 0.968) +$$
$$+ NORMDIST(T,323,8.5,1)(9 \times 10^{-4}T + 0.6811) \qquad (6.11)$$

Equation (6.11) is represented as line in figure 6.2 which shows the plots of the maximum conversion values obtained isothermally versus the curing temperature for

our studied thermosetting system Araldite 2015.This expression of α_{max} in equation (6.11) is derived following the procedure and relevant statistical considerations from the work of Samaras et al [40].

It has already been mentioned in chapter 5 that for our studied thermosetting system Araldite 2015 —

(i) A *linear relationship* between the maximum degree of conversion, α_{max} and corresponding final value of glass transition temperature is observed, obtained under relevant isothermal cure temperatures (figure 5.16).

(ii) The final value of the glass transition temperatures are always *higher* than the corresponding isothermal curing temperature and rise with increasing curing temperature almost in a *linear* fashion (figure 5.17). Basically, the curing temperature controls the glass transition temperature of the polymerization material during cure because as the glass transition temperature rises, the diffusion rate slows until the reaction becomes diffusion controlled.

These above mentioned characteristics are generally reflected in the dependence between the maximum degree of conversion, α_{max} as a function of the isothermal cure temperature, T for our studied thermosetting system as shown in figure 6.2 and expressed by equation (6.11).

Here, it can be mentioned that the dependence of T_g on the degree of conversion can be correlated by the Di Benedetto equation. This equation gives the relation between the vitrification temperature and the maximum attained degree of conversion of the form —

$$\alpha_{max}(T) = \left\{ \frac{T_{go}T_{g\infty}}{(T_{go}-T_{g\infty})} \right\}\left(\frac{1}{T}\right) + \left\{ \frac{T_{g\infty}}{(T_{g\infty}-T_{go})} \right\} \quad \text{when } T < T_{g\infty} \qquad (6.12)$$

$$\alpha_{max} = 1 \qquad\qquad \text{when } T \geq T_{g\infty} \qquad (6.13)$$

Where, T is the isothermal curing temperature. T_{go} denotes the glass transition temperature of the unreacted material when $\alpha_{max} = 0$ and $T_{g\infty}$ is the glass transition temperature of the completely cured resin when $\alpha_{max} = 1$.

Some researchers, like Gonzalez et al [41], have been used this Di Benedetto's equation for the purpose of incorporation of a relation connecting the maximum conversion to the cure temperature. However, in our case, considering that the diffusion control phenomenon is certainly governed by vitrification but could not correspond exactly to the analysis of the Di Benedetto's equation, we prefer to use the expression as in equation (6.11) to express the empirical dependence of α_{max} with T; where two simple linear temperature dependencies observed at low and high curing temperature ranges respectively, are made continuous by implementing constructed *Cumulative Normal Distribution Function*, expressed as the NORMDIST function of Microsoft Excel, which acts as a temperature dependent weighting factor for the transition from the one linear relationship to the other.

6.3.2 Estimation of Kinetic Model Parameters for Curing Reaction

To obtain an initial estimates of the three parameters (k , m , n) of the modified autocatalytic kinetic model of Kamal as in equation (6.8), we first simplify the conventional autocatalytic model (i.e. without incorporating α_{max} instead of 1) $d\alpha/dt = k\alpha^m (1 - \alpha)^n$ as in equation (3.9) by linearizing it and then used the multiple linear regression option to determine the parameter values that can then be used as the initial estimates for the non-linear regression.

Equation (3.9) can be applied to the multiple linear regression model in the following forms:

$$\ln(d\alpha/dt) = \ln(k\alpha^m) + n\ln(1 - \alpha) \tag{6.14}$$

$$\{(d\alpha/dt)/(1 - \alpha)^n\} = k\alpha^m \tag{6.15}$$

$$\ln\left\{(d\alpha/dt)/(1-\alpha)^n\right\} = \ln k + m\ln\alpha \qquad\qquad (6.16)$$

$$\ln\left\{(d\alpha/dt)/(k\alpha^m)\right\} = n\ln(1-\alpha) \qquad\qquad (6.17)$$

At first observation the reaction order n was determined from the slope of a plot of $\ln(d\alpha/dt)$ versus $\ln(1-\alpha)$, as predicted in equation (6.14).Then, using this computed n value, the reaction order m and the reaction rate constant k was determined respectively from the slope and the intercept of a plot of $\ln\left\{(d\alpha/dt)/(1-\alpha)^n\right\}$ versus $\ln\alpha$, as predicted in equation (6.16). Here, it can be mentioned that to obtain more precise values, an iterative procedure can be applied aided with computer codes. If k and m values are given, the new value of n can be determined from equation (6.17). The same iterative procedure can be repeated until apparent convergence of m and n values. The preliminary kinetic parameters thus obtained on the first trial were used as the initial values for the non-linear regression analysis software.

It can be noted that this model represented by equation (6.8) generally requires the use of an initial conversion (seed) to be numerically solved; whose size may be of importance, depending on the rate of the reaction. (It may shift the curve of α-t on the time scale).This initial conversion (seed at time = 0 e.g. 10^{-4}) is basically needed to produce changes in the fitting parameters obtained from the non-linear regression analysis.

The values of the best fit kinetic parameters determined from the non-linear regression analysis based on the autocatalytic kinetic model $\dfrac{d\alpha}{dt} = k\alpha^m (\alpha_{max} - \alpha)^n$ as in equation (6.8) for isothermal cure process of Araldite 2015 are listed in table 6.1, together with the corresponding standard errors (SE) and the squared correlation co-efficient (i.e. co-efficient of determination) for fit of model to the experimental data. Figures 6.3 (a—f) and 6.4 (a—f) illustrate the comparisons of experimental values of the isothermal reaction rates with the reaction rate curves calculated according to the predictions of autocatalytic kinetic model in equation (6.8), as a function of conversion and cure time respectively, at cure temperatures of — (a) 30°C, (b) 40°C,

(c) 50°C, (d) 60°C, (e) 70°C and (f) 80°C.

The results in the isothermal reaction rate – conversion and reaction rate – cure time plots of figure 6.3 (a—f) and figure 6.4 (a—f) respectively, show that the scientifically reasonable values of the best fit kinetic parameters based on the autocatalytic kinetic model in equation (6.8), simulate the isothermal curing experimental data of the studied commercial thermosetting system Araldite 2015 with a *reasonable degree of satisfaction*, in the range of conversion degree between 0.1 and 1.0 , at all of the six different isothermal temperatures employed in the test covering the temperature range of 30°C to 80°C, considered as a whole process map for the system.

However, at the early stages of the cure at lower conversions (on average, at $\alpha = 0 - 0.1$), near the non-typical accelerated autocatalytic peak regions, the data of the model predictions slightly deviate from that of the experimental. As we know that the experimental uncertainties are large for the initial isothermal data in this lower conversion range of $\alpha = 0 - 0.1$ (discussed in chapter 5), in view of this limitation, the agreement between the data of experimental as well as model predictions shown in figure 6.3 (a—f) and figure 6.4 (a—f) can be considered reasonable on the whole. Therefore, in spite of the slight deviations at the early stages of the cure at lower conversions (on average, at $\alpha = 0 - 0.1$, which will be discussed later on), the values of the best fit kinetic parameters of the autocatalytic kinetic model in equation (6.8), reasonably simulate the experimental data with satisfactory degree of accuracy which is reflected in the squared correlation co-efficient (i.e. co-efficient of determination) values of curve fitting as are listed in table 6.1. It is important to mention that though *contains less fitting parameters* (only one reaction rate constant) compared with Kamal model representing both *nth* order and autocatalytic reaction; the autocatalytic model with incorporation of α_{max} as in equation (6.8) almost reasonably fitted our experimental data overall. When looking at the simulation of the non-typical autocatalytic reaction rate profiles at lower conversions, this highlights an *important advantage of* DSC. *By giving access to reaction rate this technique enables us to detect complex kinetic behaviour at low conversions that would be almost undetectable by other experimental techniques.*

As mentioned in table 6.1, for this particular model in equation (6.8) an iso-conversional analysis is utilized to find out the activation energy E_a value. We preferred this iso-conversional analysis method as it *readily provides a check for the invariance of activation energy E_a with respect to conversion α* which is one of the basic assumptions in kinetic analysis of thermal analysis data, and hence, highly recommended for the reliable determination of activation energy value, which should contain information from the whole process. As only one apparent reaction rate constant k is used in the model to represent the overall cure process of the system as a single step reaction process, here, our choice of the average value of the effective activation energy E_a obtained from iso-conversional method as the activation energy value for the studied resin system, sounds more reasonable. The advantageous features reflecting the rich potential of iso-conversional analysis has mentioned details in chapter 5.

Equation (6.8) can be linearize in the following logarithmic form —

$$\ln\left(\frac{d\alpha}{dt}\right) = \ln k + m \ln \alpha + n \ln(\alpha_{max} - \alpha) \tag{6.18}$$

By fixing the value of α and letting k as a variable, this equation can be written for a fixed conversion α, as —

$$\ln\left(\frac{d\alpha}{dt}\right)_\alpha = \ln A - \frac{E_{a,\alpha}}{R} \cdot \frac{1}{T} + m \ln \alpha + n \ln(\alpha_{max} - \alpha) = constant - \frac{E_{a,\alpha}}{R} \cdot \frac{1}{T} \tag{6.19}$$

The effective activation energy $E_{a,\alpha}$ at a fixed degree of conversion can be determined from the slope of a plot of $\ln\left(\frac{d\alpha}{dt}\right)_\alpha$ versus $\frac{1}{T}$ values, for a series of isothermal DSC experiments at different temperatures, as predicted in equation (6.19). Repeating this procedure for various values of α, the effective activation energy E_a values corresponding to that different α can be obtained.

Equation (6.19), and equation (5.3) in chapter 5, both have similar general form. Therefore, obtaining effective activation energy $E_{a,\alpha}$ values utilizing iso-conversional analysis for this particular autocatalytic kinetic model in equation (6.8), is exactly

similar in every respect to that based on the conventional differential form of general

kinetic model $\dfrac{d\alpha}{dt} = k(T)f(\alpha)$ which is entitled as Differential Method, discussed

in detail with associated figures 5.8 and 5.9 (a,b) and table 5.2, in chapter 5.

Table 6.1 The values of the kinetic parameters of the Autocatalytic model
$\dfrac{d\alpha}{dt} = k\alpha^m(\alpha_{max} - \alpha)^n$ **for isothermal cure process of Araldite 2015. E_a is the average**
value of activation energy obtained from iso-conversional method.

T_{cure} (°C)	k^* (min^{-1})	m^*	n^*	$m+n$	lnA (min^{-1})	E_a (kJ/mol)	$r^2{}^{**}$
30	0.006(.000)	0.013(.002)	0.620(.003)	0.633	16.911		0.982
40	0.012(.000)	0.054(.001)	0.831(.002)	0.885	16.870		0.997
50	0.029(.000)	0.113(.001)	1.075(.002)	1.188	17.085	55.50	0.997
60	0.055(.000)	0.130(.001)	1.246(.002)	1.376	17.124		0.998
70	0.121(.001)	0.198(.002)	1.368(.004)	1.566	17.312		0.997
80	0.288(.002)	0.313(.002)	1.647(.005)	1.960	17.665		0.998
Average	0.085	0.136	1.131	1.268	17.161		

* Values in parentheses correspond to standard errors (SE).
** Squared correlation co-efficient (i.e. co-efficient of determination) of curve fitting.

As can be seen from table 6.1, the average value of the effective activation energy E_a is 55.50 kJ/mol obtained from iso-conversional analysis for this autocatalytic kinetic model in equation (6.8), calculated in the range of conversion (α) of 0.2 − 0.7, fairly consistent with the literature estimates of activation energy values for similar and comparable epoxy-amine formulations [1, 5, 7, 8, 9, 10, 11, 12, 24] which has mentioned details in table 5.3 in chapter 5.

As seen from table 6.1, the value of the overall reaction order $(m+n)$ is 0.63 and 0.88 at 30°C and 40°C and 1.18 and 1.96 at 50°C and 80°C.Therefore, the value of the

overall reaction order $(m+n)$ approaches to 2 at higher temperature, which has widely been reported in the literature for the isothermal curing kinetics of a variety of epoxy-amine systems [7, 8, 9, 13, 27, 28]. The value of m is 0.01 and 0.05 at 30°C and 40°C and 0.11 and 0.31 at 50°C and 80°C. The value of n is 0.62 and 0.83 at 30°C and 40°C and 1.07 and 1.64 at 50°C and 80°C. Almost similar values of m and n are obtained particularly at 40°C and 80°C, based on the autocatalytic kinetic model $d\alpha/dt = k\alpha^m (1-\alpha)^n$, for the isothermal cure process of stoichiometric ratio mixture epoxy(DGEBA)—amine (aliphatic triamine) system [5,7]. For each of the isothermal temperature the value of the pre-exponential factor / Arrhenius frequency factor, $\ln A$ is calculated using the values of E_a and corresponding k from the well known Arrhenius relation. The values of $\ln A$ listed in table 6.1 are also well in agreement with the values reported in literature for isothermal curing of epoxy-amine systems [5, 6, 7, 8, 9, 36].

6.3.3 Interpretation of the Temperature Dependence of Kinetic Parameters

It is evident from the table 6.1 that the value of k and n increases as the curing (reaction) temperature goes higher. Basically, the reaction rate constant k is a *measure of reaction rate in which the reaction activation energy is contained,* so the change of reaction rate constant also indicates a marked change in the reaction energies. In general, the order of reaction n, according to definition, *indicates the number of atoms, molecules, or reactive groups whose concentrations determine the reaction rate.* The increase in reaction temperature causes a distinct distribution of molecule speeds (and energies) followed by an increase in the average value of energy from reactant molecules. As a consequence, a larger number of molecules have enough energy through collision, to surpass the activation barrier, and consequently, the reaction rate increases.

Mainly, the order of the reaction n is *related to the consumption of epoxy groups.* By the shape of the reaction rate profile curve it (n) *defines the reaction type* as well as the relative contribution of the *"decay"* region of the kinetic process. As the reaction order n increases with increasing curing temperature, this implies that the consumption of epoxides is also increasing with cure temperature.

181

(a) 30°C

(b) 40°C
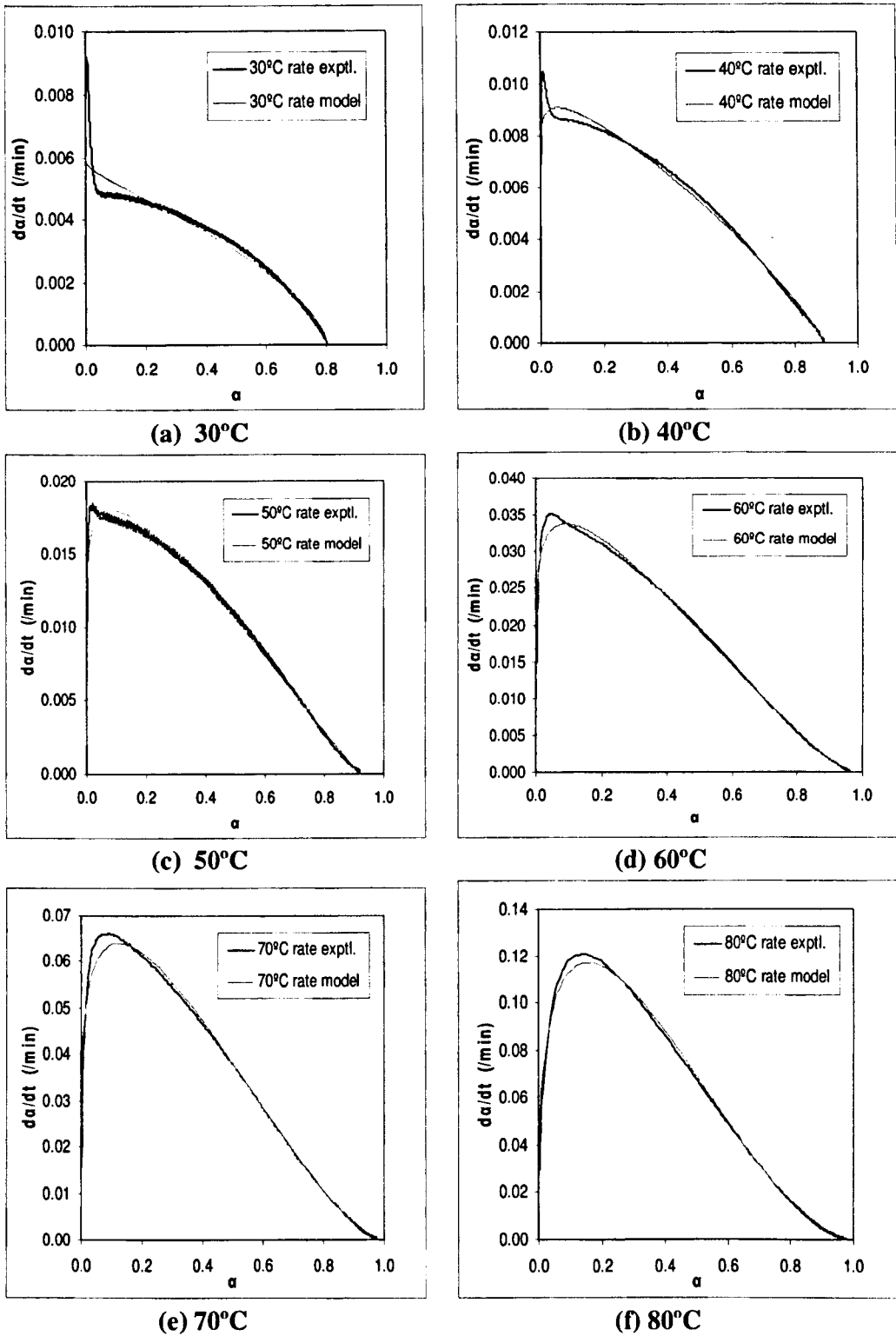
(c) 50°C

(d) 60°C

(e) 70°C

(f) 80°C

Figure 6.3 (a—f) Isothermal reaction rates as a function of conversion — comparisons of experimental data with the predictions of Autocatalytic kinetic model $d\alpha/dt = k\alpha^{m}(\alpha_{max} - \alpha)^{n}$ at cure temperatures of :(a) 30°C, (b) 40°C, (c) 50°C, (d) 60°C, (e) 70°C and (f) 80°C.
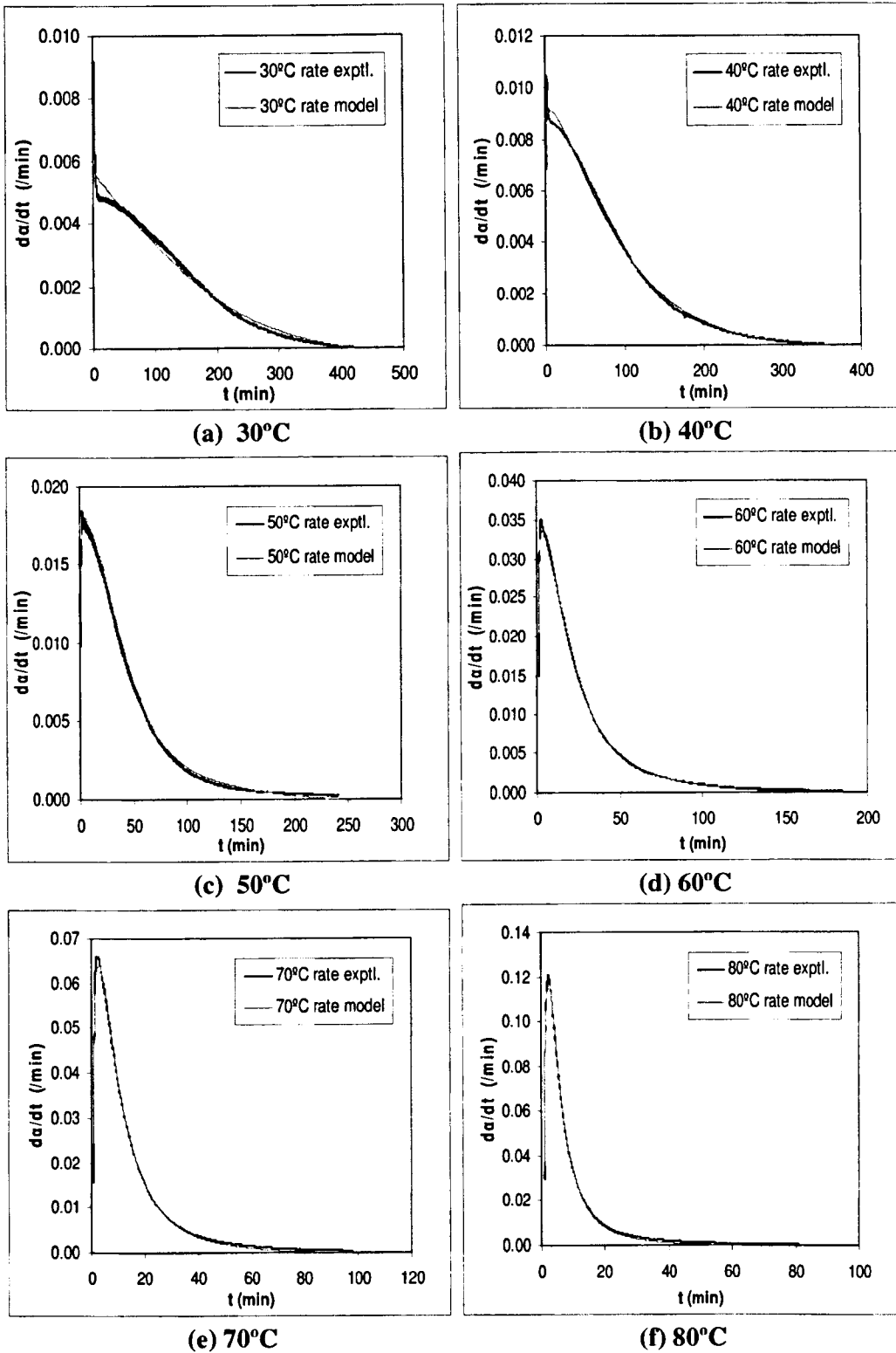
Figure 6.4 (a—f) Isothermal reaction rates as a function of cure time — comparisons of experimental data with the predictions of Autocatalytic kinetic model $d\alpha/dt = k\alpha^m(\alpha_{max} - \alpha)^n$ at cure temperatures of :(a) 30°C, (b) 40°C, (c) 50°C, (d) 60°C, (e) 70°C and (f) 80°C.

It is also seen from table 6.1 that the value of the reaction order *m* increases with increasing cure temperature, *unlike the conventional autocatalytic effect* where *m* decreases with increasing cure temperature. In fact, the order of the reaction *m* *indicates the dimension of autocatalysis contribution to the kinetics*. So, *m* is related to the autocatalytic concentration of the reaction (i.e. the concentration of —OH groups that are being generated as cure proceeds). Basically, in association with the influence of the initial rate of reaction, it (*m*) defines the relative contribution of the *"acceleratory"* region of the kinetic process and also controls the symmetry of the reaction rate profile curve. As *m* increases with increasing cure temperature, it implies that the autocatalytic effect of *m* is found not to be superseded by the effect of the thermal catalysis. As has mentioned, this is, in contrast, to data generally found in the literature for the curing of epoxy resins having conventional autocatalytic effect where *m* decreases with increasing cure temperature [7, 21, 27, 36], which generally suggests that the autocatalytic (epoxy-amine-hydroxyl) contribution decreases at high temperatures due to the difficulty of forming ternary complexes. In connection with the order of the reaction, here, it can be mentioned that a *fractional order* (as can be seen from table 6.1) is suggestive of the fact that what we observe is the overall effect of a sequence of elementary reactions and not of a single elementary reaction step.
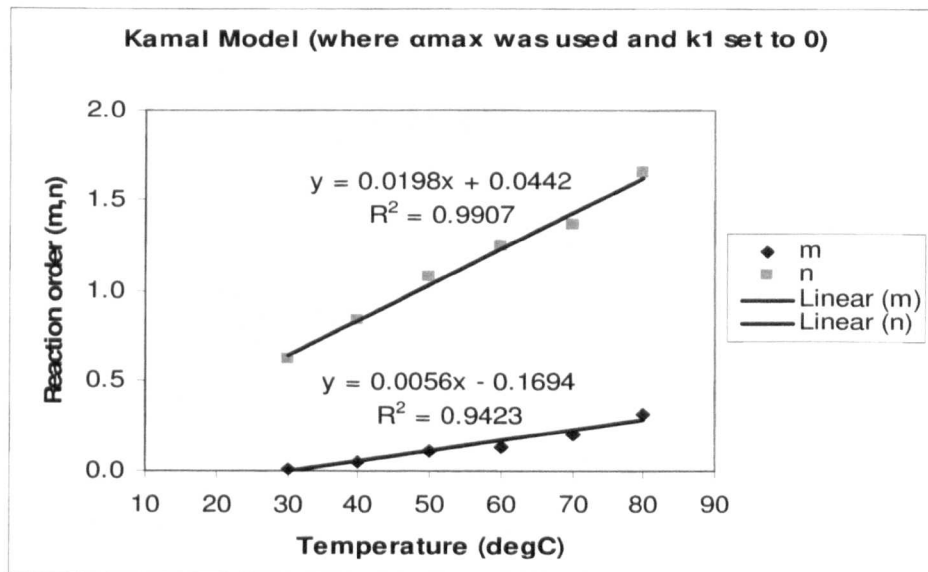
Figure 6.5 The plots showing the effect of the isothermal cure temperature on the reaction orders *m* and *n* with associated fits; based on the Autocatalytic kinetic model $d\alpha/dt = k\alpha^m (\alpha_{max} - \alpha)^n$ for isothermal cure process of Araldite 2015.

The plots of the reaction orders m and n as a function of isothermal cure temperature for the autocatalytic kinetic model in equation (6.8) is shown in figure 6.5. As seen from the figure, both of the cure reaction orders m and n increase with the increase of cure temperature following a linear relation. The corresponding equations of linear regression and their squared correlation co-efficients, R^2 (i.e. co-efficients of determination) are also presented in figure 6.5.

For epoxy-amine systems, the values of the reaction orders m and n have been observed to be temperature dependent [7, 13, 21, 27, 28, 36], exhibiting a linear relation with curing temperature [21, 27, 28, 36].The temperature variation of the reaction orders could be interpreted as an indication that the reaction mechanism in our thermosetting system may changes with temperature when it is isothermally cured at different cure temperatures, or, the temperature variation of the reaction orders m and n is purely empirical.
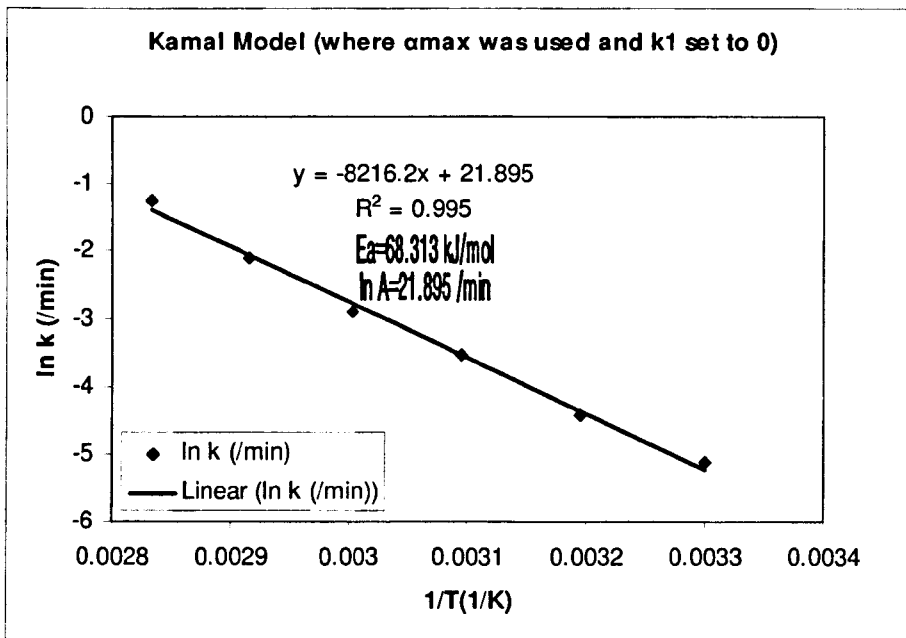
Figure 6.6 The Arrhenius plots of the temperature dependence of the isothermal reaction rate constant k determined from the non-linear regression analysis based on the Autocatalytic kinetic model $d\alpha/dt = k\alpha^m(\alpha_{max} - \alpha)^n$ for isothermal cure process of Araldite 2015.

The logarithmic plots of *ln k* as a function of 1/T is shown in figure 6.6. It is evident from the figure that the reaction rate constant *k* correlates with the reciprocal of the absolute cure temperature according to the classical Arrhenius form. The good fitting linear straight line allow to calculate the apparent activation energy from the slope of the straight line, which is 68.313 kJ/mol, as indicated in the figure.

The activation energy value obtained from iso-conversional analysis differs from that determined from the Arrhenius plots of *ln k* as a function of 1/T; where the isothermal reaction rate constant *k* obtained from fitting of experimental reaction rate data as a function of conversion to the autocatalytic kinetic model in equation (6.8) by means of non-linear regression analysis. As the apparent reaction rate constant *k*, obtained as the best fit parameter value of the kinetic model in equation (6.8) over the entire range of conversions (containing the diffusion control regime also), representing the overall cure process of the system as a single step reaction process, the activation energy value determined from the Arrhenius plots of *ln k* as a function of 1/T, differs from that obtained from the iso-conversional analysis. It can be mentioned that the iso-conversional method employed here for this kinetic model in equation (6.8), *compares the reaction rate to reach the same degree of conversion at different temperatures* to determine the E_a value for that corresponding α and thus find out the E_a value as a function of α . While the determination of E_a value from the Arrhenius plots of isothermal reaction rate constant *k* (in which the reaction activation energy is contained), obtained as the best fit parameter value of the kinetic model in equation (6.8), at different temperatures, generally *considers chemical states of different degrees of conversion.*

6.3.4 Molecular Mechanism of Cure on the Basis of Temperature Dependence of Reaction Orders

As evident from table 6.1, in general, the value of the overall reaction order $(m+n)$ increases with cure temperature. This can be reasonably attributed to the *trimolecular catalysis mechanism* associated with the formation of fairly stable donor-acceptor trimolecular transition state complexes (TSC) consisting of amine, epoxy and hydroxyl groups in the curing reaction of our modified epoxy-amine thermosetting system which will be discussed shortly.

186

Few of the hydroxyl groups in the molecular chain of the epoxy resin participate in the reaction. However, this curing reaction is not the typical catalysis mechanism. *It is favourable for the —OH group in the molecular chain of the epoxy resin to become a proton donor and participate in the reaction with the increasing curing temperature.* The reaction should follow a trimolecular mechanism with the participation of the proton. This is the reason for the increase in the $(m+n)$ values with the increase of the curing temperature as seen in table 6.1. Similar results in the isothermal curing of epoxies are reported elsewhere [17].

It is significant to discuss the general molecular mechanism for curing reaction of DGEBA/amine system and particularly for our studied thermosetting system— DGEBA/DGEBF mixture/catalyzed DETA/BDGE system, in general, in this context.

6.3.4.1 Molecular Mechanism for Curing Reaction

It is a well known fact that the interaction of epoxy compounds with amines and other nucleophiles is considerably promoted by the addition of hydroxyl-containing compounds like water, alcohols, phenols, etc. Here the reaction is supposed to proceed, initially, through a *trimolecular transition state* as Smith [19] has suggested for the reaction of epoxy compounds with amines as shown in figure 6.7.
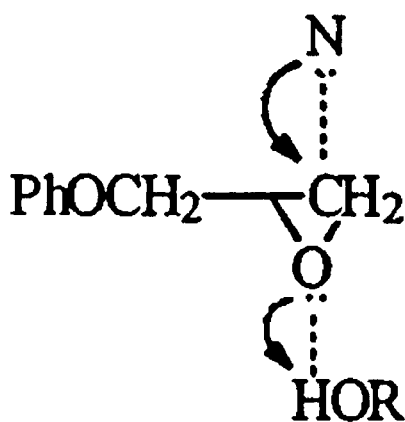
Figure 6.7 Epoxy-amine cure mechanism illustrating the formation of trimolecular transition state complex. Adapted from reference [17].

187

The reaction was found to obey an *nth* order kinetics (discussed before) as the maximum curing reaction rate was observed at $t = 0$ when carried out in the presence of a hydroxyl containing solvent. This is due to the participation of the solvent or proton in the solvent. But the cure kinetics of pure as well as modified epoxy-amine systems in the dry circumstance show a maximum reaction rate at $t > 0$, negating the simple *nth* order kinetics and the autocatalytic kinetics is observed (as in our case), which, under normal temperature and conditions, follows the reactions shown in the figure 6.8, which had discussed details in general in chapter 2.
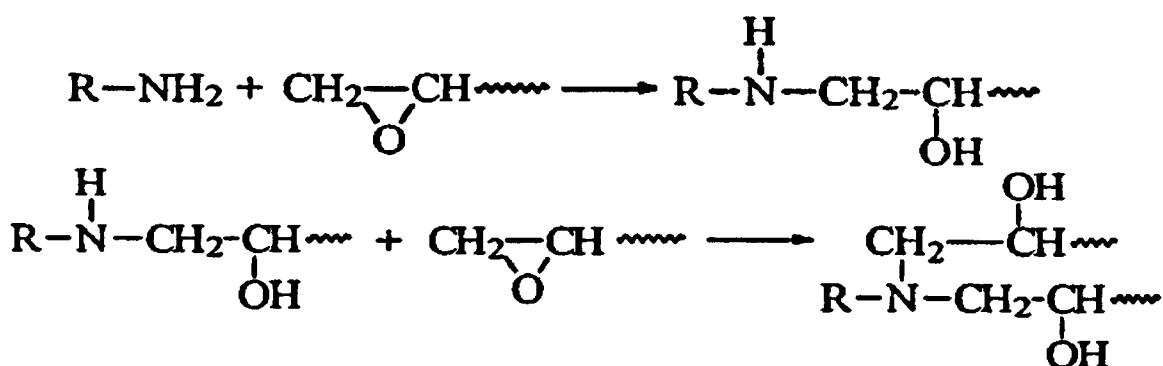
Figure 6.8 Reaction of a primary amine with an epoxy group to form a secondary amine. Reaction of a secondary amine with another epoxy group to form a tertiary amine. Adapted from reference [43].

The primary and secondary amines react with epoxy. The hydroxyl group in the formed chain, produced by the ring opening reaction of epoxide group, can react with epoxide group continually, aided opening of other epoxide ring (through hydrogen bonding in the transition state), and the catalytic hydrogen-bonded transition state complex (TSC) of epoxy can also be formed, which weakens the C—O bonds and facilitate ring opening, thereby accelerate the curing reaction rate. As the hydroxylic molecules formed as a reaction product partly protonate the oxygen atom of the epoxy group, facilitating the epoxide ring-opening reactions by hydrogen bonding in the transition state and thus serve as a catalyst, the process of cure is autocatalytic.

The source of the catalytic hydrogen-bonding species is considered to arise from *two* distinct origins [19,20]. The first source can be any external catalyst or catalytic

hydrogen-donating impurity present in the epoxy (such as moisture existing in the system, acids, Lewis acids, phenols, alcohols, hydroxyl groups in epoxy adducts etc.) while the second catalyst source can be *hydrogen bonding species* formed (e.g. hydroxyl) or depleted (tertiary amine) during the reaction. Thus, the reaction can proceed through impurity catalysis and autocatalysis. Recent studies support the formation of a termolecular intermediate consisting of the amine, the epoxy and the hydroxyl groups [1,18].

$$R_2-NH + CH_2-CH \cdots \longrightarrow R_2-N \cdots CH_2-CH \cdots$$

$$\longrightarrow R_2-N-CH_2-CH + HO-R'$$
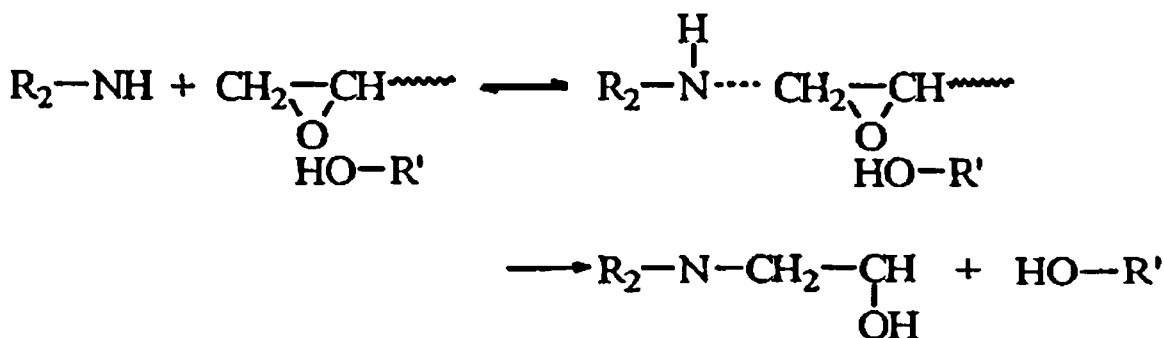
Figure 6.9 Reaction of a secondary amine with an epoxy group to form a tertiary amine through trimolecular catalytic transition state complex. Adapted from reference [43].

In the figure 6.9, HO—R' denotes the catalytic hydrogen bonding species, which are generated (or depleted) in the reaction, or are present, as external catalysts or in impurities.

In our studied commercial epoxy-amine system Araldite 2015, catalyzed triamine (DETA) cured epoxy (DGEBA/DGEBF mixture) is modified with difunctional epoxy-based reactive diluent 1,4 Butane diol diglycidyl ether (BDGE) and also contains mica which usually used as filler. Because of the presence of epoxide groups, this epoxy-based reactive diluent—aliphatic diglycidyl ether can participate, together with DGEBA and DETA, in polymerization and crosslinking reactions and thus the aliphatic chains of the reactive diluent (BDGE) are introduced into the main chain of the epoxy structure.

It can be restated here that in the case of a mono epoxy reactive diluent, it is known that the curing reaction leads to a decrease of the crosslink density of the resin. Here, in our case of *polyfunctional epoxy reactive diluent*, the behaviour of the diluent *can*

189

(a) Cure Reaction of DGEBA and DETA

(b) Chain Extension (E)

(c) Cross-linking (XL)
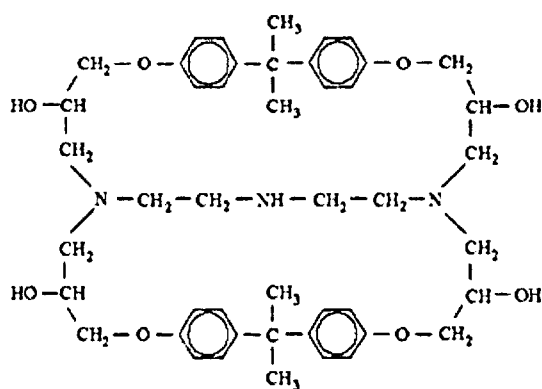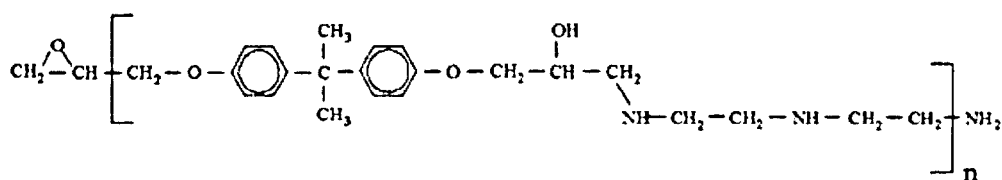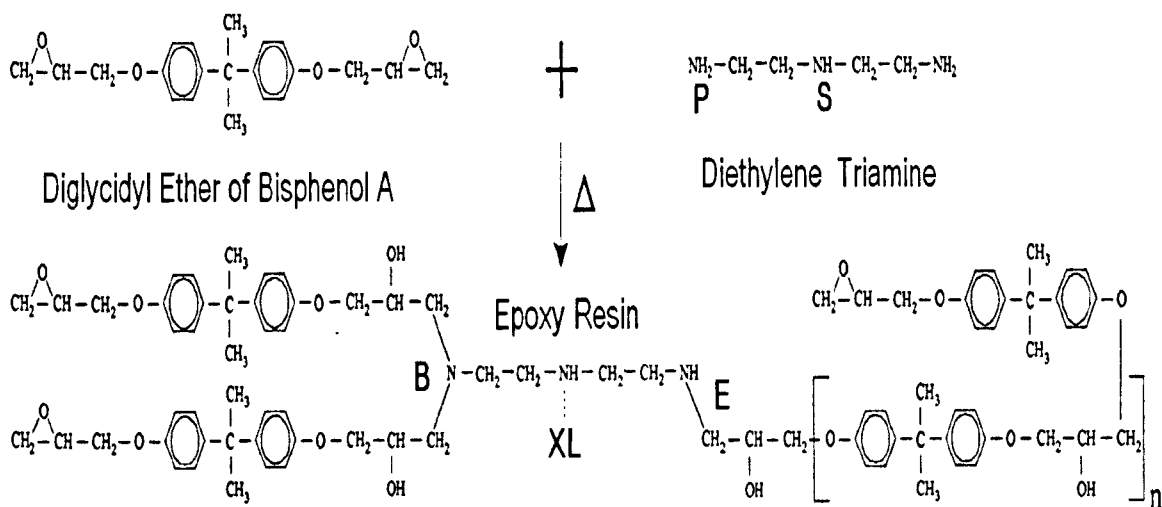
Figure 6.10 (a) Chemical structures and cure reaction of DGEBA by DETA. Possible reaction mechanisms include the epoxy oxirane ring with 1) the primary amine (P) resulting in chain extension (E), 2) the newly formed secondary amine resulting in branching (B), or 3) the mid-molecule secondary amines resulting in cross-linking (XL). (b) Chain extension (E). (c) Cross-linking (XL).Adapted from Reference [18].

be considered to be similar to that of the basic epoxy component [12,30] and the crosslink density seems not to be affected for our studied resin system. This fact is evident from figure 5.1 illustrating conversion vs. cure time plots at different temperatures, and also reflected in the obtained final values of the glass transition temperatures after the isothermal cure at these temperatures (listed in table 5.6), which already discussed in chapter 5. It has also been discussed before (in chapter 5) that the theoretical consideration of any catalytic effect of mica as filler as pointed out by Lu et al [16] can be neglected in our case.

For our studied thermosetting system the general mechanism of curing reaction considering DGEBA and DETA is shown in figure 6.10(a-c). As illustrated, the possible reaction mechanisms between DGEBA and DETA include the epoxy oxirane ring with 1) the primary amine (P) resulting in chain extension (E), 2) the newly formed secondary amine resulting in branching (B), or 3) the mid-molecule secondary amines resulting in cross-linking (XL).

To improve the fundamental knowledge of epoxy-amine curing reaction, mechanistic models have been developed based on the existence of different termolecular and tetramolecular transition state complexes (TSC) whose formation has been considered to be the rate determining step [1]. Figure 6.11 illustrates such bimolecular donor-acceptor hydrogen–bonded complexes in epoxy-amine reactions and rate-determining step (TSC = termolecular (TSC1, TSC2, TSC3, TSC4′) and tetramolecular (TSC4) transition state complex).

It can be seen from figure 6.11 that the first step includes the formation of bimolecular donor-acceptor complexes in the epoxy-amine reaction. Hydrogen-bonded complex of epoxy **1** and **2** activate the nucleophilic attack of the amine in the subsequent step. The addition of hydrogen bonded amine **3** to epoxy has also been suggested as an alternative path which should result in the same transition state as the one resulting from the 2-amine reaction. However, due to a sort of compensation effect the amine auto-association in the complex **3** has been suggested to be neglected. It can be noted that the portion of complex **3** in which the amine acts as proton donor is a stronger nucleophile while the other portion has a stronger acidity than the monoamine. Diamines are therefore more reactive than monoamine but this positive effect is said

to be compensated by the lower concentration of nucleophiles in the diamine due to association. The amine-hydroxyl complex **4** has also been considered to react with epoxy or with the epoxy-hydroxyl complex **2**. The validity of the different paths depicted in figure 6.11, is discussed here from [1], which basically based on experimental data obtained with model compounds or with simple and pure DGEBA-amine systems.

H-O—R

1

$\xrightarrow[\text{slow}]{\text{R'R''NH}}$ TSC1

H-NR'R"

2

$\xrightarrow[\text{slow}]{\text{R'R''NH}}$ TSC2

R'—N:---H—N (H, R", R', R") **3**

$\xrightarrow[\text{slow}]{}$ TSC3

R'—N:---H-O—R (H, R") **4**

$\xrightarrow[\text{slow}]{\text{1}}$ TSC4
$\xrightarrow[\text{slow}]{}$ TSC4'
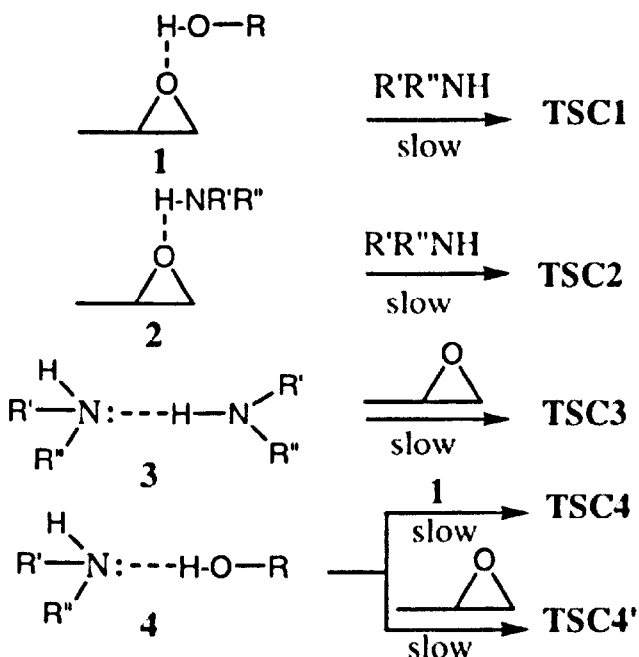
Figure 6.11 Bimolecular hydrogen-bonded complexes in epoxy-amine reactions and rate-determining step (TSC = termolecular (TSC1, TSC2, TSC3, TSC4') and tetramolecular (TSC4) transition state complex). Adapted from Reference [1].

For our studied DGEBA-triamine system (Araldite 2015), we can simplify the different paths associated with the formation of different termolecular and tetramolecular transition state complexes (TSC) shown in figure 6.11, by neglecting paths **2, 3, 4, 5** and considering path 1(TSC1) as the most appropriate one. The reasons are as follows.

It is well known that the acidity of hydroxyl compounds are much higher than that of amine. A direct effect of this fact is that the non-catalytic paths **2** and **3** in figure 6.11 were found to be significant only at the early stage of the curing reaction when the hydroxyl concentration was low. As the initial mixture of our studied thermosetting

192

system contains somewhat high amount of hydroxyl functionalities (from the external catalyst 2,4,6 - tris (dimethylaminomethyl) phenol, and the epoxy pre-polymer DGEBA/DGEBF mixture containing 1,4 Butane diol diglycidyl ether (BDGE) reactive diluent modifier); the non-catalytic reaction paths 2 and 3(TSC2 and TSC3) in figure 6.11 can be reasonably neglected. In the transition state complex 4, the lone pair of electrons on the nitrogen is already engaged in hydrogen bonding. Consequently, the nucleophilic character of amine in complex 4 is lost. So, complex 4 can be considered as an unreactive complex. At this stage, it is important to highlight that the amine-hydroxyl complex in which amine acts as the proton donor is surely formed in insignificant amounts compared to complex 4 due to the stronger acidity of a hydroxyl group compared to an amine. Therefore, path 4 (TSC4) and path 5 (TSC4') are also certainly less reasonable than path 1(TSC1) and can be neglected. This analysis regarding the validity of different paths for our studied thermosetting system, associated with the formation of different termolecular and tetramolecular transition state complexes as shown in figure 6.11, is pointed out from the very recent work of Perrin et al [1], based on — DGEBF/DGEBA mixture/Polyoxypropylene diamine (JEFF)/DETA mixture/ BPA (catalyst) system, which is almost most closely comparable to our epoxy-amine system.

The validity of our selection of the termolecular transition state complex1(TSC1) among other different transition state complexes as depicted in figure 6.11, can be further supported by the recent studies of isothermal cure of DGEBA(epoxy) and TETA (tetra-amine) by Raman Spectroscopy [18], which represents the chemical reaction of oxirane ring-amine-hydroxyl groups, providing molecular data from Raman spectra, which can be taken into account from microscopic perspective.

Figure 6.12 Illustrates the formation of a termolecular intermediate consisting of the amine, the epoxy, and the hydroxyl groups denoting the hydrogen bonded epoxy and the lone pair of electrons on the nitrogen, for isothermal cure of DGEBA and DETA.

In the epoxy-amine reaction, the hydroxyl group formed by reaction of the primary amine can catalyze the reaction of the newly formed secondary amine. The newly formed hydroxyl group can assist in opening the epoxy oxirane ring through hydrogen bonding and facilitate attack by the newly formed nucleophilic secondary amine

through the lone electron pair as shown in figure 6.12.This reaction mechanism suggests that the newly formed secondary amines may have a lower activation energy than the primary amines [18].

$$\text{Base Resin} - \underset{\text{H}}{\overset{\text{H}}{\text{C}}} - \overset{\text{H}}{\text{C}}\text{H}$$
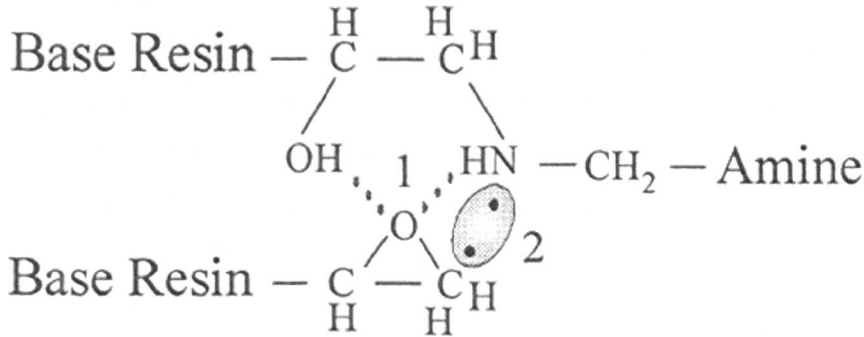
Figure 6.12 Illustration of the formation of termolecular intermediate for isothermal cure of DGEBA and DETA; showing — (1) hydrogen bonding and, (2) lone electron pair. Adapted from reference [18].

6.3.5 General Cure Mechanism on the Basis of Variation of $E_{a,\alpha}$ on α

The curing behaviour coupled with cure mechanism particularly the kinetic changes through the cure reaction could be manifested in conversion dependency of activation energy, $E_{a,\alpha}$ on α, obtained utilizing iso-conversional method inherent to this autocatalytic kinetic model in equation (6.8) which has already been discussed and analyzed comprehensively in the light of *advanced kinetic research* with associated figures 5.8 and 5.9 (a,b) and table 5.2, in chapter 5.

6.3.6 Attempt of further improvement of fit of data

We also fitted our data using the following equation proposed by Lee et al as has mentioned with particular reference in the article associated with cure kinetics modelling of epoxy resins by Skordos and Partridge [44] —

$$\frac{d\alpha}{dt} = k\left(1 - \frac{\alpha}{\alpha_{max}}\right)^n \left(\frac{\alpha}{\alpha_{max}}\right)^m \tag{6.20}$$

It can be seen from equation (6.20) that this expression basically results from the normalization of conversion of the autocatalytic model and operates in a similar way

194

like equation (6.8).When fitting our experimental reaction rate data as a function of conversion to the autocatalytic kinetic model in equation (6.20) by means of non-linear regression analysis, this approach proposed by Lee, results in best fit values for all of the model parameters almost exactly similar (except very slight deviation in the values of k only) to those as listed in table 6.1 corresponding to the autocatalytic kinetic model in equation (6.8), for all of the six isothermal temperatures employed in the test. Consequently, as listed in table 6.1 corresponding to the autocatalytic kinetic model in equation (6.8), exactly similar values of all standard errors (SE) and squared correlation co-efficients, R^2 (i.e. co-efficients of determination) of curve fitting are obtained for the model proposed by Lee in equation (6.20).

In connection with the results associated with the autocatalytic kinetic model in equation (6.8) as depicted in figures 6.3(a—f) and 6.4(a—f) it has already been mentioned that at the early stages of cure at lower conversions (on average, at α =0—0.1) near the non-typical autocatalytic peak regions, slight deviation between the data of the experimental reaction rate and that of the model predictions is observed. To improve the fit we also consider the following modified autocatalytic model given by equation (6.21) as has mentioned by Yousefi et al [42] —

$$\frac{d\alpha}{dt} = k\alpha^m \left(\alpha_{max} - \alpha\right)^n \left(1 - \alpha\right)^p \tag{6.21}$$

Basically, this model takes into account the complexity of cure process in the presence of *promoters*. In equation (6.21), p is the third reaction exponent. In some promoted systems, the cure exotherm and consequently the reaction rate profile may exhibit some deviation from a bell-shaped profile [42]. This modified reaction rate expression in equation (6.21) accounts for both maximum obtainable conversion, through α_{max}, and deviation of the cure exotherm / reaction rate profile from a bell-shaped profile by including a third term, $\left(1 - \alpha\right)^p$, in the reaction rate expression. When fitting our experimental reaction rate data as a function of conversion to this modified autocatalytic kinetic model in equation (6.21) by means of non-linear regression analysis, we obtain slightly improved fit for the rate profiles at 30°C, 50°C, 70°C and 80°C with r^2 values of 0.990, 0.998, 0.998 and 0.999 respectively instead of 0.982, 0.997, 0.997 and 0.998 as listed in table 6.1 corresponding to equation

(6.8).Goodness of fit of reaction rate profiles at 40°C and 60°C remains the same with r^2 values of 0.997 and 0.998 respectively as reported in table 6.1.However, in order to achieve these fits it is necessary to assume negative values (!) for the reaction order p at 30°C, 40°C and 50°C and negative values (!) for the reaction order m and n at 30°C and 80°C respectively as well. As the reaction orders varied in sign as a function of temperature therefore fitting is unrealistic and not possible. Again, negative values of reaction order p is obtained with similar goodness of fit of rate profiles corresponding to equation (6.21) on fitting our data with the slightly different following form of this above mentioned modified autocatalytic model expressed by equation (6.22) as mentioned in reference [45].

$$\frac{d\alpha}{dt} = k\alpha^m (\alpha_{max} - \alpha)^n [-\ln(1-\alpha)]^p \qquad (6.22)$$

Hence fitting p as a function of temperature is not possible.

In the context of the results based on the autocatalytic kinetic model in equation (6.8) as illustrated in figures 6.3(a–f) and 6.4(a–f), here, it can be mentioned that similar instance of slight underestimation in the non-typical autocatalytic peak regions by model predictions is noticed in the research work of Perrin et al [1]; where maximum reaction rate occurs nearly at 10% conversion (mentioned in table 5.1 in chapter 5) for the isothermal cure process of DGEBF/DGEBA mixture / Polyoxypropylene diamine (JEFF)/DETA mixture / BPA (catalyst) system, in the temperature range of 40°C – 80°C, which is almost closely comparable to our epoxy-amine system in respect of formulations, features and experimental window. Instance of slight underestimation in the typical autocatalytic peak regions by model predictions has also been noticed in the research work concerning modelling of isothermal cure behaviour of a commercial epoxy-amine resin system [46].In addition to the *complexity of chemistry involved in commercial thermosets, this underestimation of data by the model may be due to the fact that the shape of the reaction rate profiles is highly dependent on the cure temperature while its magnitude is highly dependent on the concentration of the catalyst/accelerator used in the formulation which should be taken into account.*

6.3.7 Comments on the Performance of the Autocatalytic Model with α_{max}

(1) It is evident that though contains only one reaction rate constant and *less fitting parameters* (*four* kinetic parameters-- $\ln A, E_a, m, n$) compared with widely used Kamal model representing both *nth* order and autocatalytic reaction; the autocatalytic model $d\alpha/dt = k\alpha^m(\alpha_{max} - \alpha)^n$ in equation (6.8) with incorporation of $\alpha_{max}(T)$, maximum value of conversion at a particular temperature, as expressed by equation (6.11) in section 6.3.1, instead of full conversion 1, very closely simulate the isothermal curing behaviour of the complex commercial epoxy (modified) thermosetting system Araldite 2015 under investigation with almost a reasonable degree of satisfaction over the entire range of conversion and temperature (30°C–80°C) studied. This model allows excellent increased accuracy at the later stages of the cure for the entire range of temperature studied. Just very slight deviations between the data of the experimental reaction rate and that of the model predictions is observed at the early stages of cure at lower conversions (on average, at $\alpha = 0$–0.1) which was elucidated and justified and also critically assessed in the context of other research work [1,46] (in section 6.3.6) consistent with similar evidence of very slight deviations between model and data for commercial epoxy-amine systems. As *no prior knowledge of a T_g model is needed* for this approach, hence this advantageous feature minimizes the experimental effort usually required for the incorporation of a T_g submodel.

(2) The validity of this kinetic model is sustained by the very good fitting of results obtained using isothermal DSC data which is reflected in the values of the squared correlation co-efficient, r^2 (i.e. co-efficient of determination) of curve fitting or the *goodness of fit* as are listed in table 6.1.It is evident from the table 6.1 that the values of the squared correlation co-efficient of curve fitting are almost *independent* of the maximum obtainable conversion, $\alpha_{max}(T)$ and hence also almost *independent* of the curing temperature as well (*will be discussed in the next section with associated figures* in comparison with conventional autocatalytic model). This is expected, as the value of the empirical term maximum obtainable conversion, $\alpha_{max}(T)$ incorporated in the autocatalytic kinetic model in equation (6.8), is determined experimentally (listed in table 5.6 in chapter 5) at a particular isothermal curing

temperature. Therefore, for the kinetic model in equation (6.8), the curing temperature and the maximum obtainable conversion, $\alpha_{max}(T)$ almost does not have any effect on the values of the squared correlation co-efficient, r^2 (i.e. co-efficient of determination) of curve fitting for our studied thermosetting system. This reveals the reliability of this kinetic model for the DGEBA-based thermosetting system under study.

(3) The values of the *four* kinetic parameters $(\ln A, E_a, m, n)$ obtained (listed details in table 6.1) are also well in agreement with the values reported in literature which has already been narrated details in that context. The average value of the overall reaction order is 1.3 and approaches to 2 at higher temperature, which is consistent with the literature estimates for the isothermal curing kinetics of a variety of epoxy-amine systems[7, 8, 9, 13, 27, 28].

(4) It is worth mentioning that in comparison to the typical data of stoichiometric ratio mixture DETA cured epoxy resins (DGEBA) without reactive diluents [1, 5, 29] and other amine cured epoxy resins (DGEBA) without reactive diluents [7, 8, 9, 13, 25], the analysis of our data in connection with the kinetic parameters obtained based on the model in equation (6.8) as reported in table 6.1, shows that most possibly, the reactive diluent increased the maximum value of calorimetric conversion (α_{max}) and the maximum value of reaction rate $(d\alpha/dt)_{max}$, while the values of activation energy (E_a), pre-exponential factor/ Arrhenius frequency factor ($\ln A$), reaction rate constant (k), and reaction orders (m,n) i.e. other process parameters remained within the typical values of epoxy formulations.

Therefore, the introduction of aliphatic segments of *difunctional* epoxy-based reactive diluent 1,4 Butane diol diglycidyl ether (BDGE) into the main chain of the epoxy based on DGEBA, does not cause a significant change in the kinetics of the overall curing process of the commercial thermosetting system under study, except contributing, most possibly, in obtaining the *relatively higher values of maximum calorimetric conversion (α_{max}) and conversion rate $(d\alpha/dt)_{max}$* observed in the investigation. The crosslink density seems not to be affected. These observations are elucidated and justified in detail with precise comparison in sections 5.1.1 and 5.2.1 in chapter 5.

(5) On the basis of kinetic parameters obtained based on the autocatalytic model in equation (6.8) as reported in table 6.1, we found that some features of reaction mechanism could be manifested in temperature dependency of kinetic exponents / reaction orders, as well as particularly in increase in the value of the overall reaction order *(m+n)* with isothermal cure temperature, which, in particular, permits the prediction of the molecular mechanism of curing reaction, consistent with the results of other recent workers[17], founded on trimolecular catalysis mechanism associated with the formation of fairly stable donor-acceptor trimolecular transition state complexes (TSC) consisting of amine, epoxy and hydroxyl groups in our modified epoxy-amine thermosetting system. Basically, *it is favourable for the* —OH *group in the molecular chain of the epoxy resin to become a proton donor and participate in the reaction following a trimolecular catalysis mechanism with the increasing curing temperature.* Interestingly, the value of the autocatalytic reaction order m is found to increase with increasing cure temperature, *unlike the conventional autocatalytic effect* where m decreases with increasing cure temperature.

(6) We found that the curing behaviour coupled with cure mechanism particularly the kinetic changes through the cure reaction could be manifested in conversion dependency of activation energy, $E_{a,\alpha}$ on α, obtained utilizing iso-conversional method inherent to the autocatalytic kinetic model in equation (6.8) as reported in table 5.2 with associated figures 5.8 and 5.9 (a,b) in chapter 5.

In the chemical controlled reaction regime between the conversion range of 0.2 and 0.7, the effective activation energy $E_{a,\alpha}$ is almost *constant* with an average value E_a=55.50 kJ/mol, satisfying the anticipated outcome of single step reaction, probably with same reaction mechanism. This value ascribed to *autocatalytic amine addition* along with $E_{a,\alpha}$=57.93 kJ/mol at α=0.1 at the beginning of the cure ascribed to *autocatalytic primary amine addition*, agrees fairly well with corresponding reported values in literature for similar epoxy-amine systems [7,8,9,33].At higher conversions, near the end of cure, the change into diffusion controlled reaction mechanism could be manifested in significant increase in the activation energy value, which is interpreted comprehensively considering the physics of *cooperative motion of the chain segments* and advanced kinetics, in chapter 5.

6.4 Kamal Model (where k_1 was set to 0)

Setting k_1 to 0 and denoting k_2 *as k,* the combined *nth* order and autocatalytic model of Kamal given by equation (3.10) takes the following form of conventional autocatalytic model which had mentioned in chapter 3 expressed by equation (3.9)

$$\frac{d\alpha}{dt} = k\alpha^m (1-\alpha)^n$$

We used this model to fit our experimental data to analyze the cure kinetics of our studied epoxy system. The object is twofold. *Firstly,* to compare the results with those obtained with the similar autocatalytic model with inclusion of α_{max} instead of complete conversion 1 as given by equation (6.8). *Secondly,* to explore the in depth information associated with the diffusion controlled kinetics due to vitrification in isothermal measurement related to our data.

To take into account of the diffusion effect on the reaction rate, the methods associated with the modifications for diffusion-controlled kinetics have discussed details in chapter 3. The modelling methodologies stated there to describe the final stages of the curing reaction are categorized into two generic groups — (i) methodologies that utilize the Rabinowitch model for serial reactions and (ii) methodologies that use maximum attained conversion expressions.

From the first generic group, the methodology we preferred was constituted defining the expression of a diffusion factor, $f_d(\alpha, T)$ obtained combining—(i) the Rabinowitch model [47] based on the addition of the reciprocal rate constants (basically sum of the characteristic times) similar to the idea of so-called *Law of the addition of kinetic Resistances,* which satisfies the actual gradual change of the onset of diffusion controlling step in the region where both chemical and diffusion factors are in control, and—(ii) the semiempirical relationship based on the fractional free volume theory proposed by Chern and Poehlein [48] for the diffusion rate constant, k_d denoting a rather abrupt change in the diffusion control from chemical control for the cure reaction after the conversion reaches the critical value, α_c .

The approximations of Rabinowitch [47] and Chern and Poehlein [48] for the overall effective rate and diffusion rate constants given by equations (3.13) and (3.18) in chapter 3 has the following forms respectively

$$\frac{1}{k_e(\alpha,T)} = \frac{1}{k(T)} + \frac{1}{k_d(\alpha,T)}$$

$$k_d = k \exp[-C(\alpha - \alpha_c)]$$

Where, k_e, k and k_d are the overall effective rate constant, Arrhenius-dependent kinetically controlled reaction rate constant and diffusion rate constant respectively. C is a constant.

Combining equations (3.13) and (3.18), the diffusion factor $f_d(\alpha,T)$ defined in equation (3.19) in chapter 3, as:

$$f_d(\alpha,T) = \frac{k_e}{k} = \frac{1}{1 + \exp[C(\alpha - \alpha_c)]}$$

So, when the cure reaction is dominated by the autocatalytic kinetic mechanism $f_d(\alpha,T) = 1$, but as the reaction becomes more diffusion controlled $f_d(\alpha,T)$ decreases exponentially.

Using the diffusion factor, the reaction rate can be expressed in the following form to account for effects of diffusion:

$$\frac{d\alpha}{dt} = k\alpha^m (1-\alpha)^n f_d(\alpha,T) = \frac{k(T)}{1 + \exp[C(\alpha - \alpha_c)]} \alpha^m (1-\alpha)^n \qquad (6.23)$$

The initial estimation process of the three parameters (k, m, n) of the kinetic model given by equation (3.9) has already been discussed before, where this equation was applied to the multiple linear regression option in the forms of equations (6.14) — (6.17) to determine the parameter values that can then be used as the initial estimates for the non-linear regression analysis.

The values of the best fit kinetic parameters determined from the non-linear regression analysis based on the autocatalytic kinetic model $d\alpha/dt = k\alpha^m(1-\alpha)^n$ for isothermal cure process of Araldite 2015 are listed in table 6.2(a), together with the corresponding standard errors (SE) and the squared correlation co-efficient (i.e. co-efficient of determination) for fit of model to the experimental data.

Figures 6.13(a,b), 6.14(a,b), 6.15(a,b), 6.16(a,b),6.17(a,b) and 6.18(a,b) illustrate the comparisons of experimental values of the isothermal reaction rates with the reaction rate curves calculated according to the predictions of autocatalytic kinetic model in equation (3.9), as a function of conversion and cure time respectively, at cure temperatures of 30°C, 40°C, 50°C, 60°C, 70°C and 80°C.

As mentioned in table 6.2 (a), for this model an iso-conversional analysis is utilized to find out the activation energy E_a value. The reliability and advantageous features of this analysis has already been discussed in the context of the autocatalytic model given by equation (6.8).As can be seen from table 6.2(a), for the isothermal temperature range of 30°C—80°C, the value of the overall reaction order $(m+n)$ is in the range of 1.65—2.09. The values of m and n are in the range of 0.12—0.32 and 1.53—1.76. The value of the overall reaction order $(m+n)$ approaches to 2 at higher temperature, which has widely been reported in the literature for the isothermal curing kinetics of a variety of epoxy-amine systems [7, 8, 9, 13, 27, 28]. All the parameter values reported in the table 6.2(a) agree well with those obtained for almost similar or comparable epoxy-amine systems [5, 6, 7, 8, 9, 13, 21].

Here, it can be mentioned that the values of the parameters k, m, n, $(m+n)$ and ln A listed in table 6.2 (a) based on conventional autocatalytic model are higher than those listed in table 6.1 obtained with autocatalytic model incorporating α_{max} instead of

complete conversion 1 as given by equation (6.8).In comparison to conventional autocatalytic model, similar trend of slightly low parameter values obtained with autocatalytic model with inclusion of α_{max} have been observed in the research work of Teil et al [14] for catalyzed DGEBA based epoxy system.

It can be seen from figures 6.13(a,b) — 6.18(a,b) that the differences between model predictions and experimental data are observed to be smaller when the curing temperature increases. Hence, the fit worsens as the cure temperature is lowered and becomes better as the cure temperature is increased. *The better degree of agreement of fit results with the experimental data at higher curing temperature indicates the temperature dependence of the diffusion and the reaction rate.* Since the mobility of the reacting groups is less hindered in high temperature, vitrification would occur until high conversions, which leading to a high α_{max}.

It is also evident from figures 6.13(a,b) — 6.18(a,b) that in the later stages of the curing reaction, i.e., at higher conversions the data of the model predictions slightly deviate from that of the experimental. This is due to the onset of vitrification where the mobility of the reactive groups is hindered and the rate of conversion is controlled by diffusion rather than by kinetic or chemical factors. *This accounts for the fact that the experimental reaction rates are lower than those predicted by the model* given by equation (3.9).Differences between model predictions and experimental data are observed to be greater when curing temperature decreases. This is reflected in figures 6.13(a,b), 6.14(a,b) and 6.15(a,b) corresponding to cure temperatures of 30°C, 40°C, and 50°C respectively. This may be related to the T_g of the fully cured material. The free volume is reduced, if the curing temperature is close to the glass transition region of the highly cured material. The segmental mobility within the polymer decreases, thereby reducing the rate of diffusion of the molecules to the reactive sites. Thus the reaction rate decreases.

Table 6.2(a) The values of the kinetic parameters of the Autocatalytic model $\frac{d\alpha}{dt} = k\alpha^m (1-\alpha)^n$ for isothermal cure process of Araldite 2015. E_a is the average value of activation energy obtained from iso-conversional method.

T_{cure} (^{0}C)	k^* (min^{-1})	m^*	n^*	$m+n$	lnA (min^{-1})	E_a (kJ/mol)	r^{2**}
30	0.008(.000)	0.120(.006)	1.531(.015)	1.651	17.199		0.917
40	0.017(.001)	0.185(.026)	1.485(.012)	1.670	17.219		0.972
50	0.033(.000)	0.183(.003)	1.522(.007)	1.705	17.214	55.50	0.987
60	0.066(.002)	0.214(.012)	1.586(.005)	1.800	17.307		0.997
70	0.141(.001)	0.266(.002)	1.634(.004)	1.900	17.465		0.998
80	0.293(.001)	0.328(.007)	1.762(.005)	2.090	17.682		0.999
Average	0.093	0.216	1.586	1.802	17.347		

* Values in parentheses correspond to standard errors (SE).
** Squared correlation co-efficient (i.e. co-efficient of determination) of curve fitting.

Table 6.2(b) The values of the Diffusion factor f_d (α,T) parameters—Co-efficient C and Critical Conversion (α_c) of the Autocatalytic model $\frac{d\alpha}{dt} = k\alpha^m (1-\alpha)^n f_d(\alpha,T)$ for isothermal cure process of Araldite 2015.

T_{cure} (^{0}C)	C^*	α_c^*
30	88.909 (2.009)	0.783 (.000)
40	103.207 (1.550)	0.868 (.000)
50	30.118 (0.314)	0.896 (.000)
60	42.824 (0.367)	0.948 (.000)
70	133.983 (7.069)	0.970 (.000)
80	183.616 (0.000)	0.999 (.000)

* Values in parentheses correspond to standard errors (SE).

Figure 6.13(a—f) Isothermal reaction rates as a function of conversion (**a, c, f**) and cure time (**b, d**)—comparisons of experimental data with the predictions of model $d\alpha/dt = k\alpha^m (1 - \alpha)^n$ at 30°C; without $f_d (\alpha,T)$, with $f_d (\alpha,T)$, and the corresponding $f_d (\alpha,T)$ as a function of conversion (**e**), as all are indicated in the figures.
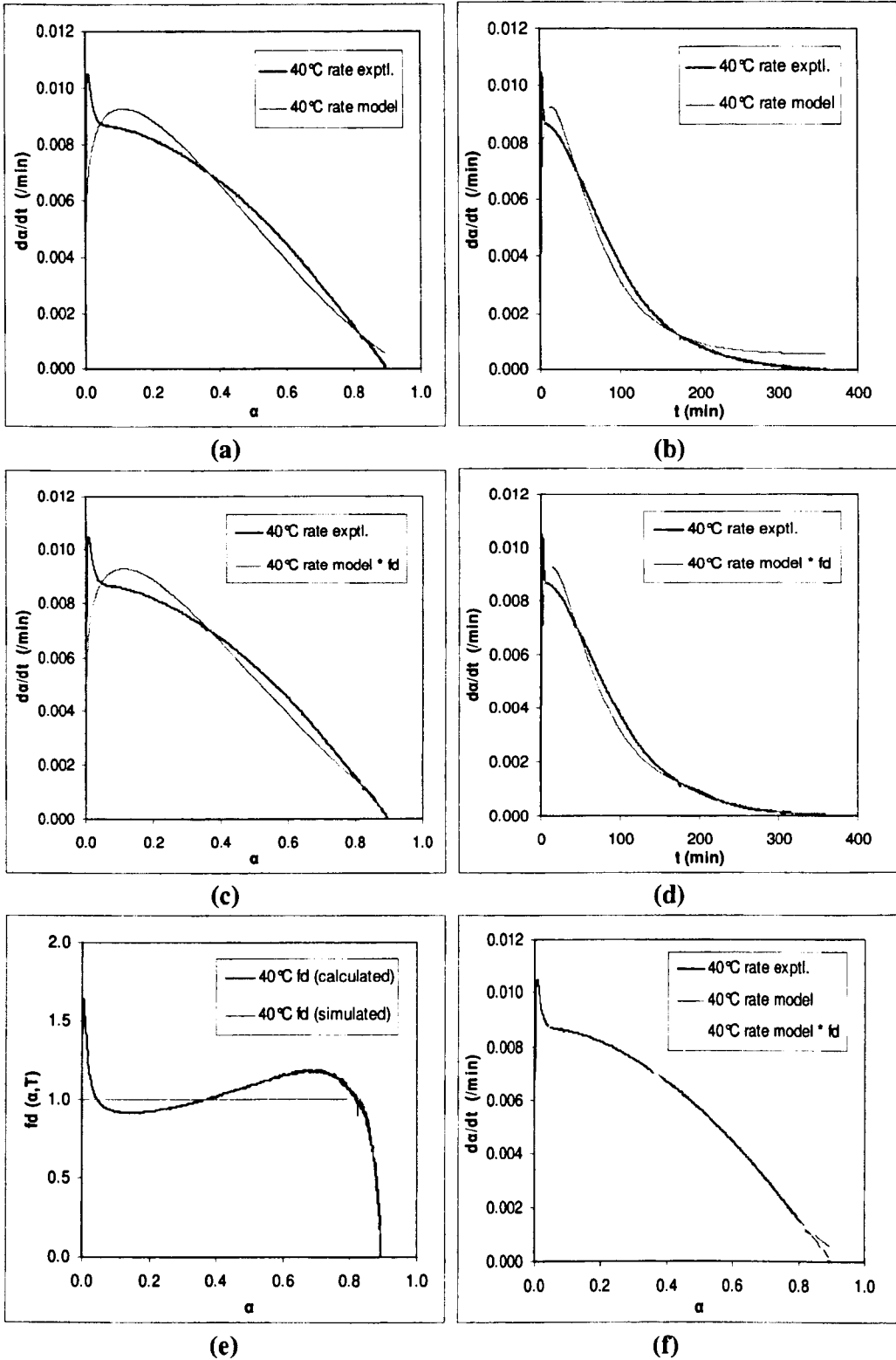
Figure 6.14(a—f) Isothermal reaction rates as a function of conversion (**a, c, f**) and cure time (**b, d**)—comparisons of experimental data with the predictions of model $d\alpha/dt = k\alpha^m(1-\alpha)^n$ at 40°C; without $f_d(\alpha,T)$, with $f_d(\alpha,T)$, and the corresponding $f_d(\alpha,T)$ as a function of conversion (**e**), as all are indicated in the figures.
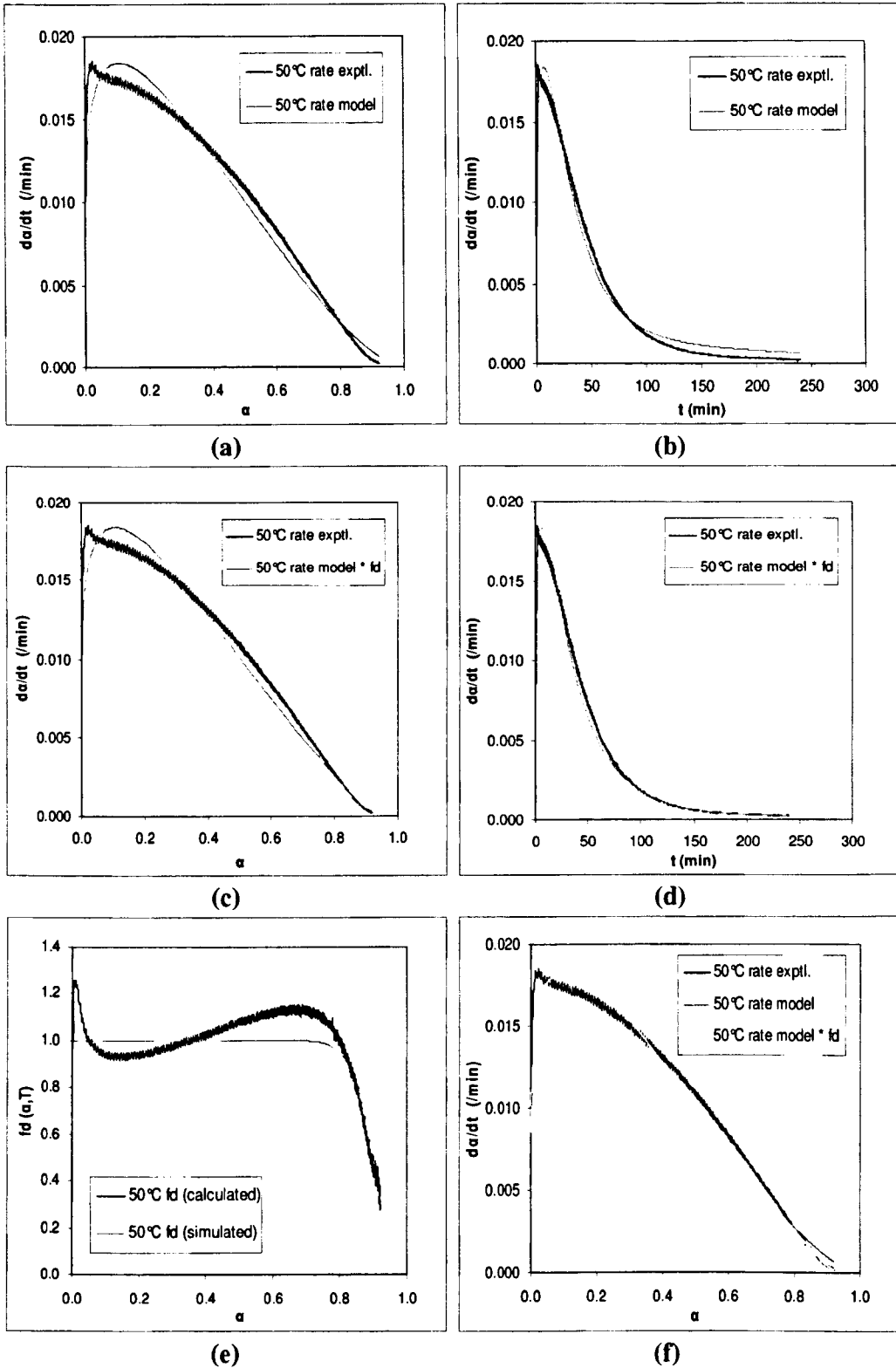
Figure 6.15 (a—f) Isothermal reaction rates as a function of conversion (**a, c, f**) and cure time (**b, d**)—comparisons of experimental data with the predictions of model $d\alpha/dt = k\alpha^m(1-\alpha)^n$ at 50°C; without $f_d(\alpha,T)$, with $f_d(\alpha,T)$, and the corresponding $f_d(\alpha,T)$ as a function of conversion (**e**), as all are indicated in the figures.
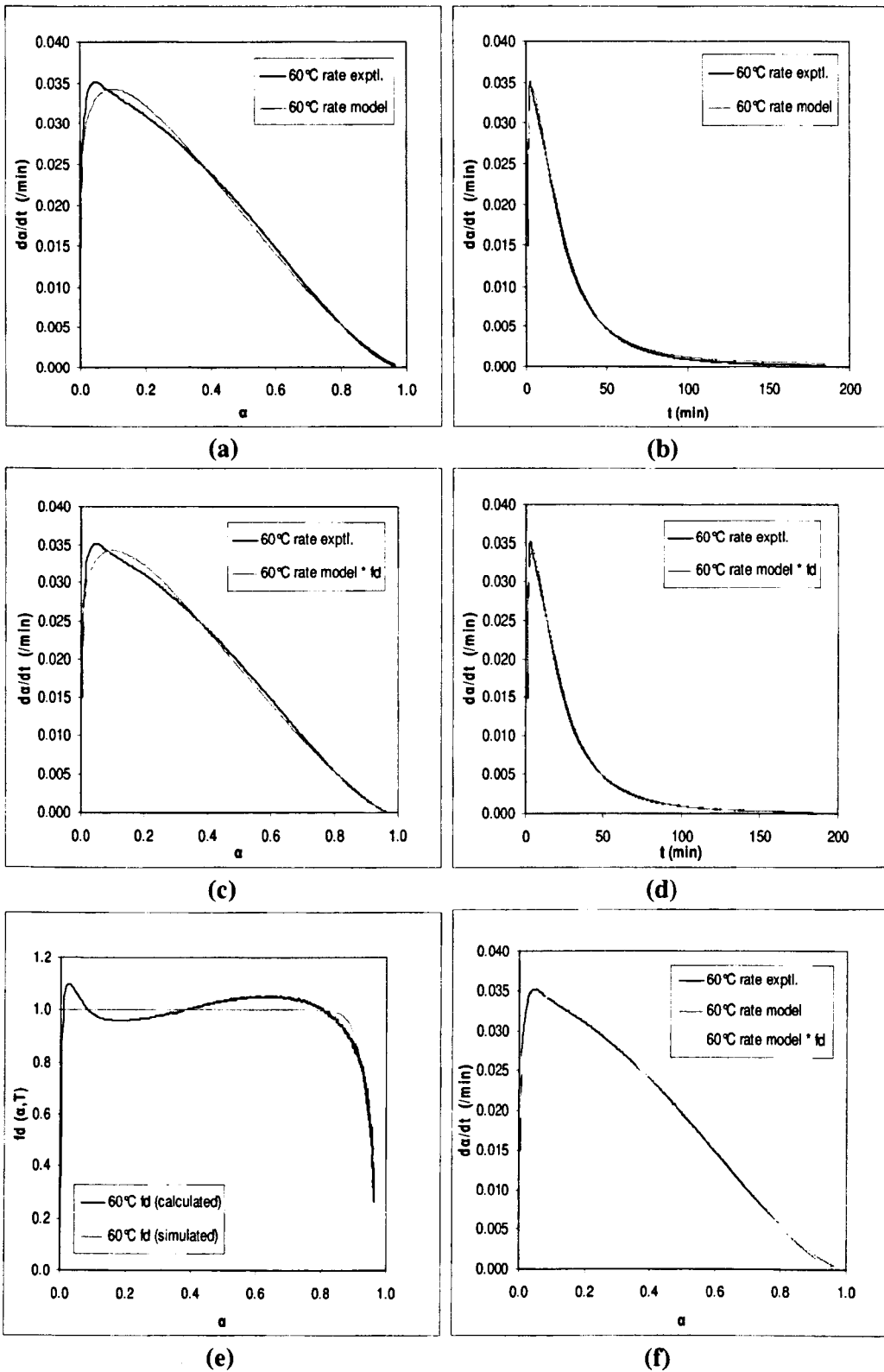
Figure 6.16 (a—f) Isothermal reaction rates as a function of conversion **(a, c, f)** and cure time **(b, d)**—comparisons of experimental data with the predictions of model $d\alpha/dt = k\alpha^m(1-\alpha)^n$ at 60°C; without $f_d(\alpha,T)$, with $f_d(\alpha,T)$, and the corresponding $f_d(\alpha,T)$ as a function of conversion **(e)**, as all are indicated in the figures.
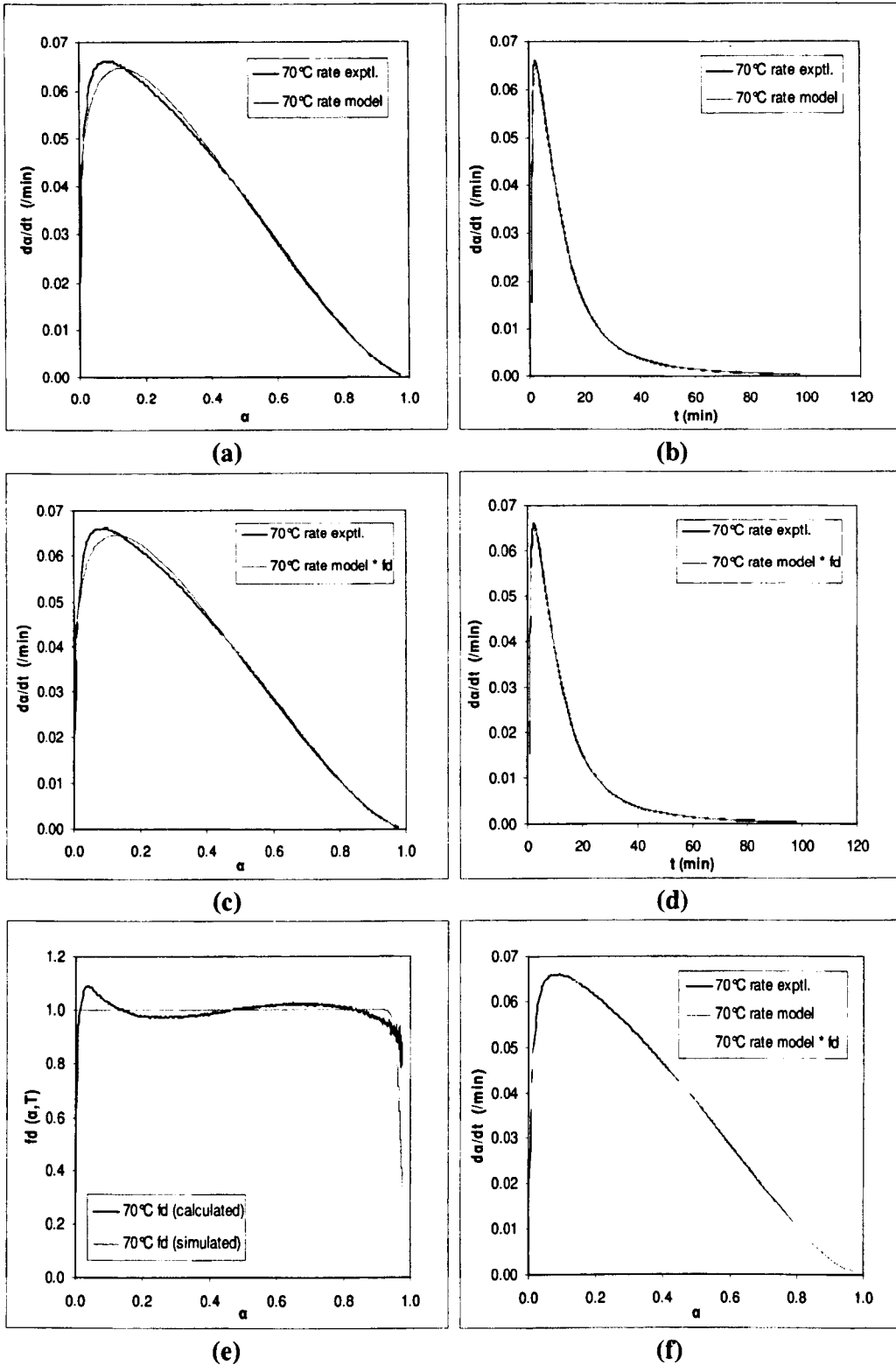
Figure 6.17 (a—f) Isothermal reaction rates as a function of conversion (**a, c, f**) and cure time (**b, d**)—comparisons of experimental data with the predictions of model $d\alpha/dt = k\alpha^{m}(1 - \alpha)^{n}$ at 70°C; without f_d (α,T), with f_d (α,T), and the corresponding f_d (α,T) as a function of conversion (**e**), as all are indicated in the figures.
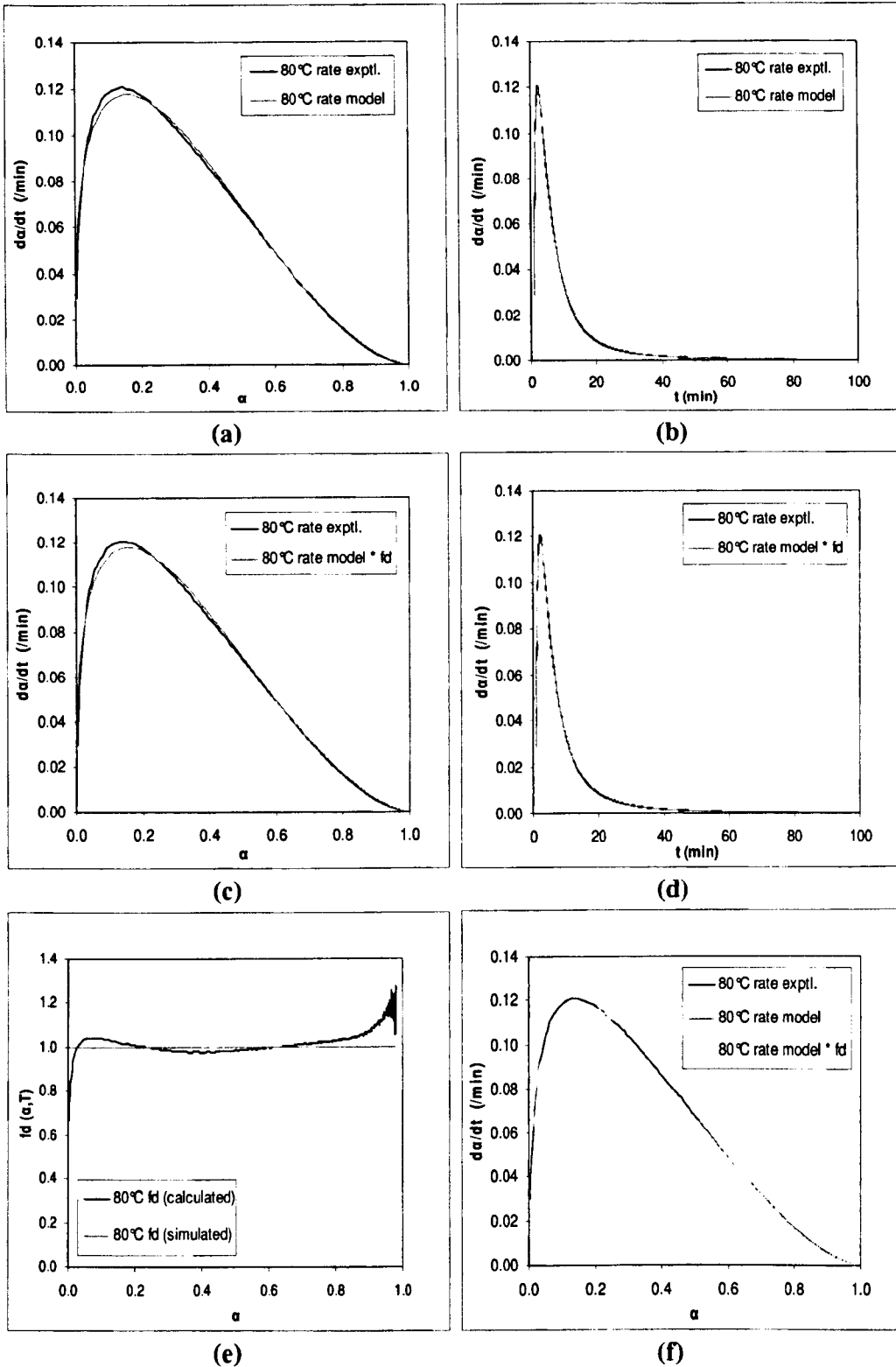
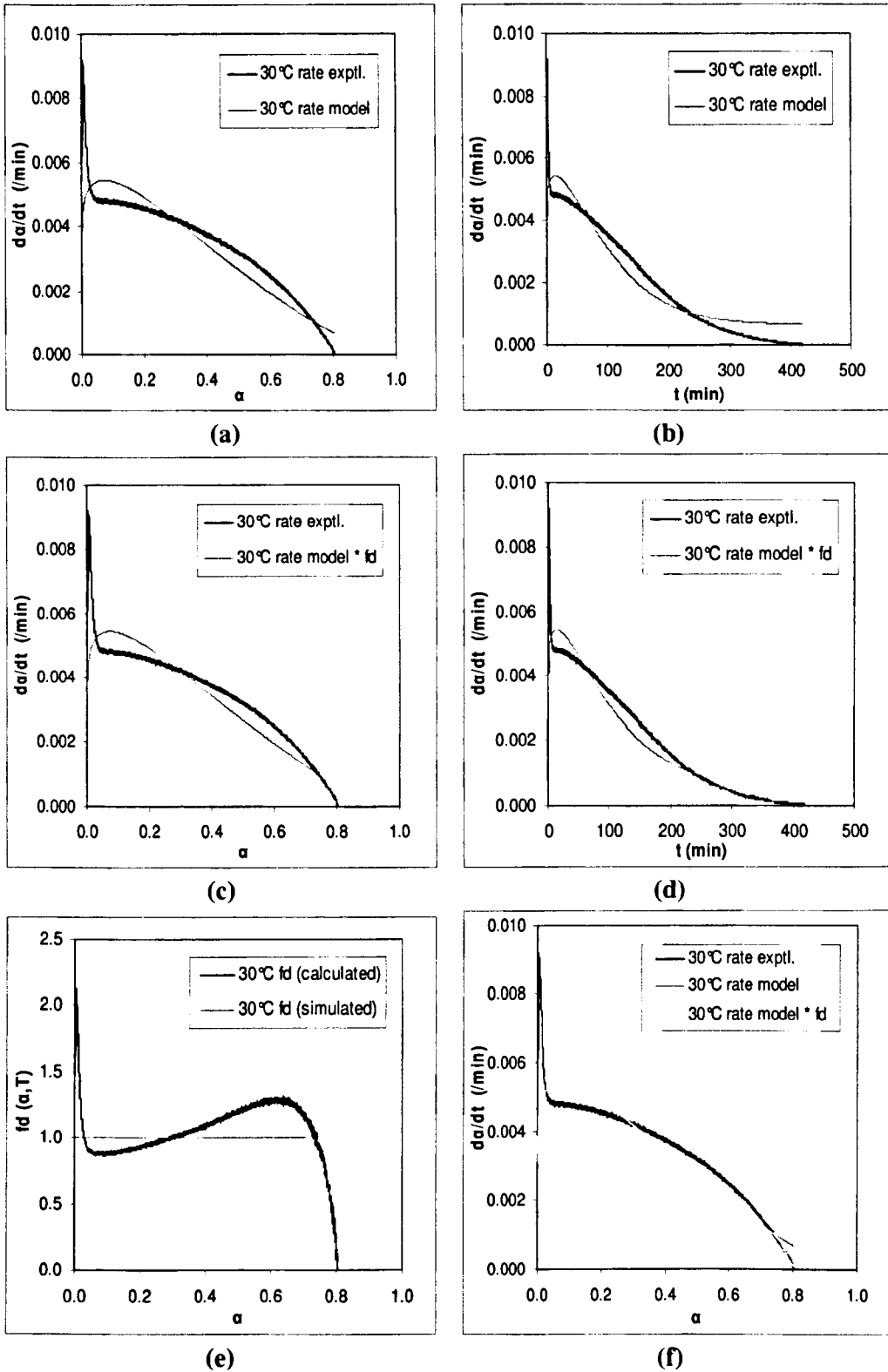**Figure 6.18(a—f)** Isothermal reaction rates as a function of conversion (**a, c, f**) and cure time (**b, d**)—comparisons of experimental data with the predictions of model $d\alpha/dt = k\alpha^m(1-\alpha)^n$ at 80°C; without $f_d(\alpha,T)$, with $f_d(\alpha,T)$, and the corresponding $f_d(\alpha,T)$ as a function of conversion (**e**), as all are indicated in the figures.

It is evident from the table 6.2(a) that the values of kinetic parameters k, m, n and $(m+n)$ based on the conventional autocatalytic model given by equation (3.9) increase with increasing cure temperature. Similar trend is observed with those kinetic parameters obtained based on the autocatalytic model with α_{max} in equation (6.8) as reported in table 6.1.The interpretation of the temperature dependence of kinetic parameters has already been described in that context. We found that the increase in the value of the overall reaction order $(m+n)$ with isothermal cure temperature, permits the prediction of the molecular mechanism of curing reaction, consistent with the results of other recent workers[17], founded on trimolecular catalysis mechanism where *it is favourable for the* —OH *group in the molecular chain of the epoxy resin to become a proton donor and participate in the reaction with the increasing curing temperature.*

The plots of the reaction orders m and n as a function of isothermal cure temperature for the conventional autocatalytic model in equation (3.9) is shown in figure 6.19. As seen from the figure, both of the reaction orders m and n increase with the increase of cure temperature following an almost linear relation. The corresponding equations of linear regression and their squared correlation co-efficients, R^2 (i.e. co-efficients of determination) are also presented in figure 6.19. Similar results have been observed for the cure of epoxy-amine systems [7, 13, 21, 27, 28, 36]. The temperature variation of the reaction orders suggest that either the reaction mechanism of the system may changes with temperature or it is purely empirical.

The Arrhenius plots of *ln k* as a function of 1/T is shown in figure 6.20. In this figure, good linear correlation is observed, which leads to calculate the apparent activation energy from the slope of the straight line, which is 63.55 kJ/mol, as indicated in the figure. The authenticity of considering the average value of apparent activation energy E_a obtained from iso-conversional analysis, instead of activation energy E_a obtained from single reaction rate constant has already been narrated before.
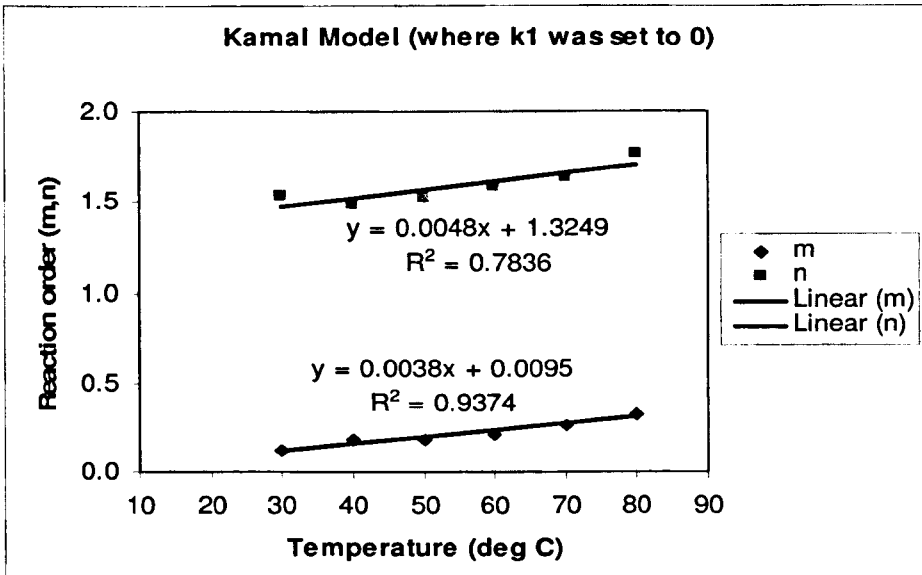
Figure 6.19 The plots showing the effect of the isothermal cure temperature on the reaction orders m and n with associated fits; based on the Autocatalytic kinetic model $d\alpha/dt = k\alpha^m (1-\alpha)^n$ for isothermal cure process of Araldite 2015.
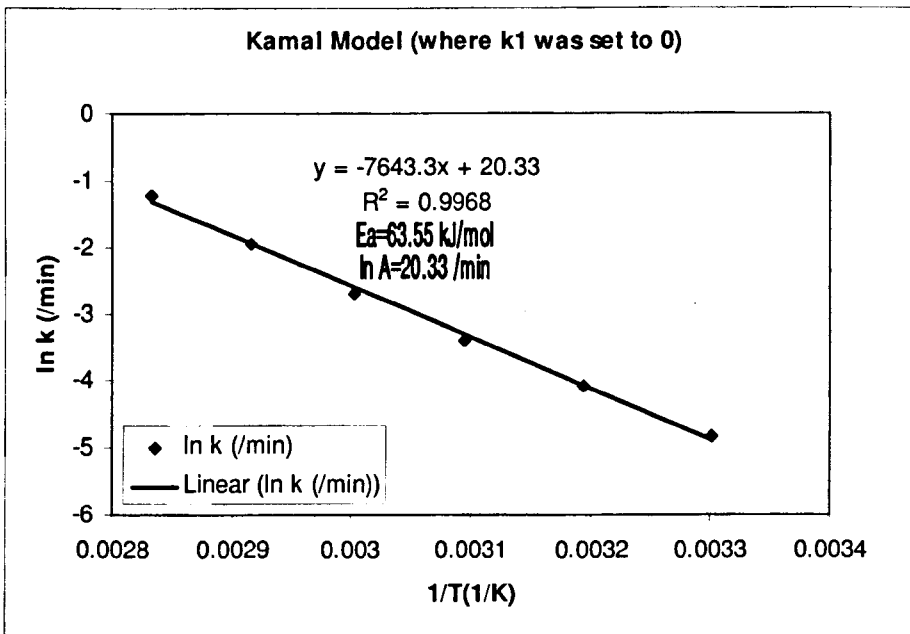
Figure 6.20 The Arrhenius plots of the temperature dependence of the isothermal reaction rate constant k determined from the non-linear regression analysis based on the Autocatalytic kinetic model $d\alpha/dt = k\alpha^m (1-\alpha)^n$ for isothermal cure process of Araldite 2015.

6.4.1 Conventional Autocatalytic Model with 1 vs. Autocatalytic Model with α_{max}

Comparing the results obtained with conventional autocatalytic model given by equation (3.9) with those obtained with the autocatalytic model as given by equation (6.8), it can be stated that the poor fit of kinetic data in the conventional model (especially at the lower temperature range of 30°C–50°C) is due to the fact that the *assumption of α_{max} =1 is overly simplified.* A *much better fit is observed* with the model given by equation (6.8) *as the constraint of the reaction going to completion is lifted.* This is illustrated in figure 6.21.
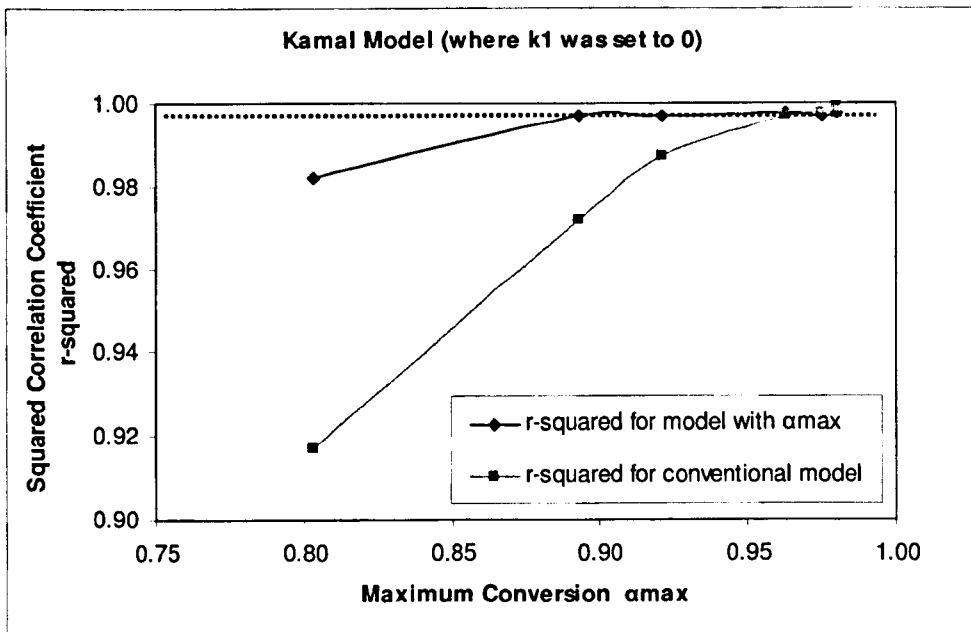
Figure 6.21 Squared correlation co-efficient (r^2) (i.e. co-efficient of determination) of curve fitting versus maximum attainable conversion of Araldite 2015 thermoset resin under several isothermal conditions.

From figure 6.21 it can be seen that the squared correlation co-efficients (r^2) (i.e. co-efficients of determination) of curve fitting for the conventional autocatalytic model appear to increase with the maximum obtainable conversion α_{max} and then approach the values for the autocatalytic model with α_{max} asymptotically. As the maximum obtainable conversion α_{max} is determined experimentally in the model with α_{max}, the squared correlation co-efficients (r^2) (i.e. co-efficients of determination) of curve fitting are found *almost to be independent of the maximum attainable conversion* α_{max}

213

as depicted in figure 6.21. The results in figure 6.21 reveal that the reliability of the kinetic model for our DGEBA based commercial thermosetting system can be greatly improved simply by taking the maximum obtainable conversion α_{max} into account in computation.

In the light of the above, we can see that incorporating α_{max} instead of complete conversion improves the goodness of fit for overall cases and particularly for the case of lower temperature range 30°C—50°C.In fact, during isothermal tests at low temperatures the polymerization reactions are not completed, and the system reaches a final value of the extent of reaction that is an increasing function of the test temperature. Basically, at low temperatures vitrification occurs earlier. So, inclusion of α_{max} instead of complete conversion (i.e. $\alpha=1$) is the appropriate case, and this *"appropriateness"* is reflected in the values of squared correlation co-efficients (r^2) (i.e. co-efficients of determination) of curve fitting — especially in the case of lower temperature range (30°C—50°C) where the implement of complete conversion suppose to cause more deviation in the model fit due to early occurrence of vitrification phenomena.

6.4.2 Diffusion Effect

It has stated earlier that it can be seen from figures 6.13(a,b) — 6.18(a,b) that in the later stages of the curing reaction, i.e., at higher conversions the data of the model predictions deviate from that of the experimental which is due to the onset of vitrification where the mobility of the reactive groups is hindered, the rate of conversion is controlled by diffusion rather than by chemical factors and *the values predicted by the model* given by equation (3.9) *are higher than the experimental data.* Deviation appears to be greater when curing temperature decreases which already has explained in terms of the T_g of the fully cured material. Here, it can be mentioned that the poor fit or the deviation between experimental rate and model predictions at lower and medium conversion ranges at the lower temperatures (30°C,40°C,50°C); most probably does not affect the vitrification region, which appears at higher conversions in the later stages of the cure.

214

To take into account the diffusion effect, in this study, the value of the diffusion factor $f_d(\alpha,T)$ is considered as the ratio of the experimental reaction rate to the reaction rate predicted by the autocatalytic chemical kinetic model given by equation (3.9) (which does not account for diffusion).

$$f_d(\alpha,T) = \frac{(d\alpha/dt)_{exptl.}}{(d\alpha/dt)_{model}} \qquad (6.24)$$

The values of the diffusion factor parameters — critical conversion α_c and co-efficient C are then obtained by applying non-linear regression to the diffusion factor $f_d(\alpha,T)$ function [defined in equation (3.19)] from a plot of $f_d(\alpha,T)$ vs. α data at each isothermal temperature as are listed in table 6.2(b).

Figures 6.13(c,d), 6.14(c,d), 6.15(c,d), 6.16(c,d), 6.17(c,d) and 6.18(c,d) illustrate the comparisons of experimental values of the isothermal reaction rates with the reaction rate curves calculated according to the predictions of autocatalytic kinetic model in equation (3.9), coupled with the diffusion factor $f_d(\alpha,T)$ [equation (3.19)], as a function of conversion and cure time respectively, at cure temperatures of 30°C, 40°C, 50°C, 60°C, 70°C and 80°C. The corresponding diffusion factors $f_d(\alpha,T)$ as a function of conversion are shown in figures 6.13(e) — 6.18(e). It can be seen that by including the diffusion factor $f_d(\alpha,T)$ in the conventional kinetic model [equation (6.25)], the agreement between experimental and predicted values of reaction rate is excellent at specific higher conversion region in the later stages of the cure, where a deviation appears due to the onset of vitrification. It is more evident at lower cure temperatures of 30°C, 40°C and 50°C, where the deviation appears to be greater.

$$\left(\frac{d\alpha}{dt}\right)_{simulated} \approx \left(\frac{d\alpha}{dt}\right)_{model} \times f_d(\alpha,T) = \left(\frac{d\alpha}{dt}\right)_{exptl.} \qquad (6.25)$$

Hence, including the diffusion factor $f_d(\alpha,T)$, the overall goodness of fit (r^2-value) of reaction rate data for the entire range of conversion slightly improves for the lower

cure temperature range (30°C—50°C) and that of higher cure temperature range (60°C—80°C) almost remains the same.

Figures 6.13(e) — 6.18(e) show the behaviour of diffusion factor $f_d(\alpha,T)$ with increasing conversion at cure temperatures of 30°C, 40°C, 50°C, 60°C, 70°C and 80°C respectively. It is of interest to follow the function $f_d(\alpha,T)$ as a function of conversion for a range of cure temperatures, as depicted in figures 6.13(e) — 6.18(e). The decrease in $f_d(\alpha,T)$ and hence, in the effective reaction rate due to onset of diffusion at higher conversions is clearly seen. It is evident from the figures that the downturn in $f_d(\alpha,T)$ at α_c increasingly occurs at higher conversions with increasing cure temperature.

When $\alpha << \alpha_c$, $f_d(\alpha,T)$ is close to unity, the reaction is kinetically controlled and the effect of diffusion is negligible. When α increases and approaches to α_c, $f_d(\alpha,T)$ begins to decrease. At $\alpha = \alpha_c$, $f_d(\alpha,T)$ becomes 0.5 and beyond this point, approaches zero as the reaction effectively stops. It shows that with increasing conversion, the effect of diffusion developed gradually. The effective reaction rate at any conversion is equal to the chemical reaction rate multiplied by $f_d(\alpha,T)$. So, when the cure reaction is dominated by the autocatalytic kinetic mechanism $f_d(\alpha,T)=1$, but as the reaction becomes more diffusion controlled, $f_d(\alpha,T)$ decreases exponentially.

It can be also seen that at a conversion greater than $\alpha = 0.7$ (basically, which is well above *theoretical gel point* $\alpha_{gel(theoretical)}$ = **0.5** for our studied system as discussed before), $f_d(\alpha,T)$ is dependent on the *conversion* and the *cure temperature* that describes the decreasing mobility of reactive units based on the inhibited reaction kinetics, associated with the onset of vitrification, which are due to the loss of free volume and molecular mobility. Basically, as the cure progresses, the resin crosslinks, and the glass transition temperature T_g of the system rise. When it approaches cure temperature, the resin passes from a rubbery state to a glassy state. At this stage, the mobility of the reacting groups is hindered and the rate of conversion is controlled by

216

diffusion rather than by chemical factors. The overall effective reaction rate constant k_e and $f_d(\alpha,T)$ are decreased with increasing conversion, and approaches zero when T_g is raised.

The onset of the vitrification of our studied thermosetting system may be detected at the point (at a conversion $\alpha > 0.75$, which is well above *theoretical gel point*), where the data of the experimental reaction rate deviates from that of the model predictions, or in other words when the diffusion factor $f_d(\alpha,T)$ becomes 0.5 (i.e. lower than 1) at $\alpha = \alpha_c$ (i.e. conversion reaches the critical value, α_c). As discussed earlier, this deviation is a consequence of the diffusion-controlled regime. *This accounts for the fact that the experimental reaction rates are lower than those predicted by the model.* Therefore, the critical conversions corresponding to the *onset of the diffusion* controlled reaction kinetics, most possibly can be considered here, at the conversions at which the *onset of vitrification* (from a theoretical point of view) occurs at the different curing temperatures below $T_{g\infty}$, the glass transition temperature of the fully cured material. As has already been mentioned that the effect of diffusion developed gradually, hence, vitrification phenomenon takes place during a time interval and not at a definite point [12].

For our studied thermosetting system, this aforementioned results suggest that *diffusion control becomes important only on vitrification and not on gelation* (which occurs at lower values of α), which is consistent with the results of other research workers [12,31,38,49,50,51] in this field. In this connection, here, it can be mentioned from Prime et al [50] that gelation does not usually inhibit cure, the reaction rate remains unchanged.

The variation of the critical conversion α_c with temperature is shown in figure 6.22. It can be seen that with increasing temperature the conversion at which diffusion control kinetics begins to dominate (onset of vitrification, from a theoretical point of view) occurs at a higher conversion. This is due to the thermosetting resin being able to stay mobile longer at the higher cure temperatures. Thus the diffusion factor

$f_d(\alpha,T)$ is a function of both conversion and temperature. The relationship of α_c with temperature can be considered *almost linear* within experimental error. The corresponding equations of linear regression and their squared correlation co-efficients, R^2 (i.e. co-efficients of determination) are also presented in figure 6.22.
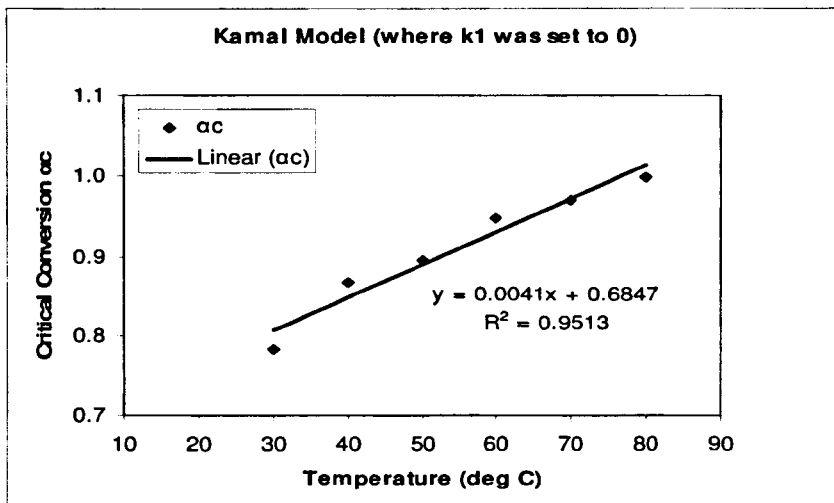
Figure 6.22 Dependence of the values of Critical conversion α_c on isothermal cure temperature based on Autocatalytic kinetic model $d\alpha/dt = k\alpha^m(1-\alpha)^n$ for cure process of Araldite 2015.
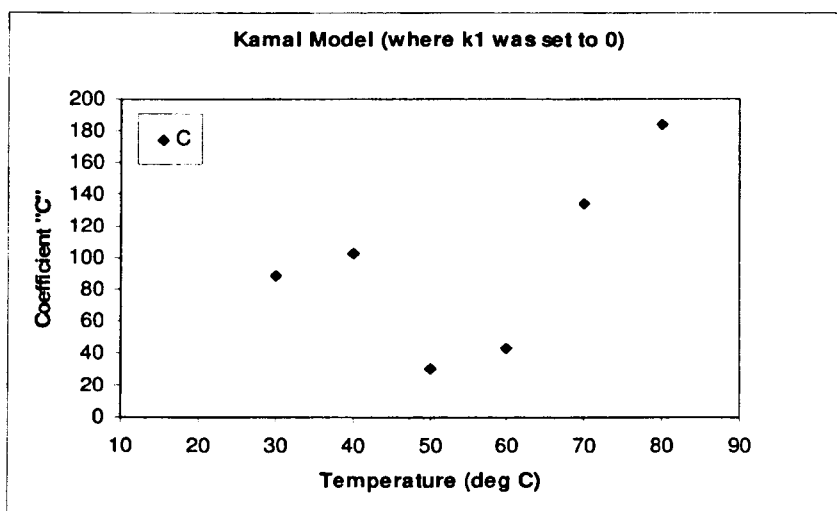
Figure 6.23 Dependence of the values of Co-efficient C on isothermal cure temperature based on Autocatalytic model $d\alpha/dt = k\alpha^m(1-\alpha)^n$ for cure process of Araldite 2015.

Figure 6.23 illustrates the variation of the co-efficient C with temperature. For the co-efficient C, there is considerably more scatter, and no discernible trend with temperature is observed. It can be noted that Cole et al [38] in their studies on epoxy-amine curing also had observed linear trend for variation of α_c with temperature, but did not observe any trend for variation of C with temperature. For diffusion factor parameters α_c and C, similar observation also have been reported by Park et al [49] for epoxy/phenol-novolac resin blend system.

It is worth mentioning that the critical conversion α_c is a particularly *useful parameter* because it specifically relates to the point at which diffusion control kinetics begins to dominate the reaction. For our studied resin system, it corresponds to the *onset of vitrification* (from a theoretical point of view) occurs at the different curing temperatures below $T_{g\infty}$. Basically, the critical conversion α_c is *not an adjustable parameter* as it reflects the onset of diffusional limitation that occurs only in the later stages of curing reaction. It is also *not an observable quantity* since the transition to the diffusion regime is gradual. As the cure proceeds, the mobility of the reacting species is reduced leading to diffusional effects. Since α_c increasingly occurs at higher conversions with increasing cure temperature, hence, α_c would *reflect the state of cure of the system as well as the temperature of cure*. Therefore, taking into account the diffusion factor $f_d(\alpha, T)$ [figures 6.13(e) — 6.18(e)] enables us to explore the in depth information associated with the diffusion controlled kinetics due to vitrification in isothermal measurement related to our data.

6.5 Autocatalytic Kinetic Model of Gonzalez-Romero (where α_{max} was used)

Gonzalez-Romero et al [41] used the following equation describing autocatalytic reaction kinetics to include the vitrification phenomenon:

$$\frac{d\alpha}{dt} = k(\alpha_{max} - \alpha)^n e^{m\alpha} \qquad (6.26)$$

In this equation, the terms have the usual definitions. From Taylor's series expansion of $e^{m\alpha}$ we get

$$e^{m\alpha} = 1 + m\alpha + \frac{(m\alpha)^2}{2!} + \frac{(m\alpha)^3}{3!} + \dots \dots \dots$$ (6.27)

From equation (6.26) it can be seen that because of the term $e^{m\alpha}$, at $\alpha = 0$ $d\alpha/dt \neq 0$.

To satisfy the *non-zero initial rate of reaction* as observed in our isothermal reaction rate profiles, we consider this autocatalytic model given by equation (6.26) to fit our experimental data to analyze the cure kinetics of our studied epoxy system. It will also enable us to compare the results with those obtained with the previous autocatalytic models we employed.

The final form of expression of α_{max} given by equation (6.11) has already been described before. The values of the best fit kinetic parameters determined from the non-linear regression analysis based on the autocatalytic kinetic model $\frac{d\alpha}{dt} = k(\alpha_{max} - \alpha)^n e^{m\alpha}$ given by equation (6.26) for isothermal cure process of Araldite 2015 are listed in table 6.3, together with the corresponding standard errors (SE) and the squared correlation co-efficient (i.e. co-efficient of determination) for fit of model to the experimental data.

Figures 6.24 (a—f) and 6.25 (a—f) illustrate the comparisons of experimental values of the isothermal reaction rates with the reaction rate curves calculated according to the predictions of autocatalytic kinetic model in equation (6.26), as a function of conversion and cure time respectively, at cure temperatures of — (a) 30°C, (b) 40°C, (c) 50°C, (d) 60°C, (e) 70°C and (f) 80°C.

It can be seen from figures 6.24 (a—f) and 6.25 (a—f) that for the entire range of conversion, the better degree of agreement of fit results with the experimental data at lower curing temperature range (30°C—50°C).In general, the differences between model predictions and experimental data are observed to be smaller when the curing temperature decreases. Hence, the fit worsens as the cure temperature is increased and becomes better as the cure temperature is lowered. At the initial stages of cure at $\alpha = 0$, the simulations show *non-zero initial rates of reaction*, the characteristic

feature which our reaction rate profiles display. However, the accuracy of simulation is poor when looking near the autocatalytic peak regions of the rate-conversion profiles at higher curing temperature range (60°C—80°C).The observed deviation due to inability to simulate the peak can be attributed to the lack of validity of the model in this region. This model allows increased accuracy at the later stages of the cure for the rate profiles of 30°C, 40°C, 50°C and 60°C (based on the model predictions). The reaction rate profiles of 70°C and 80°C suffer from poor fit of kinetic data as well as inaccuracies at the later stages of the cure.

As mentioned in table 6.3; for this model an iso-conversional analysis is utilized to find out the activation energy E_a value because of the reliability and advantageous features of this analysis which has already been discussed before. All the parameter values reported in the table 6.3 agree well with those obtained for almost similar or comparable epoxy-amine systems [5, 6, 7, 8, 9, 13, 21, 22, 46].

Table 6.3 The values of the kinetic parameters of the Autocatalytic model of Gonzalez-Romero $\dfrac{d\alpha}{dt} = k(\alpha_{max} - \alpha)^n e^{m\alpha}$ **for isothermal cure process of Araldite 2015. E_a is the average value of activation energy obtained from iso-conversional method.**

T_{cure} (°C)	k^* (min^{-1})	m^*	n^*	$m+n$	$\ln A$ (min^{-1})	E_a (kJ/mol)	r^{2**}
30	0.006(.000)	0.435(.020)	0.764(.007)	1.199	16.911		0.984
40	0.010(.000)	0.651(.007)	1.002(.003)	1.653	16.688		0.998
50	0.020(.000)	1.176(.013)	1.389(.006)	2.565	16.714	55.50	0.997
60	0.036(.000)	1.149(.024)	1.551(.012)	2.700	16.701		0.993
70	0.065(.000)	1.709(.055)	1.823(.028)	3.532	16.691		0.979
80	0.106(.001)	2.975(.100)	2.547(.054)	5.522	16.666		0.969
Average	0.040	1.349	1.512	2.861	16.728		

* Values in parentheses correspond to standard errors (SE).
** Squared correlation co-efficient (i.e. co-efficient of determination) of curve fitting.

Figure 6.24(a—f) Isothermal reaction rates as a function of conversion — comparisons of experimental data with the predictions of Autocatalytic kinetic model $d\alpha/dt = k(\alpha_{max} - \alpha)^n e^{m\alpha}$ at cure temperatures of :(a) 30°C, (b) 40°C, (c) 50°C, (d) 60°C, (e) 70°C and (f) 80°C.
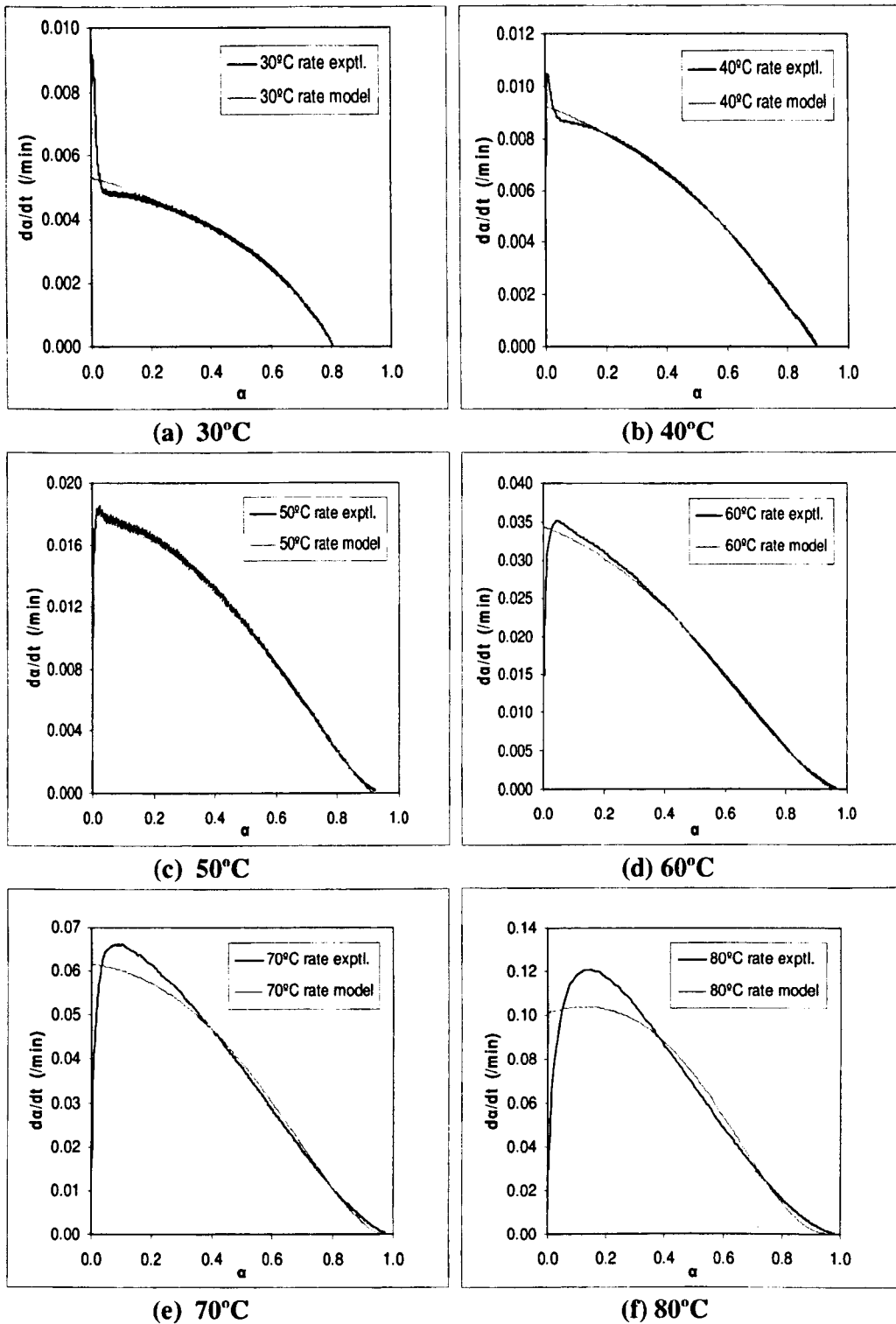
222
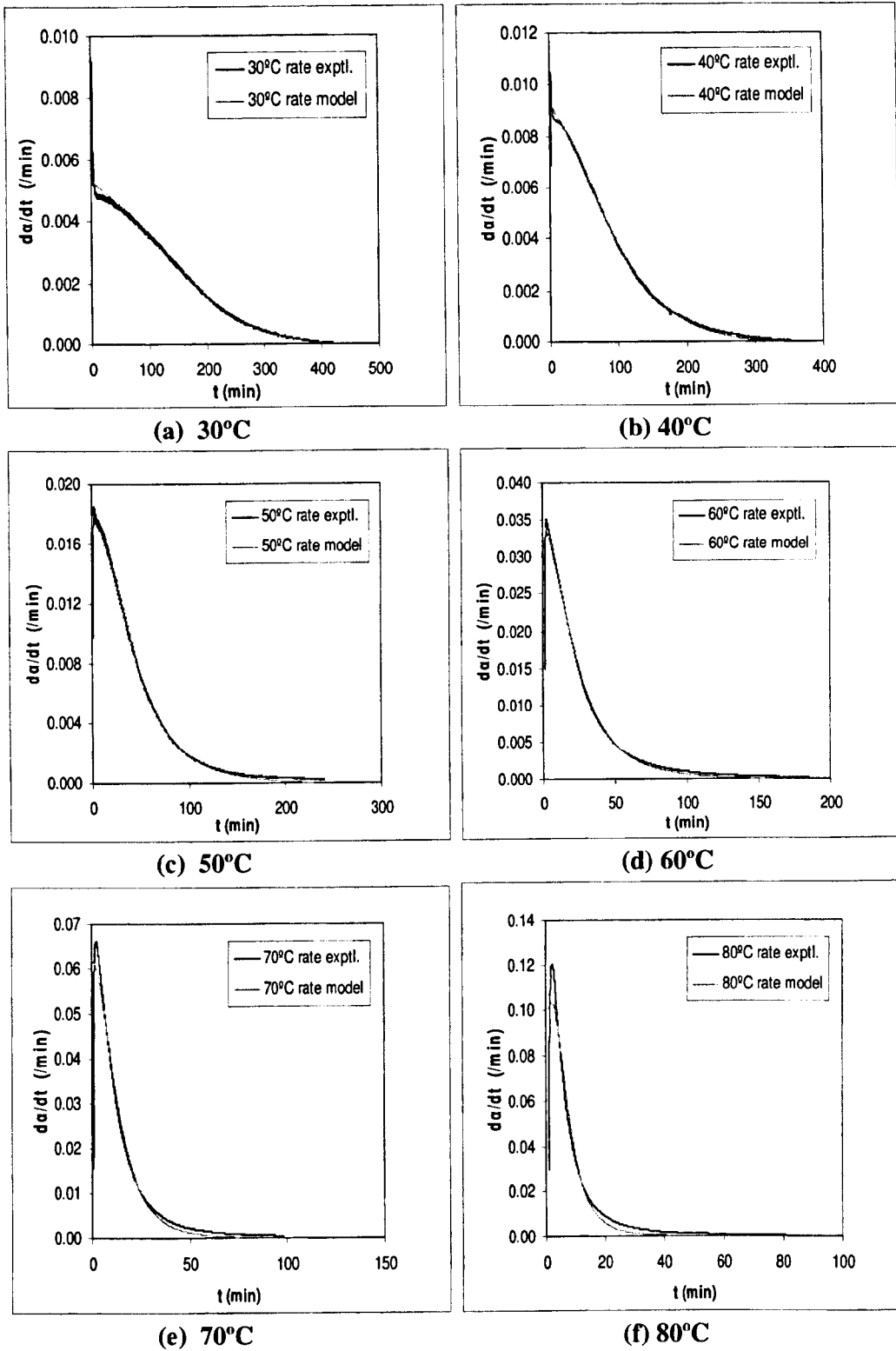
Figure 6.25(a—f) Isothermal reaction rates as a function of cure time — comparisons of experimental data with the predictions of Autocatalytic kinetic model $d\alpha/dt = k(\alpha_{max} - \alpha)^n e^{m\alpha}$ at cure temperatures of :(a) 30°C, (b) 40°C, (c) 50°C, (d) 60°C, (e) 70°C and (f) 80°C.

It can be seen from the table 6.3 that the values of kinetic parameters k, m, n and *(m+n)* based on the autocatalytic model of Gonzalez-Romero given by equation (6.26) increase with increasing cure temperature. Similar trend have already been observed with those kinetic parameters obtained based on the autocatalytic model with α_{max} in equation (6.8) as reported in table 6.1, and conventional autocatalytic model given by equation (3.9) as reported in table 6.2(a).The interpretation of the temperature dependence of kinetic parameters discussed earlier in that context. We found that the increase in the value of the overall reaction order *(m+n)* with isothermal cure temperature, permits the prediction of the molecular mechanism of curing reaction, consistent with the results of other recent workers [17], founded on trimolecular catalysis mechanism as elucidated before.

The plots of the reaction orders m and n as a function of isothermal cure temperature for the autocatalytic model of Gonzalez-Romero given by equation (6.26) is shown in figure 6.26.As suggested by these plots, the reaction order n increases with the increase of cure temperature following an almost linear relation. Similar results have been observed for the cure of epoxy-amine systems [7, 13, 21, 27, 28, 36]. But there is a great deal of scatter in the linear fit for the reaction order m. Thus the relationship is not approximately linear within experimental error, which is reflected in the R^2 value. The corresponding equations of linear regression and their squared correlation co-efficients, R^2 (i.e. co-efficients of determination) are also presented in figure 6.26. The temperature variation of the reaction orders suggest that either the reaction mechanism of the system may changes with cure temperature or it is purely empirical.

The Arrhenius plots of *ln k* as a function of 1/T is shown in figure 6.27. In this figure, good linear correlation is observed, which leads to calculate the apparent activation energy from the slope of the straight line, which is 52.248 kJ/mol, as indicated in the figure. The consideration of the average value of apparent activation energy E_a obtained from iso-conversional method, instead of activation energy E_a obtained from single reaction rate constant was justified before.

Gonzalez-Romero Model (where αmax was used)

Reaction order (m,n)

y = 0.033x - 0.3008
R^2 = 0.9492

y = 0.0453x - 1.1411
R^2 = 0.8611

◆ m
■ n
—— Linear (m)
—— Linear (n)
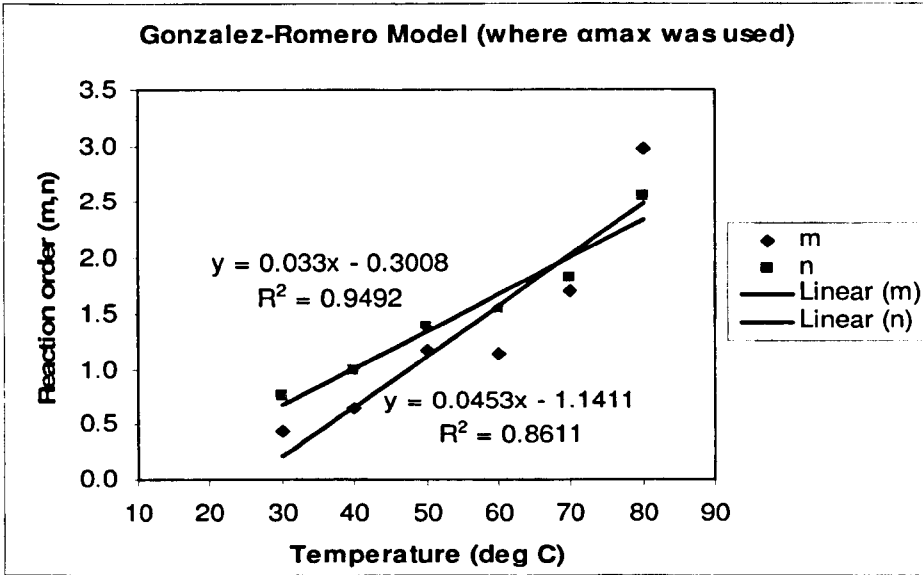
Temperature (deg C)

Figure 6.26 The plots showing the effect of the isothermal cure temperature on the reaction orders m and n with associated fits; based on the Autocatalytic kinetic model $d\alpha/dt = k(\alpha_{max} - \alpha)^n e^{m\alpha}$ for isothermal cure process of Araldite 2015.

Gonzalez-Romero Model (where αmax was used)

ln k (/min)

y = -6284.1x + 15.555
R^2 = 0.9979
Ea=52.248 kJ/mol
ln A=15.555 /min

◆ ln k (/min)
—— Linear (ln k (/min))

1/T(1/K)
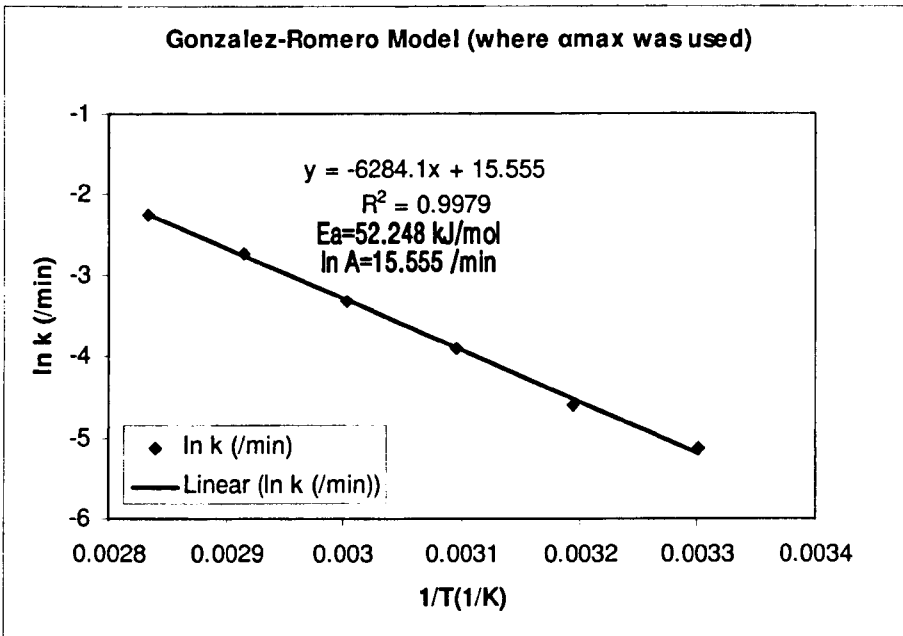
Figure 6.27 The Arrhenius plots of the temperature dependence of the isothermal reaction rate constant k determined from the non-linear regression analysis based on the Autocatalytic kinetic model $d\alpha/dt = k(\alpha_{max} - \alpha)^n e^{m\alpha}$ for isothermal cure process of Araldite 2015.

6.6 Autocatalytic Kinetic Model of Gonzalez-Romero (without α_{max})

Using conventional full conversion (i.e.1) instead of α_{max} in equation (6.26), the autocatalytic kinetic model of Gonzalez-Romero et al [41] becomes

$$\frac{d\alpha}{dt} = k(1-\alpha)^n e^{m\alpha} \qquad (6.28)$$

To satisfy the *non-zero initial rate of reaction* as observed in our isothermal reaction rate profiles, we consider this autocatalytic model given by equation (6.28) to fit our experimental data to analyze the cure kinetics of our studied epoxy system. It will also enable us to compare the results with those obtained with the similar autocatalytic model with inclusion of α_{max} instead of complete conversion 1 as given by equation (6.26) and also with the previous autocatalytic models we employed. Moreover, it may provide us with information associated with the diffusion controlled kinetics due to vitrification in isothermal measurement related to our data.

The values of the best fit kinetic parameters determined from the non-linear regression analysis based on the autocatalytic kinetic model $d\alpha/dt = k(1-\alpha)^n e^{m\alpha}$ for isothermal cure process of Araldite 2015 are listed in table 6.4(a), together with the corresponding standard errors (SE) and the squared correlation co-efficient (i.e. co-efficient of determination) for fit of model to the experimental data.

Figures 6.28(a,b), 6.29(a,b), 6.30(a,b), 6.31(a,b), 6.32(a,b) and 6.33(a,b) illustrate the comparisons of experimental values of the isothermal reaction rates with the reaction rate curves calculated according to the predictions of autocatalytic kinetic model in equation (6.28), as a function of conversion and cure time respectively, at cure temperatures of 30°C, 40°C, 50°C, 60°C, 70°C and 80°C.

As mentioned in table 6.4(a); for this model an iso-conversional analysis is utilized to find out the activation energy E_a value because of the reliability and advantageous features of this analysis which has already been discussed before. All the parameter

values reported in the table 6.4(a) agree well with those obtained for almost similar or comparable epoxy-amine systems [5, 6, 7, 8, 9, 13, 21, 22, 46].

It can be seen from figures 6.28(a,b) — 6.33(a,b) that in general, the better degree of agreement of fit results with the experimental data at lower curing temperature range (30°C–50°C). The fit worsens as the cure temperature is increased to70°C and 80°C. At the initial stages of cure at $\alpha = 0$, the simulations show *non-zero initial rates of reaction*, the characteristic feature which the reaction rate profiles of our studied thermosetting system display. However, the accuracy of simulation is poor when looking near the autocatalytic peak regions of the rate-conversion profiles at higher curing temperature range (60°C–80°C).The observed deviation due to inability to simulate the peak can be attributed to the lack of validity of the model in this region. The reaction rate profiles of 70°C and 80°C suffer from poor fit of kinetic data.

It is also evident from figures 6.28(a,b) — 6.33(a,b) that in the later stages of the cure at higher conversions the data of the model predictions slightly deviate from that of the experimental. This is due to the onset of vitrification where the mobility of the reactive groups is hindered and the rate of conversion is controlled by diffusion rather than by chemical factors.This accounts for the fact that the experimental reaction rates are lower than those predicted by the model given by equation (6.28).Differences between model predictions and experimental data are observed to be greater when curing temperature decreases. This is reflected in figures 6.28(a,b), 6.29(a,b) and 6.30(a,b) corresponding to cure temperatures of 30°C, 40°C, and 50°C respectively. This can be interpreted considering the T_g of the fully cured material in association with free volume as stated before.

As mentioned earlier using the diffusion factor, the reaction rate can be expressed in the following form to account for effects of diffusion:

$$\frac{d\alpha}{dt} = k(1-\alpha)^n e^{m\alpha} f_d(\alpha, T) = \frac{k(T)}{1+\exp[C(\alpha-\alpha_c)]}(1-\alpha)^n e^{m\alpha} \qquad (6.29)$$

Table 6.4(a) The values of the kinetic parameters of the Autocatalytic model of Gonzalez-Romero $\dfrac{d\alpha}{dt} = k(1-\alpha)^n e^{m\alpha}$ for isothermal cure process of Araldite 2015. E_a is the average value of activation energy obtained from iso-conversional method.

T_{cure} (°C)	k^* (min^{-1})	m^*	n^*	$m+n$	lnA (min^{-1})	E_a (kJ/mol)	r^{2**}
30	0.005(.000)	3.482(.059)	3.161(.034)	6.643	16.729		0.960
40	0.009(.000)	2.409(.022)	2.329(.012)	4.738	16.583		0.993
50	0.017(.000)	2.404(.016)	2.380(.009)	4.784	16.551	55.50	0.997
60	0.034(.000)	1.686(.023)	1.989(.012)	3.675	16.643		0.994
70	0.061(.000)	2.039(.054)	2.111(.029)	4.150	16.627		0.981
80	0.100(.001)	3.237(.100)	2.803(.056)	6.040	16.607		0.970
Average	0.037	2.540	2.462	5.005	16.623		

* Values in parentheses correspond to standard errors (SE).
** Squared correlation co-efficient (i.e. co-efficient of determination) of curve fitting.

Table 6.4(b) The values of the Diffusion factor f_d (α,T) parameters-- Co-efficient C and Critical Conversion (α_c) of the Autocatalytic model $\dfrac{d\alpha}{dt} = k(1-\alpha)^n e^{m\alpha} f_d(\alpha,T)$ for isothermal cure process of Araldite 2015.

T_{cure} (°C)	C^*	α_c^*
30	137.865 (2.629)	0.791 (.000)
40	167.605 (1.988)	0.880 (.000)
50	33.075 (0.435)	0.920 (.000)
60	234.358 (6.432)	0.960 (.000)
70	301.470 (7.392)	0.970 (.001)
80	334.946 (0.000)	0.999 (.000)

* Values in parentheses correspond to standard errors (SE).

Figure 6.28(a—f) Isothermal reaction rates as a function of conversion (**a, c, f**) and cure time (**b, d**)—comparisons of experimental data with the predictions of model $d\alpha/dt = k(1-\alpha)^n e^{m\alpha}$ at 30°C; without f_d (α, T), with f_d (α, T), and the corresponding f_d (α, T) as a function of conversion (**e**), as all are indicated in the figures.

229
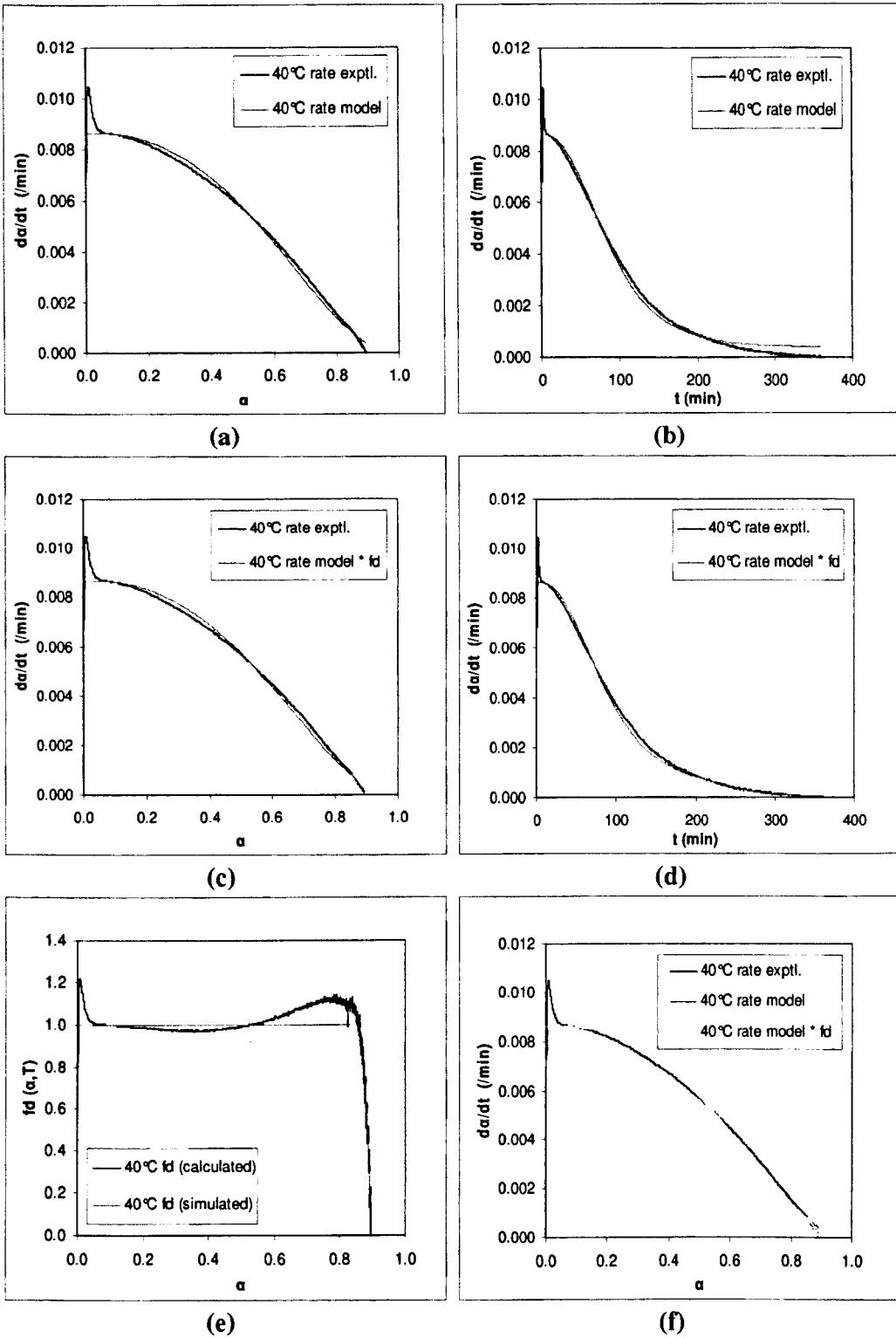
Figure 6.29(a—f) Isothermal reaction rates as a function of conversion **(a, c, f)** and cure time **(b, d)**—comparisons of experimental data with the predictions of model $d\alpha/dt = k(1-\alpha)^n e^{m\alpha}$ at 40°C; without f_d (α, T), with f_d (α, T), and the corresponding f_d (α, T) as a function of conversion **(e)**, as all are indicated in the figures.
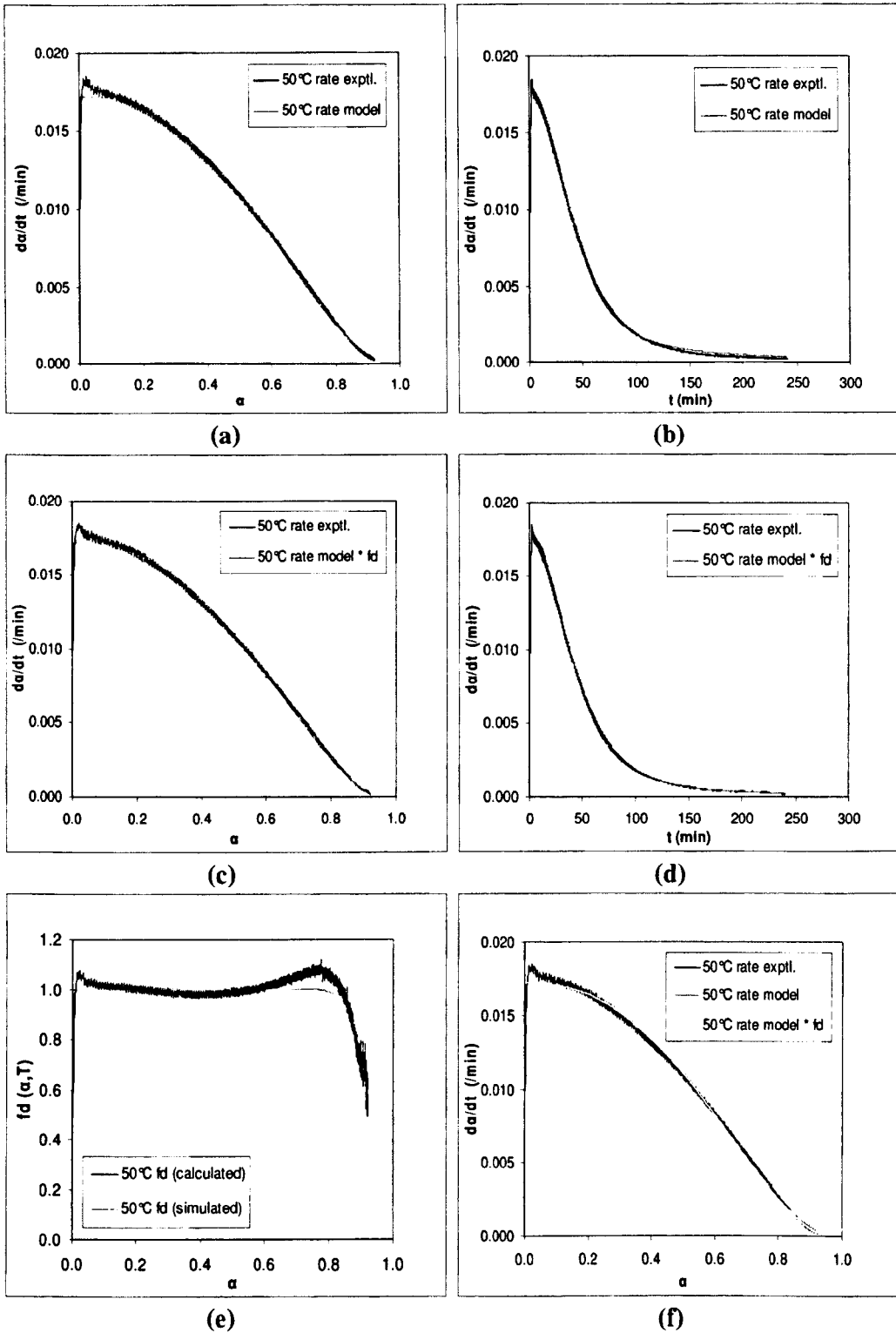
Figure 6.30(a—f) Isothermal reaction rates as a function of conversion (**a, c, f**) and cure time (**b, d**)—comparisons of experimental data with the predictions of model $d\alpha/dt = k(1-\alpha)^n e^{m\alpha}$ at 50°C; without $f_d\,(\alpha,T)$, with $f_d\,(\alpha,T)$, and the corresponding $f_d\,(\alpha,T)$ as a function of conversion (**e**), as all are indicated in the figures.

231
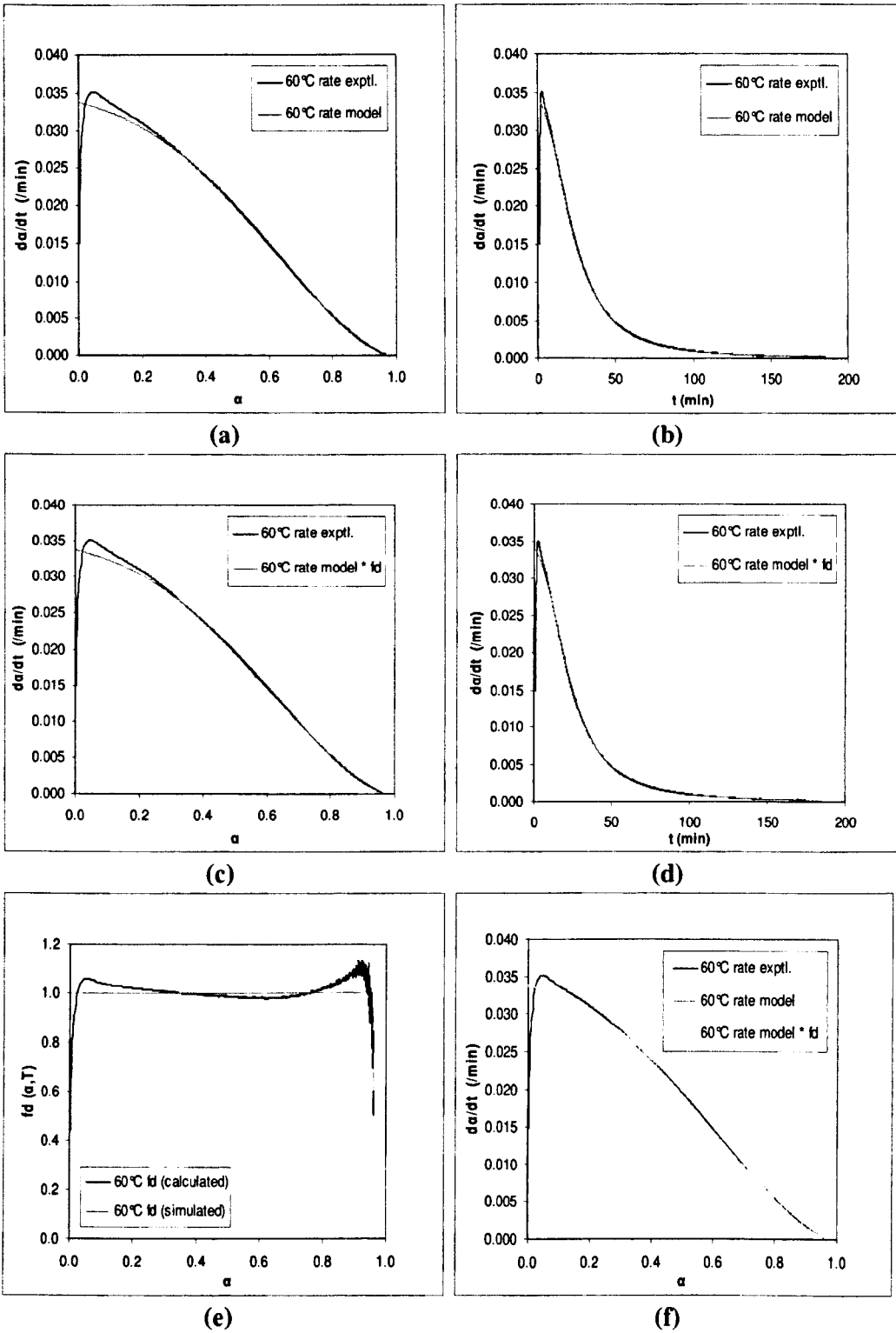
Figure 6.31(a—f) Isothermal reaction rates as a function of conversion (**a, c, f**) and cure time (**b, d**)—comparisons of experimental data with the predictions of model $d\alpha/dt = k(1-\alpha)^n e^{m\alpha}$ at 60°C; without $f_d (\alpha, T)$, with $f_d (\alpha, T)$, and the corresponding $f_d (\alpha, T)$ as a function of conversion (**e**), as all are indicated in the figures.
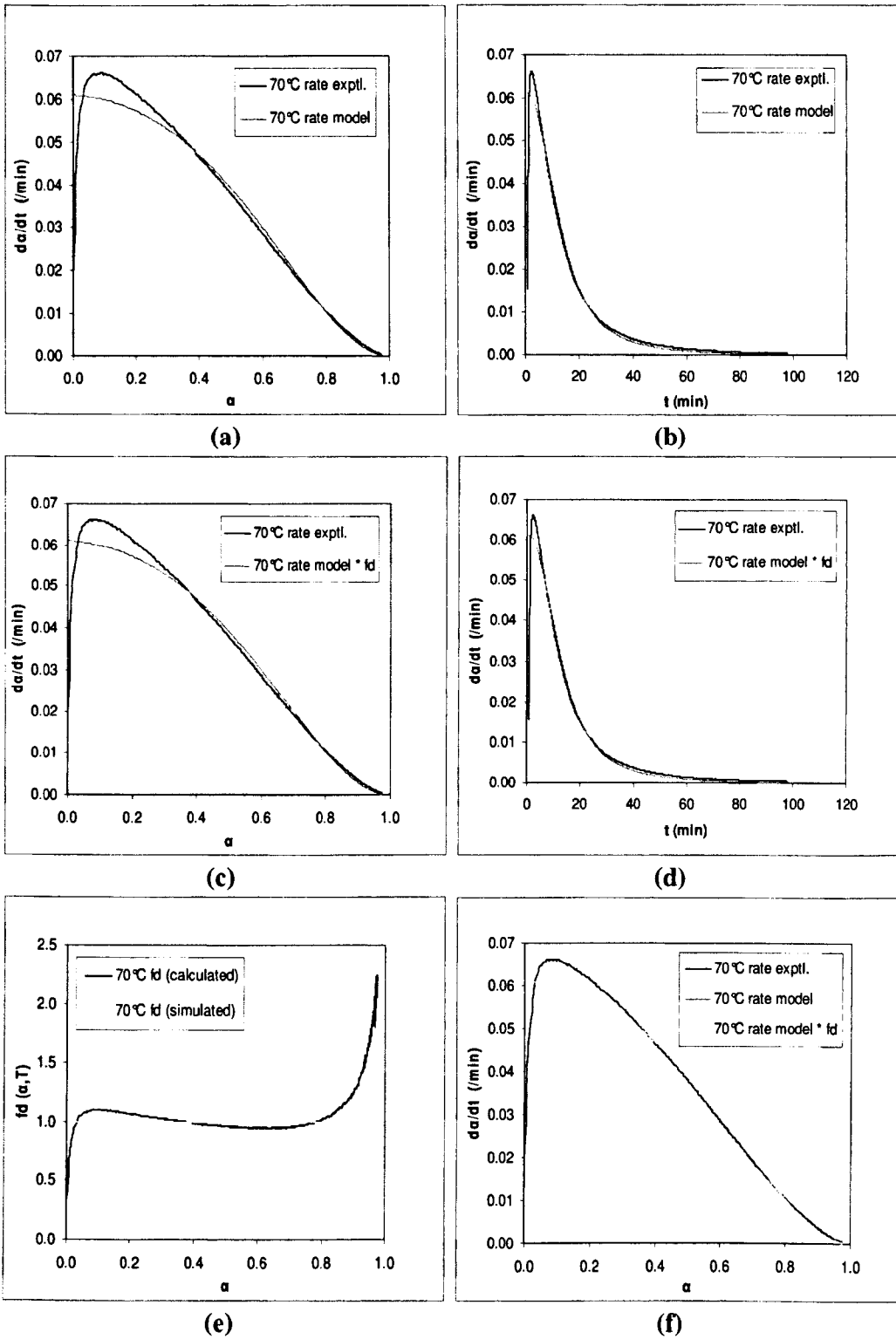
Figure 6.32(a—f) Isothermal reaction rates as a function of conversion (**a, c, f**) and cure time (**b, d**)—comparisons of experimental data with the predictions of model $d\alpha/dt = k(1-\alpha)^n e^{m\alpha}$ at 70°C; without f_d (α,T), with f_d (α,T), and the corresponding f_d (α,T) as a function of conversion (**e**), as all are indicated in the figures.
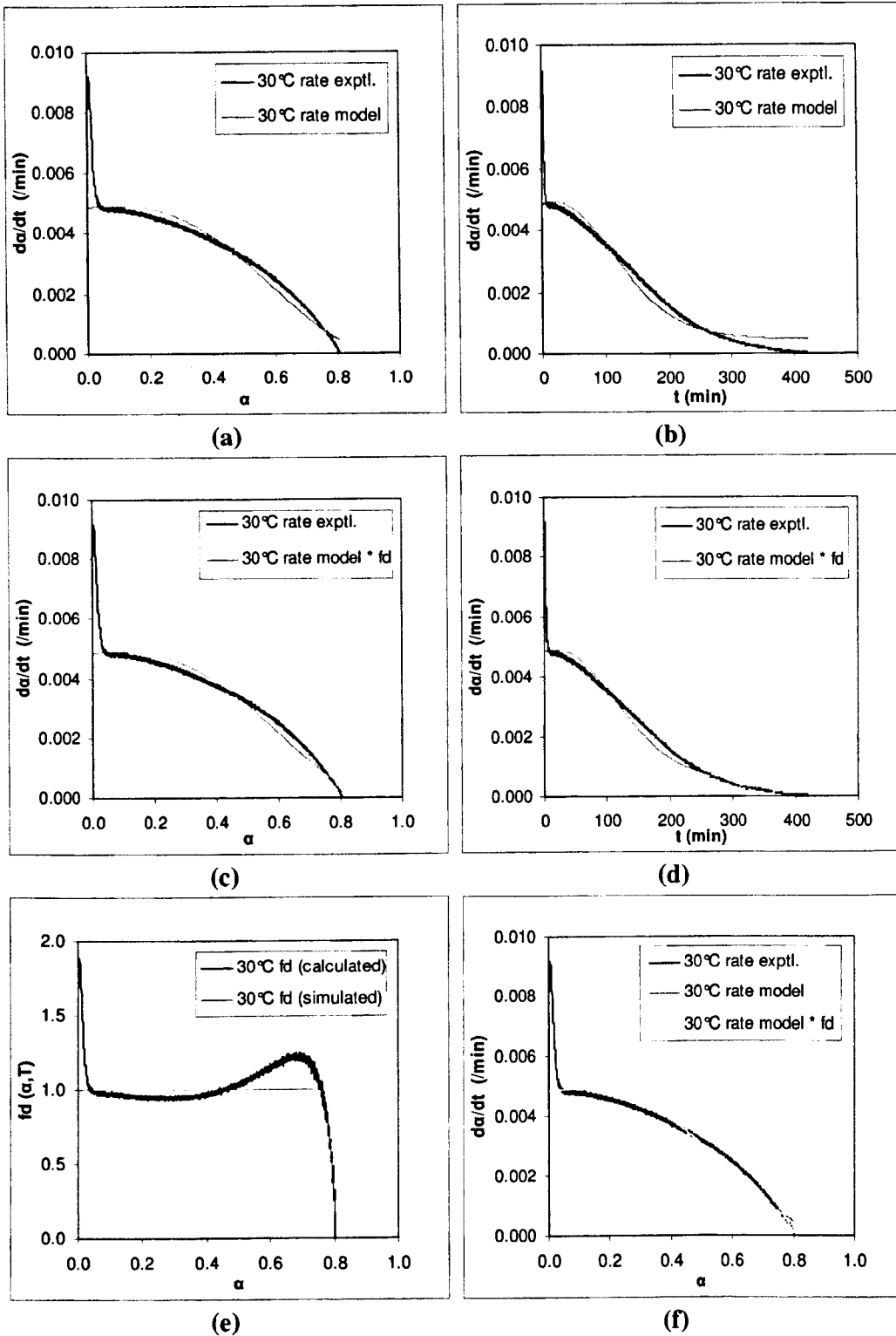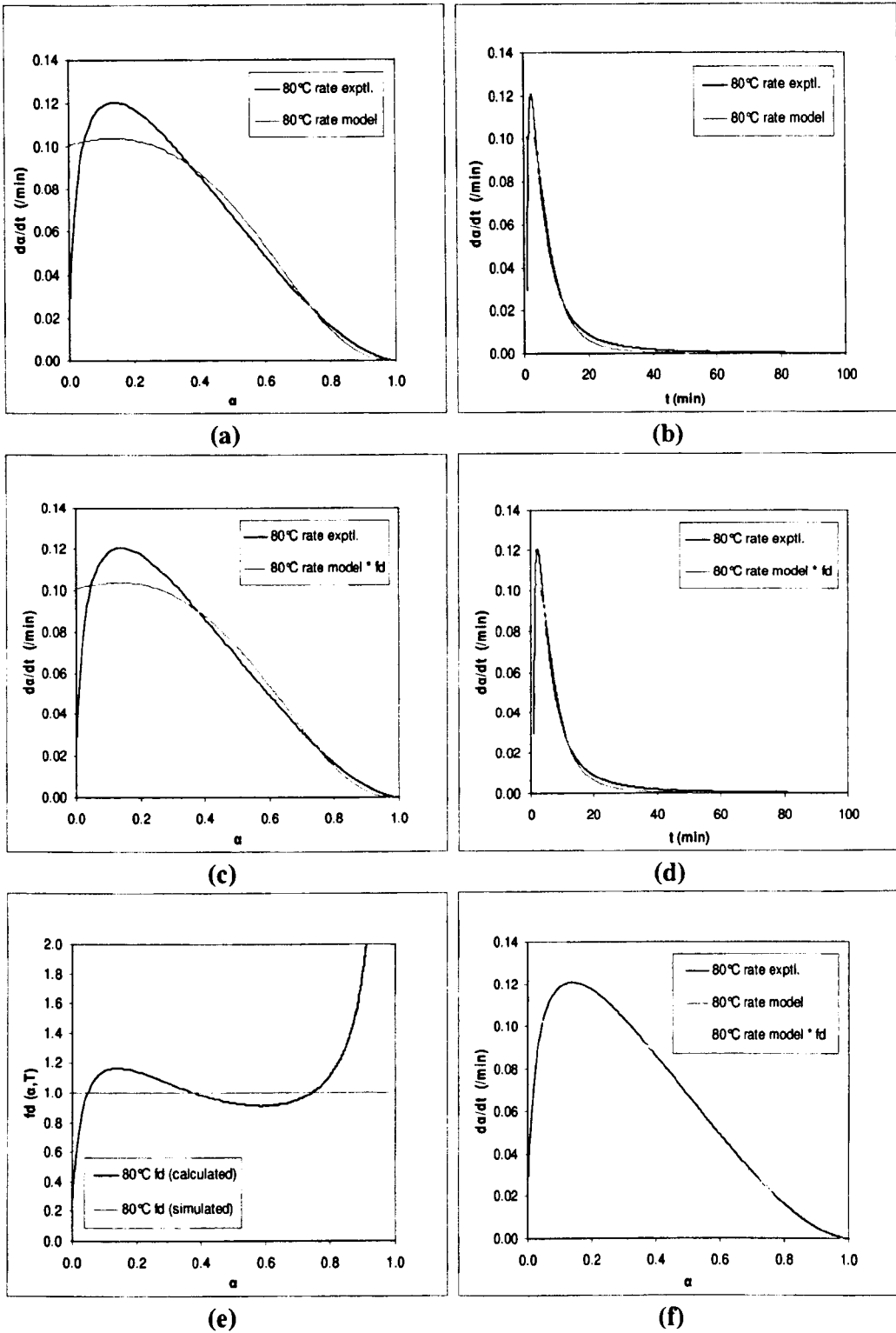
Figure 6.33(a—f) Isothermal reaction rates as a function of conversion (**a, c, f**) and cure time (**b, d**)—comparisons of experimental data with the predictions of model $d\alpha/dt = k(1-\alpha)^n e^{m\alpha}$ at 80°C; without $f_d(\alpha, T)$, with $f_d(\alpha, T)$, and the corresponding $f_d(\alpha, T)$ as a function of conversion (**e**), as all are indicated in the figures.

The plots of the reaction orders m and n as a function of isothermal cure temperature for the autocatalytic model in equation (6.28) are shown in figures 6.34(a) and (b). The dependence of m and n on temperature is not easy to discern as shown by the representative data depicted in the figures. As seen from the figures, a more complicated *fifth-order polynomial dependence* is used here to fit both of the reaction orders m and n. The corresponding equations of polynomial fit and their squared correlation co-efficients, R^2 (i.e. co-efficients of determination) are also presented in figures 6.34(a) and (b). The temperature variation of the reaction orders, especially at 70°C and 80°C, suggest that either the reaction mechanism of the system may changes with temperature which indicate may be the presence of more than one type of cure mechanism, or, it is purely empirical. The Arrhenius plots of $ln\ k$ as a function of 1/T is shown in figure 6.35. In this figure, good linear correlation is observed, which leads to calculate the apparent activation energy from the slope of the straight line, which is 54.425 kJ/mol, as indicated in the figure.

The values of the diffusion factor $f_d(\alpha, T)$ parameters — critical conversion α_c and co-efficient C of the model given by equation (6.29) obtained by applying non-linear regression to the $f_d(\alpha, T)$ vs. α data at each isothermal temperature are listed in table 6.4(b).

Figures 6.28(c,d), 6.29(c,d), 6.30(c,d), 6.31(c,d), 6.32(c,d) and 6.33(c,d) illustrate the comparisons of experimental values of the isothermal reaction rates with the reaction rate curves calculated according to the predictions of autocatalytic kinetic model in equation(6.28),coupled with the diffusion factor $f_d(\alpha, T)$ [equation (3.19)], as a function of conversion and cure time respectively, at cure temperatures of 30°C, 40°C, 50°C, 60°C, 70°C and 80°C. The corresponding diffusion factors $f_d(\alpha, T)$ as a function of conversion are shown in figures 6.28(e) — 6.33(e).It can be seen that by including the diffusion factor $f_d(\alpha, T)$ in the kinetic model, the agreement between experimental and predicted values of reaction rate is excellent at the specific higher conversion region in the later stages of the cure, where a deviation appears due to the onset of vitrification. It is more evident at lower cure temperatures of 30°C, 40°C and 50°C, where the deviation appears to be greater. Hence, including the diffusion
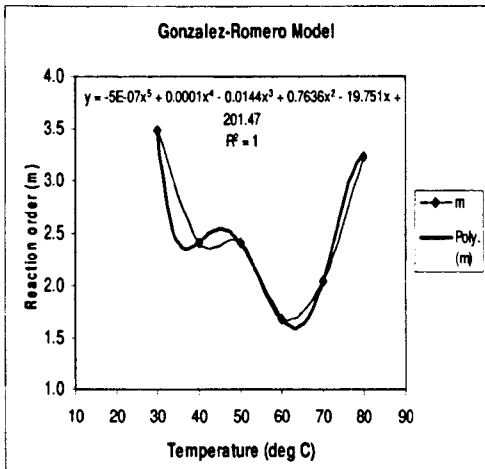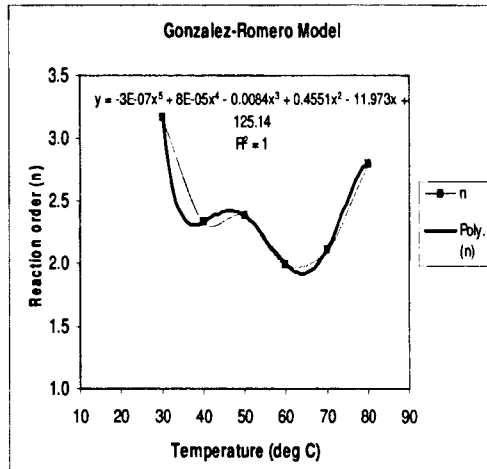
Figure 6.34 The plots showing the effect of the isothermal cure temperature on the reaction orders **(a)** m and **(b)** n with associated fits; based on the Autocatalytic kinetic model $d\alpha/dt = k(1-\alpha)^n e^{m\alpha}$ for isothermal cure process of Araldite 2015.
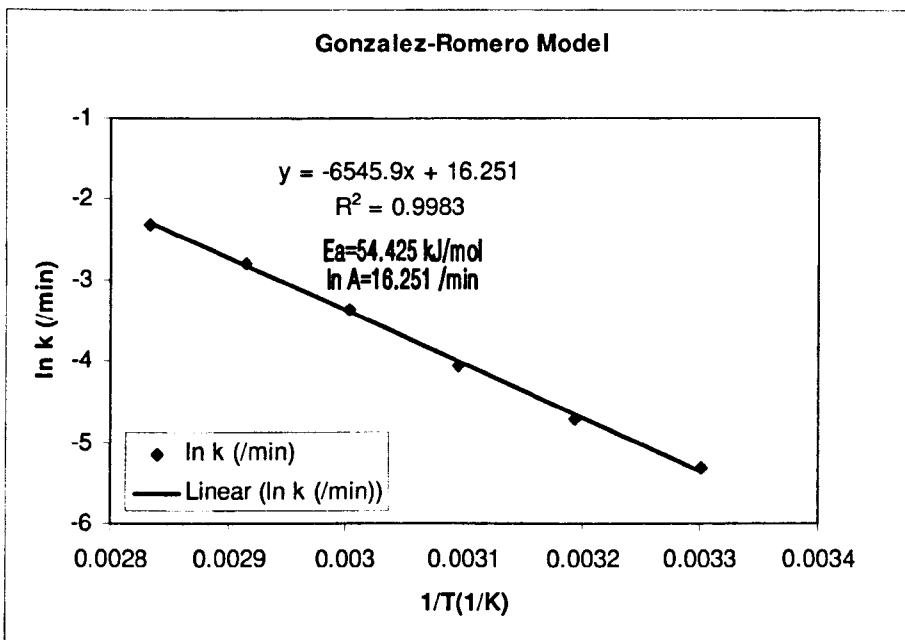
Figure 6.35 The Arrhenius plots of the temperature dependence of the isothermal reaction rate constant k determined from the non-linear regression analysis based on the Autocatalytic kinetic model $d\alpha/dt = k(1-\alpha)^n e^{m\alpha}$ for isothermal cure process of Araldite 2015.

factor $f_d(\alpha,T)$, the overall goodness of fit (r^2-value) of reaction rate data for the entire range of conversion slightly improves for the lower cure temperature range (30°C–50°C) and that of higher cure temperatures range (60°C–80°C) almost remains the same.

Figures 6.28(e) − 6.33(e) show the behaviour of diffusion factor $f_d(\alpha,T)$ with increasing conversion at cure temperatures of 30°C, 40°C, 50°C, 60°C, 70°C and 80°C respectively. It is evident from the figures that the downturn in $f_d(\alpha,T)$ at α_c due to onset of diffusion increasingly occurs at higher conversions with increasing cure temperature. Similar trend of inhibited reaction kinetics associated with the onset of vitrification at critical conversion α_c is evident with those diffusion factor parameters obtained based on the autocatalytic model in equation (6.23), consistent with the results of other research workers [12,31,38,49,50,51], which has already been discussed in details in that context in section 6.4.2.

(a)   (b)

Figure 6.36 Dependence of the values of (a) Critical conversion α_c and (b) Co-efficient C on isothermal cure temperature based on Autocatalytic kinetic model $d\alpha/dt = k(1-\alpha)^n e^{m\alpha}$ for cure process of Araldite 2015.

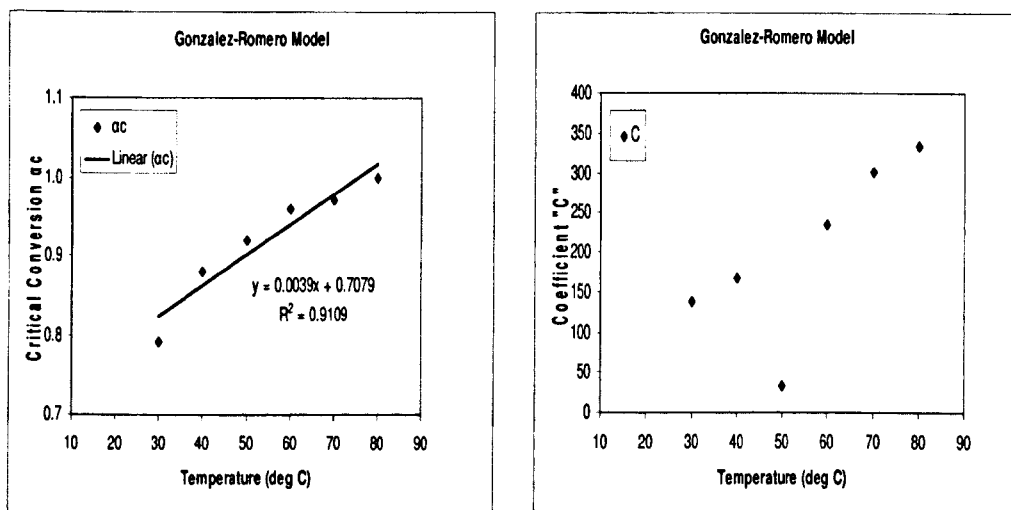The variation of the critical conversion α_c with temperature is shown in figure 6.36(a). It can be seen that with increasing temperature α_c occurs at a higher conversion as the thermosetting resin being able to stay mobile longer at the higher cure temperatures.

Thus the diffusion factor $f_d(\alpha, T)$ is a function of both conversion and temperature. The relationship of α_c with temperature can be considered *almost linear* within experimental error. The corresponding equations of linear regression and their squared correlation co-efficients, R^2 (i.e. co-efficients of determination) are also presented in figure 6.36(a). Figure 6.36(b) illustrates the variation of the co-efficient C with temperature. For the co-efficient C no discernible trend with temperature is observed. For diffusion factor parameters α_c and C, similar observations also have been reported by other authors [38,49] as mentioned earlier in section 6.4.2.

Comparing the results obtained with the both forms of autocatalytic model of Gonzalez- Romero given by equations (6.26) and (6.28) it is evident that the better degree of agreement of fit results with the experimental data at lower curing temperature range (30°C—50°C) and the fit worsens as the cure temperature is increased.

6.7 Analysis of the Isothermal Cure Kinetics Using Avrami Model

Apart from the traditional kinetic models, Avrami theory, as pointed out by Kim et al [52], has already been narrated in chapter 3. Basically, the Avrami theory is based on the phase change and most often used to describe the dynamic process of polymer crystallization since many molecular aggregates or high-molecular-weight particles have been observed during an infinite network formation as a result of crosslinking. In a broad sense, *crystallization can be considered as a physical form of cross-linking* and in some aspects the behaviour of amorphous cross-linking polymers is similar to that of crystals. Therefore, it is possible to predict the cure process of thermosets using the Avrami equation. Previous studies on the cure kinetics of the epoxy resin [52,53] using the Avrami equation show good agreement between theoretical predictions and experimental DSC data. In particular, more recently Avrami equation has also been found to account well for the autocatalytic cure kinetics of epoxy-amine systems [18].Therefore, *based on the similarity between the cure process and the crystallization process*, we consider Avrami model given by equation (3.21) in chapter 3 to fit our experimental data to analyze the cure kinetics of our studied epoxy system.

The simple Avrami expression given by equation (3.21) is as follows —

$$\alpha = 1 - \exp(-kt^n)$$

Where, α is the extent of cure at time t, k is the rate constant and n is the *Avrami exponent* which provides qualitative information on the *nature of nucleation* and the *growth processes*. The derivative form of Avrami equation is given below

$$\frac{d\alpha}{dt} = e^{-kt^n} nkt^{n-1} \tag{6.30}$$

From equation (3.21) we get,

$$\ln(1-\alpha) = \left(-kt^n\right) \tag{6.31}$$

or, $\ln[-\ln(1-\alpha)] = n\ln t + \ln k \tag{6.32}$
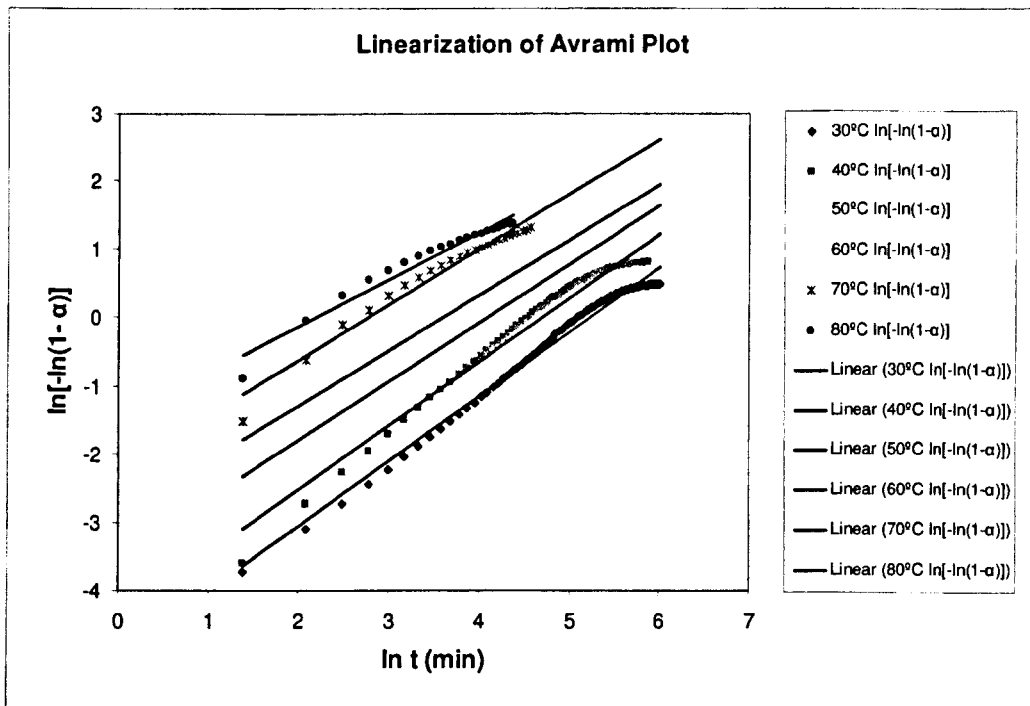
Figure 6.37 Linearization of the Avrami plots of $\ln[-\ln(1-\alpha)]$ vs. $\ln t$ at different isothermal cure temperatures for Araldite 2015.

The values of Avrami exponent n and the reaction rate constant k can be determined respectively from the slope and the intercept of the plot of $\ln[-\ln(1-\alpha)]$ vs. $\ln t$ as predicted in equation (6.32).The plots of $\ln[-\ln(1-\alpha)]$ vs. $\ln t$ are illustrated in figure 6.37 at different isothermal cure temperatures for our studied thermosetting system Araldite 2015.It can be mentioned here that probably the most popular testing method for isothermal data is an inspection of the linearity of the Avrami plot. The preliminary values computed graphically were used as initial values for the non-linear regression analysis software to find the best fit values of n and k.

The values of the best fit kinetic parameters determined from the non-linear regression analysis based on the Avrami model $\alpha = 1 - \exp(-kt^n)$ given by equation (3.21); for isothermal cure process of Araldite 2015 are listed in table 6.5, together with the corresponding standard errors (SE) and the squared correlation co-efficient (i.e. co-efficient of determination) for fit of model to the experimental data.

Table 6.5 The values of the kinetic parameters of the Avrami equation $\alpha = 1 - \exp(-kt^n)$ for isothermal cure process of Araldite 2015, obtained by applying non-linear regression to the corresponding isothermal DSC data.

T_{cure} (°C)	k^* (min^{-1})	n^*	$t_{1/2}$ (min)	E_a (kJ/mol)	$\ln A$ (min^{-1})	r^{2**}
30	0.011 (.000)	0.868 (.003)	118.32			0.983
40	0.017 (.000)	0.881 (.003)	67.28			0.984
50	0.037 (.001)	0.823 (.004)	35.18	44.834	13.265	0.978
60	0.053 (.001)	0.864 (.004)	19.60			0.985
70	0.083 (.001)	0.906 (.004)	10.40			0.988
80	0.134 (.003)	0.890 (.008)	6.33			0.975
Average	0.055	0.872				

* Values in parentheses correspond to standard errors (SE).
** Squared correlation co-efficient (i.e. co-efficient of determination) of curve fitting.

From equation (6.31) we get,

$$t_{1/2} = \left(\frac{\ln 2}{k}\right)^{1/n}$$ (6.33)

Where $t_{1/2}$, is the *half-life* or half-time of cure, and, is defined as the time at which the extent of cure is 50% complete at a certain cure temperature. It is an *important parameter* for the isothermal cure process (will be discussed later). The theoretical predictions of half-life of cure, $t_{1/2}$ at each temperature, given by equation (6.33) are also presented in the table 6.5.
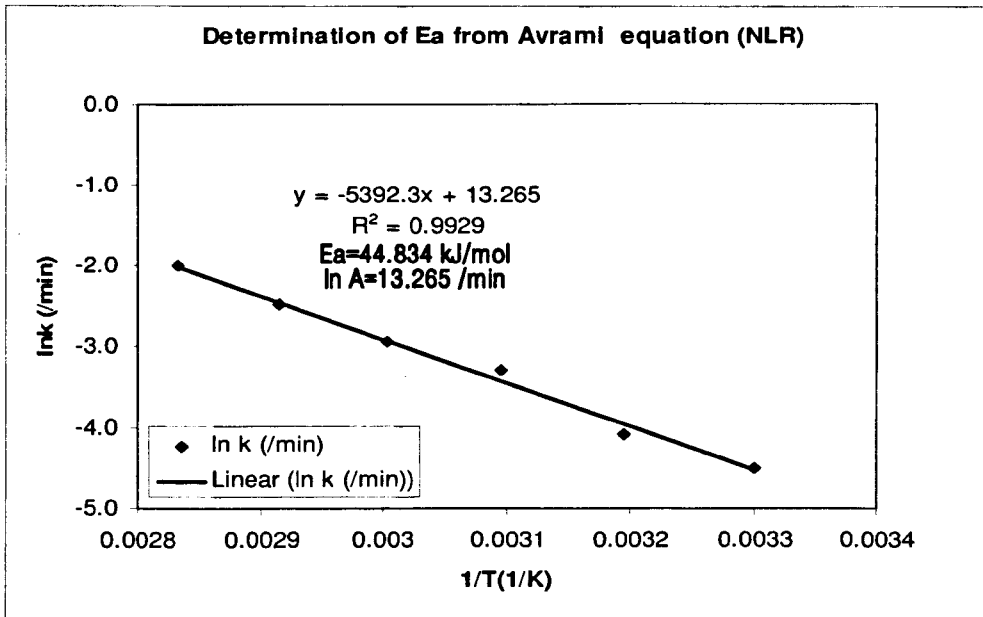
Figure 6.38 The Arrhenius plots of the temperature dependence of the isothermal reaction rate constant k determined from the non-linear regression analysis based on the Avrami model $\alpha = 1 - \exp(-kt^n)$ for isothermal cure process of Araldite 2015.

The Arrhenius plots of *ln k* as a function of 1/T is shown in figure 6.38. In this figure, good linear correlation is observed, which leads to calculate — (i) the apparent activation energy, E_a from the slope of the straight line, which is 44.834 kJ/mol, and, (ii) the pre-exponential factor or Arrhenius frequency factor, ln A from the intercept of the straight line, which is 13.265/min, as are indicated in the figure and mentioned in the table 6.5. All the parameter values reported in the table 6.5 agree well with those

241

obtained for almost similar or comparable epoxy-amine systems [5, 6, 7, 8, 9, 13, 21, 22, 46].

From table 6.5 it can be seen that the values of k are in the range of (0.01—0.13)/min and the values of k increases as the cure temperature increases which indicates that the higher the temperature, the faster the cure rate. The values of Avrami exponent n show almost a constant with an average value of 0.87. As the n values do not vary significantly with temperature, it suggests that the same cure mechanism occurs in the whole course of cure. The DSC experimental data of theoretical gel time which should occur at 50% conversion for our epoxy thermosetting system (listed in table 5.5 in chapter 5) and the theoretically predicted values of *half-life* of cure, $t_{1/2}$ [equation (6.33)] at each isothermal temperature compared very closely as shown in figure 6.39. Thus, employing Avrami expression *accurate consistency between the experimental data and the theoretically predicted values of half-life of cure*, $t_{1/2}$ at all of the six isothermal temperatures is obtained (figure 6.39). This result is consistent with the results reported by other research workers [52] on isothermal cure of DGEBA-based epoxy systems.
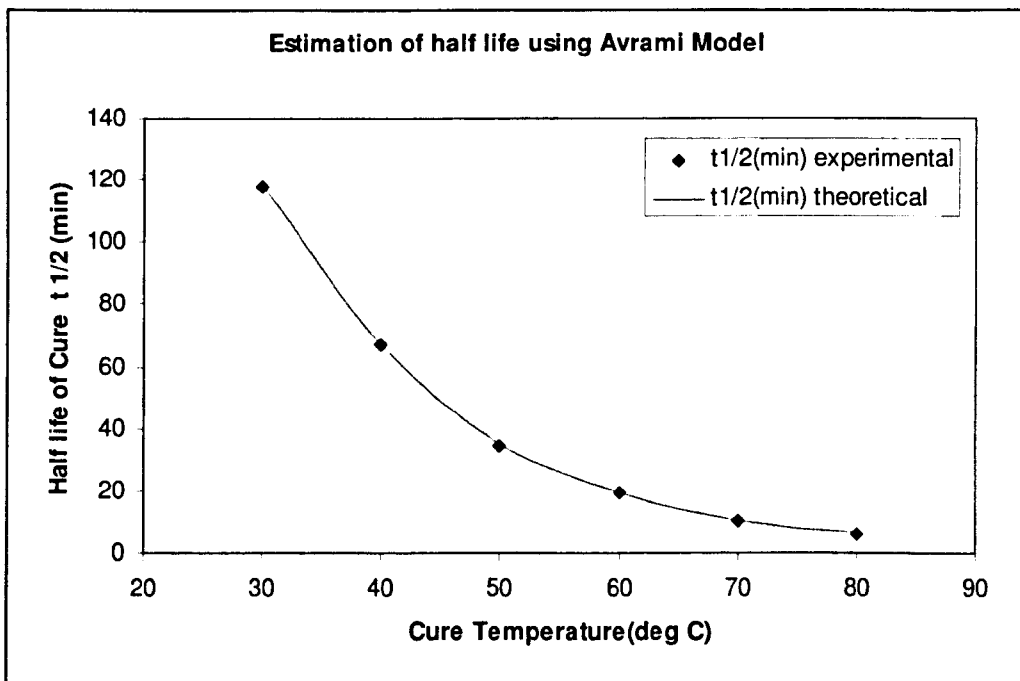
Figure 6.39 Relation of half-life of cure, $t_{1/2}$, and temperature. Solid line represents the theoretical result obtained using Avrami model. Points represent the experimental data.

It is evident from table 6.5 that the values of Avrami exponent n is in the range of 0.82—0.90 showing almost a constant with an average value of 0.87. From the formal theoretical viewpoint of transformation kinetics, the non-integral values of n cannot be explained in terms of the physical assumptions made in arriving at the Avrami equation. However, *fractional* values of n may be expected mathematically, if certain constraints are imposed such as diffusion controlled growth. The observed deviations may also be attributed to the factors — such as time-dependent nucleation, variant growth rate constants, combination of homogeneous and heterogeneous nucleation [52]. Basically, Avrami exponent n should be an *integer* ranging from 1-4. It's value is related to the morphology of polymer which provides qualitative information on the nature of nucleation and the growth processes. From the standpoint of *physical significance of n* the following information can be mentioned.

Growth Geometry	Value of n	Instant Nucleation	Sporadic Nucleation(scattered)
3-dimensional	$n = 3\text{-}4$	$n = 3/2$	$n = 5/2$
2-dimensional	$n = 2\text{-}3$	$n = 1$	$n = 2$
1-dimensional	$n = 1\text{-}2$	$n = 1/2$	$n = 3/2$

For our studied epoxy system, the values of Avrami exponent n is in the range of 0.82—0.90 showing almost a constant with an average value of 0.87. Therefore, we can see abnormality in the experimental observation of the Avrami exponent n, as it is a fractional value and is less than 1.In the light of the above, it can suggest that the cure process may involve *instantaneous nucleation* and *diffusion controlled one-dimensional growth*. For diffusion controlled process, low value of n ($n<1$) most probably due to the rapid completion of the nucleation step. Due to the fast nucleation kinetics, the overall growth rate, most possibly, governed by the mobility of the reactant species. However, in comparison to our previous results obtained with other autocatalytic kinetic models, an inspection of the r^2 values of the fits from table 6.5 based on Avrami model suggest that *the goodness of the fits are less than adequate* in representing the experimental data. Thus, the *poor fits* indicate the lack of validity of the model in representing the overall isothermal cure behaviour of our thermosetting system. It is worth mentioning that it is difficult to precisely analyze the Avrami

243

theory if the system was glassified wholly [52]. As we know, vitrification begins to occur when the $T_g = T_{cure}$, the maximum degree of cure, α_{max} depends on the cure temperature. Therefore, it is essential to conduct the isothermal experiment at little higher curing temperature to describe the whole cure process.

6.8 Analysis of the Isothermal Cure Kinetics Using Modified Avrami Model

The isothermal cure process can be analyzed using the modified Avrami equation [53].We can obtain the relationship between the degree of cure α and the curing time after the gel point $(t - t_{gel})$. Based on the similarity between the cure process and the crystallization process, we can employ the Avrami equation to analyze the cure process [53] :

$$\alpha = 1 - \exp[-k(t - t_{gel})^n] \tag{6.34}$$

$$\text{or, } \ln[-\ln(1 - \alpha)] = n\ln(t - t_{gel}) + \ln k \tag{6.35}$$

The values of Avrami exponent n and the reaction rate constant k can be determined respectively from the slope and the intercept of the plot of $\ln[-\ln(1 - \alpha)]$ vs. $\ln(t - t_{gel})$ as predicted in equation (6.35). The plots of $\ln[-\ln(1 - \alpha)]$ vs. $\ln(t - t_{gel(theoretical)})$ are illustrated in figure 6.40 at different isothermal cure temperatures for our studied thermosetting system using the data of *theoretical gel time* ($t_{gel\ (theoretical)}$) obtained from calorimetric study. The values of Avrami exponent n and the reaction rate constant k computed graphically as predicted in equation (6.35), are reported in table 6.6. An inspection of the linearity between Avrami and modified Avrami plots depicted in figures 6.37 and 6.40 respectively, indicate that at 30°C and 40°C the Avrami plots show better linearity than modified Avrami plots with corresponding R^2 values of 0.9845 and 0.9717; whereas modified Avrami plots show better linearity than Avrami plots at 50°C, 60°C, 70°C, and 80°C. The relative R^2 values are presented in table 6.6. Hence, in overall, modified Avrami plots show better linearity than Avrami plots. It generally suggests that the Avrami equation can be used to describe the cure process after $t_{gel\ (theoretical)} / t_{gel}$ to some extent.
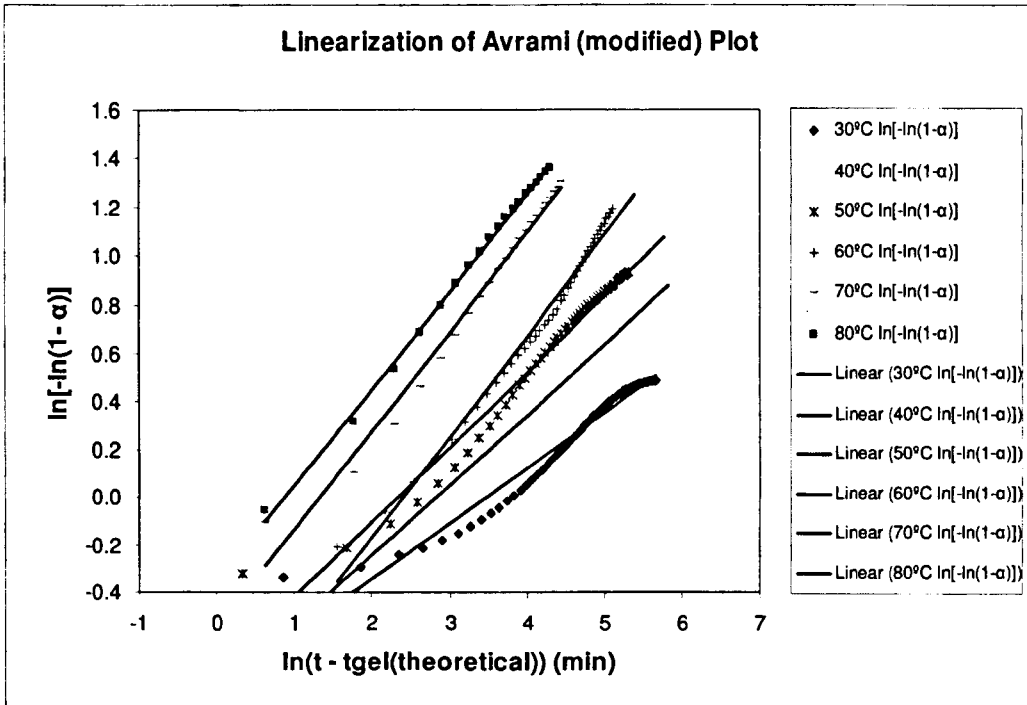
Figure 6.40 Linearization of the Avrami (modified) plots of $\ln[-\ln(1-\alpha)]$ vs. $\ln(t - t_{gel(theoretical)})$ at different isothermal cure temperatures for Araldite 2015.

Table 6.6 The values of the kinetic parameters of the Avrami (modified) equation $\alpha = 1 - \exp[-k(t - t_{gel(theoretical)})^n]$ for isothermal cure process of Araldite 2015, obtained by applying linear regression to the isothermal $\ln[-\ln(1-\alpha)]$ vs. $\ln(t - t_{gel(theoretical)})$ data graphically.

T_{cure} (^{0}C)	k (min^{-1})	n	E_a (kJ/mol)	$\ln A$ (min^{-1})	R^2 *
30	2.240	0.2320			0.9532
40	2.281	0.2915			0.9298
50	2.073	0.3127	44.200	14.046	0.9679
60	2.723	0.4177			0.9866
70	1.711	0.4079			0.9816
80	1.423	0.4015			0.9979
Average	**2.075**	**0.3438**			

* Linear regression squared correlation co-efficient (i.e. co-efficient of determination).

The activation energy can also be calculated by the Avrami method. An empirical approach can be used to describe the temperature dependence of kinetic constant k. Assuming that k is thermally activated [53]:

$$k^{1/n} = A\exp(-E_a/RT)$$ (6.36)

or, $(1/n)\ln k = \ln A - (E_a/RT)$ (6.37)

Where, the terms have their usual definitions.

The plot of $(1/n)\ln k$ as a function of 1/T is shown in figure 6.41. The activation energy and the pre-exponential factor are calculated from the slope and intercept of the straight line respectively, which are shown in the figure and also reported in the table 6.6.
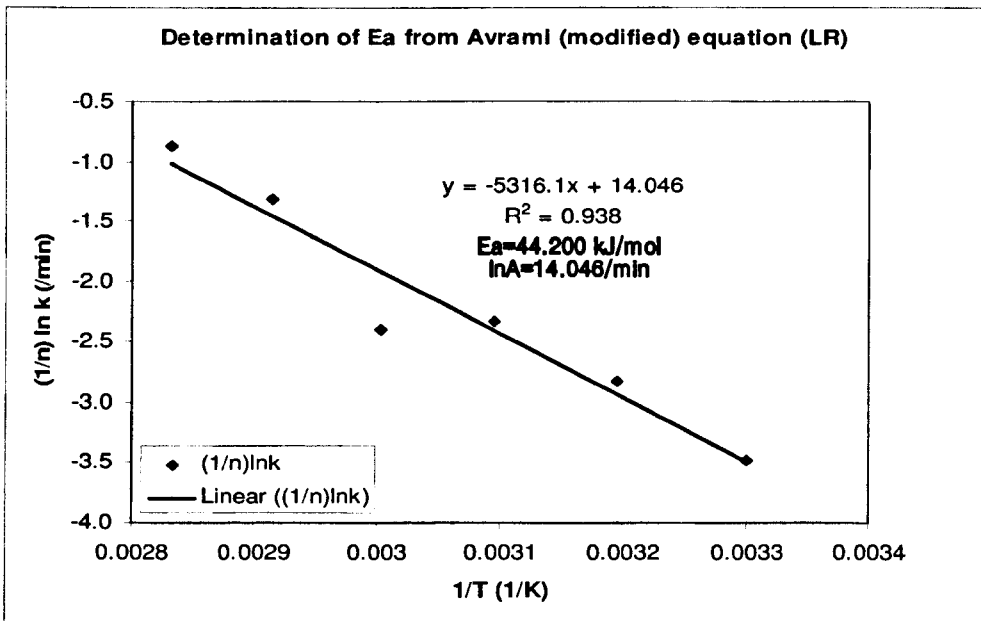
Figure 6.41 The Arrhenius plots of $(1/n)\ln k$ vs. 1/T for isothermal cure process of Araldite 2015, where, the values of Avrami exponent n and the reaction rate constant k was determined respectively from the slope and the intercept of the plot of $\ln[-\ln(1-\alpha)]$ vs. $\ln(t - t_{gel(theoretical)})$ as illustrated in the figure 6.40.

However, in comparison to our previous results obtained with other autocatalytic kinetic models, an inspection of the r^2 values of the fits from table 6.5 based on Avrami model suggest that *the goodness of the fits are less than adequate* in representing the experimental data. Thus, the *poor fits* indicate the lack of validity of the Avrami model in representing the overall isothermal cure behaviour of our studied thermosetting system. It is worth reiterating that it is difficult to precisely analyze the Avrami theory if the system was glassified wholly [52]. Therefore, it is essential to conduct the isothermal experiment at little higher curing temperature to describe the whole cure process.

6.9 Comments on Overall Performance of Models Based on Empirical Approach

Based on the aim to find a model which can *describe the reaction behaviour* of our resin system *as well as possible* and permits the prediction of the reaction course, we fitted the isothermal reaction rate curves to *ten* kinetics models. The performance of each particular model with it's associated best fit model parameters in describing the isothermal cure kinetics of the thermosetting system under study have already been discussed. The scientifically reasonable average values of the kinetic parameters of the models tested based on the empirical approach, for isothermal cure process of Araldite 2015, in the temperature range of 30°C to 80°C, obtained by applying non-linear regression to the corresponding isothermal data based on the respective model are reported in table 6.8. To demonstrate the applicability of these models, the values of the *goodness of fits* (i.e. squared correlation co-efficient, r^2(co-efficient of determination) of curve fitting) are compared in table 6.9.

6.9.1 Empirical model with best overall performance

It is evident that particularly with the autocatalytic model $d\alpha/dt = k\alpha^m (\alpha_{max} - \alpha)^n$ in equation (6.8) with incorporation of $\alpha_{max}(T)$, maximum value of conversion at a particular temperature, as expressed by equation (6.11) in section 6.3.1, instead of full conversion 1, an overall *best* fit is observed [figures 6.3(a–f) and 6.4(a–f)]. Infact, containing *four* kinetic parameters-- $\ln A, E_a, m, n$ (as listed in table 6.1) this autocatalytic model *most closely simulate* the isothermal curing behaviour of the

complex commercial epoxy (modified) thermosetting system Araldite 2015 under investigation with almost a *reasonable degree of satisfaction* over the entire range of conversion and temperature (30°C–80°C) studied. The comments on overall performance of this model have already been discussed in details in section 6.3.7 under *six* highlighted points.

Table 6.8 The average values of the kinetic parameters of the empirical models tested for isothermal cure process of Araldite 2015, in the temperature range of 30°C to 80°C, obtained by applying non-linear regression to the corresponding isothermal data based on the respective model.

Model	k (min^{-1})	m	n	$m+n$	ln$A$ (min^{-1})	E_a (kJ/mol)
$\dfrac{d\alpha}{dt} = k\alpha^m(\alpha_{max} - \alpha)^n$	0.085	0.136	1.131	1.268	17.161 ˙	55.50 *
$\dfrac{d\alpha}{dt} = k\alpha^m(1-\alpha)^n$	0.093	0.216	1.586	1.802	17.347 ˙	55.50 *
$\dfrac{d\alpha}{dt} = k(\alpha_{max} - \alpha)^n e^{m\alpha}$	0.040	1.349	1.512	2.861	16.728 ˙	55.50 *
$\dfrac{d\alpha}{dt} = k(1-\alpha)^n e^{m\alpha}$	0.037	2.540	2.462	5.000	16.623 ˙	55.50*
$\alpha = 1 - \exp(-kt^n)$	0.055	na	0.872	na	13.265	44.834

*E_a is the average value of activation energy obtained from iso-conversional method.

˙ ln A is calculated from reaction rate constant k and iso-conversional average E_a value.

6.9.2 Comparative overall performance of other empirical models

There are *some aspects of particular model fit* based on individual model tested that make the comparison interesting and useful from the perspective of kinetic modelling.

Comparing the results obtained with the autocatalytic model incorporating α_{max} instead of 1 as given by equation (6.8) with those obtained with the conventional autocatalytic model given by equation (3.9); it is evident that inclusion of α_{max} instead of complete conversion improves the goodness of fit for overall cases and particularly for the case of lower temperature range of 30°C—50°C which suffers from poor fit of kinetic data due to the fact that the *assumption of α_{max} =1 is overly simplified*. Thus *much better fit is observed with incorporating α_{max} as the constraint of the reaction going to completion is lifted*. This observation is also true for the two forms of Gonzalez-Romero model.

It is evident that the fit based on conventional autocatalytic model becomes better as the cure temperature is increased [figures 6.13(a,b) — 6.18(a,b)] which indicates the temperature dependence of the diffusion and the reaction rate.

Table 6.9 Comparison of the squared correlation coefficients of curve fitting (i.e. goodness of fit) of non-linear regression method for various empirical kinetic models tested for isothermal cure process of Araldite 2015.

Model	Squared correlation coefficient (r-squared) of curve fitting in non-linear regression method					
	T_{cure} (°C)					
	30	40	50	60	70	80
$\frac{d\alpha}{dt} = k\alpha^m(\alpha_{max} - \alpha)^n$	0.982	0.997	0.997	0.998	0.997	0.998
$\frac{d\alpha}{dt} = k\alpha^m(1-\alpha)^n$	0.917	0.972	0.987	0.997	0.998	0.999
$\frac{d\alpha}{dt} = k(\alpha_{max} - \alpha)^n e^{m\alpha}$	0.984.	0.998	0.997	0.993	0.979	0.969
$\frac{d\alpha}{dt} = k(1-\alpha)^n e^{m\alpha}$	0.960	0.993	0.997	0.994	0.981	0.970
$\alpha = 1 - \exp(-kt^n)$	0.983	0.984	0.978	0.985	0.988	0.975

By including the diffusion factor $f_d(\alpha, T)$ in the conventional kinetic model excellent fit is observed *at specific higher conversion region* in the later stages of the cure, where a deviation appears due to the onset of vitrification [figures 6.13(c,d) — 6.18(c,d)]. It is more evident at lower cure temperatures of 30°C, 40°C and 50°C, where the deviation appears to be greater. Hence, the overall goodness of fit (r^2-value) improves.

The introduction of diffusion factor $f_d(\alpha, T)$ [figures 6.13(e) — 6.18(e)] enables us to explore some in depth information associated with the diffusion controlled kinetics due to vitrification in isothermal measurement related to our data. The downturn in $f_d(\alpha, T)$ at α_c due to onset of diffusion increasingly occurs at higher conversions with increasing cure temperature is clearly evident. Our results, fairly consistent with the findings of other research workers [12,31,38,49,50,51], show that the critical conversion α_c is a *useful parameter* which specifically relates to the *onset of vitrification* for the epoxy thermosetting system under study. Thus it *reflects the state of cure of the system as well as the temperature of cure.*

The simulations with the both forms of autocatalytic model of Gonzalez-Romero [equations (6.26) and (6.28)] show *non-zero initial rates of reaction* at the initial stages of cure at $\alpha = 0$, the characteristic feature which the reaction rate profiles of our studied thermosetting system display. Interestingly, the Gonzalez-Romero model with the inclusion of α_{max} gives the *best simulation* for the particular case of kinetic data of lower cure temperature range (30°C—50°C). The fit worsens as the cure temperature is increased to 70°C and 80°C. The accuracy of simulation is poor near the autocatalytic peak regions of the rate-conversion profiles at higher curing temperature range (60°C—80°C) which implies the lack of validity of the model in this region. The reaction rate profiles of 70°C and 80°C suffer from poor fit of kinetic data for both forms of model and hence, they are less than adequate for this system at higher temperatures.

Comparing the results obtained with the introduction of diffusion factor $f_d(\alpha, T)$ in the Gonzalez-Romero model with full conversion 1 [equation (6.28)] with those obtained with the introduction of diffusion factor $f_d(\alpha, T)$ in the conventional

autocatalytic model of Kamal [equation (3.9)]; almost similar trend of overall goodness of fit (r^2-value) of reaction rate data and useful information regarding the *onset of vitrification* associated with critical conversion α_c are found.

The poor goodness of fits obtained with Avrami model indicate the lack of validity of the model in representing the overall isothermal cure behaviour of our thermosetting system. However, *accurate consistency between the experimental data and the theoretically predicted values of half-life of cure*, $t_{1/2}$ at all of the six isothermal temperatures is obtained with Avrami expression (figure 6.39). This result is consistent with the results reported by other research workers [52] on isothermal cure of DGEBA-based epoxy systems.

6.10 Analysis of Cure Kinetics Using Horie Model (Mechanistic Approach)

Horie et al [20] developed an equation based on the mechanism initially proposed by Smith [19]; which have already been discussed before in the context of interpretation of the results associated with the temperature dependence of overall reaction order *(m+n)* of autocatalytic kinetic models, in the light of *trimolecular catalysis mechanism*, in analyzing our data using empirical approach of kinetic models.

In this model of Horie et al [20], the reactions of the epoxy groups with primary and secondary amines as well as non-catalytic, catalytic (catalyst or impurity) and autocatalytic effects (hydroxyl groups generated) are explicitly taken into account. This model is expressed as:

$$\frac{d\alpha}{dt} = (k_1 + k_2\alpha)(1-\alpha)(B-\alpha) \tag{6.39}$$

Where, the rate constants k_1 and k_2 correspond respectively to catalysis by groups initially present in the thermosetting system and catalysis by hydroxyl groups formed in the reaction, and B is the ratio of primary amine N—H bonds to epoxide groups in the initial mixture i.e. stoichiometric ratio.

Assuming equal reactivity of all the amino hydrogens, the rate for a stoichiometric mixture of epoxy and amine (*similar to our case*) in this model can be expressed as:

$$\frac{d\alpha}{dt} = (k_1 + k_2\alpha)(1-\alpha)^2 \tag{6.40}$$

This simplified form of Horie model given by equation (6.40) is used here in this section to analyze our kinetic data. Logically, we do not considered the extended Horie treatment which includes side reactions like intramolecular or intermolecular etherification and epoxy homopolymerization as implemented by Cole et al [38] and other researchers [1] for epoxy-amine system cured at *high* temperature. Because it has already been discussed earlier this chapter that the resin system studied for the present investigation is taken in the stoichiometric ratio and the cure temperature employed is in the range of 30°C–80°C, which is much lower than 150°C. Hence, for our studied resin system the etherification due to epoxy/hydroxyl reaction and the epoxy homopolymerization reaction need not be considered as they have almost no possibility to occur.

Equation (6.40) considers only the chemical kinetics whereas the influence of diffusion is not taken into account. This equation can be rewritten for the analysis of the data by defining a *reduced rate* [L.H.S. of the following equation] as:

$$\frac{(d\alpha/dt)}{(1-\alpha)^2} = k_1 + k_2\alpha \tag{6.41}$$

The values of rate constants k_1 and k_2 can be determined respectively from the intercept and the slope of the plot of reduced reaction rate $(d\alpha/dt)/(1-\alpha)^2$ vs. calorimetric conversion α as predicted in equation (6.41).The plots of $(d\alpha/dt)/(1-\alpha)^2$ vs. α at different isothermal cure temperatures for our studied thermosetting system Araldite 2015 are illustrated in figure 6.44.It can be seen that the kinetics of the cure reaction can be better characterized by this plot. As shown in the figure, the reduced rate of reaction gradually increases and after it has reached a broad maximum, the reaction rate decreases rapidly. The linearity is found almost up

to a conversion close to 0.70—0.75 between 30°C—80°C. Therefore, k_1 and k_2 can be determined from this portion of the cure that exhibits autocatalytic kinetics as evidenced by this linear slope. The sudden decrease in the reduced rate at $\alpha > 0.75$ may have been caused by the onset of rate control by diffusion due to vitrification of the epoxy-amine system. It is evident that at higher cure temperatures the reaction reverts to a more autocatalytic reaction prior to vitrification. This is due to the thermosetting resin being able to stay mobile longer at the higher cure temperatures and hence, the onset of vitrification occurs at a higher conversion with increasing cure temperature.
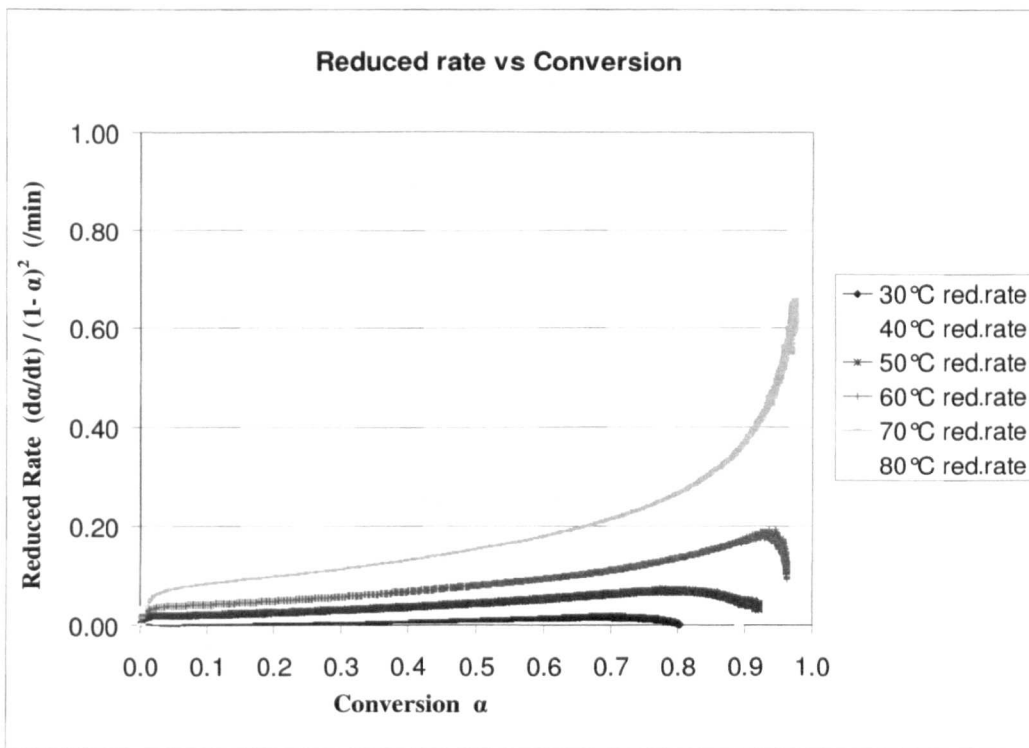
Figure 6.44 Plots of reduced reaction rate $(d\alpha/dt)/(1-\alpha)^2$ as a function of calorimetric conversion α for different isothermal temperatures based on Horie model $d\alpha/dt = (k_1 + k_2\alpha)(1-\alpha)^2$ (for the case of stoichiometric ratio, where $B = 1$) for the cure process of Araldite 2015.

The values of the reaction rate constants k_1 and k_2 obtained by applying linear regression to the isothermal reduced rate $(d\alpha/dt)/(1-\alpha)^2$ vs. α data graphically as predicted in equation (6.41), are reported in table 6.10. The corresponding Arrhenius plots are shown in figure 6.45, where excellent linear correlations are observed, which

lead to the values of parameters activation energies, $E_{a1} = 53.136\,\text{kJ/mol}$ and $E_{a2} = 59.184\,\text{kJ/mol}$ and corresponding pre-exponential factors or Arrhenius frequency factors, $\ln A_1 = 15.667/\text{min}$ and $\ln A_2 = 19.128/\text{min}$ as are indicated in the figure and also listed in table 6.10. The values of are well in agreement with the values reported in literature for isothermal curing of epoxy-amine systems [1, 3, 4, 5, 6, 7, 8, 9, 21, 22, 23, 31, 32, 36].

Table 6.10 The values of the kinetic parameters of the Autocatalytic model of Horie $\dfrac{d\alpha}{dt} = (k_1 + k_2\alpha)(1-\alpha)^2$ for isothermal cure process of Araldite 2015, where the reaction rate constants k_1 & k_2 are obtained by applying linear regression to the isothermal reduced rate $(d\alpha/dt)/(1-\alpha)^2$ vs. α data graphically using the Horie model.

T_{cure} (^{0}C)	k_1 (min^{-1})	k_2 (min^{-1})	E_{a1} (kJ/mol)	$\ln A_1$ (min^{-1})	E_{a2} (kJ/mol)	$\ln A_2$ (min^{-1})
30	0.0046	0.0145				
40	0.0081	0.0256				
50	0.0162	0.0498	53.136	15.667	59.184	19.128
60	0.0310	0.0895				
70	0.0490	0.2182				
80	0.0897	0.3803				
Average	0.0331	0.12965				

6.10.1 Critical Comments on Activation Energy Values

The obtained values of activation energies for the catalyzed (by external catalysts and impurity) and/or uncatalyzed (can be neglected) and autocatalyzed epoxy-amine reactions corresponding to the isothermal reaction rate constants k_1 and k_2 based on the Autocatalytic model of Horie are $E_{a1} = 53.136\,\text{kJ/mol}$ and $E_{a2} = 59.184\,\text{kJ/mol}$ respectively.

In the literature, the autocatalyzed reaction is usually found to have *significantly lower* activation energy than the catalyzed and/or uncatalyzed one [1,17, 27,36]. In contrast, for our modified epoxy-amine thermosetting resin system the autocatalytic and catalytic reactions have *comparable* activation energy values, 59.184 and 53.136 kJ/mol respectively. This result can be ascribed to the *specificity of the commercial modified epoxy-amine system* studied for the present investigation, which contains external catalyst 2,4,6 - tris (dimethylaminomethyl) phenol, epoxy resin (DGEBA/DGEBF mixture), triamine hardener (DETA), epoxy-based reactive diluent modifier 1,4 Butane diol diglycidyl ether (BDGE) and mica.
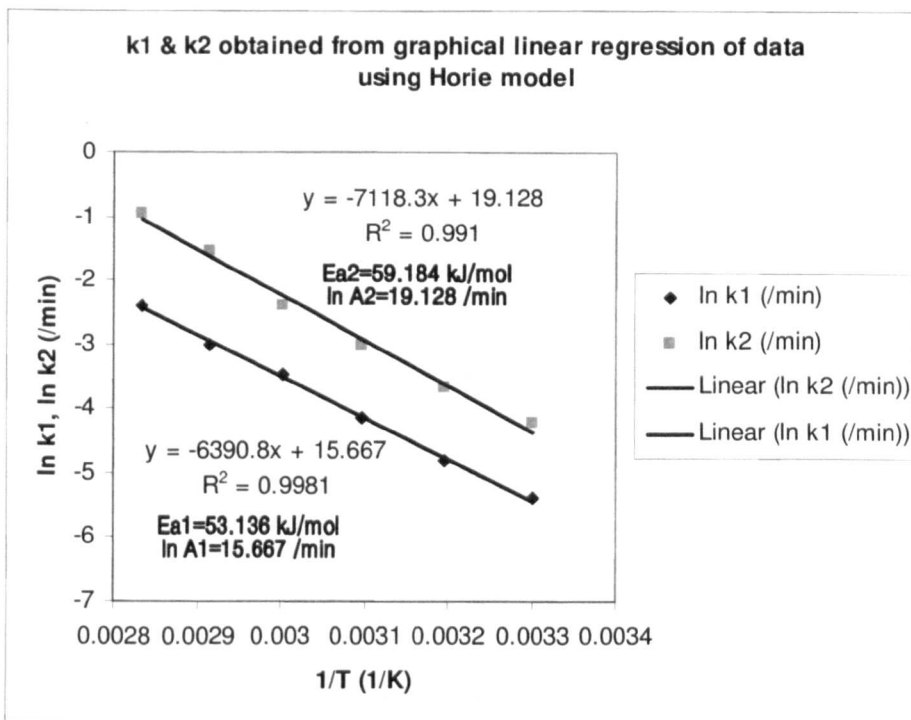
Figure 6.45 The Arrhenius plots of the temperature dependence of the isothermal reaction rate constants k_1 and k_2 obtained by applying linear regression to the reduced reaction rate $(d\alpha/dt)/(1-\alpha)^2$ vs. conversion α data graphically for different isothermal temperatures based on Horie model $d\alpha/dt = (k_1 + k_2\alpha)(1-\alpha)^2$ (for the case of stoichiometric ratio, where $B=1$) for the cure process of Araldite 2015.

Generally, the slightly higher E_{a2} value than E_{a1} value suggests that autocatalyzed reaction (reaction 2) is slightly more sensitive to the temperature than initially catalyzed reaction (reaction 1) and hence, the cure temperature has slightly more

255

effect on rate constant k_2 than k_1. The values of the activation energy in autocatalytic cure kinetics for several thermosetting resin systems are shown in table 6.11; where $E_{a1}<E_{a2}$ (i.e. the value of the activation energy of the autocatalyzed reaction is higher than that of the catalyzed and / or uncatalyzed reaction) which is non-typical. It is worth noting that the activation energies of the primary and secondary amine addition were found to be *equal* for *four* different amines, though substantially different values have also been reported [33].

Table 6.11 The values of the activation energy in autocatalytic cure kinetics for several thermosetting resin systems where $E_{a1}<E_{a2}$ (i.e. the value of the activation energy of the autocatalyzed reaction is higher than that of the catalyzed and / or uncatalyzed reaction) which is non-typical.

Investigator	System	E_a (kJ/mol)
Perrin et al [1]	DGEBF/DGEBA mixture +Amine(Poly(oxypropylene)diamine (JEFF) / DETA) + BPA (Catalyst)	E_{a1}=50 E_{a2} =58
Gualpa et al [3]	Epoxy Resin (DGEBA) + Novolak Resin	E_{a1} =41.04 E_{a2} =73.20
Han et al [22]	Biphenyl Epoxy Resin + Phenol Novolac Resin +Triphenylphosphine(TPP) (catalyst)	E_{a1} =69 E_{a2} =83
Leroy et al [23]	Dicyanate Ester Resin +Catalyst	E_{a1} =54 E_{a2} =71
Raju Thomas et al [4]	DGEBA+Anhydride hardener +Tertiary Amine (accelerator)	E_{a1} =71.20 E_{a2} =96.00

The activation energy value obtained from the theoretical gel time $E_{a\ gel\ (theoretical)}$ = **53.435 kJ/mol** (Table 5.5 in chapter 5) based on the calorimetric study is within the order of magnitude of the activation energy value for the autocatalytic reaction rate

constant k_2 (which is $E_{a2} = 59.184 \text{kJ/mol}$), and it is related to the *crosslinking reaction*. This value is also very similar to the average value of the effective activation energy E_a =55.50 kJ/mol obtained from iso-conversional analysis, which is independent of any mechanism.

A comparison of $E_{a1} = 53.136 \text{kJ/mol}$ and $E_{a2} = 59.184 \text{kJ/mol}$ values obtained from Horie model with the average value of activation energy E_a =55.50 kJ/mol obtained by the iso-conversional analysis (Differential Method) using *single-step autocatalytic models* suggests that this latter value of the activation energy most likely represents some average value between the activation energies of catalyzed or non-autocatalyzed and autocatalyzed reactions, being slightly closer to the former value of non-autocatalyzed reaction. This may be attributed to the *specificity of the commercial modified epoxy-amine system* Araldite 2015 studied for the present investigation.

6.10.2 Reaction Rate Constant Ratio

From table 6.10 it is evident that at all temperatures, k_2 values are much larger than corresponding k_1 values i.e. $k_2 >> k_1$. The difference becomes larger as the cure temperature increases. This is hardly surprising considering the fact that k_1 is for catalyzed (by external catalysts and impurity) and / or uncatalyzed (can be neglected) reactions whereas k_2 is for autocatalyzed reactions. The temperature dependence of *reaction rate constant ratio* $r_k = k_2/k_1$ is shown in figure 6.46. It can be seen that the reaction rate constant ratio is almost constant with cure temperature from 303°K(30°C) to 333°K(60°C), then rapidly increased at 343°K(70°C) and remains almost constant till 353°K(80°C).

Increasing reaction rate constant ratio results in an increase in the overall rate of reaction, which reflects a faster consumption rate of epoxy groups by secondary amines. The reaction rate constant ratio $r_k = k_2/k_1$ has great significance for the prediction of the physical and chemical characteristics in the cure system, because it works on an important factor for the development of the side-chain creation step (crosslink formation step) in the autocatalytic reaction. Some important practical

aspects of reaction rate constant ratio on kinetics based on shift or displacement of critical conversion at gelation from the ideal value (towards higher or lower values) already have discussed in the section entitled "Calorimetric Determination of Gelation (theoretical)" in chapter 5.
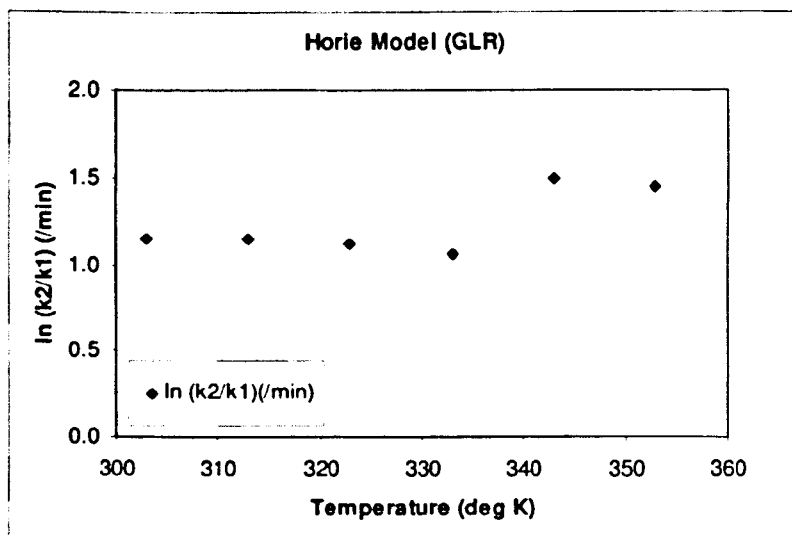
Figure 6.46 The isothermal reaction rate constant ratio (k_2/k_1) as a function of the absolute cure temperature.

It was shown experimentally and theoretically that gel conversion depends on the magnitude of the *substitution effect* [35]. When the primary amine hydrogens are much more reactive than the secondary amine hydrogens i.e. $k_1 \gg k_2$ (which is the usual case), gelation occurs of course at a conversion degree *higher* than that expected when equal reactivity of all amine hydrogens is assumed [35].In reality, the experimental value of the gel point conversion has been found to be greater than the theoretical value. As for our studied thermosetting system, $k_2 \gg k_1$, hence, most possibly gelation may occur at a conversion degree *lower* than the *theoretical gel point*, which, according to the *Flory's theory of gelation*, should occur at *50% conversion* for our epoxy system.

6.10.3 Determination of Thermodynamic Parameters

The enthalpy, entropy, and free energy of the epoxy-amine reactions can be calculated using the *Eyring equation* and the values of the activation energy E_a and Arrhenius frequency factor or pre-exponential factor ln A.

The *Eyring equation* developed by Henry Eyring relates the reaction rate to temperature like Arrhenius equation. The *Eyring equation* is used in the study of solution reactions, gas reactions, and mixed phase reactions— all places where the simple *collision model* is not very helpful.The Arrhenius equation is founded on the empirical observation that rates of reactions increase with temperature. The *Eyring equation* is a theoretical construct, based on *transition state theory*.

The linear form of the *Eyring equation* is :

$$\ln (k / T) = - (\Delta H^{\ddagger}/ R) (1/T) + \ln (k_b / h) + (\Delta S^{\ddagger}/ R) \qquad (6.42)$$

Where,

k = Reaction rate constant (/s)

T= Absolute temperature (°K)

$\Delta H^{\ddagger}$= *Enthalpy of activation* (kJ/mol)

R= Universal gas constant = 8.3145 J/°K/mol

k_b=Boltzmann constant =1.381×10^{-23} J/°K

h=Plank's constant = 6.626×10^{-34} J s

$\Delta S^{\ddagger}$ = *Entropy of activation* (J/°K/mol)

The plots of $\ln(k/T)$ vs. $(1/T)$ at different isothermal cure temperatures will give a straight line with slope = $- (\Delta H^{\ddagger}/ R)$ from which the *Enthalpy of activation* can be determined and with intercept = $\{\ln (k_b / h) + (\Delta S^{\ddagger}/ R)\} = \{23.7602 + (\Delta S^{\ddagger}/ R)\}$ from which the *Entropy of activation* can be determined as predicted in equation (6.42). The plots of $\ln(k_1/T)$ and $\ln(k_2/T)$ vs. $(1/T)$ at different isothermal cure temperatures for our studied thermosetting system Araldite 2015 are illustrated in figure 6.47. The excellent linear fits for both of the plots of reaction rate constants k_1 and k_2 allow us to determine the corresponding values of $\Delta H_1^{\ddagger}$, $\Delta S_1^{\ddagger}$ and $\Delta H_2^{\ddagger}$, $\Delta S_2^{\ddagger}$. Additionally, from thermodynamics we get,

$$\Delta G^{\ddagger} = \Delta H^{\ddagger} - T. \Delta S^{\ddagger} \qquad (6.43)$$

Where, $\Delta G^{\ddagger}$= *Free Enthalpy of activation* (kJ/mol), also known as *Gibbs free energy*.

259
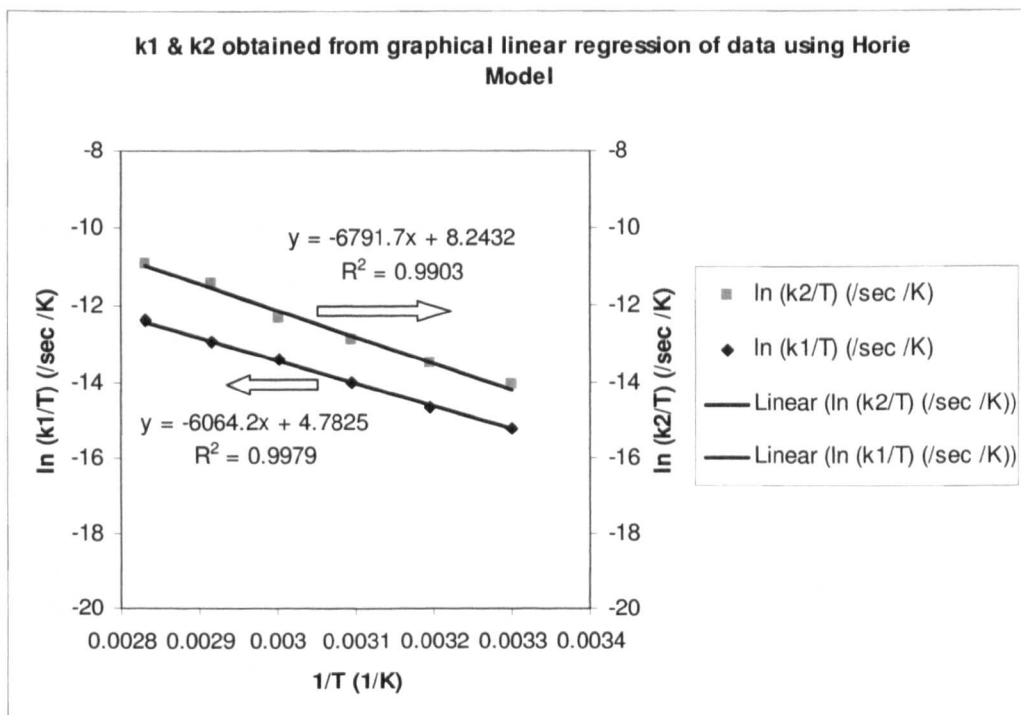
Figure 6.47 The Arrhenius plots of $\ln(k_1/T)$ and $\ln(k_2/T)$ vs. $(1/T)$ based on the linear form of *Eyring equation* of chemical kinetics for the determination of Thermodynamic parameters, where k_1 and k_2 are obtained by applying linear regression to the reduced reaction rate $(d\alpha/dt)/(1-\alpha)^2$ vs. conversion α data graphically for different isothermal temperatures based on Horie model $d\alpha/dt = (k_1 + k_2\alpha)(1-\alpha)^2$ (for the case of stoichiometric ratio, where $B = 1$)for the cure process of Araldite 2015.

The *free Enthalpy of activation (Gibbs free energy)*, $\Delta G^{\ddagger}$ may be considered to be the driving force of a chemical reaction. It determines the extent and spontaneity of the reaction.

If, $\Delta G^{\ddagger} < 0$, the reaction is spontaneous.

$\Delta G^{\ddagger} = 0$, the system at equilibrium, no net change occurs.

$\Delta G^{\ddagger} > 0$, the reaction is not spontaneous.

From equation (6.43) we can calculate the value of $\Delta G^{\ddagger}$ at a particular temperature (°K), using the obtained values of $\Delta H^{\ddagger}$ and $\Delta S^{\ddagger}$. By using the values of (already obtained) $\Delta H_1^{\ddagger}$, $\Delta S_1^{\ddagger}$ and $\Delta H_2^{\ddagger}$, $\Delta S_2^{\ddagger}$ corresponding to the reaction rate constants k_1

and k_2, we determined the related values of $\Delta G_1^{\ddagger}$ and $\Delta G_2^{\ddagger}$ at **30°C** (303°K) from equation (6.43).

The values of the Kinetic parameters (activation energy and pre-exponential factor, also mentioned before) and the Thermodynamic parameters (stated above) for the catalyzed (by external catalysts and impurity) and / or uncatalyzed (can be neglected) and autocatalyzed epoxy-amine reactions corresponding to the reaction rate constants k_1 and k_2 for the isothermal cure process of Araldite 2015, based on the Autocatalytic model of Horie [equation (6.40)] are presented in table 6.12.

Table 6.12 The values of the Kinetic parameters (activation energy and pre-exponential factor) and Thermodynamic parameters for the catalyzed (by external catalysts and impurity) and / or uncatalyzed (can be neglected) and autocatalyzed epoxy-amine reactions for isothermal cure process of Araldite 2015, based on the Autocatalytic model of Horie $\dfrac{d\alpha}{dt} = (k_1 + k_2\alpha)(1 - \alpha)^2$ where the reaction rate constants k_1 & k_2 are obtained by applying linear regression to the isothermal reduced rate $(d\alpha/dt)/(1-\alpha)^2$ vs. α data graphically using the Horie model. The Thermodynamic parameters are calculated using the Eyring equation.

	Kinetic Parameters		Thermodynamic Parameters		
	E_{a1} (kJ/mol)	$\ln A_1$ (min^{-1})	$\Delta S_1^{\ddagger}$ (J/°K/mol)	$\Delta H_1^{\ddagger}$ (kJ/mol)	$\Delta G_1^{\ddagger}$ * (kJ/mol)
k_1	53.136	15.667	-157.789	50.420	98.230
	E_{a2} (kJ/mol)	$\ln A_2$ (min^{-1})	$\Delta S_2^{\ddagger}$ (J/°K/mol)	$\Delta H_2^{\ddagger}$ (kJ/mol)	$\Delta G_2^{\ddagger}$ * (kJ/mol)
k_2	59.184	19.128	-129.015	56.469	95.560

*Calculated at **30°C**.

6.10.4 Analysis of Cure Kinetics based on Kinetic and Thermodynamic Viewpoint

6.10.4.1 Correlation between Kinetic and Thermodynamic Parameters

For the purpose of comparison the linear form of the *Eyring equation* (equation 6.42) and the *Arrhenius equation* (equation 3.4) have shown again below

$$\ln (k / T) = - (\Delta H^{\ddagger}/ R) (1/T) +\{ \ln (k_b / h) + (\Delta S^{\ddagger}/ R)\}$$

$$\ln k = - (E_a / R) (1/T) + \ln A$$

Hence, we see that $\ln A$ and $\Delta S^{\ddagger}$ on the one hand and E_a and $\Delta H^{\ddagger}$ on the other hand are analogous quantities. The *activation energy*, E_a and the *enthalpy of activation*, $\Delta H^{\ddagger}$ — these two energies are therefore frequently used interchangeably in the literature to define the activation barrier of a reaction. They are related each other by the following equation

$$E_a = \Delta H^{\ddagger} + RT \qquad (6.44)$$

Low values of E_a and $\Delta H^{\ddagger}$ implies *fast* reaction rate. *High* values of E_a and $\Delta H^{\ddagger}$ implies *slow* reaction rate. The typical values of E_a and $\Delta H^{\ddagger}$ lie between **20 — 150 kJ/mol.**

The study of the temperature dependence gives the above all mechanistically important values $\ln A$ or $\Delta S^{\ddagger}$, equivalent in their mechanistical significance. As mentioned before, basically, pre-exponential factor or frequency factor, $\ln A$ describes some physical factors related to the reaction conditions and as we know that the entropy, S denotes the extent of randomness or disorder in a system. The values of $\ln A$ and $\Delta S^{\ddagger}$, are *sensible sensors*. They give the information about the degree of order in the high-energy *transition state* (i.e. maximum of energy in the reaction path way).In the curing of epoxy thermosets this information is valuable from the *perspective of kinetic homogeneity/ inhomogeneity* which has influence on final properties.

From equation (6.43) we get,

$$\Delta G^{\ddagger} = \Delta H^{\ddagger} - T . \Delta S^{\ddagger}$$

Therefore, the higher the amount of negative entropy of activation $\Delta S^{\ddagger}$ is, the higher the free enthalpy of activation (*Gibbs free energy*) $\Delta G^{\ddagger}$, which is the driving force of a chemical reaction and determines the extent and spontaneity of it. *Higher* values of $\Delta G^{\ddagger}$ correspond to *large negative values* of $\Delta S^{\ddagger}$ is *unfavourable*. The reaction rate is *slow*. Now, from the analogy of the *Eyring equation* and the *Arrhenius equation* it can be stated that—

Low values of ln A correspond to *large negative values* of $\Delta S^{\ddagger}$ is *unfavourable*. In this case, the activated complex in the transition state has a more ordered or more rigid structure than the reactants in the ground state. This is generally the case if degrees of freedom (of translation, rotation, vibration) become "frozen" on the route from the initial to the transition state. The reaction rate is *slow*.

High values of ln A correspond to *positive values* (*less negative values*) of $\Delta S^{\ddagger}$ is *favourable*. A positive value for entropy of activation indicates that the transition state is highly disordered compared to the ground state. Translational, rotational and vibrational degrees of freedom are liberated on going from the ground state to the transition state. The reaction proceeds *fast*.

6.10.4.2 Interpretation of Cure Kinetics

A careful inspection of the values of the kinetic and thermodynamic parameters obtained (listed in table 6.12) for the catalyzed and autocatalyzed epoxy-amine reactions for isothermal cure process of Araldite 2015 based on the autocatalytic model of Horie reveals that the *catalyzed reactions k_1(* by external catalysts and impurity) are *more favourable* than the *autocatalyzed reactions k_2* in terms of *enthalpy or analogously activation energy*. This is due to the low values of $\Delta H_1^{\ddagger}$ (50.42 kJ/mol) and E_{a1} (53.136 kJ/mol) compared to $\Delta H_2^{\ddagger}$ (56.469 kJ/mol) and E_{a2} (59.184 kJ/mol) suggesting a comparatively *fast* reaction initially. However, the *entropy or analogously Arrhenius frequency factor / pre-exponential factor* for the

autocatalyzed reactions k_2 is *much more favourable* than the initially *catalyzed reactions*. This is due to the *positive values* (less negative values) of $\Delta S_2^{\ddagger}$ (-129.015 J/°K/mol) compared to $\Delta S_1^{\ddagger}$ (-157.789 J/°K/mol) or *high values* of ln A_2 (19.128/min) compared to ln A_1 (15.667 /min) which suggests that the high-energy *transition state* (i.e. maximum of energy in the reaction path way) is highly disordered compared to the ground state. Translational, rotational and vibrational degrees of freedom are liberated on going from the ground state to the transition state. The reaction proceeds *fast*.

Therefore, when both *enthalpy* and *entropy* are taken into account, the *entropy factor overcomes the enthalpy factor*. As a consequence, the *free enthalpy of activation or free energy* (*Gibbs free energy*) for the autocatalyzed reactions $\Delta G_2^{\ddagger}$ (95.56 kJ/mol) is *lower* than that for the initially catalyzed reactions $\Delta G_1^{\ddagger}$ (98.23 kJ/mol). This indicates that the *autocatalyzed reactions*, k_2 *are much more favourable* (i.e. lower $\Delta G_2^{\ddagger}$ value) than the *initially catalyzed reactions*, k_1 (non- autocatalytic reactions).

The calculated value of *entropy* of the epoxy-amine reaction (listed in table 6.12) for our studied system is *lower* than those reported in the literature for other epoxy-amine systems *without reactive diluent* [1]. In comparison to our system, the *large entropy effect* observed in other epoxy-amine systems *without reactive diluent* [1], most probably may be due to the fact that the reaction mixture is very *viscous*, though including this fact, other causes may also account for the effect.

6.10.4.3 Effect of Reactive Diluent (modifier) in Cure kinetics of Araldite 2015

As our commercial epoxy-amine system Araldite 2015 is *modified* with difunctional epoxy-based reactive diluent 1,4 Butane diol diglycidyl ether (BDGE); therefore, the introduction of the aliphatic segments of the reactive diluent into the main chain of the epoxy structure, in general, enables to *reduce viscosity* in order to aid general processability, which is well known. This is reflected in the considerably *lower* values of *entropy* reported in table 6.12 in comparison to other epoxy-amine systems *without reactive diluent* [1]. Therefore, in comparison to other epoxy-amine system without reactive diluent, the analysis of our Thermodynamic data shows that most probably the reactive diluent reduced the viscosity which is its conventional effect. From the

values of entropy and pre-exponential factor listed in table 6.12 it is evident that at the early stages of the cure, reactions are more *homogeneous*. As the cure proceeds, kinetic homogeneity becomes less pronounced and reactions become more *inhomogeneous*.

It is worth noting that in comparison to the typical data of stoichiometric ratio mixture DETA cured epoxy resins (DGEBA) without reactive diluents [1, 5, 29] and other amine cured epoxy resins (DGEBA) without reactive diluents [7, 8, 9, 13, 25], the analysis of our data (conversion and reaction rate profiles) in connection with the kinetic parameters obtained based on the Horie model [equation (6.40)] as reported in table 6.10, shows that most possibly, the reactive diluent increased the maximum value of calorimetric conversion (α_{max}) and the maximum value of reaction rate ($d\alpha/dt$)$_{max}$, while the values of activation energies (E_{a1}, E_{a2}), pre-exponential factors/ Arrhenius frequency factors ($\ln A_1$, $\ln A_2$), reaction rate constants (k_1, k_2), and process parameters remained within the typical values of epoxy formulations.

Therefore, the introduction of aliphatic segments of reactive diluent into the main chain of the epoxy does not cause a significant change in the kinetics of the overall curing process of the commercial thermosetting system under study, except —

(i) contributing, most possibly, in obtaining the *relatively higher values of maximum calorimetric conversion* (α_{max}) *and conversion rate* ($d\alpha/dt$)$_{max}$ observed in the investigation. The crosslink density seems not to be affected. These observations are elucidated and justified in detail with precise comparison in sections 5.1.1 and 5.2.1 in chapter 5.

(ii) *Reducing viscosity* associated with the considerably *lower* values of *entropy* as stated here, which is the most familiar effect of reactive diluent.

6.10.4.4 Advantages of Thermodynamic Reasoning in Cure Kinetics

The *Thermodynamic reasoning* coupled with its *kinetic viewpoint* founded on the analogy between the *Eyring equation* (which is a theoretical construct) and the *Arrhenius equation* (which basically based on empirical observation) are implemented here to analyze the kinetics of our studied thermosetting system. The potential of this

approach associated with its mechanistical and kinetic significance can *contribute* towards the in depth critical understanding of the cure reaction and in particular, can provide us with information of kinetic homogeneity / inhomogeneity associated with reaction phase and the properties of the end product which is important to control the reaction kinetics to attain desired / good properties in the end material.

6.10.5 Diffusion Effect

As mentioned earlier using the diffusion factor, the reaction rate can be expressed in the following form to account for effects of diffusion:

$$\frac{d\alpha}{dt} = (k_1 + k_2\alpha)(1-\alpha)^2 f_d(\alpha, T) \qquad (6.45)$$

Where, the diffusion factor $f_d(\alpha, T)$ defined in equation (3.19) in chapter 3, as:

$$f_d(\alpha, T) = \frac{k_e}{k} = \frac{1}{1 + \exp[C(\alpha - \alpha_c)]}$$

To take into account the diffusion effect, in this study, the value of the diffusion factor $f_d(\alpha, T)$ is considered as the ratio of the experimental reaction rate to the reaction rate predicted by the autocatalytic chemical kinetic model of Horie given by equation (6.40) (which does not account for diffusion). The values of the diffusion factor $f_d(\alpha, T)$ parameters — critical conversion α_c and co-efficient C of the model given by equation (6.45) obtained by applying non-linear regression to the $f_d(\alpha, T)$ vs. α data at each isothermal temperature are listed in table 6.13.

Figure 6.48 shows the behaviour of diffusion factor $f_d(\alpha, T)$ [(a) calculated, (b) simulated] with increasing conversion at cure temperatures of 30°C, 40°C, 50°C, 60°C, 70°C and 80°C respectively based on Horie model. It is clearly evident from the figure that the downturn in $f_d(\alpha, T)$ at α_c due to onset of diffusion increasingly occurs at higher conversions with increasing cure temperature. As discussed before, for the studied thermosetting system, our results consistent with the findings of other research workers [12,31,38,49,50,51] suggest that *diffusion control becomes important only on vitrification and not on gelation* (which occurs at lower values of α), and that the *critical conversion α_c* specifically relates to the *onset of vitrification.*

Table 6.13 The values of the Diffusion factor f_d (α,T) parameters-- Co-efficient C and Critical Conversion (α_c) of the Autocatalytic model $\dfrac{d\alpha}{dt} = (k_1 + k_2\alpha)(1-\alpha)^2 f_d(\alpha,T)$ (Horie model coupled with Diffusion factor)for isothermal cure process of Araldite 2015.

| T_{cure} (^{0}C)	C*	α_c*
30	90.501 (1.433)	0.784 (.000)
40	232.992 (7.909)	0.880 (.000)
50	47.206(1.476)	0.920 (.001)
60	182.504 (2.085)	0.950 (.001)
70	331.539 (2.056)	0.970 (.001)
80	257.191 (2.833)	0.975 (.001)

* Values in parentheses correspond to standard errors (SE).

Figure 6.44 illustrating plots of reduced rate vs. conversion and figure 6.48 (b) illustrating plots of diffusion factor (simulated) vs. conversion are reproduced together for a *better representation of the diffusion control phase*. The reduced rate of reaction gradually increases and after it has reached a broad maximum, the reaction rate decreases rapidly caused by the onset of rate control by diffusion due to vitrification of the epoxy-amine system. The portion of the cure that exhibits *autocatalytic* kinetics is evident by the *linear* slope. It can be seen from the $f_d(\alpha,T)$ vs. α plots that the downturn in $f_d(\alpha,T)$ at α_c is due to onset of vitrification . When $\alpha << \alpha_c$, $f_d(\alpha,T)$ is close to *unity*, the reaction is controlled by *autocatalytic* kinetics which is *analogous to the linear portion* of the reduced rate vs. conversion plots. When α increases and approaches to α_c, $f_d(\alpha,T)$begins to decrease similar to the rapid decrease in reduced reaction rate vs. conversion plots.
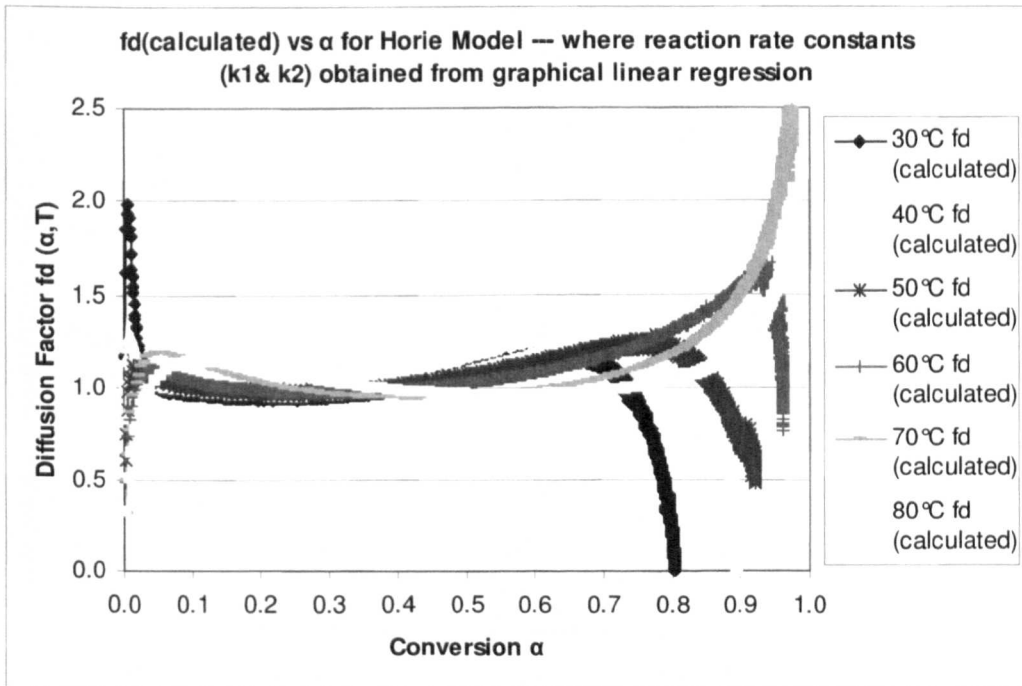
(a)
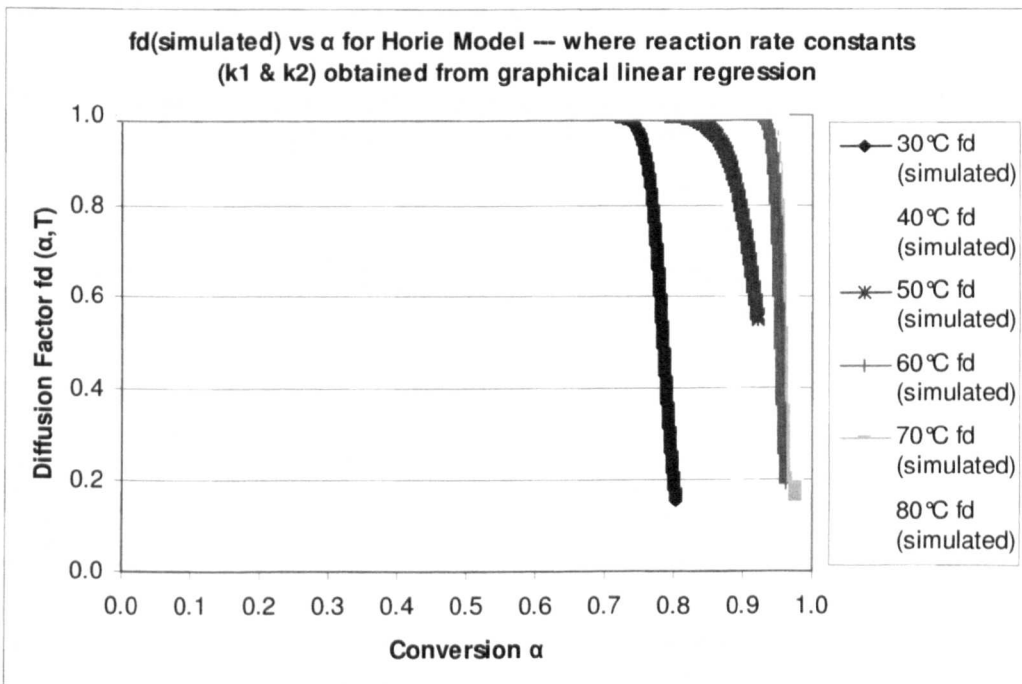
(b)

Figure 6.48 Variation of Diffusion factor [**(a)** calculated,**(b)** simulated] with calorimetric conversion at different isothermal temperatures based on Horie model $d\alpha/dt = (k_1 + k_2\alpha)(1-\alpha)^2$ where k_1 and k_2 are obtained by applying linear regression to the reduced reaction rate vs. conversion data graphically for the cure process of Araldite 2015.
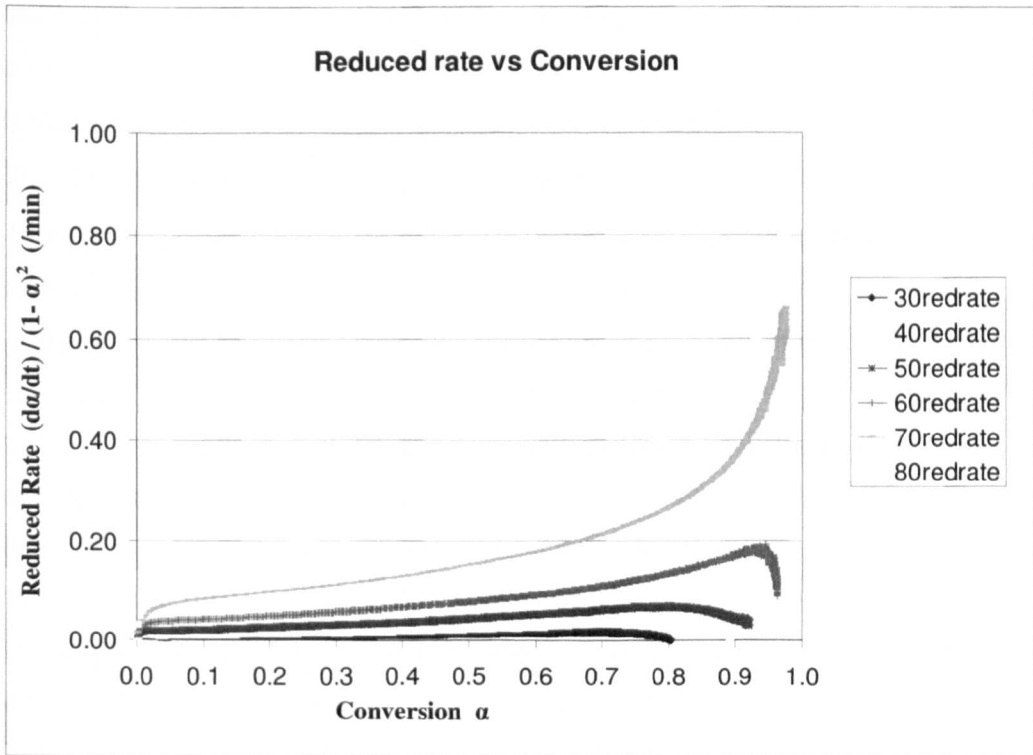
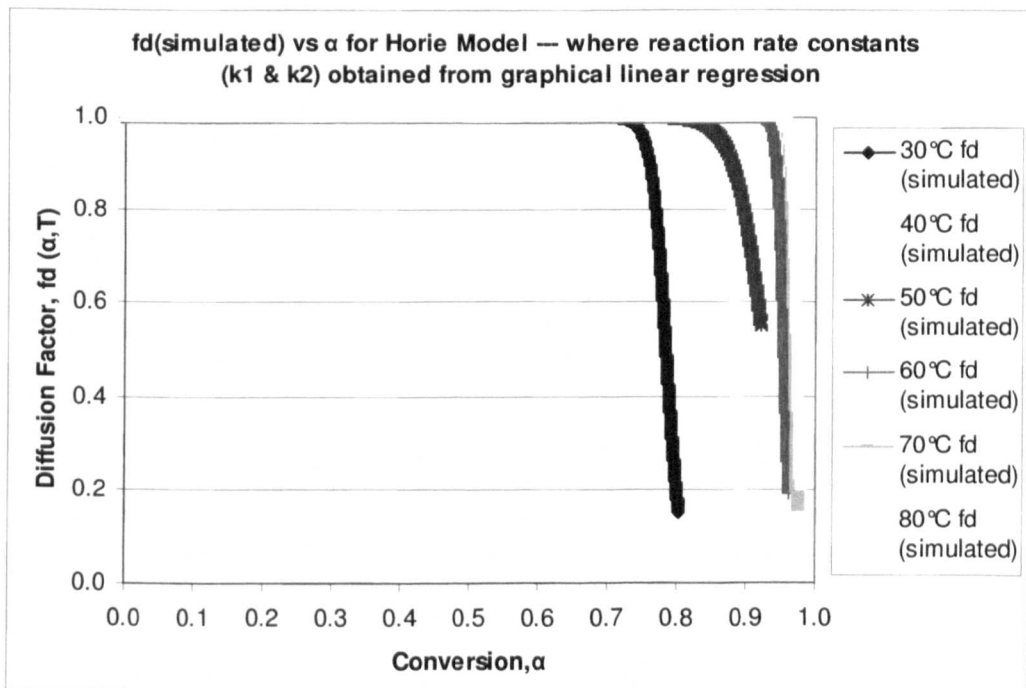**Figure 6.44 (Reproduced)** Plots of reduced rate vs. conversion.

Figure 6.48 (b) (Reproduced) Plots of Diffusion factor vs. conversion.

Figures 6.44 and 6.48 (b) (Reproduced) An illustration of diffusion control phase.

269

The variation of the critical conversion α_c with temperature is shown in figure 6.49(a). It can be seen that with increasing temperature α_c occurs at a higher conversion as the thermosetting resin being able to stay mobile longer at the higher cure temperatures. Thus the diffusion factor $f_d(\alpha,T)$ is a function of both conversion and temperature. There is considerable scatter in the linear fit for the critical conversion α_c. Thus the relationship is not approximately linear within experimental error, which is reflected in the R^2 value. The corresponding equation of linear regression and their squared correlation co-efficients, R^2 (i.e. co-efficients of determination) are also presented in figure 6.49(a). Figure 6.49(b) illustrates the variation of the co-efficient C with temperature. For the co-efficient C, there is considerably more scatter, and no discernible trend with temperature is observed. It can be noted that Cole et al [38] in their studies on epoxy-amine curing had observed linear trend for variation of α_c with temperature, but did not observe any trend for variation of C with temperature. For diffusion factor parameters α_c and C, similar observation also have been reported by Park et al [49] for epoxy/phenol-novolac resin blend system.
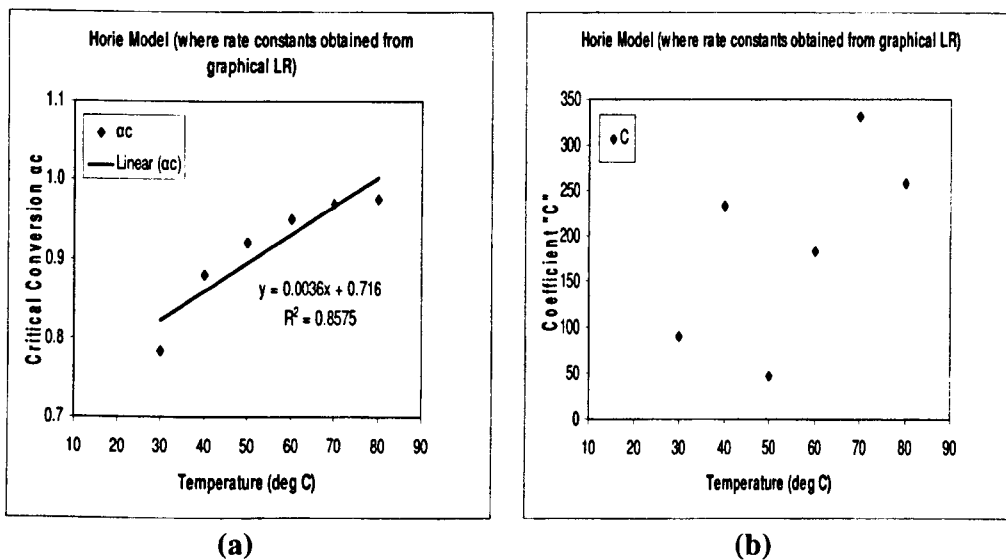

(a)

(b)

Figure 6.49 Dependence of the values of **(a)** Critical conversion α_c and **(b)** Co-efficient C on isothermal cure temperature based on the kinetic model of Horie $d\alpha/dt = (k_1 + k_2\alpha)(1-\alpha)^2$ for cure process of Araldite 2015.

6.11 Further Characterization of Cure Kinetics

6.11.1 Half-life ($t_{1/2}$) of Cure

Corresponding to the maximum degree of cure (α_{max}) at each isothermal cure temperature, there exists a maximum cure time (t_{max}). The values for the maximum cure time at different isothermal cure temperatures are very different. The relationship between the maximum cure time and the isothermal cure temperature for our studied thermosetting system is shown in figure 6.50.
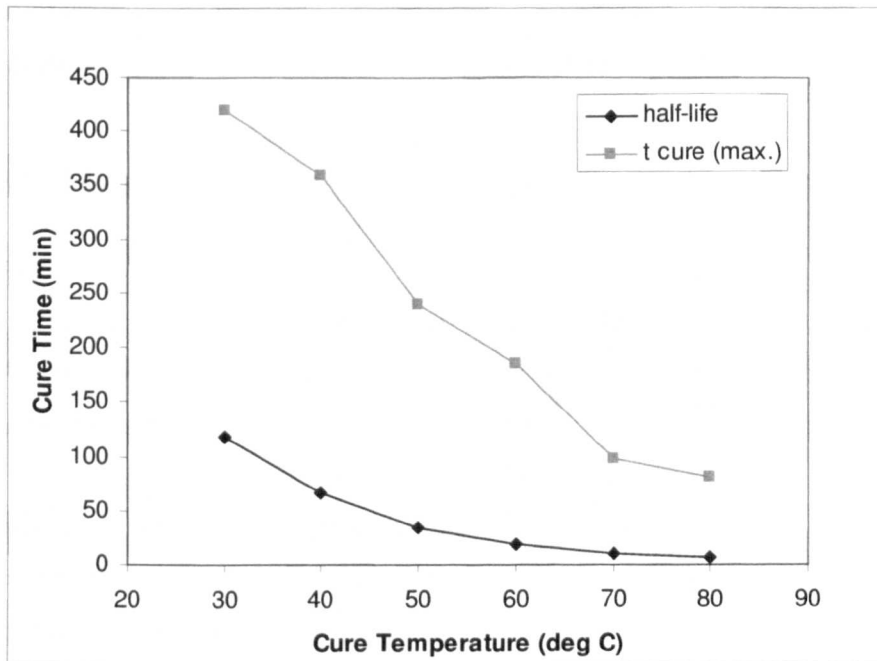
Figure 6.50 Half-life ($t_{1/2}$) and the maximum cure time (t_{max}) for the isothermal cure process of Araldite 2015 as a function of isothermal cure temperature.

Half-life ($t_{1/2}$) or half-time of cure is another *important parameter* for the isothermal cure process. It is the time required to reach 50 percent conversion at a certain cure temperature. The relationship between the half-life and isothermal cure temperature is also given in figure 6.50. It is actually an iso-conversional plot of cure time vs. temperature at degree of cure of 0.5. By comparison, it is clear that half-life is much smaller than the maximum cure time at the same isothermal temperature. This is not difficult to understand. At the same temperatures, the cure rate in the later cure stage

becomes much smaller. So it needs much more time in the late cure stage than in the early cure stage to increase the same value of degree of cure. The curves suggest that both the maximum cure time and half-life decay exponentially with respect to the isothermal cure temperature. Half-life temperature is very useful to verify DSC thermal cure results.

Two interesting points can be mentioned here. *Firstly*, in figure 6.50, the half-life $(t_{1/2})$ curve also represents the *theoretical* gelation curve for our epoxy thermosetting system which should occur at a conversion of 0.5 as discussed before. *Secondly*, employing Avrami model *accurate consistency between the experimental data and the theoretically predicted values of half-life of cure*, $t_{1/2}$ at all of the six isothermal temperatures is obtained (figure 6.39) as stated earlier.

6.11.2 Isothermal TTT Cure Diagram (Theoretical) of Araldite 2015

In chapter 3 the details of Time Temperature Transformation diagram was discussed in the context of time temperature and cure. Ideally, a thermosetting TTT cure diagram permits cure time-temperature paths to be chosen properly, so that the different material state transitions occur in a controlled manner and consequently give rise to predictable properties. From the cure process of our studied thermosetting system Araldite 2015 performed in isothermal conditions, it is possible to follow experimentally the transition from the liquid state to the rubbery state, and then to the glassy state as a function of time.

6.11.2.1 Gelation Curve

Gelation and vitrification times can be either experimentally evaluated using rheological measurement methods or determined by both the reaction kinetics and the consideration of the system component chemistry [14]. The experimental gel point of the cure process is closely related to rheological properties which can be associated with an *iso-viscous* state. An isothermal viscosity measurement could be used to determine the gel point. Due to limitation of the equipments in our laboratory, this experiment could not be performed at this stage.

The isothermal gelation (theoretical) curve (figure 6.51) is constructed from the values of *theoretical gel time* listed in table 5.5 in chapter 5 obtained from calorimetric study which has already been discussed in details. However, these *theoretical gel time* values do not hold the traditional *rheological or viscometric signature of gelation.*

6.11.2.2 Vitrification Curve

For a given isothermal cure, the vitrification point represents the cessation of reaction, as the increased viscosity and/or molecular weight prevent further reactive group interactions. Basically, the study of the vitrification process by DSC is based on the data of variation of the degree of conversion, α and the glass transition temperature, T_g as a function of cure time, t_{cure} at a particular cure temperature T_{cure}. As discussed earlier, the T_g is a function of degree of conversion only and is independent of cure temperature. So the relationship between T_g and the isothermal cure time can be determined. The system vitrifies when $T_g = T_{cure}$. Thus, at each isothermal cure temperature, T_{cure} the cure time, t_{cure} required for T_g to rise to the cure temperature, T_{cure} can be obtained which is equal to the vitrification time, $t_{vitrification}$. The relationship between isothermal cure temperature and the vitrification time is represented by the vitrification curve.

For our thermosetting system, the isothermal theoretical vitrification curve (onset) (figure 6.51) is constructed from the obtained values of the critical conversion (α_c) [listed in table 6.2(b)] based on the autocatalytic kinetic model of Kamal [equation (3.9)] coupled with the diffusion factor $f_d(\alpha,T)$ [equation (3.19)], i.e.

$$\frac{d\alpha}{dt} = k\alpha^m (1-\alpha)^n f_d(\alpha,T)$$ [equation (6.23)] for the series of isothermal temperatures

of 30°C, 40°C, 50°C, 60°C, 70°C and 80°C, employed in the test which was elucidated and justified in details in section 6.4.2.

6.11.2.3 TTT Cure Diagram (Theoretical) for Araldite 2015

For the isothermal cure process of our studied thermosetting system DGEBA/DETA the relationship between isothermal cure temperature and the theoretical gel time is

represented by the theoretical gelation curve. The theoretical vitrification curve represents the relationship between isothermal cure temperature and the onset of vitrification time obtained theoretically based on autocatalytic model of Kamal coupled with the diffusion factor. By plotting the theoretical gelation and vitrification curves in the same graph, the isothermal TTT cure diagram (theoretical) of our modified epoxy-amine system is constructed. It is shown in figure 6.51. From the figure it can be seen the transition from the liquid region to the rubbery region, and then to the glassy region as a function of time. Depending on the isothermal cure path with respect to temperature and time, the cure process is controlled by *kinetics* in the liquid and rubber regions and is controlled by *diffusion* in the glass region.

Figure 6.52 illustrates the generalized Time-Temperature-Transformation phase diagram (discussed details in chapter 3) based on isothermal cure of DGEBA with DETA. The TTT diagram re-drawn and adopted from references [2,18,50]. Basic regions and the gelation and vitrification curves are depicted in the figure. Chemical structures are included to indicate the extreme cases of predominantly crosslinked (top) and chain extension (bottom).

6.11.2.4 Fundamentals of Fixation of Cure Cycle

The TTT diagram aids a manufacturer in selecting a heat schedule to produce a cured resin with the desired properties. In order to get optimum overall properties, the best possible cure cycle should be fixed. As discussed in chapter 2 and 3, degradation and undercure play a crucial role. On top of it, formation of microgels before gelation, phase separation or partial segregation and development of inhomogeneity are to be taken into account.

In the cure of any thermoset, the first cure temperature must be low enough to build a homogeneous network but not too low to keep a suitable curing time. In order to define the second cure temperature (in the case of high temperature cure) or the post cure temperature (in the case of low temperature cure) maximum crosslinking density is to be taken into account.
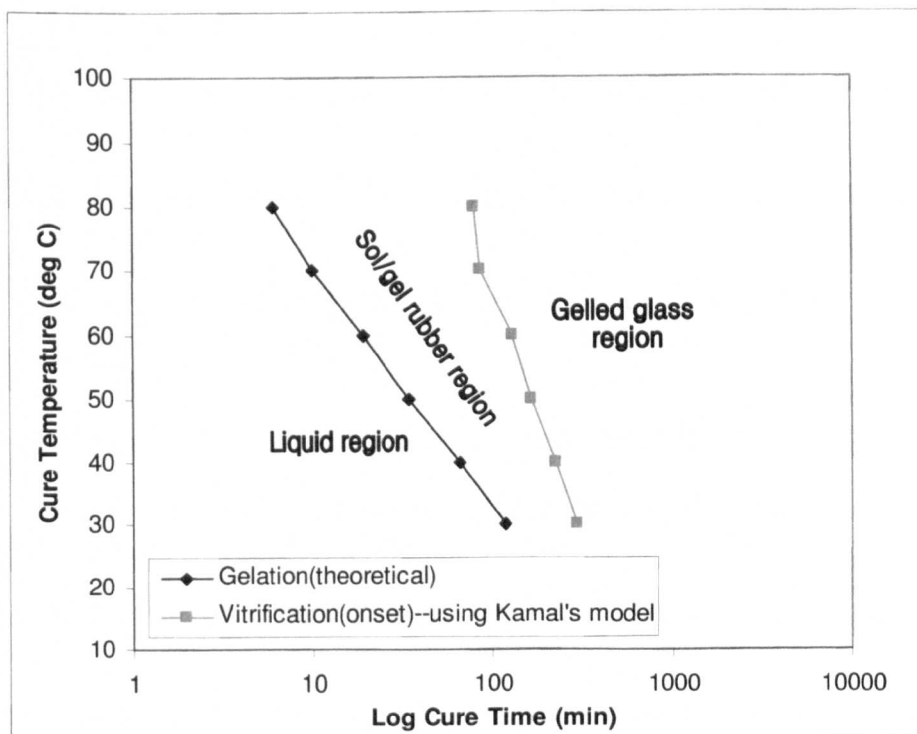
Figure 6.51 A simple theoretical TTT cure diagram for the isothermal cure process of Araldite 2015 (DGEBA/DGEBF/DETA) system.

Log Cure Time

Figure 6.52 Generalized Time-Temperature-Transformation phase diagram based on isothermal cure of DGEBA with DETA. Note regions and gelation and vitrification curves are shown. Chemical structures are included to indicate the extreme cases of predominantly crosslinked (top) and chain extension (bottom). TTT diagram re-drawn and adopted from references [2,18,50].

6.12 References

[1— 37]. Exactly are the same as that of mentioned in section 5.10 references in chapter 5.

38. Cole, K.C., Hechler, J. J., and Noel, D., Macromolecules,vol.24, 1991, 3098-3110.
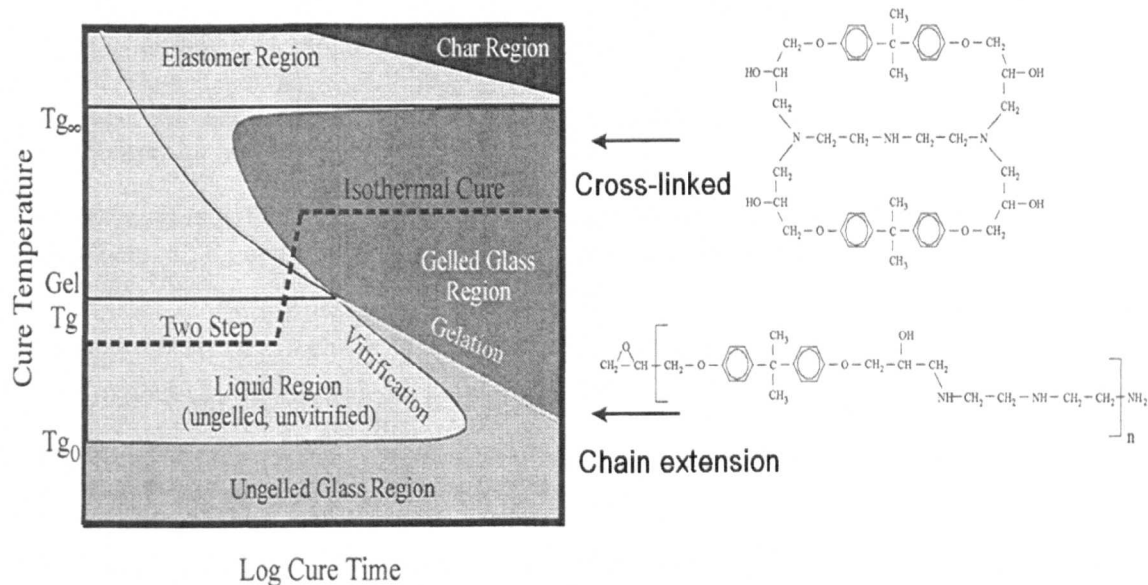
39. Hargis, M., Grady, B.P., Aktas, L., Bomireddy, K.R., Howsman, S., Altan, M.C., Rose, T., and Rose, H., Journal of Composite Materials, vol.40, no.10, 2006, 873-897.

40. Samaras, Z.I., PhD Thesis, University of Carnfield, United Kingdom, 2005.

41. Gonzalez-Romero, V.M., and Casillas, N., Polymer Engineering and Science, vol.29, no.5, 1989, 295-301.

42. Yousefi, A., Lafleur, P.G., and Gauvin, R., Polymer Composites, vol.18, no.2, 1997, 157-168.

43. Wise, C.W., Cook, W. D., and Goodwin, A. A., Polymer, vol. 38, no. 13, 1997, 3251- 3261.

44. Skordos, A.A., and Partridge, I.K., Polymer Engineering and Science, vol.41, no.5, 2001, 793-805.

45. Flammersheim, H. J., Opfermann, J. R., Macromolecular Material Engineering, vol.286, no.3, 2001, 143-150.

46. Dusi, M. R., Lee, W. I., Ciriscioli, P. R., and Springer, G.S., Journal of Composite Materials, vol.21, 1987, 243-261.

47. Rabinowitch, E., Transactions of the Faraday Society, vol. 33, 1937, 1225.
48. Chern, C. S., and Poehlein, G. W., Polymer Engineering and Science, vol. 27, 1987, 782.

49. Park, S. J., Seo, M. K., Lee, J. R., Journal of Polymer Science: Part A: Polymer Chemistry, vol. 38, 2000, 2945-2956.

50. Prime, R. B., Thermal Characterization of Polymeric Materials, 2nd edition, Turi, E. A., ed., vol. 2, 1379-1766.

51. Eom, Y., Boogh, L., Michaud, V., Sunderland, P., and Manson, J.A., Polymer Engineering and Science, vol. 40, no. 6, 2000, 1281-1292.

52. Kim, S. W., Lu, M. G., and Shim, M. J., Polymer Journal, vol. 30, no. 2, 1998, 90-94.

53. Yiyun, C., and Pingsheng, H., Journal of Composite Materials, vol.40, no.13, 2006, 1215-1223.

Chapter 7 Ultrasonic Wave Propagation in Curing Thermosets

7.1 Introduction

This chapter presents the theory and fundamentals of ultrasonic wave propagation in thermosets, reviews viscoelasticity and relaxation in polymers along with various viscoelastic models of wave propagation and distribution of relaxation times. This chapter also critically reviews typical ultrasonic results related to evolution of structure in curing thermosets, the effect of temperature and frequency on ultrasound data and the potential of ultrasonic technique in defining gelation and vitrification. The purpose is to identify the most important observations that have been made during the cure cycle.

7.2 Wave propagation in an absorbing medium

A linearly elastic solid having a linear single-valued relation between stress and strain over a complete cycle of oscillatory stress, displays no damping or losses. In such a case stress and strain are always in phase. Real materials may show deviations from ideal Hookian and Newtonian behaviour. This is illustrated in figure 7.1.
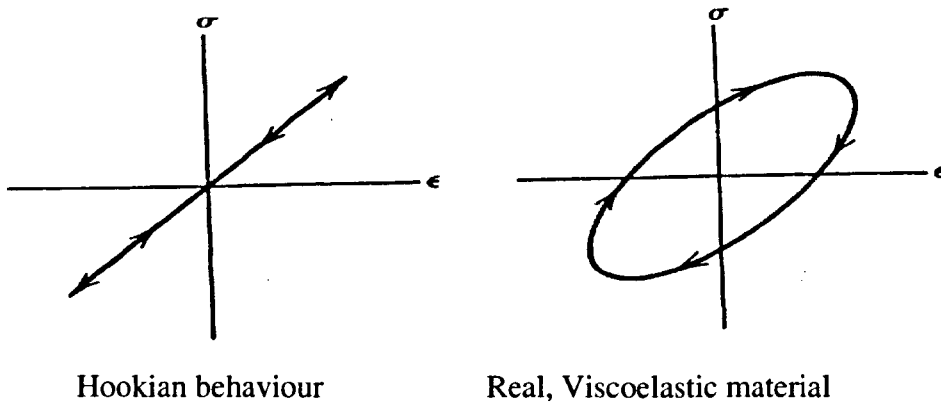

Hookian behaviour   Real, Viscoelastic material

Figure7.1 Simple dynamic relationships between stress(σ) and strain(ε).

In a viscoelastic solid internal friction mechanisms dissipate energy. Elastic waves propagating in an absorbing medium will experience a frequency dependent damping. In this case, the stress and strain are not just a linear single-valued functions of one another for a complete cycle of vibration, in addition there exists the time derivatives of stress and/or strain in the equation relating stress and strain. This hysteresis effect can be represented by the use of both elastic and viscous terms in the equation of motion for an elastic solid.

There are many derivations for acoustic wave propagation in an absorbing medium, some of which depend on specific models of the loss mechanisms [59]. Here, in the derivation of acoustic wave propagation in viscoelastic medium we have used the work of McSkimin[9] which incorporates loss mechanisms in the form of a generalized complex frequency dependent elastic modulus. As the expressions describing the viscoelastic behaviour of the material *do not depend on any assumed model for the loss mechanism*, it is therefore possible to carry out direct calculation of the mechanical properties of the adhesive material from measurements of absorption coefficient, phase velocity and density. The equations of motion for a perfectly elastic media presented here below are available in many textbooks and for the background and detailed derivations the reader is referred to the informative texts of Kolsky [51] and Ewing et al [52].

The equations of motion for an ideal elastic solid may be decoupled into the well known equations adequately describing compression and shear wave motion, thus

$$\frac{1}{v_c^2} \frac{\partial^2 \varphi}{\partial t^2} = \nabla^2 \varphi \qquad (7.1)$$

$$\frac{1}{v_s^2} \frac{\partial^2 \overline{\psi}}{\partial t^2} = \nabla^2 \overline{\psi} \qquad (7.2)$$

where v_c and v_s are the compression and shear wave velocities respectively which are functions of the material properties of stiffness and density, t is time and φ and $\overline{\psi}$

are the scalar and vector *displacement potentials* which are solutions of the wave equation. The wave velocities depend only on the Lamé constants λ and μ and density ρ by the following equations

$$v_c^2 \rho = \lambda + 2\mu \tag{7.3}$$

$$v_s^2 \rho = \mu \tag{7.4}$$

$$(v_c^2 - 2v_s^2)\rho = \lambda \tag{7.5}$$

It is useful to define the common elastic moduli of a solid in terms of the Lamé constants. So, equations (7.3), (7.4) and (7.5) may be written,

$$C = v_c^2 \rho = \lambda + 2\mu \tag{7.6}$$

$$G = v_s^2 \rho = \mu \tag{7.7}$$

$$K = C - \frac{4}{3}G = \lambda + \frac{2}{3}\mu = [v_c^2 - \frac{4}{3}v_s^2]\rho \tag{7.8}$$

where C, G and K are the compression (also known as the longitudinal wave modulus), shear and bulk moduli respectively.For the case of elastic solid C, G, K are wholly real and for a viscoelastic solid, C, G, K will be complex and the exact form of the modulus depends on the nature of the viscoelastic model used in the equation of motion. This is explained later.

In two-dimensional space (x_1, x_2) in an isotropic homogeneous medium the general plane wave solution to equations (7.1) and (7.2) for a displacement potential P is,

$$P = A \exp\{j(\omega t - k \sin\theta \, x_1 + k \cos\theta \, x_2)\} \tag{7.9}$$

Where A is the wave amplitude, ω is the angular frequency, k is the complex wave number, θ is the angle of propagation with respect to the x_2-axis, and j is the complex operator equivalent to $\sqrt{-1}$. In the case of an elastic solid the wave number (k) is wholly real and is defined by

$$k = \frac{\omega}{c} \qquad (7.10)$$

where c is the speed of the wave. For a viscoelastic medium we need to introduce loss terms as the medium always exhibits loss. Therefore, in an absorbing medium the Lamé constants may be extended by loss terms $(\lambda_r + j\lambda_i)$ and $(\mu_r + j\mu_i)$ resulting in a complex wave number $(k_r + jk_i)$ with real (k_r) and imaginary (k_i) parts

$$k_r = \frac{\omega}{c(\omega)} \qquad (7.11)$$

$$k_i = \alpha(\omega) \qquad (7.12)$$

where $c(\omega)$ and $\alpha(\omega)$ are the phase velocity and the absorption co-efficient respectively which are functions of frequency.

Previously it was shown that, in an isotropic viscoelastic medium, three complex moduli are related to the compression and shear phase velocities. In the work of McSkimin[9], the complex wave number is derived in terms of a generalized complex frequency dependent elastic modulus $M(\omega)$, with real part $M_r(\omega)$ and imaginary part $M_i(\omega)$

$$M(\omega) = M_r(\omega) + jM_i(\omega) \qquad (7.13)$$

and $M_r(\omega) = \rho c^2(\omega) \dfrac{1 - \alpha^2(\omega)c^2(\omega)/\omega^2}{[1 + \alpha^2(\omega)c^2(\omega)/\omega^2]^2} \qquad (7.14)$

$$M_i(\omega) = 2\rho c^2(\omega) \frac{\alpha(\omega)c(\omega)/\omega}{[1+\alpha^2(\omega)c^2(\omega)/\omega^2]^2} \tag{7.15}$$

The form of $M(\omega)$ will depend on whether compression or shear motion is being considered, and the nature of the viscoelastic solid used to give the form of the complex modulus. For compression waves $M(\omega)$ would be equivalent to compression modulus C and for shear waves it would be equivalent to G, both C and G are complex and frequency dependent.

7.3 Viscoelastic models of wave propagation

Historically, there are various viscoelastic models which describes the viscoelastic behaviour in real solids.

Following McSkimin [9] it can be shown that

$$k_i^2 = \alpha^2 = \frac{\omega^2 \rho}{2M_r}[\frac{F-1}{F^2}] \tag{7.16}$$

$$k_r^2 = [\frac{\omega}{c(\omega)}]^2 = \frac{\omega^2 \rho}{2M_r}[\frac{F+1}{F^2}] \tag{7.17}$$

where $F = \frac{|M(\omega)|}{M_r(\omega)}$ and $F^2 = 1+[\frac{M_i(\omega)}{M_r(\omega)}]^2 \tag{7.18}$

From equation (7.17) we obtain the phase velocity

$$c^2(\omega) = \frac{2M_r(\omega)}{\rho}\frac{F^2}{(F+1)} \tag{7.19}$$

Using equation (7.16) & (7.17) absorption per wavelength is obtained noting that

$$\alpha(\omega)\lambda = \frac{2\pi\alpha}{k_r} = \frac{\alpha 2\pi c(\omega)}{\omega}$$

$$\alpha(\omega)\lambda = 2\pi[\frac{F-1}{F+1}]^{1/2} \tag{7.20}$$

In this chapter our main concern is with ultrasonic wave propagation in polymeric materials which brings the need for analytical models by which wave absorption and phase velocity may be estimated as functions of frequency. So, it would be useful to identify a simple mechanical model which represents the viscoelastic state of the curing material. This would enable ultrasonic propagation data to be parameterized into a few variables that could be used to track and monitor the cure process. Various models are invented explicitly to provide a method of mathematical analysis of polymeric viscoelastic behaviour. Though scientifically long outmoded, we consider classical phenomenological models of viscoelasticity based on springs and dashpots(as bases for working approximations to reality) to make it clear about their applicability as engineering approximations to wave propagation in polymers.

In the following section brief derivations and short analysis of viscoelastic behaviour for three phenomenological models (Maxwell, Kelvin-Voigt and Zener) are presented. It is worthnoting that each of the models of viscoelasticity imply a particular form of $M(\omega)$ and F and through these the behaviour of the absorption co-efficient and phase velocity as functions of frequency can be obtained.

7.3.1 Maxwell model

Maxwell [56] was the first one who had attempted to describe the behaviour of a real liquid. According to him, a real liquid exhibits both elastic and viscous behaviour and under shear stress the deformation of the liquid is the sum of an elastic response (Hookian) and a viscous response (Newtonian). The response is described by a mechanical model consists of an elastic element (M_0) in series with a viscous (loss) element (η) which is shown in figure 7. 2(b). In this case, both the spring and the dashpot are subjected to the same stress but are permitted independent strains.
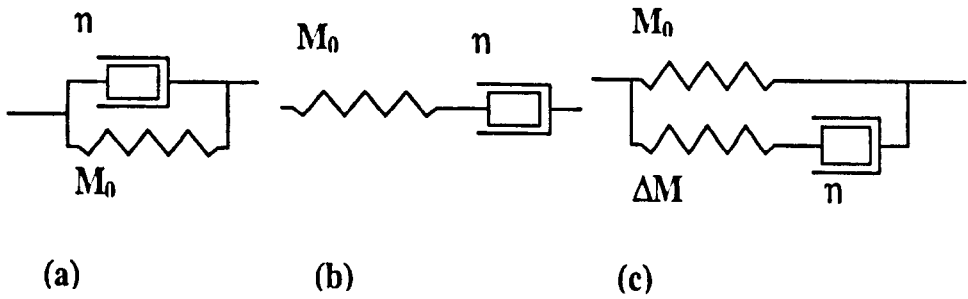
Figure 7.2 Phenomenological models of viscoelasticity: (a) Kelvin-Voigt, (b) Maxwell, and (c) the anelastic solid (Zener).

From the mechanical model the following relationship for the modulus can be derived.

$$M = \frac{M_0 \, j\omega\eta}{M_0 + j\omega\eta} \tag{7.21}$$

Assuming a relaxation time τ given by $\dfrac{\eta}{M_0}$ the complex modulus is written,

$$M = M_0 \left[\frac{j\omega\tau}{1 + j\omega\tau} \right] \tag{7.22}$$

The magnitude and the real part of the complex modulus is given by,

$$|M| = M_0 \frac{\omega\tau}{(1 + \omega^2\tau^2)^{1/2}} \qquad M_r = M_0 \left[\frac{\omega^2\tau^2}{1 + \omega^2\tau^2} \right] \tag{7.23}$$

With appropriate manipulations of equations (7.16) – (7.20) yields phase velocity, attenuation per wavelength and attenuation thus with $c_0^2 = \dfrac{M_0}{\rho}$ we get [2],

$$c(\omega) = c_0 \left[\frac{2\omega\tau}{\omega\tau + (1 + \omega^2\tau^2)^{1/2}} \right]^{1/2} \tag{7.24}$$

$$\alpha(\omega)\lambda = 2\pi \left[\frac{(1+\omega^2\tau^2)^{1/2} - \omega\tau}{(1+\omega^2\tau^2)^{1/2} + \omega\tau} \right]^{1/2} \tag{7.25}$$

$$\alpha(\omega) = \frac{\omega}{c_0} \left[\frac{(1+\omega^2\tau^2)^{1/2} - \omega\tau}{2\omega\tau} \right]^{1/2} \tag{7.26}$$

Where c_0 is the low frequency velocity.

Challis et al have shown [2] that the Maxwell model cannot support compression wave propagation in polymers at all at low frequency. Phase velocity tends to zero at low frequency ($\omega\tau \ll 1$) and reaches a high frequency value of $c_0 = (\frac{M_0}{\rho})^{1/2}$ governed by the elastic element and material density. Attenuation ($\alpha\lambda$) is highest at low frequency (6 Nepers per wavelength) and approaches to zero at high frequency. Neither of these attenuation and velocity behaviours have been observed in polymers.

7.3.2 Kelvin-Voigt model

The Maxwell model was extended independently by Kelvin[57] and Voigt[58]. The model consists of an elastic element in parallel with a viscous element shown in figure 7.2(a). In the Maxwell model, both the spring and the dashpot are subjected to the same stress but are permitted independent strains. The inverse is true for the Kelvin-Voigt model. Here, the stress is related to strain and the rate of change of strain. For this model the complex modulus is given by,

$$M = M_0 + j\omega\eta = M_0(1 + j\omega\tau) \tag{7.27}$$

where relaxation time $\tau = \frac{\eta}{M_0}$

The magnitude and real part of modulus are given by,

$$|M| = M_0(1+\omega^2\tau^2)^{1/2} \qquad\qquad M_r = M_0 \tag{7.28}$$

With appropriate manipulations of equations (7.16) – (7.20) we obtain [2],

$$c(\omega) = c_0 \left[\frac{2(1+\omega^2\tau^2)}{(1+\omega^2\tau^2)^{1/2}+1} \right]^{1/2} \qquad (7.29)$$

$$\alpha(\omega)\lambda = 2\pi \left[\frac{(1+\omega^2\tau^2)^{1/2}-1}{(1+\omega^2\tau^2)^{1/2}+1} \right]^{1/2} \qquad (7.30)$$

$$\alpha(\omega) = \frac{\omega}{c_0} \left[\frac{(1+\omega^2\tau^2)^{1/2}-1}{2(1+\omega^2\tau^2)} \right]^{1/2} \qquad (7.31)$$

This model, in principle, could support compression wave propagation in polymers at low frequency. Challis et al have shown [2] that the phase velocity can take a realistic value at low frequencies, but would be expected to rise indefinitely (approximates to $c_0(2\omega\tau)^{1/2}$) at high frequencies, a behaviour not observed in practice. In most polymers the phase velocity rises from a low frequency value to a slightly higher value (+ 3% say) at frequencies $>> \frac{1}{\tau}$. Further, it can be shown [2] that the wave attenuation per wavelength $\alpha(\omega)\lambda$ travelled by a wave at high frequency rises asymptotically and approaches to 2π Nepers (54dB) which is also not observed in polymers. In most polymers $\alpha(\omega)\lambda$ peaks around $\omega\tau=1$ and falls as frequency increases thereafter, the peak value is generally around an order of magnitude less than 2π.

7.3.3 Zener model/Anelastic Solid model

The Maxwell model describes the stress relaxation of a ploymer to a first approximation whereas the Kelvin-Voigt model similarly describes creep. A logical step forward is therefore to find some combination of these two basic models which can account for both phenomena. A simple model which does this is known as the anelastic solid or Zener model. It is a further modification to the Kelvin-Voigt model suggested by Zener [59] where there are time derivatives in both the stress and strain terms of the equation of motion.

In this case a Maxwell element and spring are in parallel which is shown in figure 7.2(c). The presence of the second spring will stop the tendency of the Maxwell element undergoing simple viscous flow during creep loading, but will still allow the stress relaxation to occur [26].

From the figure7.2(c) we see that this model consists of an elastic element (M_0) in parallel with the Maxwell combination of an incremental elastic element (ΔM) and a viscous element(η). Its stress-strain relationship is

$$\sigma + \frac{\tau}{a}\frac{\partial \sigma}{\partial t} = M_0(\varepsilon + a\tau \frac{\partial \varepsilon}{\partial t}) \tag{7.32}$$

Where σ and ε are compressive stress and strain in the element, τ is the relaxation time and a is a measure of the relaxation strength. Challis et al and Cocker [3] had carried out a detailed analysis of this system which is not fully discussed here.

The complex modulus is given by,

$$M = M_0\left[\frac{1 + j\omega\tau_2}{1 + j\omega\tau_1}\right] \tag{7.33}$$

Where the two relaxation times are given by,

$$\tau_1 = \frac{\eta}{\Delta M} \qquad \tau_2 = \eta\frac{M_0 + \Delta M}{M_0\Delta M} \tag{7.34}$$

Using the relationship $\tau = (\tau_1\tau_2)^{1/2}$ equation (7.33) may be written,

$$M = M_0\left[\frac{1 + j\omega\tau a}{1 + j\omega\tau/a}\right] \tag{7.35}$$

Where, $\tau = \frac{\eta}{\Delta M}\left[\frac{M_0 + \Delta M}{M_0}\right]^{1/2}$ i.e. $\tau = \frac{a\eta}{\Delta M}$

and $\quad a^2 = \dfrac{\tau_2}{\tau_1} = \dfrac{(M_0 + \Delta M)}{M_0}$ \hfill (7.36)

ΔM is the increment in compression wave modulus between the low frequency and the infinite frequency values and M_0 is the low frequency compression wave modulus. Generally, $\Delta M << M_0$ giving the relaxation strength parameter $a \approx 1$. The magnitude and the real part of the modulus are given by,

$$|M| = M_0 \left[\frac{1 + \omega^2 \tau^2 a^2}{1 + \omega^2 \tau^2 a^{-2}} \right]^{1/2} \quad \text{and} \quad M_r = M_0 \left[\frac{1 + \omega^2 \tau^2}{1 + \omega^2 \tau^2 a^{-2}} \right] \hfill (7.37)$$

From earlier work of Challis et al [2,4] we get,

$$c(\omega) = c_0 \left[\frac{1 + \omega^2 \tau^2 a^2}{1 + \omega^2 \tau^2} \right]^{1/2} \hfill (7.38)$$

$$\alpha(\omega)\lambda = \pi(a^2 - 1) \frac{\omega\tau}{1 + a^2 \omega^2 \tau^2} \hfill (7.39)$$

$$\alpha(\omega) = \frac{(a^2 - 1)}{2c_0} \frac{\omega^2 \tau}{1 + \omega^2 \tau^2} \hfill (7.40)$$

From equation (7.38) we see that the phase velocity has a low frequency value $c_0 = (M_0 / \rho)^{1/2}$ which rises to a high frequency asymptote given by $c_\infty = ac_0$. As the high frequency phase velocity is a times the two frequency value and the value of the relaxation strength parameter a is close to unity, and certainly less than about 1.2 [3], clearly it can be seen that the phase velocity rises from a low frequency value to a value slightly greater at high frequencies. The attenuation behaviour at a given frequency as τ increases is particularly interesting. From equation (7.40) we see that the attenuation function is zero at low frequency, rises to a high frequency asymptotic value $\alpha_\infty = (a^2 - 1)/2c_0\tau$ corresponding to a peak at around $\omega\tau = 1$ and then falls off as τ increases.

From equation (7.39) we get the loss tangent which corresponds to the attenuation per wavelength traveled by the wave and characterizes the material as the ratio of the imaginary to the real parts of the modulus M governing propagation. We get,

$$\tan\delta = \frac{\alpha\lambda}{\pi} = (a^2-1)\frac{\omega\tau}{1+a^2\omega^2\tau^2} \qquad (7.41)$$

The peak value occurs when $a\omega\tau = 1$ and is given by

$$\frac{1}{2}\left[a-\frac{1}{a}\right] \cong \left[\frac{c_\infty-c_0}{c_0}\right] \qquad (7.42)$$

Experimental evidence shows the typical behaviour of loss modulus in epoxy adhesives which has a low value at low frequencies, rises to a peak and then falls again at higher frequencies. This behaviour can be explained in terms of the anelastic solid (Zener) model shown in figure7.2(c) where we assumed that a single high frequency relaxation process governed the wave propagation in polymer.

At low frequency, the dash–pot is able to slide freely and thus the modulus of the material is equal to the elastic modulus of the spring M_0. At higher frequencies, the dash-pot appears rigid and the modulus of the whole incorporates both springs, M_0 and ΔM, and the polymer appears to be more rigid.

These behaviours are observed in a wide range of polymers. As previously stated, the Kelvin-Viogt and Maxwell models were shown [2] to be inappropriate when these are applied to ultrasonic wave propagation in polymers as they give non-physical results for both wave velocity and absorption. The anelastic solid or Zener model which represents a single relaxation (Debye formulation) gives physically realistic results in terms of wave velocity, and an observed peak in absorption or acoustic loss tangent corresponding to an α–relaxation[2,3,4,7] process which will be described later. However, according to this simple Debye formulation of Zener model, ultrasonic absorption would be expected to rise will the square of the frequency (f^2). But much experimental results show that the relationship is close to linear.

In past Challis et al [3] have demonstrated that this Zener model, which represents a simple Debye process can qualitatively describe the behaviour of the number of adhesive polymers over a frequency of 1-60 MHz.

But the fact is that simple relaxational models of polymer behaviour are not universally applicable. More rigorous approaches, such as based on the correspondence principle, have greater universality [10]. However, for the restricted frequency range of interest for conventional ultrasonic NDT, the simple relaxation model can be used as a means to make estimates of wave phenomena in an engineering context [3].

Many amorphous polymers would be expected to exhibit absorption and phase velocity behaviour that would vary over a wider range of frequencies than the predictions of the Zener model representing single relaxation time. By taking into account a distributed system of relaxation processes corresponding to a multiple relaxation time system, these behaviours , in principle, could be modelled, to which many approximations exist (this is discussed later). This requires further development of the governing equations of single relaxation time Zener model.

There have been many attempts at devising more complex models which can give a better representation of the viscoelastic behaviour of polymers. As the number of elements increases the mathematics becomes more complex. It must be stressed that the mechanical models only give a mathematical representation of the mechanical behaviour and as such do not give much help in interpreting the viscoelastic properties on a molecular level.

7.4 Polymer and Viscoelasticity- an overview

As materials, the most marked feature of polymers lies in their viscoelastic character. Before going through Ultrasonic wave propagation in polymer, a brief description of the basic viscoelastic behaviour of polymeric material is in order.

7.4.1 Polymer

Basically, polymers are constituted of large molecules, comprising a large number of repeating units which are covalently linked together to form chains. In turn, the attraction between the chains is provided by secondary bonds, which, depending on the nature of the molecules, may be Van-der-Waals forces, dipole-dipole interactions, hydrogen bonds and, if crosslinking is present, covalent bonds.

7.4.2 Viscoelasticity

Bulk polymers combine elastic and viscous properties in both the fluid and the solid state. Therefore they are generally addressed as 'viscoelastic' and, in fact, polymers are the main representatives of this special class of materials. Because of the long chain nature of polymeric materials, their viscoelastic characteristics come to the forefront. This is especially true when the times for molecular motion are of the same order of magnitude as an imposed mechanical motion.

Viscoelastic behaviour does not just mean a superposition of independent viscous and elastic forces but it includes in addition a new phenomenon known as " anelasticity", where both become coupled. It becomes apparent in the observation that part of the deformation, although being reversible, requires a certain time (relaxation time) to become established when a load is applied.

7.4.3 Relaxation in Polymer

This relaxation behaviour of polymers are related to their molecular structure and motion, the latter parameter being a function of temperature. The main modes of molecular motions are movement of branch point, rotation of side groups, cranckshaft motion and segmental motion. In epoxy resins three types of relaxation are possible, α, β and γ. α-relaxations are the primary relaxations and are associated with the motion of the whole molecule. β and γ are known as secondary relaxations and are associated with local

segmental motion. In epoxy resins the β- relaxation is associated with motion of either the hydroxyether group or the diphenylproprane unit and the γ -relaxation is associated with the motion of the epoxide group.

Polymer relaxation processes occur over a wide range of time and length scales. This range of scales makes mechanical relaxations, plasticity, structural transitions and other kinetic phenomena both interesting and difficult to study. The contributions of perfect elasticity, anelasticity and viscous flow to the total mechanical response of a sample possess different weights for different polymers and, in particular, they greatly vary with temperature. This strong temperature dependence represents another characteristic property of polymeric materials.

7.5 Fundamentals of ultrasonic wave propagation in thermosets

Ultrasonic disturbances are propagated through a material as high frequency elastic stress waves, corresponds to a dynamic mechanical deformation imposed to the material. This deformation produces an oscillation (vibrational motion) or displacement around the equilibrium position of atoms and chain segments in the nm range, so the information that can be obtained from the ultrasonic measurements in polymer is related to small – scale mobility of short segments between entanglements. These waves obey the wave equation and therefore the phenomena that take place with electromagnetic waves have counterparts in acoustic systems.

The structure of adhesive materials is particularly complex on a scale that would be expected to bring about complex interactions with alternating time-dependent deformation at ultrasonic frequencies. The ultrasound method measures this complex interaction on a " macroscopic scale " where microscopic inhomogeneity (non-uniform structure of polymeric systems induced by inter-chain reactions and density fluctuations [49]) in a forming solid may appear to be macroscopically homogeneous. Macroscopically, a " detectable " change is observed which can be related to a simple case of single characteristic time only, which goes back to Debye. But things are not so

simple and it must be stressed that the time dependence of a macroscopic relaxation process always reflects the underlying microscopic dynamics which is more complex. During cure complex changes in molecular state occurs and one would expect these to bring about observable changes in ultrasonic wave propagation, through the available " experimental window " which could provide such informations. To characterize completely material properties, the acoustic behaviour over a wide range of frequencies must be examined.

7.5.1 Modes of propagation- compression and shear waves

In isotropic materials, the oscillations (caused by dynamic mechanical deformation) can occur either parallel or perpendicular to the propagation direction of the disturbance. These disturbances can propagate in solids, liquids and gases. However, in liquids and gases, shear stresses cannot be supported, and only a single mode of ultrasonic propagation, the longitudinal mode, can exist. This mode displaces particles in a direction parallel to the direction of ultrasonic wave propagation. Since compressional and dilational forces are active in these waves, they are also called pressure or compressional waves. They are also sometimes called density waves because their particle density fluctuates as they move.

In solids (and some liquids of very high viscosities) shear stresses can be supported and in these cases both the longitudinal mode and a transverse, or shear, mode (in which the particle is displaced perpendicular to the direction of ultrasonic wave propagation) can be propagated. Shear waves are relatively weak when compared to longitudinal wave. In fact, an ultrasonic longitudinal wave contains both shear and compressional components and shear waves are usually generated in materials using some of the energy from longitudinal waves. The velocity of both modes is governed by the materials modulus and density.

7.5.2 Effect of shear and compression wave propagation

When a material is subjected to a shear strain, no volume change occurs (that's why shear waves are known as isovoluminous waves), hence no temperature change would be expected. This has been confirmed experimentally in metals[13]. When a shear wave is applied to a viscoelastic medium there should be no simultaneous temperature variation – the temperature rise in the medium resulting from viscous flow appears as a random increase in the translational energy of the molecules of the medium and not as a temperature variation in phase with the applied strain. This is in marked contrast to the situation with an ultrasonic longitudinal wave.

In case of longitudinal wave temperature gradients are set up in the medium between regions of compression and of rarefaction leading to a flow of heat, accompanied by a production of entropy and a dissipation of energy (thermoelastic effect) which results in an attenuation of the wave amplitude[13].

7.5.3 Advantageous feature of compression wave ultrasound

It can be mentioned that the propagation of shear waves is restricted by the very high damping properties of polymers which often leads to a complete attenuation of the wave through the material. On the other hand, the propagation of longitudinal elastic waves is easily observed in polymers as well as in reactive mixtures of monomers [6].

As compression waves are supported in both liquids and solids, ultrasonic compression wave data could be recorded throughout the cure. This continuous measure of compression wave attenuation and phase velocity has potential to monitor the adhesive cure [7].Though shear wave ultrasound is simpler in technology and concept, it is not easy to apply the engineering of on-line shear wave measurements. In order to propagate bulk shear waves through a sample shear wave transducers are usually used which require the use of high viscosity couplant. On the other hand, compression wave

ultrasound systems in adhered assemblies are relatively convenient, adequately cheap and portable for on-line process applications.

7.5.4 Advantageous feature of shear wave ultrasound

As temperature sensitive equilibria in a medium is not affected by a shear wave, it can be used to study molecular diffusional motion free from the complication of other relaxation processes in the medium[14]. The medium may respond to the shear wave by viscous flow (i.e. a liquid), by elastic deformation (solid) or by some combination of the two (viscoelastic body). The change from viscous to elastic behaviour (viscoelastic relaxation) occurs when the period of the shear wave becomes comparable to the time for an elementary diffusive motion of the molecules of the medium. The shear modulus (which can be measured when shear waves propagated through a medium) is the most sensitive to the physical changes from liquid to solid state during cure reaction. So, measuring the elastic properties, particularly the shear modulus, can be regarded as the most reliable method of testing the homogeneity of an epoxy resin[21].

Another advantageous feature of shear waves in comparison to longitudinal waves, is their higher resolution associated with their lower propagation velocity. As for example, the shear waves travel at approximately half the velocity of a longitudinal wave. Thus measurements taken in the temporal domain using a bipolar 5 MHz frequency shear wave pulse have the same resolution as a bipolar 10 MHz longitudinal wave[21].

7.5.5 Simple Molecular picture of viscoelastic relaxation

Due to anelasticity, the response of a polymeric material to a dynamic mechanical deformation (stress) imposed to it by ultrasonic wave propagation is not instantaneous but develops by relaxation processes that are characterized by a relaxation time, τ. If the period of the ultrasonic wave is much longer than the time constant i.e. $f \ll \tau$ (or material's relaxation time τ) for the alteration of the position of equilibrium, material's elastic response is able to remain in phase with the stress throughout the applied cycle

and the medium is disturbed by the wave. All of the driving energy is dissipated and no energy is stored elastically. By contrast, if the period of the wave is much shorter than the relaxation time i.e. $f \gg \tau$, the anelastic component of strain is unable to respond to the rapidly changing applied stress and the wave will not 'see' the equilibrium which consequently remains undisturbed. In this case no energy is dissipated. Instead the energy is stored elastically and the material appears to stiffen. At some intermediate frequency, where the period of the wave is comparable to the relaxation time, changes in the velocity of propagation and absorption co-efficient of the elastic wave occur and the material shows both viscous and elastic properties. The change from viscous to elastic behaviour with increasing frequency is known as viscoelastic relaxation.

7.5.6 Ultrasonic velocity and attenuation

As the typical ultrasonic frequencies of analysis range from the hundreds of KHz to the tens of MHz, the deformaion rate imposed to a material by ultrasonic wave propagation is very high. As discussed, when an alternating time-dependent deformation at the ultrasonic frequencies is applied to a material, the velocity of propagation elastic waves (called ultrasonic or acoustic velocity) and the attenuation of the amplitude of the waves (called ultrasonic or acoustic attenuation) can be measured.

Meaningful determinations of the propagation constants of ultrasonic longitudinal waves in liquids can only be made at frequencies above 1 MHz [14]. The molecular theories of the viscoelasticity of polymers show that the period of such an ultrasonic wave is much shorter than many of the relaxation times for the motion of polymer chains.Therefore, with longitudinal waves of frequency greater than 1 MHz it is only possible to study rapid, localized motions of polymer chains.

Basically, the acoustic propagation characteristics of a material are determined by both the elastic properties and the density of the material. The attenuation of acoustic wave energy caused by non-ideal elastic behaviour of the propagation medium is known as acoustic absorption. Generally, the acoustic absorption characteristics of a material are a

strong function of frequency and this can be used as an indirect means of studying the chemical or physical structure of a material[15]. At the molecular level the wave energy can be converted into vibrational modes within the material leading to molecular absorption[14].

In polymeric materials, the predominant source of acoustic wave attenuation is due to viscoelastic absorption which is caused by frictional losses as chains of molecules move relative to each other. Generally, the effect of absorption is an increase in acoustic attenuation with increasing frequency and this is accompanied by small changes in the acoustic propagation velocity which is a weak function of frequency. It is expected that ultrasonic wave propagation would depend on the polymer matrix. Many engineering polymers include filler particles for toughen and/or property modification and scattering at fillers brings about a significant increase in ultrasound absorption [2] and also restricts the molecular mobility of the macromolecules. Thus, the presence of particulate fillers or gas filled voids in the adhesive can also have measurable effects on the ultrasonic phase velocity and attenuation[50].

7.5.7 Significance of the ultrasonic velocity and attenuation measurement

As the propagation of the acoustic wave is known to be sensitive to the macroscopic polymer structure and the mechanical properties of the material, the evolution of attenuation and velocity during reaction is related to the strong physical changes occuring during the cure process. In this connection it can be mentioned that ultrasonic absorption has the potential to be sensitive to the molecular and configurational state of the curing material and ultrasonic propagation velocity is sensitive to the elastic moduli and shows the development of elastic behaviour. So, ultrasonic attenuation measurements can be interpreted in terms of the structural development of the polymeric material during cure (progress of cure) and the velocity measurements give a useful indication of the development of mechanical properties of the curing material. Any given values of absorption and velocity could result from a number of molecular states which depends on the detailed nature of the cure reaction.

7.5.8 Basic requirement of sample dimension for ultrasonic measurement

The measurements of ultrasonic velocity and attenuation can be performed only if the samples are sufficiently larger than the wavelength, typically higher than 0.17 mm for a polymer at a frequency of 10 MHz, and sufficiently small to allow the detection of the wave traveling from the ultrasonic transducer to the receiver [18,19,20].

7.5.9 Practical validity of ultrasonic measurements of polymer

The actual strains involved in ultrasonic measurements are very small ($\Delta\varepsilon/\varepsilon \approx 10^{-5}$), so the problem of strain dependence or creep, which is important for polymers, is virtually eliminated. Also, owing to various structural relaxation mechanisms in the material, the elastic properties of polymers may depend on the rate at which the strain is imposed [18,20].In polyethylene, torsion pendulum measurements [16] at 1 Hz show the existence of a relaxation process centered near 20^0 C. However, experience shows [17] that because of the high frequencies, ultrasonic measurements at 20^0 C, are not influenced by this relaxation. *The ultrasonic moduli can thus be discussed in terms of elasticity alone.* The main applications of the ultrasonic technique will be in studying local motions of polymer chains to provide information complementary to that obtained from dielectric relaxation and nuclear magnetic relaxation[14].

However, the particular problem for investigation of polymers is the relatively high sound attenuation in this class of substances. Due to limitations of available bandwidth and signal to noise ratio (SNR), ultrasonic techniques can only be used over a restricted frequency range. Therefore, to characterize completely material properties, the acoustic behaviour over a wide range of frequencies must be examined.

7.6 Ultrasonic wave propagation in curing thermoset

In this section, the discussion is presented in three distinct steps. At first, a brief overview of ultrasonic wave propagation in terms of elasticity parameters is presented.

Secondly, a detail description and interpretation of typical ultrasonic measurements related to evolution of structure during the cure is given in connection with supportive research analysis and critics. Thirdly, the general aspects and a discussion is presented regarding distribution of relaxation times.

7.6.1 The stages of cure

As a thermoset cures it passes through many different states of polymerization which lead to changing viscoelastic properties in the material. The stages of cure may be classified mainly as liquid phase, gelation, postgelation and vitrification which already have discussed details in chapter 3.The time scale on which these stages occur is dependent on the used hardener type and the cure temperature. In all of the states of polymerization during cure and post cure the material is viscoelastic in nature.

7.6.2 Ultrasonic wave propagation

As discussed before, the propagation of bulk ultrasonic waves in polymeric materials is associated with the complex wave number

$$k = \frac{\omega}{c(\omega)} + j\alpha(\omega) \tag{7.43}$$

Where $c(\omega)$ is phase velocity and $\alpha(\omega)$ is the absorption co-efficient. They are functions of frequency and depend on complex elastic modulus $M(\omega)$ [$M(\omega) = M_r(\omega) + j\, M_i(\omega)$] .equation (7.13)] governing wave propagation. The real part [$M_r(\omega)$] of the complex modulus is often called the *storage modulus* because it can be identified with the in-phase elastic component of the deformation. Elastic materials 'store' energy during deformation and release it on unloading. The imaginary part [$M_i(\omega)$] is sometimes called the *loss modulus* since it gives a measure of the energy dissipated during each cycle. It provides the evidence of molecular relaxation mechanisms that relate to losses in high frequency wave motions.

In a curing material, as the behaviour of $M(\omega)$ with respect to frequency results from various relaxation mechanisms on a molecular scale, it is convenient to express the modulus in terms of a frequency function $H(\omega)$ and the values of the modulus when fully relaxed M_o and in the unrelaxed state M_∞. In comparison with the centre frequencies of mechanical relaxations present in the material, M_o and M_∞ can be regarded as asymptotically limiting values of modulus at very low and very high frequencies respectively.

$$\frac{M_\infty - M(\omega)}{M_\infty - M_o} = H(\omega)$$

(7.44)

It is also useful to introduce a parameter which represents the strength of the relaxation process (or processes) which takes place in the curing material.

$$a^2 = \frac{M_\infty}{M_o}$$

(7.45)

Now, the elastic modulus can be expressed in frequency domain by the following equations [4],

$$M(\omega) = M_o\left[a^2 - \left(a^2 - 1\right)H(\omega)\right]$$

(7.46)

$$M_r(\omega) = -M_o\left[a^2 - \left(a^2 - 1\right)H_r(\omega)\right]$$

(7.47)

$$M_i(\omega) = -M_o\left[\left(a^2 - 1\right)H_i(\omega)\right]$$

(7.48)

Where $H_r(\omega)$ and $H_i(\omega)$ are the real and imaginary parts of $H(\omega)$. At any instant in the cure process M_o, M_∞ and $H(\omega)$ can give an indication of the viscoelastic state of the material.

In the case of shear waves propagation $M(\omega)$ is interpreted as the shear modulus G, and for compression waves it takes the combined form $\left(K + \frac{4}{3}G\right)$ where K is the bulk

modulus. Since compression waves are supported in both liquids and solids, compression mode is observable throughout all the stages of the cure. As shear strains and thus in phase stresses can only be supported by solid materials, during the initial stages of cure when the resin is a viscous liquid shear waves are not supported by the medium. After the 'gel' point when the material begins to solidify and becomes crosslinked enough to support shear stress, shear mode is observable.

Taking into account the assumption that $\alpha(\omega) << \dfrac{\omega}{c(\omega)}$, which is a realistic case for most resin materials in states where ultrasonic measurements are possible (i.e. as in most practical applications), and using the work of McSkimin [9] and Challis et al [22] from equation (7.14) and (7.15) it can be shown that [5]

$$c^2(\omega) = \frac{M_r(\omega)}{\rho} \tag{7.49}$$

and $\quad \alpha(\omega) = \dfrac{\omega[M_i(\omega)]}{2\rho[c^3(\omega)]}$ (7.50)

Knowing the material density ρ and the measured quantities $\alpha(\omega)$ and $c(\omega)$ for either wave mode one can calculate $M_r(\omega)$ and $M_i(\omega)$ at times during the cure.

7.6.3 Changes during the cure

During the cure modulus M_o and M_∞ increase as the material solidifies. This brings about corresponding increases in both compression and shear wave phase velocities (C_o and C_∞). $H(\omega)$ also changes as the molecular arrangements within the material develop.

As cure proceeds $\alpha(\omega)$ rises to a peak and falls again. As the frequency of the test is increased, the peak occurring earlier in the cure cycle. This can be interpreted as the passage of the centre frequency of a broad α-relaxation process through the measurement

range during the cure cycle [5,7]. This interpretation of ultrasonic absorption data given by Challis et al [5,7] will be discussed in the next section.

From the phenomenological point of view, the relaxation is associated with at least, a relaxation time τ_M .Previously we discussed simple molecular picture of viscoelastic relaxation. The analysis has much in common with the classical Debye theory of dielectrics and there is often a close, if not one to one, relationship between mechanical and dielectric relaxation phenomena.

Both mechanical and dielectric relaxation effects in polymers have been discussed at length in the book by McCrum et al [23] where an alternative description of mechanical loss phenomena is given. It considers the equivalent relaxation in the complex compliance modulus $\left(\dfrac{1}{M}\right)$ which is associated with the compliance relaxation time (τ_c).

Generally, $\tau_c > \tau_M$. It is convenient to consider the loss tangent as a measure of mechanical loss as this is associated with mechanical relaxation time $\bar{\tau}_M = (\tau_M \tau_C)^{1/2}$ which is independent of whether complex compliance or complex modulus are used as the experimental variable [23]. The mechanical loss tangent is given by

$$\tan \delta_M = \frac{M_i}{M_r} = \frac{1}{\pi}\alpha(\omega)\lambda = \frac{2\alpha(\omega)c(\omega)}{\omega} \qquad (7.51)$$

For a simple Debye process we get [23]

$$\tan \delta_M = \frac{M_\infty - M_o}{(M_\infty M_o)^{1/2}} \frac{\omega\bar{\tau}_M}{1+\omega^2\bar{\tau}_M{}^2} \qquad (7.52)$$

From this equation it is seen that during the cure cycle, considering stationary $\bar{\tau}_M$, as a function of frequency $\tan \delta_M$ is expected to peak at $\omega = \dfrac{1}{\bar{\tau}_M}$. At a fixed frequency and considering $\tan \delta_M$ as a function of $\bar{\tau}_M$, a similar peak occurs. On the basis of dielectric measurements [5], it is known that as cure proceeds the increasing molecular size brings

about an increase in the α-relaxation times from a few ns in the liquid state to orders of seconds in the final solid state. Therefore, if $\bar{\tau}_M$ increases during the cure cycle, $\tan \delta_M$ is expected to exhibit a peak as a function of time into the cure process. Thus at any time in the cure process we can estimate $\bar{\tau}_M$ if we know the frequency at which $\tan \delta_M$ reaches its peak value [5].

Around the middle of the cure the material is highly viscoelastic and shows as an increase in the loss tangent at that time as the relaxation strength parameter a increases. In this state, the number of different types of partially polymerized molecules increases and the polydispersity in molecular type could imply many degrees of mechanical freedom on the molecular scale which would lead to a multiple relaxation time system which will be discussed later.

7.6. 4 Analysis of typical ultrasonic responses during cure

Starting with an overview of general curing kinetics, under respective headings, this section gives a detail description, interpretation and critics of typical ultrasonic compression and shear wave velocity and attenuation characteristics related to the structural development of a thermoset during cure.

7.6.4.1 Ultrasonic compression wave velocity during cure

It has been shown [5,6,7] that ultrasonic compression wave velocity increases gradually in an 'S' shaped curve as a function of cure time with no significant inflections (figure 7.3(a)). As stated above, it indicates a steady growth of the real part of the compression modulus $\left(K + \dfrac{4}{3}G \right)$ of the curing adhesive as it solidifies. Lindrose[42] and Alig et al [24] explain the results observed as being partly due to an increase in mechanical modulus (which is directly linked to the number density of cross-links), and partly due to an increase during the initial phase of cure of the macroscopic viscosity and during the

later stages an increase in the 'internal' viscosity or the molecular and network relaxation times.
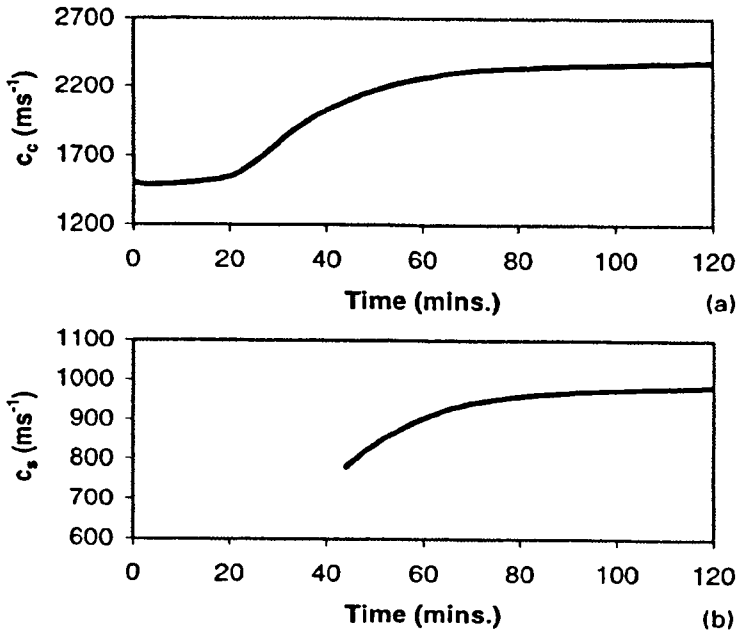

Figure 7.3 Ultrasonic (a) compression wave velocity and (b) shear wave velocity as a function of cure time (after Challis et al [7]).

The compression wave phase velocity is moderately dependent on the frequency. Due to the viscoelastic nature of the material, a small dispersion between low and high frequency values is observed in experiments. It is important to mention that as the compression wave propagation velocity provides a continuous measure of the evolving modulus $\left(K + \dfrac{4}{3} G \right)$, it has the potential to monitor the adhesive cure [7].

7.6.4.2 Ultrasonic shear wave velocity during cure

Shear waves are not observable early in cure. As solid material begins to form shear waves are observable. From that point, the shear wave velocity starts to increase as cure proceeds (figure 7.3(b)).The subsequent increase in the shear wave velocity follows the

development of the real part of the shear modulus G as solidification progresses. It can be mentioned that low values of shear modulus are associated with rubbery materials.

7.6.4.3 Necessity of both compression and shear wave identification

Both compression and shear wave characterization can give a complete picture of the elastic moduli of an adhesive material. In this connection, the work of Freemantle and Challis [1] can be mentioned. In that work, they had found very small difference in compression wave velocity (only 3%) between a high modulus (2013) and low modulus (2017) adhesives despite the fact that they have different shear moduli and that the high modulus (2013) material has a much higher (33%) shear wave velocity. This result reveals the necessity of measuring both the wave mode for complete analysis. Previously the fundamental aspects and useful practical features of ultrasonic compression and shear wave propagation mode had mentioned.

7.6.4.4 Ultrasonic compression wave attenuation characteristics

The wave absorption is caused by ultrasound energy loss in the adhesive. At the early stage of cure, the reaction produces chains composed of resin and hardener which grow in the still liquid phase of adhesive. This liquid stage contains small relatively inflexible molecules of unreacted resin and hardener and larger more flexible chains of partially reacted material. Ultrasound attenuation occurs when the travelling pressure disturbance excites the molecules of the medium into motion that does not remain in phase with the wave [15].

7.6.4.5 Attenuation behaviour as a function of frequency

Most experimental evidence show [1,5,7] that ultrasonic compression wave attenuation co-efficient shows particularly *'interesting'* behaviour during the cure of thermoset. *'Interesting'* in the sense that in lieu of increasing as the square of the ultrasonic

frequency observed in classical absorption of ultrasonic longitudinal wave, the attenuation increases *approximately linearly* with frequency right through the cure cycle. The rate of increase is observed to be highly dependent on the cure state and the function rises to a maximum slope around the gel point of the material. This linear behaviour of attenuation versus frequency suggests that the attenuation effect cannot be explained by classical viscothermal absorption or relaxation theory. Such type of behaviour was found previously for some highly viscous liquids, for solid polymers and for biological tissue.

7.6.4.6 Attenuation behaviour as a function of cure time

Typical data of ultrasonic compression wave attenuation co-efficient at fixed frequencies as a function of cure time shows that early in cure the compression wave absorption increases rapidly, rises to a peak and then falls thereafter to a nearly constant value(figure 7.4(a)).
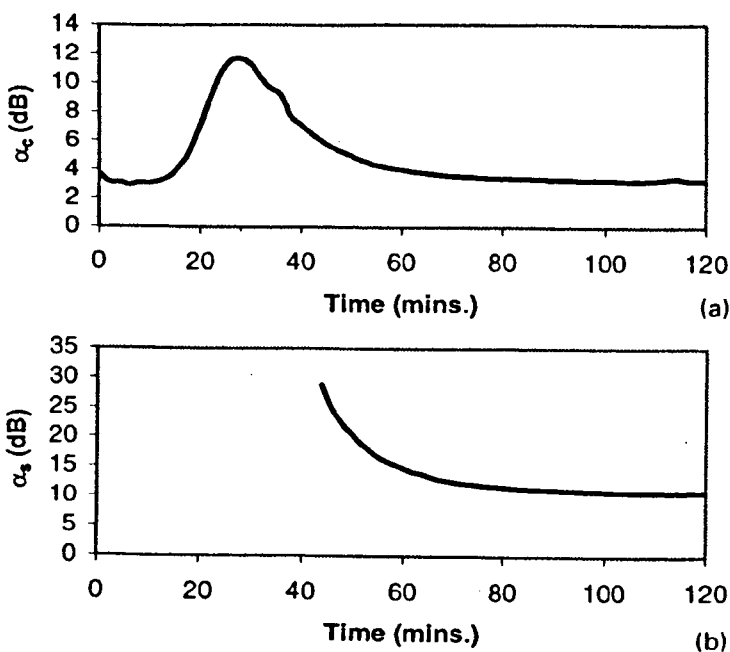
Figure 7.4 Ultrasonic (a) compression wave attenuation and (b) shear wave attenuation as a function of cure time (after Challis et al [7]).

7.7 Significance of the absorption peak in defining gelation

Comparisons with equivalent data from other cure monitoring techniques suggest that the compression wave absorption peak occurs at a time equivalent to gelation [5]. Emery et al [27] define this point of gelation or gel-point as " *the point at which the liquid reaction mixture ceased to flow in an inverted tube* " i.e. the point at which sufficient structure has developed for the material to support its own weight.

Experimental results show that a point of inflection exists on the compression wave phase velocity curve at the gel-time. Alig et al [28] explain that the magnitude of the effect of gelation on propagation depends upon the degree of cross-linking in the system, the more cross-linked the greater the effect.

However, the determination of gel-time from the compression wave absorption curve is often contradictory. In his first paper published in 1992 Alig et al [24] define the gel-point as being the *end of the absorption peak* whereas later in 1992, in his second paper, Alig et al [28] define the gel-point as being at the *beginning of the absorption peak* . In the work of Maffezzoli et al [6] it is shown that the gel-time occurs after the onset of rapid increase in longitudinal velocity and before the peak of the loss modulus. Maffezzoli states that the position of the gel-time along the longitudinal velocity vs cure time and the longitudinal storage modulus vs cure time characteristics (curves) highlight the fact that the steep increase of velocity can be associated with the development of elastic properties in the curing material. In a nut shell, it can be mentioned that the characteristic times corresponding to the compression wave attenuation peak and rapid increae in compression wave velocity, marking incipient and fully achieved gelation can indicate the interval in which gelation occurs.

7.7.1 Detection of shear wave

After the initial compression wave absorption peak i.e. after gelation when the absorption decreases, shear waves become evident (figure 7.4(b))which reflects the fact that the

material is developing a shear stiffness and has changed from a rubber gel-like phase to a more solid one. It is, therefore, interesting to note that the compression wave attenuation characteristics varies during cure in a way that enables one to determine the approximate time when shear waves are supportable, and possibly the time at which a material reaches a defined lap- shear strength [1].

7.8 Significance of the absorption peak in defining vitrification

Previously we discussed about the convenient consideration of the loss tangent where it is considered as a measure of mechanical loss. Maffezzoli et al [6] suggest that the ultrasonic attenuation may be considered as equivalent to the damping factor associated with dynamic mechanical studies [19] in which a peak is observed around the transition to a glassy state (vitrification).

In their work of low frequency (1Hz) shear dynamic-mechanical studies of an epoxy system, Babayevsky and Gillham [29] observed two peaks in the damping factor. The first (weaker) one was attributed to gelation and the second (stronger) one to the vitrification. In the ultrasonic studies of thermoset cure by Lairez et al [30], Matsukawa et al[31] and Alig et al [28]; the observed peak in ultrasonic absorption is attributed to vitrification. However, it is important to mention that the higher frequencies (MHz range) used in ultrasonic measurements indicate that the observed absorption peaks due to vitrification would be expected at lower degree of cross-linking corresponding to looser network than would be the case in low frequency dynamic mechanical measurements.

Furthermore, there remains the scope of debate. In low frequency rheological methods, mostly the shear wave propagation is involved. In contrast, ultrasonic measurements involve both shearing action (shear waves) [21] and combined shearing and compression action (longitudinal waves) [1,8]. From this point of view question can be raised [32,33] about the origin of the losses associated with longitudinal waves. In this connection, some past experimental results associated with both compression and shear wave measurements can be mentioned which can highlight this subject to some extent. The

results associated with *pure* compression waves showed that there were energy or viscous losses [34] and that these structural relaxation [35] losses could in fact be comparable [36,37] or even larger [38] than losses associated with *pure* shear waves.

7.9 Interpretation of the attenuation peak in terms of relaxation

Previously, in the overview of ultrasonic wave propagation section we had mentioned the most likely hypothesis of ultrasonic compression wave absorption peak given by Challis et al [5,7]. To shed some light on this interpretation, here, the subject is presented in three different steps. A logical approach in the first step co-relates the attenuation peak as the centre frequency of a relaxation process passing through the measurement range during the cure cycle. In the second step, the linear dependence of attenuation on frequency is interpreted as a broad distribution of relaxation times. Finally, experimental evidences are presented which suggest that the absorption peak is associated with α-relaxation.

7.9.1 First step

The simple molecular picture of viscoelastic relaxation was described before. At the initial stage of the cure, when the polymer is in liquid state, the relaxation frequencies would be expected to be much higher than the test frequency. So, the small molecular segments can follow the excitation. As the lengths of the molecular segments increase, relaxation times would be expected also to increase, with corresponding characteristic frequencies reducing. So, for relatively short unreacted resin and hardener molecules the frequency of maximum absorption would be expected to be high and beyond the range of the measurement. As molecular entanglement and cross-linking occurs, the relaxation frequencies would fall and would be expected to enter in the measurement range (around the centre frequency of transducer). As a consequence, both modulus and damping increases. As cure proceeds further, the relaxation frequencies would fall to below the centre frequency of transducer, polymeric material would continue to stiffen and eventually damping would decrease. Therefore, the peak in compression wave

attenuation can be interpreted [7] as the centre frequency of a relaxation process passing through the measurement range from high frequency to low frequency, as cure proceeds.

7.9.2 Second step

The ultrasonic attenuation behaviour in polymer is described in the Anelastic solid (Zener) model where we assumed that a single high frequency relaxation process associated with a single discrete relaxation time governed the propagation in the polymer. The attenuation co-efficient is sigmoidal in shape with a low frequency asymptote and increases to a high frequency asymptotic value above the centre frequency of relaxation. This characteristic feature exhibits a peak in the attenuation $\times$ wavelength ($\alpha\lambda$) function at the relaxation frequency [14].

The near-linear dependence of attenuation on frequency observed in thermosets suggests that this behaviour corresponds to flat functions or frequency independent functions for ($\alpha\lambda$) rather than peaks about a relaxation centre frequency. Previously we mentioned that this anomalous ultrasonic absorption cannot be explained by classical viscothermal absorption or relaxation theory. This relationship between attenuation and frequency implies a broad distribution of relaxation times governing ultrasonic propagation in the MHz frequency range.

7.9.3 Third step

Alig et al [24] suggested that during the cure, at each instant, the resin would be expected to relax with at least α and β- relaxations at temperatures at or below its T_g , but with only one relaxation at temperatures above its T_g , when the two relaxations become at least partially merged. Thus as cure proceeds and the structure of the resin changes from liquid ($T_{cure} > T_g$; associated with one relaxation) to a solid ($T_{cure} \leq T_g$; associated with two relaxations). This would mean that initially during cure there would be contributions from the β- relaxation process only, with the contributions from the two process α and β

varying as cure proceeds. At frequencies of the order of MHz the α and β- relaxation processes will become merged. Alig showed that the primary relaxation time τ increases with cure time. However, in this [24] work, a shoulder is observed in the attenuation-cure time characteristics. This shoulder is explained as probably being due to γ-relaxation process. Its contribution showing only in part of the curing process as it probably becomes merged, at longer cure times, with the α-contribution in the same way as the β-contribution did. This bimodal distribution of relaxation times [24] associated with α and β- relaxation processes as stated above, also have been identified by Matsukawa et al [39].

Further research carried out by Alig et al [28] involved both dynamic light scattering and ultrasonic techniques to study the curing process of DGEBA with butane-1,4-diol. Previously he showed [24] that the primary relaxation time τ increases with cure time. In this work, the hypersonic (GHz) Brillouin scattering experiments enabled the measurements of τ associated with faster relaxations at earlier stages of cure. At higher curing times, a shoulder and second small maximum in the absorption peak was observed which was attributed to secondary relaxations. They are more clearly defined in this system because of the co-components due to the presence of the diol. Alig et al [28] conclude that the extent of cure follows a single reduced Vogel- Fulcher- Hesse- Tamann equation which describes the segmental mobility of the material during the cure.

The recent research of the dielectric behaviour of polymerizing systems by Williams et al [40] further highlights on this subject. According to him, at the beginning of the cure when the relaxation frequencies are much higher than the test frequency, the α- and β-relaxation processes would be expected to coincide at frequencies in the GHz region.

As cure progresses, the centre frequency of the α- relaxation process would fall to a low value of the order of mHz (milli hertz) towards the end of cure. William et al [40] suggest that the centre frequency of the β-relaxation would separate from that of the α-relaxation but would nevertheless fall down to an intermediate value ~ 1MHz during cure.

In view of the discussed experimental outcome [24,28,39,40] the compression wave absorption peak can be interpreted as the passage of the centre frequency of a broad α-relaxation process (which is associated with large scale conformational changes of the polymer backbone) through the measurement range [5,7] and the residual attenuation observed at higher curing times, can be attributed to a broad β-relaxation process [7] (which is associated with the motions of short molecular segments).

7.10 Ultrasonic shear waves absorption during cure

During the cure when the material begins to cross-link and as a consequence starts to display some shear rigidity, at that point shear waves can be supported by the material and from that time follow the same trends observed in the compression wave absorption which is described before. But the absorption is generally higher for shear waves (that's why shear waves are known as viscous waves)than for compression waves [1,7] because of the viscoelastic nature of the material.

Experimental results show [1,7] that when shear waves are first observed the associated absorption co-efficient is high. From the phenomenological point of view Challis et al [7] give the explanation of this behaviour. According to him, this is possibly, due to the development of an imaginary component of the viscosity or the early development of the real part of the rigidity modulus G which at that time is associated with a relatively large imaginary part due to the strongly viscoelastic nature of the part-cured material. Work done on commercial adhesives shows [1] that the time at which shear waves are first observed in resin and hardener mixtures, generally corresponds to the manufacturer's specification to a minimum time to a usable, but low, lap shear strength, typically ~ 10 MPa [7].

As cure progresses and the material becomes more solid in nature, the shear wave absorption reduces and the shear wave propagation velocity increases reflecting the fact that the real part of shear modulus G develops and the imaginary part of G reduces. Towards the end of cure shear wave absorption falls rapidly as vitrification takes place.It

can be mentioned that low values of shear wave absorption are associated with brittle materials [41]. The detailed relationship between ultrasonic propagation phenomena and evolving molecular structure will require further investigation.

7.11 The effect of temperature and frequency on ultrasound data

For successful application of ultrasonic waves to in-process cure monitoring two basic questions have to be answered. **First**, how do the frequency of measurements and temperature of cure affect ultrasonic data ? **Second,** how are ultrasonic data related to static polymer properties, such as resin viscosity in a liquid stage and its mechanical properties in a solid stage? The previous section can help one to get the basic answer of the second question. Now, the effect of temperature and frequency on ultrasonic measurement is discussed.

Previous work [1,6,47] has shown that ultrasonic technique is also sensitive to changes in the cure temperature. An increase in the cure temperature leads to an increase in reaction rate and as a consequence, adhesive cures faster with increased temperature. This is seen in the experimental data, by a narrowing of the compression wave absorption peak which occurs earlier in time with increased cure temperature. Also, the times to reach gel-point and solidification (the onset of velocity increase) is observed to reduce as the cure temperature increases [1,6,47].Similar behaviour is observed in the studies by Matsukawa et al [31] who considered the change in compression wave absorption with the reaction rate which was controlled by the resin-hardener stoichiometric ratio.

The earlier arrival of the attenuation peak at higher cure temperature reflects a more rapid development of intermediate molecular chains. Also, the more rapid decay of the relaxation peak [1] with respect to cure time for higher temperature cure, indicates a more rapid cross-linking which, in turn, implies the inhibition of the motions of long intermediate molecular chains. On the contrary, the relatively late arrival of the peak and longer decay time associated with lower cure temperatures can be attributed to slower chain formation and slower cross-linking [1]. It is important to note that these effects

observed in ultrasonic studies by many workers [1,6,31,47], are quite marked for relatively small differences in cure temperature. Therefore, ultrasound could be used to detect changes in cure behaviour due, for example, to temperature fluctuations in an autoclave.

In the ultrasonic study done by Alig et al [24], the changes observed in ultrasonic longitudinal velocity and attenuation during cure were found to be similar to changes previously observed when measurements were made as a function of temperature at a fixed frequency or as a function of frequency at a fixed temperature on a cured resin. Alig et al [24] suggest this implies that the changes observed on curing of the resin are mechanically analogous to an increase in frequency or a decrease in temperature and that the two effects are phenomenologically equivalent.

7.12 Distribution of relaxation times--- a general overview and critics

7.12.1 Relaxation – the basic concept

In mechanistic terms one could say that, a system which at first, when having an enhanced free energy, is 'strained', 'relaxes' while going to the equilibrium. Correspondingly, all the retarded transitions into a new equilibrium are generally addressed as 'relaxation processes'. In fact, the name includes even more, namely the underlying microscopic motions as well. So, the notion 'relaxation' has a broad meaning and not all restricted to only one special case of stress relaxation.

7.12.2 Molecular polydispersity and it's effect

The time dependence of a macroscopic relaxation process always reflects the underlying microscopic dynamics. The cure reaction leads to complex changes in molecular state, and macroscopically, a detectable change is observed through the available ultrasonic experimental window which is related to a single characteristic time only [2,4,7] . It goes

back to Debye, who proposed it in a famous work on the dielectric properties of polar liquids, based on a statistical mechanical theory.

Previously we had stated the different stages of the cure. Around the 'gel' state, we mentioned that there will be a continuously changing mixture of partially polymerized molecular segments whose size and local entanglements may vary considerably at any given time within the mixture. As solidification progresses, there will be many molecular sub species which may be physically entwined with each other in complex and varied ways. This polydispersity in molecular type could imply many degrees of mechanical freedom on the molecular scale. Therefore, one would expect the mechanical responses of the polymerizing mixture to vary locally, from molecule to molecule or from molecular cluster to molecular cluster [4].

Here, it can be mentioned that for a given sample, the ratio $\dfrac{[M_w]}{[M_n]}$ is referred to as the heterogeneity index (HI) and is a measure of polydispersity. Here, $[M_w]$ represents weight average molecular weight and $[M_n]$ represents number average molecular weight and the terms are defined as $[M_n] = \sum n_i M_i$ and $[M_w] = \sum w_i M_i$ where n_i is the mole fraction, w_i is the weight fraction and M_i is the molecular weight of the ith fraction or component.

It is thus expected that in response to ultrasonic waves such molecular polydispersity would lead to a broad distribution of relaxation processes associated with multiple relaxation time system throughout the material. As a consequence, the result would be a broadening of the phase velocity and attenuation functions in the frequency domain.

7.12.3 Phenomenological functions for distribution of relaxation times

In equation (7.44) we expressed the modulus in terms of the frequency domain function $H(\omega)$. For the simple Debye case of a single relaxation process or a group of identical relaxation processes $H(\omega)$ can be expressed as

$$H(\omega) = \frac{1}{1 + j\omega\tau} \qquad (7.53)$$

In this model, it is assumed that the molecular arrangements are monodisperse and that mechanical interactions are characterized at all points in the material by single time constants. In order to account for polydispersity in molecular arrangement and the subsequent broadening of measured responses associated with distribution of relaxation processes, as functions of frequency or time, many alternative phenomenological models of frequency dependence have been suggested in dielectric studies [23,43,44,45] of polymers over many years. The most commonly adopted forms for $H(\omega)$ based on these phenomenological functions are—

Cole- Cole [43] $\qquad H(\omega) = \dfrac{1}{1 + (j\omega\tau)^{\beta}} \qquad\qquad (7.54)$

Cole- Davidson [44] $\qquad H(\omega) = \dfrac{1}{(1 + j\omega\tau)^{\beta}} \qquad\qquad (7.55)$

Havriliak- Negumi [45] $\qquad H(\omega) = \dfrac{1}{\left[1 + (j\omega\tau)^{\beta}\right]^{\gamma}} \qquad (7.56)$

The Cole-Cole [43] frequency dependence has been most commonly applied to polymerising systems. β is a parameter which represents the distribution of relaxation times about a notional centre value. The range of β is between 0 to 1.when $\beta=0$, $H(\omega)$ is independent of frequency and when $\beta=1$, $H(\omega)$ (for Cole-Cole and Cole- Davidson) represents the single time constant Debye case. The dispersion curves for mechanical or dielectric parameters show the same symmetry about $\omega\tau=1$ for $\beta\neq1$ as for $\beta=1$ [23]. Estimates of the developing relaxation time during a cure process made on the basis of the position of a peak in the measured data would still remain valid under the Cole-Cole model or related models [5].

Challis et al[2,3] showed that the anelastic solid model(Debye formulation) representing viscoelasticity gives a qualitative description of the wave propagation in a curing thermoset but that formal fits of the model to measured data are poor [4] and that the

Cole-Davidson [44] extension of the model gave better agreement with experiment although there were some inconsistencies [4].

In that work [4], it was shown that the Cole-Davidson parameter β has the effect of broadening the frequency range over which phase velocity and attenuation change for a given relaxation strength a. It provides a subtle means to give an index of the breadth of the distribution of relaxation times as cure proceeds and an indirect measure of molecular polydispersity in the curing material.

Challis showed that at the beginning of cure the relaxation strength a is relatively low and β =0.8, close to unity which indicates relaxation mechanisms close to the single relaxation time Debye case with limited degrees of freedom. Around gelation a increases to a maximum and β falls to a minimum value of 0.4, reflecting a broad distribution of relaxation times associated with highly disperse molecular mixture of longer molecular chains with minimal cross-linking. As cross-linking proceeds and the molecular structure 'tightens up' there are fewer degrees of mechanical freedom on the molecular scale, a reduces and β increases to its final value around 0.9, indicating that at the end of cure the material is again close to Debye in its behaviour. Therefore, the work [4] shows that it is possible to track the cure by following relaxation strength a and molecular polydispersity β -- these two parameters over the cure cycle.

7.13 Experimental verification and limitation of ultrasound method

Due to the limitations of signal to noise ratio, ultrasound measurement bandwidths are generally restricted to 20 MHz in studies of curing adhesive. Therefore, it is not generally possible to identify which, if any, of the phenomenological functions used to represent multiple relaxation time systems, best matches ultrasonic wave propagation data obtained in a real experiment. However, they do provide a useful basis to explore the characteristics of such data in broad terms. As viscoelastic relaxation in curing adhesives can occur over many decades of frequency, there remains the requirement to develop wider bandwidth techniques to provide detailed experimental verification and the basis for determining the distribution of relaxation times.

In this connection, the basic principle of the method of reduced variables (or time-temperature superposition principle) can be mentioned which was originally developed empirically for polymers in order to reduce the experimental results for viscoelastic relaxation at different temperatures to a common curve. In order to extend the available frequency range it is usual to vary the temperature of the polymer solution being studied. As for example, a decrease in temperature will slow down the molecular relaxation processes under investigation and enables a given instrument to observe processes which would have been too rapid at the higher temperature. This method may also be applied where a distribution of relaxation times exists provided that all the relaxation times in the distribution have the same dependence on temperature [14].

7.14 Validity of distribution of relaxation times—a critic

The interpretation of relaxation phenomena in dielectrics has been based, traditionally [23], on the concept of a system of independent relaxing species—where the relaxation of independent polar units originates from their individual reorientational motions, modified when necessary, to allow for a distribution of parameters affecting the relaxation rates. This postulation results in a distribution of relaxation times, each contributing a relaxation peak and thus accounting for the much broader peak than that attributable to a single relaxation time process.

A serious drawback to this approach is its lack of physical reality. Researches show [11] that there exists discrepancy between the prediction of the classical Debye expression of mechanical relaxation response function [equation (7.53)] and experimental data for polymers and a wide range of other materials. It is now recognized [46] that the exponential decay of polarization fluctuations regressing to an equilibrium, as predicted by Debye in 1912, is not obeyed by most liquids and solids. The individual dipoles and their environment do not remain independent during the regression of fluctuation. It is shown [11] that non-exponential relaxation characterizes the dynamics of polymers, particularly near T_g . There is an extensive body of theoretical work [46] that explains these non-exponential relaxations. Therefore, there is now considerable doubt about the

validity of the postulation of distribution of relaxation times as it implicitly assumes each relaxation process to be exponential.

Basically, compared to the dielectric response, mechanical response is more complex. In mechanical relaxation of a rubber a different situation occurs, which is related with transitions between the different conformations of a chain and not with individual movements of single groups. Rather than having one process only, in this case, a large number of different 'modes' exist, and these may vary over a wide range in the characteristic times which cannot be associated with a single time constant only, but is of a complex nature. There is also a simple situation equivalent to the dipole reorientations in mechanical behaviour. In glassy polymers, large scale conformational changes are inhibited but there remains the possibility of localized conformational transitions [48]. These can be observed, for example, for polymers with side groups.

7.14.1 Inabilities of the traditional models of dielectric spectroscopy

Previously we mentioned that the *anomalous* ultrasonic absorption (near linear dependence of attenuation on frequency) observed in thermosets cannot be explained by classical viscothermal absorption or relaxation theory. Using the traditional models of dielectric relaxation phenomena does not yields the linear behaviour of attenuation versus frequency. It must be emphasized that all such distribution functions are purely empirical—they form a convenient way of describing experimental results mathematically, but are in no way a theoretical treatment of the relaxation process. Future demands to establish a model which can fully give physically realistic results for both attenuation and velocity as functions of frequency.

7.15 Conclusion

In the conclusion, it can be mentioned that ultrasonics should prove to be a useful and powerful tool for polymer studies, although a great amount of work is still required before the full potential of the technique is established. However, not so clear are the

relationships between the observed changes in the ultrasonic propagation functions and the key points in the cure cycle such as *gelation* and *vitrification*. This sets the scene for the experimental aspects of the current work, the aims of which are to:

(i) Relate observations of attenuation and phase velocity, and other variables derived from them, to gelation and vitrification.

(ii) Achieve this for a range of cure temperatures.

(iii) Relate the ultrasonic observations to the extent of conversion (α) curves obtained from the DSC – with a view to using ultrasonic measurements as a mimic of the DSC.

7.16 References

1. Freemantle,R.J., and Challis,R.E., Meas. Sci. Technol. vol-9, 1998, 1291-1302.

2. Challis,R.E., Freemantle,R.J., and Holmes,A.K., Proc. Institute of Acoustics (UK), vol-17, 1995, 23-30.

3. Challis,R.E., and Cocker,R.P., Ultrasonics, vol-33, no-4, 1995, 311-319.

4. Challis,R.E., and Unwin,M.E., American Institute of Physics Conf. Proc., CP 657, Review of Quantitative Nondestructive Evaluation, vol-22, ed. by Thompson, D.O., and Chimenti, D.E., 2003,1657-1664.

5. Challis,R.E., Unwin,M.E., Chadwick,D.L., Freemantle,R.J., Partridge,I.K., Dare,D.J., Karkanas,P.I., Journal of Applied Polymer Science, vol-88, 2003, 1665-1675.

6. Maffezzoli,A., Quarta,E., Luprano,V.A.M., Montagna,G., Nicolais,L., Journal of Applied Polymer Science, vol-73,1999,1969-1977.

7. Challis,R.E., Freemantle,R.J., Cocker,R.P., Chadwick,D.L., Dare,D.L., Martin,C., Mahendrasingam,A., and Fuller,W., Plastics, Rubber and Composites, vol-29, no-3, 2000, 109-118.

8. Dixon,S., Jaques,D., and Palmer,S.B., Journal of Physics D : Applied Physics, vol-36, 2003, 753-759.

9. McSkimin,H.J., Ultrasonic methods for measuring the mechanical properties of liquids and solids, Physical Acoustics, vol-1, 1964, ed W P Mason (New York: Academic).

10. Beltzer,A.K., Acoustics of Solids, Springer-Verlag, 1988, 81-84.

11. Almond,D.P., Braddell,O.G., and Harris,B., Polymer, vol-33, no-10, 1992, 2234-2237.

12. Hartmann,B., ultrasonic measurements Methods of Experimental Physics: Polymers vol –16 C, 1980, Marton,ed.L., and Marton,C., (London : Academic), 59-90.

13. Truell,R., Elbaum,C., Chick,B.B., Ultrasonic Methods in Solid State Physics, 1969, Academic Press New York and London.

14. Matheson,A.J., Molecular Acoustics, Wiley, London, 1971.

15. Bhatia,A.B., Ultrasonic Absorption, Dover Publications, London,1986.

16. Illers,K.H., Brever,H., Journal of Colloid Science, vol-18, 1, 1963.

17. Adachie,K., Harrison,G., Lamb,J., North,A.M., Pethrick,R.A., Polymer, vol-22, 1981, 1032.

18. Krautkramer,J., Krautkramer,H., Ultrasonic Testing of Materials, Springer- Verlag : Berlin, Germany, 1977.

19. Ferry,J.D., Viscoelastic Properties of Polymers, Wiley,J., & Sons: New York, 1980.

20. Perepechko,I., Acoustic Methods of Investigating Polymers, Mir Publishers : Moscow, 1975.

21. Dixon,S., Edwards,C., and Palmer,S.B., Meas. Sci. Technol. vol-12, 2001, 615-621.

22. Challis,R.E., Alper,T., Holmes,A.K., Cocker,R.P., Meas. Sci. Technol. 1991, vol-2, 59-68.

23. McCrum,N.G., Read,B.E., Williams,G., Anelastic and Dielectric Effects in Polymeric Solids, Wiley: New York, 1967.

24. Alig,I., Lellinger,D., and Johari,G.P., J. Appl. Polym. Sci : Part B, vol –30, 1992, 791-799.

25. Cocker,R.P., Chadwick,D.L., Dare,D.J., Challis,R.E., International Journal of Adhesion and Adhesives, vol-18, 1998, 319-331.

26. Young,R.J., and Lovell,P.A., Introduction to Polymers, 2nd Edition, Chapman and Hall,1996.

27. Emery,J.R., Durand,D., Tabellout,M., and Pethrick,R.A., Polymer, vol-28, 1987,

1436.

28. Alig,I., Lellinger,D., Nancke,K., Rizos,A., and Fytas,G., J. Applied Polymer Science, vol-44,1992, 829.

29. Babayevsky,P.G., Gillham,J.K., J. Appl. Polym.Sci. vol-17, 1973, 2067.

30. Lairez,D., Durand,D., Emery,J.R., Chem,M., Symp,M., vol-45, 1991,31.

31. Matsukawa,M., Nagai,I.,, J. Acoust. Soc. Am. vol-99,1996, 2110.

32. Mason,W., Baker,W., McSkimin,H.J., and Heiss,J., Phys. Rev., Vol-73, 1948, 1074.

33. Nolle,A.W., and Sieck,P.W., J. Appl. Phys. vol-23, 1952, 888.

34. Cunningham,J.R., and Ivey,D.G., J. Appl. Phys. vol-27, 1956, 967.

35. Herzfeld,K.F., and Litovitz,T.A., Absorption and Dispersion of Ultrasonic waves, Academic Press, New York, 1959.

36. Kono,R., J. Phys. Soc. Jpn., vol-16, 1961, 1580.

37. Marvin,R.S., Aldrich,R., and Sack,H.S., J. Appl. Phys. vol-25, 1954, 1213.

38. Kono,R., J. Phys. Soc. Jpn. vol-15, 1960, 718.

39. Matsukawa,M., Okabe,H., and Matsushige,K., J. Appl. Polym. Sci. vol-50, 1993, 67-73.

40. Williams,G., Smith,I.K., Holmes,P.A., and Varma,S., J. Phys. A, Condens. Matter, vol-11, 1999, 57-74.

41. Chadwick,D.L., PhD Thesis, Keele University,1992.

42. Lindrose,A.M., Experimental Mechanics, 1978, 227.

43. Cole,K.S., and Cole,R.H., J. Chem. Phys. vol-9, 1941, 341-351.

44. Davidson,D.W., and Cole,R.H., J. Chem. Phys. vol-19, 1951, 1484-1490.

45. Havriliak,S., and Negami,S., Polymer, vol-8, 1967, 161-173.

46. Scherer,G.W., J. Non-Crys. Solids, vol-123, 1990, 75.

47. Lionetto, F., Rizzo, R., Luprano, V.A.M., Maffezzoli, A., Materials Science and

Engineering A, vol. 370, 2004, 284-287.

48. Strobl,G.R., The Physics of Polymers, 2nd Edition, Springer, 1997.

49. Irzhak,V.I., Kuzub,L.I., Irzhak,T.F., Relaxation properties of the Kargin-Slonimsky-Rouse non-uniform chains.

50. Challis,R.E., Holmes,A.K., J S Tebbutt,J.S., and Cocker,R.P., J. Acoust. Soc. Am., vol-103,1998, 1413-1420.

51. Kolsky, H., Stress Waves in Solids, Dover, New York, 1963.

52. Ewing, W.M. et al, Elastic Waves in Layered Media, Mc Graw Hill,New York, 1957.

53. Miller, D.R., Macosko,C.W., Macromolecules, vol-9, 1976, p-206.

54. Macosko,C.V., Miller, D.R., Macromolecules, vol-9, 1976, p-199.

55. Finney, R.L., and Thomas, G.B., Jr Calculus. Addison-Wesley, New York,1990.

56.Maxwell, J.C., Philos. Trans.R. Soc. Vol.157,49,1867.

57. Kelvin, L., Encyclopedia Britannica., 1875.

58. Voigt, W., Ann. D. Phys., Vol. 47, 671, 1892.

59. Zener, C., Elasticity and anelasticity of metals. Univ. of Chicago Press. Chicago, 1948.

Chapter 8   Experimental Apparatus and Techniques of Ultrasonic Measurements

8.1 Introduction

This chapter describes the apparatus used to measure ultrasonic wave attenuation and phase velocity in thin epoxy samples. It was originally developed by Freemantle [1-3] for measurements at relatively low temperatures, in the range of 20°C to 80°C. Usually, shear wave transducers are used to propagate bulk shear waves through a test material which require the use of high viscosity couplant. Thus it would not be possible to make almost simultaneous measurements of both the compression and shear wave propagation characteristics as a change of transducers would be required. The instrument employs a goniometer so that by using the mode conversion technique to excite pure shear waves by compression waves incident at an oblique angle on a thin sample of resin where mode conversion takes place the measurements of absorption and phase velocity for both propagating modes can be made.

8.2 Operating principle

The principle by which both compression and shear waves are excited in a slab of material is illustrated in figure 8.1.
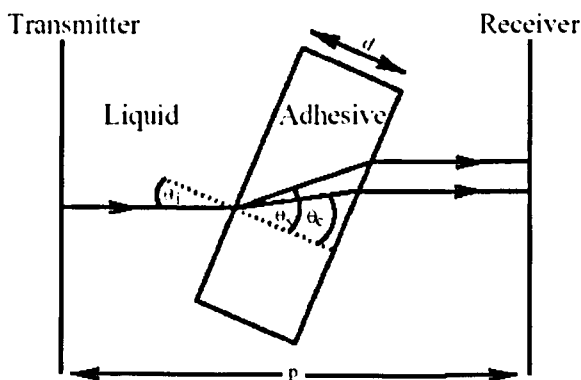
Figure 8.1 Excitation of compression and shear waves in a slab sample immersed in a liquid between an ultrasonic transmitter and receiver.

Compression waves are excited on one side of the test cell, travel through the liquid (water) to the test sample boundary, where for non normal incidence they mode convert into compression and shear modes. After passage through the sample these wave convert back again to compression waves at the second boundary of the sample. If the incidence angle is zero only compression waves will traverse the sample. With suitable adjustment of this angle the compression wave in the sample can be cut off, leaving just the shear wave. At the exit boundary of the sample the transmitted compression wave propagates through the liquid to the receiving transducer.

Assuming an isotropic medium, the angles of refraction (θ_c and θ_s) in the sample for the compression and shear wave respectively are determined by the Snell's law, thus

$$\theta_c(\omega) = \sin^{-1}\left(\frac{\sin\theta_i}{c_l}c_c(\omega)\right) \tag{8.1}$$

$$\theta_s(\omega) = \sin^{-1}\left(\frac{\sin\theta_i}{c_l}c_s(\omega)\right) \tag{8.2}$$

Where θ_i is the angle of incidence, c_l is the compression wave velocity in the surrounding liquid, assumed to be independent of frequency, and c_s and c_c are the compression and shear wave velocities in the sample.

If the angle of incidence is sufficiently high it is possible to eliminate the compression wave in the sample and excite a pure shear wave. The angle at which this occurs is dependent upon the compression wave velocity in both the liquid and solid and is given by the following equation:

$$\theta_k(\omega) = \sin^{-1}\left(\frac{c_l}{c_c(\omega)}\right) \tag{8.3}$$

In epoxies the maximum compression wave velocity is typically 2500ms^{-1}, and so an angle of 50° is sufficient for pure shear waves to be excited into the sample. Referring to figure 8.1 and considering a compression wave incident on the sample at an angle of 0°, the signal received at the receiver transducer ($C(\omega)$), for ideal broad-band

excitation should then be described as a function of frequency by the following equation:

$$C(\omega) = T_x(\omega)R_x(\omega)\exp\{-j\omega[(\frac{p}{c_l}) - (\frac{d}{c_l})]\}$$
$$\times tcc_{01}(\omega)tcc_{10}(\omega)\exp\{-j\omega(\frac{d}{c_c(\omega)})\}\exp\{-\alpha_c(\omega)d\}$$

(8.4)

where:

$T_x(\omega)$ and $R_x(\omega)$ are the transmitter and receiver transducer responses.

tcc_{01} is the compression to compression transmission coefficient at the liquid-sample interface.

tcc_{10} is the compression to compression transmission coefficient at the sample-liquid interface.

For a compression wave incident on the sample at $\theta_i > \theta_k$ (i.e. compression wave mode converted into pure shear wave) the received signal in shear mode at the receiver transducer $(S(\omega))$ is given by

$$S(\omega) = T_x(\omega)R_x(\omega)\exp\{-j\omega[(\frac{p}{c_l}) - (\frac{d\cos(\theta_i - \theta_s(\omega))}{c_l\cos\theta_s(\omega)})]\}$$
$$\times tcs_{01}(\omega,\theta_i)tsc_{10}(\omega,\theta_i)\exp\{-j\omega(\frac{c_s(\omega)d}{\cos\theta_s(\omega)})\} \times \exp\{-\alpha_s(\omega)(\frac{d}{\cos\theta_s(\omega)})\}$$

(8.5)

where:

tcs_{01} is the compression to shear transmission coefficient at the liquid-sample interface.

tsc_{10} is the shear to compression transmission coefficient at the sample-liquid interface.

Equation (8.5) takes into account the lateral displacement of the shear wave as it exits the sample, which shortens the path length in the water to the receiver transducer.
It is important to note that the transmission coefficients are not constants but are

325

dependent on the density, wave phase velocity and angle of incidence. Freemantle [1-3] has used analytical expressions derived by Brekhoviskikh [4] to calculate the coefficients at the liquid-solid and solid-liquid interface for incident compression and shear waves as functions of the wave phase velocity and wave propagation angle. From equations (8.4) and (8.5) the absorption coefficient and phase velocity in both compression and shear mode can be calculated.

8.3 System hardware (mechanical)

The mechanical parts of the system consist of three essential components – the sample holder, the test cell in which the liquid is held, and a goniometer stage which is used to rotate the sample in order to adjust the incidence angle. These are described separately in the following paragraphs.

8.3.1 Sample holder

The sample holder is shown in figure 8.2. It is used to mount either solid cured samples of adhesive or liquid curing samples in the test cell. Post cure samples can be tested in the goniometer test cell, simply by cutting the cured sample into the shape of the sample holder.
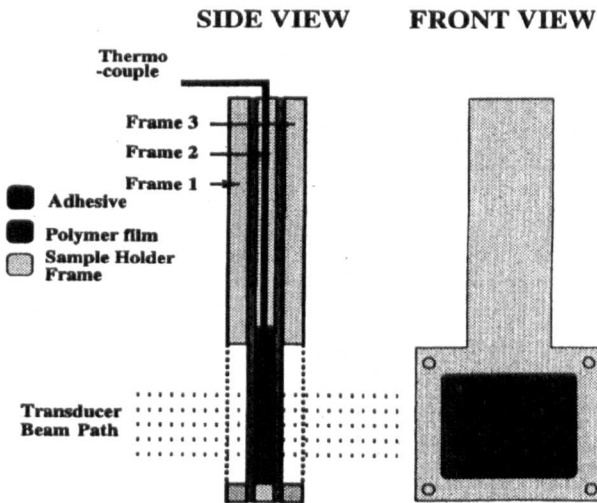
Figure 8.2 The sample holder for liquid-curing samples.

It consists of a frame and two thin (100 microns) sheets of polyimide film on either side of the frame to contain the initially liquid epoxy. Two further frames placed outside of the films to maintain them in liquid tight contact with the main frame. The distance between the two films sets the thickness of the epoxy sample, normally 1.5mm. The sample cures in this chamber formed by the frame and the polyimide films.

It has been found that the variation in the thickness in the cured samples is better than ±0.1mm. A small thermocouple is placed in the sample, outside of the propagation path. Freemantle [1-2] investigated the effect of the two films in the signal path and found it to be negligible. There were two reasons for this – The films were very thin, and any expected (half-wave) resonances would be well outside the frequency range of the transducers. Also, the strength of these resonances was very weak on account of the good acoustic match with the materials either side of them. Freemantle calculated that the maximum variation due to resonance in the films was 0.43dB at 12 MHz, which would result in an error in attenuation measurement of around 2%.

8.3.2 Test cell

The test cell is shown on figure 8.3.
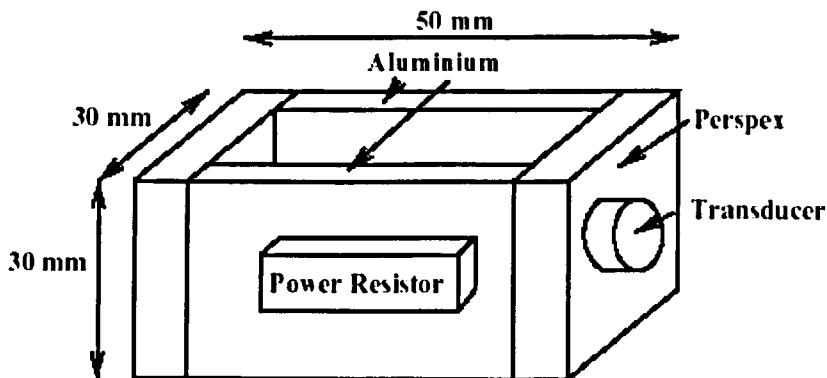
Figure 8.3 The test cell.

It consisted of two aluminium side walls 5mm thick. The end walls were of Perspex, 5mm thick, on to which were clamped transmitting and receiving transducers. It was important to maintain these end walls parallel to each other to avoid the band limiting

effects of oblique incidence on the transducers [5]. In practice, they were aligned parallel to within ±0.01°. The cell could be heated by two 12W power resistors mounted on the aluminium side plates. A temperature feedback proportional-integral-derivative (PID) controller(RS 344-574) controls the temperature with a temperature probe (pt 100, RS 158-985) mounted in the water. The PID controller switches the power to the resistors. The temperature could be set in the range from room temperature (approx. 20°C) up to 80° C. The transducers were of type tmp3 (Sonatest Ltd, UK); their centre frequency was 10 MHz, with a bandwidth of 12MHz extending between 4MHz and 16MHz.

8.3.3 Goniometer stage

The test cell and sample holder are placed within a goniometer and micrometer stage as shown in figure 8.4.
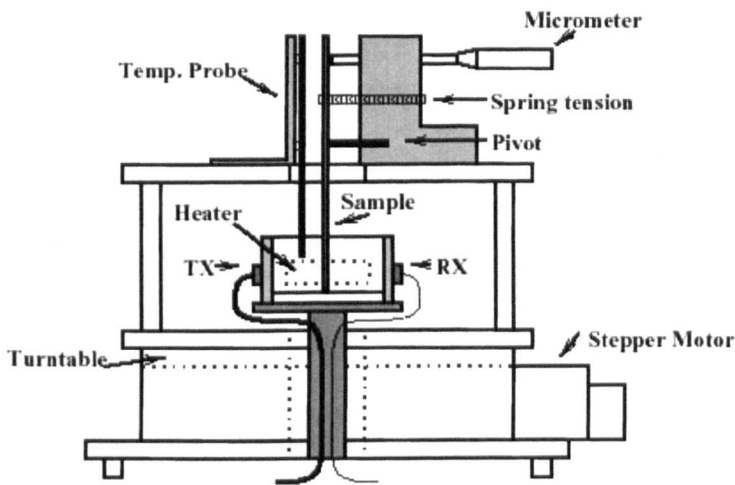
Figure 8.4 Goniometer and micrometer stage assembly.

The goniometer is mounted on a high- precision (±0.01° resolution) rotary table (Time and Precision Ltd) which is driven by a stepper motor and controlled by a PC via the parallel port. By this means, the sample can be aligned very accurately (±0.04°) in the horizontal plane for angles up to 360°. The sample is aligned in the vertical plane by the use of a micrometer and pivot arrangement and can be set with the same degree of accuracy as the rotating stage. Alignment in the vertical plane is checked using the system in pulse echo mode, with a metal reflector placed in the

sample holder. The reflected pulse reaches a maximum amplitude and minimum rise time when the sample is perpendicular to the incident wave. Once set the vertical alignment need not to be readjusted.

8.4 System hardware (electronic)

The transducers were connected to a standard pulser-receiver (EUI, NDT Solutions Ltd, Chesterfield, UK). The receiver output was connected to a digital storage oscilloscope (DSO, LeCroy Inc, USA), which was also used to calculate 1000 coherent averages of each signal, improving the signal to noise ratio (SNR) by 30 dB. The sampling rate was 320 MHz, giving better resolution in the frequency domain than would have been the case if the basic Nyquist rate had been used. The DSO communicated with the host PC by a GPIB interface. The whole system was controlled by the **WinAFG** software package designed by Freemantle [1]. Data processing is done on-line, yielding plots of attenuation coefficient and phase velocity on a PC screen virtually in real time. The basic ultrasonic data capture time is 5s per record. When adjustment of the goniometer is included the maximum time between measurements was around 50s.

8.5 Initial data processing
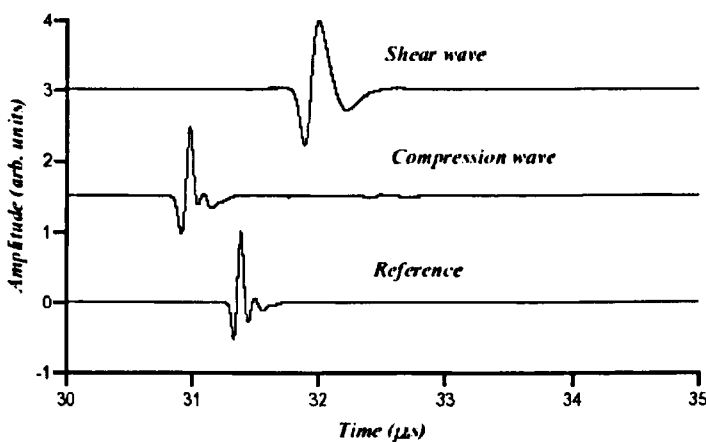
Figure 8.6 Typical pulses received: reference, compression wave in sample and shear wave in the sample.

Figure 8.6 shows typical pulses received from the test cell in three situations: The reference pulse is obtained by transmitting a pulse across the cell with the adhesive sample removed (water propagation path); the compression wave excitation is obtained placing the sample at normal incidence, and the shear wave excitation is obtained by placing the sample at oblique incidence to the transducer.

The arrival times of all three pulses are referenced to the original trigger time of the pulser. So, this arrival time includes the transit time through the Perspex buffers, the water path, and the sample. The phase velocity and absorption coefficient are calculated in a number of signal-processing steps.

The first task is to find the exact position of the centre of the main peak in the received pulses. This is achieved using a peak finding algorithm which picks up successively each point and compares the last point to the previous maximum point. If the last point is larger than the previous maximum then the program saves this new point as the maximum point. Sometimes, where there is poor signal to noise ratio, the pulses may not start and/or end on the baseline, in which cases the offset must be taken off before further processing to avoid spectral leakage in subsequent frequency domain processing. This is achieved by averaging the first and last 50 data samples in each record, and then subtracting this averaged value from the signal, figure 8.7.
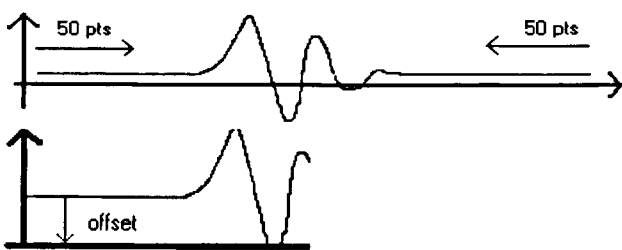
Figure 8.7 Offset removal.

A further Hanning window with a 10% taper of duration 86 μs is then used to extract each received pulse. The phase lag of the pulse is then minimised by applying a circular shift to the data within its storage array. This placed the received pulse in a near symmetrical orientation about the first point in the array, the notional origin of

330

time for the FFT. The section of the pulse that appears in 'negative time' due to this manoeuvre ends up on the right hand side of the array. The FFT thus has as its time domain input what is effectively one period of a periodic signal which will be of minimum phase; the process is illustrated in figure 8.8.
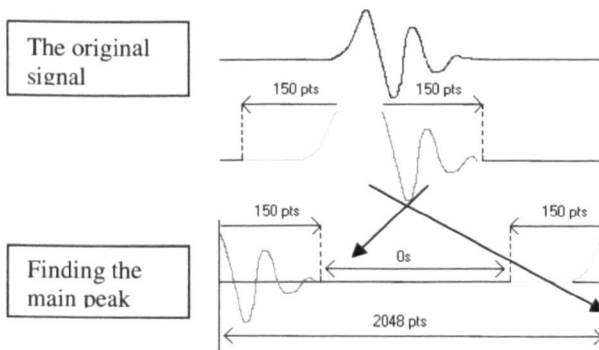
Figure 8.8 Time shifting to achieve minimum phase.

8.6 Calculation of absorption and phase velocity

The equations for calculating the compression and shear wave absorption coefficient and phase velocity are derived from equations (8.4) and (8.5). It is possible to work out approximate values of the compression and shear wave velocities by the time of flight method, using the peak arrival times of the compression, shear and reference (compression) wave signals. The method is illustrated in Figure 8.9.
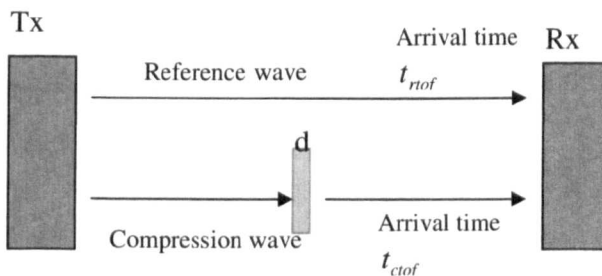
Figure 8.9 Time of flight method.

The time to traverse the sample is

$$t_{ctof} - t_{rtof} - \left(\frac{d}{v_l} \right)$$ (8.6)

An approximate value of the compression wave velocity is then

$$c_{ctof} = \frac{d}{\left[t_{ctof} - t_{rtof} - \dfrac{d}{c_l} \right]}$$ (8.7)

Where d is the sample thickness, c_l is the compression wave velocity in the water, and t_{ctof} and t_{rtof} are the measured arrival times of the compression wave pulse and reference pulse respectively.

The calculation of the shear wave arrival time is more complex since the path length in the sample is dependent on the shear wave angle of refraction (equation (8.2)). This depends on the shear wave velocity which is unknown. In this case, the velocity is calculated iteratively by comparing the predicted arrival time (equation (8.8)) to the measured time (equation (8.9)) as a function of shear wave velocity.

$$t_s = \left[\frac{d}{c_s \cos\theta_s} \right] - \left[\frac{d\cos(\theta_i - \theta_s)}{c_l \cos\theta_s} \right]$$ (8.8)

$$t_s = t_{stof} - t_{rtof}$$ (8.9)

Here, θ_i and θ_s are the angles of incidence and shear wave refraction respectively, and t_{stof} is the measured arrival time of the shear wave pulse.

To obtain the phase velocity as a function of frequency, we need to know the effective arrival times of each of the Fourier domain frequency components. This time can easily be determined from the phase spectra of the signals, obtained from the FFT output. Therefore, the way of calculating this phase velocity is done in much the same way.

t_{ctof} is changed to $\dfrac{\phi_c(\omega)}{\omega}$ and t_{rtof} to $\dfrac{\phi_r(\omega)}{\omega}$, where $\phi_c(\omega)$ and $\phi_r(\omega)$ are the phase spectra obtained from the Fourier transforms of the windowed signals for the compression wave pulse and the reference pulse respectively.

Finally, the compression wave phase velocity as a function of frequency can be calculated by the following equation:

$$c_c(\omega) = \cfrac{d}{\left[\dfrac{\phi_c(\omega)}{\omega} - \dfrac{\phi_r(\omega)}{\omega} - \dfrac{d}{c_l}\right]} \tag{8.10}$$

The shear wave phase velocity is calculated in the same manner as for the time of flight, by comparing the predicted frequency dependent arrival times (equation (8.11)) with the measured times (equation (8.12)), in an iterative procedure.

$$t_s(\omega) = \left[\cfrac{\omega d}{c_s(\omega)\cos\theta_s(\omega)}\right] - \left[\cfrac{d\cos(\theta_i - \theta_s(\omega))}{c_l\cos\theta_s(\omega)}\right] \tag{8.11}$$

$$t_s(\omega) = \frac{\phi_s(\omega) - \phi_r(\omega)}{\omega} \tag{8.12}$$

where $\phi_s(\omega)$ is the measured phase response of the shear wave pulse.

As a small change in temperature in the sample cell could cause a significant change in the wave velocity through water, time delay errors may occur in the above calculations in some cases where the temperature might change between two measurements. For example, if the measurements are not made successively, or if we want to monitor the evolving properties of the adhesive during cure which might last for long time (over 2 hours). Therefore, for each measurement the water temperature is measured and the water velocity is calculated from an equation based on experimental measurements of water velocity versus temperature [6].

$$c(\tau) = 1402.7 + 488\tau - 482\tau^2 + 135\tau^3 + (15.9 + 2.8\tau + 2.4\tau^2) \tag{8.13}$$

where: $\tau = T/100$ and T is temperature in $^{\circ}$C.

Once the compression and shear wave velocities, and the density of the sample are known (the density of the sample can be determined using a density bottle) it is then possible to calculate the compression and shear wave transmission coefficients, and these are used to correct the frequency domain amplitudes of the compression and shear wave pulses.

Calculation of the attenuation coefficients (in units of dB/mm) is achieved by dividing the modulus frequency response of the compression and shear wave by that of the water reference using the following equations:

$$\alpha_c(\omega) = 20\log_{10}\left[\frac{A_c(\omega)}{A_r(\omega)tcc_{01}(\omega)tcc_{10}(\omega)}\right]\left(\frac{1}{d}\right) \qquad (8.14)$$

$$\alpha_s(\omega) = 20\log_{10}\left[\frac{A_s(\omega)}{A_r(\omega)tcs_{01}(\omega,\theta_i)tsc_{10}(\omega,\theta_i)}\right]\times\left[\frac{\cos\theta_s(\omega)}{d}\right] \qquad (8.15)$$

Where $A_r(\omega)$, $A_c(\omega)$, and $A_s(\omega)$ are the frequency domain amplitudes of the reference, compression and shear wave pulses respectively.

After carrying out the above analysis, the attenuation coefficient and the phase velocity data can then be plotted as a function of frequency or alternatively, data at particular frequencies can be plotted as a function of cure time.

In order to demonstrate the validity of the technique, Freemantle [1-2] used a frequency domain transfer matrix model to verify the results. The model supports compression and shear wave motions with complex wavenumbers and has been extensively verified against other workers' simulations and experimental data. The derivations used in the model are very different from those used above. Therefore, the model provided a reliable means to validate the results of equations (8.6-8.15).

8.7 Use of the system

In this project, the system was used to obtain compression wave attenuation and phase velocity data during the cure of Araldite 2015 epoxy adhesive material. Records were obtained at two minutes intervals during cure cycles at temperatures 30 °C, 40 °C and 50 °C, and at one minute interval during cure cycles at temperatures 60 °C and 70°C.

8.8 References

1. Freemantle, R.J., PhD thesis, University of Keele, UK, 1995.

2. Challis,R.E., Alper, T., Freemantle, R.J., Crean,G., and Zhang, D., Rev. Sci. Inst. Vol. 64(5), 1993, 1271-1273.

3. Freemantle, R.J., Alper, T., and Challis, R.E., Meas. Sci. Technol, Vol. 4, 1993,1129-1137.

4. Brekhoviskikh, L.M, Waves in Layered Media, Academic Press, New York, 1980.

5. Challis, R.E., Acustica, Vol. 50, 1982, 221-225.

6. Del Grosso, V.A., and Mader, C.W., J. Acoust. Soc. Am, Vol. 52(2), 1972,1442-1446.

Chapter 9   Results and Discussions of
Ultrasonic Cure Monitoring and Comparison and Correlation with
DSC Cure Monitoring

9.1 Ultrasonic Compression wave velocity and attenuation

As discussed in chapter 7 both velocity and attenuation of ultrasound are known to be sensitive to the viscoelastic properties and the structure of polymers. Therefore, measurements of ultrasound absorption and phase velocity lead to important information about the extent of thermoset curing reaction, mechanical modulus, mechanical relaxation processes, phase transition phenomena and structural or morphological information in polymer systems.

In order to track the cure process of our studied thermosetting system Araldite 2015 the compression wave phase velocity and attenuation coefficient data have been considered in this chapter at a *fixed frequency* of 5MHz as a function of cure time at isothermal temperatures of 30°C, 40°C, 50°C, 60°C, and 70°C.Secondary calculations also have been carried out from the velocity and attenuation data at 5MHz at the various isothermal temperatures so as to produce derived functions like real and imaginary parts of ultrasonic compression wave modulus and ultrasonic loss tangent using equations (7.49),(7.50) and (7.51) respectively as have already been mentioned in chapter 7 . These parameters provide information of the material state and the cure process which will be discussed later.

The effect of frequency on the velocity and attenuation data have been narrated. *Frequency dependent* compression wave velocity and attenuation at various times throughout the cure process for this studied epoxy system also have been discussed. The development of the *central relaxation time* of this epoxy thermoset Araldite 2015 during the cure process also have been demonstrated as a useful measure of the progress of the structural development.

9.2 Fixed-frequency Ultrasonic Compression wave velocity

As mentioned before the ultrasonic longitudinal velocity is a measurement of the density and elastic response of the material to the oscillating pressure and provides information regarding its molecular organization. The velocity change corresponds to contributions of *modulus* and *density*, while the velocity itself is related to the real component of the modulus. Basically, ultrasonic compression wave velocity responds to changes in material's adiabatic Bulk modulus [=(adiabatic compressibility)$^{-1}$] and density which are dependent on pressure and temperature. Ultrasonic shear wave velocity in solid responds to changes in material's rigidity (Shear modulus), Bulk modulus [=(compressibility)$^{-1}$] and density. Thus, ultrasonic velocity is closely related to the elastic moduli of materials and the elastic coefficients of materials are influenced by the ultrasound velocity. In addition, the *continuity of the macromolecular chains, intermolecular interactions* and *temperature* affect the ultrasound velocity. As the shrinkage of epoxy resins is comparatively small (1.5%-2%) during polymerization, the increase in density exhibited during cure is at most a few percent and is neglected here.

Figure 9.1 shows the variation of ultrasonic compression wave phase velocity at 5MHz as a function of cure time during the cure process of Araldite 2015 at cure temperatures of 30°C, 40°C, 50°C, 60°C, and 70°C. Because of the nature of the ultrasonic wave's propagation, ultrasonic technique directly measures the relation between ultrasonic wave behaviour and material characteristics (here, the changes in mechanical properties of the material Araldite 2015 during the cure process and correspondingly in the physical / thermo-physical state of it) on *microscopic scale*.

From figure 9.1 it can be seen that all of the shapes of the velocity curves follow a general trend, all starting at a low value due to the initial fluid like state of the mixture until the gel point is reached and then rapidly increasing with curing time to a high value as the mixture solidifies and hardens through crosslinking, following as S-shaped curve, levelling in a plateau up to a limiting value around which time the rate of increase becomes very gradual, corresponding to the end of the cure process due to

the vitrification. After vitrification, further reaction depends on a diffusion-controlled mechanism as discussed details in chapter 3.
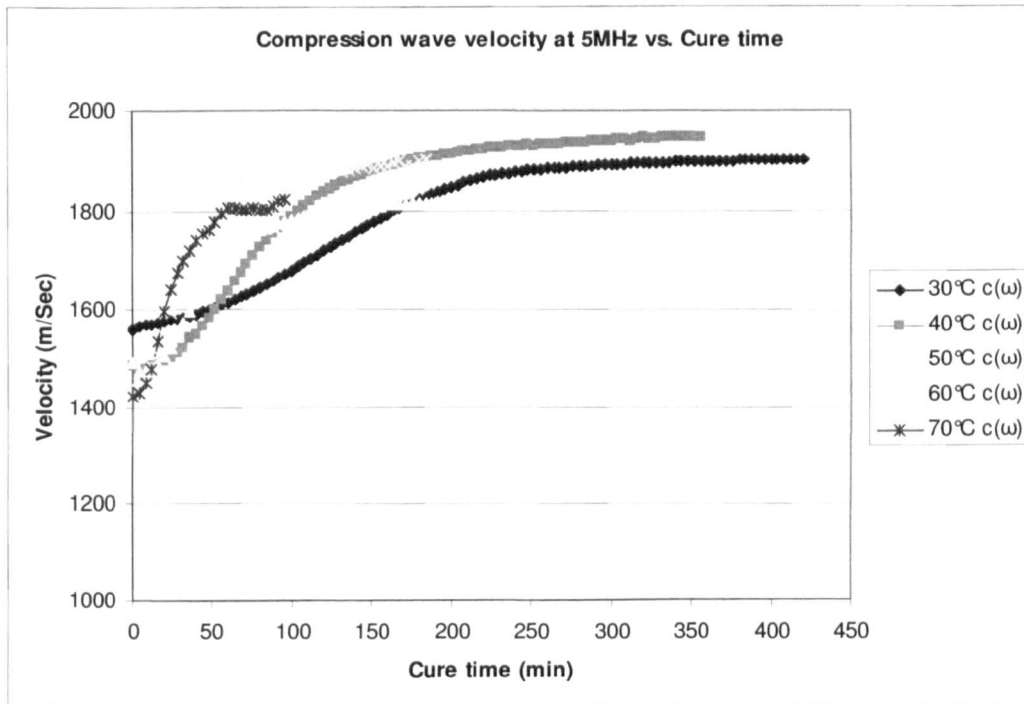
Figure 9.1 Ultrasonic Compression wave phase velocity at 5MHz as a function of cure time at cure temperatures of 30°C, 40°C, 50°C, 60°C, and 70°C.

From the perspective of elastic property development the general trend of the velocity curves can be explained further. From the sigmoidal curve we see that at the beginning of the cure, while the molecular weight starts to grow and the resin appears as a viscous liquid, the compression wave velocity shows a very limited increase. Then, corresponding to the gelation time, the maximum rate of change in the velocity occurs. A steep increase in velocity—a true jump of its derivative can be thought to be associated with the build-up of bulk and shear modulus as a consequence of the incipient formation of a cross-linked structure. Basically, at that point, the growing branched molecules can be characterized by extensive entanglements which are capable of providing an elastic response associated with this significant growth of velocity. At the end of the cure, the velocity reaches a stable value which reflects the development of highly cross-linked structure and, in turn, the achievement of the final values of modulus. Hence, the gradual increase of ultrasonic compression wave velocity in an S-shaped curve as a function of cure time indicates a steady growth of

the real part of the compression modulus $\left(K + \dfrac{4}{3}G\right)$ of the curing thermosetting system (Araldite 2015) as it solidifies.

Ultrasonic Compression wave phase velocity at 5MHz as a function of cure time at five different cure temperatures (30°C, 40°C, 50°C, 60°C, and 70°C) are reported in the figure 9.1. The effect of temperature on the compression wave velocities is clearly evident from the figure as it is reflected in the shape of the velocity curves.

The *initial velocity values decrease with increasing temperature*. This decrease of the initial velocity as the cure temperature increases most possibly can be attributed to a *reduction of the bulk modulus and of the density* of the unreacted resin with temperature. Intermolecular forces play a vital role in characterizing the physical properties of liquid systems. This observed phenomenon can be explained in terms of *intermolecular interactions*. The decrease in bulk modulus and density of the unreacted resin and in the corresponding initial velocity with temperature suggest decrease in intermolecular forces as a result of increase in thermal energy, which causes increase in kinetic energy and volume expansion. The increase in kinetic energy causes *lowering in viscosity*. Similarly increase in volume causes lowering in the density of the mixture and hence increase in intermolecular free length. The initial velocity of the curve for 30°C cure (1551 m/sec) is significantly higher than the others, probably due to the fact that the colder material exhibits a higher bulk modulus. The initial velocity decreases in relatively small steps as the cure temperature is increased.

Therefore, in view of the above discussion we see that for the studied epoxy thermosetting system, temperature dependence of ultrasonic longitudinal velocity is very sensitive to changes in intermolecular interactions and molecular organization and capable to detect this *initial rheological behaviour* of lowering in bulk modulus, density and viscosity of the unreacted resin with temperature during cure. Interestingly, referring to the isothermal DSC conversion traces in figure 5.1 in chapter 5, it appears that the *DSC is insensitive to this phenomenon.*

The initial and final values of ultrasonic longitudinal wave velocities, corresponding change between them and the characteristic time to attain the final value of the velocity at different cure temperatures are presented in table 9.1.

Table 9.1 The initial and final values of ultrasonic longitudinal wave velocities, corresponding change between them and the characteristic time to attain the final value of the longitudinal wave velocity all based on 5MHz ultrasonic frequency obtained at different isothermal cure temperatures for the isothermal cure process of Araldite 2015.

T_{cure} (°C)	30	40	50	60	70
Initial longitudinal velocity (m/Sec)	1551	1484	1491	1447	1422
Final longitudinal velocity (m/Sec)	1902	1946	1824	1900	1822
Relative change in velocity (m/Sec)	351	462	333	453	400
$t_{final\ velocity\ (5MHz)}$ (min)	420	356	240	184	97

From figure 9.1 it is evident that the gradient of the cure time versus compression wave velocity curve is steeper the higher the cure temperature. This indicates that the reaction rate increases as cure temperature is increased and that the modulus increases more rapidly at higher cure temperatures. Thus, *the shape of the velocity curves reflect the rate of the chemical reaction*. It is clear from the figure that the time taken to attain the final value of the longitudinal wave velocity (i.e. to complete cure) is reduced at higher cure temperatures.

It can be seen that the velocity changes from liquid to solid state are less at higher temperatures of curing (50°C, 60°C, 70°C) in spite of high crosslink density at these temperatures due to the fact that the curing reaction stops when the thermoset achieves the crosslink structure having static glass transition temperature equal to the temperature of curing because of vitrification as all of the cure temperature employed

are less than the $T_{g\infty}$ of the fully cured system (described in details in the context of DSC results and modelling in chapters 5 and 6).This suggests that in spite of high crosslink density at these temperatures (50°C, 60°C, 70°C) the crosslinkage network is not fully developed most possibly due to the cure process occurring quickly because of the increased rate of reaction and the diffusion-controlled phase of cure stopping the cure reaction.

Basically, the temperature of the curing affects the value of the velocity by changing the reaction kinetics and by affecting the viscoelastic state for a given time of cure. Therefore, the velocity values cannot be compared directly from figure 9.1, because the cure reaction proceeds differently at different temperatures and consequently different types of network structure have formed, hence, points with the same velocity on different kinetic curves will correspond to different structures. In general, temperature not only controls cure rates, but also reaction pathways. Low cure temperatures favour chain-extension producing flexible material, while high temperatures favour cross-linking producing rigid material. The effect of temperature on the absolute final values of velocities are difficult to interpret, it would appear that the 40°C cure temperature produces the resin with the highest modulus. However, both *compression wave* (sensitive to *stiffness*) and *shear wave* (sensitive to *density*) characterization can provide a complete picture of the elastic moduli developed.

Any comparison with literature should be dealt with caution. The results in figure 9.1 refer to measurements made at the curing temperature (*not* at room temperature) and one would expect the velocities / moduli of epoxy resins to be temperature dependent. Our results indicate that the epoxy thermosetting system used in this study is more sensitive to crosslink density changes than to bulk density changes. So, our results are in good agreement for the extent of reaction as a function of cure time, i.e. reaction rate is found to be higher at higher temperatures with completion of cure being achieved more quickly at higher temperatures. *This is in good agreement with DSC conversion and reaction rate results as a function of cure time* (figure 5.1 and 5.3 in chapter 5) which again show increased reaction rates and decreased times to attain the final degree of cure at higher cure temperatures. Furthermore, it is interesting to mention that the evolution of S-shaped compression wave velocity curves follow an

initial dramatic increase in rate and then orient to a stationary state. Thus, the first stage of the reaction is characterized by an *acceleration* followed by a *de-acceleration* which is indicative of *autocatalytic* reaction kinetics and *is in excellent agreement with the DSC kinetics modelling results.*

9.3 Fixed-frequency Ultrasonic Compression wave attenuation

As we know the adiabatic passage of a sound wave is associated with a fluctuation in the local temperature of the transmitting medium. So, during propagation of a sound wave, the oscillation of acoustic pressure is coupled with *adiabatic temperature oscillations* which is very similar to a temperature-modulated calorimetric experiment and important in understanding the attenuation behaviour of ultrasound. Ultrasound attenuation occurs when the travelling pressure disturbance excites the molecules of the medium into motion that does not remain in phase with the wave. When viscothermal processes lead to heat transport between the peaks and troughs of this fluctuation, there arises classical viscothermal absorption familiar in all homogeneous media. In more complex systems like polymers or systems with different phases, the contributions from *relaxation, classical viscosity, thermal conductivity,* and *sound scattering* for inhomogeneous systems can add up to the attenuation of sound.

Attenuation which is a measure of the energy loss in the compressions and decompressions produced as an ultrasonic wave passes through a material can give information on the *microscopic structural organization* of the material. Basically, attenuation is governed in a complex fashion by interactive effects of density, hardness, viscosity and molecular structure and normally increases with frequency in a given material. This already has been discussed in chapter 7. Figure 9.2 shows the variation of ultrasonic compression wave attenuation at 5MHz as a function of cure time during the cure process of Araldite 2015 at cure temperatures of 30°C, 40°C, 50°C, 60°C, and 70°C and corresponding to the velocity data on figure 9.1. The observed attenuation can be ascribed mainly to viscoelastic relaxation, which results from thermally stimulated jump processes involving molecules or molecular segments.
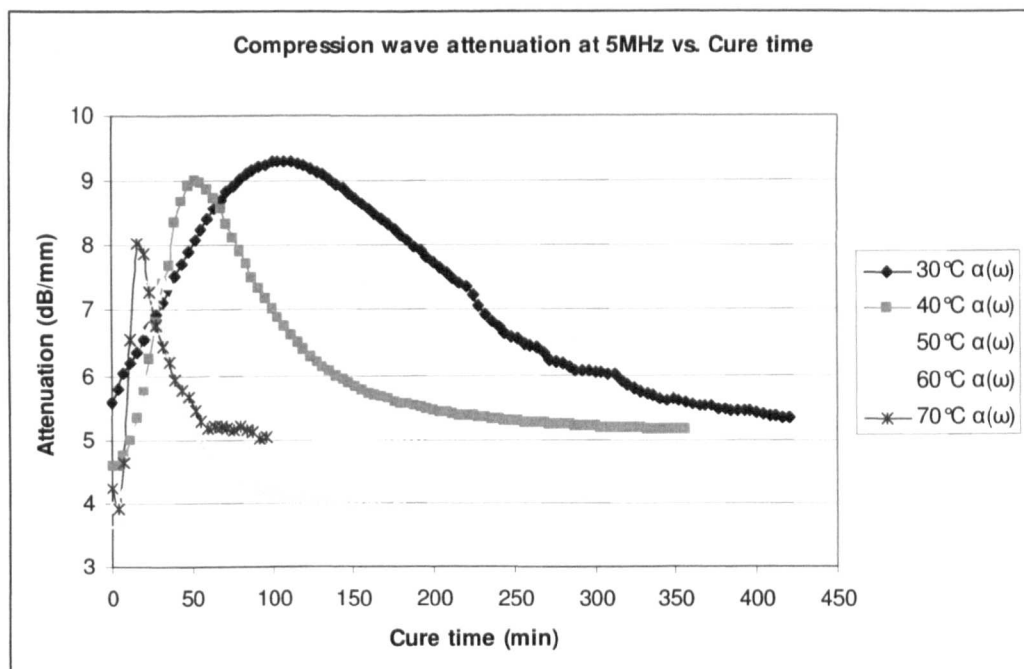
Figure 9.2 Ultrasonic Compression wave attenuation at 5MHz as a function of cure time at cure temperatures of 30°C, 40°C, 50°C, 60°C, and 70°C.

From figure 9.2 it can be seen that the general shape of all of the attenuation curves remain similar, with the curves initially starting at a low value and increasing rapidly rising to a distinct peak as cure reaction progresses and thereafter decreases gradually in dependence on cure time to a nearly constant value indicating the final glass polymer has formed.

This observed behaviour of the compression wave absorption co-efficient can be interpreted in terms of the structural development of the polymeric material during cure. Early in the cure, the observed sharp increase in attenuation can be attributed to polymerization. Initially, as the chains begin to form and elongate, because of their size and flexibility, they interact strongly with the ultrasound causing significant signal loss and eventually increasing attenuation. The observed peak is reached when most of the polymer chains have formed and have the greatest degree of freedom. According to Freemantle and Challis [1], this characteristic peak in the compression wave absorption is an indicator of the start of cross-linking after initial polymer chain formation and the *position* and *width* of this peak is related to the *rate* of polymerization and *cross-linking*. After reaching the peak, the attenuation decreases as the polymer chains begin to cross-link and their movement becomes restricted. The

long intermediate molecules become constrained along their length and there is no significant signal loss due to interactions with ultrasound. As cure proceeds, increased cross-link density causes increased chain stiffness and density, and as a consequence, a change in the energy absorbing interaction between the solid chains and ultrasound occurs. The signal loss lessens which explains the subsequent decrease in the observed attenuation behaviour. The final value of attenuation depends on the type of network formed and the cure schedule which has produced it.

Ultrasonic Compression wave attenuation at 5MHz as a function of cure time at five different cure temperatures (30°C, 40°C, 50°C, 60°C, and 70°C) are illustrated in the figure 9.2. The effect of temperature on the compression wave attenuation is clearly evident from the figure as it is reflected in the shape of the attenuation curves.

The *initial attenuation values decrease with increasing temperature*. It is also noted that a small downward change in the attenuation can be seen at the very beginning of the cure which is particularly prominent for the higher temperature cures. This decrease of the initial attenuation coupled with this downward curvature / drop at the beginning of the cure most possibly is the result of the epoxy losing its viscosity as the cure temperature increases. The reduction in viscosity at the initial stages of curing is due to the exothermic heat of reaction. There are two competing mechanisms affecting the viscosity. A higher temperature reduces viscosity and the reduced viscosity increases mobility of the mixture thus briefly accelerating the cure rate. Advancing cure decreases viscosity. The final viscosity and hence the attenuation depend on the temperature and the degree of cure. This observed phenomenon has already been explained in terms of *intermolecular interactions* in correspondence with the explanation of initial decrease of velocity with increasing temperature.

Therefore, we see that for this epoxy system, temperature dependence of ultrasonic compression wave attenuation is very sensitive to changes in intermolecular interactions and molecular organization and capable to detect this *initial rheological behaviour* of lowering in attenuation and viscosity with temperature during cure. This again agrees with the corresponding velocity data previously discussed in this chapter, indicating that the initial velocity decreased associated with reduction of bulk modulus, density and viscosity with increasing temperature. Interestingly, referring to

the isothermal DSC conversion curves in figure 5.1in chapter 5, it appears that the *DSC is insensitive to this phenomenon.*

It can be seen from figure 9.2 that an increase in the cure temperature leads to an increase in reaction rate and as a consequence, the adhesive cures faster with increased temperature. This is observed in the experimental data, by a narrowing of the compression wave absorption peak which occurs earlier in time with increased cure temperature. This occurrence of the absorption peak over a shorter period of time with increased cure temperature, indicates that the part of the reaction in which large conformational changes take place occurs in a shorter time period the higher the curing temperature. This signifies that the higher the curing temperature the faster the reaction rate, the faster the attenuation reaches the peak value, and the earlier in time the attenuation peak occurs. Similar behaviour is observed in the studies by Matsukawa et al [2] who considered the change in compression wave absorption with the reaction rate which was controlled by the resin-hardener stoichiometric ratio.

The earlier arrival of the attenuation peak at higher cure temperature reflects a more rapid development of intermediate molecular chains. Also, the more rapid decay of the relaxation peak with respect to cure time for higher temperature cure, indicates a more rapid cross-linking which, in turn, implies the inhibition of the motions of long intermediate molecular chains. On the contrary, the relatively late arrival of the peak and longer decay time associated with lower cure temperatures can be attributed to slower chain formation and slower cross-linking. The peak attenuation values also change with different cure temperatures, with lower cure temperatures exhibiting high values of peak attenuation indicating a rubbery state in the curing polymer, whereas higher temperature cure shows a lower value of peak attenuation characteristic of a more glassy state in the material. The final value of the attenuation data tends to be higher for lower curing temperatures indicating that lower curing temperatures result in resins that are more rubbery. But this must be viewed with caution as the absorption of an epoxy resin will be temperature dependent.

The temperature dependence compression wave attenuation results are in excellent agreement with the corresponding temperature dependence compression wave velocity results previously discussed in this chapter, indicating that the reaction rate is

found to be higher at higher temperatures with completion of cure being achieved more quickly at higher temperatures. *This is in good agreement with DSC conversion and reaction rate results as a function of cure time* (figure 5.1 and 5.3 in chapter 5) which again show increased reaction rates and decreased times to attain the final degree of cure at higher cure temperatures. Our results based on the temperature dependence of compression wave velocity and attenuation data are consistent with the results of previous workers [1,2,3] and suggest that ultrasonic technique is sensitive to changes in the cure temperature. It is important to note that these effects observed in ultrasonic studies are quite marked for relatively small differences in cure temperature. Therefore, ultrasound could be used to detect changes in cure behaviour due, for example, to temperature fluctuations in an autoclave.

9.4 Development of Moduli during cure

Epoxy resin adhesives cure with little change in volume which implies that the density does not change significantly during cure. Assuming constant density, we know that the square of the phase velocity of the propagating wave in the material is proportional to the modulus of the material for the particular wave mode. So, as the material cures, following the trends in compression and shear wave phase velocities we can get the information of the changes in elastic behaviour of the material as cure proceeds. It is of interest to calculate the complex moduli as this gives an indication of the viscoelastic state of the material during and after cure. Figures 9.3 and 9.4 show the real and imaginary parts of the ultrasonic compression wave modulus at 5MHz for the Araldite 2015 adhesive as a function of cure time at cure temperatures of 30°C, 40°C, 50°C, 60°C, and 70°C.The real and imaginary parts of the compression wave modulus are calculated from the attenuation and velocity data at 5MHz.

From figure 9.3 it can be seen that the shapes of the real part of the compression wave moduli or storage moduli curves follow a general trend which is similar to the development of velocity as described before in this chapter. The real part of the compression modulus $\left(K + \frac{4}{3}G \right)$ of the curing adhesive evolves in a continuous steady growth fashion as it solidifies. The characteristics of the temperature

dependence of moduli are similar to the characteristics of the temperature dependence of velocities as narrated before.

From figure 9.4 it can be seen that the shapes of the imaginary part of the compression wave moduli or loss moduli curves follow a general trend all rapidly increase to some maximum value followed by a gradual reduction. With increasing temperature the initial slope of rising becomes steeper. At the early stages of cure, the initial value of both storage and loss moduli decrease with increase in cure temperature, a feature similar to velocity and attenuation which narrated before in this chapter.

The development of the compression modulus $\left(K + \frac{4}{3} G \right)$ during cure results from contributions from both the developing shear modulus and the developing bulk modulus. This can be explained in terms of the degree of molecular cross-linking during the cure.

After the gel-point, as cure proceeds, the evolving shear modulus can be thought to be clearly related to the increasing molecular cross-linking due to the fact that a molecular network then possesses an increased shear rigidity with increased bond number in the network. Therefore, it is evident that shear modulus increases with cure time.

The adiabatic bulk modulus (K_s) has an energy dependent form given by (from the second law of Thermodynamics) the following thermodynamic relationship

$$K_s = V \left(\frac{\partial^2 E}{\partial V^2} \right)_s \qquad (9.1)$$

Where subscript S is entropy, E is energy and V is volume. Equation (9.1) relates the bulk modulus with *intermolecular potential* which is expected to increase with increased molecular cross-linking as the cure progresses. This gives the explanation of the increase of bulk modulus during the cure. So, we can see that both the evolving bulk and shear moduli are related to the degree of molecular cross-linking. Which modulus will undergo the largest percentage increase depends on the adhesive type and cure condition.
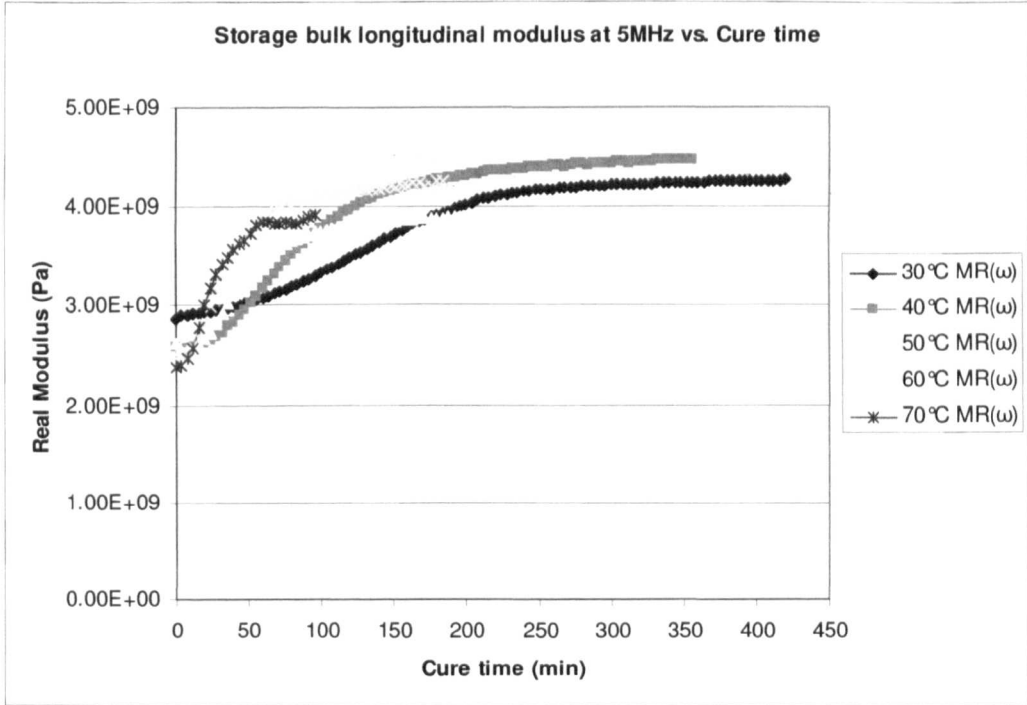
Figure 9.3 Real part of Ultrasonic Compression wave modulus at 5MHz as a function of cure time at cure temperatures of 30°C, 40°C, 50°C, 60°C, and 70°C.
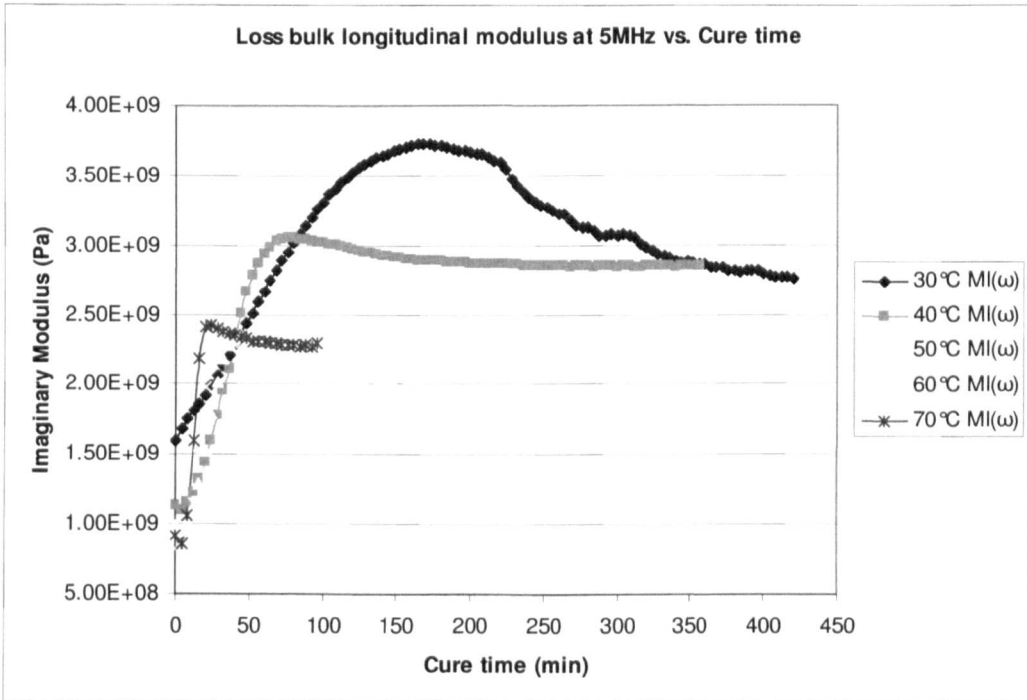
Figure 9.4 Imaginary part of Ultrasonic Compression wave modulus at 5MHz as a function of cure time at cure temperatures of 30°C, 40°C, 50°C, 60°C, and 70°C.

9.5 Ultrasonic loss tangent

Ultrasonic loss tangent (tanδ) is the ratio of the imaginary part of compression modulus (loss modulus) to the real part of compression modulus (storage modulus). Ultrasonic loss tangent calculated from compression wave velocity and attenuation data at 5MHz for the curing of Araldite 2015 epoxy adhesive as a function of cure time at five different cure temperatures is shown in figure 9.5.
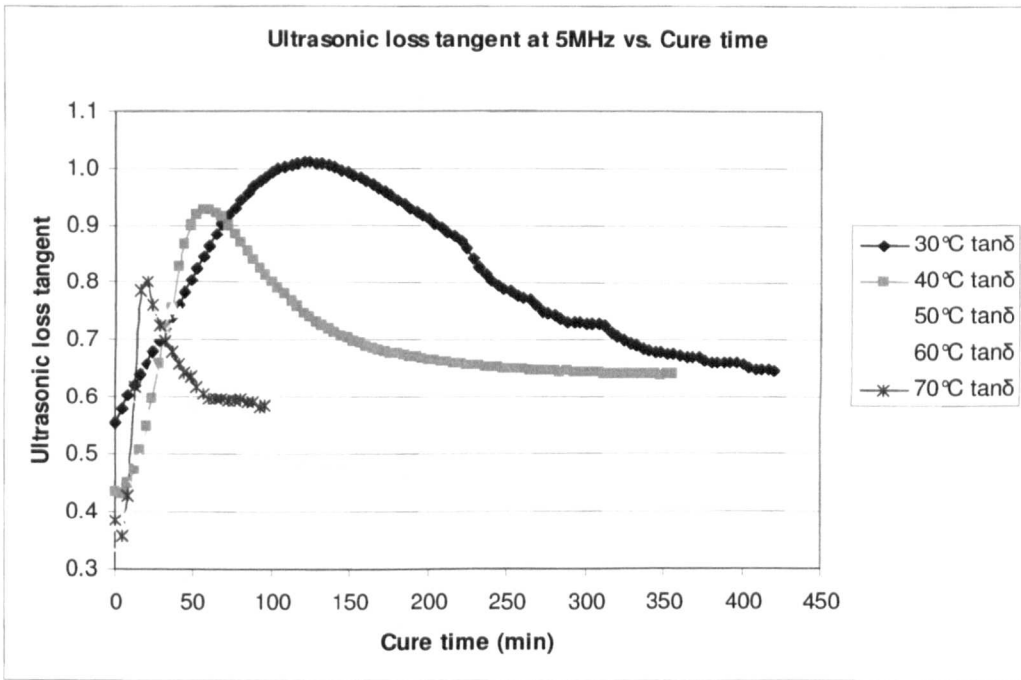
Figure 9.5 Ultrasonic Compression wave loss tangent at 5MHz as a function of cure time at cure temperatures of 30°C, 40°C, 50°C, 60°C, and 70°C.

From the figure it can be seen that all the loss tangent curves at different temperatures follow exactly similar trends like attenuation curves as a function of cure time. Interestingly, the initial, peak and final values of loss tangent curves at different temperatures also follow the same trends like attenuation curves. At the beginning of the cure ultrasonic loss tangent values are higher at lower cure temperatures and decreases as cure temperature increases which is associated with reduction of viscosity, bulk modulus and density (described before in the context of velocity and attenuation).During cure the loss tangent shows a peak in the data which becomes narrower and occurs earlier in time as cure temperature increases which suggests the

increased rate of reaction as the temperature increases. The maximum of loss tangent is slightly delayed with respect to the attenuation peak (data will be shown later). The final value of the loss tangent data tends to be higher for lower curing temperatures, most probably suggesting that lower curing temperatures result in resins that are more rubbery. Basically, at the lowest cure temperature the cure reaction is unlikely to have been completed fully leading to the formation of a more rubbery solid. At the higher cure temperature the low value of loss tangent is likely to indicate a well formed, highly crosslinked, glassy solid has been formed. Therefore, from the above results it is evident that ultrasonic loss tangent sensitive to progress of the cure reaction. It can give information about relaxation and micro-structural properties which will be discussed later.

9.6 Longitudinal Velocity and Ultrasonic prediction of Gelation and Vitrification

Ultrasonic methods are ideal process sensors. As ultrasonic spectroscopy characterizes the *thermo-physical* properties of materials using the response to a high frequency mechanical wave, hence, ultrasound can be used as a measure of the *rheological* properties of a material and thus in determination of on-line rheological properties of materials.

The previously discussed results of us show that ultrasonic compression wave velocity provides a continuous measure of the evolving modulus$\left(K + \frac{4}{3}G \right)$ and has the potential to monitor the adhesive cure. It follows the cure by monitoring changes in the *physical properties* of the system. Basically, it provides us with the information of *degree of mechanical* (more precisely *thermo-mechanical*) *property development* during the cure of a material as it is sensitive to *elastically effective physical and chemical crosslinks.*

Figure 9.6 (a—e) seperately shows the relative variation of ultrasonic longitudinal velocity and attenuation at 5MHz as a function of cure time at cure temperatures of :(a) 30°C, (b) 40°C, (c) 50°C, (d) 60°C, and (e) 70°C corresponding to figures 9.1 and 9.2.
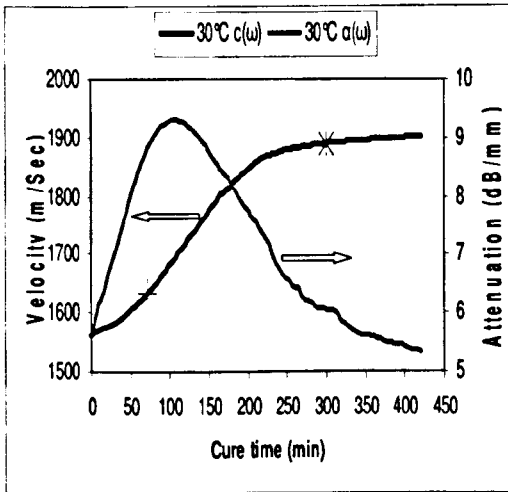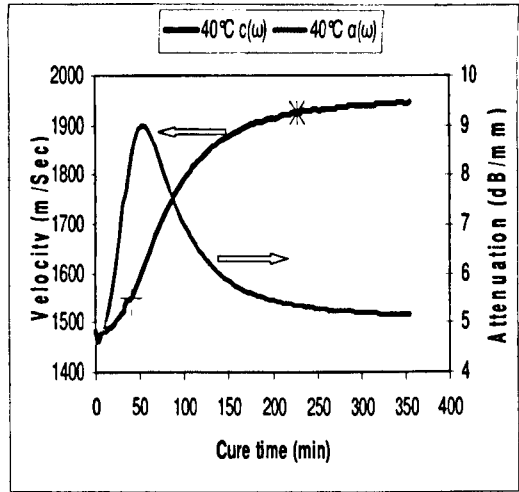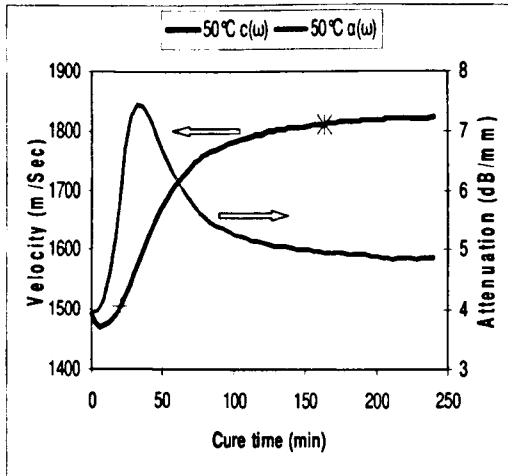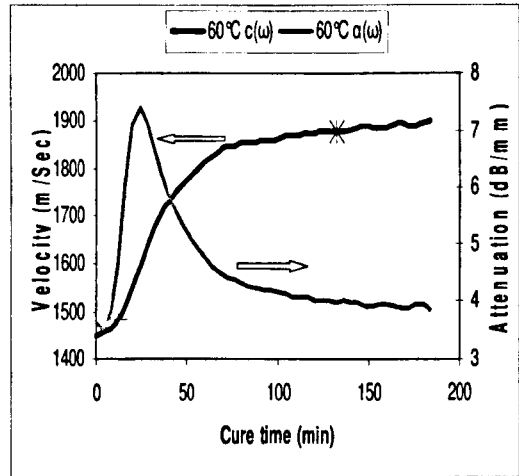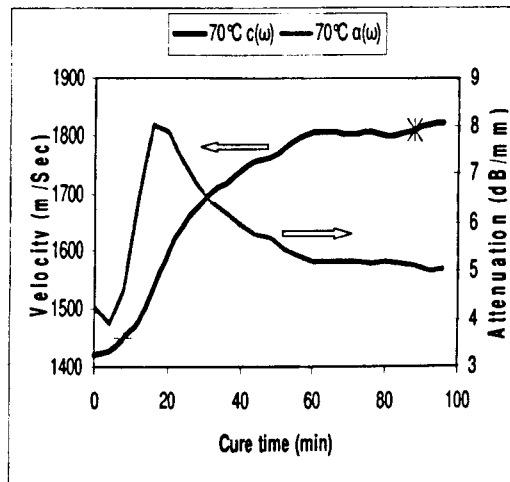
Figure 9.6 (a—e) Longitudinal velocity and attenuation at 5MHz as a function of cure time at cure temperatures of :(a) 30°C, (b) 40°C, (c) 50°C, (d) 60°C, and (e) 70°C.

In figure 9.6 (a—e) on the ultrasonic velocity curves, at the early stages of cure, the onset of velocity increase times (which here, most probably we predict as *gelation time (ultrasonic gelation time)*) are shown with ' **+**' symbol. In the later stages on the plateau regions on velocity curves the *vitrification (onset)* times obtained from DSC study utilizing the empirical autocatalytic model of Kamal have also been marked with ' **✕**' symbol correspondingly (i.e. on corresponding time).

The onset of gelation occurs during the sol-gel transition, which is a transition of connectivity. The gelation occurs through the growth of branched polymer units. As the reaction proceeds, the viscosity increases and diverges for a critical reaction extent at which an infinite cluster is formed and a static modulus appears. The increase of connectivity leads to a decrease in mobility and thus to an increase of the glass transition temperature.

Figure 9.6 (a—e) indicates that the time at which the ultrasonic longitudinal velocity rapidly starts increasing can be used to detect gelation for our studied epoxy resin system Araldite 2015. Close to this point, the significant increase of velocity is detected, which is due to the growing branched molecules presenting a considerable elastic response reflecting the build up of bulk and shear moduli. The times corresponding to the onset of velocity increase at cure temperatures of **30°C, 40°C, 50°C, 60°C, and 70°C** are **70, 40, 20, 12 and 6 minutes** respectively corresponding to a conversion of 0.32 irrespective of temperature (i.e. *iso-conversion* point).Very interestingly, this prediction of gel time, is in *fairly good agreement* with literature data reported by Xu et al [4] for almost similar epoxy-amine formulation. According to the data reported by Xu et al [4], the *rheological data* of gel time for stoichiometric ratio mixture DGEBA/DETA system (similar to our resin-hardener formulation but without reactive diluent modifier) at isothermal cure temperatures of **40°C, 50°C, 60°C, and 70°C** are **40.01, 19.83, 11.93 and 3.01 minutes** respectively.

As has already been discussed in chapter 5, according to Flory's theory of gelation, for our *difunctional* epoxy resin and *pentafunctional* aliphatic amine hardener in a stoichiometric ratio mixture, which react in *ideal* conditions, the *theoretical* gel point should achieved at a conversion of 0.5.

The difference between the theoretical and experimental value of the gel point conversion most possibly due to *various non-ideal reaction conditions*. In an *ideal* case, i.e. in absence of the *substitution effect*, the *reactivity ratio* $r_k = \dfrac{k_2}{k_1} = 1$ or, $k_1 = k_2$, where k_1 and k_2 are respectively the reaction rate constants of the primary amine and secondary amine hydrogens, and the gel point depends on this *ideal reactivity ratio*. In this case, the reaction rate constants are related to the hydrogen of the amino group. Basically, the reaction rate constants are related to the molecule and

$r_k = \dfrac{k_2}{k_1} = \dfrac{1}{2}$ or, $2k_2 = k_1$ i.e. $k_1 > k_2$, in an ideal case, because the primary amino

group contains two hydrogen atoms and hence, react about twice as fast as secondary amino group. Indeed, it was shown experimentally and theoretically that gel conversion depends on the magnitude of the *substitution effect*. When the primary amine hydrogens are much more reactive than the secondary amine hydrogens i.e. $k_1 \gg k_2$ (which is the usual case), gelation occurs of course at a conversion degree *higher* than that expected when equal reactivity of all amine hydrogens is assumed.

In chapter 6, based on Horie model, for our epoxy-amine system, we obtain $k_2 \gg k_1$, which implies that gelation will occur most possibly at a conversion degree *lower* than the expected ideal or theoretical value i.e. α =0.5.Our epoxy system contains *external catalyst* 2,4,6 - tris (dimethylaminomethyl) phenol and hence, it is likely that the catalyst had the effect of speeding up the cure reaction in the pre-gel state leading to a gelation time shorter than predicted ideally, as the effect of catalyst is not taken into account in Flory's equation. It has discussed in chapter 5 that most probably the reactive diluent has some catalytic effect on the conversion rate, which may also contribute to some extent leading to a shorter gel time.Our epoxy formulation consists of two difunctional epoxies and a difunctional aliphatic reactive diluent.The shift or displacement of critical conversion at gelation from the ideal value towards lower value also can occur due to the possible difference in reactivity between the same types of functional groups, and the possibility that the curing system may be affected by other non-ideal reaction conditions, such as the presence of higher polyfunctional impurities in the monomers.

Figure 9.7 illustrates the cross plots of ultrasonic longitudinal velocity and calorimetric conversion data measured by DSC observed at the same cure times. It can be seen that at the early stage of cure the velocity changes almost *linearly* with conversion, which holds for approximately $\alpha=0.32$. Above $\alpha=0.32$ chain entanglements become significant, causing a change in behaviour, consequently, the velocity changes at a continuously increasing rate with conversion until the fully achieved gelation. These data indicate that velocity is mainly sensitive to the increasing crosslink density occurring after gelation rather than to the number of reacted groups and a *non-linear* correlation between velocity and conversion is observed.
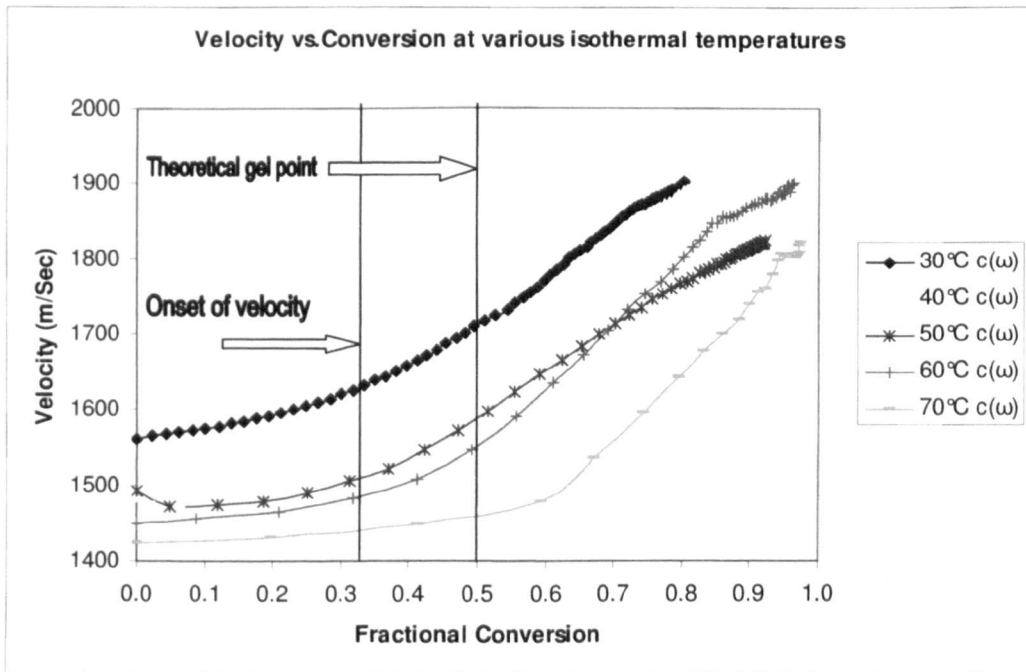
Figure 9.7 Ultrasonic Longitudinal velocity at 5MHz as a function of calorimetric conversion measured by DSC at cure temperatures of 30°C, 40°C, 50°C, 60°C, and 70°C.The theoretical gel point obtained from Flory's theory of gelation and the onset of ultrasonic velocity increase (ultrasonic prediction of gelation) corresponding to $\alpha=0.50$ and $\alpha=0.32$ respectively are also shown in the figure.

This prediction of gelation based on the velocity onset point where the longitudinal velocity starts to increase sharply is consistent with the results of other workers [3,5].This estimation of velocity onset time can be done by plotting the lines of initial slope and maximum slope on velocity curves in figure 9.6 (a—e) and taking the time of the intersection of these as the velocity onset.

In figure 9.6 (a—e) in the later stages on the plateau regions on velocity curves the *vitrification (onset)* times obtained from DSC study utilizing the empirical autocatalytic model of Kamal coupled with the introduction of *diffusion limitation* (associated with the values of *critical conversion* α_c) also been marked with ' ✕' symbol correspondingly (i.e. on corresponding time). From a general assumption of ultrasonic determination of vitrification we can estimate the vitrification time as the velocity offset time on velocity curve which can be estimated by plotting the lines of the final slope and maximum slope on velocity curves in figure 9.6 (a—e) and taking the time of the intersection of these as the velocity offset. Basically, these are the points on the velocity curves around the shoulder before the plateau or velocity saturation regions. It can be roughly predicted from figure 9.6 (a—e) that these points should appear to some extent earlier than the vitrification times (onset) estimated from the DSC data as mentioned.

9.7 Comparison of Activation Energies

Figure 9.8 shows the plots of the ln t_{gel} (ultrasonic prediction) versus 1/T and the corresponding equation and correlation coefficient of linear fit along with calculated activation energy value E_a = 52.798 kJ/mol. The excellent linear fit allow us to calculate this. As an Arrhenius expression did an excellent job of describing the data; this also shows that the *Arrhenius behaviour of the reaction could be followed by the ultrasonic technique.* This activation energy value calculated from the ultrasonic prediction of gelation time based on the onset of velocity increase time, is within the order of magnitude of the activation energy value E_{a2} = 59.184 kJ/mol for the autocatalytic kinetic constant k_2, obtained from Horie model (discussed details in chapter 6) and *it is related to the crosslinking reaction.* The activation energy value based on ultrasonic prediction of gelation also agrees well with the activation energy

355

value obtained from theoretical gel time based on the calorimetric study $E_{agel\,(theoretical)}$ = 53.435 kJ/mol (discussed in chapter 5).
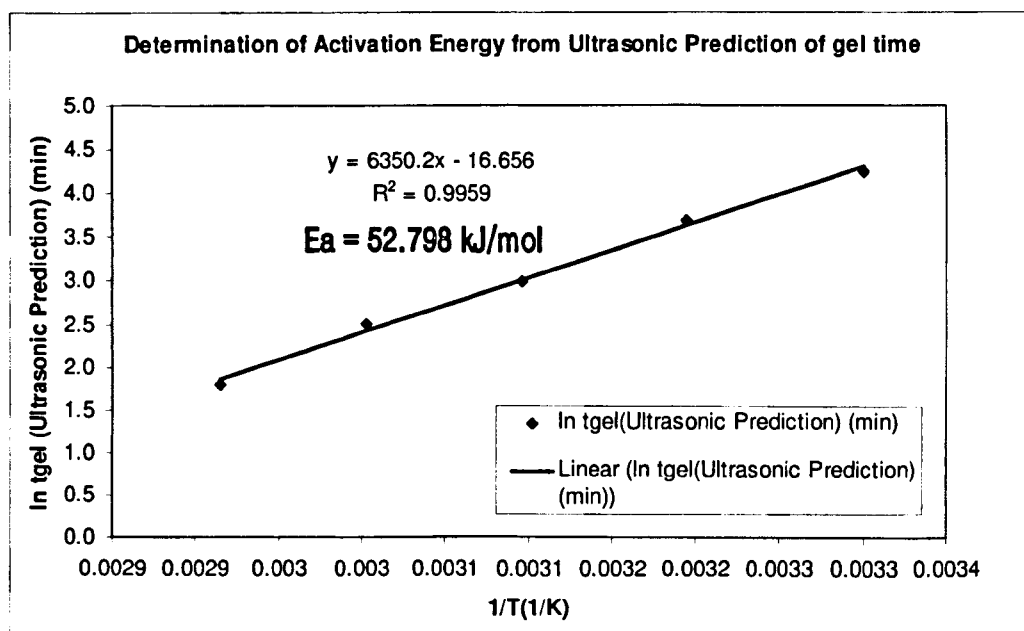
Figure 9.8 Plots of ultrasonic prediction of gel time obtained from the observation of onset of ultrasonic longitudinal velocity (at 5MHz) increase as a function of the reciprocal of the absolute cure temperature. The corresponding equation and correlation coefficient of linear fit along with calculated activation energy value are also presented in the figure.

Comparison of activation energies from ultrasonic prediction of gel time measurements can be made with activation energies from *enthalpic measurements*, since ideally conversion is determined by the fraction of functional groups reacted for both. However, the slight difference in activation energy value may simply imply that the two measurements do not reflect the same phenomena.

Each technique measures a different property of the system. So, they are sensitive to very different things. The gel time represents a change in *physical state* (*domain formation*) through *sol-gel transition*. Ultrasound monitors the *physical and mechanical* properties of the material. As the mechanical properties of the polymer are greatly changed on crosslinking, reasonably it can be assumed that the changes in velocity/modulus are more affected by the crosslinking reaction. The calorimetry represents a chemical *reaction*/cure reaction (epoxy/oxirane ring-amine-hydroxyl

356

groups) based on the *heat of reaction*. Basically, ultrasonic technique is sensitive to *elastically effective physical and chemical crossslinks* associated with elastically effective degree of crosslinking and *mechanical fractional conversion*, while differential scanning calorimetry technique is able to detect *chemically effective crossslinks* associated with *chemical fractional conversion*. Clearly the two phenomena occur at different time during cure.

9.8 Longitudinal storage modulus and Loss factor

Longitudinal storage modulus and loss tangent calculated from longitudinal wave velocity and attenuation data at 5MHz as a function of cure time at cure temperatures of :(a) 30°C, (b) 40°C, (c) 50°C, (d) 60°C, and (e) 70°C are shown in Figure 9.9 (a—e).

The changes of storage modulus and loss tangent as a function of cure time cannot be easily interpreted due to their complex nature arising from the combination of bulk and shear moduli. As previously discussed in the section associated with development of moduli, we already have explained that both the evolving bulk and shear moduli are related to the degree of molecular cross-linking. Which modulus will undergo the largest percentage increase depends on the adhesive type and cure condition.

The time dependence of storage modulus follows the same trend like the velocity in figure 9.1. The limited changes of storage modulus observed at the beginning of the cure process may be associated with a slight increase of bulk modulus in the liquid resin while the shear modulus gives a significant contribution to the storage modulus only when a rubbery gel is formed. The time dependence of loss tangent follows almost the same trend like the attenuation in figure 9.2. The maximum of the loss tangent peak is slightly delayed with respect to the attenuation peak (data will be reported later). Figures 9.9(a—e) and 9.6 (a—e) can be compared easily as they follow almost the same behaviour as functions of cure time.
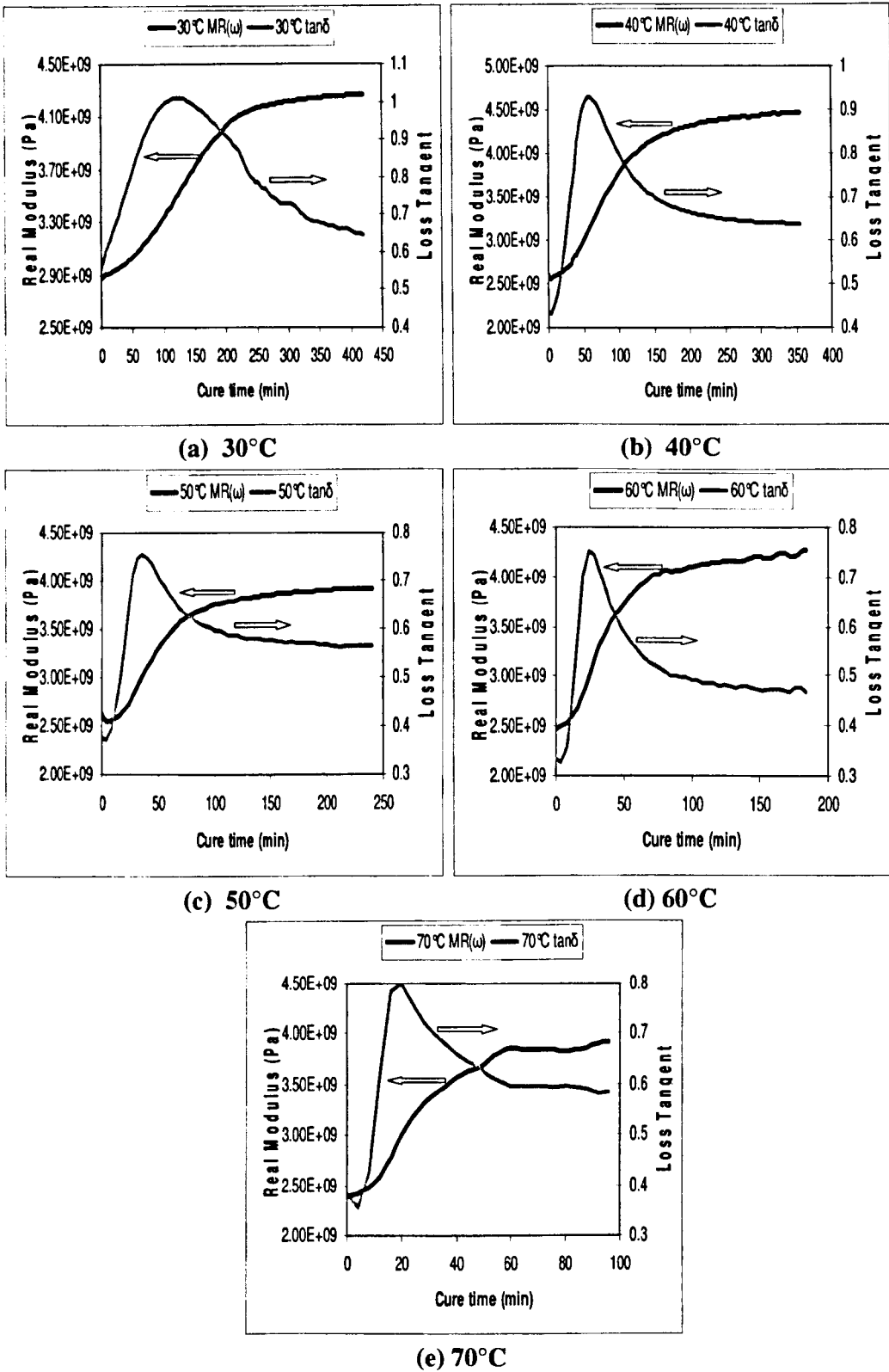
Figure 9.9 (a–e) Longitudinal storage modulus and loss tangent at 5MHz as a function of cure time at cure temperatures of :(a) 30°C, (b) 40°C, (c) 50°C, (d) 60°C, and (e) 70°C.

9.9 Effect of cure temperature upon time to various ultrasonic cure events

To show the sensitivity of the ultrasonic technique to changes in the reaction rate brought about by changes in the cure temperature, the time to various features on the cure curves is plotted as a function of cure temperature as depicted in figure 9.10. The events chosen are —

the onset of compression wave velocity increase [t-c(ω)onset(UT tgel)], the final value of the compression wave velocity [t-c(ω)final], the compression wave attenuation peak [t-α(ω)peak], the compression wave loss tangent peak [t-tanδ(ω)peak], the imaginary part of the compression wave modulus (loss modulus)peak [t-MI(ω)peak].
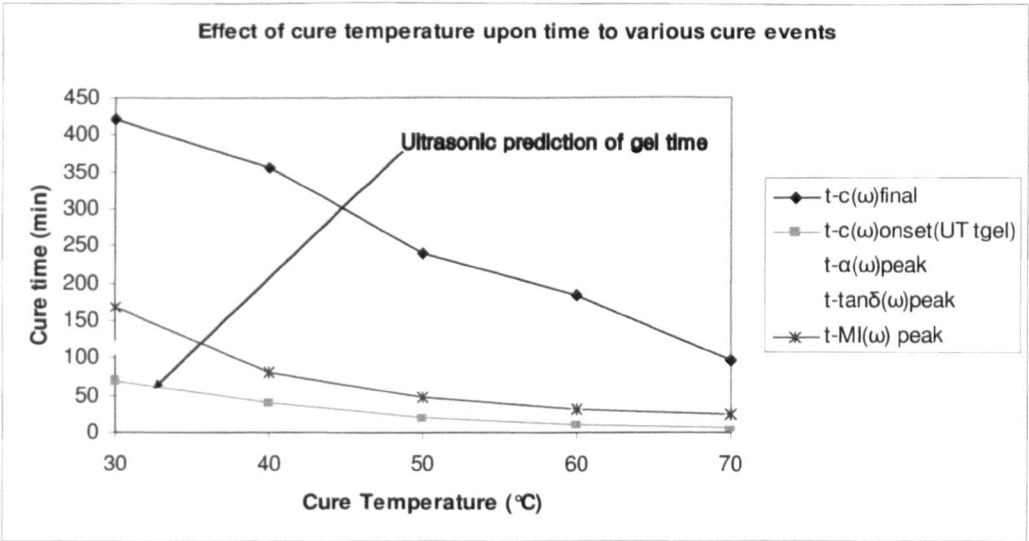
Figure 9.10 The effect of cure temperature upon time to various cure events based on Ultrasonic frequency at 5MHz.The events shown are — the onset of compression wave velocity increase [t-c(ω)onset(UT tgel)], the final value of the compression wave velocity [t-c(ω)final], the compression wave attenuation peak [t-α(ω)peak], the compression wave loss tangent peak [t-tanδ(ω)peak], the imaginary part of the compression wave modulus (loss modulus)peak [t-MI(ω)peak]. All of the curves show a decrease in gradient as the cure temperature is increased.

The above mentioned events along with theoretical gel time obtained from DSC study with corresponding time and temperature are listed in table 9.2.

Table 9.2 Theoretical gel time obtained from calorimetric study (where critical conversion at gelation was calculated from Flory's theory of gelation for the resin system) along with the characteristic time of ultrasonic attenuation peak, loss tangent peak, imaginary modulus peak , the onset of longitudinal velocity increase and the final value of the compression wave velocity all based on 5MHz ultrasonic frequency obtained at different isothermal cure temperatures for isothermal cure process of Araldite 2015 are presented.

T_{cure} (°C)	30	40	50	60	70
$t_{gel\ DSC\ (theoretical)}$ (min)	117.66	67.10	34.62	19.29	10.14
$t_{attenuation\ peak\ (5MHz)}$ (min)	112	54	34	24	18
$t_{loss\ tangent\ (tan\delta)\ peak\ (5MHz)}$ (min)	120	58	36	24	19
$t_{onset\ of\ velocity\ increase\ (5MHz)}$ $\equiv t_{gel\ Ultrasonic}$ (min)	70	40	20	12	6
$t_{imaginary\ modulus\ peak\ (5MHz)}$ (min)	168	80	48	32	24
$t_{final\ velocity\ (5MHz)}$ (min)	420	356	240	184	97

Figure 9.10 shows the effect of curing temperature upon time to the various cure events. It can be seen that they all follow the same general trend — *a decrease in the gradient of the curve as the cure temperature is increased.* This implies that higher cure temperatures increase the reaction rate.

The curve associated with the time of onset of compression wave velocity increase [t-c(ω)onset(UT tgel)], which we predicted as ultrasonic gel time curve, is indicated in figure 9.10 with an arrow. Reducing the cure temperature decreases the rate of reaction and the gel point is shifted on the time axis. The *percent of crosslink connections in the gel point is a material property* and is not affected by temperature. Therefore a shift of the gel point on the time axis characterizes *quantitatively* the variation in the reaction rate as a function of the temperature.

In connection with the previous discussions in this chapter associated with the effect of temperature on the above mentioned cure events, the following principal conclusions can be made:

1. Higher cure temperatures cause an increase in the rate of reaction.

2. Time taken to complete cure is reduced at higher cure temperatures.

3. Time taken to reach gelation is reduced at higher cure temperatures.

4. Conformational changes take place over a shorter time period at higher cure temperatures.

5. Changes in the cure cycle and the resulting changes in the physical and mechanical properties caused by changes in the different cure temperatures are well within the detection capability of the ultrasonic technique employed.

6. Events 1, 2, 3 are well agreed by DSC data. Basically, by monitoring the polymerization reactions at different temperatures, the *Arrhenius behaviour of the crosslinking reaction is confirmed* by both ultrasonic and DSC data.

Thus, the ability of both the ultrasound and DSC techniques to detect the effects of changing cure temperature upon the cure cycle have been demonstrated. The ultrasonic results agree well with those found previously by other authors [1,2,3,5] and suggest that ultrasonic technique is sensitive to changes in the cure temperature. It is important to note that these effects observed in ultrasonic studies are quite marked for relatively small differences in cure temperature. Therefore, ultrasound could be used to detect changes in cure behaviour due, for example, to temperature fluctuations in an autoclave.

9.10 Effect of frequency on velocity and attenuation

Figure 9.11 shows ultrasonic compression wave (a) velocity and (b) attenuation at frequencies of 3.75MHz, 5MHz and 8.75MHz as a function of cure time for Araldite 2015 at cure temperature of 50°C.
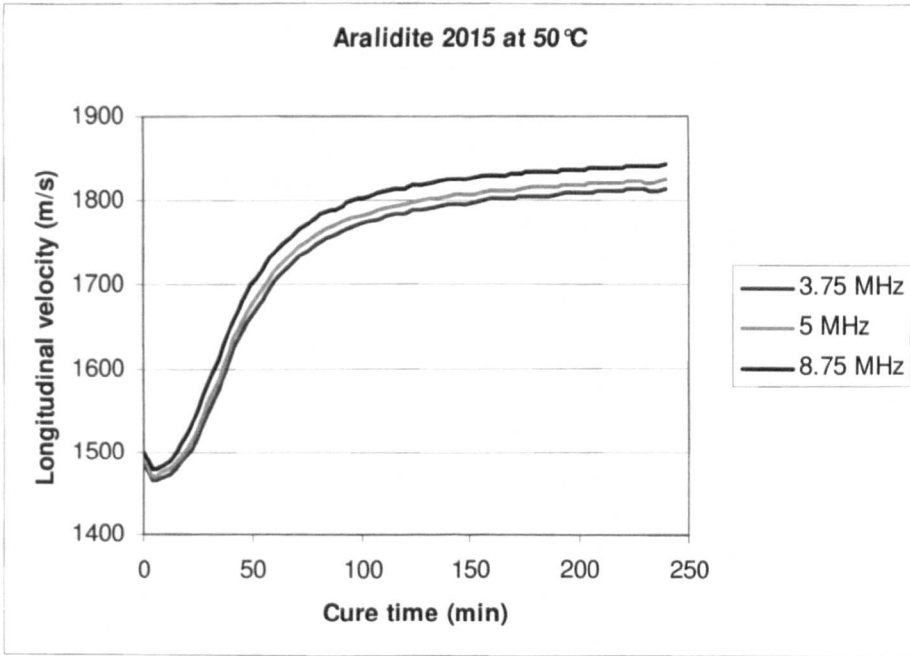
(a)
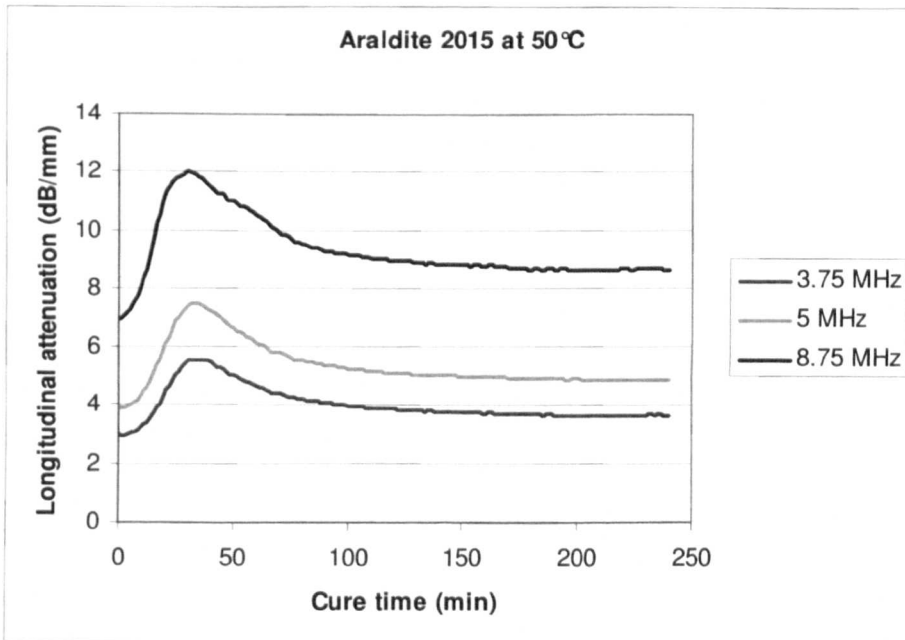
(b)

Figure 9.11 Ultrasonic compression wave **(a)** velocity and **(b)** attenuation at frequencies of 3.75MHz, 5MHz and 8.75MHz as a function of cure time at cure temperature of 50°C.

It can be seen from the figure that as stated before, ultrasonic velocity changes with time according to an S-shaped curve. It is moderately dependent on the frequency and increases moderately with increasing frequency (i.e.moderate velocity dispersion). Attenuation is highly dependent on frequency and increases to higher values with increasing frequency. It can be seen that there is no observable shift of the attenuation maximum on the time scale due to changes in frequency (in the frequency range under study).

These results lead to an important practical conclusion that in the frequency range 1-14 MHz there is no observable effect of the frequency of ultrasonic measurements on kinetic curves such as the dependence of velocity and attenuation on cure time. Hence, the selection of frequency may be dictated by experimental convenience. As a general behaviour can be observed in all frequencies, it is logical to use a single frequency component to represent the observed changes. As mentioned before, for both compression wave phase velocity and attenuation we have chosen a fixed frequency 5 MHz to illustrate the curing behaviour at various isothermal temperatures. Experimental evidence shows that 5MHz ultrasound sensitive throughout the cure process.

9.11 Frequency dependent velocity and attenuation

Figures 9.12 and 9.13 illustrate ultrasonic compression wave phase velocity and attenuation coefficient respectively as a function of frequency for different time stages (in minutes) during the cure reaction of Araldite 2015 at cure temperature of 50°C. These results are typical. It can be seen that the general trend is for the velocity to increase (shown by an arrow in the figure 9.12) during cure as the modulus of the adhesive increases. The trend is for the slope of the attenuation to reduce (shown by an arrow in the figure 9.13) during cure. Therefore, we see that both frequency dependent velocity and attenuation has the potential to track the cure process.

It can be seen that the attenuation appears to nearly increase linearly with frequency at all stages of the cure reaction from viscous liquid to solid state with no suggestion of relaxation peaks.
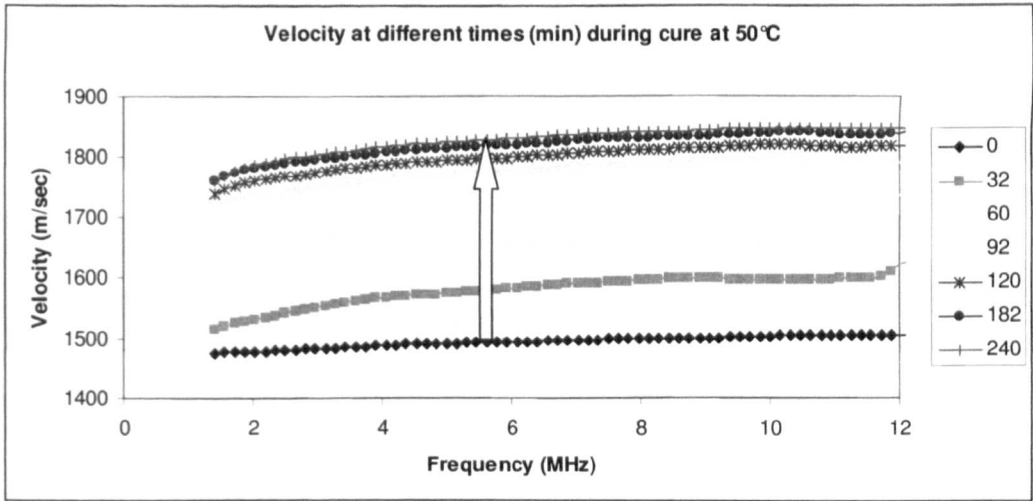
Figure 9.12 Ultrasonic compression wave phase velocity as a function of frequency for different time stages (in minutes) during the cure reaction of Araldite 2015 at cure temperature of 50°C.
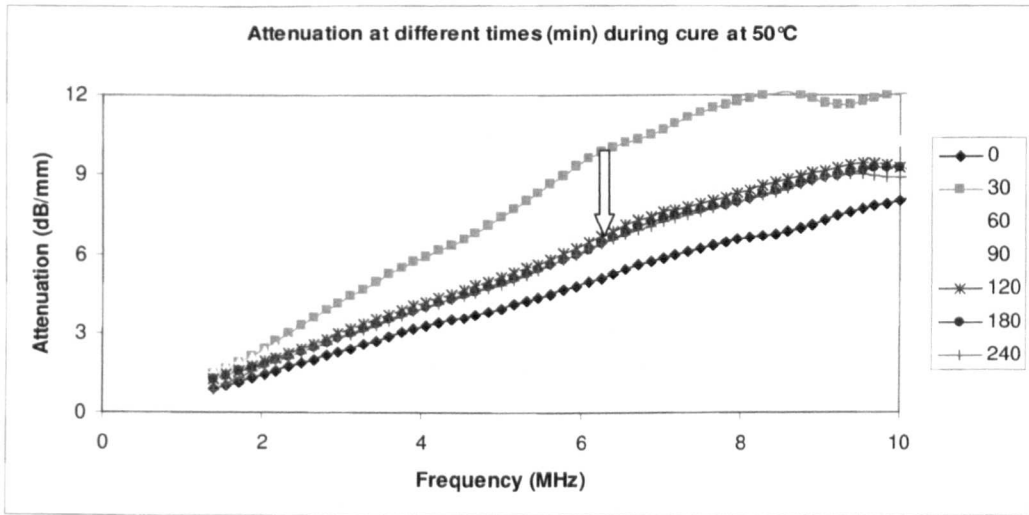

Figure 9.13 Ultrasonic compression wave attenuation coefficient as a function of frequency for different time stages (in minutes) during the cure reaction of Araldite 2015 at cure temperature of 50°C.

This linear behaviour of attenuation versus frequency suggests that the attenuation effect cannot be explained by classical viscothermal absorption or relaxation theory. More comprehensive relaxation theories which use continuous or discrete *distribution of relaxation times*, also have difficulties in describing experimental data for strongly viscous liquids. Such type of behaviour was found previously for some highly viscous liquids, for solid polymers and for biological tissue. In this context, it is worth mentioning that in chapter 7, almost at the end, under the heading *"validity of distribution of relaxation times—a critic"* a critical discussion is presented, which can shed some light regarding its applicability in explaining the anomalous behaviour of sound attenuation.

9.12 Effect of frequency on loss tangent

Figure 9.14 shows ultrasonic compression wave loss tangent at frequencies of 2.5MHz and 5MHz as a function of cure time during the cure reaction of Araldite 2015 at cure temperature of 40°C. From this figure we see a fairly observable shift of the loss tangent peak on the time scale due to changes of frequency (in the frequency range under study). From this data we can calculate what we have termed a *central relaxation frequency* corresponding to the peak in the data. This relaxation can then be tracked during the cure and we can see a gradual increase of relaxation time as the molecular structure develops during the cure process.

Suppose, a loss tangent at f MHz frequency. Corresponding to the peak in the loss tangent we get *central relaxation time* $\tau = \dfrac{1}{2\pi f}$ at time t. From values of the loss tangent at different frequencies, relaxation times can be calculated corresponding to cure time and then the calculated values of τ are plotted against the cure time. Thus, the relaxation times corresponding to the peaks in loss tangent for a range of frequencies.

Figure 9.15 shows ultrasonic relaxation times as a function of cure time during the cure reaction of Araldite 2015 at cure temperature of 50°C. The change in relaxation time during cure is clearly seen. A gradual increase of relaxation time is noticeable as

the molecular structure develops during the cure process. As discussed before, ultrasonic loss tangent sensitive to progress of the cure reaction. Also it can provide information about relaxation and micro-structural properties. The development of the
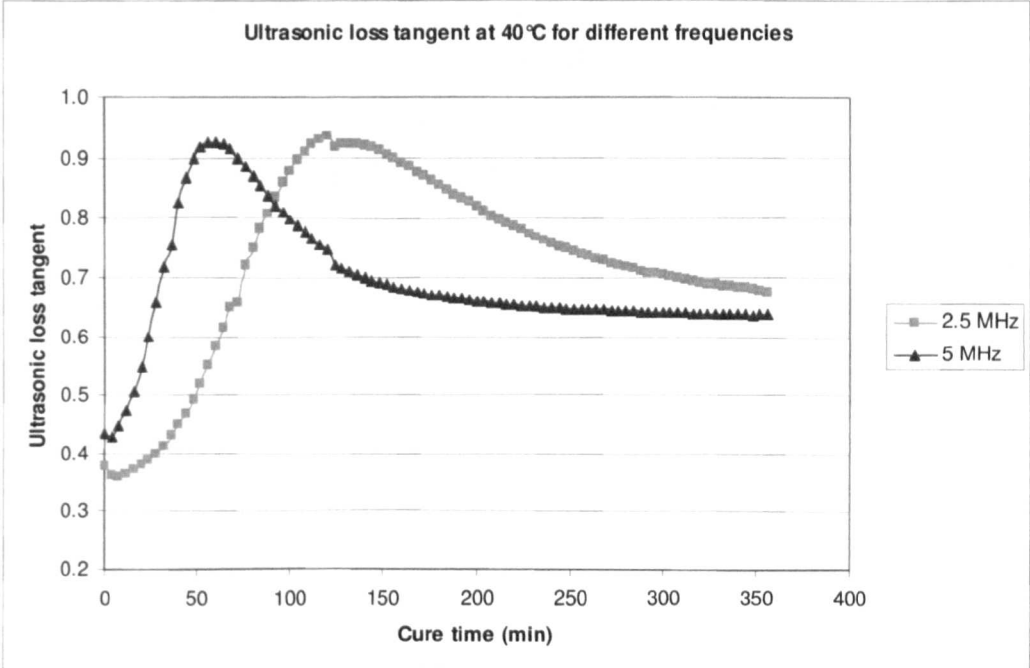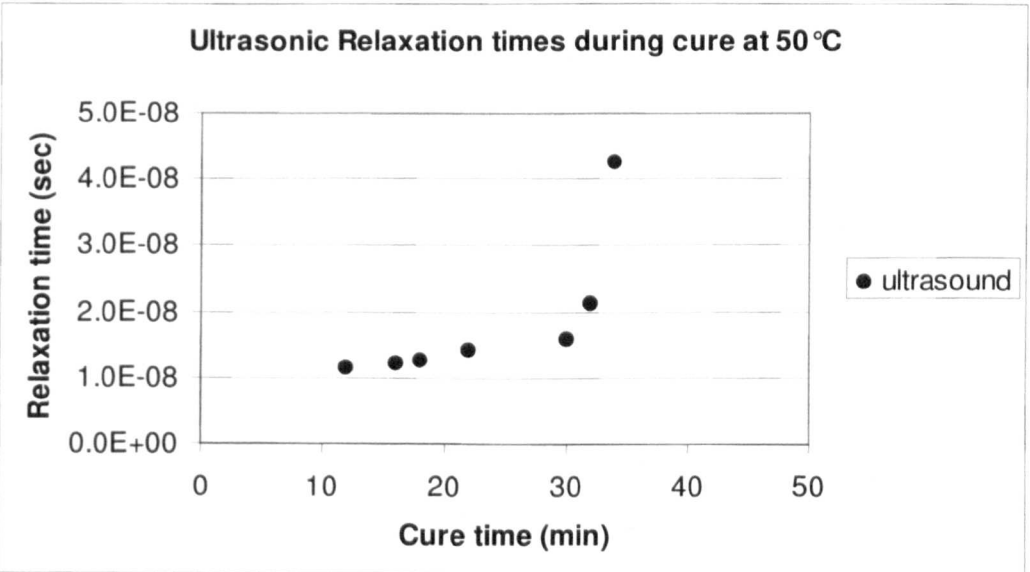

Figure 9.14 Ultrasonic compression wave loss tangent at frequencies of 2.5MHz and 5MHz as a function of cure time during the cure reaction of Araldite 2015 at cure temperature of 40°C.

Figure 9.15 Ultrasonic relaxation times as a function of cure time during the cure reaction of Araldite 2015 at cure temperature of 50°C.

central relaxation time of the thermoset during the cure process is a useful measure of the progress of the structural development. In the early stages of the cure process this relaxation time is relatively small corresponding to the small molecules of the resin and hardener. As cure proceeds and the polymer chains form, branching and crosslinking occur, the relaxation time increases by several orders of magnitude to a value in seconds at the end of cure. However, due to the somewhat limited bandwidth of the ultrasonic technique only a *snap shot* of this process can be seen.

9.13 Correlation between Ultrasonic Velocity and Calorimetric Conversion

The ultrasound velocity is directly related to both elastic modulus and density. In epoxies, the ultrasound velocity changes as they harden. Thus, ultrasonic velocity measurements, which denotes *ultrasonic cure index*, can be correlated to the degree of curing. It is worth to notice that the evolution of ultrasonic compression wave velocity $c(t)$ and the calorimetric conversion α at similar isothermal temperature almost follow the same pattern as shown in figure 9.1 and figure 5.1(chapter 5) — an initial dramatic increase in rate, then both $c(t)$ and α orient to a stationary state. The first stage of the reaction is characterized by an acceleration followed by a de-acceleration.

From close inspection it can be observed that the time course of the calorimetric conversion curves as observed by differential scanning calorimetry is akin to those of the velocity profiles, but not identical. It generally appears that the calorimetric conversion curve leads the compression wave velocity curves roughly by some amount of time shift.

However, in an effort to draw correlations between the ultrasonic and DSC data sets, at *first instance*, we *normalized* the compression wave velocity values using the following equation which characterizes the cure state:

$$c_{Normalized}(t) = \frac{c(t) - c_{initial}}{c_{final} - c_{initial}} \qquad (9.2)$$

In equation (9.2), $c_{Normalized}(t)$ is the normalized velocity as a function of time, $c(t)$ is the velocity value as a function of time, $c_{initial}$ is the initial value of the velocity, and c_{final} is the final value of the velocity.
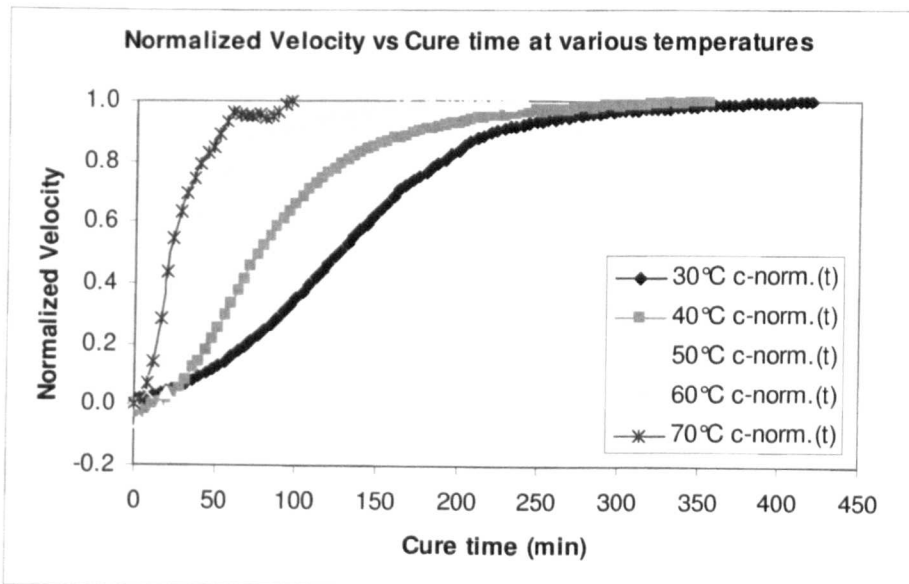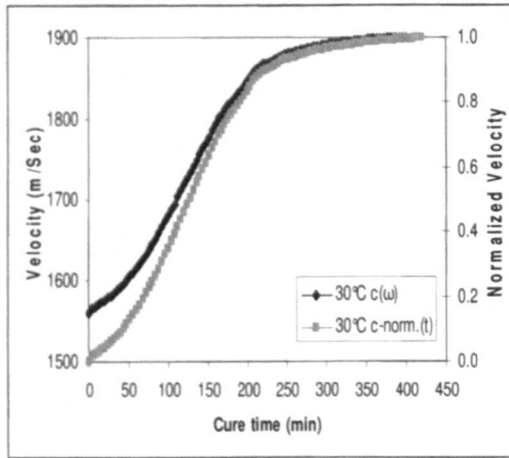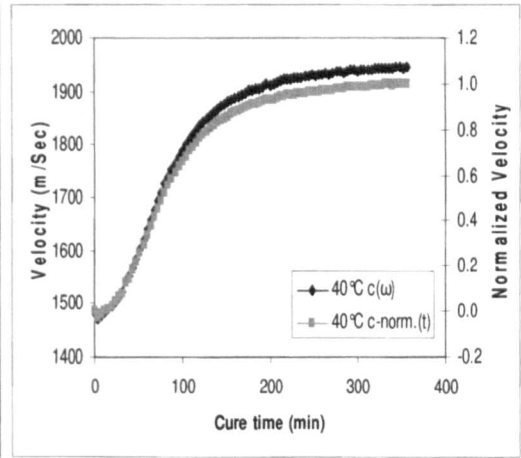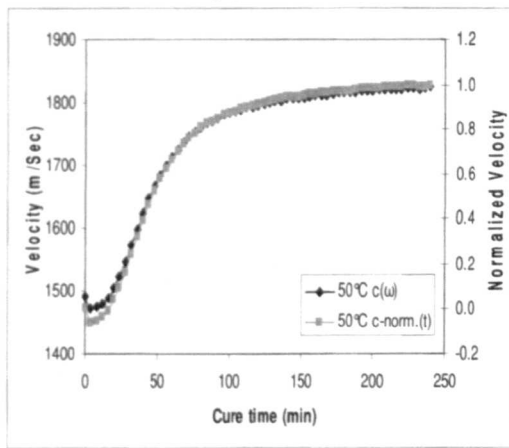
Figure 9.16 shows the evolution of the Normalized values of ultrasonic longitudinal velocities at 5MHz as a function of cure time at cure temperatures of 30°C, 40°C, 50°C, 60°C, and 70°C for the isothermal cure process of Araldite 2015. It clearly indicates *excellent sensitivity* to the state of cure in all cases of the isothermal temperatures employed in the test. We can see that as the curing progresses, *the normalized velocity values increase in magnitude until approaching unity*. The data also show that as the cure temperature increases, the rate of increase in the normalized velocity values, and thus the rate of cure increases. It is interesting to mention that all the normalized velocity curves are sigmoidal in shape where a change in curvature occur at the early stages of the cure. Basically, the point of curvature change corresponds to the velocity onset time which we predicted as gelation. Referring to the isothermal DSC conversion curves in figure 5.1 in chapter 5, it is worth mentioning that it appears that the DSC is insensitive to this phenomenon.

Figure 9.16 The Normalized values of ultrasonic longitudinal velocities at 5MHz as a function of cure time at cure temperatures of 30°C, 40°C, 50°C, 60°C, and 70°C for the isothermal cure of Araldite 2015.
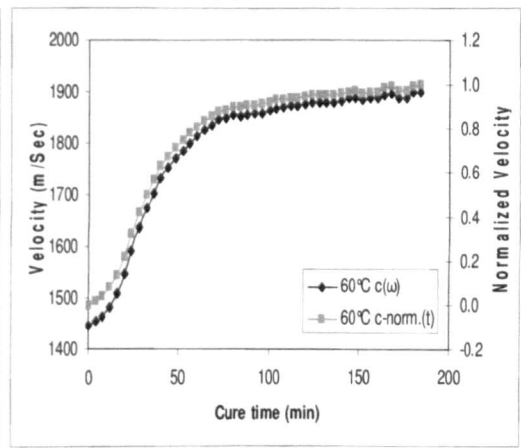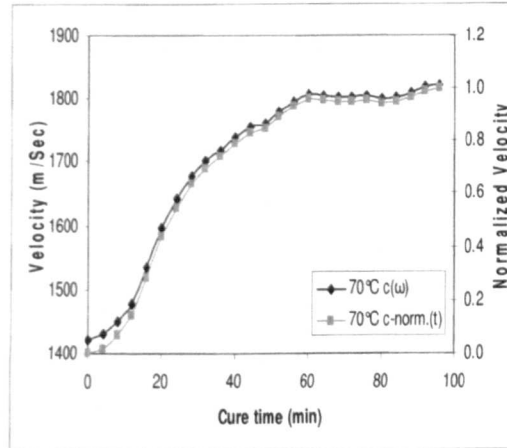
Figure 9.17 (a—e) The ultrasonic longitudinal velocities at 5MHz are compared with their Normalized values as a function of cure time at cure temperatures of : (a) 30°C, (b) 40°C, (c) 50°C, (d) 60°C, and (e) 70°C for the isothermal cure of Araldite 2015.

The ultrasonic longitudinal velocities at 5MHz reported in figure 9.1 are compared in Figure 9.17 (a—e) with their normalized values as a function of cure time at cure temperatures of : (a) 30°C, (b) 40°C, (c) 50°C, (d) 60°C, and (e) 70°C for the isothermal cure of Araldite 2015. From the figure it is evident that the normalized velocity curves almost superimposed on the original velocity curves indicating *similar sigmoidal shape with a linear correlation.*

It has already been mentioned that it generally appears that the calorimetric conversion curve leads the compression wave velocity curves roughly by some amount of time shift. To illustrate this, in the **second instance**, the normalized velocity curves (having final amplitude of unity) as a function of cure time are scaled to match the final amplitude of the calorimetric conversion curves using the following equation:

$$c_{Normalized}(t) = \frac{c(t) - c_{initial}}{c_{final} - c_{initial}} \alpha_{max}$$

(9.3)

Where, α_{max} denotes the final or maximum value of the calorimetric conversion.

The existing time lag between the DSC calorimetric conversion curves and ultrasonic normalized velocity curves imply that the two measurements do not reflect the same phenomena. As narrated before, each technique measures a different property of the system and are sensitive to very different things. Ultrasound monitors the *physical and mechanical* properties of the material. The calorimetry represents a chemical *reaction* (epoxy/oxirane ring-amine-hydroxyl groups) based on the *heat of reaction.* Basically, ultrasonic technique is sensitive to *elastically effective physical and chemical crosssslinks* associated with elastically effective degree of crosslinking and *mechanical fractional conversion*, while differential scanning calorimetry technique is able to detect *chemically effective crosssslinks* associated with *chemical fractional conversion*. Clearly the two phenomena occur at different time during cure.

However, further effort to draw correlations between ultrasonic and DSC data is based on this *time lag* factor. To investigate the comparison further, all of the

370

normalized velocity curves were advanced in time by an *optimum* amount which would render the *velocity curve to superimpose on the conversion curve best possibly* or *optimally* removing the existing time lag between them. The choice of the optimum applied time shift has been made entirely on a trial and error basis. In this case, the updated normalized equation becomes:

$$c_{Normalized}(t) = \frac{c(t - t_{lag}) - c_{initial}}{c_{final} - c_{initial}} \alpha_{max}$$ (9.4)

Where, t_{lag} is the applied time shift on the normalized velocity curve.

Figures **9.18–9.22(a–c)** very clearly demonstrates this correlation between ultrasonic and DSC data for the cure temperature of **30°C ,40°C, 50°C ,60°C, and 70°C** . Each figure includes the previously discussed *three* steps of this correlation procedure corresponding to equations **(9.2)–(9.4)**. The three steps are: **(a)**Normalized ultrasonic longitudinal velocity at 5MHz [corresponding to equation **(9.2)**] and calorimetric conversion as a function of cure time, **(b)** The normalized velocity profile as a function of cure time has been scaled to match the final amplitude of the calorimetric conversion profile[corresponding to equation **(9.3)**], **(c)** The normalized velocity profile has advanced in time by an applied time shift to remove the time lag[corresponding to equation **(9.4)**].

It will be clear from the figure that the shifted velocity curves optimally superimposed on the DSC curves at all the five temperatures indicating that for our particular epoxy thermosetting system Araldite 2015, the normalized ultrasonic longitudinal wave velocity data shows an excellent agreement with DSC conversion data for all of the five temperatures (30°C ,40°C, 50°C ,60°C, and 70°C) employed in the test showing excellent quantitative correlation between ultrasonic longitudinal velocity data and calorimetric conversion data. However, this quantitative correlation is system specific.
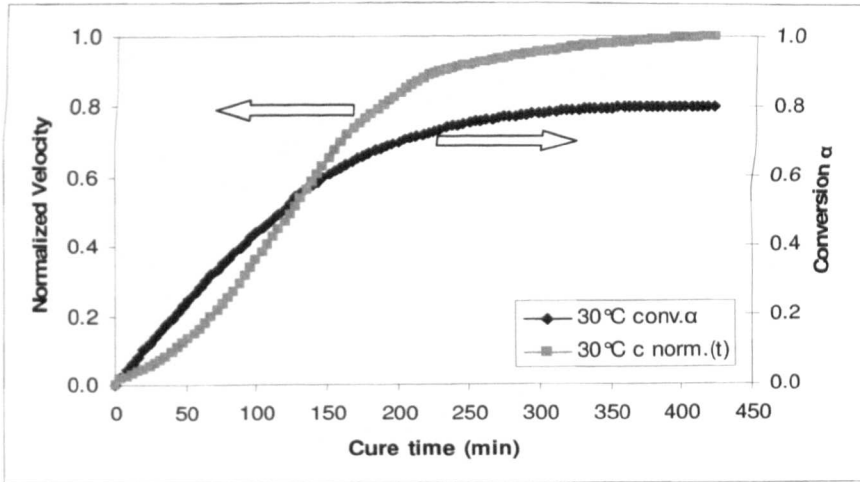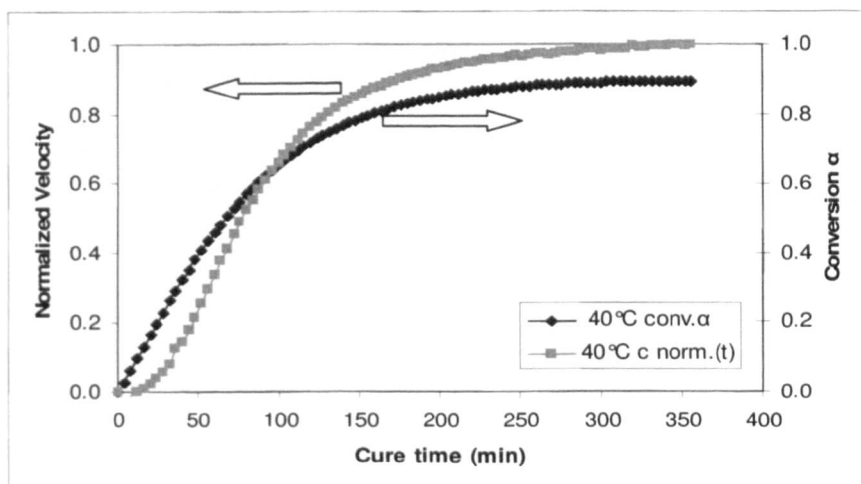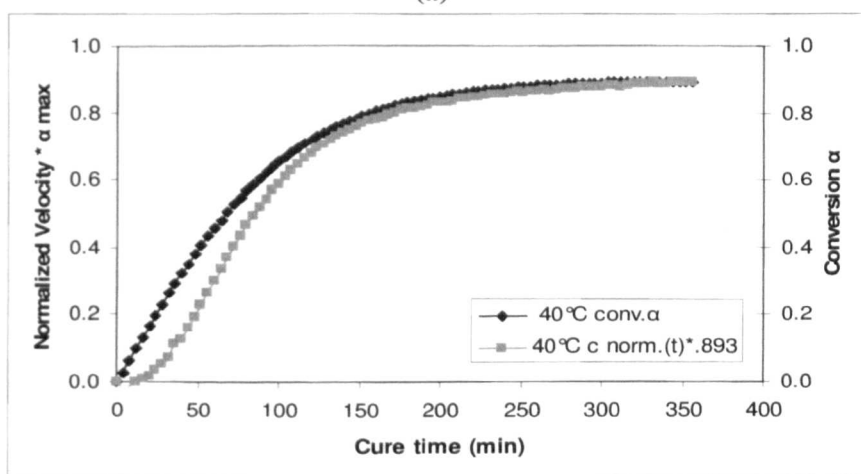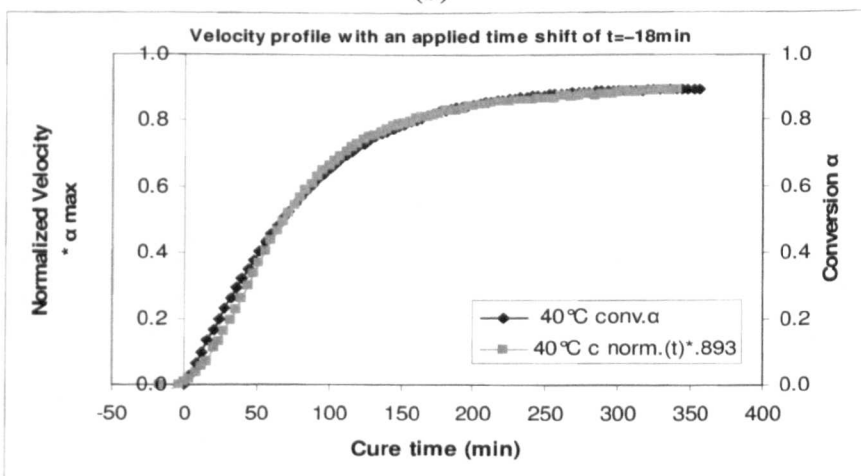
(a)
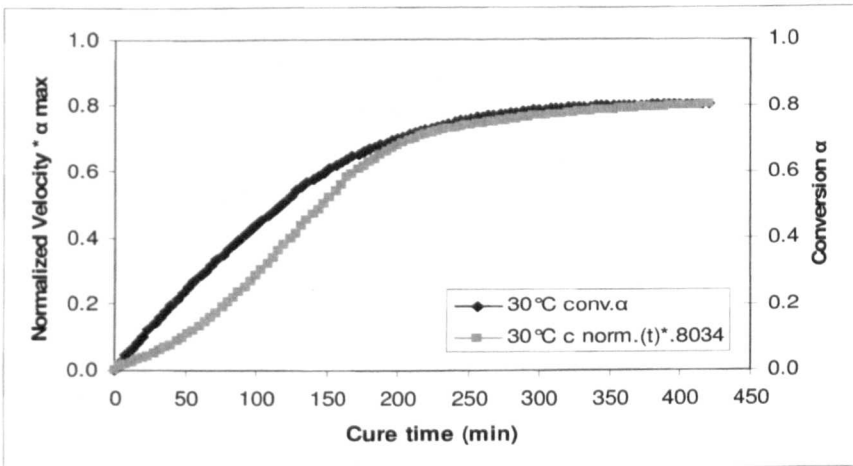
(b)
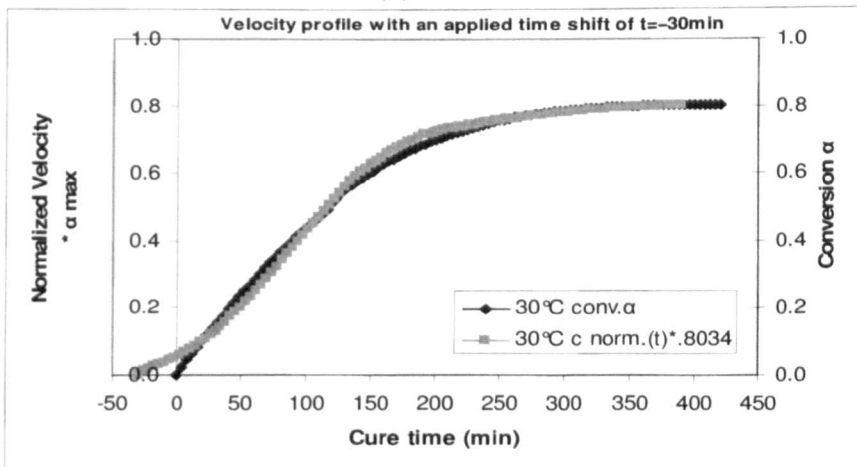
(c)

Figure 9.18 (a–c) (a) Normalized ultrasonic longitudinal velocity at 5MHz and calorimetric conversion as a function of cure time at 30°C, **(b)** The normalized velocity profile as a function of cure time has been scaled to match the final amplitude of the calorimetric conversion profile, **(c)** The normalized velocity profile has advanced in time by an applied time shift of t=– 30 min to remove the time lag.
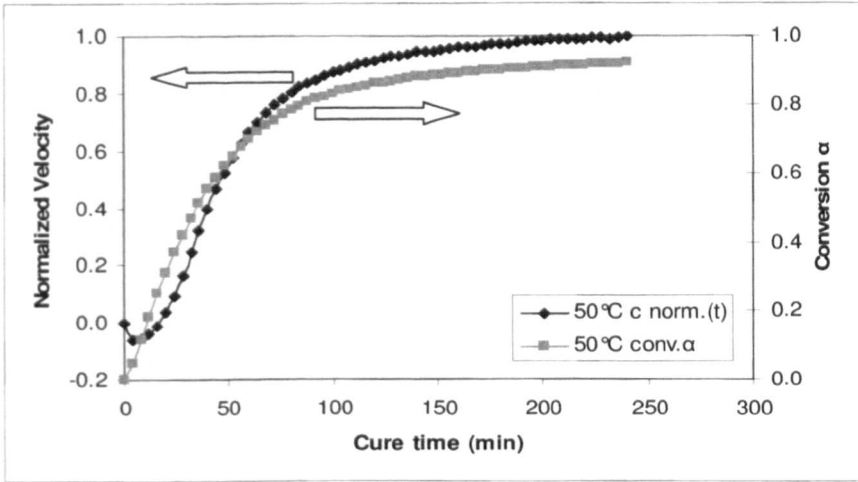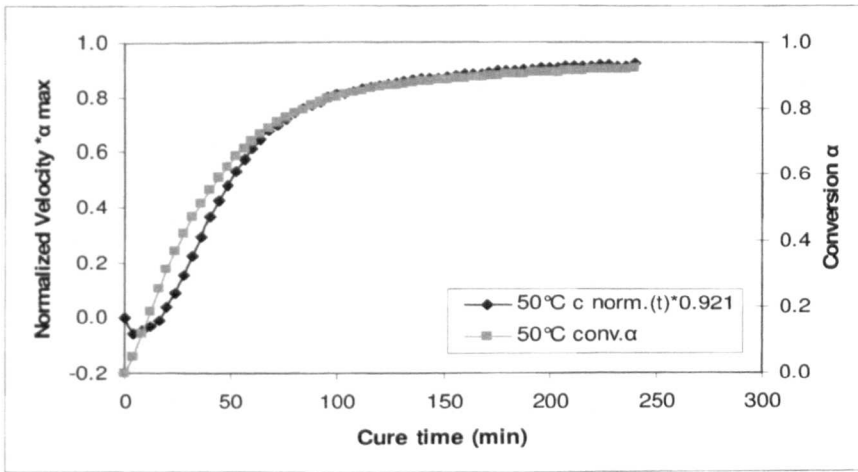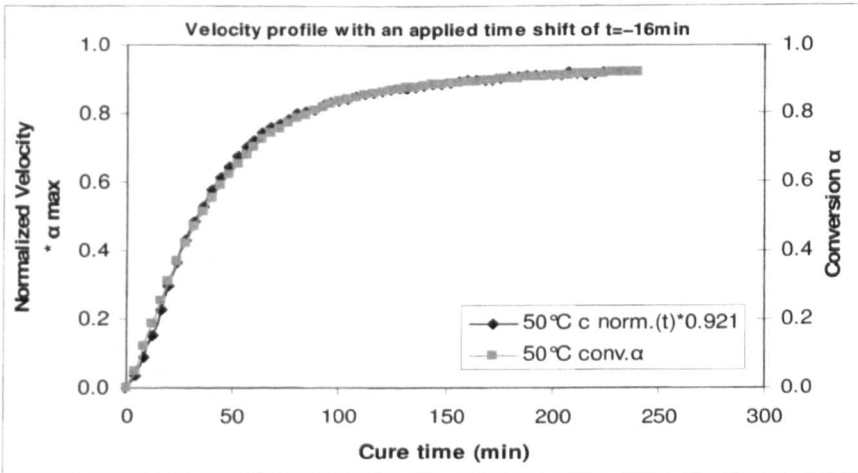
(a)

(b)

(c)

Figure 9.19 (a—c) (a) Normalized ultrasonic longitudinal velocity at 5MHz and calorimetric conversion as a function of cure time at 40°C, **(b)** The normalized velocity profile as a function of cure time has been scaled to match the final amplitude of the calorimetric conversion profile, **(c)** The normalized velocity profile has advanced in time by an applied time shift of t=− 18 min to remove the time lag.
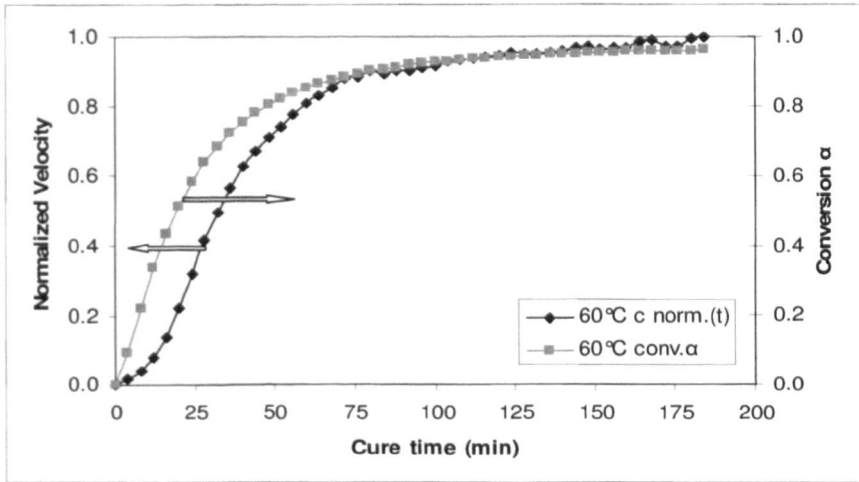
373

(a)

(b)

(c)

Figure 9.20 (a—c) (a)Normalized ultrasonic longitudinal velocity at 5MHz and calorimetric conversion as a function of cure time at 50°C, **(b)** The normalized velocity profile as a function of cure time has been scaled to match the final amplitude of the calorimetric conversion profile, **(c)** The normalized velocity profile has advanced in time by an applied time shift of t=− 16 min to remove the time lag.
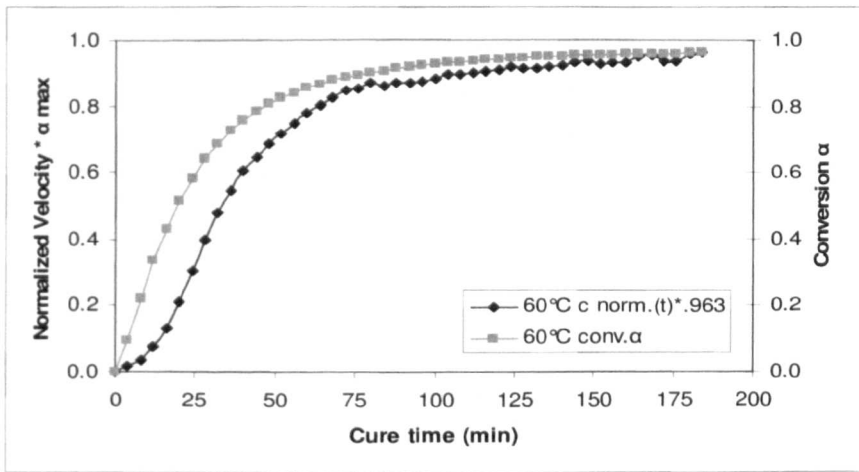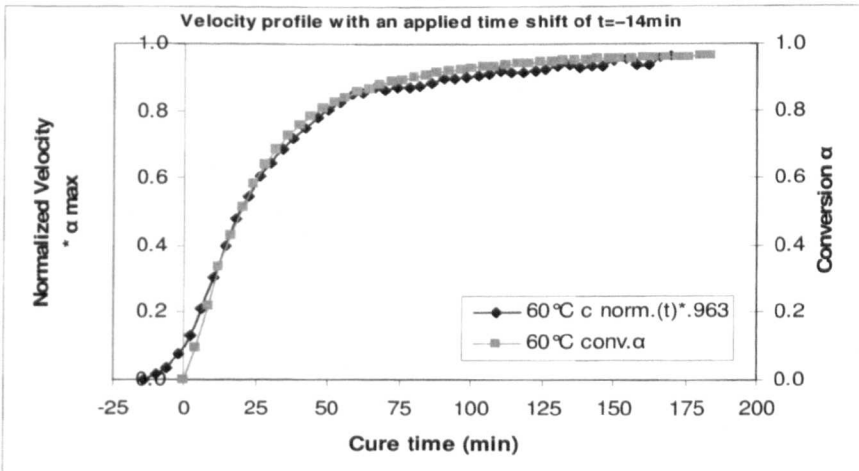
Figure 9.21 (a—c) (a)Normalized ultrasonic longitudinal velocity at 5MHz and calorimetric conversion as a function of cure time at 60°C, **(b)** The normalized velocity profile as a function of cure time has been scaled to match the final amplitude of the calorimetric conversion profile, **(c)** The normalized velocity profile has advanced in time by an applied time shift of t=−14 min to remove the time lag.

(a)

(b)

(c)

Figure 9.22 (a–c) (a) Normalized ultrasonic longitudinal velocity at 5MHz and calorimetric conversion as a function of cure time at 70°C, **(b)** The normalized velocity profile as a function of cure time has been scaled to match the final amplitude of the calorimetric conversion profile, **(c)** The normalized velocity profile has advanced in time by an applied time shift of t=−12 min to remove the time lag.
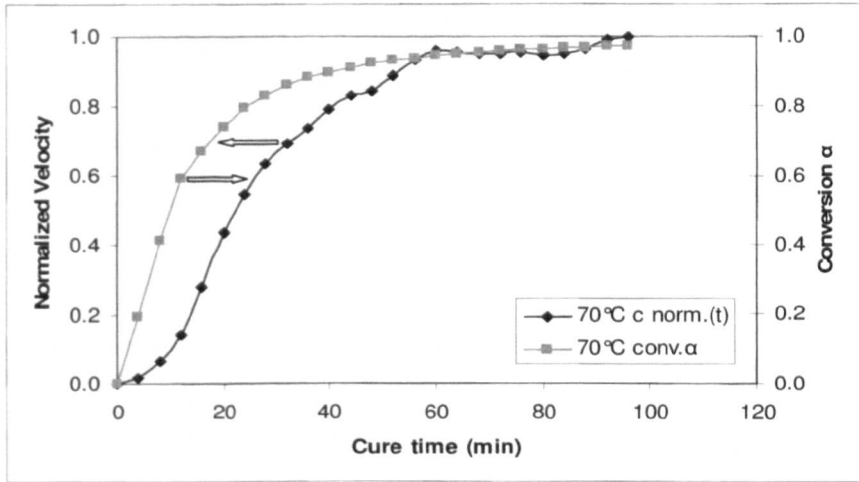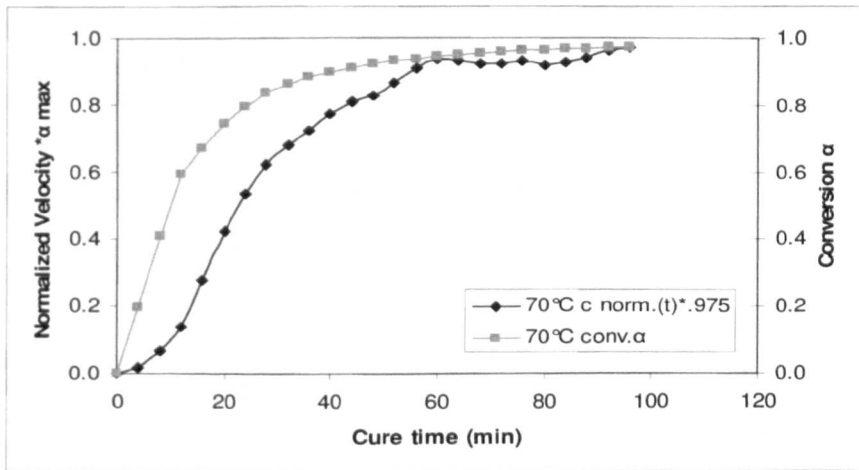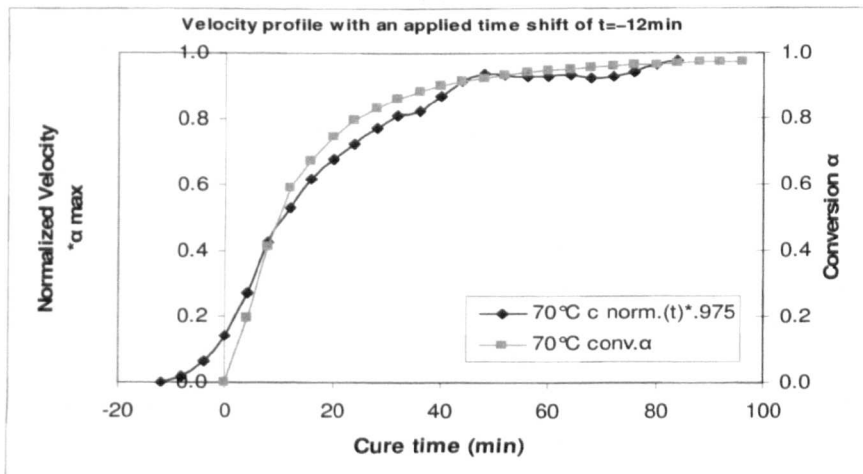
The optimum values of time shift are listed in table 9.3 and are plotted in figure 9.23 as a function of temperature. The time lag reduces with temperature. The time shift temperature curve can be ideally modelled by a fourth order polynomial as shown in figure.

Table 9.3 Time shift of velocity ($-t_{lag}$) and corresponding temperature dependent Shift factor (a_T) at different isothermal cure temperatures obtained for correlating between calorimetric conversion and ultrasonic longitudinal wave velocity during isothermal cure process of Araldite 2015.

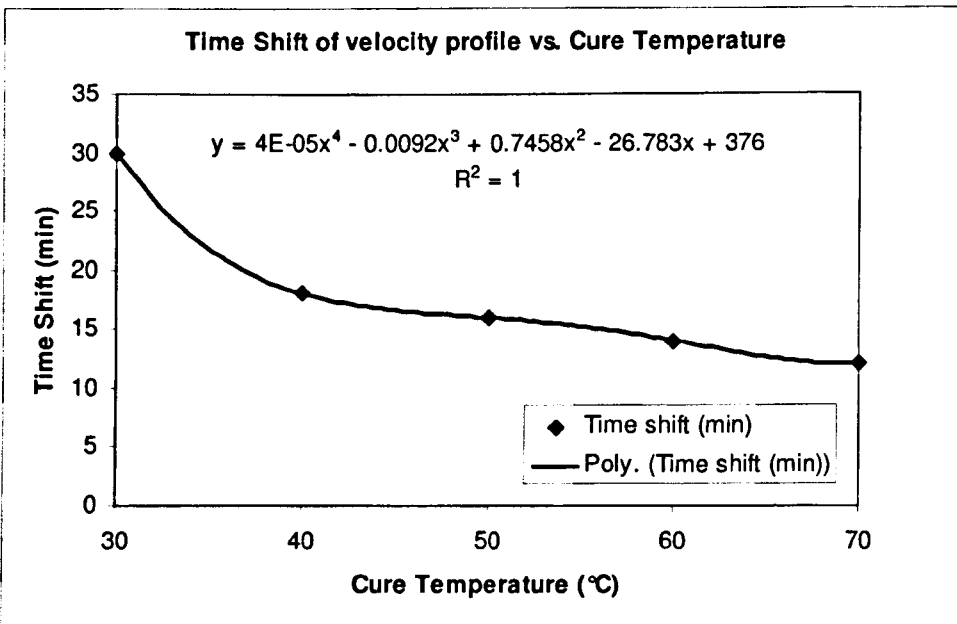| T_{cure} (°C)	30	40	50	60	70
Time shift of velocity ($-t_{lag}$) (min)	30	18	16	14	12
Shift factor (a_T)	1.0	0.60	0.533	0.466	0.40

Figure 9.23 Applied time shifts on normalized ultrasonic velocity profiles at 5MHz as a function of isothermal cure temperature. The corresponding equation of fit and its correlation coefficient are also presented in the figure.

It can be seen from figures 9.18—9.22(a,b) that the DSC curve always lead the normalized velocity curve. This has already been explained. At the beginning of the cure, due to the high concentration of reactive groups in the liquid reactive mixture, the calorimetric conversion increases more rapidly than the velocity, since the mechanical properties of the resin before the gel point are scarcely affected by the growth of the molecular weight. Therefore, the time lag exists between the two curves. Near gelation, the growing branched molecules show a considerable elastic response, which is detectable by a significant increase in velocity and modulus. After that when the cure is fully developed both curves levels off to a plateau. Hence, it is found that the DSC is much more sensitive to changes occurring at the early stages of the cure but is relatively insensitive to the changes occurring at the latter stage, especially after vitrification. The observed time lag between DSC conversion and ultrasonic velocity traces indicate delays in the development of velocity, giving greater sensitivity towards the end of cure. This raises the possibility of using ultrasonic velocity to predict calorimetric conversion. In fact, ultrasonic compression wave velocity shows a better sensitivity at the end of the cure.

It can be mentioned here that there have been other attempts to correlate the evolution of ultrasonic compression modulus during cure to conversion measured by DSC [3,5,6] and broadly almost similar qualitative correlation was demonstrated. This is expected as the modulus follows the square of the velocity. However, in our case, the velocity data gave very much closer agreement with the conversion curves.

Basically, the relationships between ultrasonic wave propagation phenomena and reaction kinetics are complex and difficult to determine. We found that the real part of the elastic modulus, as represented by ultrasonic longitudinal phase velocity $c(t)$ could be used as an indicator of fractional conversion α, by normalizing $c(t)$ and imposing a scaling term α_{max} and time lag (t_{lag}) between α and $c(t)$ following the equation (9.4). So, we see that the link between fractional conversion and the ultrasonic phase velocity contained a time lag and a scaling term which could be variable and would therefore have to be set for each material and set of process conditions before it could be used to track chemical reaction. Also, each material has a specific sound velocity like a finger print, depending on its reactivity and chemical composition and processing condition. Thus, our results indicate that ultrasonic compression wave

velocity has potential not only to monitor the cure process but also to map other methods of cure tracking, particularly the DSC. This suggests that it may be possible to use ultrasonic compression wave velocity as a predictor of calorimetric conversion measurements observed by DSC.

Though system specific, the initial study with this preliminary results indicate the promise of being able to measure the degree of cure from the longitudinal velocity for commercial resin system. Our study is based on making a series of different measurements at different temperatures for a group of isothermal cure cycles of a commercial epoxy resin with ultrasonic and conventional DSC technique. A more careful study needs to be done to better understand this potential. Studies of other wide varieties of epoxy/amine systems have been begun to determine if they follow this same trend and they can be shaped under the same methodology applied. This may constitute promising future work. Although system specific and non-conventional this methodology based on equation (9.4), to some extent, constitutes a *novel way* of quantifying the degree of cure of a thermoset network from ultrasonic longitudinal velocity measurements which is interesting. This relationship is of potential importance for cure monitoring, since it is possible to measure ultrasonic longitudinal velocity, but not the degree of cure online.

Matsukawa et al [2] once stated *"simple ultrasonic investigations suffer from the disadvantage of not knowing the relationship between changes in elastic properties(determined from ultrasonic velocity) and extent of chemical reaction"*. Combining ultrasound and differential scanning calorimetry to study the cure of a commercially important epoxy thermosetting system this research work has, at least in part, *addressed this disadvantage and thus answered this statement*, and shown that *ultrasonic compression wave velocity could be used as an indicator of calorimetric extent of cure measurements* and that physical and mechanical changes observed ultrasonically can be corroborated with changes observed by DSC.

Moreover, the ability of both the ultrasound and DSC technique to detect the effects of changing cure temperature upon the cure cycle have been demonstrated. The ultrasonic results agree with those found previously by other authors. Apart from the correlation between velocity and conversion, the rest of the work presented earlier in

this chapter expands the body of knowledge by corroborating the effect of cure temperature upon physical changes during cure, observed ultrasonically, with changes observed using DSC.

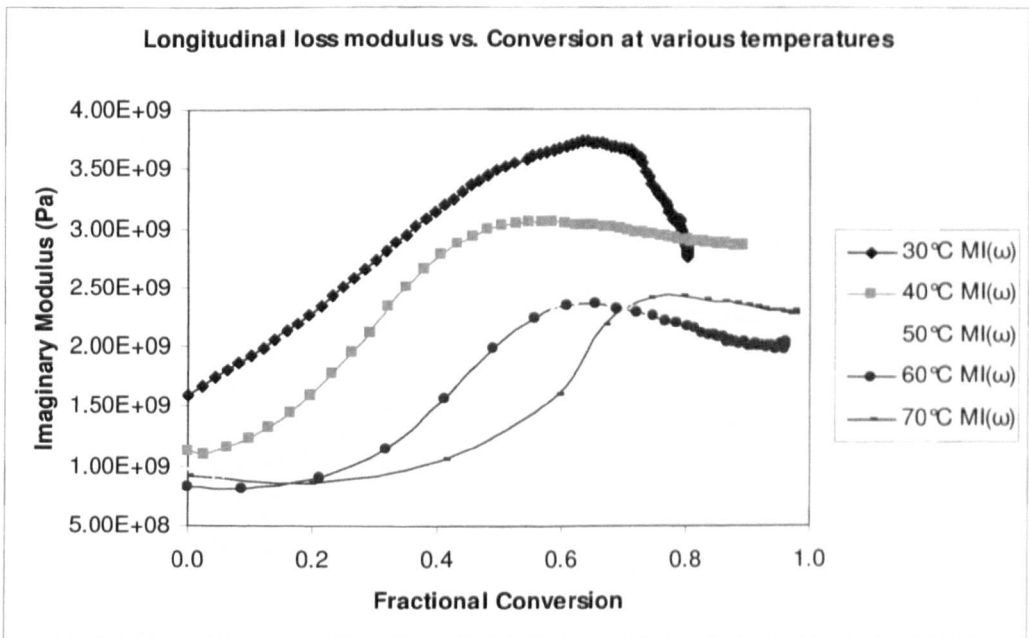## 9.14 Storage and loss modulus versus conversion

Figure 9.24 illustrates Ultrasonic Longitudinal (a) storage modulus and (b) loss modulus at 5MHz as a function of calorimetric conversion at cure temperatures of 30°C, 40°C, 50°C, 60°C, and 70°C. From this results we get some qualitative picture of development of modulus as the cure progresses. Hence viscoelastic information also could be extracted. The development of bulk and shear moduli during cure have already been discussed early in this chapter. The storage modulus follows the same trend shown by velocity. The limited change of storage modulus at the early stages of cure most probably associated with a slight increase of bulk modulus in the liquid resin while shear modulus gives a significant contribution to the storage modulus when a rubbery gel is formed. After the gelation conversion chain entanglements become significant causing a change in behaviour. These data indicate that the storage modulus mainly sensitive to the increasing crosslink density occurring after gelation rather than to the number of reacted groups. So, a strong nonlinear correlation between storage modulus and conversion is observed. The loss modulus gradually increases to a peak from the early stages of cure corresponding near gelation and then decreases as the mechanical properties developed.

9.15 Attenuation versus conversion

Figure 9.25(a—e) shows ultrasonic attenuation at 5MHz as a function of calorimetric conversion at cure temperatures of :(a) 30°C, (b) 40°C, (c) 50°C, (d) 60°C, and (e) 70°C. From the early discussions of this chapter we know that the attenuation data can provide us with qualitative information on the reaction rate, as observed by the width and shift of the attenuation peak. From the figure we can see that attenuation value gradually increases with conversion, reaches to a peak and then gradually decreases. At higher temperatures an initial decrease of attenuation coupled with a downward shift is due to the reduction of viscosity because of exothermic heat of reaction. The conversions corresponding to the attenuation peaks can be seen from the figure.
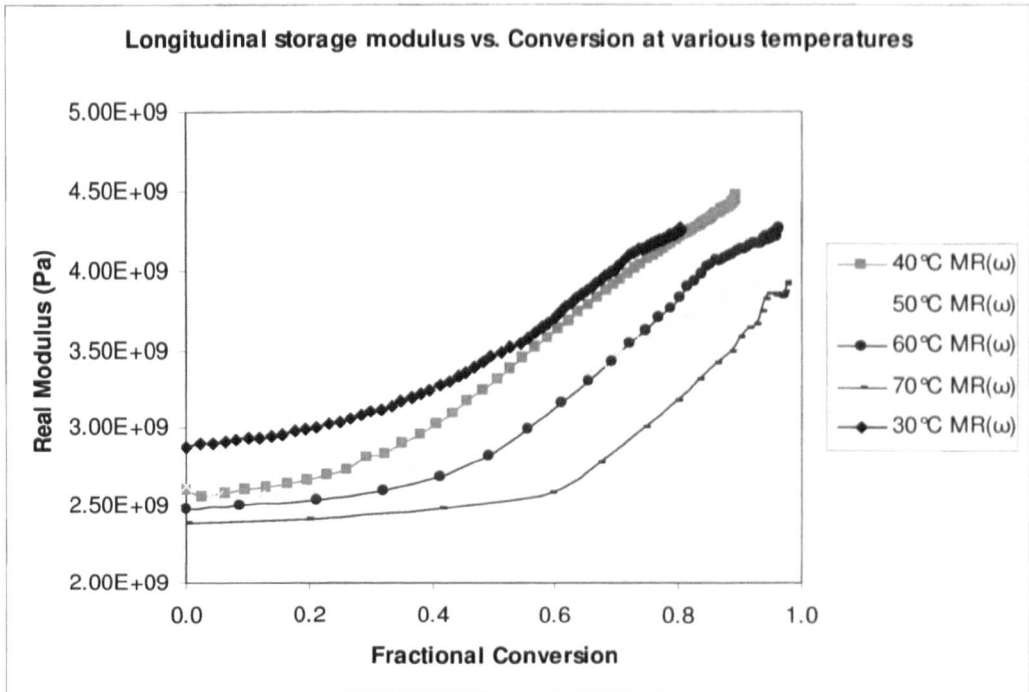
(a)

(b)

Figure 9.24 Ultrasonic Longitudinal **(a)** storage modulus and **(b)** loss modulus at 5MHz as a function of calorimetric conversion at cure temperatures of 30°C, 40°C, 50°C, 60°C, and 70°C.
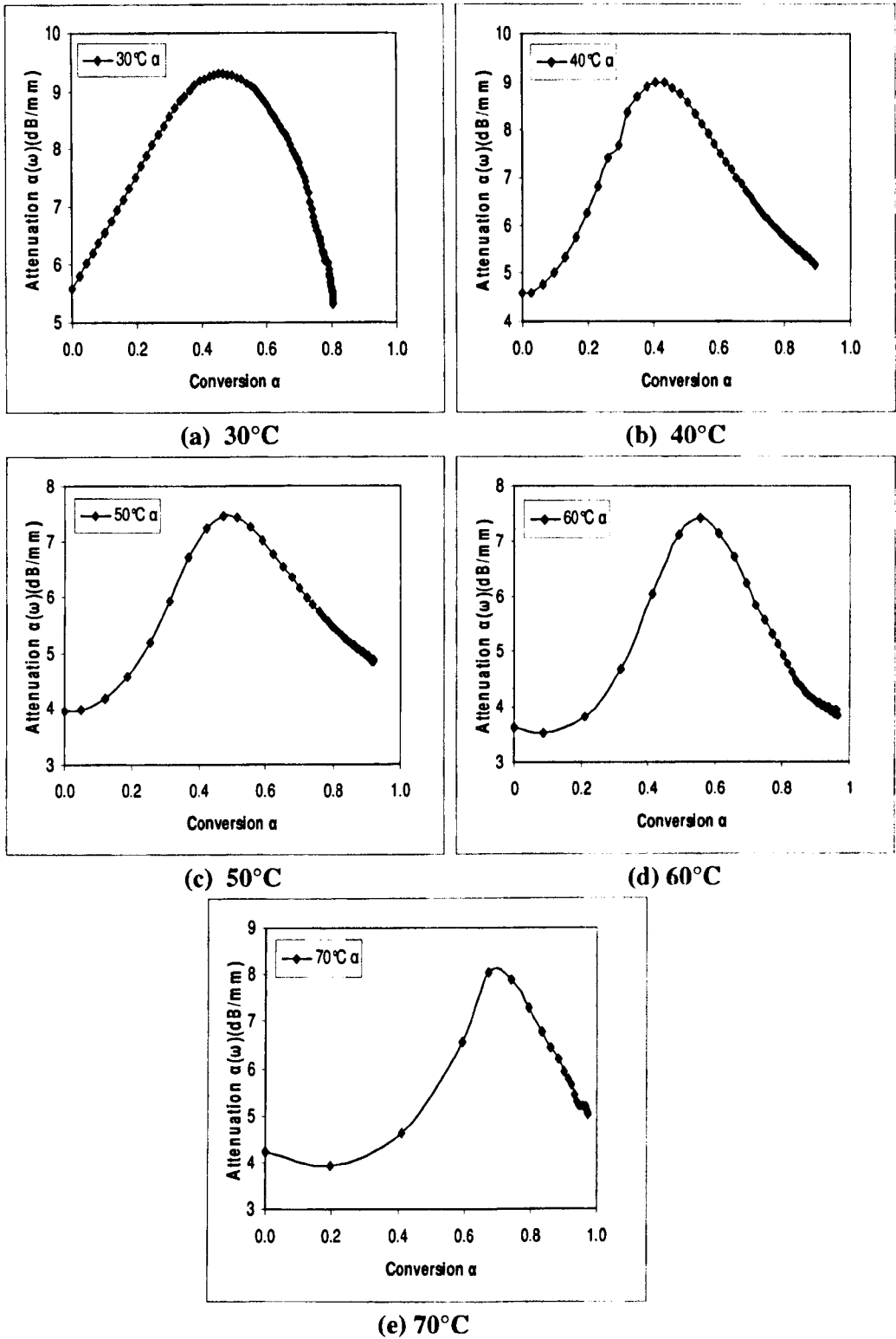
Figure 9.25 (a—e) Ultrasonic attenuation at 5MHz as a function of calorimetric conversion at cure temperatures of :(a) 30°C, (b) 40°C, (c) 50°C, (d) 60°C, and (e) 70°C.

382

9.16 References

1. Freemantle, R.J., and Challis, R.E., Meas. Sci. Technol. vol-9, 1998, 1291-1302.

2. Matsukawa, M., Nagai, I., J. Acoust. Soc. Am. vol-99, 1996, 2110.

3. Maffezzoli, A., Quarta, E., Luprano, V.A.M., Montagna, G., Nicolais, L., Journal of Applied Polymer Science, vol-73,1999,1969-1977.

4. Xu et al, J. Therm. Anal. Cal., 78, 2004.

5. Lionetto, F., Rizzo, R., Luprano, V.A.M., Maffezzoli, A., Materials Science and Engineering A, vol. 370, 2004,284-287.

6. Pindinelli, C., Montagna, G., Luprano, V.A.M., and Maffezzoli, A., Macromolecular Symposia, vol. 180, 2002, 73-88.

Chapter 10   Conclusions and Suggestion for Future Work

A summary of the conclusions drawn from this investigation in connection to its objectives along with suggestion for future work are presented in this chapter.

10.1 Potential Overview of the Present Investigation

(1)Both *monitoring* and *modelling* are valuable for optimizing the cure process. The predictive ability of the simulation can be used as a part of the process design, while monitoring constitutes a potential tool for on line control. Therefore, the need for a combination of modelling and monitoring has arisen. Combining the cure kinetics modelling and thermal (DSC) and ultrasonic cure monitoring to characterize the cure state of a commercial epoxy thermosetting system of industrial importance under study, this research work, at least in part, has been met this need.

(2)The cure kinetics of the catalyzed multifunctional unmodified epoxy-amine system has been described by various authors, but there is less information when both catalyst and reactive diluent is used in the formulation of two epoxy resin mixture. Both external catalyst and aliphatic reactive diluent modifier in the formulation of two epoxy resin mixture (along with diethylene triamine hardener and mica) keep this complex system under study odd from others and to some extent *a new one* to report cure kinetics to the best of our knowledge.

10.2 Thermo-kinetic characterization and cure kinetics modelling using DSC

(3) We found that the curing behaviour coupled with cure mechanism particularly the kinetic changes through the cure reaction could be manifested in *conversion dependency of activation energy*, $E_{a,\alpha}$ on α obtained utilizing *iso-conversional analysis* coupled with the light of *physics of advanced kinetics research*. The experimentally evaluated values of $E_{a,\alpha}$ are *reasonable* and *fairly consistent with the literature estimates* for the activation energies of the *autocatalytic primary amine addition* (at $\alpha \rightarrow 0$) and of *autocatalyzed epoxy-amine addition* and assure adequate statistical soundness of their validity.

(4) It is evident that the autocatalytic model $d\alpha/dt = k\alpha^m(\alpha_{max} - \alpha)^n$ in equation (6.8) with incorporation of $\alpha_{max}(T)$, maximum value of conversion at a particular temperature, as expressed by equation (6.11) in section 6.3.1, instead of full conversion 1, *most closely simulate* the *non-typical autocatalytic* isothermal curing behaviour of the complex commercial epoxy (modified) thermosetting system Araldite 2015 under investigation with almost a reasonable degree of satisfaction over the entire range of conversion (under both chemical controlled and diffusion controlled conditions) and temperature (30°C–80°C) studied without the *a priori need of knowledge of a glass transition temperature model*. This *advantageous feature* minimizes the experimental effort usually required for the incorporation of a T_g submodel. This model allows excellent increased accuracy at the later stages of the cure for the entire range of temperature studied.

(5)The values of the squared correlation co-efficient, r^2 (i.e. co-efficient of determination) of curve fitting or the *goodness of fit* are found to be *almost independent of the maximum obtainable conversion*, α_{max} and hence also almost *independent* of the curing temperature as well. This reveals the *reliability of this kinetic model* for the DGEBA-based commercial thermosetting system under study.

(6) The *non-conventional autocatalytic effect, some features of reaction mechanism* and prediction of the *trimolecular catalysis mechanism* of curing reaction founded on *trimolecular* transition state complexes (TSC) was found to be manifested in *temperature dependency of reaction orders* based on the autocatalytic kinetic model in equation (6.8), which was elucidated and justified critically and comprehensively. This in depth interpretation added potential weight. *Interestingly,* the value of the autocatalytic reaction order *m* is found to increase with increasing cure temperature, *unlike the conventional autocatalytic effect* where *m* decreases with increasing cure temperature. Utilizing iso-conversional method inherent to the autocatalytic kinetic model in equation (6.8) the cure behaviour along with cure mechanism could be exhibited in *conversion dependency of activation energy* as has been mentioned above in point (3).

(7)Some interesting features of other individual model tested can be mentioned here which are useful from the perspective of kinetic modelling. **(i)** It is evident that *much better fit is observed with incorporating α_{max} as the constraint of the reaction going to completion is lifted* and particularly for the case of lower temperature range of 30°C–50°C which suffers from poor fit of kinetic data due to the fact that the *assumption of α_{max} =1 in the conventional model is overly simplified.* **(ii)**The simulations with the both forms of autocatalytic model of Gonzalez-Romero [equations (6.26) and (6.28)] show *non-zero initial rates of reaction* at $\alpha = 0$, the feature which the reaction rate profiles of the studied thermosetting system display. **(iii)** The Gonzalez-Romero model with the inclusion of α_{max} gives the *best simulation* for the particular case of kinetic data of lower cure temperature range (30°C–50°C). **(iv)** Interestingly, *accurate consistency between the experimental data and the theoretically predicted values of half-life of cure*, $t_{1/2}$ at all of the six isothermal temperatures is obtained with Avrami model (figure 6.39).

(8) Implementing diffusion factor $f_d(\alpha,T)$ in conventional autocatalytic kinetic model excellent fit is observed *at specific higher conversion region* in the later stages of the cure, where a deviation appears due to the onset of vitrification. It is more evident at lower cure temperatures where the deviation appears to be greater. Hence, the overall goodness of fit improves. This introduction of diffusion factor enables us to explore some in depth useful information associated with the diffusion controlled kinetics related to our data. The downturn in $f_d(\alpha,T)$ at α_c due to onset of diffusion increasingly occurs at higher conversions with increasing cure temperature is clearly evident. Our results show that the critical conversion α_c is a *useful parameter* which specifically relates to the *onset of vitrification* for the epoxy thermosetting system under study. Thus it *reflects the state of cure of the system as well as the temperature of cure.*

(9)It has clearly demonstrated that the kinetics of the isothermal cure reaction comprising chemical and diffusion control phases *can be better characterized by* the reduced reaction rate $[(d\alpha/dt)/(1-\alpha)^2]$ vs. conversion[α] plot based on autocatalytic model of Horie along with corresponding diffusion factor (simulated) $[f_d(\alpha,T)]$ vs. conversion [α] plot.

(10)The cure kinetics was also analyzed comprehensively from both kinetic and thermodynamic viewpoint based on the correlations between their associated parameters evaluated in the context of Horie model. This approach of *thermodynamic reasoning* founded on Eyring equation coupled with kinetic correlations which we employed, is, to some extent uncommon, can **contribute** towards a **new way of characterization** and can add potential weight in critical understanding of the cure reaction from the *micro-kinetic standpoint* providing information of the overall effect of reactive diluent on kinetics, regarding reaction pathways, kinetic homogeneity / inhomogeneity associated with reaction phase and the properties of the end product which is important to control the reaction kinetics to attain desired properties in the end material, thus can **contribute** in expanding current body knowledge.

(11) (i) In contrast to the literature estimates the catalytic and autocatalytic reactions based on Horie model have found to have *comparable* activation energy values which is *non-typical* and ascribed to the *specificity of the complex commercial epoxy-amine system* under investigation. The analysis of our data from both kinetic and thermodynamic perspective indicates that (ii) the *autocatalyzed reactions, k_2 are much more favourable* than the *initially catalyzed reactions, k_1* (non- autocatalytic reactions), and that (iii) at the early stages of the cure reactions are more *homogeneous* and as the cure proceeds kinetic homogeneity becomes less pronounced and reactions become more *inhomogeneous*. All the findings were explained and justified.

(12)It is worth noting that in comparison to the data of other epoxy resins without reactive diluents, the analysis of our data in connection with the kinetic and thermodynamic parameters obtained based on the Horie model shows that most possibly the reactive diluent — (i) increased the maximum value of calorimetric conversion (α_{max}) and reaction rate $(d\alpha/dt)_{max}$ .The crosslink density seems not to be affected. These observations are elucidated and justified in detail with precise comparison in sections 5.1.1 and 5.2.1 in chapter 5. (ii) Reduced the viscosity in order to aid general processability which is its most conventional effect. This is reflected in the considerably *lower* values of *entropy* discussed in section 6.10.4.3 in chapter 6. While the values of

activation energies (E_{a1}, E_{a2}), pre-exponential factors (lnA_1, lnA_2), reaction rate constants (k_1, k_2), and process parameters remained within the typical values of epoxy formulations. Therefore, except the above mentioned effects the introduction of aliphatic segments of reactive diluent into the main chain of the epoxy *does not cause a significant change in the kinetics of the overall curing process* of the commercial thermosetting system under study.

(13) A TTT diagram of the cure process of this system under study was constructed. Such a diagram might form the basis of a molecular model to select a cure schedule (time-temperature).

(14) When looking at the non-typical autocatalytic reaction rate profiles at lower conversions, this highlights an **important advantage of** DSC. *By giving access to reaction rate this technique enables us to detect complex kinetic behaviour at low conversions that would be almost undetectable by other experimental techniques.*

10.3 Ultrasonic characterization of curing and comparison with DSC results

(15) The ultrasonic compression wave velocity (at 5 MHz) has been demonstrated to be the *most interesting* and *potential parameter* for monitoring and characterizing the cure process at all stages (from the very beginning to the end) which provided with the information of *degree of mechanical property development* of the curing material and *can detect gelation and vitrification* that occur during cure. Therefore, ultrasonic velocity measurement could be exploited for **non-destructive on-line process control** in an industrial environment. The *sigmoidal* shaped velocity profile also is a signature of autocatalytic reaction kinetics.

(16) The *onset* points where a change in curvature occur on the curves of ultrasonic compression wave phase *velocity* (at 5MHz) versus cure time at different isothermal temperatures all appear to be *iso-conversional* as observed by DSC, irrespective of cure temperature, and according to our prediction, fairly *consistent* with the literature data, it is most likely to be *indicative of gelation* for the epoxy thermosetting system under study.

The *theoretical gelation* and *ultrasonic prediction of gelation* have also been elucidated and justified.

(17)The activation energy value calculated from the ultrasonic prediction of gelation time, is within the order of magnitude of the activation energy value for the autocatalytic reaction rate constant k_2, obtained from Horie model and *it is related to the crosslinking reaction*. Comparison of activation energies from *ultrasonic* prediction of gel time *measurements* can be made with activation energies from *enthalpic measurements*, since ideally conversion is determined by the fraction of functional groups reacted for both.

(18)The *offset* points on the curves of ultrasonic compression wave phase *velocity* (at 5MHz) versus cure time at different isothermal temperatures, roughly which should occur around the shoulders before the plateau or velocity saturation regions, could be an indication, less precisely, to the onset of vitrification, which seems to appear to some extent earlier than the vitrification times (onset) estimated from the DSC data based on critical conversion of diffusion factor associated with empirical kinetic model of Kamal.

(19)It has been demonstrated that ultrasonic compression wave velocity (at 5MHz) could be used as a predictor of calorimetric conversion measurements for commercially important epoxy thermosetting system and thus can be used *to track chemical reaction on-line non-destructively* which is of *potential importance* for cure monitoring, since it is possible to measure ultrasonic longitudinal velocity, but not the degree of cure *online*.

(20)Though system specific, the methodology we utilized (based on normalizing the velocity $c(t)$ and imposing a scaling term α_{max} and   time lag (t_{lag}) between conversion α and velocity $c(t)$ following equation (9.4)), to some extent, constitutes a *novel way* of quantifying the degree of cure of a commercial epoxy thermoset network from ultrasonic longitudinal velocity measurements which is interesting and provide an exciting and promising opportunity for process monitoring.

(21) It is interesting to note that Matsukawa et al [1] once wrote *"simple ultrasonic investigations suffer from the disadvantage of not knowing the relationship between changes in elastic properties (determined from ultrasonic velocity) and extent of chemical reaction"*. Combining ultrasound and differential scanning calorimetry techniques to characterize the cure state of a commercial epoxy thermosetting system of industrial importance this research work has, at least in part, **addressed this disadvantage and thus answered this statement**, and shown that *ultrasonic compression wave velocity could be used as an indicator of calorimetric extent of cure measurements* and that physical and mechanical changes observed ultrasonically can be corroborated with changes observed by DSC.

(22) It has also been demonstrated that the fixed frequency (5MHz) ultrasonic compression wave attenuation, real and imaginary parts of compression modulus, ultrasonic loss tangent and associated central relaxation time, these parameters also provide with the information of the material state, progress of the structural development and the cure process as well. Our results indicate that ultrasonic loss tangent (at 5MHz) can provide information about *relaxation* and *micro-structural* properties. The development of the *central relaxation time* of the thermoset during the cure process is a useful measure of the progress of the structural development. However, due to the somewhat limited bandwidth of the ultrasonic technique only a *snap shot* of this process can be seen. *The end of cure ultrasonic data, in general, provide a convenient assessment of final product quality.*

(23) It has also been shown that *frequency-dependent* ultrasonic compression wave phase velocity and relative attenuation coefficient have the *potential to track the cure process at all stages of the cure* from viscous liquid to solid state. The attenuation was *close to a linear function of frequency* and this was associated with a small dispersion in phase velocity across the frequency range.

(24) The effect of temperature and frequency on the velocity, attenuation and loss tangent data have been narrated. Changes in the cure cycle and the resulting changes in the

390

physical and mechanical properties caused by changes in the different cure temperatures are well within the detection capability of the ultrasonic technique employed. From the attenuation profile, *qualitative information on the reaction rate* can be obtained, as observed by the *narrower width* and *shift of the attenuation peak* to shorter cure times with increasing cure temperature. *The shape of the velocity curves also reflect the rate of the chemical reaction.* It is evident that the gradient of the cure time versus compression wave velocity curve is steeper the higher the cure temperature and thus the reaction rate.

(25)It was found that the DSC is much more sensitive to changes occurring at the *early* stages of the cure but is relatively insensitive to the changes occurring at the latter stage especially after vitrification. Ultrasonic compression wave velocity shows a better sensitivity at the *end of the cure.*

(26)The ability of both the ultrasound and DSC technique to detect the effects of changing cure temperature upon the cure cycle have been demonstrated. The ultrasonic results agree fairly well with those of DSC. The principal conclusion follows from the results are — higher cure temperatures **(i)** increase the reaction rate, **(ii)** reduce the time taken to complete cure, **(iii)** reduce the time taken to reach gelation. Basically, by monitoring the polymerization reactions at different temperatures, the *Arrhenius behaviour of the crosslinking reaction is confirmed* by both ultrasonic and DSC data.

10.4 Suggestions for future work

(1) The complexity of our epoxy system requires more extensive study to draw any further conclusion. In our opinion, a more precise model of the cure mechanism in such complex epoxy-amine system would require techniques like Fourier Transform Infrared Spectrometry (FTIR) to determine the *concentrations* of the various species involved in the reaction. By following the changes in the concentration of the primary and secondary amines and epoxide, the information on the relative reactivities of the primary and secondary amines with the epoxide can be obtained which may enable to develop such

precise model. It is worth mentioning that the effect of reactivity ratio between primary and secondary amino hydrogens is still among the most hotly debated question.

(2) Though system specific, the initial study with the preliminary results associated with the quantitative correlation between ultrasonic velocity and calorimetric conversion, indicate the promise of being able to measure the degree of cure from the longitudinal velocity for commercial resin system. A more careful study needs to be done to better understand this potential. Studies of other wide varieties of epoxy/amine systems have been begun to determine if they follow this same trend and they can be shaped under the same methodology applied. This may constitute promising future work.

(3) Based on the isothermal data, further work should attempt non-isothermal curing of the similar epoxy system to have a complete in depth kinetics study and understanding.

(4) Future work should attempt to develop a deeper understanding of the relationships between the measured ultrasonic and thermal parameters, with the evolution of macromolecular structure. Also, we should attempt to develop some fundamental investigations on observed *anomalous* behaviour of ultrasonic attenuation in our resin system.

(5) Future work should attempt to gain an enhanced understanding of the changes to the physical properties of the resins caused by changes in stoichiometry and cure temperature.

10.5 References

1. Matsukawa, M., Nagai, I., J. Acoust. Soc. Am. vol-99, 1996, 2110.

"In science, self-satisfaction is death. Personal self-satisfaction is the death of the scientist. Collective self-satisfaction is the death of the research. It is restlessness, anxiety, dissatisfaction, agony of mind that nourish science."
— Jacques-Lucien Monod